A REVIEW OF SELECTED SMALL SCALE SEAWATER INTAKES IN SOUTH AFRICA AND AN INVESTIGATION INTO ABSTRACTION FROM THE SURFZONE ON ROCKY COASTLINES, BY MEANS OF THE HORIZONTAL WELL METHOD

By

Arivindra Brahmin

Submitted in partial fulfilment of the requirements for the degree of
Master of Science in Engineering
in the
Department of Civil Engineering
University of Stellenbosch

Mr G. Toms
Study Leader

Stellenbosch September 2011

Declaration

The work described in this dissertation was carried out in the Department of Civil Engineering, University of Stellenbosch, under the supervision of Mr Geoff Toms and is in accordance with the requirements of the University for the Award of Master of Science in Engineering.

This dissertation represents the original work by the author and has not otherwise been submitted in any form for any degree or diploma to any tertiary institution. Where use was made of work done by others, it has been duly acknowledged in the text.

_____ 23rd September 2011

A. Brahmin

Synopsis

South Africa is a relatively dry country with an annual average rainfall of 464mm compared to a world average of 860mm (WSA, 2009). Water shortages and droughts are fairly common to the western and high lying of regions South Africa. Due to its population growth and the rapid development, like the rest of the world, there has been an increased demand for water.

Due to increasing costs of procuring water and its decreasing availability, the option of using seawater as a source for freshwater or directly in industrial processes has become competitive, especially in the arid parts of the world. The design of seawater intakes forms an integral part of providing a secure source of seawater.

The objective of this thesis is to aid in the development of guidelines for the design of small scale seawater abstraction systems on rocky coastlines using the Horizontal Well Method. Recommendations for guidelines will be given.

Acknowledgements

I wish to extend my thanks to Mr G Toms for his patience, support and guidance during the compilation of this thesis. I would like to thank Mr DE Bosman for opening up a world of opportunity.

I would like to thank the staff of the Hydraulics laboratory and the Workshop at the Civil Engineering department: Stellenbosch University, for their assistance and direction. I could have not carried out these experiments without their immense help.

I would like to thank RLH Consulting Engineers for proposing this dissertation topic and supporting me with time off during the testing phase.

Finally, an enormous thank you to my wife Anneita (and the *outlaws*), whose love, sacrifice and understanding was never in short supply for the duration of this thesis.

A REVIEW OF SELECTED SMALL SCALE SEAWATER INTAKES IN SOUTH AFRICA AND AN INVESTIGATION INTO ABSTRACTION FROM THE SURFZONE ON ROCKY COASTLINES, BY MEANS OF THE HORIZONTAL WELL METHOD

TABLE OF CONTENTS

Declaration	ii
Synopsis	iii
Acknowledgements	iv
Table of Contents	v
List of Tables	ix
List of Figures	xiii
List of Symbols	xx
List of Abbreviations	xx
Chapter 1 INTRODUCTION	
1.1 Background	1
1.2 Present Situation	2
1.3 Objectives and Aims	3
1.4 Thesis Presentation Structure	3
Chapter 2 LITERATURE REVIEW	
2.1 Introduction	4
2.2 Uses of Extracted Seawater: Overview	4
2.2.1 Cooling	5
2.2.1.1 Cooling at Power Stations	5

2.2.1.1 Cooling for Air conditioning 8
2.2.2 Desalination 9
2.2.3 Fish Processing 10
2.2.4 Mariculture 12
2.2.5 Scientific Facilities 14
2.2.6 Recreational Facilities 15
2.2.7 Environmental 16
2.3 Seawater Intake Systems 17
2.3.1 Direct Intakes 17
2.3.2 Sub-bottom Abstraction 19
2.3.3 Surf Zone Abstraction (including) 20
2.3.3.1 Sandy Coastlines 20
2.3.3.2 Rocky Coastlines 22
2.4 Hydraulic Review 23
2.4.1 Introduction 23
2.4.2 Sub-Surface Seawater Abstraction from a Sandy Beach 23
2.4.2.1 Beach Wells 23
2.4.2.2 Horizontal Beach Galleries 24
2.4.2.3 Infiltration Galleries with Horizontal well-screens 25
2.4.2.4 Seabed Filtrations 26
2.4.3 Basic Groundwater Flow Theory 28
2.4.4 Groundwater Abstraction 30
2.4.4.1 Well Hydraulics 30
2.4.4.2 Unconfined steady flow well hydraulics 31
2.4.4.3 Pumping Tests 33
2.4.5 Hydraulic Conductivity of Filter and Porous Material 35
2.4.5.1 Introduction 35
2.4.5.2 Absolute Permeability 36
2.4.5.3 Hydraulic Conductivity: Empirical Relations 36
2.4.5.4 Hydraulic Conductivity: Turbulent Flow 39
2.4.6 Hydraulic Design Guidelines: Sub Surface Seawater Abstraction 41
2.4.6.1 Introduction 41
2.4.6.2 General Hydraulic Design Criteria 42
2.4.6.3 Backflushing 42
2.4.6.4 General Design Criteria: Horizontal Screens in Seawater Intakes 43

2.4.7 Filter Design 44
2.4.7.1 Introduction 44
2.4.7.2 Internal Erosion of Granular Material 45
2.4.7.3 Interface Stability of a Granular Filter 46
2.4.7.4 Permeability Requirements of a Granular Filter 47
2.4.7.5 Interface Stability of a Geotextile Filter 48
2.4.7.6 Requirements on Permeability of a Geotextile Filter 49

Chapter 3 REVIEW OF SELECTED SEAWATER INTAKES ALONG THE SOUTH AFRICAN COASTLINE

3.1 Introduction 50
3.2 Hermanus: Mariculture 50
3.3 Sea Fisheries Aquarium: Research 55
3.4 Two Oceans Aquarium: Research/Public Education 57
3.5 Sea World Aquarium: Research/Public Education 61
3.6 Paternoster: Mariculture 66
3.7 Britannia Bay: Mariculture 72
3.8 St Helena Bay: Mariculture 77
3.9 Summary of Problems Experienced 81

Chapter 4 CASE STUDY: INVESTIGATION OF INTAKE PIPES FOR A HORIZONTAL WELL SYSTEM, FOR ABSTRACTING SEAWATER FROM THE SURFZONE ON ROCKY COASTLINES

4.1 Introduction 84
4.2 Conceptual Design and Layout of Seawater Intake on a Rocky Coastline 86
4.2.1 Background 86
4.2.2 Proposed Seawater Intake 87
4.2.3 Cross Section Design of Seawater Intake 88
4.2.4 Structural Design of Seawater Intake 89
4.2.5 Filter Design of Seawater Intake 89
2.4.5.1 Interface Stability of a Closed Granular Filter 91
2.4.5.2 Permeability Requirements of a Granular Filter 92
4.3 Specific Aims of Investigation 94
4.3.1 Overall Objectives 94
4.3.2 Flow regime and Filter Objectives 94

4.4 Hydraulic Physical Model 95
4.4.1 Model Design Objectives 95
4.4.2 Intake Pipes 96
4.4.3 Types of Test 97
4.4.4 Basic Methodology of Tests 97
4.4.4.1 Test 1: Hydraulic test with water only 97
4.4.4.2 Test 2: Hydraulic test with Pipe in 19mm Stone Bedding 99
4.4.4.3 Test 3: Hydraulic test with Pipe in 19mm Stone and Sand Bedding 100
4.4.5 Three Methods used for Estimating Intake Pipe Bedding Headloss 101
4.4.6 Minor losses in the Model 103

Chapter 5 CASE STUDY: TEST RESULTS FOR DETAIL INVESTIGATION OF INTAKE PIPES IN HYDRAULIC PHYSICAL MODEL

5.1 Slotted PVC Pipe Abstraction Model 106
5.1.1 Synopsis 106
5.1.2 Test 1: Water Only Test 107
5.1.3 Test 2: Water and Stone Test 108
5.1.4 Test 3: Water, Stone and Sand Test 110
5.1.4.1 Introduction 110
5.1.4.2 Testing 111
5.1.5 Backflushing 113
5.1.5.1 Introduction 113
5.1.5.2 Design of Flushing System 113
5.1.5.3 Augmentation of Flushing System 114
5.1.6 Test 4: Water, Stone and Sand Test after Back Flushing 118
5.2 Perforated PVC Pipe Abstraction Model 119
5.2.1 Synopsis 119
5.2.2 Test 1: Water Only Test 121
5.2.3 Test 2: Water Only Test with Extra Perforation 122
5.2.4 Test 3: Water and Stone Test 123
5.2.5 Test 4: Water, Stone and Sand Test 124
5.2.5.1 Introduction 124
5.2.5.2 Testing 124
5.3 Metal Wire Pipe Abstraction Model 129
5.3.1 Synopsis 129

5.3.2 Test 1: Water Only Test 130
5.3.3 Test 2: Water and Stone Test 131

Chapter 6 DISCUSSIONS OF CASE STUDY TEST RESULTS

6.1 Introduction 133
6.2 Water Only Tests 133
6.2.1 Test Results 133
6.2.2 Porosity versus Flowrate Test 135
6.3 Tests with Stone Bedding 137
6.4 Test with Stone + Sand Bedding 139
6.4.1 Slotted PVC Pipe 139
6.4.2 Extra Perforated PVC Pipe 141
6.5 Estimating losses due to Stone Bedding 143
6.6 Estimating losses due to Sand and Stone Bedding 147
6.7 Comparison of Three methods used to estimate Stone Bedding losses 147
6.8 Concluding Summary and Recommendations 150

Chapter 7 DESIGN RECOMMENDATIONS FOR SMALL SCALE SEAWATER INTAKES ON A ROCKY COASTLINE USING THE HORIZONTAL WELL SYSTEM

7.1 Introduction 151
7.2 Design Steps 151
Step 1: End Usage Requirements 151
Step 2: Site Specific and Physical Conditions 153
Step 3: Adjacent Landuse 153
Step 4: Lateral location of Seawater Intake 154
Step 5: Seawater Intake per Coast Type 154
Step 6: Design of a Seawater Intake for Rocky Coastlines 155
Step 7: Structural Design of Seawater Intake 156
Step 8 Hydraulic Design of Seawater Intake & Protection 156
Step 8.1 General Hydraulic Design 156
Step 8.2 Empirical Relations for Estimating Hydraulic Conductivity 157
Step 8.3 Hydraulic Conductivity: Turbulent Flow 157
Step 8.4 Hydraulic Design of Horizontal Intake Pipe & Stone bedding Combination 157
Step 9: Environment Impacts on a Seawater Intake 158

REFERENCES 159

APPENDICES

Appendix A: Design of Model 163

Appendix B: Calibration of V Notch Weir 168

Appendix C: Soil Grading 175

Appendix D: Slotted PVC Pipe Abstraction Model 177

Appendix E: Perforated PVC Pipe Abstraction Model 242

Appendix F: Metal Wire Pipe Abstraction Model 328

Appendix G: Summary of Results 377

Appendices D, E, F and G are added as electronic copies. These can be found on CDs, situated at the end of thesis.

LIST OF TABLES

Table 2.1: Aspects relevant for a seawater intake location selection
Table 2.2: Porosity and hydraulic conductivity: natural material. (Roberson, et al, 1998)
Table 2.3: Hydraulic conductivity of various materials (Schwartz, 2000)
Table 2.4: Permeability of granular materials (CIRIA, CUR, CETMEF, 2007)
Table 4.1: Details of material sizing for armour protection of seawater Intake
Table 4.2: Material sizes for armour protection of seawater Intake [meters]
Table 4.3: Calculation of Permeability for armour protection of seawater Intake
Table 6.1: Results of Water Only Test carried on the four test pipe
Table 6.2: Relationship between porosity versus the flowrate divided by the associated headloss for the four test pipes
Table 6.3: Results of Water and Stone bedding Test carried on the 3 test pipes
Table 6.4: Pressure loss and Flowrate vs. time relationship for the Slotted PVC Pipe with sand and stone bedding
Table 6.5: Pressure Loss vs. Flowrates for: Extra perforated PVC Pipe with sand + stone bedding and Extra perforated PVC Pipe with stone bedding only (WST + WSST)
Table 7.1: Pressure loss - flow relationship for intake pipes

Table B1: Flow vs. Height for V Notch Weir
Table B2: Flow vs. Height for 90° V Notch Weir
Table C1: Soils grading for combined Phillipi and Granular Filter sand
Table D1: The physical aspects of the HPM and Intake Pipeline
Table D2: Total headloss and initial flow rate for Water Only test
Table D3: Total headloss and flow rate incorporating losses
Table D4: Disaggregation of pressure losses
Table D5: Perforation friction (Loss A) flowrate Half and Full pipeline
Table D6: Inflowing velocity of water flowing into the pipe, over the length of the Intake Pipeline
Table D7: Calculated flowrate from all segments of the Pipeline
Table D8: The physical aspects of the HPM and Intake Pipeline
Table D9: Total Headloss and initial flow rate for Water and Stone test
Table D10: Total headloss and flow rate incorporating losses for Water and Stone Test
Table D11: Disaggregation of pressure losses for Water and Stone test
Table D12: Perforation (Loss A), and Stone Bedding friction, Half flowrate and Full pipeline flowrate
Table D13: Inflowing velocity of water flowing into the pipe, over the length of the Intake Pipeline
Table D14: Calculated Flowrate from all segments of the Pipeline
Table D15: ø250mm Slotted pipe test: Pressure loss due to Stone Bedding Only
Table D16: ø250mm Slotted Pipe, Water and Stone Bedding Test: Flow through segments

Table D17: Summary: Calculating the Hydraulic conductivity
Table D18: Segment 1: Averaging of Areas
Table D19: Segment 1: Velocity and cumulative headloss
Table D20: Segment 2: Averaging of Areas
Table D21: Segment 2: Velocity and cumulative headloss
Table D22: Segment 3: Averaging of Areas
Table D23: Segment 3: Velocity and cumulative headloss
Table D24: Segment 4: Averaging of Areas
Table D25: Segment 4: Velocity and cumulative headloss
Table D26: Segment 5: Averaging of Areas
Table D27: Segment 5: Velocity and cumulative headloss
Table D28: Summary of 15 Headloss Tests. Results from Tables 15 to 24
Table D29: Summary of maximum headloss versus flow rates
Table D30: Total Headloss and initial flow rate for Sand and Stone Bedding
Table D31: Total headloss and flow rate incorporating losses
Table D32: Disaggregation of pressure losses
Table D33: Loss A+ sand + stone bedding with corresponding flowrates
Table D34: Total Headloss and initial flow rate for Sand and Stone Bedding
Table D35: Total headloss and flow rate incorporating losses
Table D36: Disaggregation of pressure losses
Table D37: Loss A + sand + stone bedding with corresponding flowrates
Table E1: Perforated PVC Pipe: Variables and Values
Table E2: Extra Perforated PVC Pipe: Variables and Values
Table E3: The physical aspects of the HPM and Initial Intake Pipeline
Table E4: Total Headloss and initial flow rate for Initial Water Only test
Table E5: Total headloss and flow rate incorporating losses
Table E6: Disaggregation of pressure losses
Table E7: Perforation friction (Loss A) flowrate for Half and Full pipeline
Table E8: The physical aspects of the HPM and Initial Intake Pipeline
Table E9: Total Headloss and initial flow rate for Initial Water Only test
Table E10: Total headloss and flow rate incorporating losses
Table E11: Disaggregation of pressure losses
Table E12: Extra Perforation friction (Loss A) flowrate for Half and Full pipeline
Table E13: Inflowing velocity of water flowing into the pipe, over the length of the Intake Pipeline
Table E14: Calculated Flowrate from all segments of the Pipeline
Table E15: Pressure losses over length of Intake Pipeline
Table E16: Total Headloss and initial flow rate for Water and Stone test
Table E17: Total headloss and flow rate incorporating losses for Water and Stone Test
Table E18: Disaggregation of pressure losses for Water and Stone test

Table E19: Perforation (Loss A), and Stone Bedding friction, flowrate for Half and Full pipeline
Table E20: Inflowing velocity of water flowing into the pipe, over the length of the Intake Pipeline
Table E21: Calculated Flowrate from all segments of the Pipeline
Table E22: Pressure losses over length of Intake Pipeline
Table E23: ø250mm perforated pipe test: Pressure loss due to Stone Bedding only
Table E24: ø250mm Perforated pipe, Water and Stone Bedding Test: Flow through segments
Table E25: Summary: Calculating the Hydraulic conductivity
Table E26: Segment 1: Averaging of Areas
Table E27: Segment 1: Velocity and cumulative headloss
Table E28: Segment 2: Averaging of Areas
Table E29: Segment 2: Velocity and cumulative headloss
Table E30: Segment 3: Averaging of Areas
Table E31: Segment 3: Velocity and cumulative headloss
Table E32: Segment 4: Averaging of Areas
Table E33: Segment 4: Velocity and cumulative headloss
Table E34: Segment 5: Averaging of Areas
Table E35: Segment 5: Velocity and cumulative headloss
Table E36: Summaries of results for Tables 26 to 35
Table E37: Summary of maximum headloss versus flow rates
Table E38: Total Headloss and initial flow rate for Sand and Stone Bedding
Table E39: Total headloss and flow rate incorporating losses
Table E40: Disaggregation of pressure losses
Table E41: Loss A + sand + stone bedding with corresponding flowrates
Table E42: Inflowing velocity of water flowing into the pipe, over the length of the Intake Pipeline
Table E43: Calculated Flowrate from all segments of the Pipeline
Table E44: Pressure losses over length of Intake Pipeline
Table E45: ø250mm perforated pipe test: Pressure loss due to Stone Bedding only
Table E46: ø250mm Perforated pipe, Sand and Stone Bedding Test: Flow through segments
Table E47: Summary: Calculating the Hydraulic conductivity
Table E48: Segment 1: Averaging of Areas
Table E49: Segment 1: Velocity and cumulative headloss
Table E50: Segment 2: Averaging of Areas
Table E51: Segment 2: Velocity and cumulative headloss
Table E52: Segment 3: Averaging of Areas
Table E53: Segment 3: Velocity and cumulative headloss
Table E54: Segment 4: Averaging of Areas
Table E55: Segment 4: Velocity and cumulative headloss
Table E56: Segment 5: Averaging of Areas

Table E57: Segment 5: Velocity and cumulative headloss
Table E58: Summaries of results for Tables 48 to 57
Table E59: Summary of maximum headloss versus flow rates
Table F1: Metal Wire Pipe: Variables and Values
Table F2: The physical aspects of the HPM and Intake Pipeline
Table F3: Total Headloss and initial flow rate for Water Only test
Table F4: Total headloss and flow rate incorporating losses
Table F5: Disaggregation of pressure losses
Table F6: Perforation friction (Loss A) flowrate for Half and Full pipeline
Table F7: Inflowing velocity of water flowing into the pipe, over the length of the Intake Pipeline
Table F8: Calculated Flowrate from all segments of the Pipeline
Table F9: Total Headloss and initial flow rate for Water and Stone test
Table F10: Total headloss and flow rate incorporating losses for Water and Stone Test
Table F11: Disaggregation of pressure losses for Water and Stone test
Table F12: Perforation (Loss A), and Stone Bedding friction, flowrate for Half and Full pipeline
Table F13: Inflowing velocity - water flowing into the pipe, over the length of the Intake Pipeline
Table F14: Calculated Flowrate from all segments of the Pipeline
Table F15: ø250mm Grooved Metal Wire pipe test: Stone bedding friction only: Method1
Table F16: ø250mm Grooved Metal Wire Pipe, Water and Stone Bedding Test: Flow through segments
Table F17: Summary: Calculating the Hydraulic conductivity
Table F18: Segment 1: Averaging of Areas
Table F19: Segment 1: Velocity and cumulative headloss
Table F20: Segment 2: Averaging of Areas
Table F21: Segment 2: Velocity and cumulative headloss
Table F22: Segment 3: Averaging of Areas
Table F23: Segment 3: Velocity and cumulative headloss
Table F24: Segment 4: Averaging of Areas
Table F25: Segment 4: Velocity and cumulative headloss
Table F26: Segment 5: Averaging of Areas
Table F27: Segment 5: Velocity and cumulative headloss
Table F28: Summary of 15 Headloss Tests. Results from Tables 15 to 24
Table F29: Summary of maximum headloss versus flow rates
Table F30: Summary of maximum headloss versus flow rates
Table G1: Summary of results for all the Water only tests
Table G2: Summary of results for the Stone Bedding tests
Table G3: Summary of results for the Slotted PVC Pipe: Sand + Stone bedding tests
Table G4: Summary of results for the Extra Perforated PVC Pipe: Sand + Stone bedding tests

Table G5: Method 1 and 2: Headloss due to Stone bedding
Table G6: Method 1 and 2: Headloss due to Stone bedding
Table G7: Method 1 and 2: Headloss due to Stone bedding
Table G8: Method 1 and 2: Headloss due to Sand and Stone bedding

LIST OF FIGURES

Figure 2.1: Koeberg nuclear power station (NPPW 2008)
Figure 2.2: South Bay Power Plant in Chula Vista, California (San Diego Union Tribune 2008)
Figure 2.3: Temperature profile for deep oceans in the tropics (Makai, 2008a)
Figure 2.4: Typical flow diagram for seawater used in air conditioning (Makai, 2008b)
Figure 2.5: General layout of a Desalination system (IECM: 2004)
Figure 2.6: Fish processing plants close to harbour and quay wall. (Bosman, 2005)
Figure 2.7: Schematic sketch of Ikamva Lethu Fishing Intake Jetty and Pumping Configuration
Figure 2.8: Intake Jetty for Ikamva Lethu Fishing. (WSPACE, 2007)
Figure 2.9: Abalone (DEAT, 2001)
Figure 2.10: Brown Mussel (DEAT, 2001)
Figure 2.11: Scallops (DEAT, 2001)
Figure 2.12: Natal Rock Oyster (DEAT, 2001)
Figure 2.13: Ushaka Marine World in Durban South Africa
Figure 2.14: Paddling pools and Rachael Finlayson pool (left) in Durban SA. (Google 2008)
Figure 2.15: uShaka World in Durban, South Africa
Figure 2.16: De Gama Estuary and Beach well at Muizenberg (Adapted from Google 2008)
Figure 2.17: Majung Power Station seawater intake structure (ZLH 2008)
Figure 2.18: Majung Power Station seawater connecting culverts on land. (ZLH 2008)
Figure 2.19: Majung Power Station seawater connecting culvert being floated and placed into position. (ZLH 2008)
Figure 2.20: Typical sub-surface seawater abstraction (Reynolds & Maley, 2008)
Figure 2.21: Position of radial beach wells shown on Long Beach, California. (Wang, 2009)
Figure 2.22: Section through a horizontal/ radial beach well (Adapted from Prandtl 2007)
Figure 2.23: Seawater intake on a rocky shore. (Thiess 2006)
Figure 2.24: Layout and typical section of Beach wells (Schwarz, 2000)
Figure 2.25: Layout and Section of a typical Horizontal Beach Gallery (Schwarz, 2000)
Figure 2.26: Infiltration galleries with horizontal well screens (Basson, 2005)
Figure 2.27: Seabed Filtration (Schwarz, 2000)
Figure 2.28 Flow through a conduit filled with permeable material (Roberson, et al, 1998)
Figure 2.29: Most common section of a borehole well (Roberson et al, 1998)
Figure 2.30: Axially symmetrical flow into a well in an uncontrolled aquifer (Roberson et al, 1998)
Figure 2.31: Variation of velocity *v* with hydraulic gradient *i* (Das, 2000)
Figure 2.32: Results of Permeability Tests for C_u = 1-3(Das, 2000)
Figure 2.33: Results of Permeability Tests for C_u>3(Das, 2000)
Figure 2.34: Permeability of granular soils (Das, 2000)
Figure 2.35: Permeability versus grain or stone sieve size (CIRIA, CUR, CETMEF, 2007)

Figure 2.36: Factors to consider when developing a sub surface seawater intake
Figure 2:37: Particle size distribution characteristics relevant to internal stability (CIRIA, CUR, CETMEF, 2007)
Figure 2.38: Interface stability of granular materials (CIRIA, CUR, CETMEF, 2007)
Figure 2.39: Design chart for the interface stability of granular filters (CIRIA, CUR, CETMEF, 2007)
Figure 3.1: Clock wise from top left, Western Province SA, Hermanus with a breakwater protruding north east from the new harbour, Abagold seawater intake, situated south west of the breakwater. Note the 2 pump houses can be clearly seen as white rectangles at the end of the intake. (Adapted from Google Earth 2008)
Figure 3.2: Schematic section of Abagold seawater intake
Figure 3.3: Looking seawards, the back end of the rotating screen can be seen in the fore ground and the concrete screen wall in the rear
Figure 3.4: Strategically blasted rock sitting at the entrance of the intake Gulley
Figure 3.5: Abagold's Seawater Intake Basin
Figure 3.6: Clock wise from top left, Cape Peninsula, Cape Town with a breakwater protruding north east from the harbour, Sea Fisheries Aquarium can be seen as the long red roofed structure (Adapted from Google Earth 2008)
Figure 3.7: Clock wise from top left, Cape Peninsula, Cape Town harbour, V&A Waterfront showing the Two Oceans Aquarium (Adapted from Google Earth 2008)
Figure 3.8: The intake for the Two Oceans Aquarium. The intake is situated opposite the canal from the Nelson Mandela Museum
Figure 3.9: The first intake pipe for the Two Oceans Aquarium, a ø250mm slotted PVC screen
Figure 3.10: The second intake for the Two Oceans Aquarium, a ø250mm specially manufactured PVC pipe utilizing Nylon mesh
Figure 3.11: TOA - ø75mm intake pipeline and colony of Barnacles
Figure 3.12: Construction of Jetty at Ushaka Marine World with the extra amount of purposed built jetty piles being constructed at the head of the Jetty
Figure 3.13: Layout of Well points with North and South Suction Legs
Figure 3.14: Well Point Downpipe
Figure 3.15: Well points showing Aerobic and Anoxic Zones
Figure 3.16: Paternoster Oyster with the shoreline to the west and the Oyster ponds clearly visible (Adapted from Google Earth 2008)
Figure 3.17: Paternoster Oyster: Sectional Elevation - 2No. Beach Well Subsoil intake units
Figure 3.18: Paternoster Oyster: Layout of Beach Well abstraction infrastructure
Figure 3.19: New Beach Well. Stitched geofabric covering the perforated intake pipe
Figure 3.20: New Beach Well. Inside of the specially constructed perforated intake pipe
Figure 3.21: The method by which air and sand displaces sand allows the metal sleeve to settle
Figure 3.22: The set of pipes/jets used to displace sand

Figure 3.23: The metal sleeve with a bell end that has already been driven in to the sand
Figure 3.24: Clock wise from top left, Western Province SA, Britannia Bay, West coast Abalone seawater intake pump house can be seen as a rectangle in the top left portion of the image. Note the abalone production facilities can be seen in the bottom right (Adapted from Google Earth 2008)
Figure 3.25: Schematic section of West Coast Abalones Seawater Intake
Figure 3.26: Centrifugal pumps, at Intake for West Coast Abalone
Figure 3.27: Slurry pumps, at Intake for West Coast Abalone
Figure 3.28: Intake for West Coast Abalone
Figure 3.29: Clock wise from top left, Western Province SA, The western peninsula. St Helena Abalone is situated south east of harbour. (Adapted from Google Earth 2008)
Figure 3.30: The intake pipelines for St Helena Abalone, 2No. ø300mm HDPE pipelines
Figure 3.31: Schematic section of St Helena Abalone Seawater Intake
Figure 3.32: The pumping infrastructure for St Helena Abalone
Figure 3.33: Wastewater is discharged in the area where the intake pipelines cross the shore. Discharged water can be seen as white water, above and to the right of the collar on the HDPE Intake Pipeline
Figure 4.1: Seawater Abstraction and disposal System: Option 1 (ZLH 2008a)
Figure 4.2: Seawater Abstraction and disposal System: Option 2 (ZLH 2008a)
Figure 4.3: Seawater Abstraction and disposal System: Option 3 (ZLH 2008a)
Figure 4.4 Seawater Abstraction and Disposal System: Final Layout (ZLH 2008a)
Figure 4.5: Proposed Seawater Intake System
Figure 4.6: Cross-sectional of Breakwater (CEM, 2007).
Figure 4.7: Material Grain Distribution for armour protection material of seawater Intake
Figure 4.8: Physical Hydraulic Model for testing of Seawater Intake pipework
Figure 4.9: Flow diagram depicting the loss of pressure head in the (HPM)
Figure 4.10: Relationship between flow and the associated pressure loss for Test 1 (water only, no stone bedding)
Figure 4.11: Relationship between flow and the associated loss of pressure head due to the intake pipe AND Stone bedding in the HPM
Figure 4.12: Relationship between flow and the associated loss of pressure head due to the intake pipe, Stone AND Sand bedding in the HPM
Figure 4.13: Loss of pressure head in the HPM (Water Only)
Figure 4.14: A leak in the first half of WC2 of the HPM
Figure 4.15: A dam constructed around the HPM
Figure 5.1: View of inner section of half a ø250mm slotted PVC Pipe
Figure 5.2: ø250mm slotted pipe in the Physical model
Figure 5.3: Headloss, (Loss A) versus the flowrate for a fully flowing ø250mm Slotted pipe
Figure 5.4: ø250mm slotted pipe with stone bedding and blanket

Figure 5.5: Headloss due to Slot Friction and Stone bedding including Slot friction
Figure 5.6: Partial grading curve for combined Phillipi and Granular Filter sand
Figure 5.7: Sand and stone material surrounding the intake pipe
Figure 5.8: Headloss and rate of flow for a 3 hour test period
Figure 5.9: Horizontal section through middle of Intake Pipeline
Figure 5.10: 15mm flushing pipe. Note the holes/ports and black spacers that hold the pipe in the centre of the Intake pipeline
Figure 5.11: Plan view of water column 1. Sand and 19mm stone mix after flushing with water. Note the Intake pipe runs along the upper edge
Figure 5.12: A manifold used to create a mixture of water and air
Figure 5.13: Air and water mixture flowing out the flushing pipe, Flow of air from holes seen as white plumes
Figure 5.14: Plan view of water column 1. Sand and 19mm stone mix after Flushing with water and air. Note the Intake pipe runs along the upper edge
Figure 5.15: Oblique view of water column 1. Sandbar on Bedding after Back flushing with air and water. Intake pipe runs along the left edge
Figure 5.16: Headloss and Rate of Flow for a 6.5hour test period. After back flushing
Figure 5.17: Typical Perforated PVC Pipe, similar to pipe used in Test 2
Figure 5.18: Section and Elevation of ø250mm Perforated PVC Pipe
Figure 5.19: Section and Elevation of Extra Perforated ø250mm Perforated PVC Pipe
Figure 5.20: Headloss due to perforation (Loss A) versus the flowrate for a fully flowing ø250mm perforated pipe
Figure 5.21: Headloss due to extra perforation (Loss A) versus the flowrate for a fully flowing ø250mm Perforated pipe
Figure 5.22: Headloss due to Perforation Friction only and Stone bedding including perforation friction
Figure 5.23: Sand ingress into Intake Pipeline before testing can commence
Figure 5.24: Sand ingress into Intake Pipeline when testing commences
Figure 5.25: The growth of sand mounds within the Intake Pipeline
Figure 5.26: Development of front face of ‘dune’ seen as angular stratified layers of sand
Figure 5.27: Front face of the dune has reached WC1 and the Intake pipeline has started to scour clean
Figure 5.28: Headloss due to Perforation Friction; Headloss due to Perforation friction and Stone bedding; and Headloss due to Perforation friction, Stone and Sand bedding.
Figure 5.29: Internal View of half a ø250mm Metal Wire Pipe
Figure 5.30: External View of half a ø250mm Metal Wire Pipe
Figure 5.31: Headloss due to the Slots (Loss A) versus the flowrate for a fully flowing ø250mm Metal Wire pipe
Figure 5.32: Headloss due to Slot Friction and Stone bedding including Slot friction

Figure 6.1: Perforation friction for all three intake pipe types
Figure 6.2: Plot of Relationship between porosity and the flowrate divided by the associated headloss for the four test pipes
Figure 6.3: Perforation friction for all three intake pipe
Figure 6.4: Pressure loss and Flowrate vs. time relationship for the Slotted PVC Pipe with sand and
Figure 6.5: Pressure Loss vs. Flowrate for Extra perforated PVC Pipe (WST + WSST)
Figure 6.6: Slotted PVC Pipe-Method 1, 2 and 3: Headloss due to the stone bedding
Figure 6.7: Extra Perforated PVC Pipe- Method 1, 2 and 3: Headloss due to the stone bedding
Figure 6.8: Metal Wire Pipe- Method 1, 2 and 3: Headloss due to the stone bedding
Figure 6.9: Perforated PVC Pipe-Method 1, 2 and 3: Headloss due to the stone bedding
Figure 6.10: Comparison of Method 1 for all three pipe types
Figure 6.11: Comparison of Method 2 for all three pipe types
Figure 6.12: Comparison of Method 3 for all three pipe types
Figure 7.1: Design Step Guide for a Seawater Intake
Figure 7.2: Conceptual Seawater intake for Kidd's Beach
Figure 7.2: Cross-sectional of Breakwater (CEM, 2007).
Figure 7.3: Particle size distribution characteristics relevant to internal stability (CIRIA, CUR, CETMEF, 2007)
Figure 7.4: Interface stability of granular materials (CIRIA, CUR, CETMEF, 2007)
Figure 7.5: Design chart for the interface stability of granular filters
Figure 7.6: Material Grain Distribution for armour protection material of seawater Intake
Figure 7.7: Permeability versus grain or stone sieve size (CIRIA, CUR, CETMEF, 2007)
Figure 7.8: Conceptual Seawater intake for Kidd's Beach
Figure 7.9: Permeability for the Armour, Under Layers and Core Material versus grain or stone sieve size (CIRIA, CUR, CETMEF, 2007)
Figure 7.10: Headloss vs. Flowrate for the Seawater Intake in Figure 8.5

Figure A1: Hydraulic Model for testing intake pipework.
Figure A2: V Notch weir inside the second water column.
Figure A3: Tubing to measure height of water in a column.
Figure A4: Outlet and Inspection window to Water Column 2
Figure A5: Construction Drawing of Hydraulic Model
Figure B1: V notch weir used for flow calculations
Figure B2a: V Notch Weir
Figure B2b: Flow augmenting structure adjacent to V notch weir on the right
Figure B3: V notch weir and additional structure depicting flow pattern
Figure B4: V notch weir with Measuring Needles
Figure B5: V notch weir, additional structure and measuring needle orientation

Figure B6: Flow vs. Height for 90 V Notch Weir
Figure B7: Flow vs. Height curves for Calibrated and Conventional outflow calculation
Figure C1: Partial grading curve for Phillipi sand.
Figure C2: Partial grading curve for Granular Filter sand.
Figure C3: Partial grading curve for combined Phillipi and Granular Filter sand
Figure D1: Slotted PVC Pipe Abstraction Model: Areas of interest
Figure D2: Areas of Water Leakage
Figure D3: Headloss due to the slots (Loss A) versus the flowrate for a fully flowing ø250mm slotted pipe
Figure D4: Segmented HPM with notional EGL flow that enters WC1 and exits from WC2
Figure D5: Plot of EGLs at the centre of the Intake Pipeline
Figure D6: The EGL in the HPM for all nineteen tests
Figure D7: Headloss due to the slots (Loss A) and Stone bedding versus the flowrate for a fully flowing ø250mm slotted pipe
Figure D8: Segmented HPM with notional EGL flow that enters WC1 and exits from WC2
Figure D9: Plot of EGLs at the centre of the Intake Pipeline for Water and Stone Bedding Test
Figure D10: ø250mm Slotted pipe-Water and Stone Bedding Test: Pressure loss due to Stone Bedding Only
Figure D11: ø250mm Slotted pipe -Water and Stone Bedding Test: Segmentation of Stone Bedding area
Figure D12: Notional flow path of a stone bedding segment
Figure D13: Typical grading curve for nominally single-sized 19mm Stone (Alexander & Mindess, 2005)
Figure D14: Graphical plot of Hydraulic conductivity Equation (Das, 2000)
Figure D15: Results of Headloss due to Stone Bedding, within WC1
Figure D16: Method 1 and Method 2: Headloss due to the stone bedding
Figure D17: Plot of Pressure due to the slots, +sand + stone bedding and corresponding flowrate for a fully flowing ø250mm slotted pipe
Figure D18: Headloss and rate of flow for a 3hour test period
Figure D19: Plot of Pressure due to the slots, +sand + stone bedding and corresponding flowrate for a fully flowing ø250mm slotted pipe after flushing
Figure D20: Headloss and rate of flow for a 6.5hour test period
Figure D21: Headloss and rate of flow for test Before Back Flushing (BBF) and After Back Flushing (ABF)
Figure E1: Perforated PVC Pipe Abstraction Model: Areas of interest
Figure E2: Areas of Water Leakage
Figure E3: Headloss due to perforation (Loss A) versus the flowrate for a fully flowing ø250mm Perforated pipe
Figure E4: Headloss due to extra perforation (Loss A) versus the flowrate for a fully flowing ø250mm Extra Perforated pipe

Figure E5: Segmented HPM with notional EGL flow that enters W1 and exits fromWC2
Figure E6: Plot of EGLs at the centre of the Intake Pipeline. Legend: Flowrates
Figure E7: Headloss due to perforation (Loss A) and Stone bedding versus the flowrate for a fully flowing ø250mm Perforated pipe
Figure E8: Segmented HPM with notional EGL flow that enters WC1 and exits from WC2
Figure E9: Plot of EGLs at the centre of the Intake Pipeline for Water and Stone Bedding Test
Figure E10: Method 1- ø250mm Perforated pipe, Water and Stone Bedding Test: Pressure loss due to Stone Bedding ONLY
Figure E11: ø250mm Perforated pipe, Water and Stone Bedding Test: Segmentation of Stone Bedding area
Figure E12: Notional flow path of a stone bedding segment
Figure E13: Typical grading curve for nominally single-sized 19mm Stone (Alexander & Mindess, 2005)
Figure E14: Graphical plot of Hydraulic conductivity Equation (Das, 2000)
Figure E15: Results of Headloss due to Stone Bedding, within WC1
Figure E16: Method 1 and Method 2: Headloss due to the stone bedding
Figure E17: Plot of Pressure loss due to the slots, +sand + stone bedding flowrate for Full ø250mm perforated pipe
Figure E18: Plot of EGLs at the centre of the Intake Pipeline for Sand and Stone Bedding Test
Figure E19: ø250mm Perforated pipe, Sand and Stone Bedding Test: Pressure loss due to sand and Stone Bedding ONLY
Figure E20: Typical grading curve for nominally single-sized 19mm Stone (Alexander & Mindess, 2005)
Figure E21: Graphical plot of Hydraulic conductivity Equation (Das, 2000)
Figure E22: Results of Headloss due to (sand and) Stone Bedding, within WC1 (Legend: Flowrates)
Figure E23: Method 1 and Method 2: Headloss due to the stone bedding
Figure F1: Metal Wire Pipe Abstraction Model: Areas of interest
Figure F2: Areas of Water Leakage
Figure F3: Headloss due to the slots (Loss A) versus the flowrate for a fully flowing ø250mm Metal Wire pipe
Figure F4: Segmented HPM with notional EGL flow that enters WC1 and exits from WC2
Figure F5: Plot of EGLs at the centre of the Intake Pipeline Legend: Flowrate
Figure F6: Headloss due to the slots (Loss A) and Stone bedding versus the flowrate for a Full flowing ø250mm Metal Wire pipe
Figure F7: Plot of EGLs at the centre of the Intake Pipeline for Water and Stone Bedding Test
Figure F8: ø250mm Metal Wire Pipe, Water and Stone Bedding Test: Pressure loss due to Stone Bedding Only-Method 1

Figure F9: ø250mm Metal Wire pipe, Water and Stone Bedding Test: Segmentation of Stone Bedding area
Figure F10: Notional flow path of a stone bedding segment
Figure F11: Typical grading curve for nominally single-sized 19mm Stone (Alexander & Mindess, 2005)
Figure F12: Graphical plot of Hydraulic Conductivity Equation (Das, 2000)
Figure F13: Results of Headloss due to Stone Bedding, within WC1
Figure F14: Headloss due to Stone bedding ONLY versus the flowrate for a Full flowing ø250mm Metal Wire pipe-Method 2
Figure F15: Method 1 and Method 2: Headloss due to the stone bedding
Figure G1: Perforation friction for all three intake pipe types
Figure G2: Perforation and Stone Bedding Friction for all three intake pipe types
Figure G3: Pressure loss and Flowrate vs. time relationship for the Slotted PVC Pipe with sand and stone bedding
Figure G4: Pressure Loss vs. Flowrate for Extra perforated PVC Pipe with sand and stone bedding
Figure G5: Slotted PVC Pipe-Method 1 and Method 2: Headloss due to the stone bedding
Figure G6: Perforated PVC Pipe-Method 1 and Method 2: Headloss due to the stone bedding
Figure G7: Metal Wire Pipe Method 1 and Method 2: Headloss due to the stone bedding
Figure G8: Perforated PVC Pipe Method 1 and Method 2: Headloss due to the sand and stone bedding

LIST OF SYMBOLS

C_d : Coefficient of Discharge

d : Depth (m)

d_m : Minimum depth (m)

F : Froude Number (dimensionless)

g : acceleration due to gravity (m/s^2)

LIST OF ABBREVIATIONS

BBF : Before Back Flushing

ABF : After Back Flushing

CD : Chart Datum

DEA : Department of Environmental Affairs

DEAT : Department of Environmental Affairs and Tourism

HDPE : High Density Poly Ethylene

HPM : Hydraulic Physical Model

HWM : Horizontal Well Method

ID : Inner Diameter

LAT : Lowest Astronomical Tide

MCM : Marine and Coastal

MSL : Mean Sea Level

MWP : Metal Wire Pipe

mPVC : modified Poly Vinyl Chloride

OD : Outer Diameter

PPP : Perforated PVC Pipe

PVC : Poly Vinyl Chloride

RO : Reverse Osmosis

SFA : Sea Fisheries Aquarium

SPP : Slotted PVC Pipe

SWL : Still Water Level

SWAC : Sea Water Air Conditioning

SWA : Sea World Aquarium

TLB : Tractor-Loader-Backhoe

UMW : Ushaka Marine World

UMP : Ushaka Marine Park

WC1 : Water Column 1

WC2 : Water Column 2

Chapter 1

1. INTRODUCTION

1.1 Background

South Africa (SA) is a relatively dry country with an average annual rainfall of only 464mm, compared to a world average of 860mm (African Sky, 2005). Water shortages and droughts are fairly common to the western and high lying of regions South Africa.

Due to increased development in SA, the demand for water has steadily increased; hence new sources of water are required. At present the vast majority of land based, human activity requires fresh water. Water for consumption is of significant importance. However the largest consumer of water is Industry.

The quantity of water used, is dependent on the type of Industry concerned. Typically, large industries the likes of mining and power generation consume vast quantities of water. With the expansion of such facilities, which is the current situation in South Africa, there is increase in water demand.

One option that would decrease the water demand is the recycling of water. However, based on the activity, the costs for recycling might be fairly large and prove to be unsustainable; hence a new cost effective water source is required

In the past decade, the use of seawater has increased due to the decrease in fresh water resources. Many industries now use seawater where possible. Seawater is mainly used for: cooling purposes, drinking water, fish processing, mariculture, scientific and recreational facilities. These are discussed further in Chapter 2.2

Hence the use of seawater has provided growth for many sectors of industry. An investigation into seawater intake systems would assist in securing this limitless resource.

1.2 Present Situation

At present in South Africa, there are many industries that use seawater as their medium. Activities the likes of fish processing, mariculture, scientific and recreational facilities operate in a saline environment. These facilities are usually found close to the shoreline hence the use of nearby seawater is favorable. With screening and filtration this source of seawater becomes complimentary.

Another sector of industry is the power generation industry. This sector uses large volumes of seawater for cooling purposes. Hence power plants are purposely situated near the shoreline in order to make use of the nearby seawater. Situated on the west coast of South Africa, the Koeberg Power station uses seawater for cooling purposes. This power station has a direct surface intake and has an intake flowrate of 80m^3/s (ESKOM, 2010a)

Another significant use of seawater is the production of potable water from seawater. At present most potable water is delivered to its end users, via a municipality. The municipality usually treats water from a freshwater source and then delivers the water via a network of pipelines. However with the increase in development, there has been an increased demand for potable water. Hence municipalities have to now deliver a larger quantity of water, over larger distances. This has a significant impact on the cost of the water. Hence new developments have to now consider more cost effective methods of providing potable water.

One such method is the desalination of seawater to produce potable water. The most common technology used for desalination is Reverse Osmosis (RO). In arid countries, a large portion of potable water is produced from seawater. By comparison, the demand for potable water in South Africa via desalination is very small. However this technology has been used for small developments. Desalination for producing potable water has been used at Sedgefield, Western Cape, South Africa. Here beach wells are used to abstract seawater from the sandy shoreline. Water is abstracted at a rate of 156.25m^3/hour. With a recovery of 40% , this produces potable water at a rate of 62.3m^3/hour (Roussow, 2010) This system has proven to be effective in providing potable water to smaller developments and is now being considered by other developments/ residential communities. New plants were recently constructed at Mossel Bay, Knysna and Sedgefield while others at Port

Nolloth, Lamberts Bay and Saldanha are in the design phase. Hence it is into this branch of Coastal Engineering that investigations are required, in order to secure a reliable seawater intake system.

1.3 Objective and Aims

The objective of this thesis is to investigate the hydraulics of a proposed seawater abstraction system using the Horizontal Well Method (HWM) on rocky coastlines. The next objective is to provide recommendations for design guidelines for small scale seawater abstraction systems on rocky coastlines using the HWM.

1.4 Report Presentation Structure

Chapter 2: Literature Review. This chapter first documents information on different seawater intake systems and the manner in which seawater is collected. Thereafter this section investigates the hydraulic sphere of seawater intakes.

Chapter 3: Review of existing seawater Intakes along South African coastline. This chapter looks at a few South African seawater intakes and details their unique conditions.

Chapter 4 Case Study: Investigation of a horizontal well for abstracting seawater from the surf zone on rocky coastlines. This chapter examines how the horizontal well method can be used on a rocky coastline. The specific aims for a laboratory investigation are drawn. The parameters and procedures for the laboratory tests are agreed upon.

Chapter 5: This chapter contains the results of the Case Study tests. These results include the testing of the three seawater intake pipes types which were tested in the Hydraulic Physical Model (HPM).

Chapter 6: This chapter discusses the case study test results.

Chapter 7 This chapter proposes a methodology on how to plan and design a small scale seawater abstraction system from the surfzone of a rocky coastline. It uses information gathered from the preceding chapters.

Chapter 2

2. LITERATURE REVIEW

2.1 Introduction

The oceans have long been seen as untapped resources. The effective use of seawater intakes will increase the accessibility of this resource. Chapter 2.2 lists the most common uses of seawater. Chapter 2.3 shows the various types of seawater intakes that are employed to abstract seawater. Chapter 2.4 is a hydraulic review that examines in finer detail, the areas that are of particular concern with small scale seawater abstraction in the coastal zone.

2.2 Uses of Extracted Seawater: Overview

Due to development and advances of technology, there are numerous ways in which seawater can now be utilised. With supply being almost unlimited, this resource can be considered secure into the future. However, as history shows, man has severely affected multitudes of ecosystems with the uncontrolled use of a resource. Hence particular heed should be paid to the environmental impact of abstraction, usage and discharge of this seemingly unlimited resource.

The following are the main usages of seawater. This is not an exclusive list and can be augmented to include specialised water demands.

A. Cooling:	1. Cooling at power stations
	2. Air conditioning
B. Desalination:	Potable water for human consumption
C. Fish Processing:	Processing of fish for commercial consumption.
D. Mariculture:	Farming of oceanic fauna and flora.
E. Scientific Facilities:	Seawater used for facilities like aquariums
F. Recreational Facilities:	Seawater used for pools
G. Environmental:	Seawater is used to augment natural systems.

The uses for seawater listed above are discussed separately under the respective headings below with examples in South Africa and elsewhere.

2.2.1. Cooling

2.2.1.1 Cooling at Power Stations

The majority of electricity generated in the world, is done so via the burning of fossil fuel. Some electricity generating plants use gas turbines while a few use petroleum or nuclear energy (ESKOM, 2010a). However the large majority of electricity generating plants are coal based. Here coal is used to create pressurised steam which is used to turn turbines connected to electricity generators (ESKOM, 2010b).

However as part of the process, large quantities of water are heated. This water is then cooled before being recovered or discharged into the environment (ESKOM, 2010c). The cooling of this water is usually done in the huge parabolic shaped cooling towers, synonymous with coal powered stations. Hence the usage of seawater for cooling purposes would eliminate these cooling towers.

There are a number of variables that describe the quality of seawater. Some of the basic variables are water temperature, pH, turbidity, dissolved oxygen, salinity, hardness, and suspended sediment. (Hatzikos et al, 2007). These criteria need to be fully understood as they affect the filtration process and the associated costs.

The amount of water required by electricity generating plants is large; hence the intake structures typical for such power stations are large as well. The type of intake for a power station is dependent on the coastline properties and many other factors (Desalination Issues Assessment Report, 2003). Table 2.1 below contains a few of these factors.

Pictured in Figure 2.1 is Koeberg nuclear power station which is situated on the west coast of South Africa, 8km north of Cape Town. The plant uses a large amount of seawater for cooling hence it has a large intake/stilling basin which is flanked by two rubble mound breakwaters. It has a large intake rate of $80m^3/s$ (ESKOM, 2010b). The water is pumped into the condenser where it aids in cooling down (ESKOM, 2010b). After water passed through the condenser, it discharge back into a water body. The discharged water is typically 5 to 15 degrees higher than the ambient seawater (Lattermann and Höpner, 2007). In the case of Koeberg, this is done via a canal just south of the southern breakwater, Figure 2.1.

Table 2.1: Aspects relevant for a seawater intake location selection

Beneficial uses of surrounding waters and beach area
Environmental sensitive areas
Recreational areas
Port demarcated areas (i.e. vessel navigation)
Industrial use (i.e. proximity existing industrial ocean outfalls)
Physical characteristics of the intake
Intake type
Required water depth
Required flow
Water quality
Meteorological conditions
Oceanographic conditions (i.e. seabed slope, bathymetry)
Environmental processes
Waves (i.e. construction constrains, intake structure stability, turbidity at intake works)
Currents (i.e. construction constrains, intake structure stability)
Sediment processes
Environmental impacts
Pollution
Fouling
Aesthetic considerations (i.e. could change character and appearance of beaches)
Marine biology (i.e. Impact on shore and benthic marine organisms in the area of the intake,
Entrainment issues (area rich in marine species))

Figure 2.1: Koeberg nuclear power station (NPPW, 2008)

Figure 2.2, below is of the South Bay Power Plant situated in Chula Vista, California. The power plant is situated adjacent to a relatively calm bay. Hence the seawater intake which is not in the surf zone, is not subjected any dynamic forces for example, wave action. This intake allows for vast quantities of sea water to be abstracted with minimal impact of undesirable contaminants. This power facility provides electricity for 700,000 households and has a seawater intake flowrate of up to 22m^3/s (The San Diego Union-Tribune, 2006).

Figure 2.2: South Bay Power Plant in Chula Vista, California (The San Diego Union-Tribune, 2006)

2.2.1.2 Cooling for Air conditioning

In the same manner that seawater is used for power plants, it can also be used for air conditioning. The common terminology for this process is termed Sea Water Air Conditioning (SWAC). However the incoming water has to be at a significantly lower temperature (Makai, 2008a). The figure below shows the temperature profile in the tropics for a typical deep ocean.

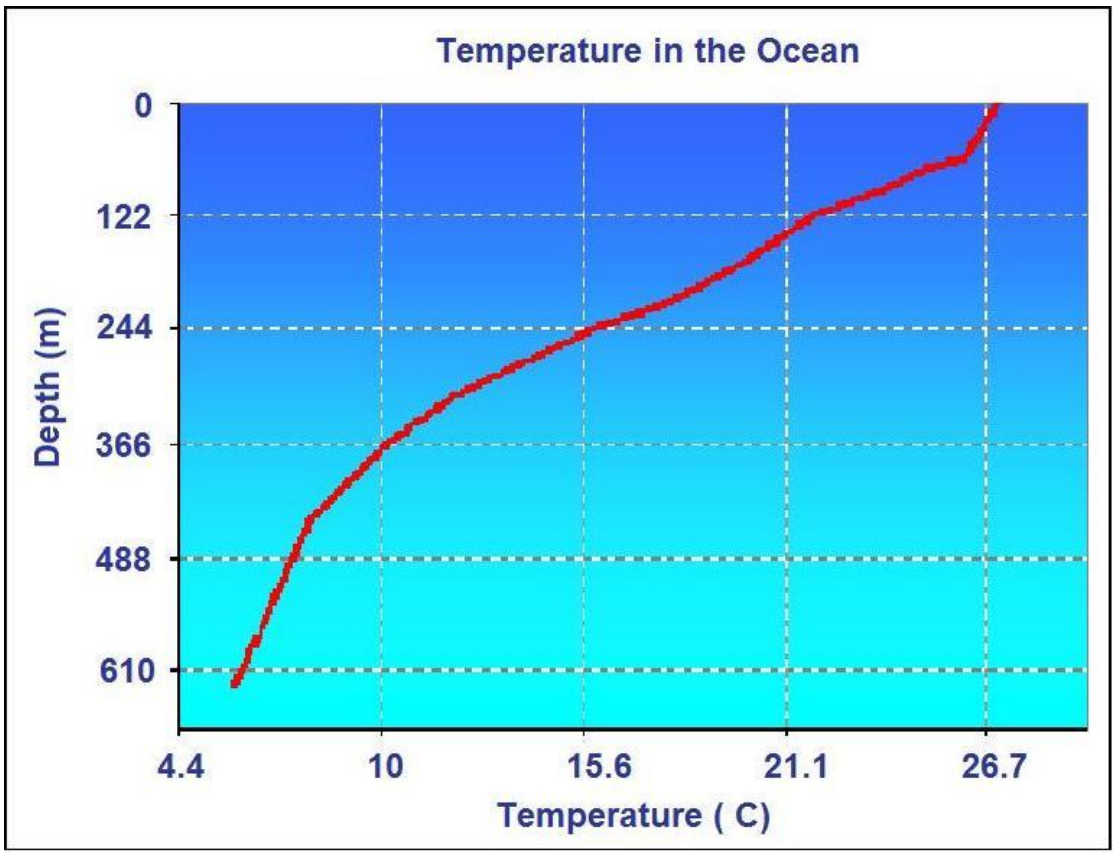

Figure 2.3: Temperature profile for deep oceans in the tropics (Makai, 2008a)

The flow diagram for the use of this cold seawater can be seen in Figure 2.4 below. Cold water is drawn from the sea and passes through a Heat Exchanger. The water is then warmed and enters the Chiller Unit (Makai, 2008b). Thereafter the heated water is gravitated/pumped back to the sea.

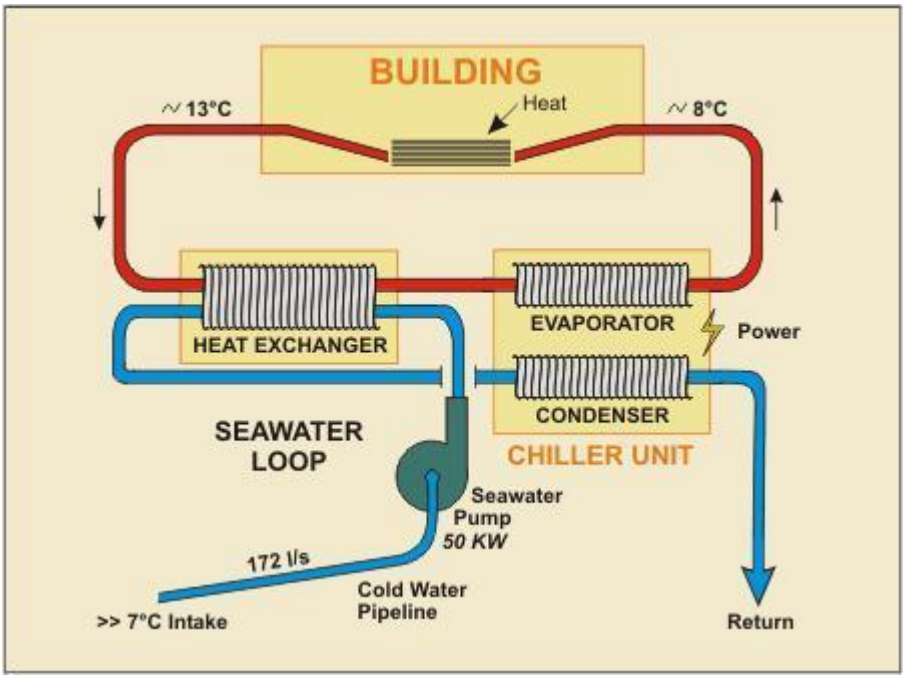

Figure 2.4: Typical flow diagram for seawater used in air conditioning (Makai, 2008b)

This system has its draw backs. The most adverse factor is the depth at which pipes have to go, in order to abstract sufficiently cold water. For coastlines with a fairly wide continental shelf, this would not be a viable option. Pipelines would have to be very long in order to reach the depths at which these cold waters are found.

2.2.2 Desalination

Desalination is the process by which potable water is extracted from seawater. With the decreased availability of fresh water, desalination is used to augment water needs. Large-scale desalination typically uses extremely large amounts of energy as well as specialized, expensive infrastructure, making it very costly compared to the use of fresh water (Mora Associates, 2007).

Due to the growth of development and population, there been rapid growth in desalination technology and research into this field. This technology has grown to an advanced stage; hence package desalination plants are now available “off the shelf” (Aqualyng AS, 2009).This advance in technology now allows for mass amounts of water to be desalinated. Figure 2.5 shows the schematic flow of seawater in such a

system. This system has two pre-filter modules before the water enters the desalting process.

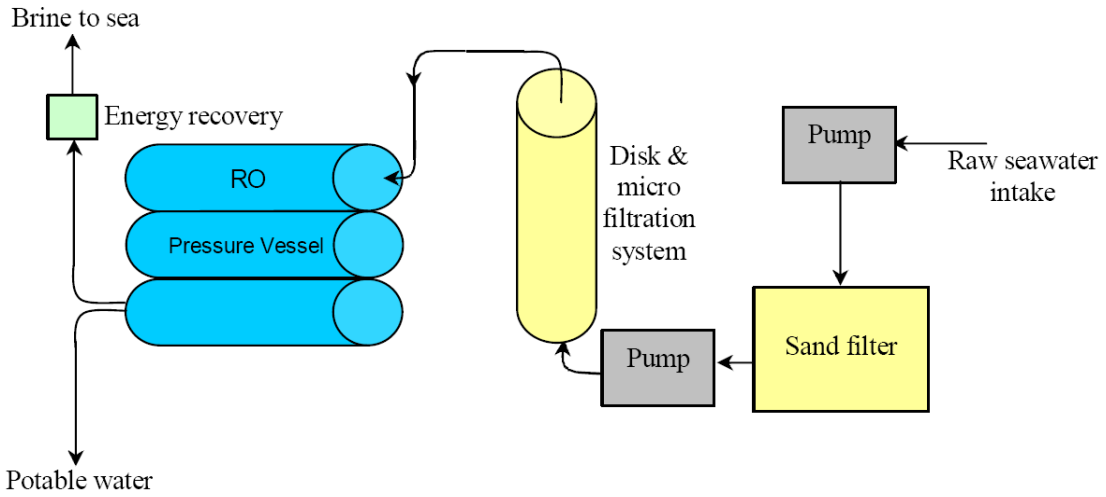

Figure 2.5: General layout of a Reverse Osmosis Desalination system (Prankratz, 2008).

Currently, the preferred method of desalination is Reverse Osmosis. Here salt water is forced through a membrane. The membrane allows H_2O molecules through and the bigger salt crystals are flushed away as brine concentrate. Desalination systems do however have certain requirements. These requirements determine if the desalination process is financially viable. When considering desalination the assessment should consider all constituents that may impact plant operation and process performance. A thorough review of historical water quality data including seawater temperature, total dissolved solids (TDS), total suspended solids (TSS), and total organic carbon (TOC) is crucial (Prankratz, 2008).

2.2.3 Fish Processing

South Africa has two oceans that flank three sides of the country. The Benguela current, in the Atlantic Ocean, is fed from the Antarctic sea. This current is extremely high in nutrients. Hence the coastline it influences is rich with marine life. This in turn supports a large fishing industry.

Most fish caught by fishing vessels are brought to shore for processing. As part of their operation, fish processing factories use seawater for the preparation and canning of fish products. Depending on their location, seawater is taken from the harbour or the neighbouring coastline. These processing plants are usually situated

close to the shore line in order to reduce the cost of transporting seawater to the processing plants. The economically viable option for sighting a fish processing plant would be to place it as close as possible to the mooring quays. Figure 2.6, Shows the fish processing plants situated near the quay wall at Elandsbaai, Northern Cape, South Africa. (Bosman, 2005)

Figure 2.6: Fish processing plants close to harbour and quay wall. (Bosman, 2005)

In Hout Bay, Western Cape, South Africa, Ikamva Lethu Fishing operates a fish processing plant that utilises seawater from the adjacent bay. Figure 2.7 is a schematic sketch of the Ikamva Lethu Fishing Jetty and seawater Intake configuration. Water is abstracted via this jetty that extends 18m in to the bay, Figure 2.8.

This jetty contains the pipework and the pumps used for pumping seawater to the fish proceeding plant. The pumps are situated at the end of the jetty with the intake pies extending a further 30m into the bay. This jetty is 40 years old and is in a state of disrepair (WSPACE, 2007). With regards to the flow of seawater within the factory, the current system is a flow through system with an in flowrate of 20l/s (ZLH, 2007).

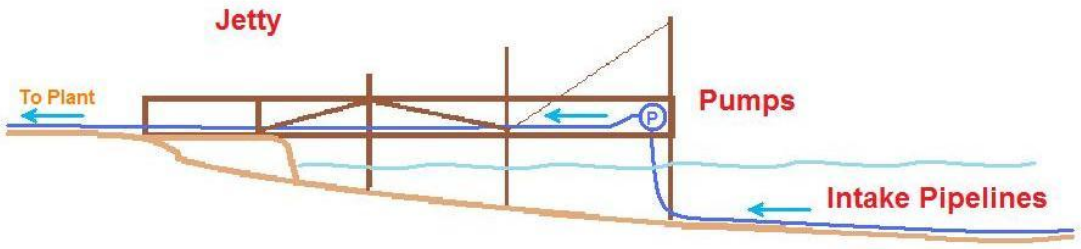

Figure 2.7: Schematic sketch of Ikamva Lethu Fishing Jetty and Pumping Configuration

Figure 2.8: Intake Jetty for Ikamva Lethu Fishing. (WSPACE, 2007)

2.2.4 Mariculture

Mariculture is in general, the farming of sea life for human consumption. Previously known as aquaculture, this branch of farming with seawater has subsequently become known as mariculture. Due to the depletion of natural fish stocks, mariculture can meet the increasing demand for seafood.

As the world developed into a global economy, other sea creatures from the coasts of South Africa have become desirable. Hence mariculture, which started with the farming of fish, has grown to include, Abalone, Mussels, Scallops, Clams, Oysters, Limpets Crayfish, Lobster and lately even Sea cucumbers. Figures 2.9 to 2.12 (DEAT, 2001)

Figure 2.9:Abalone (DEAT, 2001)

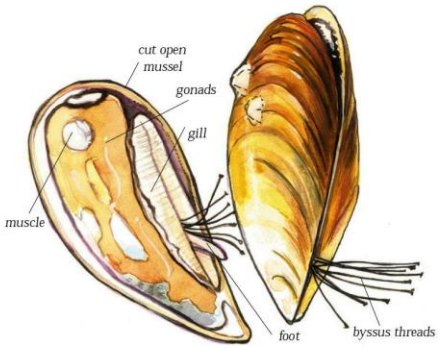

Figure 2.10:Brown Mussel (DEAT, 2001)

Figure 2.11:Scallops (DEAT, 2001)

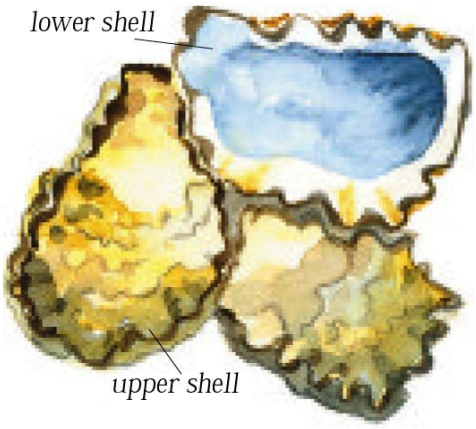

Figure 2.12:Natal Rock Oyster (DEAT, 2001)

Early mariculturists placed fish farms in sheltered bays and lagoons. Here wave action is at a minimum. The continuous flow of fresh seawater past the farm is a basic natural requirement.

However farms in the ocean or at the shoreline were still subjected to extreme events like, storms and red tides. Additionally, the cost of equipment maintenance is extremely high. Hence farming moved to land based operations where the feed seawater could be monitored and controlled. There are numerous examples of mariculture in South Africa. Some of these are described in further detail in chapters, 3.2, 3.6, 3.7 and 3.8.

2.2.5 Scientific Facilities

Due to development, there are severe pressures on marine life. Hence much research is conducted to ensure that sea life is protected and is not severely impacted by man. This is done by several means. One alternative is the general informing of the public. This is done in the most convincing way by means of an Aquarium. Here the public can view sea life in their most natural habitat. The two major aquariums in South Africa being the Two Oceans Aquarium in Cape Town and the Sea World Aquarium, Figure 2.13, at Ushaka Marine World, in Durban. These two facilities will be discussed further in Chapters 3.4 and 3.5 respectively.

Broad spectrum aquatic research is however conducted at specialised research aquariums. Here the scientific communities study the entire pelagic and benthic community in order to better understand and protect marine colonies. While research is carried out in the above two aquariums, specialised research is carried out in small dedicated aquariums. Two such facilities of note are the Sea Fisheries Aquarium in Sea Point, Cape Town and the Natal Sharks Board in Mhlanga Durban.

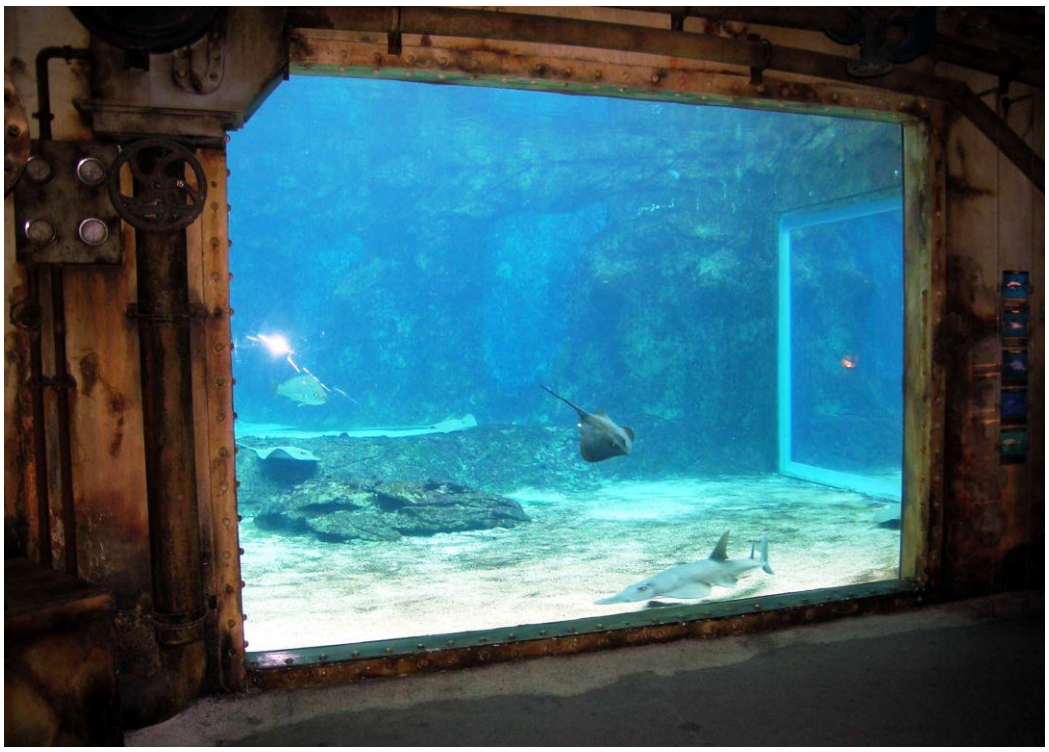

Figure 2.13: uShaka Marine World in Durban, South Africa

2.2.6 Recreational Facilities

Recreational facilities which use large quantities of seawater are usually situated close to the shoreline. Majority of swimming pools along the Durban coastline, Figure 2.14, use seawater. Seawater is extracted by means of beach wells and circulated via submersible pumps (Wenlock, 2009). The resident time for water in the small circular public paddling pools is 2 hours, Figure 2.14. The larger rectangular, Rachel Finlayson pool has a sea water resident time of 4hours. Ushaka Marine World (UMW), Figure 2.15, also utilises seawater for its marine activities. The seawater intake for UMW is discussed chapter 3.5.

Figure 2.14: Paddling pools and Rachael Finlayson pool (left) in Durban SA (Google 2008)

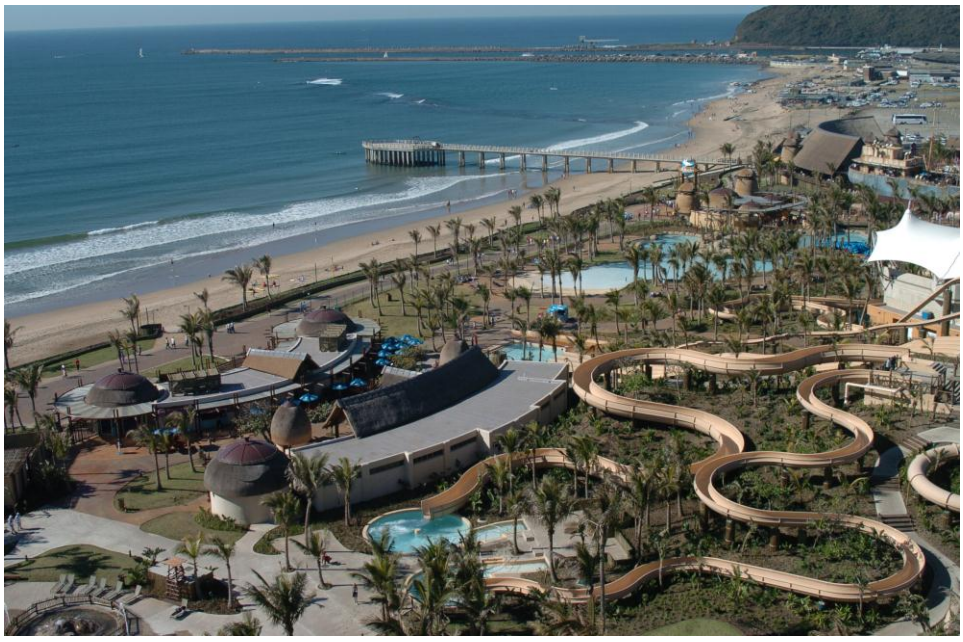

Figure 2.15: uShaka Marine World in Durban, South Africa

2.2.7 Environmental

Seawater can be used to augment natural systems when extreme conditions are encountered. Seawater is used to enhance natural or man implemented systems and can even be used to create extreme events like flash floods.

Figure 2.16 below is of the Zandvlei estuary near Muizenberg, Cape Town. Prior to development the estuary was frequently flushed by the rainfall runoff and diluted by the tidal action. However, at one time, the situation became extremely critical when the concentrate of pollutants in the estuary and the de Gama development became very high. Hence measures were taken to stabilise the amount of concentrates in the estuary.

Seawater from False Bay was used to dilute the estuarine waters. A beach well was installed 100m east of the estuary mouth. This then fed into a pipeline which then delivered sea water to the estuary the de Gama development, hence causing a dilution of the water (Samson, 2010).

Figure 2.16: De Gama Estuary and Beach well at Muizenberg. (Adapted from Google, 2008)

2.3 Seawater Intake Systems

There are numerous types of seawater intakes, with their designs being influenced by three major criteria, viz., 1.) the intended use of seawater, 2.) the coastal geology of the region and 3.) the coastal/wave climate of the area. Hence each seawater intake system is unique, due to the above three factors.

2.3.1 Direct Intakes

Direct seawater abstraction normally occurs at or near the seabed floor. Here a physical structure draws seawater directly into its connecting pipe work. These systems are typically designed to extract large volumes of seawater, hence the larger intake heads. The intakes for these systems are more often than not placed past the surf zone where sediment loads; erosion as well as wave forces, are reduced.

Depending on the surf zone characteristics, the connecting pipe work lies above, partially or completely below the seabed. The connecting pipe work passes the breaking zone and terminates into a structure. These systems can either work via gravity or pumps. Figure 2.17 shows the inlet structure, and Figures 2.18 and 2.19 show the pipe work during installation (submergence) for a power station in Majung, Malaysia respectively. The intake structures lie on the seabed and the 'pipe work' comprises a concrete box culvert with 3 channels. This system is fairly large with a capacity of approximately 88.2m^3/s (ZLH, 2008).

Figure 2.17: Majung Power Station seawater intake structure (ZLH, 2008a)

Figure 2.18: Majung Power Station seawater connecting culverts on land (ZLH, 2008a)

Figure 2.19: Majung Power Station seawater connecting culvert being floated and placed into position (ZLH, 2008a)

2.3.2 Sub-bottom Abstraction

Sub-bottom abstraction is the removal of seawater, with the intake structure occurring below the seabed, also referred to as “Partially direct” intake of seawater. Hence this implies that the floor is porous being either a non-cohesive soil or porous rock. Gravity is the flow driving mechanism. Seawater flows into the intake structure and then into the connecting pipework.

The seawater then flows into a collection well where it is usually transferred to land via pumps. The one added benefit of such systems is that they provide seawater that has had a degree of filtration due the natural medium that they have had to flow through.

Figure 2.20 below, shows a section of a Sub-bottom seawater abstraction system. Seawater flows down, through the seabed, into the intake pipes. Water then flows via a pipe to a collection sump that is beyond the shore zone. Seawater is then pumped out the collection sump to its end use. (Reynolds & Maley, 2008) This abstraction system is usually augmented for a particular environment and is based on the availability of material and plant equipment.

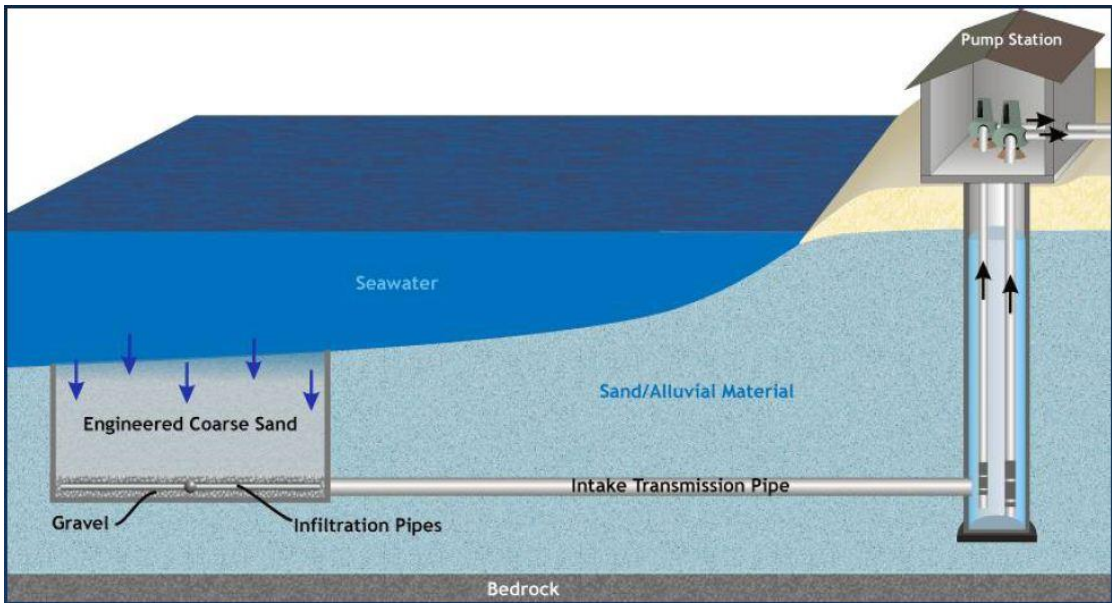

Figure 2.20: Typical sub-surface seawater abstraction (Reynolds & Maley, 2008)

2.3.3 Surf Zone Abstraction

The surf zone is not a good location when abstracting seawater. This is due to the dynamically turbulent nature of the surf zone and the abundant quantity of suspended sediments and high wave forces. This portion of the seafloor also normally contains a higher quantity and diversity of sea life, hence the environmental impacts on seawater intakes at the shoreline, can be potentially negative.

The coastlines are numerous in their geology and topography but are essentially either sandy or rocky. Sandy coastlines imply beaches of fine grain material and rocky coastlines implying rock strata, outcrops and headlands. Hence there are various approaches to abstracting seawater in these two coastal types.

2.3.3.1 Sandy Coastlines

Sandy coastlines make up a significant portion of the South African coastline. Coupled with the South African climate, these areas have a high recreational value. Hence, seawater abstractions in these areas, apart from other factors, have had to consider the aesthetic design of such systems.

The most common seawater abstraction systems used at sandy shores, for large discharges, are intake basins (e.g. Koeberg Ch.2.2.1.1). For smaller discharges, radial beach wells are used. Figure 2.21 shows radial beach wells on a sandy beach at Long Beach, California (Wang, 2009). Figure 2.22 is a typical section through the sump of a radial beach well (Wang, 2009).

It can be seen that subsurface pipes are placed in suitable material, at a sufficiently subterranean depth. The water then flows under gravity, through the sand, into the pipes and into a collection sump. This water is then pumped out using submersible pumps.

Figure 2.21: Position of radial beach wells shown on Long Beach, California (Wang, 2009)

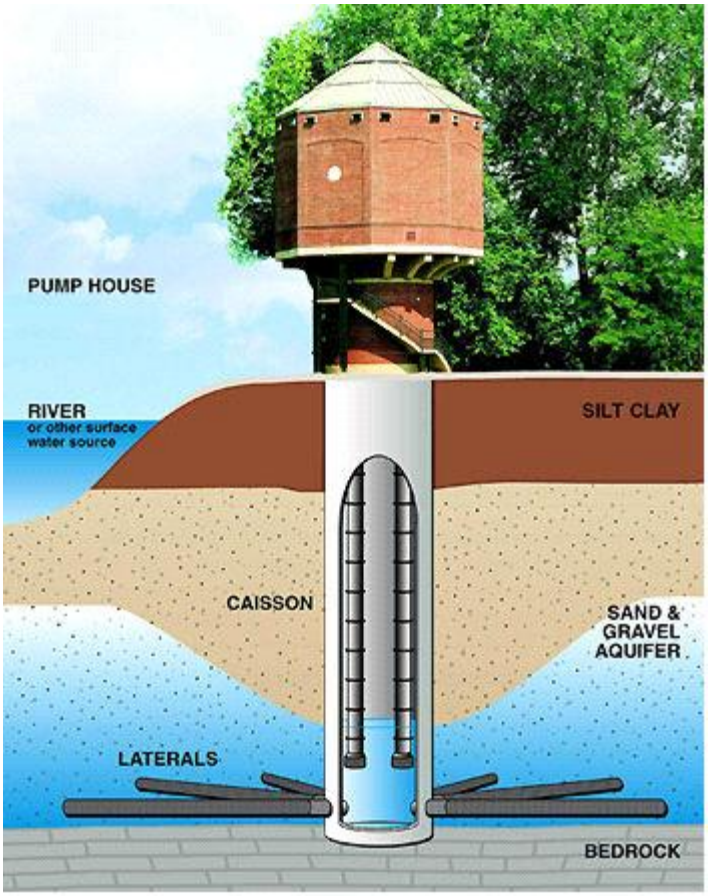

Figure 2.22: Section through a horizontal/ radial well (Wang, 2009)

2.3.3.2 Rocky Coastlines

A coastline is considered rocky when the vast majority of the shoreline is composed of rock. Due to the dynamic nature of shorelines, pockets of sand might be present.

When abstracting seawater, rocky coastlines are not the preferred topography; as working in the surf zone within a hard material is fairly complicated. If the rock is found to be fairly pervious, then a subsurface abstraction system approach is preferred and drilling horizontal wells into the surf zone is the favourable method by which seawater can be collected.

Another method is the excavation of a trench out from the shoreline into the surf zone. In Figure 2.23 an example of a concrete compartmentalized section is used to filter sea water into a collection sump.

Figure 2.23: Seawater intake on a rocky shore. (Thiess, 2006)

2.4 Hydraulic Review

2.4.1 Introduction

This Chapter reviews a few hydraulic processes concerned with small scale seawater abstraction in the coastal/aquifer zone. Chapter 2.4.2.examines general methods for subsurface seawater abstracted from a sandy beach. Chapter 2.4.3 depicts the basic principles of ground water flow while Chapter 2.4.4 examines groundwater abstraction theory. Chapter 2.4.5 looks at the hydraulic conductivity of material as this is critical for the design of non surface, seawater intake systems. Chapter 2.4.6 examines current seawater intake planning and design criteria for small scale abstraction. Chapter 2.4.7 will focus on filter design criteria

2.4.2 Subsurface Seawater Abstraction from a Sandy Beach

The following general methods of abstraction depict the different ways seawater is abstracted from a sandy beach. Each examined intake has its own particular method for abstraction and is as follows.

2.4.2.1 Beach Wells

Figure 2.24 shows the typical section and layout of a Beach well. A Beach well characteristically consists of casing pipes that line boreholes with screened sections usually at their lower parts. Due to economics, the diameters of well screens are usually 15 to 30cm. A turbine pump is lowered into the casing below the water table in the well. The pump motor, integrated with the pump can be submerged. The motor can also be installed at the top, driving the pump via a long shaft (Schwarz, 2000).

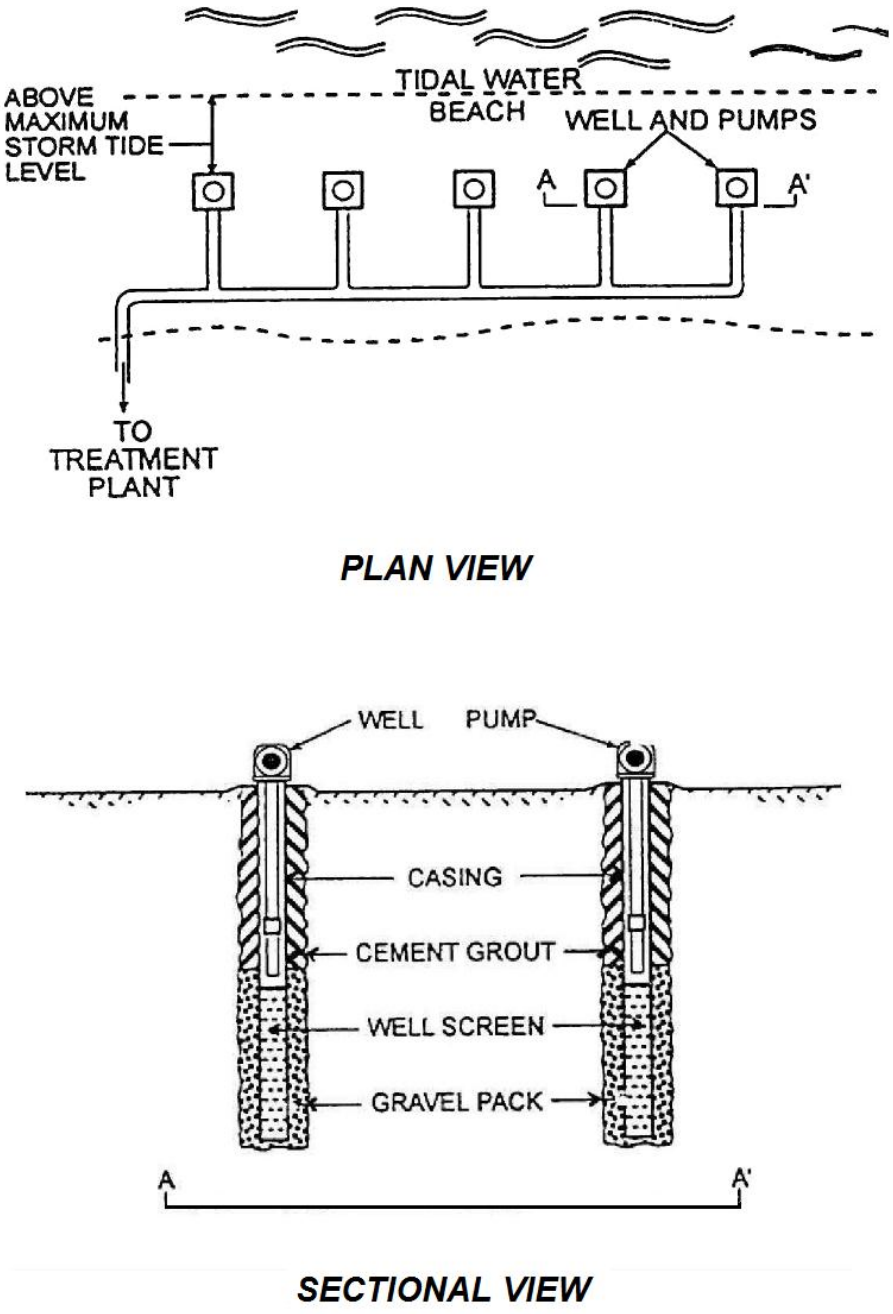

Figure 2.24: Layout and typical section of Beach wells (Schwarz, 2000)

2.4.2.2 Horizontal Beach Galleries

A horizontal beach gallery, Figure 2.25, is an alternative to Beach wells when the thickness of the water bearing formation is small or when its permeability is low. It is constructed by digging a ditch on the beach parallel to the coast. In the majority of cases, the ditch is filled with graded gravel in which a screened pipeline collector is installed. Beach sand is used to fill the ditch above the gravel layer. Water is pumped up from the gallery via well points and submersible pumps (Schwarz, 2000).

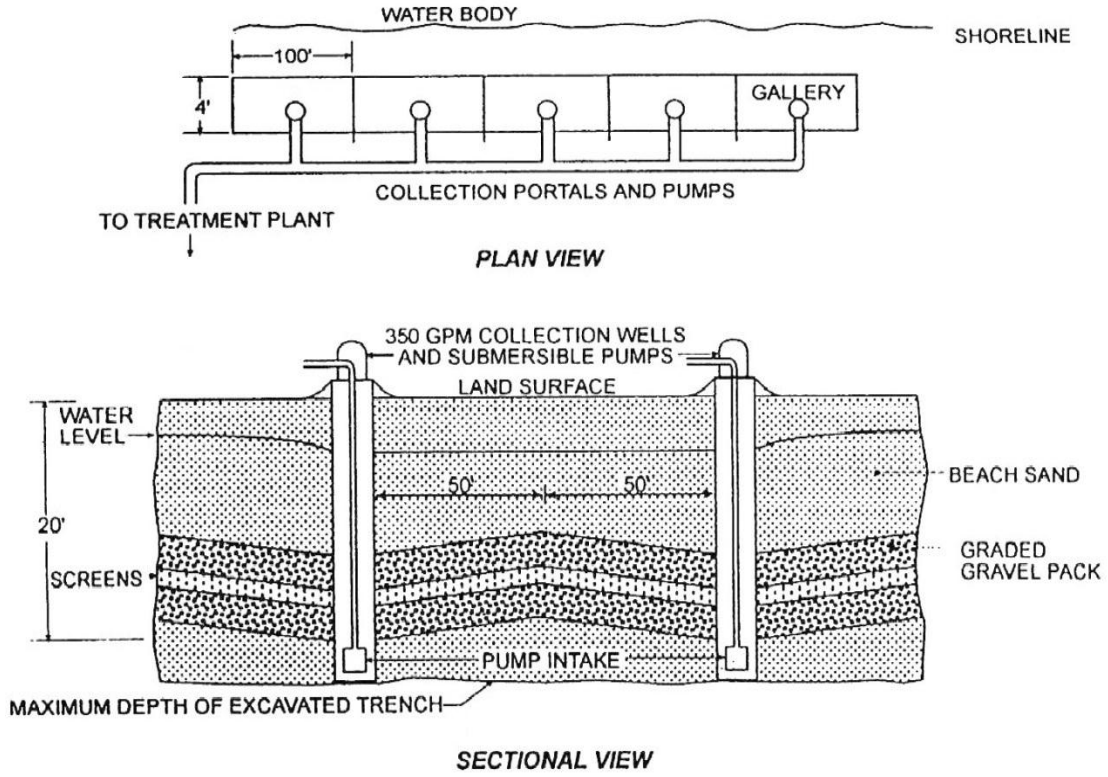

Figure 2.25: Layout and Section of a typical Horizontal Beach Gallery (Schwarz, 2000)

2.4.2.3 Infiltration Galleries with Horizontal well-screens

Infiltration galleries incorporate a horizontal gallery installed out of the surfzone. Horizontal well screens are then connected to the gallery, near the invert of the gallery. These well screens project into the sandy beach at a predetermined depth. The well screens are normally parallel to each other, although screens at the ends of the gallery, can be projected at an angle. A typical infiltration gallery with horizontal well screens is shown in Figure 2.26.

The length, diameter and slot size of the well screens is determined by the parameters of the sand, and the required yield of the system. The screen diameter is also governed by the need to minimise head loss for flow through the screen pipe (Basson, 2005).

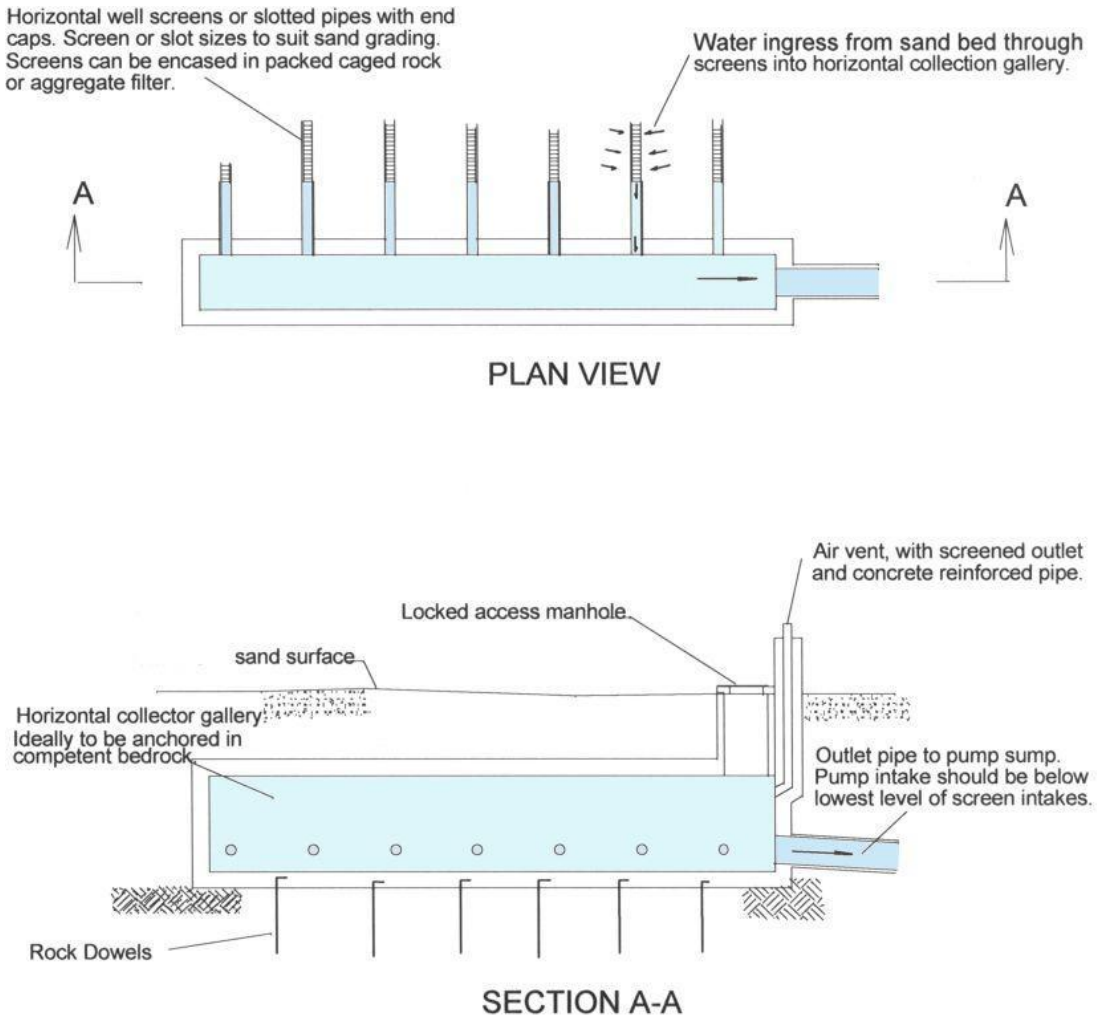

Figure 2.26: Infiltration galleries with horizontal well screens (Basson, 2005)

2.4.2.4 Seabed Filtrations

Figure 2.27 shows an example of Seabed Filtration. This intake system is mainly used when the hydraulic conductivity of the surrounding material is very low. The Seabed filtration system is constructed by dredging or trenching the seabed bottom parallel to the coastline. The gallery is placed at an appropriate depth below the seabed. Pipelines connect the gallery to the coast. The trench is filled with a graded gravel and sand pack (Schwarz, 2000).

The system operates similarly to a slow sand filter. In order to regenerate capacity after clogging, the upper sand layer of 3 - 5 cm is removed and replaced periodically. The seabed filtration system can be used as a seawater intake but can also be used in riverbeds for abstraction of fresh water (Schwarz, 2000).

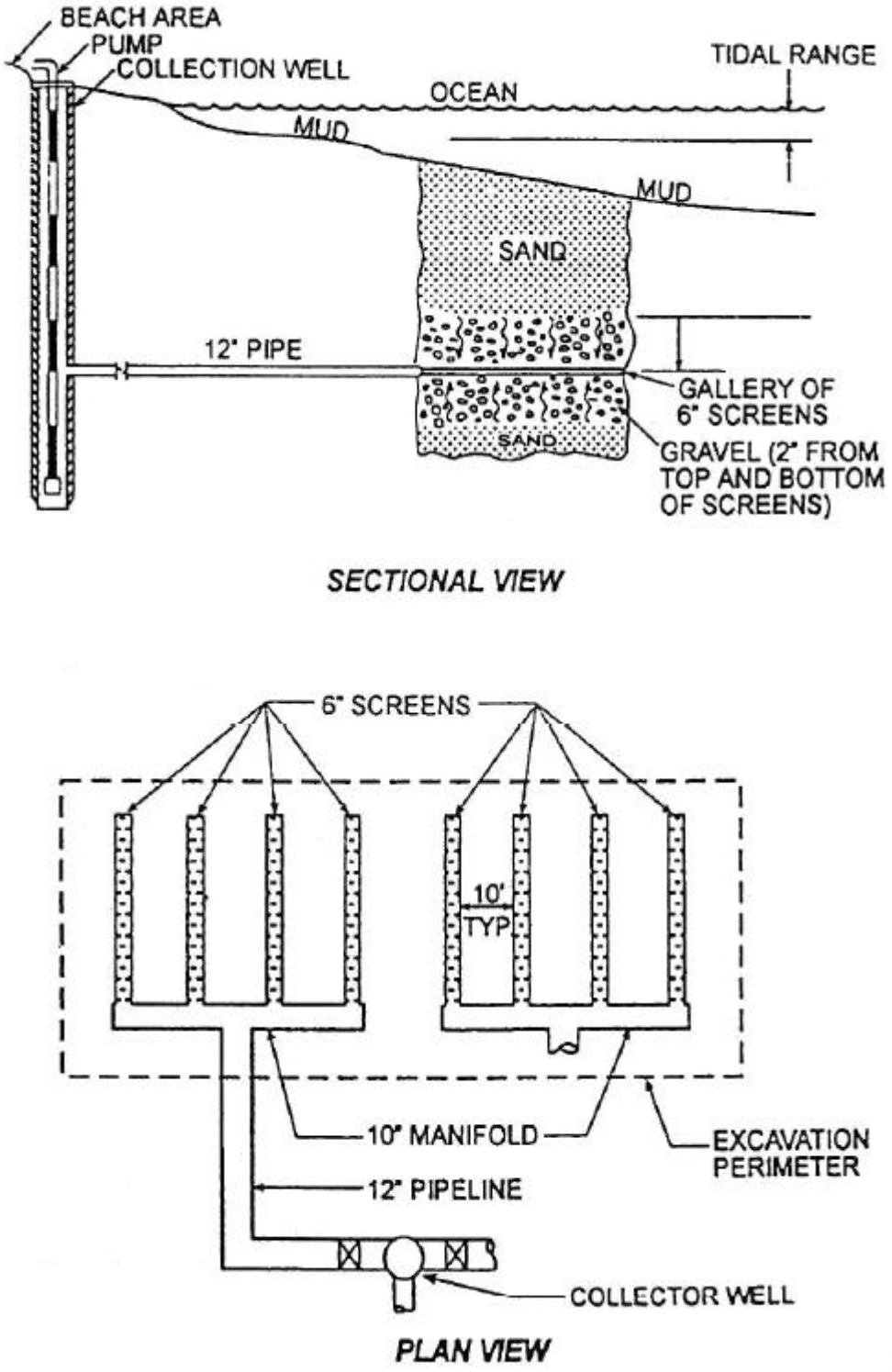

Figure 2.27: Seabed Filtration (Schwarz, 2000)

2.4.3 Basic Groundwater Flow Theory

Water and most other liquids, can flow through all natural material. The velocity at which the water moves is inversely proportional to the size of the openings through which it moves Roberson, et al, 1998). Figure 2.28 below shows water flowing from one reservoir to another, through a conduit filled with a permeable material (Roberson et al, 1998).

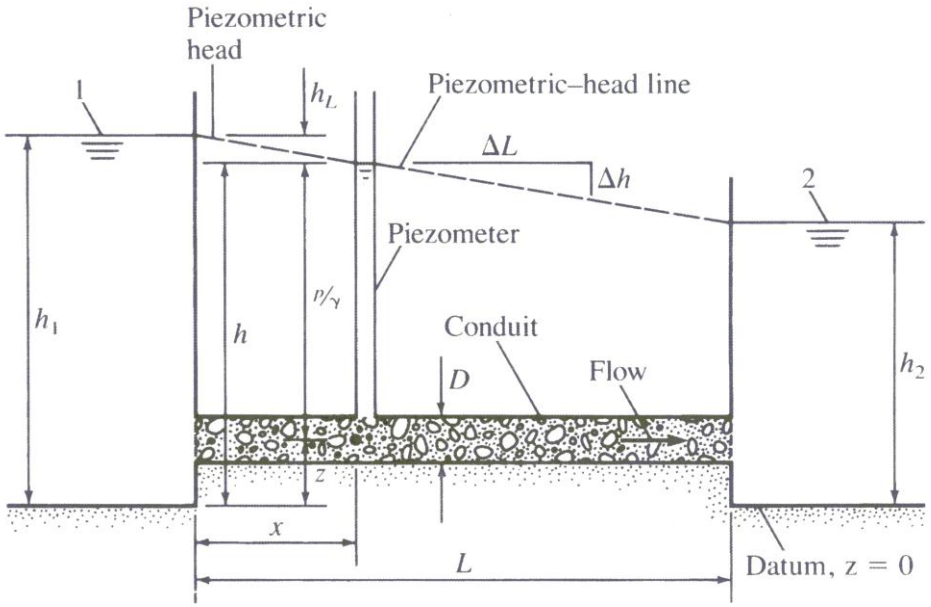

Figure 2.28 Flow through a conduit filled with permeable material (Roberson et al, 1998)

It was found that for small velocities, the flow is laminar and the energy loss is linearly proportional to the velocity *V*:

$$h_L = \frac{LV}{k} \qquad \text{(Eqn LR1)}$$

Where:

h_L = Headloss due to friction
L = The length of the conduit
V = Velocity
k = The proportionality constant / Hydraulic conductivity constant

k is a function of the size and shape of the voids between the particles making up the porous material as well as the viscosity of the liquid. Table 2.2 shows the porosity and range of hydraulic conductivity for various natural materials.

Substituting $h_L = h_2 - h_1$ into LR2 produces

$$V = k\frac{h_2 - h_1}{L} = k\frac{\Delta h}{L} = ki \qquad \text{(Eqn LR2)}$$

Where:

i = Hydraulic gradient

This equation (LR2) is known as Darcy's law. Darcy concluded that the flow velocity through a porous material was directly proportional to the gradient of the piezometric head (hydraulic gradient). Note that Darcy's law is only valid for laminar flow.

Table 2.2: Porosity and hydraulic conductivity: Natural Material (Roberson et al, 1998)

Material	Porosity	Hydraulic conductivity
		m/day
Soil	0.55	10^{-3} to 5
Clay	0.5	10^{-7} to 10^{-4}
Sand	0.25	0.06 to 120
Gravel	0.2	100 to 7000
Limestone	0.2	10^{-4} to 500
Sandstone	0.11	10^{-5} to 0.5
Basalt	0.11	10^{-8} to 1000
Granite	0.001	10-^{8} to 5

As can be seen in Table 2.2 above, there can be, a wide variation of hydraulic conductivity for a particular material. Basalt for example can vary in hydraulic conductivity from 10^{-8} to 1000m per day. The lower number is applicable to unfractured basalt in its natural state. The higher number is indicative of basalt that has under gone fracturing. Large hydraulic conductivity is typical of a highly fractured rock. (Roberson et al, 1998)

Note that the flow regime investigated is laminar. Turbulent flow as well as empirical methods to determine hydraulic conductivity, is presented in Chapter 2.4.5.6

2.4.4 Groundwater Abstraction

2.4.4.1 Well Hydraulics

Wells are the most common method used to extract water from the earth. The well in Figure 2.29 is the most common layout of a borehole well. Figure 2.24 shows how these wells can be connected to a manifold. Wells are designed to be drilled to a depth where water can be found. The area that contains a saturated concentration of water is termed an aquifer.

A casting is usually installed to line a borehole. For these wells, a short piece of casing would be grouted in the top of the well to protect against the unwanted inflow from layers of soil that contain undesirable elements. (Roberson et al, 1998) A grout seal at the surface prevents surface runoff from entering the borehole and reaching the source aquifer. The bottom of the well contains the well screen which allows water to enter the well.

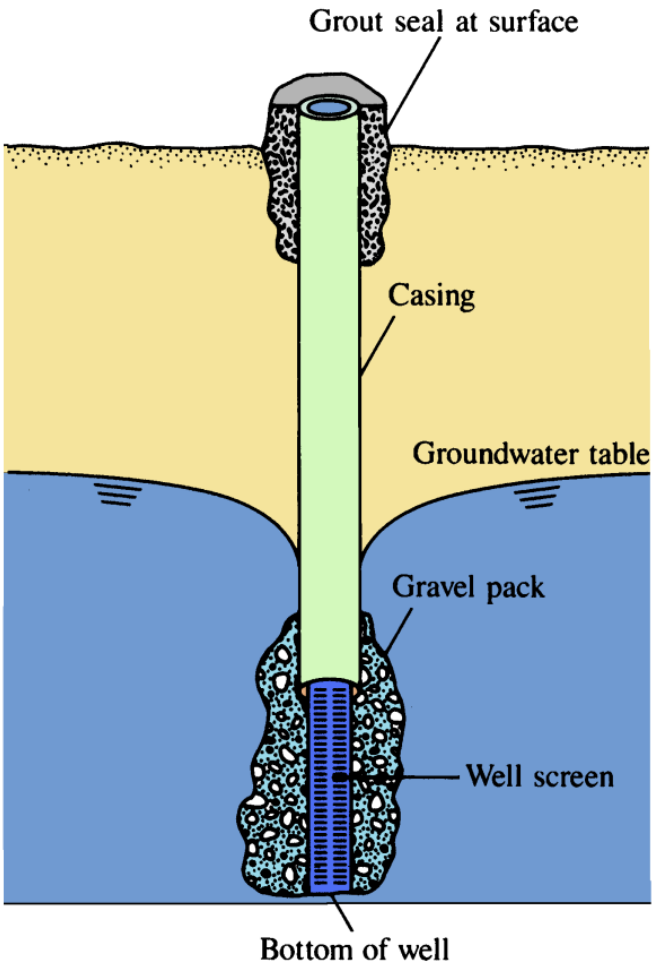

Figure 2.29: Most common section of a borehole well (Roberson et al, 1998)

A well screen is typically surrounded with a gravel pack. These packs are usually zones of large hydraulic conductivity which enhance flow into the well screen. This is true of normal boreholes, where the surrounding material is finer than the gravel pack. However this is not the case when wells are situated in sandy beaches. Here the gravel packs act more like filters to stop the intrusion of fine material as opposed to creating an area of higher hydraulic conductivity

2.4.4.2 Unconfined steady flow Well hydraulics

From equation LR2, the following equations show how axially symmetrical flow into a well can be analysed. Figure 2.30 below shows the manner in which it is done.

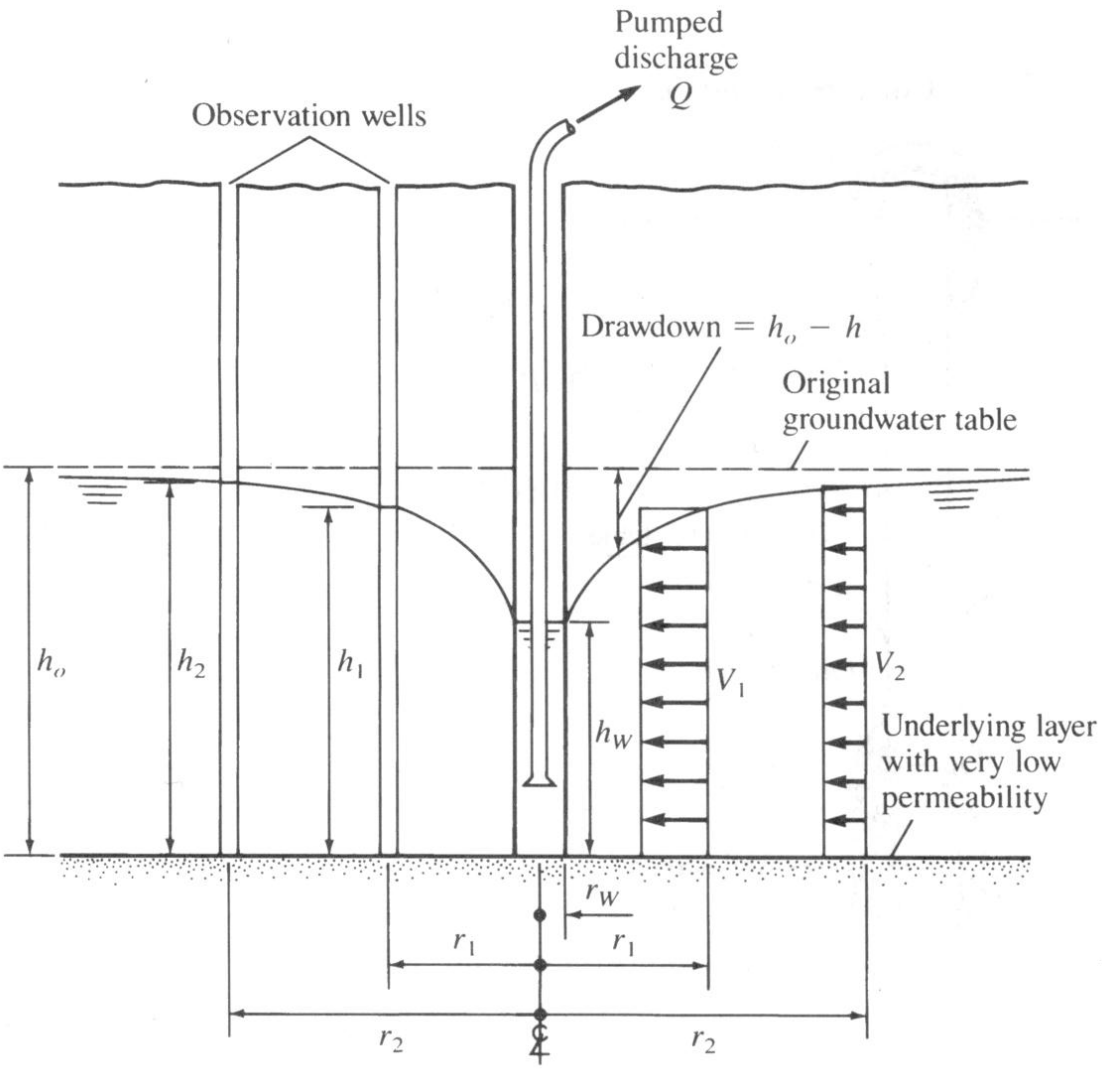

Figure 2.30: Axially symmetrical flow into a well in an uncontrolled aquifer (Roberson et al, 1998)

The velocity of the flow is steady and equal to *V* at a distance *r* from the centre of the well. The depth of the flow at that point is *h*. The original depth of groundwater is h_0. The radius of the well is r_w, and the steady state height of the water in the well is h_w. It is assumed that the flow is steady. The aquifer is homogenous and underlain by an impervious layer, but unconfined on top.

From equation LR2, if the area A of inflow is $2\pi rh$ then LR2 becomes

$$Q = 2\pi rhK\frac{dh}{dL} = 2\pi rhK\frac{dh}{dr} \qquad \text{(Eqn LR3)}$$

Since *dh/dr = dh/dL*

Hence if equation LR3 is integrated as

$$Q\int_{r_1}^{r_2}\left(\frac{1}{r}\right)dr = 2\pi K\int_{h_1}^{h_2} h\,dh \qquad \text{(Eqn LR4)}$$

to yield

$$Q = \frac{\pi K(h_2^2 - h_1^2)}{ln\left(\frac{r_2}{2r_1}\right)} \qquad \text{(Eqn LR5)}$$

Due to pumping, the drawdown of the water table is h_o - *h* and the vertical distance at a point *r* distance from the well centreline. The development of equation LR5 has assumed that the velocity is steady and that water moves continually towards the well from some undefined surrounding source so that he water level remains at a constant level *h* at a distance *r* from the well.

In reality, this seldom occurs as the flow of water from surrounding sources can vary over time. In general, equation LR8 gives reasonably accurate results if the maximum drawdown is not more than about one half the aquifers depth. As drawdown becomes too great, the assumptions of horizontal flow are violated and Equation LR5 is no longer applicable.

Equation LR8 can also be used to calculate the hydraulic conductivity of an aquifer. To calculate this value, a pumping test is required. This is discussed further in

Chapter 2.4.4.3. The following Table 2.3 contains estimation of the order of magnitude of *k* values for some material.

Table 2.3: Hydraulic conductivity of various materials (Schwartz, 2000)

Material	Hydraulic conductivity
	m/day
Clay	10^{-5} to 10^{-7}
Silt	10^{-1}
Fine Sand	10^{-1} to 10
Course Sand	10^{0} to 2 x 10^{2}
Gravel	10^{0} to 10^{3} or more

2.4.4.3 Pumping Tests

The most significant aspect of quantitatively predicting the movement of groundwater or in determining the yield of a well is accurate knowledge of the aquifer characteristics. These characteristics include: the hydraulic conductivity *k,* the aquifer thickness *B,* and the storage coefficient *S*.

In simple cases, drawdown and discharge data can used to estimate aquifer characteristics. The basic tool for collecting this data is the pumping test. This test consists of pumping directly from one well while water levels are recorded in one or more observation wells. These wells are drilled solely for observing the drawdown as pumping of the test well proceeds. Having at least three observation wells, each at different distances from the pumped well, is desirable (Schwarz, 2000).

In general, it is desirable to space the wells at approximately at 1.5, 2, and 4 times the thickness of the aquifer away from the test well (Schwarz, 2000). Experience has shown that a concept called the radius of influence can often be invoked where the surface of the groundwater table at an appreciably large distance from the well, (usually 500* Well radius (r_w) or approximately 300m) is assumed to be at a constant elevation (Roberson et al, 1998).

Equation LR5 can be used to estimate the hydraulic conductivity of an aquifer with information obtained from a pumping test. A well, constructed as shown in Figure

2.30, and smaller observation wells, are drilled at a distance such as r_1 and r_2 from the well (Roberson et al, 1998). The water levels are observed and recorded before pumping at a known rate begins. Thereafter the approximately steady state values achieved after continuous pumping are recorded. These values are then substituted into Equation LR5 to obtain estimates of *k.*

Note that due to the shape of the drawdown surface varying with time, values of *k* determined through using Equation LR5 must be considered approximations. If the groundwater levels go down slowly, the calculated hydraulic conductivity can be reasonable. However, if the groundwater levels continue to fall rapidly, the flow is obviously very unsteady, and errors in the value of hydraulic conductivity, as determined from the steady-state equations, can be significant (Roberson et al, 1998).

Several techniques have been developed for approximately evaluating local aquifer characteristics using so-called rate of use or slug tests. In the absence of observation wells, valuable information can be obtained from the pumped well observations. One of the techniques requires that a volume of water is quickly removed from the well, and the rate of rise of the water surface in the well is carefully observed after the water removal. The rate of rise can then be related to the local value of the hydraulic conductivity. These techniques are much cheaper and quicker to perform than pumping tests and are valuable for use in preliminary investigations (Schwarz, 2000).

2.4.5 Hydraulic Conductivity of Filter and Porous Material

2.4.5.1 Introduction

Basic ground water flow theory was covered in Chapter 2.4.3. This introduced the linear relationship between the flow velocity *v*, the permeability *k* and the hydraulic conductivity *i*. This can be seen in equation LR2

When the size of the material starts to become larger, Darcy's Law for laminar flow starts to become invalid. Looking at Figure 2.31, when the hydraulic gradient is increased, the flow remains laminar in Zones I and II. With the line being fairly straight in this portion, the velocity is linearly proportional to the hydraulic gradient (Das, 2000).

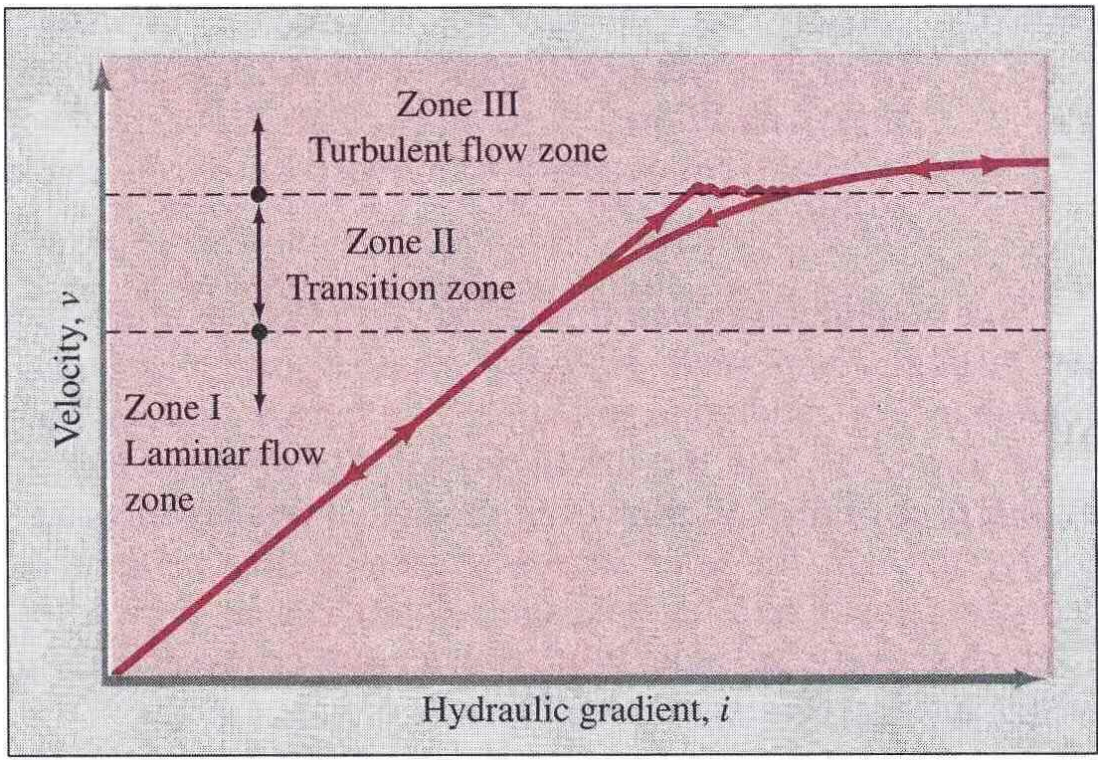

Figure 2.31: Variation of velocity *v* with hydraulic gradient *i* (Das, 2000)

At a higher hydraulic gradient, the flow becomes turbulent (Zone III). Thereafter, when the hydraulic gradient is decreased, laminar flow is only once again attained in Zone I. Thereafter, it is deemed that laminar is found to occur in Zone I only.

2.4.5.2 Absolute Permeability

The hydraulic conductivity *k* of soils are dependent on many factors. These are mainly: grain size distribution, pore-size distribution, void ration, fluid viscosity, roughness of material particles and degree of saturation. Hence for similar element the hydraulic conductivity *k* can vary. Therefore is understood that *k* would vary for different materials (Das, 2000).

The viscosity of a fluid flowing through a porous material will affect the hydraulic conductivity *k* of a material. This hydraulic conductivity is dependent on the Absolute Permeability *k* and defined by equation LR6 below. The relevance of this equation becomes evident in the following section

$$k = \frac{\gamma_w}{\eta} \mathfrak{k} \qquad \text{(Eqn LR6)}$$

Where:

k = Hydraulic Conductivity

γ_w = Unit weight of water

η = Viscosity of water

$\boldsymbol{\mathfrak{k}}$ = Absolute Permeability

2.4.5.3 Hydraulic Conductivity: Empirical Relations

In the past, several empirical methods have been derived for estimating the hydraulic conductivity. A few of these equations and associated methods are presented below (Das, 2000).

Hazen

Hazen proposed the following empirical relationship for the hydraulic conductivity of sand that was fairly uniform in nature. This equation was formulated based on Hazen's observations of loose, clean, filter sands. The equation is as follows:

$$k = cD_{10}^2 \qquad \text{(Eqn LR7)}$$

Where:

k = Hydraulic Conductivity

c = Constant that varies from 1.0 to 1.5

D_{10} = Effective size, in mm

Kenny, Lau and Ofoegbu

As was mentioned previously in Chapter 2.4.5.1, Darcy's formula is valid for laminar flows only. Hence equation LR2 would not be applicable. However it was found that under low hydraulic gradients, laminar flow conditions can be found in in very coarse sands and gravels. Kenny, Lau and Ofoegbu conducted laboratory tests on granular soils in which the particle sizes in various specimens ranged from 0.074 to 25.4mm. The uniformity coefficients, C_u varied between 2 and 12. These tests showed that for laminar conditions,

$$k = (0.05 \; to \; 1)D_5^2 \qquad \text{(Eqn LR8)}$$

Where:

k = Absolute Permeability

D_5 = the effective size, in mm

Equation LH8 is based on results shown in the following Figures 2.32 and 2.33

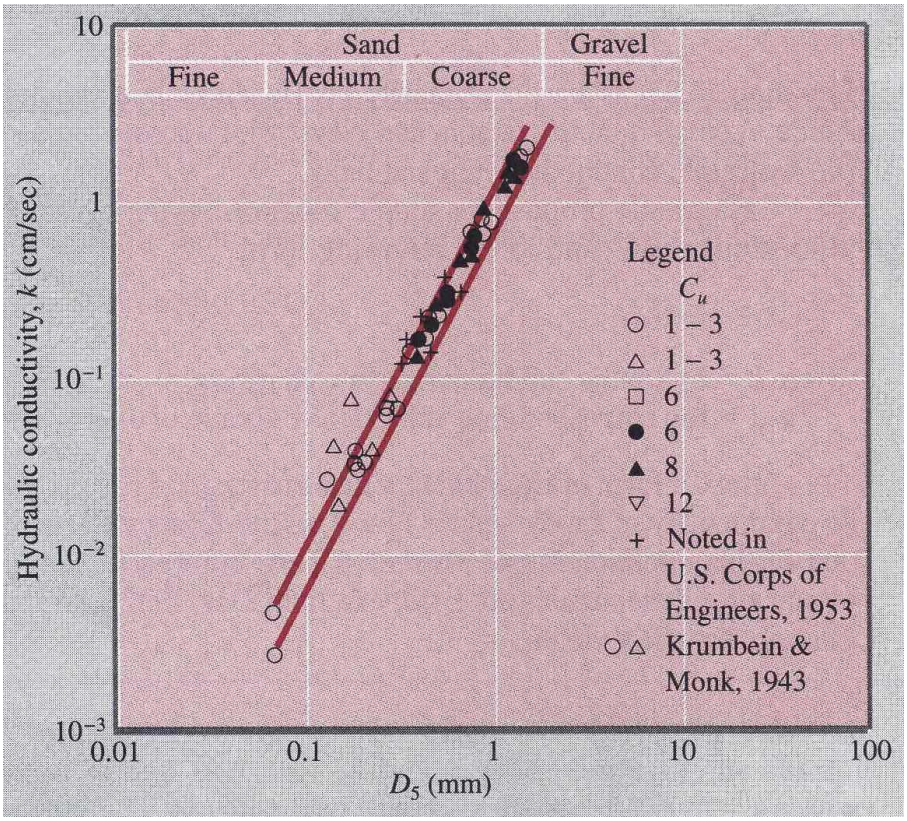

Figure 2.32: Results of Permeability Tests for C_u = 1-3 (Das, 2000)

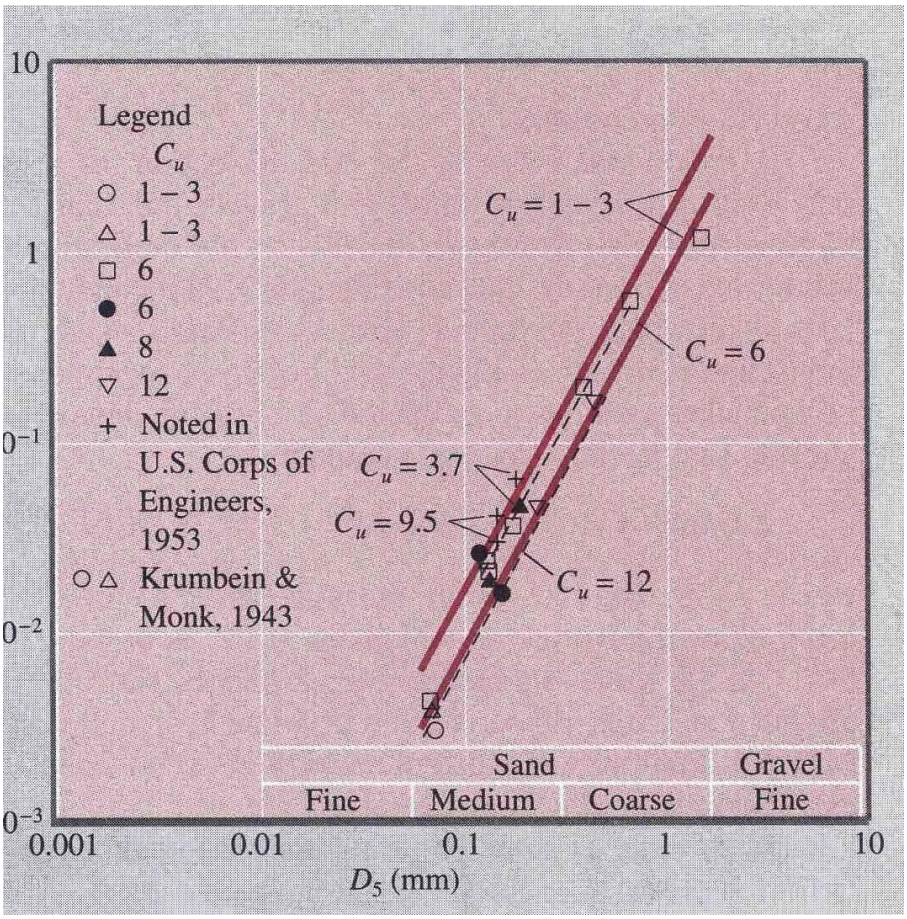

Figure 2.33: Results of Permeability Tests for C_u>3 (Das, 2000)

2.4.5.4 Hydraulic Conductivity: Turbulent Flow

As mentioned in Chapter 2.4.5.2, the flow of water through most soils is laminar. However, as material size increases, for example rockfill, the flow though the larger voids is found to be turbulent. In Darcy's law the Flow velocity *V* and the Hydraulic gradient *i* share a linear relationship. When the flow becomes turbulent, this equation has to be replaced by a non linear relationship. This is summarised by Forchheimer's Equation LR9 below: (CIRIA, CUR, CETMEF, 2007)

$$i = A_{For}V + B_{For}V|V| \qquad \text{(Eqn LR9)}$$

where,

i = Hydraulic gradient

V= Flow velocity

and A_{For} and B_{For} are coefficients that can be estimated from the median stone of D_{n50} and the volumetric porosity n_v by using the following Equations:

$$A_{For} = \propto_{For} \frac{(1-n_v)^2}{n_v^3} \frac{v_w}{gD_{n50}^2} \qquad \text{(Eqn LR10)}$$

$$B_{For} = \beta_{For} \frac{1-n_v}{n_v^3} \frac{v_w}{gD_{n50}} \qquad \text{(Eqn LR11)}$$

Where

α_{For} ≈ 1000 to 2000

β_{For} ≈ 1.0 to 1.5 at least for fairly uniform material

D_{n50} = Diameter of the average particle making up the porous material

v_w = Kinematic viscosity of the fluid≈ 10^{-6} m^2/s

n_v = Volumetric porosity

In equation LR9, the first "A_{For}" term is dominant when the flow velocity between the voids is small enough to be laminar. The second "B_{For}" term becomes dominant when flow through that medium becomes turbulent.

It is often practical to simplify the Forchheimer's relationship by linearisation to form the equation LR12. Some general values for the resulting permeability, *k* can be found in Table 2.4. Figure 2.34 provides experimental results for several types of granular material.

$$k_{eq} = \frac{1}{0.5A_{For} + \sqrt{0.25A_{For}^2 + B_{For}|i|}} \qquad \text{(Eqn LR12)}$$

Table 2.4: Permeability of granular materials (CIRIA, CUR, CETMEF, 2007)

Particle Type	Diameter (D) Range	Permeability, k
	mm	m/s
Large stone	2500-800	1 (turbulent)
'One-man stone'	300-100	0.3 (turbulent)
Gravel	80-10	0.1 (turbulent)
Very course sand	3-1	0.01
Course sand	2-0.5	0.001
Medium sand	0.5-0.25	0.001
Sand with gravel	10-0.05	10^{-4}
Fine sand	0.25-0.05	10^{-5}
Silty sand	2-0.005	10^{-6}
Sandy clay	1-0.001	10^{-7}

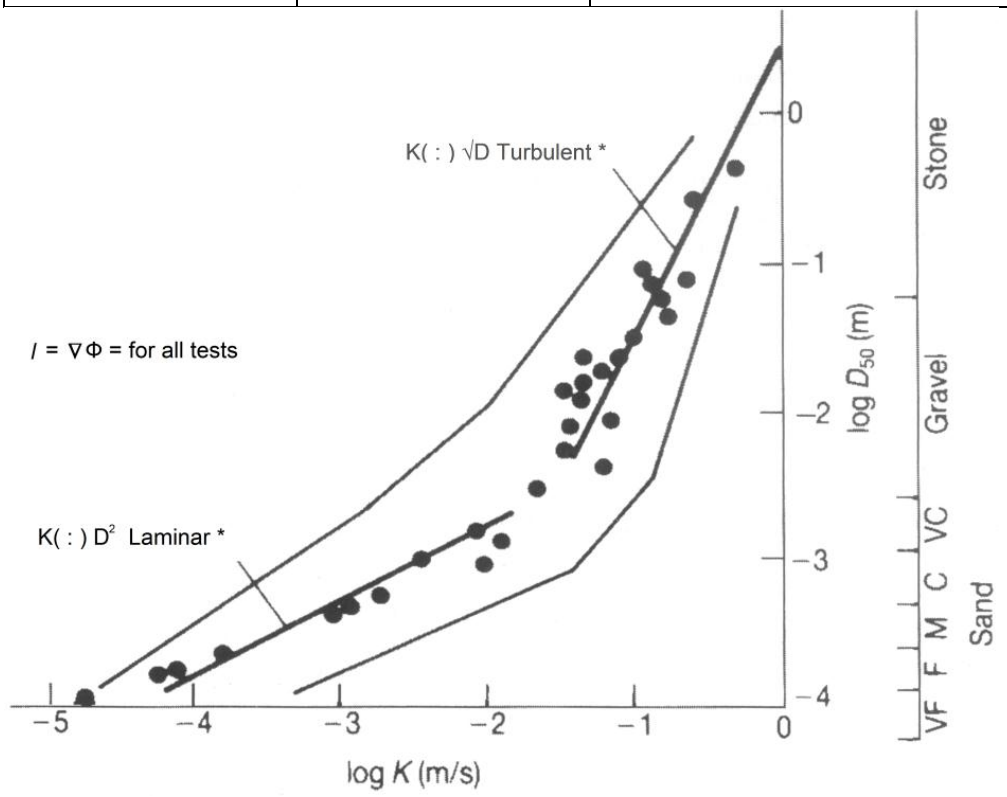

Figure 2.34: Permeability versus grain or stone sieve size (CIRIA, CUR, CETMEF,2007)

2.4.6 Hydraulic Design Guidelines: Sub Surface Seawater Abstraction

2.4.6.1 Introduction

There are numerous guidelines that aid in the design of seawater intakes. In order to meet the objectives of this thesis, only the quintessential guidelines with respect to hydraulic design of subsurface seawater abstraction will be reviewed.

In order to provide a brief, concise review, it is best to distinguish the design guidelines from the planning guidelines (of a subsurface intake). Note that the planning guideline will be mentioned in brief, where appropriate, but will not be further investigated. This review will mainly cover a) the hydraulic design guidelines associated with the intake types documented in Chapter 2.4.2.and b) the proposed seawater intake in Chapter 4.

Note that the hydraulic design of an intake is only part of the entire design/planning process. The hydraulic design of a seawater intake cannot be removed as a separate component from the total design process. The hydraulic design of a seawater intake is a list of guidelines that address an array of hydraulic situations. Figure 2.35 is a representation of most hydraulic factors that must be understood, when developing a sub-surface seawater intake. This review will concentrate on the, “Hydraulics within Seawater Intake” component.

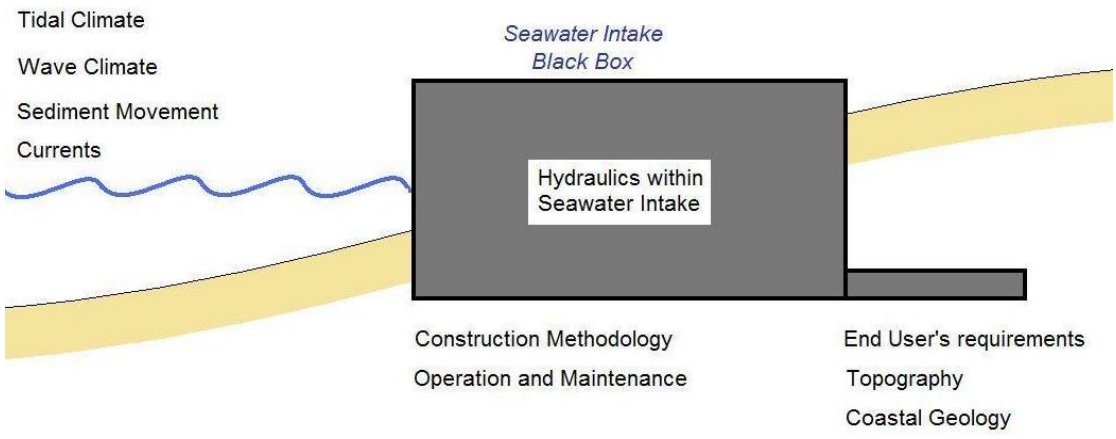

Figure 2.35: Factors to consider when developing a sub surface seawater intake

2.4.6.2 General Hydraulic Design Criteria

The following are general design criteria when designing a small scale seawater intake. Due to the settlement of material, the Infiltration rates from areas with minimal wave action will ordinarily decrease with time when compared with areas with constant wave action. It is advantageous when the wave activity is particularly vigorous. Hence the screens and filter pack material used for infiltration galleries may become partially plugged with sediment over time. Thus, it is good engineering practice to estimate the plugging potential and allow for excess entrance area to maintain the required flow. To maintain yield over time, the actual open area of the screens should be twice the required open area, i.e. the screen length should be doubled (Basson, 2005).

The length, diameter and slot size of the well screens will be determined by the parameters of the sand, and the required yield of the system. The screen diameter is also governed by the need to minimise head loss for flow through the screen pipe. It is recommended that the well screens be connected to the manifold by a length of flexible pipe (helical). This will allow for some movement of the well screens without shearing the screens at the manifold (Basson, 2005).

2.4.6.3 Backflushing

It has generally been found that systems that are backwashed regularly as part of normal operation procedures fare better than systems that are not backwashed (Basson, 2005).

Backflushing of the screens will remove any fines that have accumulated in the screens and will assist in breaking down and controlling the development and build up of scale and / or biofilm in the screens (Basson, 2005). Backflushing techniques include:

- gravity backflushing,
- piping and valve systems to pump from several screens while backflushing others, and
- air backflushing (Basson, 2005).

It is recommended that where possible, the system be designed such that it can be backwashed. This can either be done by incorporating a return flow from storage tanks or by incorporating a circular return system, whereby water abstracted from one screen is pumped back into another screen to backwash it.

Problems can arise if fines and biofilm etc. being washed out of the screen being backwashed is sucked into the screen that is being used to abstract the water for backflushing. This could lead to clogging of some of the screens (Basson, 2005).

Based on the laboratory tests conducted by Basson (2005), the following backflushing recommendations are made:

Backwashing should be done when the abstraction capacity decreases by 10% or when the negative pressure of the suction head of the hydraulic pump drops below a specified value. These are some of the measures used to protect the pump.

• For a well screen longer or shorter than 3m, only the duration of this backwash procedure and the pressure of the air backwash must be altered, not the capacity of water backwash. Water backwash should be equal to twice the abstraction rate.

2.4.6.4 General Design Criteria: Horizontal Screens in Seawater Intakes

A major design principle for infiltration galleries involves the orientation of the Intake screen relative to the surface water or groundwater flow directions. For swash zone galleries, the screen is oriented perpendicular to the shoreline. For non swash zone galleries, the screen is placed perpendicular to the groundwater flow to minimize the head loss; that is, the screen is located parallel to the beach. Important design criteria of infiltration galleries include: (Basson, 2005).

a) Entrance velocity through the screen slot openings should be 0.03 m/s or less.

b) Axial velocity inside the screen should be 0.9 m/s or less, so that the head loss, *h*, will be 0.3 m or less(Basson, 2005).

c) Screen slot size is based on the grain-size distribution of the surrounding material. I.e. The slot size should be smaller than D_1 (Basson, 2005).

d) Use 304 stainless steel for fresh water, and 316 stainless steel for salt water.

2.4.7 Filter Design

2.4.7.1 Introduction

Filter design is usually required when there is a need to introduce a transition between a layer of course material and a layer of finer particles. In coastal engineering this situation is most typically encounter in the multiple layers of a breakwater or revetment. The main objective of this type of design is to ensure that all material (layers) remain intact. This transition is usually achieved by means of a granular or geotextile filter (CIRIA, CUR, CETMEF, 2007).

The local flow of pore water may pass on fine (subsoil) particles of granular materials through the pores of coarse granular materials or through those of geotextiles. This is termed filter instability and may lead to deterioration of the structure as well as change in the permeability.

The three types of filter instability are noted as follows:

1) **Internal erosion**: the finer particles are conveyed through the voids associated with the coarse particles *within the same layer*. This can only occur with wide-graded materials
2) **Interface instability with granular filters**: if the particles of one base layer are conveyed through the pores between the particles of *another* (usually the overlying) *filter layer*
3) Interface instability with geotextile filters: if the particles of the base layer are conveyed through the pores of a *geotextile filter*.

Geometrically Tight Filters

Geometrically tight (or closed) filter design can be characterised as design which implies that pore (grains) or opening (geotextiles) sizes be made small enough not to allow the fine grains to pass through. Such filters are moderately simple to design and only knowledge of the grain size distributions and the pore or opening size distributions of the filter is required.

Geometrically Open Filters

Geometrically open filter criteria is based on the principle that the hydraulic load must be too small to initiate erosion of the fine material. These criteria, however, require more detailed knowledge of the hydraulic loads on the filters, caused by the water movement along and inside the structure.

Each filter has two functions. The first of these functions is *Filter Stability* which is the prevention of the transport of fine particles. The second functional requirement is *Filter Permeability*. This function ensures that a filter must allow for the transport of water through a material, mainly to prevent excess pore pressures.

2.4.7.2 Internal Erosion of Granular Material

Kenney and Lau (1985): formulated a good criterion for geometrically tight (or closed) filters. This can be found as equation LR13 below:

$$\left[\frac{F_{4D}}{F_D} - 1\right]_{\min} > 1.3 \qquad \text{(Eqn LR13)}$$

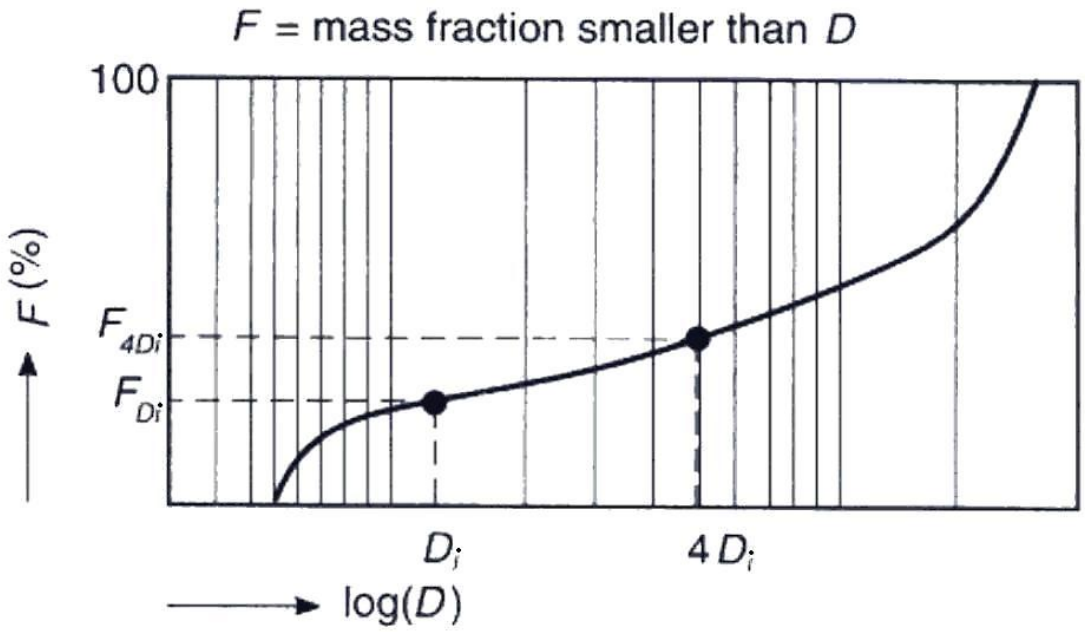

Figure 2:37: Particle size distribution characteristics relevant to internal stability (CIRIA, CUR, CETMEF, 2007)

where F_{4D} and F_D are two (dependent) characteristics (cumulative mass percentage) of the grain size distribution curve can be seen in Figure 2.37. Moving along the curve, values of [F_{4D}/F_D -1] will vary and the minimum value of [F_{4D}/F_D -1] is found at the flattest part of the grain size distribution curve (CIRIA, CUR, CETMEF, 2007).

Pilarczyk (1998) formulated a similar acceptability criterion for the assessment of the internal stability of geometrically tight filters. This criterion is given here as Equation LR14. The value of [D_{60}/D_{10}] is known as the grading width coefficient of uniformity, *Cu* ,of the filter material

$$\frac{D_{60}}{D_{10}} < 10 \qquad \text{(Eqn LR14)}$$

2.4.7.3 Interface Stability of a Granular Filter (CIRIA, CUR, CETMEF, 2007)

The filter stability at the interface of two different granular materials is called interface stability. As is described in Figure 2.38C, the layer with the finer of the two materials is termed the *Base* layer while the coarser layer is termed, *Filter*. (CIRIA, CUR, CETMEF, 2007)

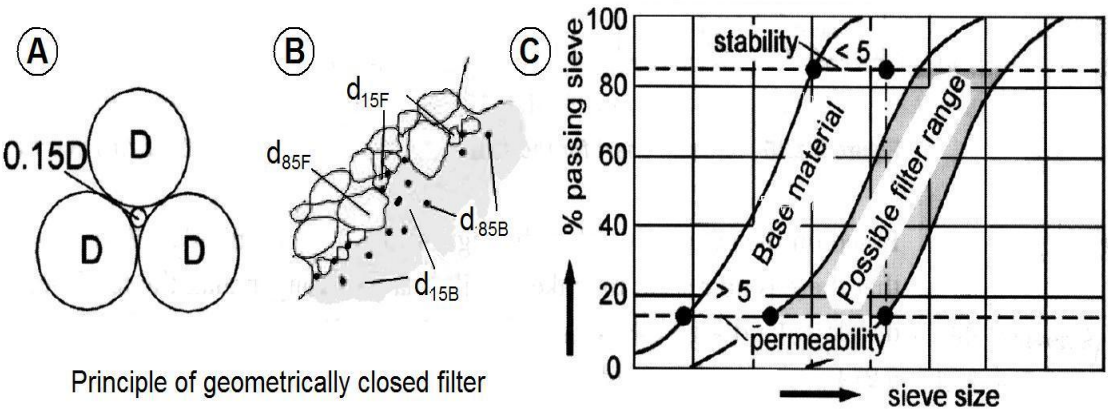

Figure 2.38: Interface stability of granular materials (CIRIA, CUR, CETMEF, 2007)

Geometrically Tight Filters (CIRIA, CUR, CETMEF, 2007)

The geometrically tight (or closed) criterion is best described in the following Equation LR15. This equation can be applied if both materials are rather uniformly graded, i.e. Equation LR15 is found to hold true.

$$\frac{D_{15f}}{D_{85b}} < 5 \qquad \text{(Eqn LR15)}$$

Where the indices "*b*" and "*f*" are used for the base and filter materials respectively and numbers refer to the particle size distribution curve. When the "filter" is a cover layer the base ("*b*") is a secondary armour or filter layer.

Geometrically Open Filters

The use of geometrical tight criteria can be summarised in Figure 2.38, below. Note that i_{cr} refers to i_n and n_b is the porosity of the base material (CIRIA, CUR, CETMEF, 2007).

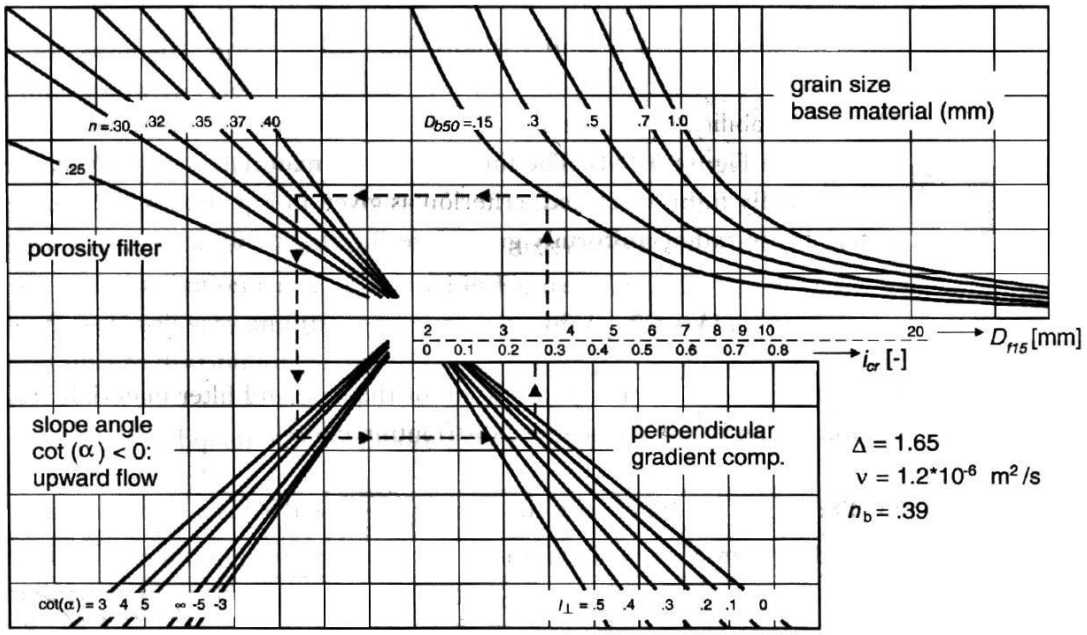

Figure 2.38: Design chart for the interface stability of granular filters (CIRIA, CUR, CETMEF, 2007)

2.4.7.4 Permeability Requirements of a Granular Filter

Water conveyance or drainage is the other major function of a filter. This particular investigation focussed on filters in rock structures. The general permeability requirement for such filters is that the flow resistance is small enough to prevent pore pressures contributing to instability of the structure.

The permeability requirement can be simplified to the expression given by Equation LR16. Figure 2.38 refers.

$$\frac{D_{15f}}{D_{15b}} > 4\ to\ 5 \qquad \text{(Eqn LR16)}$$

This filter criteria corresponds to the requirement that the permeability of the filter layer, k_f, is much larger than that of the base, k_b . In cases of laminar flow, which is for example the case with sand as the base material, see Figure 2.37, the following Equation LR17 applies.

$$\frac{k_f}{k_b} > 16\ to\ 15 \qquad \text{(Eqn LR17)}$$

The permeability criterion given above as Equation LR16 and illustrated in Figure 2.38 is especially secure for all kinds of filters. These include their use in the design of filters for drainage pipes, drinking water wells etc.

This criterion is generally readily achieved with appropriate selection of uniformly graded material for the filter layer(s). Where wide graded material is to be used as a filter, then this criterion can be relaxed. This corresponds to the requirement of $k_f > k_b$.

2.4.7.5 Interface Stability of a Geotextile Filter

The criterion for interface stability of a geotextile filter is predominantly formulated according to the geometrically tight principle. A common criterion can be found in Equation LR18 below:

$$D_{min} \leq O_{90,w} \leq D_I \qquad \text{(Eqn LR18)}$$

Where:

$O_{90,w}$ = Filtration opening size of the geotextile filter : ENISO12956:1999

D_I = Indicative diameter of the soil particles to be filtered, corresponding to the soil skeleton size to be stabilised

D_{min} = is the minimum value of the geotextile opening size corresponding to the largest fine particles being transported in suspension. Giroud et al (1998) estimated this minimum value to be: $D_{min} \approx 50, \mu m$

D_I is defined by Equation LR19 below and is sourced from the standard NF G38061: 1993

$$D_I = CD_{85b} \quad \text{(Eqn LR19)}$$

For a geotextile filter used in coastal or bank protection under a granular layer, this standard provides for a uniform distribution curve of the underlying subsoil. The following values for the coefficient *C*: *C* =0.4 if the soil is in a loose state and *C* = 0.6 if the soil is in a dense state. The coefficient of uniformity C_u is defined by
$C_u = D_{60b} / D_{IOb}$ with $C_u < 5$.

2.4.7.6 Requirements on Permeability of a Geotextile Filter

General permeability requirements for a geotextile filter are the same as those for a granular filter layer. Certain limits pertaining to the ratio of k_f / k_b, with k_f being the permeability of the Filter layer and k_b , the permeability of the Base layer determine the stability of a layer.

The permeability criteria for such layers and hence ratio values, are as follows:

- $k_f \geq 100\ k_b$ for coastal protection structures (Giroud, 1996)
- $k_f \geq 50\ k_b$ for silty soils (BAW, 1993)
- $k_f \geq 10\ k_b$ for hardly silty soils (BAW, 1993)
- $k_f \geq 20\ k_b$ (Lafleur *et al*, 1993).

The values of the factors proposed by Giroud and BAW for silty soils are much higher than the factors "16 to 25". This is due to a considerable reduction of the filter permeability, k_f, during the lifetime of the structure owing to blocking and/or clogging, especially with silty soils. Another reduction of the filter permeability might be accounted to the flow resistance of the combination of geotextile and soil that may differ from the sum of the flow resistances of both materials separately. It is important to take the long-term reduced value of the filter permeability into account and determine its value via an internationally agreed methodology.

Chapter 3

3. REVIEW OF SELECTED SEAWATER INTAKES ALONG THE SOUTH AFRICAN COASTLINE

3.1 Introduction

In order to investigate the practical implementation of intakes along the South African shoreline, it was decided to review some of South Africa's seawater intakes in more detail. Adjacent seawater end-users might have the very same water requirements, but their methodology for seawater abstraction might be highly varied. This approach to investigating seawater intakes would then bring to light any indigenously designed systems, their particular problems and the associated solutions.

3.2 Hermanus: Mariculture

3.2.1 Introduction

The coastal town of Hermanus is situated in the Western Cape (Figure 3.1) and it best known for its whale sightings. One of the main industries apart from tourism is fishing and mariculture. Abagold which farms abalone is the company operating one of the larger mariculture farms/companies in the country.

Hence their seawater intake was investigated. The various components of the seawater system are the seawater intake, filtration, the flow of seawater for operation of a hatchery, rearing of abalone, and finally the treatment and disposal of wastewater. At Abagold, the seawater intake flowrate is approximately 3000m^3per hour (De Wit, 2008)

Figure 3.1: Clock wise from top left, Western Province SA, Hermanus with a breakwater protruding north east from the new harbour, Abagold seawater intake, situated south west of the breakwater. Note the 2 pump houses can be clearly seen as white rectangles at the end of the intake. (Adapted from Google Earth, 2008)

3.2.2 Description

Water requirements vary as per the life cycle of the abalone. All abstracted seawater is first screened via a 1mm screen (De Wit, 2008). The seawater is then further screened and distributed as required. One requirement of the sea water intake is to deliver water that is suitable to be used on 1mm screens, i.e. particles in the incoming water should be small enough that the 1mm screens do not clog (De Wit, 2008).

Abagolds' seawater intake is situated at the end of a natural gully. The gully has however been augmented over time, in order to secure a more reliable source. Figure 3.2 below shows a schematic section of the intake.

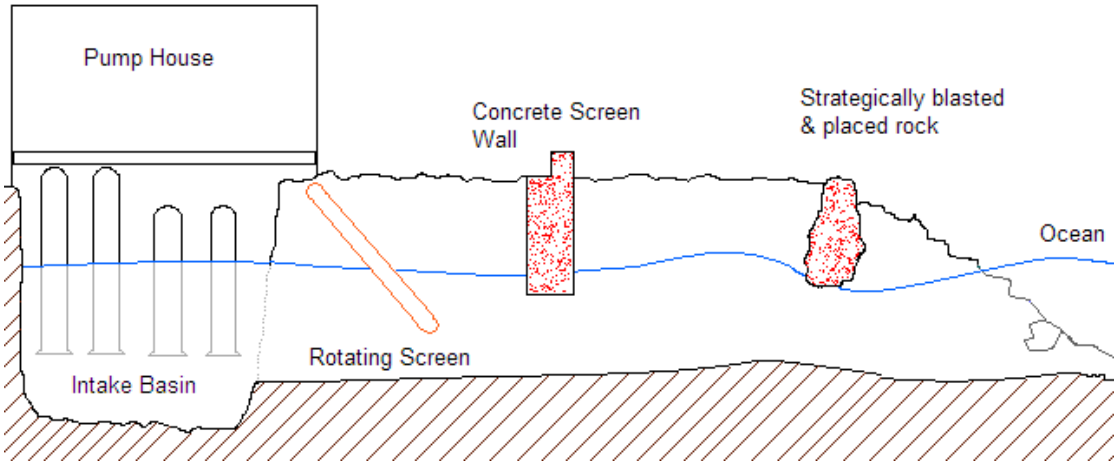

Figure 3.2: Schematic section of Abagold seawater intake

Waves enter the intake via Walker Bay. Here the shallow seabed allows for only small broken waves to enter the intake. Water passes under a placed (blasted) rock, under a concrete screen-wall, through a rotating screen and into the intake basin.

Figure 3.3: Looking seawards, the back end of the rotating screen can be seen in the fore ground and the concrete screen wall in the rear

One of the early modifications in the history of Abagold's seawater intake gully, was the construction of a concrete screen, Figure 3.3. This was for two purposes. The first was to channel the water through a rotating screen. The second purpose was to help remove the air entrained in the water. This method proved to be moderately helpful (De Wit, 2008).

The intake at the sea end was enlarged to increase the gully width. Here a rock was strategically blasted into place at the entrance. The purpose of this was to force the flow of seawater down and under the rock. Hence the rock would dampen the wave action and reduce the amount of white water entering the intake. As can be seen in Figure 3.4, this has not worked very well.

Figure 3.4: Strategically blasted rock placed at the entrance of the intake gulley

Due to the amount of air still contained in the water, it was decided to construct another, concrete wall at this widened entrance, hence reinforcing bars were epoxied into the drilled holes, Figure 3.4. The wall would then allow for an extension of the intake and for the use of additional screens.

After the widening of the entrance channel, the intake basin was then enlarged as additional intake pipes were commissioned. As can be seen in Figure 3.5, the initial two intakes can be seen in the lower center. Thereafter new twin intakes, slightly higher up, were added. Thereafter the remaining pipes were added for usage by an adjacent sea farm. It is also evident that air is still entrained the water.

Although the channel has been widened, the amount of water entering the basin is still equal to the amount being extracted. The flow of water into the Intake basin is determined by the contraction of the channel at the rotating screen. Due to the flow cross section being restricted at the concrete screen wall and the rock in the entrance channel, the flow velocity in the gulley is quite high at these locations. Hence this does not allow for air to be removed before entering the Intake basin. This problem is most acute at low tide when the negative head, that is required to be overcome by the pumps, is at its highest. The entrainment of air in the water serves to further worsen conditions, as the entrained air aids cavitation at the pumps' impellors.

Figure 3.5: Abagold's Seawater Intake Basin

In conclusion, this seawater intake demonstrates that air entrainment can have a significant influence in such a seawater intake system.

3.3 Sea Fisheries Aquarium: Research

3.3.1 Introduction

The Sea Fisheries Aquarium (SFA) is a research facility which falls under Marine and Coastal Management (MCM) which is component of the Department of Environmental Affairs (DEA). The aquarium is situated in Sea Point; Cape Town The core function of this aquarium is the research of sea life along the South African Coast. This information is used in managing our coastal resources and the interaction between the marine, land and human activity.

The various components with respect to seawater usage, varies from seawater abstraction, filtering, the operation of a hatchery, the rearing of marine life, and finally the disposal of wastewater.

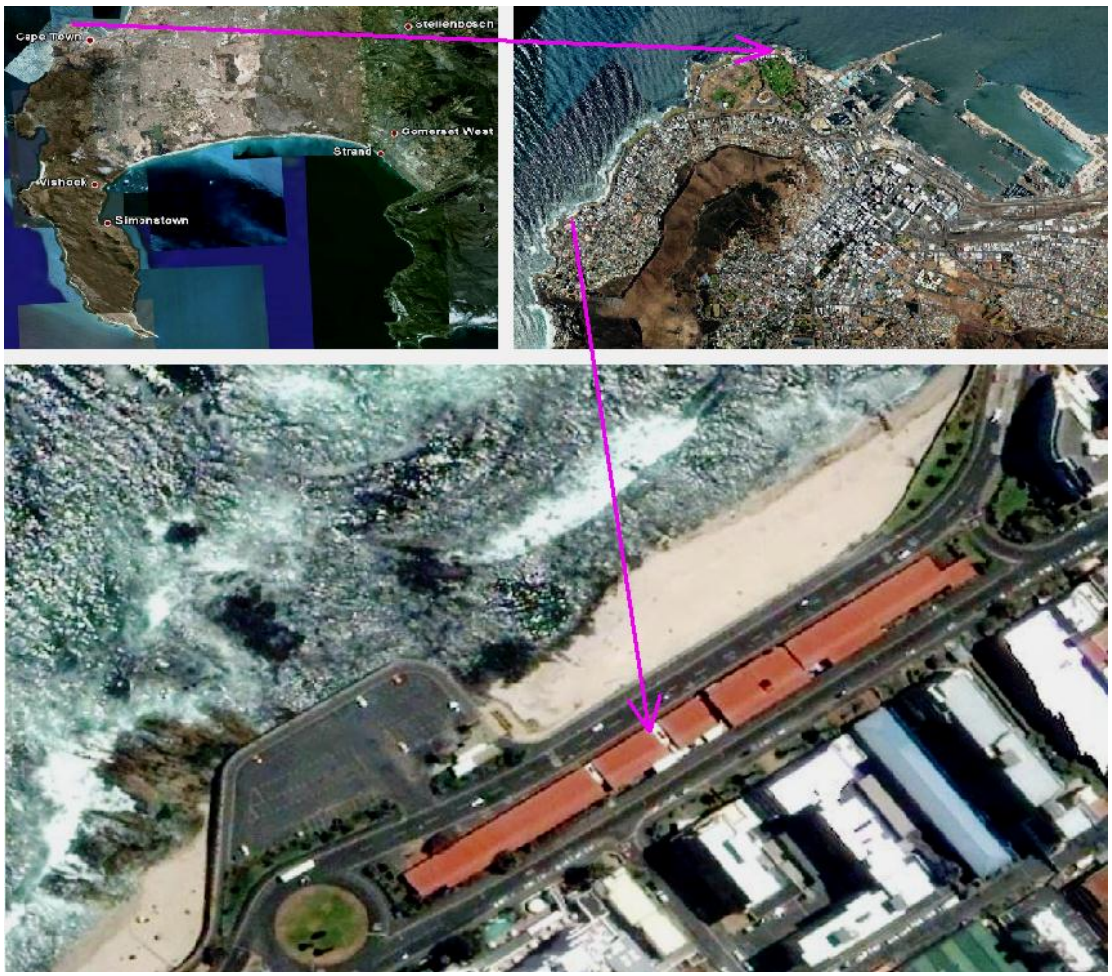

Figure 3.6: Clockwise from top left, Cape Peninsula, Cape Town with a breakwater protruding north east from the harbour, Sea Fisheries Aquarium can be seen as the long red roofed structure at Seapoint, southwest from the breakwater (Adapted from Google Earth, 2008

3.2.2 Description

The majority of coastline along the Cape Town Atlantic seaboard is rocky. This nutrient rich coastline is fed by the cold Benguela current. These are the conditions that exist at the seawater intake for SFA. The inlet for the intake is situated on a rocky shore with kelp beds in close proximity.

The intake to the facility is implemented via two ±ø1m diameter pipes (Busby, 2008). These pipes are connected to intake manifolds which are pipes with holes cut into them. The holes start at a larger diameter towards the seaward end and reduce as they move landwards (Busby, 2008). This is done in an attempt to equal the amounts of water fed into the pipe. The holes are cut out the bottom of the pipe, so as to reduce air entrainment.

The pipe manifolds are situated in fairly shallow water. There is approximately 400mm cover during low tide and the intake is visible during very low spring tides (Busby, 2008). The manifolds are situated on a concrete plinth and have a metal cage to act as a screen against ingress of marine life. The mesh openings are 50mm squares which keeps the majority of pelagic life out. The water quality is highly seasonal, with the nutrient loading being far higher in summer than in winter (Busby, 2008).

Twice a year during the spring low tides, the intake manifolds are usually replaced as part of routine maintenance. The old screens set is removed and refurbished and another set put is in its place. The most significant impact is the accretion of marine growth along the intake manifold. Upon closer examination of the screening cage which surrounds the intake manifold. The cage is found to be teeming with marine growth. Crayfish can be seen to hang perched to the underside of the manifold. This appears to be a good breeding area as the passing water provides ample nutrients to the resident sea life (Busby, 2008).

In conclusion, this seawater intake draws into significance the impact that pelagic marine growth can have on an intake system. In areas of high marine growth this factor cannot be ignored as it can reduce the capacity of the intake to a fraction of its initial design values as seen in the case of SFA.

3.4 Two Oceans Aquarium : Research/Public Education

3.4.1 Introduction

The Two Oceans Aquarium (TOA) which is situated at Cape Town's V&A Waterfront, is a public unit which seeks to inform and educate the general public about marine life. Although research is conducted on a smaller scale, it contributes largely to marine conservation and awareness (Templar, 2008).

The various components which utilise seawater include abstraction, filtration, circulation, treatment and disposal of wastewater. The water requirements at TOA differ dramatically, Hence the pretreatment of water is a necessity, as opposed to mere filtration. Harbour contaminants further justify the need for pretreatment.

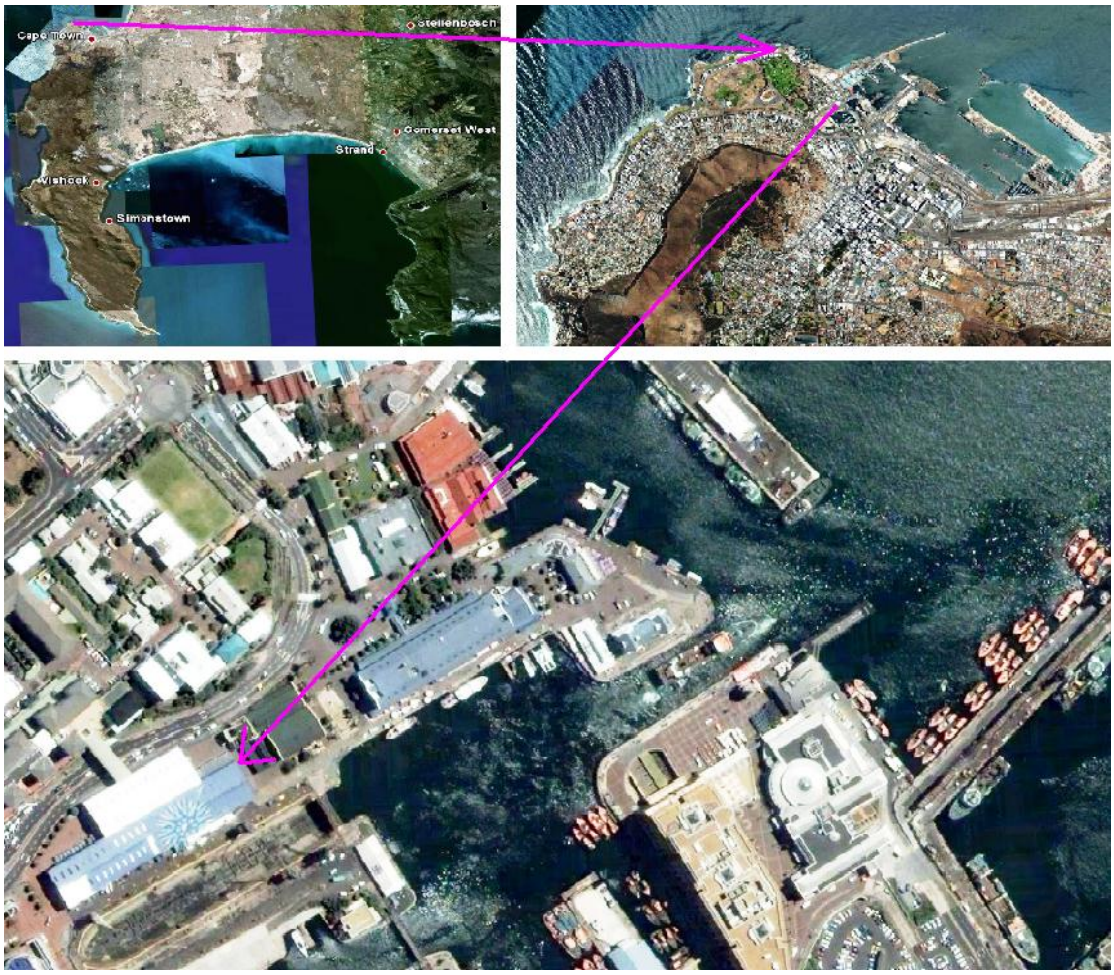

Figure 3.7: Clockwise from top left, Cape Peninsula, Cape Town harbour, V&A Waterfront showing the Two Oceans Aquarium (Adapted from Google Earth, 2008)

3.4.2 Description

The seawater abstraction point for the TOA is situated within Cape Town's harbour. Although the intake is not contained within a surf zone and not subjected to wave influence, it is still susceptible to chemical and biological attack.

Water is abstracted using submersible well pumps as the water is considered to be free of sand particles, Figure 3.9. A perforated High Density Poly Ethylene (HDPE) screen is used as a precaution (Templar, 2008).

Figure 3.8: The intake for the Two Oceans Aquarium. The intake is situated opposite the canal from the Nelson Mandela Museum.

When the aquarium was first commissioned, a slotted Poly Vinyl Chloride (PVC) screen was used, Figure 3.9, however this screen proved infective due to marine growth and a second specially manufactured screen was used. This screen was constructed of stacked PVC pipe which used Nylon mesh to filter any large particles, Figure 3.10. This nylon mesh has a larger diagonal which measure 30mm across.

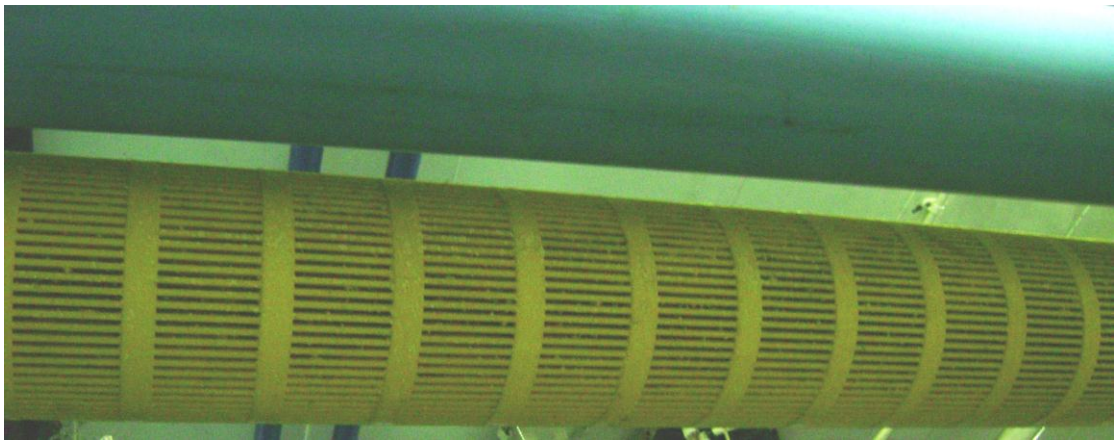

Figure 3.9: The first intake pipe for the Two Oceans Aquarium, a ø250mm slotted PVC screen

Figure 3.10: The second intake for the Two Oceans Aquarium, a ø250mm specially manufactured PVC pipe utilising Nylon mesh

After an initial period, the capacity of the pumps had reduced significantly. The intake pipes were then inspected. Upon the inspection and retrieval of the screens it was found that entire colonies of sea cucumbers had taken up residence inside the screens. This occurred for both PVC pipe screens (Templar, 2008).

When such screens are designed, the velocities through the screens are kept at a minimum in order to minimize the loss of pressure. The sea cucumbers entered the screen whilst smaller than 1mm and had grown to significant sizes. The low velocities provided opportune locations for sea cumbers as they could anchor easily and make use of the passing water which is high in nutrients (Templar, 2008).

The growth of marine life within intake pipework cannot be completely prevented but managed. By using antifouling paints and mechanical pigging of the line, marine growth can be kept to a minimum Barnacles are the most predominant form of marine life and as such can be seen colonising the TOA intake pipework, Figure 3.11.

Figure 3.11: TOA - ø75mm intake pipeline and colony of Barnacles.

As part of regular maintenance, the pipe lines are cleared via a rotor router. This device uses pressure to rotate and drive a metal head forward within a pipeline. This router then removes all marine life by coring it out. This system has proved to work effectively for the Two Oceans Aquarium with coring of the intake pipeline required every four months. The intake screens for the seawater Intake, function adequately and are only replace one a year (Templar, 2008).

3.5 Sea World Aquarium: Research/Public Education

3.5.1 Introduction

Ushaka Marine World (UMW) is located at the Point, Durban, KwaZulu Natal. The center facilitates the Sea World aquarium (SWA), dolphinarium, and recreational areas. The various SWA operations with respect to seawater usage includes seawater abstraction, filtration, circulation, care control and rearing of marine life, operation of hatcheries, operations within a dolphinarium and finally the treatment and disposal of wastewater.

The SWA intake is unique as it is a sub-bottom abstraction system. Some of the problems encountered by the intake system over its initial two year period of operation are documented later in this chapter (CBI, 2007).

The intake for UMW is a well point system situated in Vetches Bay beneath the jetty, Figure 3.12. The well point system, Figure 3.13 is split into two halves, a North and South suction leg. The well point system consists of sixty individual submersible pumps which are fixed to the purpose built jetty piles. Only the pumps are attached to the jetty piles, the connecting pipework is embedded in the sand.

Figure 3.12: Construction of Jetty at Ushaka Marine World with the extra amount of purposed built jetty piles being constructed at the head of the Jetty.

The well points are in-between 0.5m to 3m apart and extend to a depth of 6m below the seabed. The lower 3m of the wells, contain the submersible pumps which draw in the seawater. Hence the layer of soil through which the seawater needs to pass is always more than 3m.

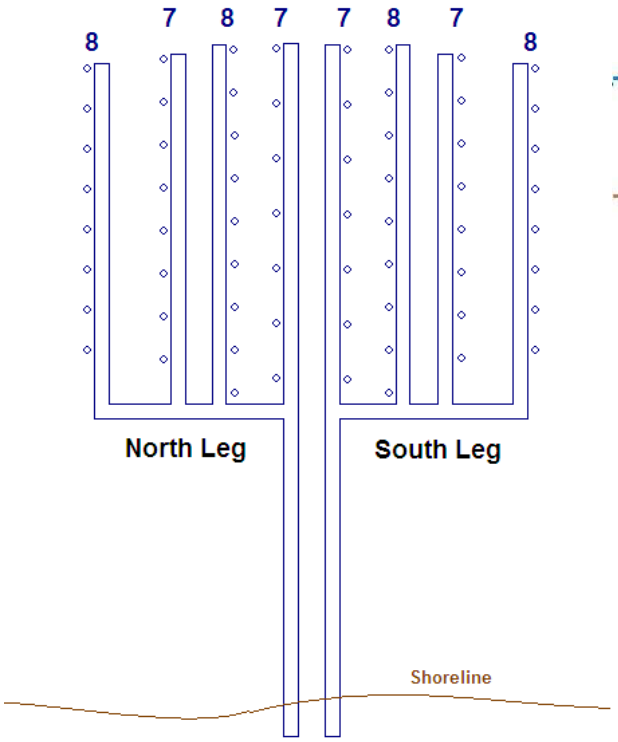

Figure 3.13: Layout of Well points with North and South Suction Legs

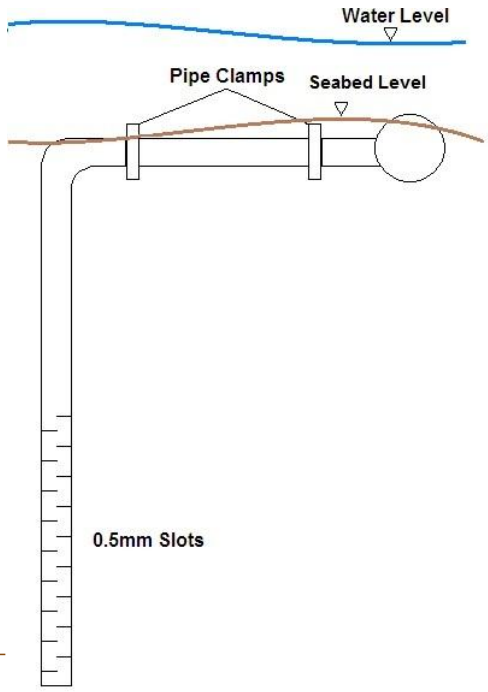

Figure 3.14: Well Point Downpipe

The well points are connected to the Suction legs via a bellows system of flexible hoses and steel clamps. However sixteen wells now use a flanged system of connection.

The system runs on a flow rate of 0.65Ml/hour. There are two Gormann Rupp pumps which provide the suction head. The system can be spilt with only one of the suction arms working during times of low demand.

The problems experienced at SWA can be split into two categories: Hydraulic and Biological. The hydraulic part encompasses the problems experienced by the pumps, pipeline and screens while the major part of Biological problems are due to the processes involved with benthic marine life.

3.5.2 Hydraulic Problems

3.5.2.1 Pumps and Cavitation

The pumps work on maintaining a suction pressure of 40kPa. With the rise and fall of the sea level, the pumps were changed over to a variable speed system in order to maintain this pressure. This system was installed and thereafter it was found that pumps would cavitate during periods of low tide. The increased rate of cavitation led to impellers having to be replaced every three to six months.

3.5.2.2 Connection system

The well points are connected via a system of flexible hoses and steel clamps. However this has not proven effective and has led to air entrainment. Hence sixteen wells now use a flanged system of connection.

3.5.2.3 Air entrainment and super saturation

It was found that a large barrage of bubbles was being sucked up from the well points and introducing air into the system. These bubbles then cause the pumps to cavitate or force air into the saturation. This in turn causes the super saturation of nitrogen. If leaking, joints, clamps and joint movements are eliminated this would reduce the amount of air taken in.

It was found that high negative pressures suck the gases out of solution. This occurs, when two wells are in close proximity with each other and have areas of overlapping pressure. These localized areas cause the formation of bubbles in the well point pipework. This is supported by the following events. Prior to rebedding of the well points, the negative pressure needed to deliver 0.65Ml/hr. during the high tide period was 70kPa. However, after rebedding this dropped to 40kPa for a similar high tide period (CBI, 2007).

3.5.3 Biological Problems

3.5.3.1 Iron Build-up

Over a two year period, there have been two incidents of high Iron Oxide precipitate coming through the seawater intake. This is due to high dissolved iron concentrations, in the incoming water, passing through an anoxic zone in the sand bed. Here the iron is reduced and made soluble. Thereafter the seawater passes through an area of higher oxygen, relative to the sand bed, and this causes the iron hydroxide to precipitate out. The main serious outcome of this is that iron promotes the growth of algae. Any uncontrollable algal growth can be detrimental to the water quality of sensitive systems like those of aquariums (CBI, 2007).

3.5.3.2 Ammonia

In October 2005 there was apprehension over the levels of ammonia entering the intake as higher than normal levels of ammonia had been measured in the surf. Tests conducted on the incoming seawater revealed that the level of ammonia was on average 36% more than that found in the surf (CBI, 2007).

The most likely explanation for this is attributed to the biological process within the sand bed. Here water is sucked into the intake past the seabed. Through bacterial decomposition of particulate matter, the nutrients are converted to ammonia. The main process being that the bacteria feed upon the nutrients and excrete predominantly ammonia (CBI, 2007).

3.5.3.3 Low Oxygen

Water entering the well points has an oxygen concentration of 40 to 60%. This is low in comparison to the surround surf which had an oxygen concentration of 95%. When rebedding occurs i.e., the sand is lifted using air and water pumped into the sand strata and the sand density is decreased, this problem is alleviated to a degree, as is noted by Oxygen levels then climbing to 70-75%. Low oxygen concentration is part of a larger biological problem which is discussed in detail, in the next point (CBI, 2007).

3.5.3.4 Anaerobic activity in Sand

During rebedding, anoxic staining was found on the bottom of most well points. This indicated that water did not flow equally into the well point. Instead, most of the water entered via the upper half. This action implies that water containing oxygen did not pass through the lower layer. Hence the growth of aerobic bacteria was stunted in this region. The little flow that permeated through the anoxic zone is oxygen free as all the oxygen would have been used up by bacteria in the upper zone (CBI, 2007).

Therefore it is possible for ammoniated water to reach the anoxic zone and be converted further. Through denitrification, the anoxic zone produces Nitrogen (N_2), Nitric Oxide (NO), or Nitrous Oxide (N_2O), Figure 3.15. Oxygen is known to suppress the enzymes that are responsible for denitrification. Therefore as the concentration of oxygen is lowered, the production of nitrogen gases intensifies (CBI, 2007).

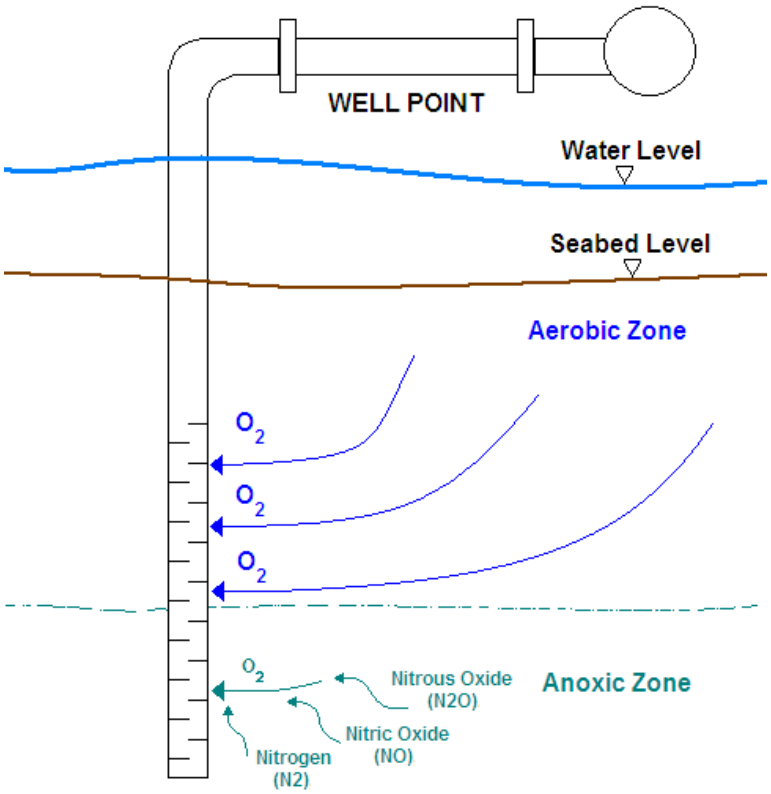

Figure 3.15: Well points showing Aerobic and Anoxic Zones

When designing a sub-bottom abstraction system, it is clear that, physical, chemical and biological processes have to be considered. In the UMW case it shows that Biological and Chemical have a large impact on the design of sub-bottom seawater abstraction.

3.6 Paternoster : Mariculture

3.6.1 Introduction

Paternoster Oyster Co. (Pty) Ltd is situated 2km north of the residential holiday area of Paternoster. It is a commercial unit that farms Oysters. The operation lies in a naturally low lying area. It is approximately 150m from the Atlantic Ocean. The farm consists of 8 fairly large ponds that are approximately 7 hectares (ha) in total (Smith, 2008).

Regarding the seawater usage, water is used on a 'once through' basis. Some of the water flows first through the nursery and on to the other pond. The majority flows directly into the ponds and out back to sea. A substantial portion of the flow is lost to seepage and evaporation. One clear difference between this type of mariculture and others is that the oysters are filter feeders. The feeder food for this operation is algae as opposed to seaweed or kelp which was the feeder food for abalone farming.

Figure 3.16: Paternoster Oyster mariculture farm with the shoreline to the west and the Oyster ponds clearly visible (Adapted from Google Earth, 2008)

3.6.2 Description

3.6.2.1 Current system

Seawater for the farm is abstracted from a sandy beach west of the operations, Figure 3.16. The current system abstracts water from the surf zone using a pumping system and subsoil perforated intake pipes. This water is abstracted at a depth of -5m MSL. The sand is course grained with the beach profile being dynamic.

The abstracted seawater has been described as being very clear with no turbidity or undesirables (Smith, 2008). Hence there is no pre-treatment of the water, even for nursery purposes. The current system uses ø110mm subsoil intake pipes to abstract the water from the adjoining soil. This is then feed into the ø 200mm, collector lines via an ø50mm HDPE connecter pipe. See Figures 3.17and 3.18 below

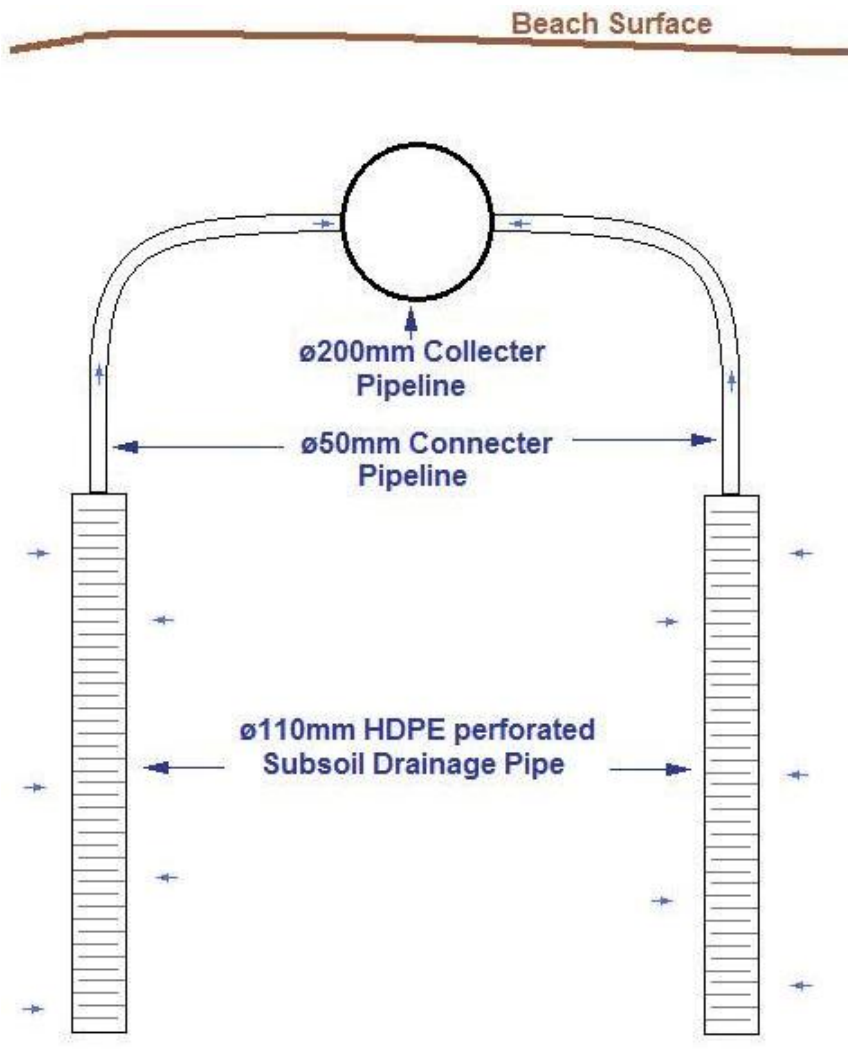

Figure 3.17: Paternoster Oyster: Sectional Elevation - 2No. Beach Well Subsoil intake units

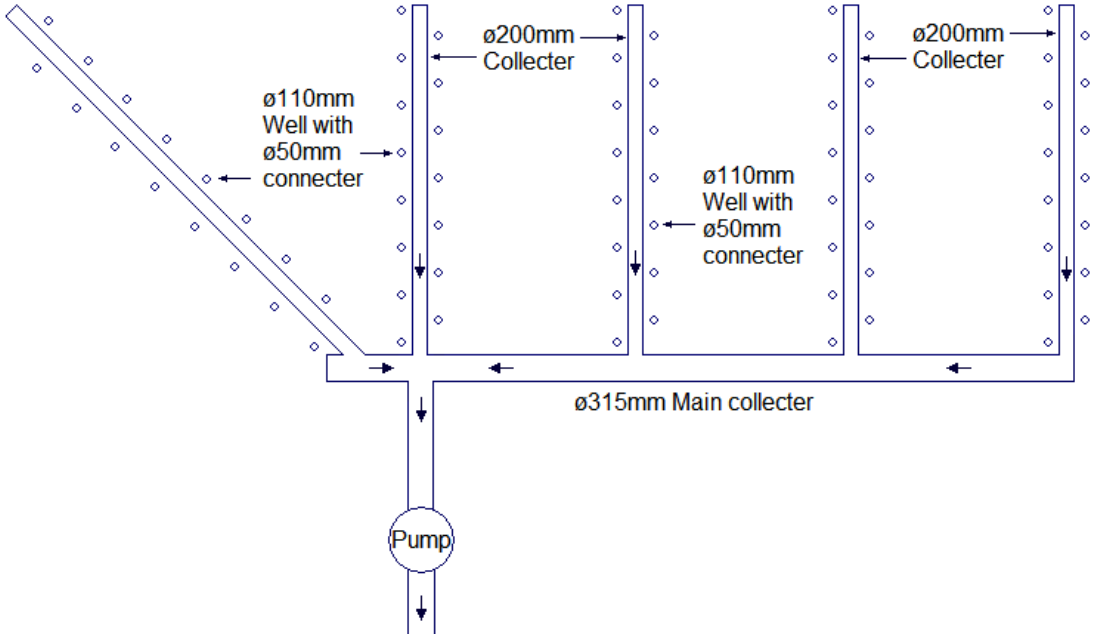

Figure 3.18: Paternoster Oyster: Layout of Beach Well abstraction infrastructure

3.6.2.2 New System

The current system provides 200m^3/hour however due to evaporation, this amount is below the amount of 350m^3/hour, required to farm the entire 7ha of ponds. Hence the owner has configured a new supplementary system using the same concept. The new wells are made from a perforated drain. These components are derived from a commercial French intake outlet Figure 3.20. The -perforated pipe is housed in a geo-fabric in order to filter the incoming seawater, Figure 3.19 (Smith, 2008).

3.19: New Beach Well. Stitched geofabric covering the perforated intake pipe

3.20: New Beach Well. Inside of the specially constructed perforated intake pipe

The owner has had very good results from this system. With the connecting pipe work being upgraded from a 50mm to a 110mm pipe, the flow estimated from one of the units is 20l/s (72m^3/hour). Installation of 5 beach wells would augment the supply to the 350m^3 needed per hour. This is the flow rate required to operate all 7ha of the operation (Smith, 2008).

3.6.2.3 Installation method of the New System

The beach wells are ø900mm. There are no conventional commercial methods available in order to install the wells; thus the owner has devised his own system (Smith, 2008). This method is simple. As shown in Figure 3.21 a round metal sleeve that can accommodate the perforated intake pipe, is required. This should be large enough to generously accommodate the beach well and “drilling” equipment (Smith, 2008).

The ‘drilling’ equipment which is a set of pipes / jets, Figure 3.22, is placed within the metal sleeve. These pipes deliver water and air. By method of airlifting and suspension, the material at the bottom of the metal sleeve is displaced and flows out over the metal sleeve. This allows the sleeve to be driven into the sand with minimum force. Figure 3.23 shows a metal sleeve that has already been driven in to the soil (Smith, 2008).

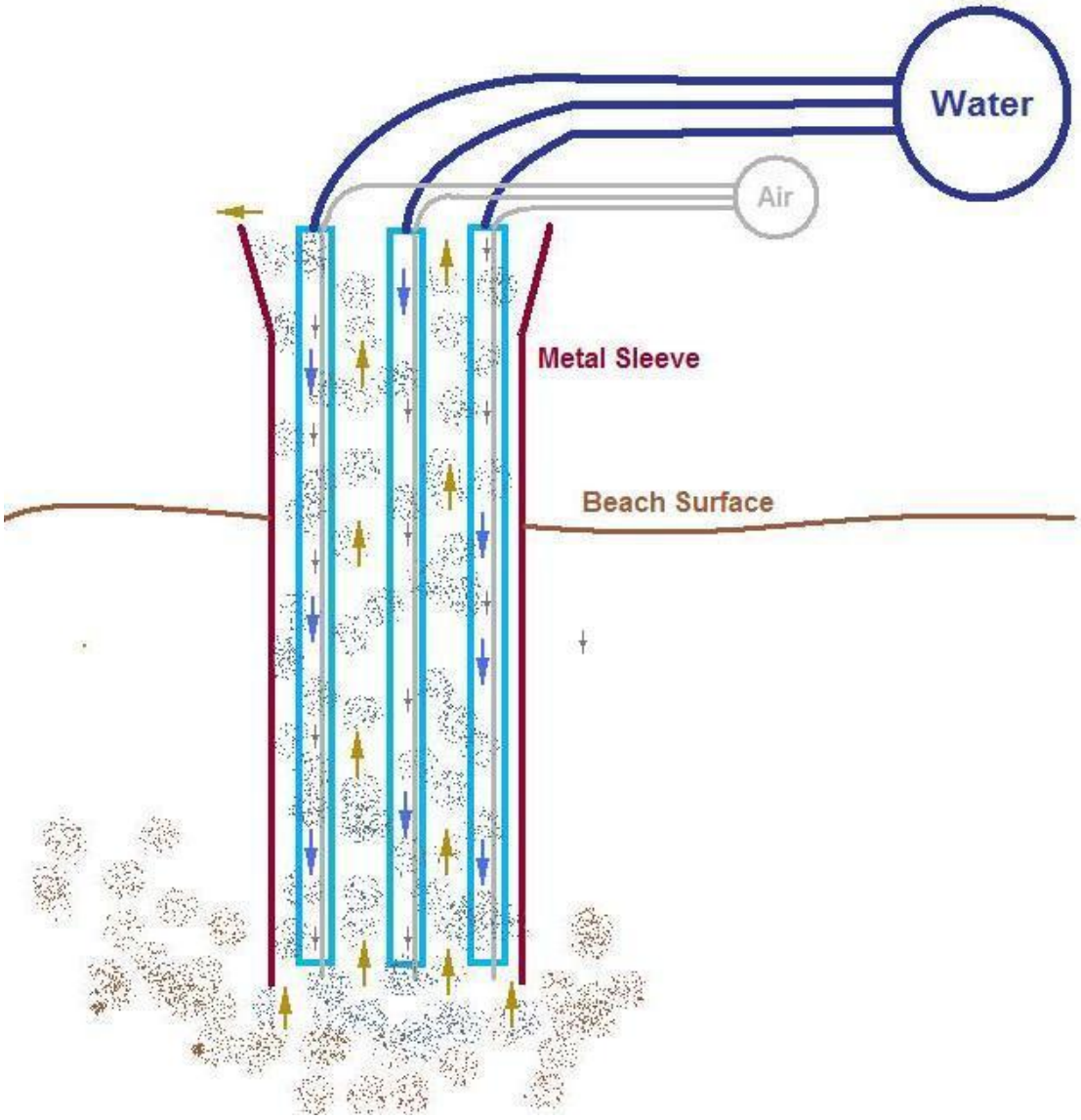

Figure 3.21: The method by which air and sand displaces sand allows the metal sleeve to settle

Figure 3.22: The set of pipes/jets used to displace sand

Figure 3.23: The metal sleeve with a bell end that has already been driven in to the sand

After the well is installed, the metal sleeve is removed with a Tractor-Loader-Backhoe (TLB). The connecting pipe is then buried during low tide periods (Smith, 2008).

3.7 Britannia Bay : Mariculture

3.7.1 Introduction

Britannia Bay is situated on the West Coast in the Western Cape SA. A large majority of the area is residential, with West Coast Abalone (WCA) being the only type of mariculture in the immediate vicinity. West Coast Abalone's main concern is the farming of Abalone on a commercial scale. Seawater is abstracted at a rate of 2500m^3 per hour. Various operations are conducted on seawater viz, seawater abstraction, filtering, operation of a hatchery, rearing of abalone, and treatment and disposal of wastewater (Whyte, 2008).

Figure 3.24: Clock wise from top left, Western Province SA, Britannia Bay, West coast Abalone seawater intake pump house can be seen as a rectangle in the top left portion of the image. Note the abalone production facilities can be seen in the bottom right (Adapted from Google Earth, 2008)

3.7.2 Description

As the abalone goes through entire life cycle at WCA, the water has to be treated specifically as per the phase of the abalones life cycle. At WCA, bulk water is abstracted and screens are used as per the water requirement.

The seawater intake for WCA is situated on a rocky coastline. The intake pipes are situated in a modified natural gulley, Figure 3.25. Water enters the gulley via a side entrance. Here, the initial filtering is done via a course grated screen 50mm square holes. Thereafter the water passes through a grated metal screens which contain the Intake Pipelines. The mesh holes are diamond in shape with the smaller diagonal being 20mm in opening length (Whyte, 2008).

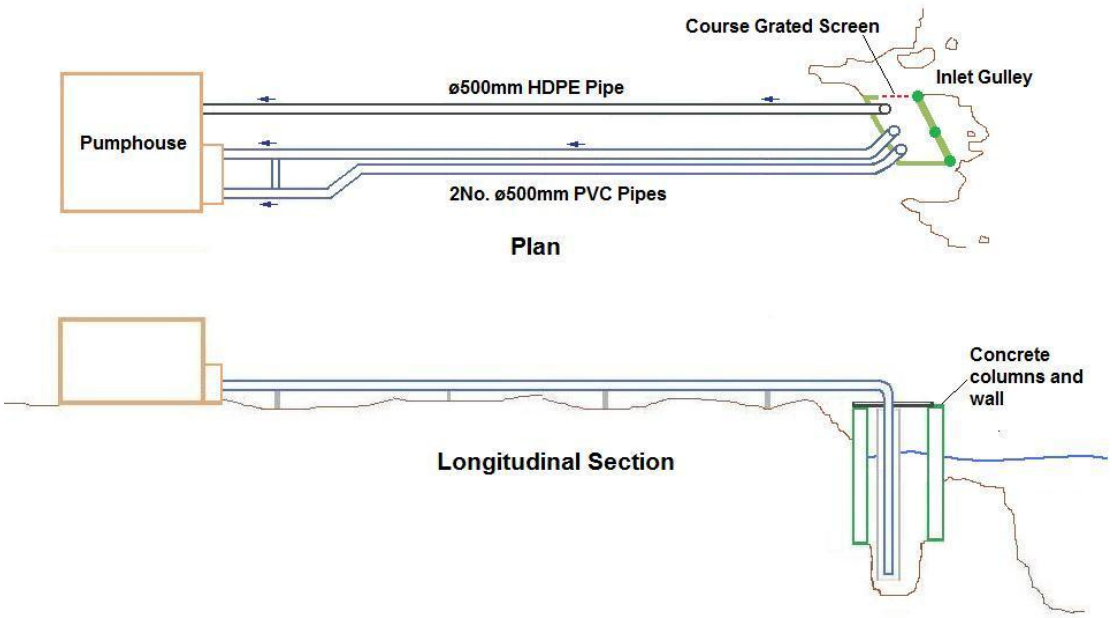

Figure 3.25: Schematic section of West Coast Abalones Seawater Intake

The intake pipes which are ø500mm comprised a single HDPE pipe and two modified Poly Vinyl Chlorine (mPVC) pipelines. There are two pumps situated within the pump house. Each pump is dedicated to a particular line type. A smaller centrifugal pump abstracts seawater via the HDPE line, while a large Slurry pump services the two mPVC pipelines (Whyte, 2008).

3.7.2.1 Pumping Operation

At present, each pump supplies approximately 90l/s (324m^3/hour). The difference between the pumps, at 2m MSL, and the free water surface of the ocean, induces a negative pressure of between 0.1 to 0.3 bars. These conditions are barely acceptable as negative suction heads add complications (Whyte, 2008).

One of the first requirements of such a system is that the incoming pipelines are primed before pumping can occur. For pumping to occur the pipe has to be filled with water and a negative pressure has to be induced into the pipeline, thus creating a suction of the seawater. Priming of a pipe is a long complicated operation that is resource and time consuming. Hence any break in operation sees priming occur each time before the system can run again. This is highly undesirable.

Another problem due to negative suction head is cavitation. On low suctions head cavitation does not occur, however when the negative pressures become too large, air is pulled of saturation and the implosion of these air bubbles cause miniature explosions that destroy the adjoining material. The entrainment of air in the water at lower pressures will increase the likelihood for cavitation as well.

This problem has existed at WCA for the past few years. Previously all units were smaller centrifugal pumps, Figure 3.26. These pumps were high revving pumps which exacerbated the cavitation problem. Due to the pumps casings being constructed of cast iron and the impeller being constructed of steel, the pumps did not last very long. A change of impellers was required every few months (Whyte, 2008).

This problem was solved with the installation of a slurry pump Figure 3.27. This pump is larger and has a stainless steel impeller. The pump is lower revving, which aids in keeping cavitation events to a minimum (Whyte, 2008).

3.7.2.2 Intake Arrangement

Three major problems were experienced at the Intake, Figure 3.27. These were:

- Too little water entering the stilling basin.
- Too much white water entering the stilling basin
- Too much seaweed entering/obscuring the stilling basin

Figure 3.26: Centrifugal pumps, at Intake for West Coast Abalone

Figure 3.27: Slurry pumps, at Intake for West Coast Abalone

The side entrance into the stilling basin is only 1m across with the depth varying in between 0.5m to 2m, excluding wave action (Whyte, 2008). This creates an area of ±2m^2 for water to flow through into the stilling basin. However when the physical grate, which covers the opening is considered, the area for water to flow into the stilling basin is fairly small. Hence the water level in the stilling basis drops and this in turn creates additional strain on the pumps (Whyte, 2008).

As this intake sits in the surf zone, white water is expected. However due to wave action and the surrounding rock, additional white water enters the stilling basin. This white water then enters the intake pipelines and aids in the cavitation of pumps (Whyte, 2008).

Due to the nutrient rich waters off the west coast, flora is prominent along the coastline. In particular, seaweed and sea grass can be found in abundance. However this causes varies problems when attempting to abstract water from the sea. In this particular case, seaweed tends to block up the entrance of the stilling basin and reduces the flow of seawater into the basin (Whyte, 2008). Seaweed that enters the stilling basin is found wrapped around the intake and due to the constant suction force, is never dislodged (Whyte, 2008). Hence maintenance intervals, for the intake, have been reduced to once a week (Whyte, 2008).

Figure 3.28: Intake for West Coast Abalone

3.8 St Helena Bay: Mariculture

3.8.1 Introduction

St Helena Bay is situated on the small east coast of a peninsula that is on the west coast of South Africa, Figure 3.29. One of the main industries is commercial fishing with commercial fishing company: I&J utilising varies facilities along the coast.

St Helena Abalone is the only abalone farm in the St Helena the area. This company has been in existent for approximately 10 years and is unique as it is one of the few, in the country, that work on a recirculation system (Denis, 2008).

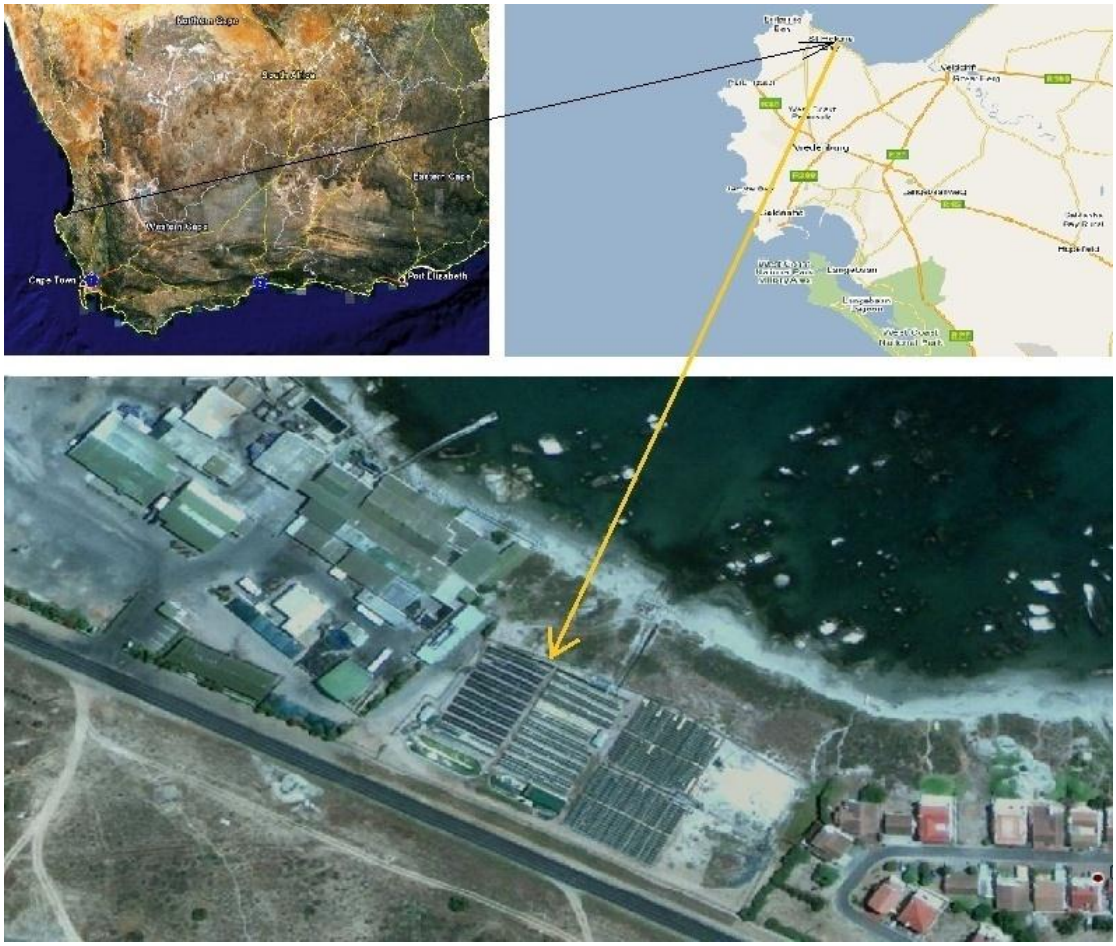

Figure 3.29: Clock wise from top left, Western Province SA, The western peninsula. St Helena Abalone is situated south east of harbour (Adapted from Google Earth, 2008)

3.8.2 Description

Water is abstracted from the adjoining bay via two ø300mm HDPE pipelines, Figure 3.30. These pipes are semi buoyant and lie just below the surface. Their positions are controlled by two drums. The first drum is located at the beginning of the pipelines and the other is at the half way point. These drums are partially filled with water and anchored to concrete blocks. The drums ensure that the pipeline stays off the seafloor and just below the water surface, Figure 3.31 (Denis, 2008).

Due to its geographic location, storms do not affect the pipeline as the wave climate is very docile all year round (Denis, 2008).

Figure 3.30: The intake pipelines for St Helena Abalone, 2No. ø300mm HDPE pipelines

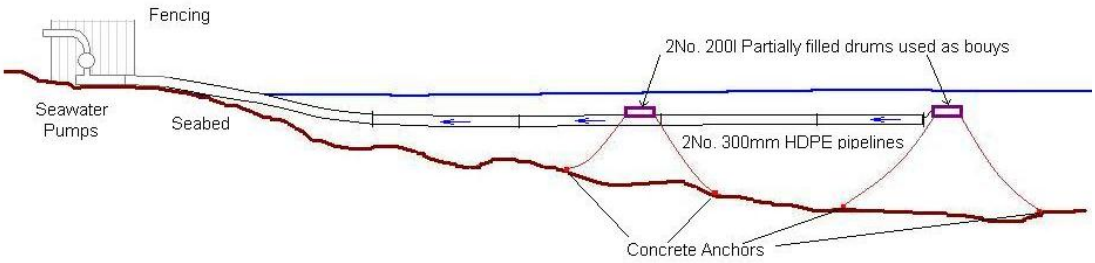

Figure 3.31: Schematic section of St Helena Abalone Seawater Intake (Denis, 2008).

3.8.2.1 Pumping Operation

Each ø300mm HDPE intake pipeline has a single centrifugal pump. A third and fourth pump were installed as backup pumps. All pumps deliver 45l/s (162m^3/hour) into a common manifold which is then pumped into the reticulation system, Figure 3.32. There is a small difference in between the level of the pumps, at 0.7m MSL and the free water surface of the ocean. Hence this induces a very small negative pressure in the intake pipelines which is acceptable for operation of this intake system.

Figure 3.32: The pumping infrastructure for St Helena Abalone

3.8.2.2 Problems Experienced

The first problem is due to the nutrient rich waters and the abundance of flora. In particular, seaweed and sea grass can be found in profusion. These two types of flora can cause various problems. In particular, the seaweed tends to block up the intake pipe openings (100mm square) and reduce the flow through of water. Due to the constant suction force, the seaweed is never dislodged.

The second problem is the short circuiting of the system or recirculation which is the ingress of discharged waste water into the intake pipelines. This is attributed to the following two circumstances:

1) Due to the inherent position of St Helena Bay, the surf zone is fairly inactive. I.e. the waves and tidal action are small. In addition, any currents in the area can be considered negligible. Hence mixing in the sea area adjacent to St Helena Abalone is very poor.
2) The discharge of waste water is done with minimal effort. Wastewater is discharged via gravity onto rocks that lie above the high water mark, Figure 3.33. Discharged water can be seen as white water, above and to the right of the collar on the HDPE Intake Pipeline. There is no mixing and the denser wastewater enters the sea at low velocities. This wastewater then fills the surrounding area until the end of the plume reaches the head of the intake pipeline and re-enters the system.

Figure 3.33: Wastewater is discharged on the shore

3.9 Summary of Problems Experienced

As can be seen for the seven seawater intake cases visited, there are numerous configurations to a seawater intake. Unfortunately none of these was a horizontal well a rocky shoreline. The seawater intake at Sea Fisheries Aquarium, Two Oceans Aquarium and Sea World Aquarium have formal designs which were undertaken by Professional Engineers. The remaining four cases do not employ any professional assistance. All design and construction is undertaken by the owner/operator.

It should be noted that the seawater intakes that did not have a formal design, did not fare better or worse than seawater intakes designed by professionals. A particular trend noticed with not formally designed seawater intakes, is that the operator is usually the owner, the designer and the contractor, hence his practical experience helps him converge on solutions timorously.

The seawater intakes are reviewed as per type of intake.

The first type to be discussed is the offshore direct seawater intake where water is gathered from an unrestricted water column. This occurs for the seawater intake at St Helena Abalone, St Helena Bay.

The St Helena Abalone seawater intake draws water from a water column that is offshore. Hence it is always guaranteed unlimited feed water. The seawater intake is not robust. However, the wave climate at St Helena is very docile and hence allows for such an intake to be used. The downside of this situation is that without wave action and the induced turbulence, there is no mixing in the surf zone, hence waste water that is deposited on the shore, sometimes re-enters the system. Therefore when designing a intake system, potentially harmful discharges (brine or waste water) in the vicinity of the proposed seawater intake, should be well documented.

The second type of seawater intake is the onshore direct seawater intake where seawater is gathered from a water column in the surf zone. This occurs for the four seawater intakes at Abagold, Hermanus, Sea Fisheries Aquarium, Seapoint, Two Oceans Aquarium (TOA), Cape Town Harbor and West Coast Abalone, Britannia Bay.

With the exception of TOA, these intakes occur in the relatively open surf zone while the intake for TOA is in a harbor. The most common factor in the latter three intakes is the impact of marine life. Hence when designing the hydraulics of a seawater intake, accommodation should be made for the growth of marine life. This is akin to designing a pipeline and compensating for deterioration of the inner surface of the pipe over a large time period.

With marine growth being inevitable in seawater intakes, two methods can be employed to reduce marine growth. The first is the use of antifouling paints. These paints discourage marine growth on a surface; however they might also be detrimental to the seawater end user. This method is not recommended if the end user is part of a marine environment.

If the seawater end user is part of a marine environment, then the mechanical method of clearing the seawater intake is recommended. Here, the intake pipe(s)can be cleared via pigging or rotor routing. This method ensures that there is no change in the chemical composition of the abstracted water. When designing a seawater intake, allowance should be made for this maintenance action

At Abagold the seawater can be considered direct as it abstracts water from a water column. However this water column is in an intake basin that is at the end of a gully, hence there are a few extra factors that affect the intake. The main problem at Abagolds seawater intake is air entrainment and the low quantity of feed water. This cause's additional strain to the pumps as there is additional negative pressure head to pump against. With air being present in the feed water, this causes cavitation to the pump impellors. Hence it should be noted that when designing a seawater intake, the quantity of available water must be guaranteed and that the design should eliminate air from entering the pumping system.

The third type of seawater intake is the sub-bottom seawater intake. This occurs at Sea World Aquarium, UMW, Durban and Paternoster Oyster, Paternoster.

At Paternoster Oyster the entrepreneurial skills of the owner/operator should be noted. The beach wells are unique to the owner as he designed them himself. His method of installation of the beach wells is commendable as they stem from his practical experience and not any formal education.

The second sub-bottom intake is situated at UMW. Here water is abstracted for use at Sea World Aquarium. Here the design of a seawater intake is considered to be in one of three categories, they are: Hydraulic/Physical, Biological and Biochemical. Each category is discussed briefly

Hydraulic

When designing a pumping system the rise and fall of the sea level must be considered and hence a variable speed pump system should be used. Similar to the case at Abagold, air entrainment should be considered. At SWA, It was found that a large barrage of bubbles was being sucked up from the well points and the air caused cavitation of the pumps.

Physical

When the filter material through which the seawater flows become too compact, the negative suction pressure become so large that gases are drawn out of solution. The occurrence of these gases is undesirable.

Biological and Biochemical

There are numerous assumptions made when designing a sub-bottom intake. It is often assumed that the sand would act as a filter agent and that the physical quality of the water would be better. This might occur, however the myriad of biological and chemical reactions within the filter material must be considered. Chapter 3.5.3 covers a few scenarios that occurred at SWA seawater intake. Hence these should also be considered when designing a sub-bottom seawater intake. The use of a marine biologist to analyse the biological and biochemical reactions that occur in the sand matrix surrounding a beach well is recommended.

Chapter 4

4. CASE STUDY: INVESTIGATION OF INTAKE PIPES FOR A HORIZONTAL WELL FOR ABSTRACTING SEAWATER FROM THE SURFZONE ON ROCKY COASTLINES

4.1 Introduction

The feasibility of constructing a desalination facility at Kidd's Beach, near East London, Eastern Cape was undertaken by ZLH Consulting Engineers (ZLH, 2008). This entailed the design of all associated pipework, abstraction and disposal systems. The design parameters of water demand and relative locality were predetermined. The flowrate of required potable water is 40l/s (144m^3/hour); hence due the desalination plant providing a 50% return, an abstraction rate of 80l/s (288m^3/hour) is required. Three main options were proposed. These were located near the Kidd's Beach main bathing area and can be seen in Figures 4.1 to 4.3

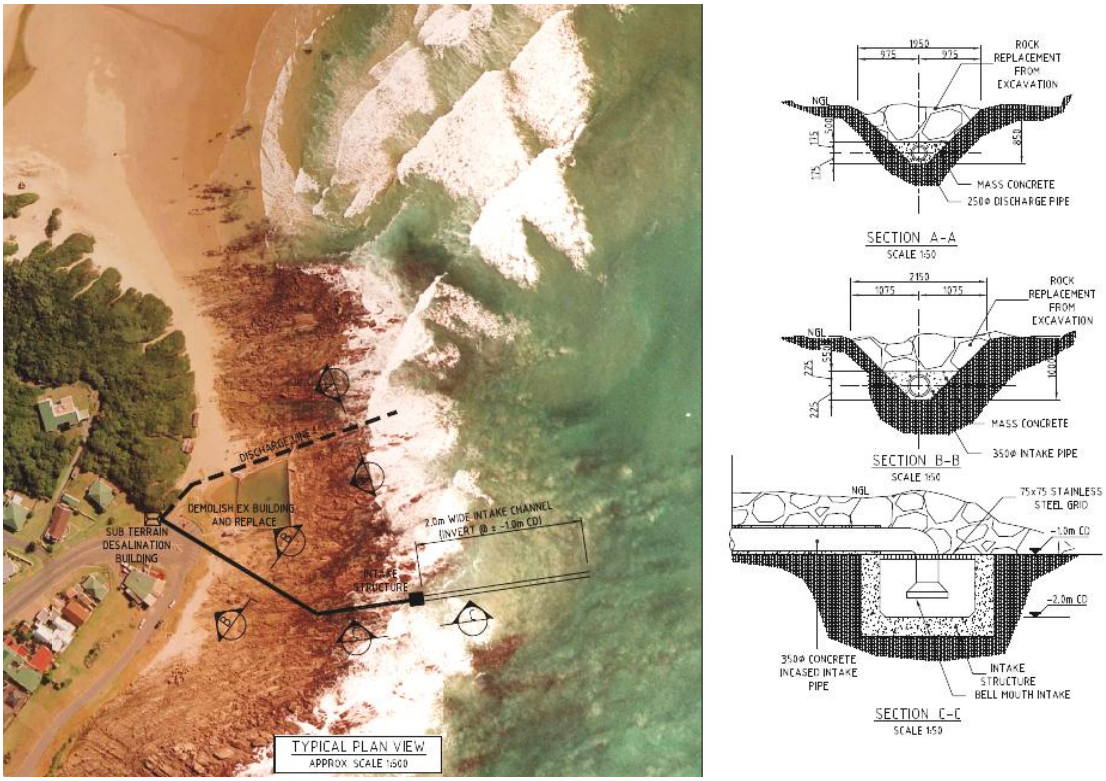

Figure 4.1: Seawater Abstraction and disposal System: Option 1 (ZLH, 2008)

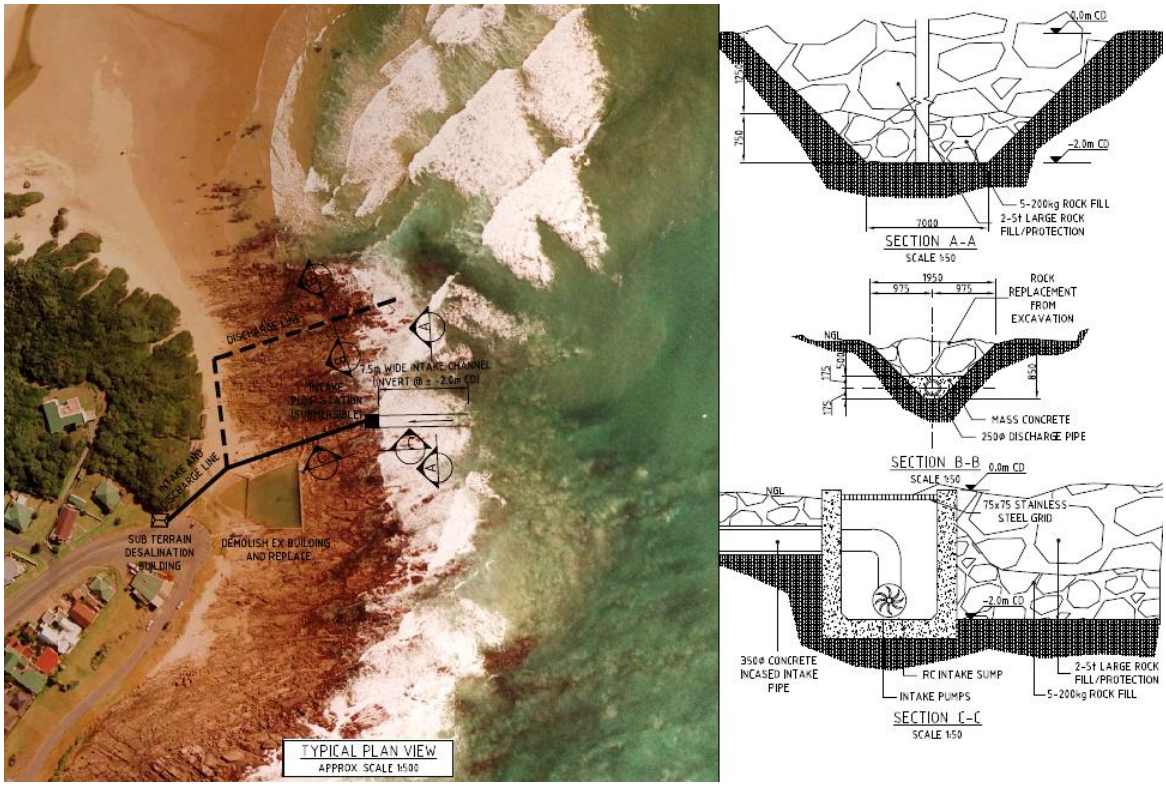

Figure 4.2: Seawater Abstraction and disposal System: Option 2 (ZLH, 2008)

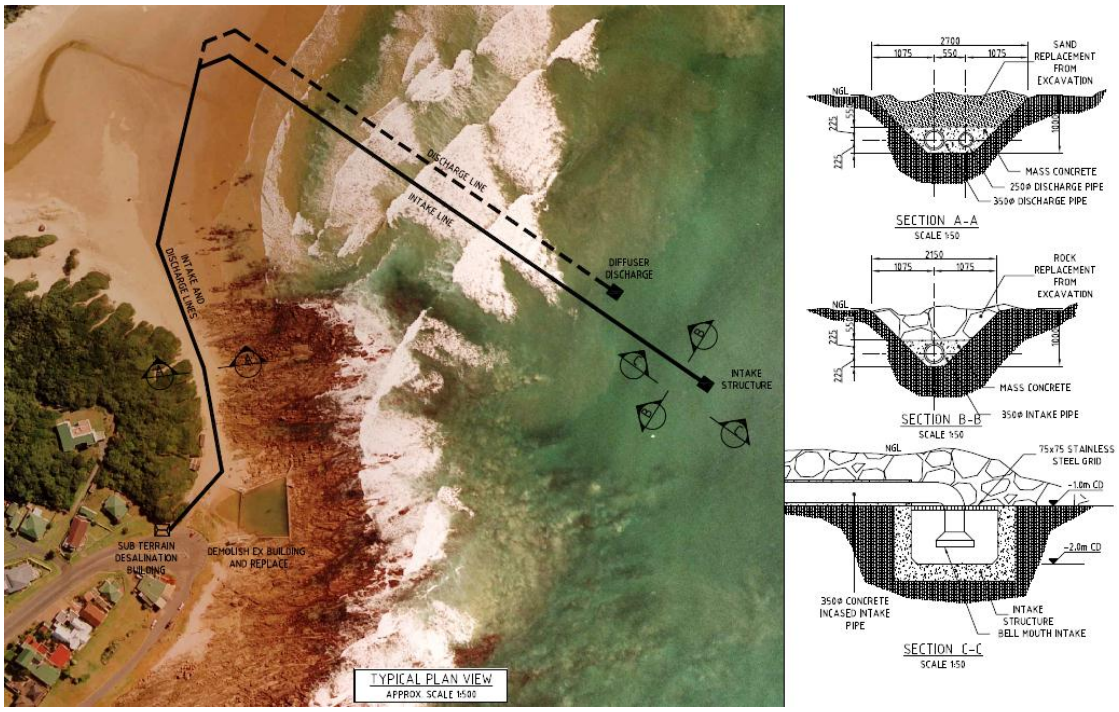

Figure 4.3: Seawater Abstraction and disposal System: Option 3 (ZLH, 2008)

Due to growing environmental and tourism pressure, these options were rejected. The final design had to consider 1) environmental impacts & 2) the concern of Kidd's Beach residents who found the intakes to be visually unacceptable (ZLH, 2008)

4.2 Conceptual Design & Layout of Seawater Intake on a Rocky Coastline

4.2.1 Background

The new location for the seawater abstraction/disposal area was approximately 1km south west of the main bathing beach. The area is far enough from the residential areas but close to the new potential desalination site. The coastline in this area is composed only of rocky shoreline that is populated with numerous parallel gulleys. Seawater is to be abstracted and disposed from this area, with minimal visual and environmental impact to the shoreline (ZLH, 2008).

The desalination facility will be situated behind the natural vegetation. Seawater will be pumped from the abstraction point to the desalination plant. The concentrated brine will be pumped from the plant via the disposal infrastructure, back into the surf zone. A newly constructed wooden foot path will to be used to alleviate visual impact. As shown in Figure 4.4, Turquoise indicates the Intake system, Yellow the Disposal system and Green the Wooden Footpath (ZLH, 2008).

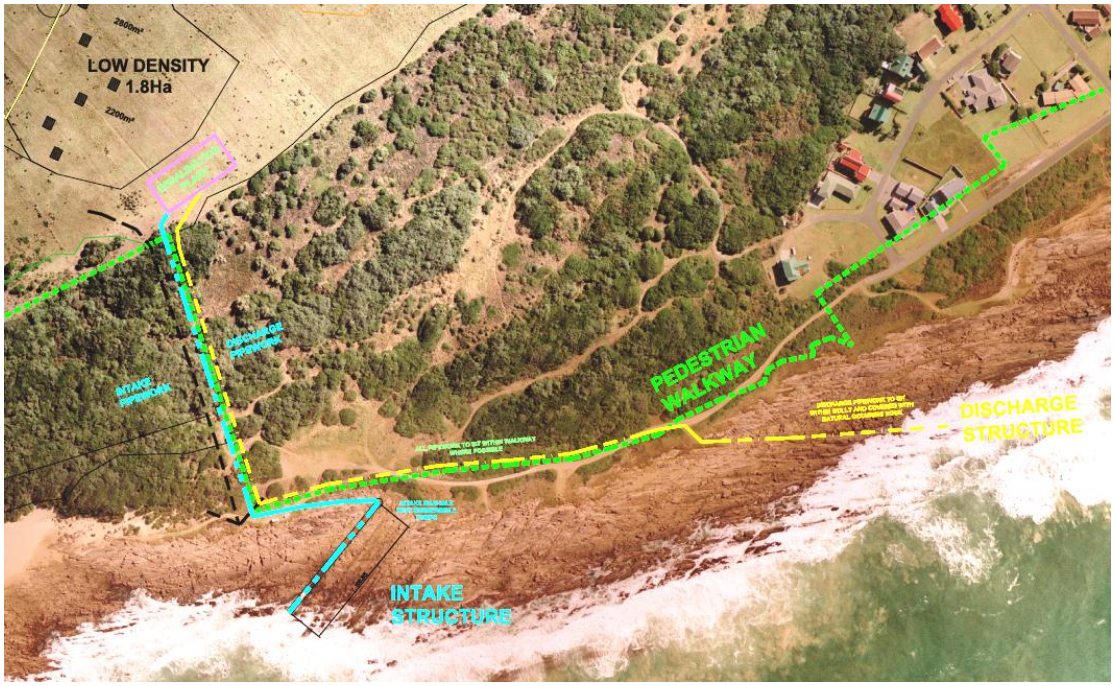

Figure 4.4: Seawater Abstraction and Disposal System: Final Layout (ZLH, 2008)

Due to the wave climate, and to negate recirculation, the disposal point is situated north east of the abstraction point. The presence of sand in the rocky shoreline is confirmed by the plumes of sand in the surf zone, Figure 4.4 above. The final design incorporates a few aspects from the initial options. One design criteria was to blend the seawater intake into the natural environment. Another suggestion was for the intake and disposal infrastructure to make use of the existing gulley's.

4.2.2 Proposed Seawater Intake

To draw water from sandy beaches, a well point system, as noted in Chapter 2.3.3.1, can be used. Intake pipes with small perforation can be used to collect seawater. Under gravity; this water flows through the sand bed and intake pipes into a collection well (ZLH, 2008).

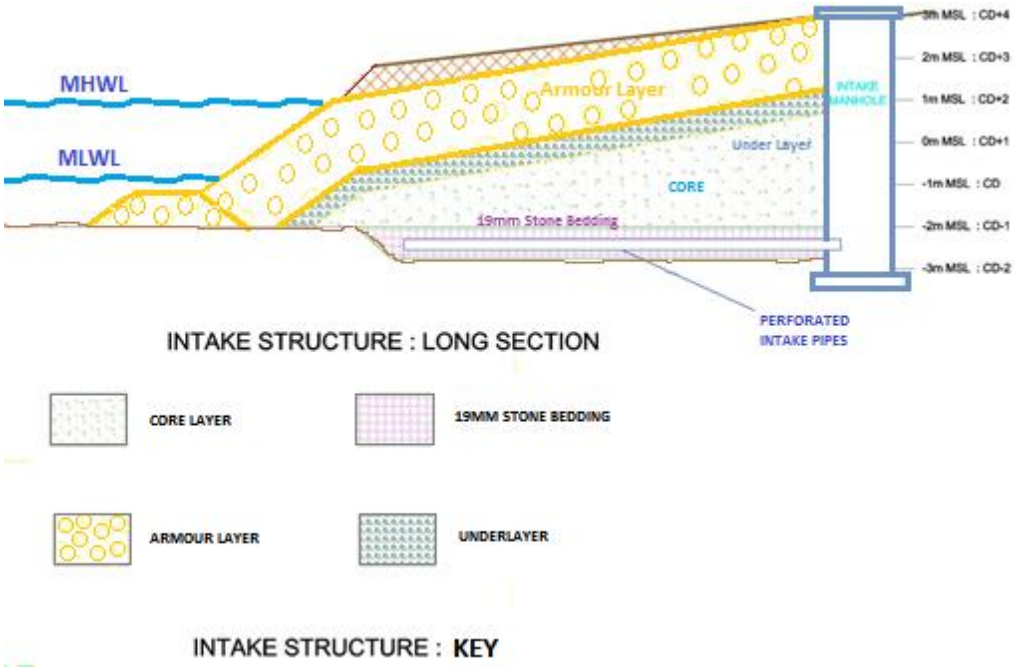

Figure 4.5: Proposed Seawater Intake System

The basis of this seawater intake was to use the same type of horizontal well to collect seawater and gravity feed this into a sump The above design long section, Figure 4.5, was proposed. (ZLH, 2008). Referring to Figure 4.5 above, the intake structure would be designed / constructed as follows. An existing gulley would be excavated to ensure that the intake would lie parallel to the existing rock strata. A screen pipe would be bedded in 19mm stone bedding. Above this is a core and under layer. Thereafter the seawater intake would terminate with a rock armour layer.

4.2.3 Cross Section Design of Seawater Intake

With respect to structural stability, the armour layer would be the most vital component. Due to economics, rock armour is almost always used, at the steepest slope possible. The use of low sloped armour units is not common. Hence analysis of the armour rock at a low gradient is not required as it can be assumed that tradition analysis of a steep slope revetment would be more than adequate. Figure 4.6 below shows two sections of a breakwater.

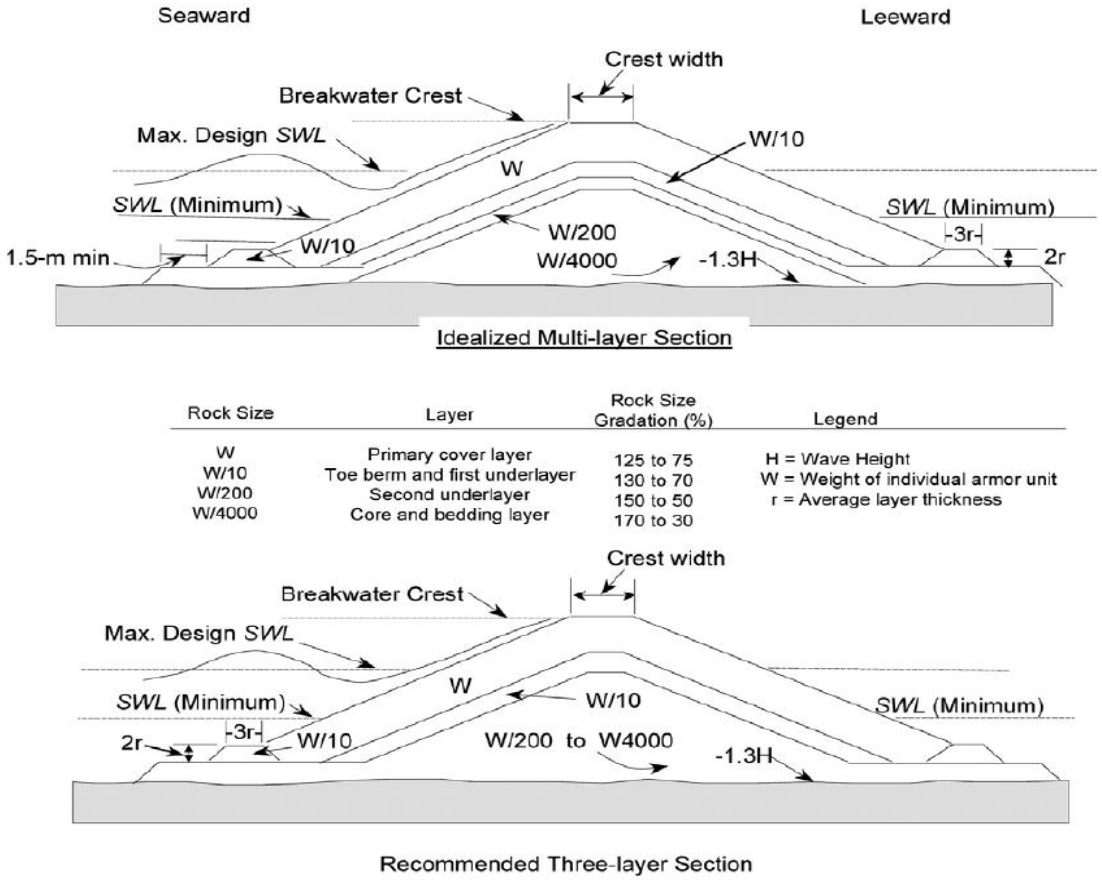

Figure 4.6: Cross-sectional of Breakwater (CEM, 2007).

The upper section of Figure 4.6 shows a complex idealized cross section. The lower part of Figure 4.6 depicts a recommended cross section. The idealized cross section provides more complete use of the range of materials typically available from a quarry, but it is more difficult to construct. The recommended cross section takes into account some of the practical problems involved in constructing submerged portions of the structure (CEM, 2007). Hence the second, recommended section will be used.

4.2.4 Structural Design of Seawater Intake

To calculate the armour size, Van Gents' method is used (CIRIA, CUR, CETMEF, 2006). Equation CS1 below. shows Van Gents method when calculating rubble mound armour size for shallow foreshore conditions.

$$\frac{H_S}{\Delta D_{n50}} = 1.75\sqrt{cot\alpha}\left(1 + \frac{D_{n50-core}}{D_{n50}}\right)^{\frac{2}{3}}\left(\frac{S_D}{\sqrt{N}}\right)^{0.2} \qquad \text{(Eqn CS1)}$$

For a depth limited wave in 2 meters of water, an armour slope of 1 over 1.5. This resulted in an armour rock size of M_{50} = 1.45 tons at the toe of the revetment. Utilising Figure 4.6, the design values for the cross section are found in Table 4.1below. It is assumed that the rock material has a density of 2500kg/m^3. The relevance of this information below, will be utilized further on.

Table 4.1: Details of material sizing for armour protection of seawater Intake

Layer		Armour	Underlayer	Core	Core	Bedding
Size Notation		W	W/10	W/200	W/4000	W/150000
Weight	kg	1450	145	7.25	0.36	0.010
Rock Density	kg/m^3	2500	2500	2500	2500	2500
$D_{n50}{}^3$	m^3	0.58	0.058	0.0029	0.00015	3.87E-06
D_{n50}	m	0.834	0.387	0.143	0.053	0.0157
Rock Size Gradation (%)	from	125%	130%	150%	170%	170%
	to	75%	70%	50%	30%	30%
Upper Weight Limit	kg	1813	189	10.9	0.6	0.016
Lower Weight Limit	kg	1088	102	3.6	0.11	0.003
D_{n100}	m	0.898	0.422	0.163	0.063	0.019
D_{n0}	m	0.758	0.344	0.113	0.035	0.011

4.2.5 Filter Design of Seawater Intake

After the structural strength has been confirmed, the next important step is to undertake a filter design. The basic principle of this design, is to ensure that no material is lost. The finer details of this can be found in Chapter 2.4.7.For the purposes of this thesis the following conditions are assumed:

- There is no internal erosion of granular material
- Only 1) Interface Stability of a Closed Granular Filter will be checked
  2) Permeability Requirements of a Granular Filter will be checked
- A layer will only comprise of material that lies between the two, predetermined outer limits of that layer
- D_n size of a particular layer will be linearly interpolated from these two limits

Table 4.2, which is sourced from Table 4.1, shows the information required to perform the filter test. The blue figures are interpolated from Figure 4.7 which is a graphical plot of the data in Table 4.1.

Table 4.2: Material sizes for armour protection of seawater Intake[meters]

Layer	Armour	Underlayer	Core upper	Core Lower	Core Mixture	Bedding
D_{n50}	0.834	0.387	0.143	0.053	0.100	0.0157
D_{n100}	0.898	0.422	0.163	0.063	0.163	0.019
D_{n0}	0.758	0.344	0.113	0.035	0.035	0.011
D_{n85}	0.879	0.413	0.157	0.062	0.146	0.018
D_{n15}	0.781	0.357	0.122	0.041	0.055	0.012

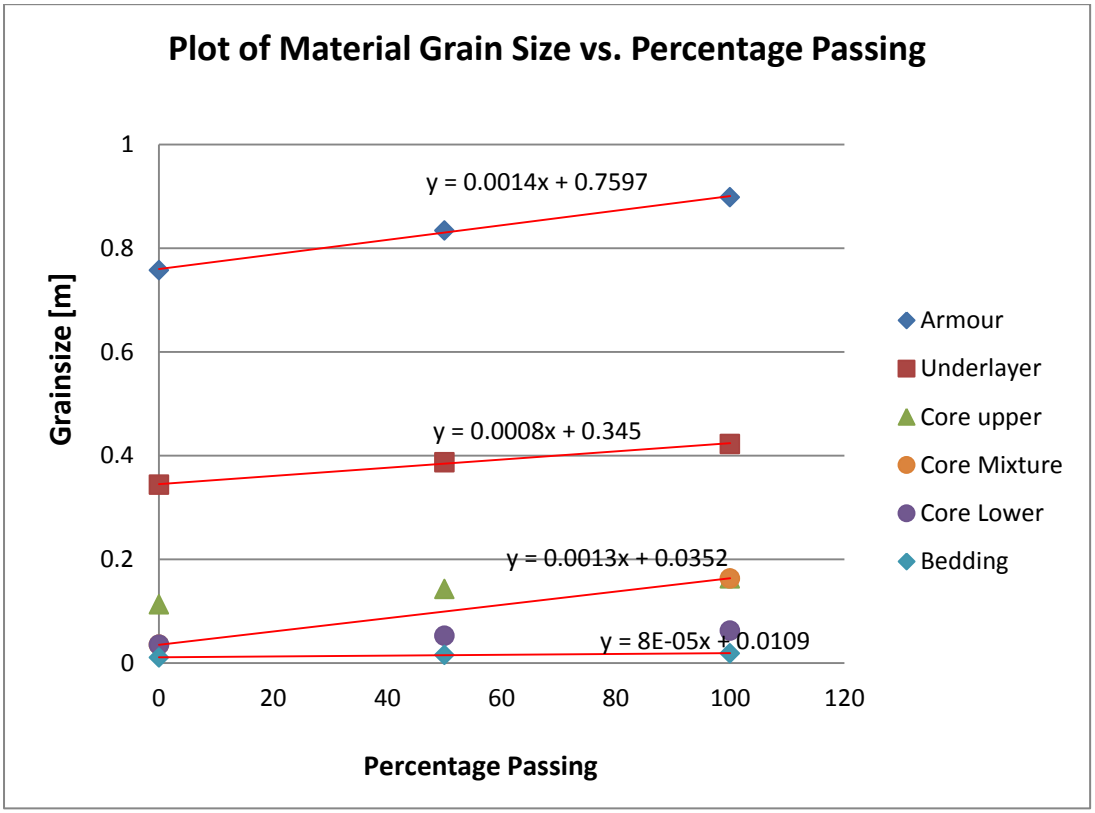

Figure 4.7: Material Grain Distribution for armour protection material of seawater Intake

4.2.5.1 Interface Stability of a Closed Granular Filter

The check with regards to Interface Stability of a Granular Filter is done with Equation LR17 below

$$\frac{D_{15f}}{D_{85b}} < 5 \qquad \text{(Eqn LR17)}$$

The indices "*b*" and "*f*" are used for the base and filter materials respectively and numbers refer to the particle size distribution curve. The filter "f" layer is at the top and the base "*b*" is the lower layer.

Filter Check between Armour and Underlayer

From Table 4.2, D_{15f} = 0.781m and D_{85b} =0.413. Applying Equation LR17,

$$\frac{D_{15f}}{D_{85b}} = \frac{0.781}{0.413} = 1.89 < 5$$

Hence the interface between the Armour layer and Underlayer is stable.

Filter Check between Underlayer and Core

From Table 4.2, D_{15f} = 0.357m and D_{85b} =0.146. Applying Equation LR17,

$$\frac{D_{15f}}{D_{85b}} = \frac{0.357}{0.146} = 2.45 < 5$$

Hence the interface between the Underlayer and Core is stable.

Filter Check between Core and Bedding

From Table 4.2, D_{15f} = 0.055m and D_{85b} =0.018. Applying Equation LR17,

$$\frac{D_{15f}}{D_{85b}} = \frac{0.055}{0.0186} = 2.96 < 5$$

Hence the interface between the Core and Bedding layer is stable.

4.2.5.2 Permeability Requirements of a Granular Filter

The general permeability requirement for such filters is that the flow resistance is small enough to prevent pore pressures contributing to instability of the structure. This criterion is automatically met if the material in a layer is stabile.

This filter criteria corresponds to the requirement that the permeability of the filter layer, k_f, is much larger than that of the base, k_b . In cases of laminar flow, the following Equation LR19 applies.

$$\frac{k_f}{k_b} > 16 \; to \; 15 \qquad \text{(Eqn LR40)}$$

The indices "*b*" and ''*f*' are used for the base and filter materials respectively and numbers refer to the particle size distribution curve. The filter "f" layer is at the top and the base "*b*" is the lower layer. The permeability criterion given above as Equation LR19 and illustrated in Figure 2.39 below, is especially secure for all kinds of filters. Table 4.3 below shows the manner in which Figure 2.39 is used to determine the permeability of each layer

Table 4.3: Calculation of Permeability for armour protection of seawater Intake

Layer		Armour	Underlayer	Core Mixture	Bedding
D_{n50}	m	0.834	0.387	0.100	0.0157
Log (D_{50})	m	-0.08	-0.41	-1.00	-1.80
Log *k* (from fig. 2.39)	m/s	-0.28	-0.44	-0.74	-1.16
k	m/s	0.525	0.363	0.182	0.069

Permeability Check between Armour and Underlayer

From Table 4.2, D_{50f} = 0.834m and D_{50b} =0.387. From Figure 2.39, k_f =0.525 and k_b =.363. Applying Equation LR19,

$$\frac{k_f}{k_b} = \frac{0.834}{0.387} = 2.15$$

This is less that the ratio stated by equation LR 19, However the permeability of the filter layer is twice that of the base layer and hence the permeability is acceptable.

Permeability Check between Underlayer and Core Layer

From Table 4.2, D_{50f} = 0.387m and D_{50b} =0.1. From Figure 2.39, k_f =0.363 and k_b =0.182. Applying Equation LR19,

$$\frac{k_f}{k_b} = \frac{0.387}{0.182} = 2.13$$

This is less that the ratio stated by equation LR 19, However the permeability of the filter layer is twice that of the base layer and hence the permeability is acceptable.

Permeability Check between Core Layer and Bedding Layer

From Table 4.2, D_{50f} = 0.1m and D_{50b} =0.0157. From Figure 2.39, k_f =0.182 and k_b =0.069. Applying Equation LR19,

$$\frac{k_f}{k_b} = \frac{0.182}{0.069} = 2.64$$

This is less that the ratio stated by equation LR 19, However the permeability of the filter layer is more than twice that of the base layer and hence the permeability is acceptable.

4.3 Specific Aims of Investigation

4.3.1 Overall Objectives

The main objectives of this thesis are found in Chapter 1.3. They are summarized as follows:

1. Survey selected seawater abstraction facilities in South Africa.
2. Investigate the hydraulics of a proposed seawater abstraction system using the Horizontal Well Method (HWM)on rocky coastlines.
3. Provide recommendations for design guidelines for small scale seawater abstraction systems on rocky coastlines using the HWM.

The first objective was addressed in Chapter 3. Proposed solution and guidelines to the investigated abstraction facilities are made in the Chapter 3.9.

The third objective is addressed in the final Chapter 7. It is a culmination of the seawater abstraction facilities survey and the findings of the Hydraulic Physical Model (HPM) tests

4.3.2 Flow regime and Filter Objectives

In Chapters 2.4.6 and 2.4.7, the literature review concentrated on the, “Hydraulics within Seawater Intake” component. Thereafter, identification of areas that require more in depth investigation is required.

The hydraulics of the intake pipes is the bottle neck as the area of perforation dictates the flow and the associated losses through the opening. Hence better understanding of the screen pipe is required. The relationship of flow versus headloss will help determine the screen pipe invert level and thus, the entire seawater intake.

The first part of the study, investigates the relationship between flow and headloss in a seawater intake pipe. The second part of the study, investigates the effect of filter/bedding material around the Intake pipeline. The effect of this material on flow, and headloss in the seawater pipe intake is to be better understood. The project at Kidd’s beach did not past the scoping stage. However the information on seawater intakes on rocky shores will prove valuable in the future.

4.4 Hydraulic Physical Model

4.4.1 Model Design Objectives

As, mentioned in chapters 4.2 & 4.3, there are various components that require attention when designing a seawater intake. By drawing up a conceptual design, the number of components to be designed is better managed. Certain components of the intake would have established design guidelines, whilst some are still in the experimental stage. With supporting literature, the list of design items to be investigated in this thesis has been reduced to two viz.:

- The relationship between flows, pressure driving flow and headloss in the seawater, pipe intake.
- The effect of material surrounding the intake pipeline, on flow, pressure driving the flow and headloss in the seawater pipe intake.

With these design objectives established, a summary of the design and construction of the Hydraulic Physical Model (HPM) follows. Appendix A contains more detailed information on the layout and dimensions of the HPM.

The requirements of the model had to satisfy the following conditions.

The model:

- should allow for easy calculation of head loss.
- should ensure that variable flow is attainable.
- should allow for material to surround the intake pipe

The model should also:

- ensure that all flows can be measured.
- ensure that all losses are accounted for.
- ensure that any material (sand) conveyed by water is measurable.
- maximise visual viewing of flow.

Figures 4.8 and 4.9 below show the Hydraulic Physical Model setup as used for testing.

Figure 4.8: Physical Hydraulic Model for testing of Seawater Intake pipework

4.4.2 Intake Pipes

Three intake pipes of 250mm diameter were tested. 250mm diameter pipes, being not commonly used in practice, were used as they were the only size available for all three pipe types. These pipe types where chosen as they are the only perforated pipe types available in South Africa. The three pipes tested were as follows:

- A Slotted PVC Pipe
- A Perforated PVC Pipe
- A Metal Wire (Johnson Screen) Pipe

The first pipe tested was a slotted PVC pipe with 1mm slots. These slots take up half the area of the pipe wall in the form of five slots. The second pipe tested was a PVC pipe into which 8mm diameter holes were drilled. The third pipe was a circularly wound, metal wire pipe. These pipes will be described in greater detail in the subsequent sub chapters.

4.4.3 Types of Test

Considering the conceptual design in chapter 4.2, flow is restricted by the perforation of the pipe, and the material surrounding the intake pipe. The core and armour material were deemed large enough not to impede the flow of water. Hence the following tests were conducted as they were designed to illicit only the specific information required. They were as follows:

Test 1: Hydraulic test with water only
Test 2: Hydraulic test with Intake Pipe in 19mm Stone Bedding
Test 3: Hydraulic test with Intake Pipe in 19mm Stone and sand bedding.

The following chapters will describe the above tests in greater detail

4.4.4 Basic Methodology of Tests

Method

Referring to Figure 4.8 and 4.9, water enters the larger Water Column 1 (WC1). Under gravity, the water moves through the slots/perforation into the intake pipe. Thereafter water travels through the intake pipe into the first half of Water Column 2 (WC2a). The water flows upwards until it encounters the V notch weir. The water then flows over the weir into the second half of WC2, noted as WC2b. Due to the V notch being calibrated; the flowrate through the model is easily calculated. Two tubes that connect to the bottom of WC1 and WC2 are placed on either side of a measuring scale in order to accurately measure their respective water level and thus the head difference between both water columns

4.4.4.1 Test 1: Hydraulic test with water only

Figure 4.9 below is a simple flow diagram depicting the loss of pressure head as water flows through the Hydraulic Physical Model (HPM). The 19mm stone bedding is shown for reference purposes and is not used in the first test. Figure 4.10 shows the relationship between headloss due the pipe openings and the rate of flow.

For steady state flows, the difference of Water Level in Column 1 (WC1) and Column 2 (WC2) is the total loss of pressure head (ΔP_{TOTAL}) through the model. The total loss is the sum of pressure loss due to:

A) Openings in the intake pipe
B) Skin friction in the portion of intake pipe where there is water ingression and transportation
C) Skin friction in the portion of intake pipe where there is water transportation only
D) Exit loss as water exits the intake pipe and enters WC2a
E) Skin friction as water flows up WC2a

Chapter 4.4.6 and Figure 4.13 describe the minor losses in greater detail

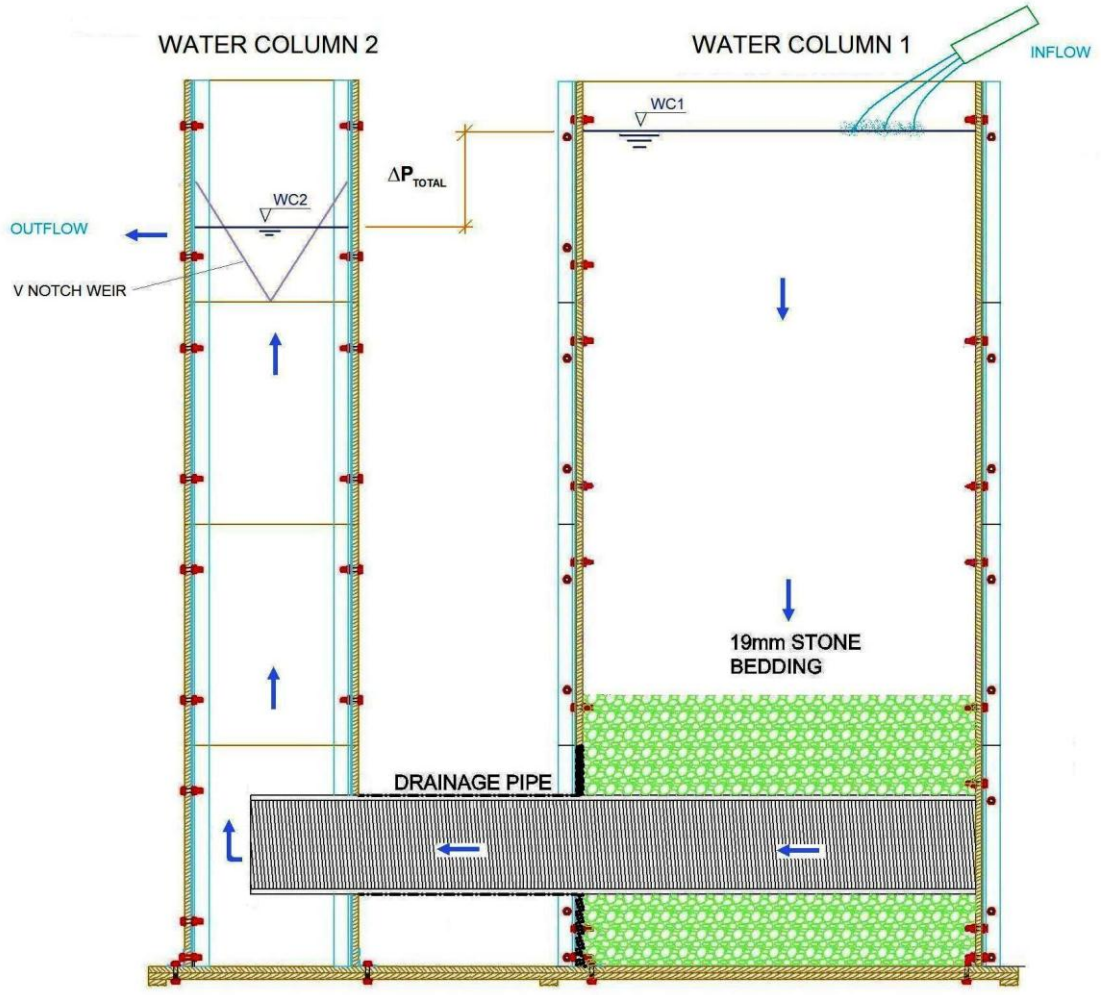

Figure 4.9: Flow diagram depicting the loss of pressure head in the (HPM)

The losses associated with the openings in a pipe (Loss A), is easily calculated as ΔP_{TOTAL} minus (B+C+D+E). Hence for various flows, the relationship between the loss in pressure due to the intake pipe openings and flow can be established.

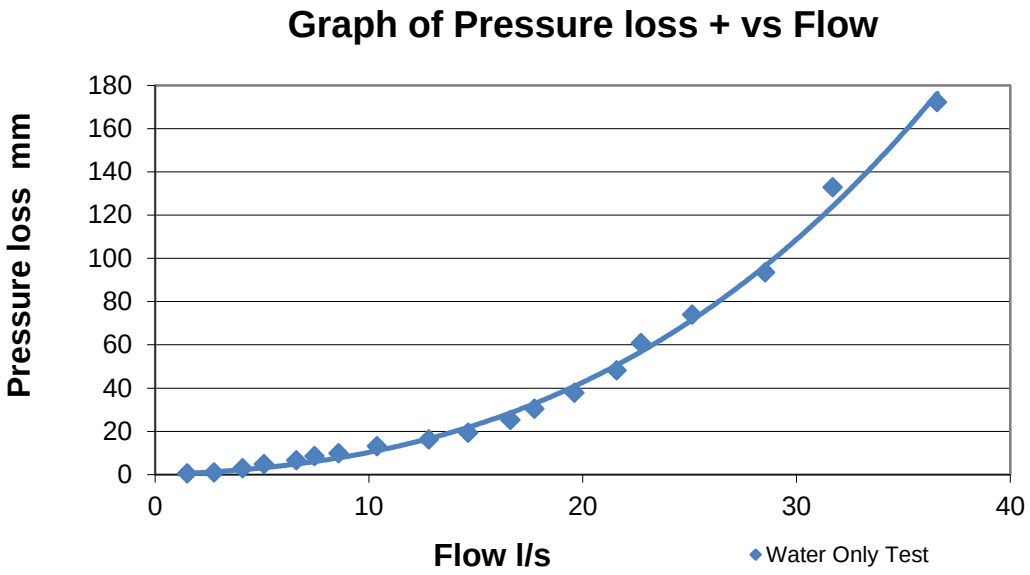

Figure 4.10: Relationship between flow and the associated pressure loss for Test 1 (water only, no stone bedding)

4.4.4.2 Test 2: Hydraulic test with Pipe in 19mm Stone Bedding

The second test is conducted in a similar manner as the first test. For steady state flows, the difference of Water Level in Column 1 (WC1) and Column 2 (WC2) is the total loss of pressure head (ΔP_{TOTAL}) through the model. The total loss is the sum of pressure loss due to:

A) The stone bedding surrounding the intake pipe.
B) Openings in the intake pipe
C) Skin friction in the portion of intake pipe where there is water ingression and transportation
D) Skin friction in the portion of intake pipe where there is water transportation only
E) Exit loss as water exits the intake pipe and enters WC2a
F) Skin friction as water flows up WC2a

Figure 4.11 shows the typical relationship between flow and the associated pressure loss plotted with the results of Test 1 (water only). Note that the higher line is the sum of the pressure loss due to the intake pipe and the stone bedding. Hence the space between both lines is the actual physical headloss due to stone bedding alone.

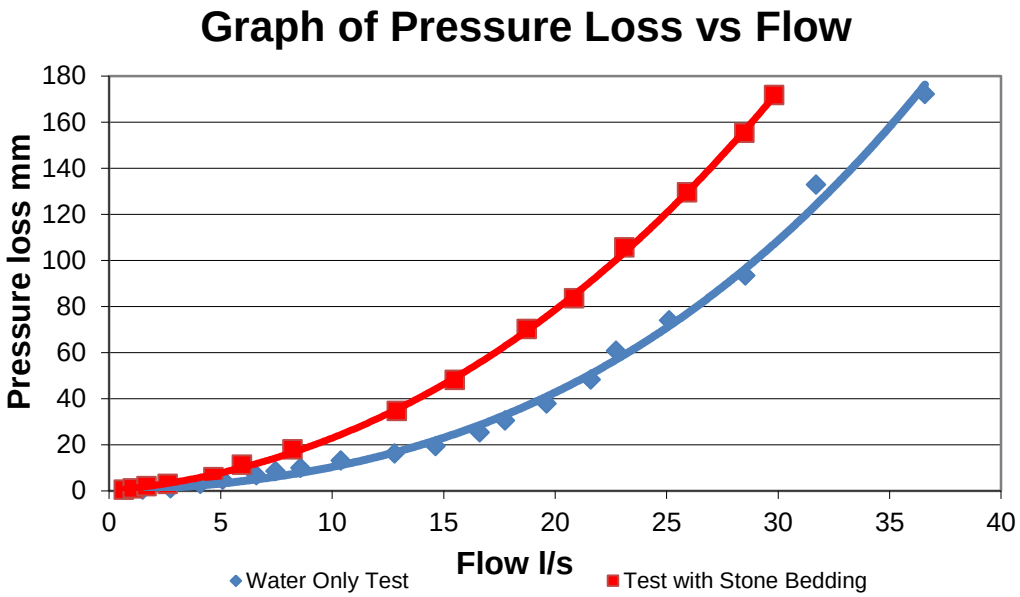

Figure 4.11: Relationship between flow and the associated loss of pressure head due to the intake pipe AND Stone bedding in the HPM

4.4.4.3 Test 3: Hydraulic test with Pipe in 19mm Stone and Sand

The third test is conducted in a similar manner as the first two. For steady state flows, the difference of Water Level in Column 1 (WC1) and Column 2 (WC2) is the total loss of pressure head (ΔP_{TOTAL}) through the model. The total loss is the sum of pressure loss due to:

A) The stone and sand bedding surrounding the intake pipe.
B) Openings in the intake pipe
C) Skin friction in the portion of intake pipe where there is water ingression and transportation
D) Skin friction in the portion of intake pipe where there is water transportation only
E) Exit loss as water exits the intake pipe and enters WC2a
F) Skin friction as water flows up WC2a

Figure 4.12 shows the typical relationship between flow and the associated pressure loss. Note that the middle line (Test 2) is the sum of the pressure loss due to the intake pipe and the stone bedding (no sand) and the lower line is the result of Test 1 (water only). The green line is the sum of the pressure loss due to the intake pipe, stone bedding and sand mixture Hence the space between the highest and lowest lines is the pressure loss due to the stone AND sand bedding.

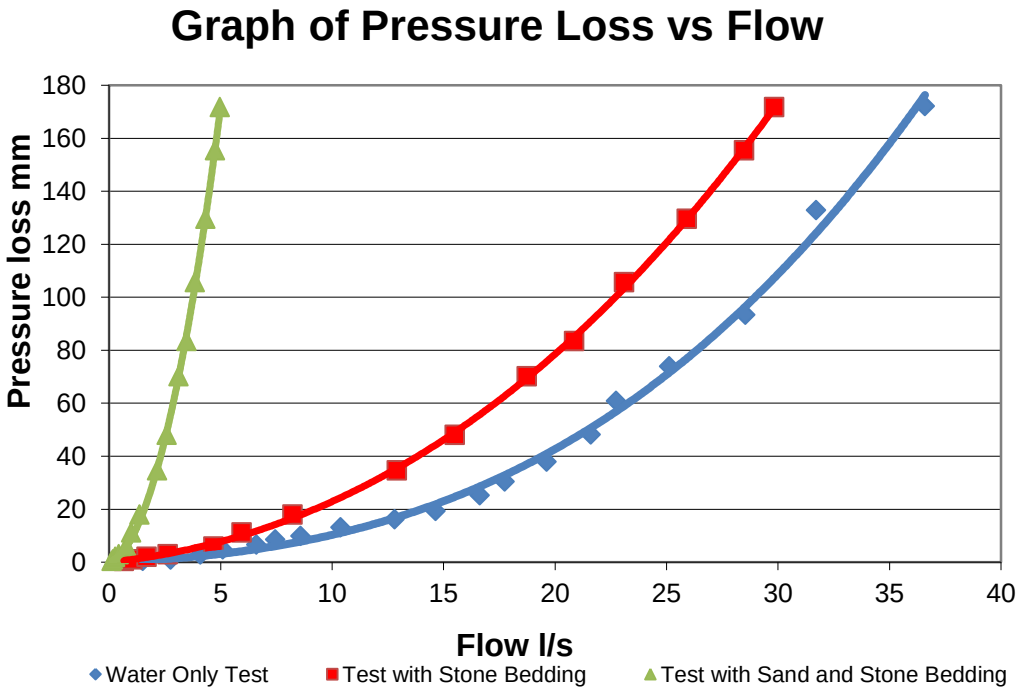

Figure 4.12: Relationship between flow and the associated loss of pressure head due to the intake pipe, Stone AND Sand bedding in the HPM

4.4.5 Three Methods used for Estimating Headloss by Bedding

Three methods where investigated when calculating the headloss due to the stone bedding surrounding the intake pipes. The three methods are compared in order to establish which would be most appropriate for the application of Seawater Intakes on a rocky coastline. Detailed calculations with reference to the, Slotted, Perforated and Metal Wire pipe can be found in Appendices D, E and F respectively

Method 1: Simple method for determining stone bedding loss

In this simplistic method, the results of the “Water Test only: is plotted. Curve line 1 is fitted to the results and an equation characterising the line and hence the pipe, headloss characteristics is formulated.

Thereafter, the results of the “Stone and water test” is plotted. Curve line 2 is fitted to the results and an equation characterising the line and hence the pipe and surrounding bedding, headloss characteristics is formulated.

The loss due to the stone bedding only, Curve line 3, is determined by subtracting Curve line 2 from Curve Line 1. This data is then plotted to show graphically the relationship between the headloss caused by the bedding.

Method 2: Method for determining stone bedding loss : Hydraulic conductivity: Kenny, Lau and Ofoegbu

The second method used to determine the loss of pressure due to Stone bedding, looks at the hydraulic conductivity of stone bedding. The following equation LR16 and Figures, 2.32 and 2.33 by Kenny, Lau and Ofoegbu are used to estimate stone bedding headloss.

$$\text{ƙ} = (0.05\ to\ 1)D_5^2 \qquad \text{(Eqn LR16)}$$

Method 3: Method for determining stone bedding loss : Hydraulic conductivity: Forchheimer

The third method used to determine the loss of pressure due to Stone bedding, stems from work carried out by Forchheimer. Figure 2.35, chapter 2.4.5.4 was used to estimate the permeability of the stone bedding and hence the headloss.

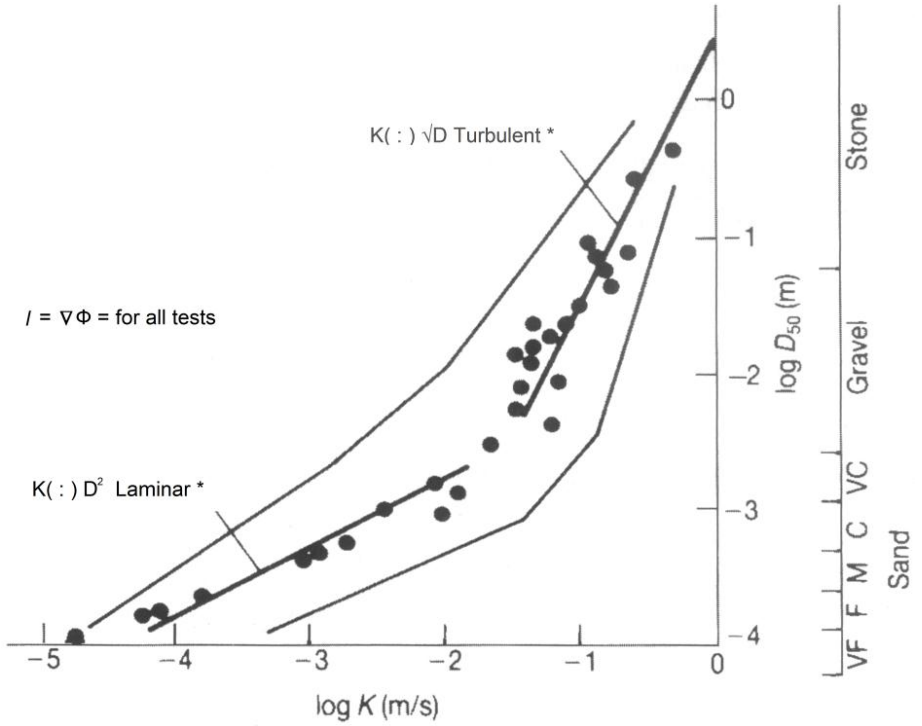

Figure 2.35: Permeability versus grain or stone sieve size (CIRIA, CUR, CETMEF, 2007)

4.4.6 Minor losses in the Model

There are two types of losses that occur in the PHM. The first type is minor pressure losses due to the resistance to flow. The second loss is physical loss of water due to model leakage.

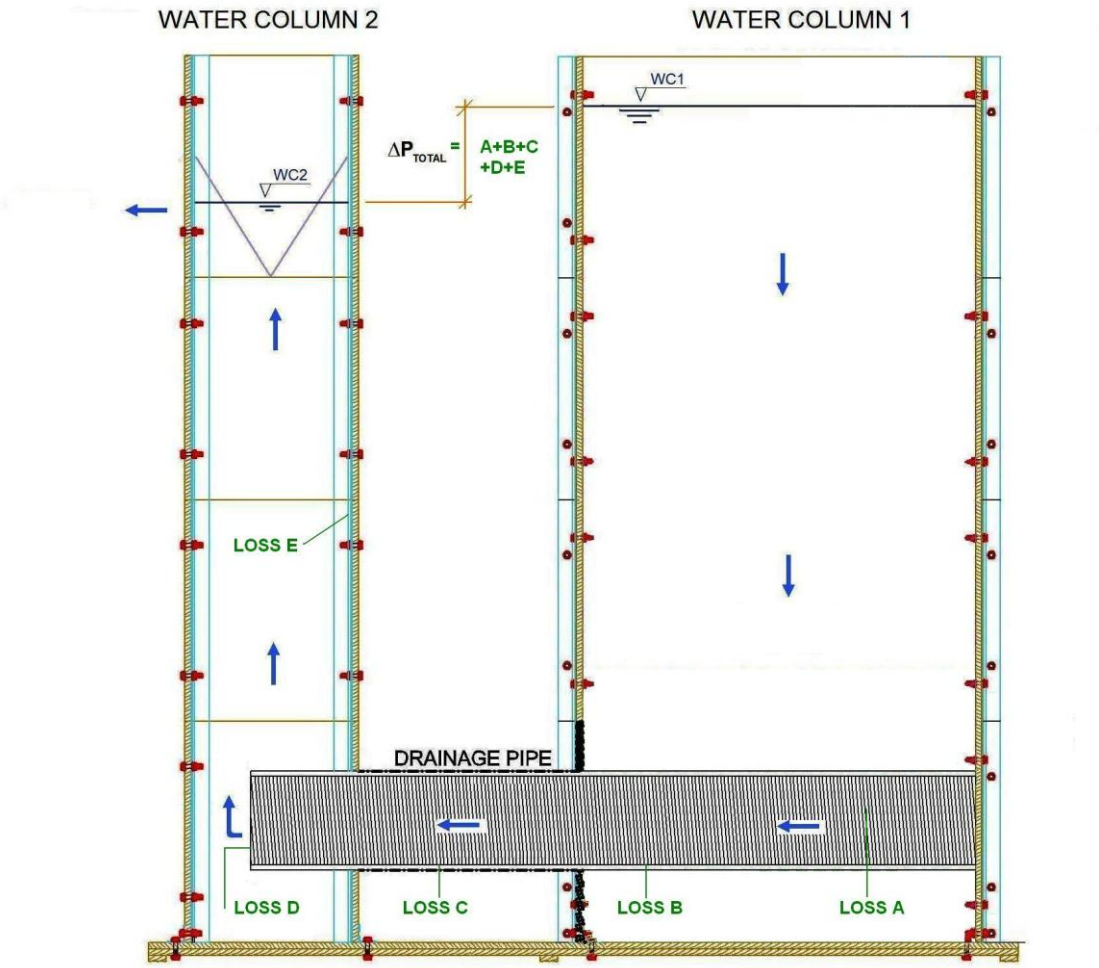

Figure 4.13: Loss of pressure head in the HPM (Water Only)

4.4.6.1 Minor Pressure Losses

Figure 4.13 shows the local for the major loss A and the minor losses B, C, D, and E. As mentioned in the previous sub chapter, subsequent minor losses are calculated as follows, Loss A is the friction due to the intake pipes perforation and is not considered a minor loss.

Loss B: Skin friction in the portion of intake pipe where there is water ingression and transportation. The skin friction in this is calculated using Manning's Method. A pipe of ø250mm is used as the conduit size. However, the skin friction in this area is halved as theoretically the flow is at its maximum as it exits WC1 and zero at the start of the line (Right hand side of Figure 4.10)

Loss C: Skin friction in the portion of intake pipe where there is water transportation only. The skin friction in this chapter is calculated using Manning's Method. A pipe of ø250mm is used as the conduit size.

Loss D: Exit loss as water enters WC2a. For the flow exiting the intake pipe, and then turning 90 degrees, a coefficient of K_e = 1.0 is used as in the calculation of the pressure loss which is equal to $K_e*V^2/2g$

Loss E: Skin friction as water flows up WC2a. The skin friction in this chapter is calculated using the Manning's Method. A rectangular section of 600mm by 250mm is used as the conduit size.

All of these losses are be quantitatively estimated in the detailed calculations contained in Appendices D, E and F.

4.4.6.2 Loss of water due to leakage

All HPM's have the potential to leak, Figure 4.14. Hence the ability to quantify the leakage is crucial as this would affect the measurement of flow through the model. The method used in this HPM, was to measure the flow rate of the leakage for each increment of flow through the model.

This was done by constructing a dam around the HPM, Figure 4.15. The leaked flow was then guided to a water canal and collected in a measuring vessel over a specified time period. Hence for a steady flow conditions, the leakage flow rate was easily established and the actual flow rate in the model calculated. Ultimately the leakage flow rate was found to be insignificant in comparison to the flow rate in the HPM.

Figure 4.14: A leak in the first half of WC2 of the HPM

Figure 4.15: A dam constructed around the HPM

Chapter 5

5. CASE STUDY: TEST PROCEDURES AND RESULTS FOR DETAIL INVESTIGATION OF INTAKE PIPES IN HYDRAULIC PHYSICAL MODEL

5.1 Slotted PVC Pipe Abstraction Model

5.1.1 Synopsis

The following is a chronological summary of the tests conducted on the Slotted PVC Pipe, Figure 5.1. The first test was conducted utilising water only. Figure 5.2 describes the HPM. The test pipe has been cut in half and placed against a Perspex sheet. For the second test, 19mm stone bedding was placed around the pipeline. The third test involved sand being used to fill the voids of the 19mm stone bedding

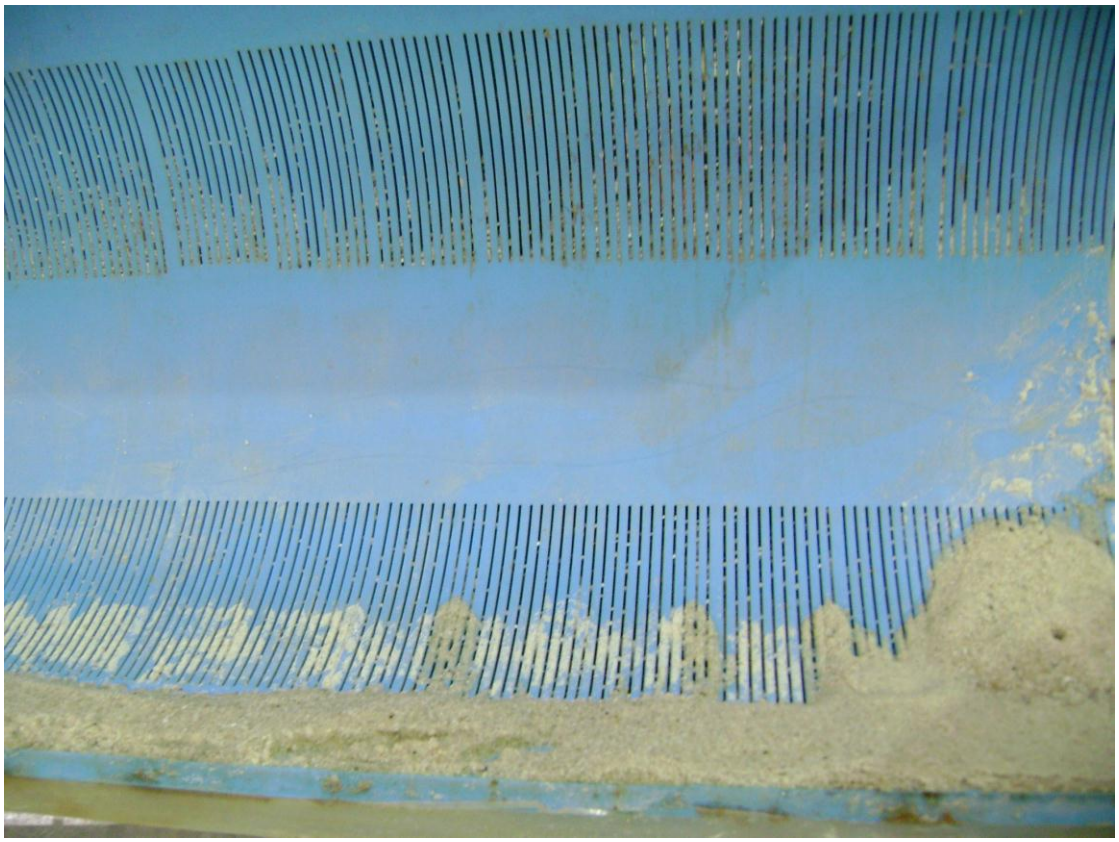

Figure 5.1: View of inner section of half a ø250mm slotted PVC Pipe

The first two tests proceeded well. In the third test, the sand and stone mixture constricted the flow to a fraction of those in the former two tests. At this point, a system of back flushing was introduced in order to dislodge the sand and restore the initial flow rates. This system proved to be moderately successful. Subsequent chapters discuss the tests and results in finer detail.

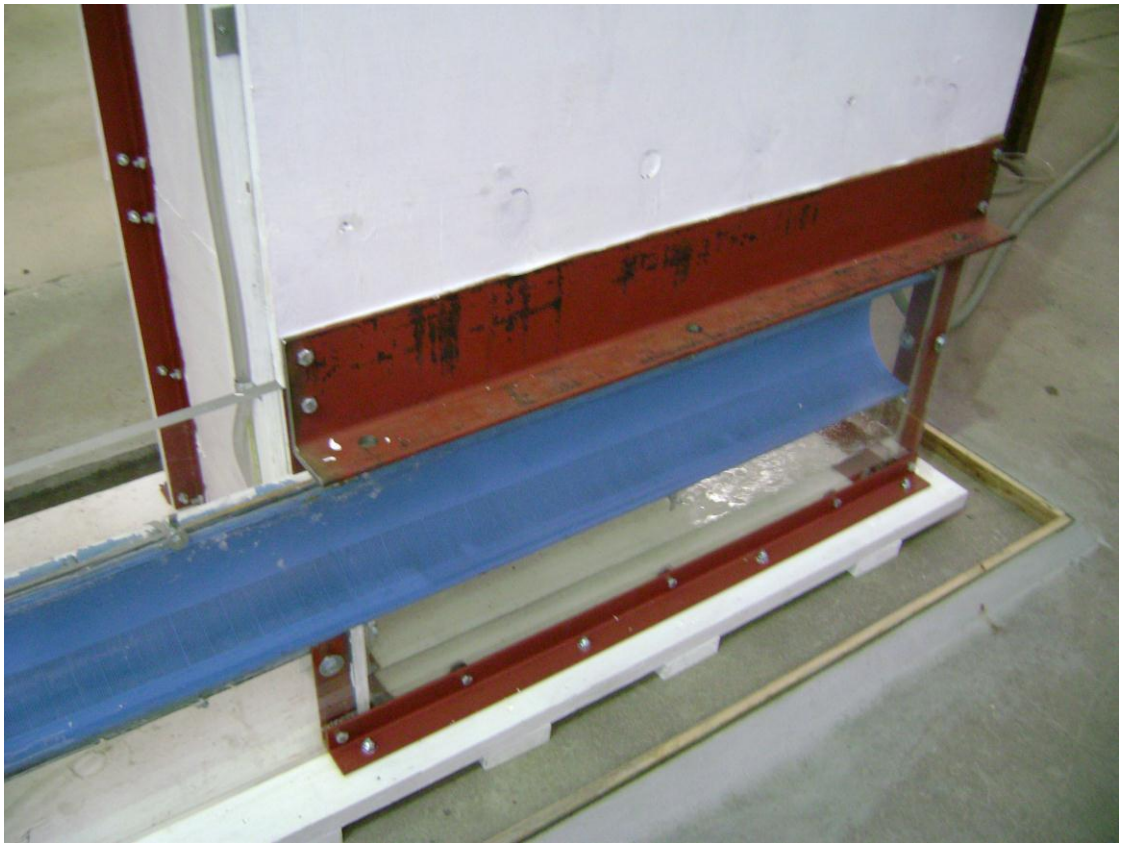

Figure 5.2: ø250mm slotted pipe in the Physical model

5.1.2 Test 1: Water Only Test

The first test proceeded without incident. Figure 5.3 below describes graphically the headloss due to the slots (Loss A) versus the flowrate for a fully flowing ø250mm slotted pipe.

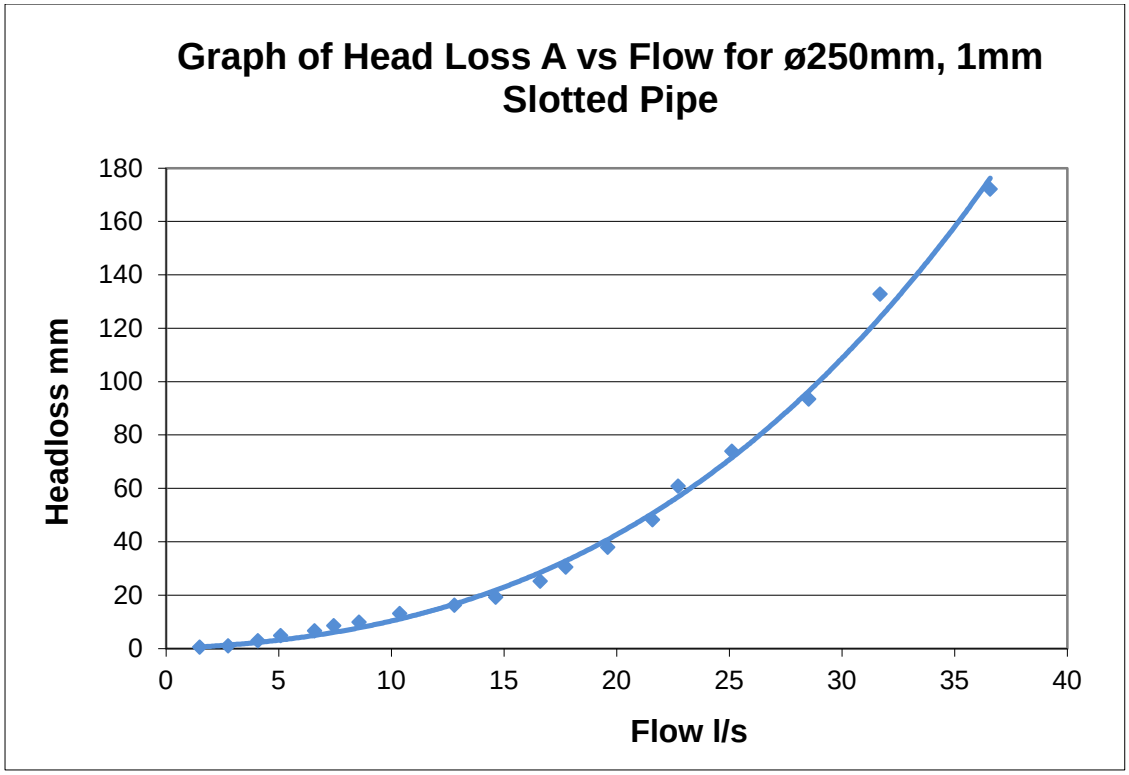

Figure 5.3: Headloss, (Loss A) versus the flowrate for a fully flowing ø250mm Slotted pipe

The equation below describes the relationship between headloss due to slot friction and flowrate

$$\Delta P = 0.05178Q^2 + 0.32059Q \qquad \text{(Eqn1)}$$

With

ΔP = Headloss due to slot friction in mm

Q = Flowrate in litres/second

5.1.3 Test 2: Water and Stone Test

The second experiment saw the use of 19mm stone as bedding and blanketing material. The intake pipe was entirely contained within 19mm Stone benching medium, Figure 5.4. This experiment process was uncomplicated and similar to the previous experiment. Figure 5.5 describes the headloss due to the slots (Loss A) and the loss due to stone and slot friction, versus the flowrate for a fully flowing ø250mm slotted pipe.

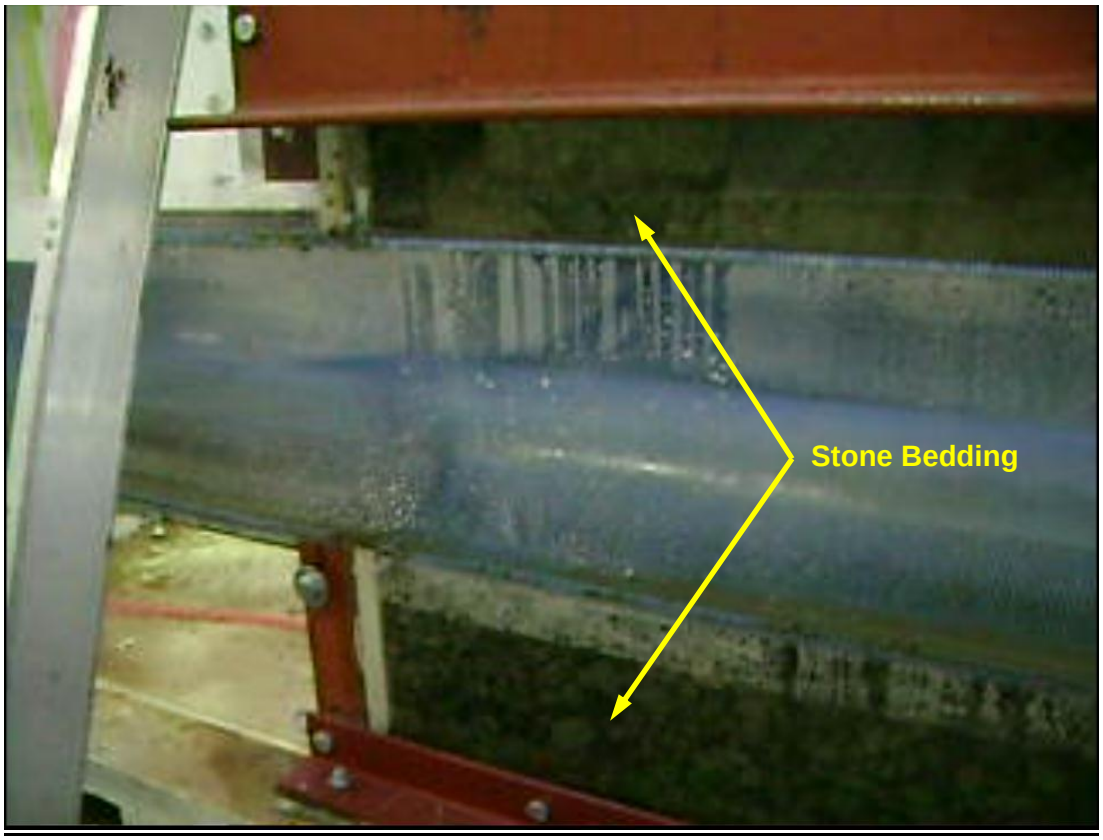

Figure 5.4: ø250mm slotted pipe with stone bedding and blanket

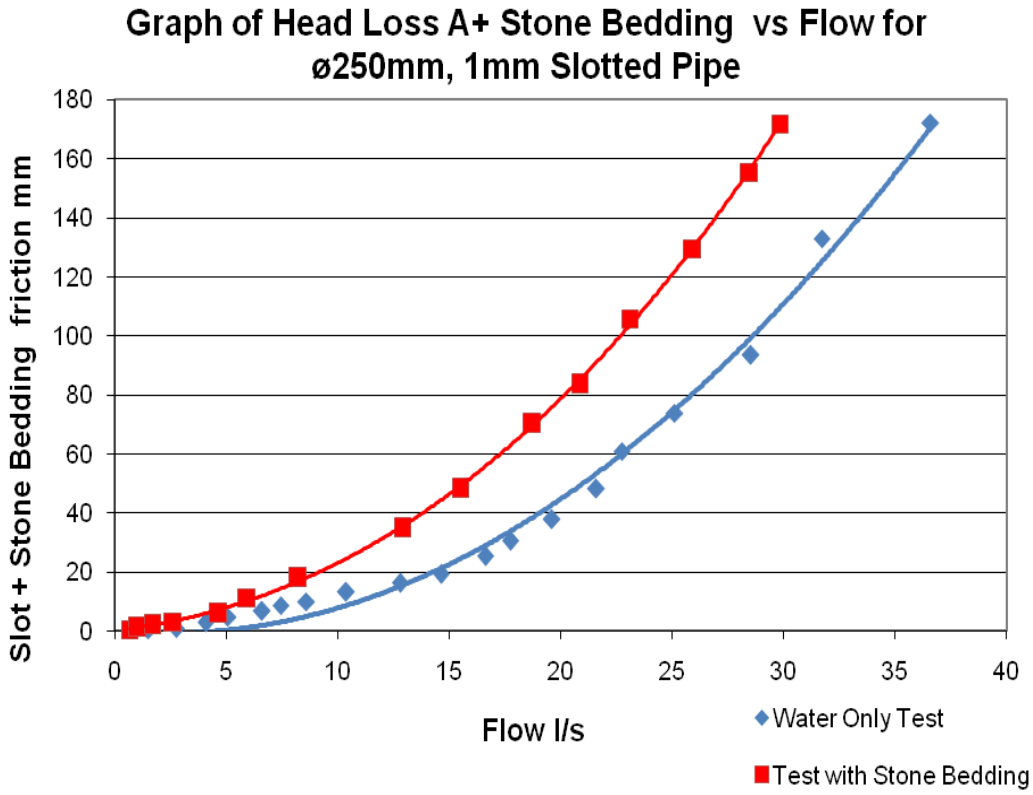

Figure 5.5: Headloss due to Slot Friction and Stone bedding including Slot friction

The equation below describes the relationship between headloss due to Stone Bedding and slot friction versus flowrate

$$\Delta P = 0.13092Q^2 + 0.87249Q \quad \text{(Eqn 2)}$$

The equation below describes the relationship between headloss due to slot friction only versus flowrate

$$\Delta P = 0.05178Q^2 + 0.32059Q \quad \text{(Eqn 1)}$$

With
ΔP = Headloss due to slot friction in mm
Q = Flowrate in liters/second

Hence using Method 1, the loss due to the Stone bedding alone (Equation 3), would be Equation 1 minus Equation 2

$$\Delta P = 0.07914Q^2 + 0.5519Q \quad \text{(Eqn 3)}$$

5.1.4 Test 3: Water, Stone and Sand Test

5.1.4.1 Introduction

Although the seawater intake is to be installed in a rocky coastline, due to the highly dynamic nature of coastlines, the presence of sand can be expected. Hence the ingress of sand into the seawater intake should be considered.

For design purposes, a conservative approach was taken. In the HPM, the stone bedding surrounding the slotted pipeline was considered to be saturated with sand. The sand is a mixture of a fine grained ‘beach’ sanded called Philippi and a ‘single sized’ granular filter sand which is normally used as filter material. The grading in Figure 5.6 below, shows the grading of the sand. More details concerning the sand can be found in Appendix C

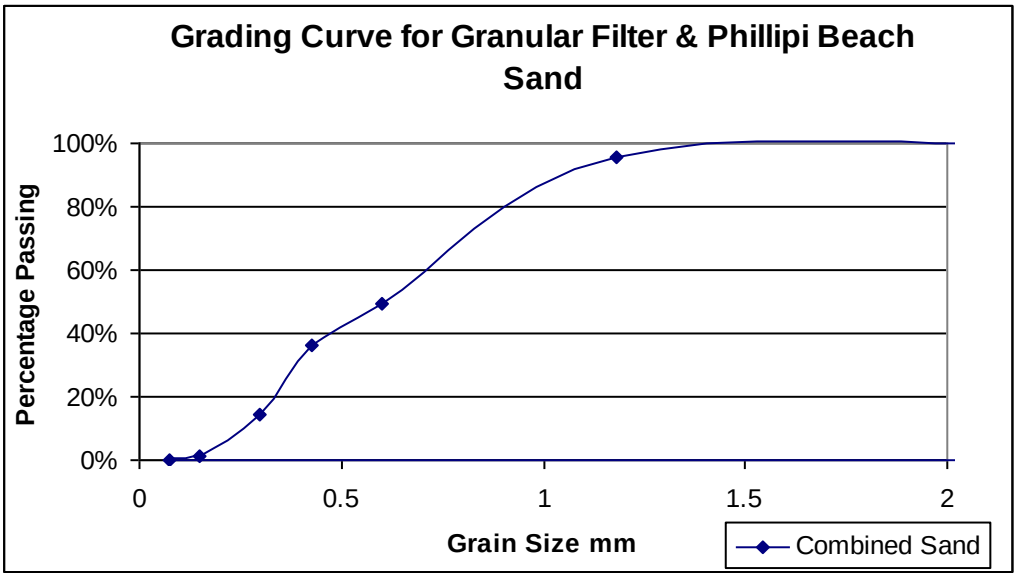

Figure 5.6: Partial grading curve for combined Phillipi and Granular Filter sand

5.1.4.2 Testing

The test commenced with the sand and stone mixture insitu. However considering
1) the slot widths for the intake pipe to be 1mm and
2) the grading curve of the sand content, Figure 5.6,

clogging of the seawater intake pipe was inevitable.

Figure 5.7 below shows the sand and stone material surround the intake pipe. It can be seen that the fine material from below, has seeped into the pipe. This material is still in suspension due to the flow in the pipe being very slow. Increasing the driving head had no effect on the rate of flow through the HPM which remained below 0.5l/s. Figure 5.8 shows the headloss and flowrate the over a 3 hour test period.

Figure 5.7: Sand and stone material surrounding the intake pipe

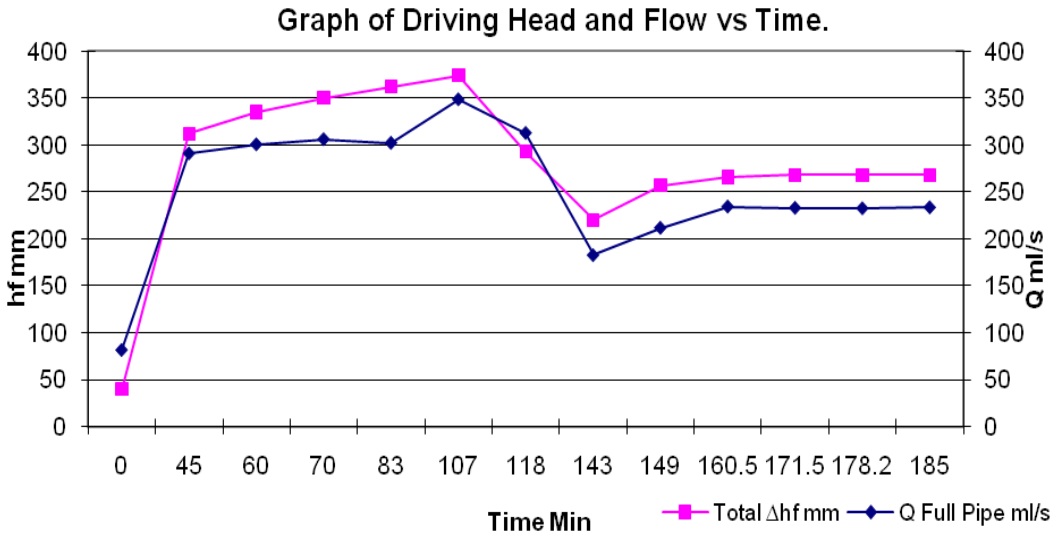

Figure 5.8: Headloss and rate of flow for a 3 hour test period

Due to the severely restricted flow, it was impossible to decipher a flow versus headloss relationship. Hence the design of such a Seawater Intake pipeline was considered a failure, as the flow rate was a fraction of the 80l/s design flowrate.

In order to make the Seawater Intake operational an augmentation or entire redesign of the intake had to be undertaken. It was decided that an augmentation of the design would be undertaken and hence a back flushing system was proposed. The aim of the back flushing system is to dislodge sand from the voids in between the stone bedding and pipe perforations.

5.1.5 Backflushing

5.1.5.1 Introduction

The process of backflushing is fairly common and is used to dislodge material that has become lodged in another medium. Water is the most common element used to conduct back flushing, although gases are sometimes used. The main attributes in the various types of back flushing are namely the velocity and the flowrate of the material used. Depending on their requirement, high velocity flows are usually used to physically dislodge material while high flow rates are indicative of the volume of material that has to be displaced.

5.1.5.2 Design of Flushing System

It was initially decided that the high velocity option would be used as this would remove all sand particle lodged in the slots of the intake pipeline. The design concept was to insert a 15mm pipe down the entire length of the intake pipeline. Small diameter holes were drilled down the length of the pipe in order to create high velocity flows. The flushing pipe would be centralised with the aid of spacers. Pumps then delivered water at a pressure of 7 bar.

In order to have positive radial flushing flow, it was important to seal the open end of the intake pipe during the flushing operation. Figures 5.9 and 5.10 describe the flushing apparatus layout.

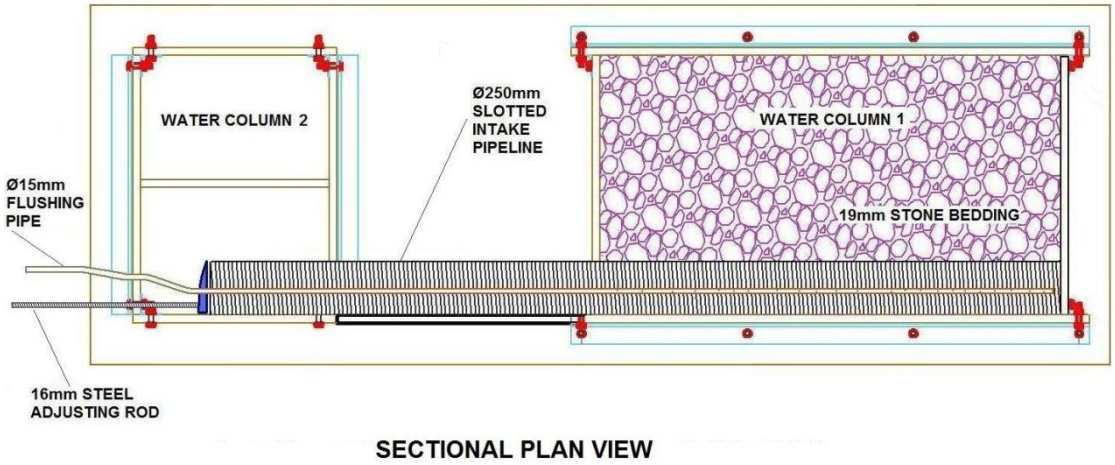

Figure 5.9: Horizontal section through middle of Intake Pipeline

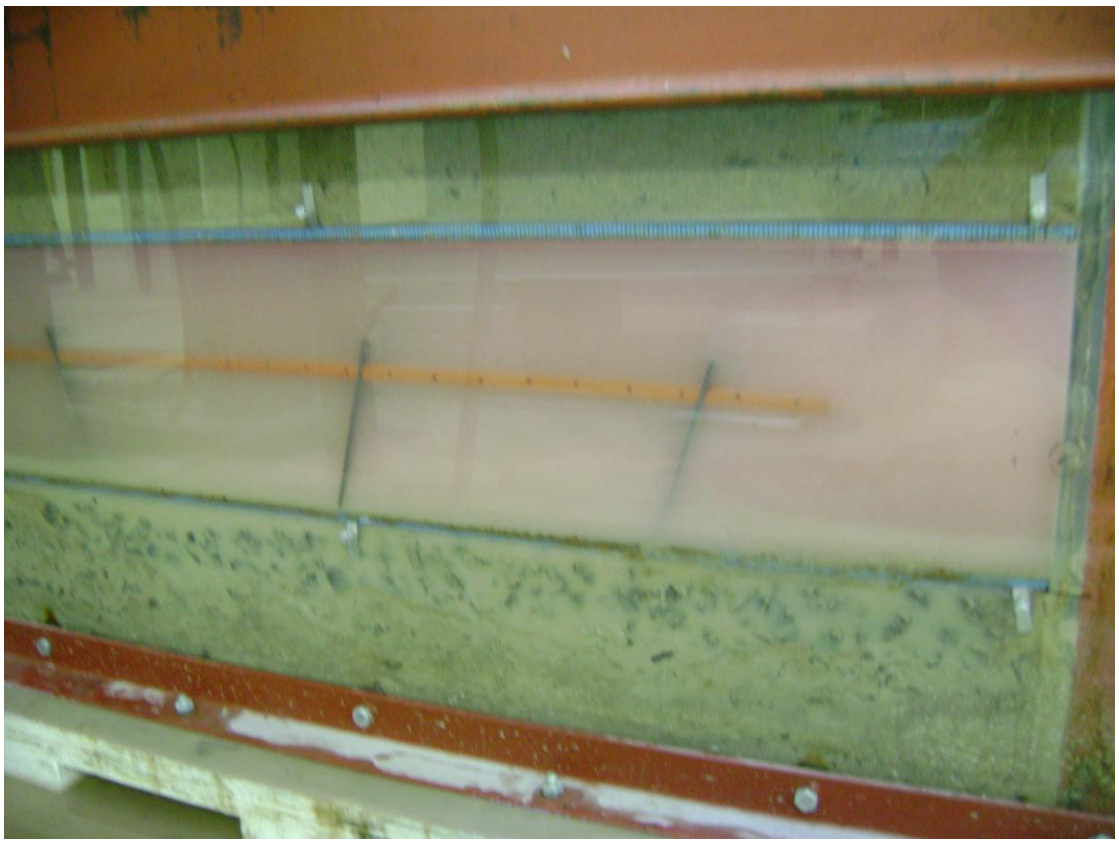

Figure 5.10: 15mm flushing pipe. Note the holes/ports and black spacers that hold the pipe in the center of the Intake pipeline

5.1.5.3 Augmentation of Flushing System

The initial flushing system, did not function satisfactorily as it did not provide the required results. Figure 5.11 below shows the plan view of Water Column 1 after the first backflushing event. At 7 bar of pressure, the flushing flow flowed vertical through certain pathways and only managed to dislodge a very small portion of the sand from the sand and stone mixture.

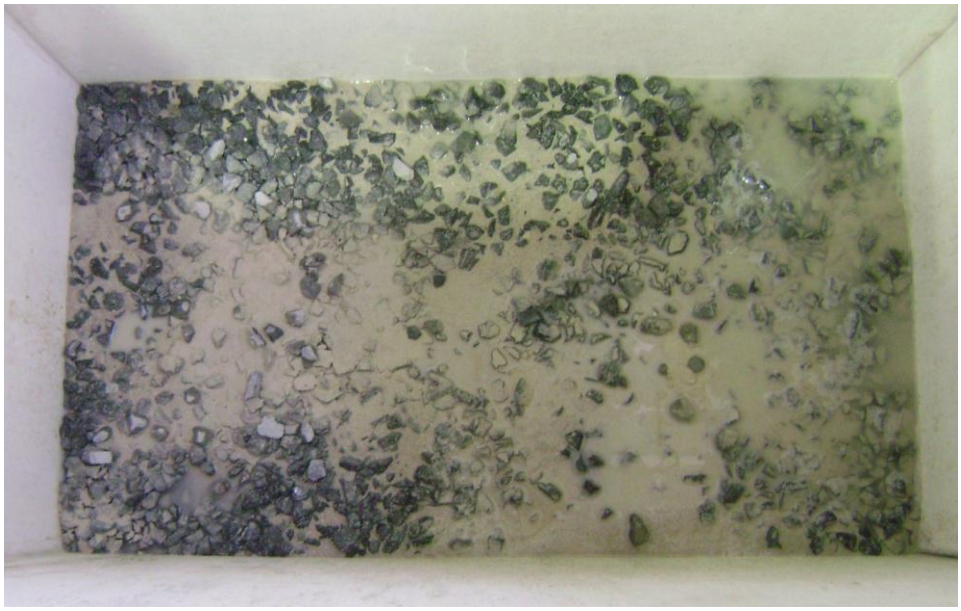

Figure 5.11: Plan view of water column 1. Sand and 19mm stone mix after flushing with water. Note the Intake pipe runs along the upper edge

As can be seen in Figure 5.11 above, the use of high velocity water is not effective in removing the sand from the stone bedding. Hence a method was required that would physically displace the sand. Increasing the flow was not an option as the increased volume of water rose to the surface via the already established pathways. Hence it was decided that air be used to aid with the removal of sand from the bedding.

The first hurdle was to ensure that the delivery of the air and water components of the flow, were equal. Due to the pressure difference between the delivered air and water, a manifold was used to create a mixture of water and air, Figure 5.12. With the pressure of water being preset at 7 bars, the pressure and flow of the air had to be adjusted.

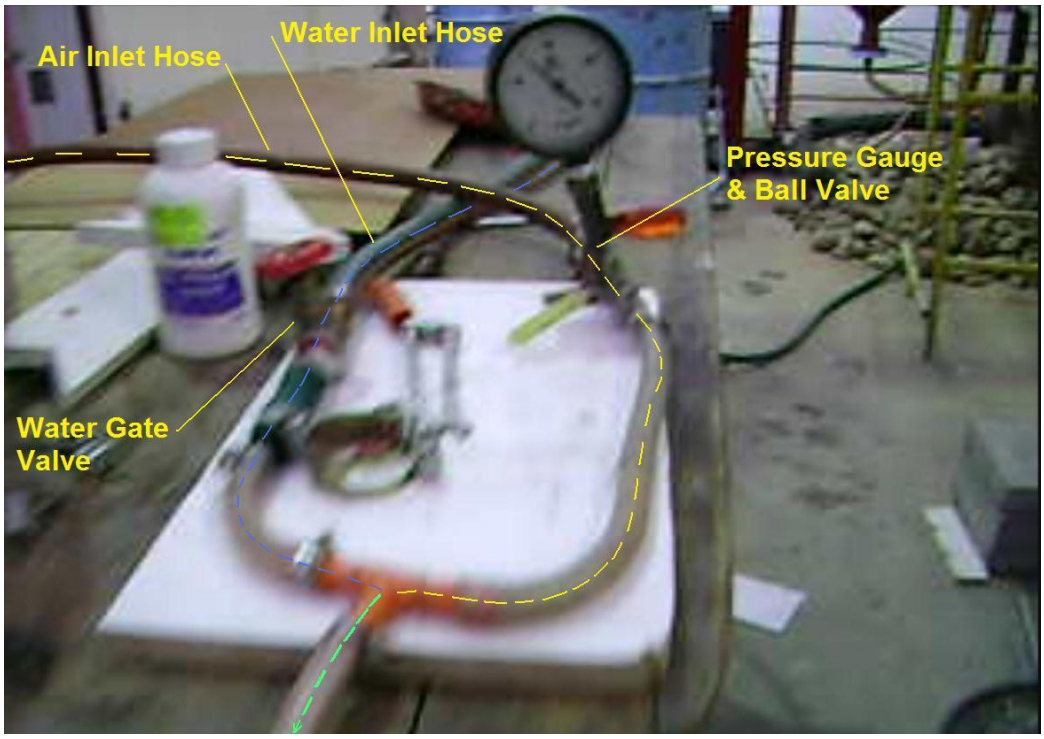

Figure 5.12: A manifold used to create a mixture of water and air

The mixture of air and water was feed into the flushing line. Figure 5.13, the addition of air helped dislodge sand from the bedding. This can be identified in Figure 5.13 as the dark portions of the bedding where sand has been removed

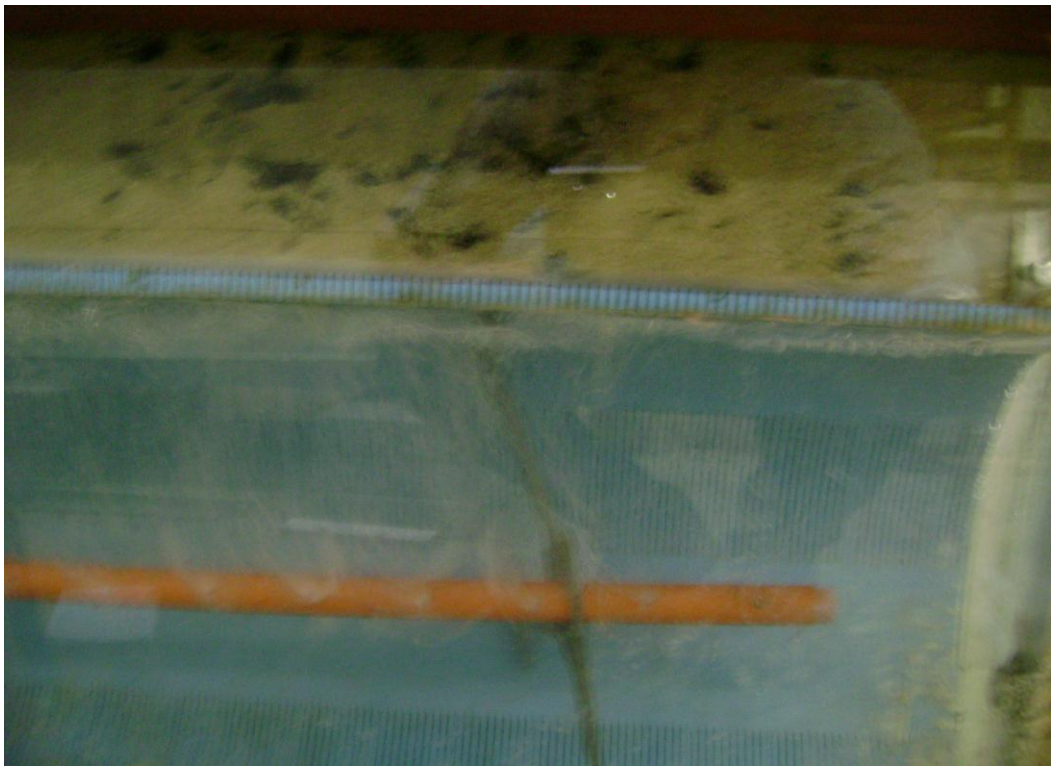

Figure 5.13: Air and water mixture flowing out the flushing pipe, Flow of air from holes seen as white plumes

The combined use of air and water proved advantageous. The flushing flow eventually removed all the sand immediately above the Intake pipeline, Figure 5.14, This sand was then deposited as a sand bank which was formed parallel to the Intake pipeline. The oblique view in Figure 5.15 is of WC1 taken in the easterly direction. This shows the sand bed to be 30mm at its highest point.

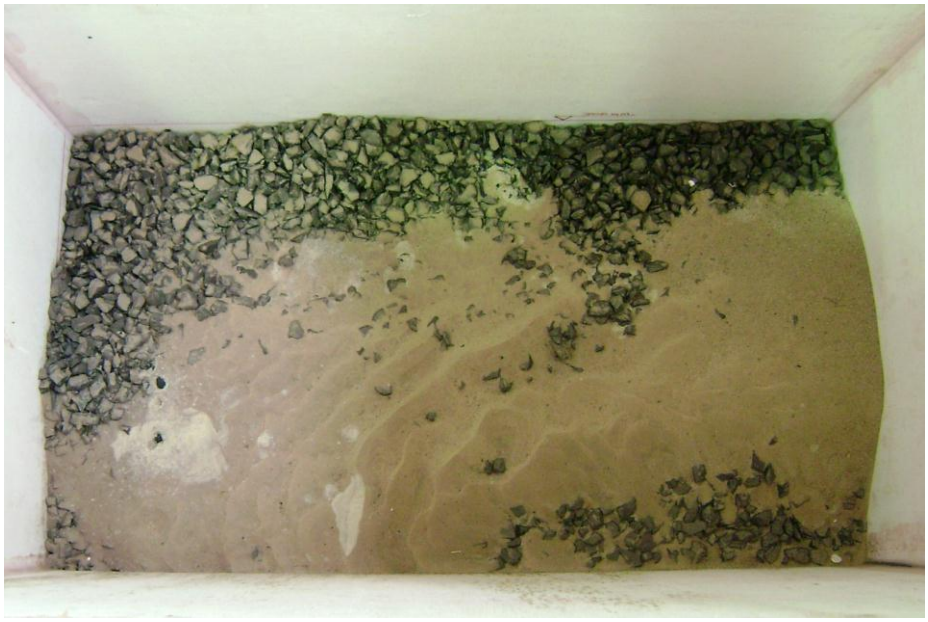

Figure 5.14: Plan view of water column 1. Sand and 19mm stone mix after Flushing with water and air. Note the Intake pipe runs along the upper edge

Figure 5.15: Oblique view of water column 1. Sandbar on Bedding after Back flushing with air and water. Intake pipe runs along the left edge

5.1.6 Test 4: Water, Stone and Sand Test after Back Flushing

After examining the results of Test 3 (Before Back Flushing), a steady flow of approximately 0.23l/s was attained for a driving head of 0.175m. This was far less than the required flow. This low flow was due to the presence of sand in the bedding which effectively reduces the number of pathways allow water to flow through.

After back flushing with water alone proved ineffective, air was added to the back flushing water and it evident from Figures 5.14 and 5.15 that sand was physically removed from areas above the intake pipeline. Thereafter Test 4 was conducted. In relation to Test 1 and Test 2, this test was time based. Figure 5.16 below shows the results of the test.

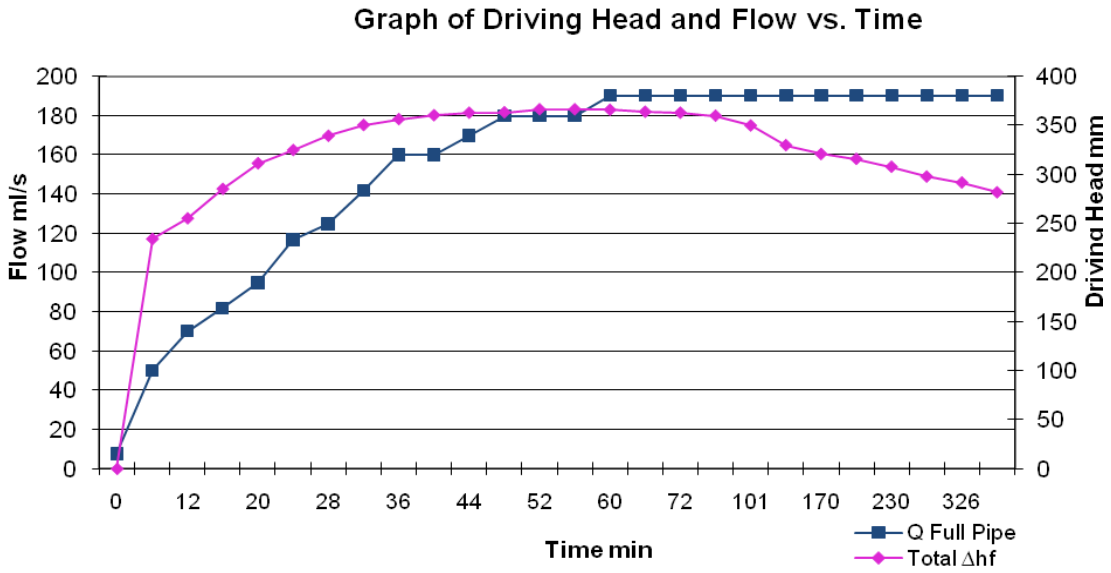

Figure 5.16: Headloss and Rate of Flow for a 6.5hour test period. After back flushing

The results of Test 4 show that after an hour, a steady flow of approximately 0.19l/s (0.38l/s for a full pipe) was attained. After an hour, the driving head was approximately 0.36m. However this decreases until the driving head is 0.28m after 6.5hours. This is far less than the flow rate before the back flushing (0.23l/s). A possible explanation for this lower flow rate is as follows. During the back flushing, sand was removed from the area directly above the pipe. This sand settles on the adjacent area, effectively sealing a portion of the surface. Seen in Figure 5.14, 70% of the surface is covered with sand. Hence the numbers of flow paths have been significantly reduced, thus lowering flow through the model. Hence it can be concluded that since back flushing was not successful, this pipe type would not be successful if a sand-rock mixture was encountered.

5.2 Perforated PVC Pipe Abstraction Model

5.2.1 Synopsis

The following is a chronological summary of the tests conducted on the Perforated PVC Pipe. Figure 5.17 shows a typical perforated PVC pipe. All holes are ø8mm. Figure 5.18 shows the pipe used in the first test. This test was conducted utilising water only. This test showed that the flow was comparatively low. It was approximately half the flow rate of the Slotted PVC pipe.

For Test 2, more holes were then drilled into the pipe in order to increase the flow rate, Figure 5.19. For the third test, 19mm stone bedding was placed around the pipeline. The fourth test saw sand being used to fill the voids between the stone bedding

Figure 5.17: Typical Perforated PVC Pipe, similar to pipe used in Test 2

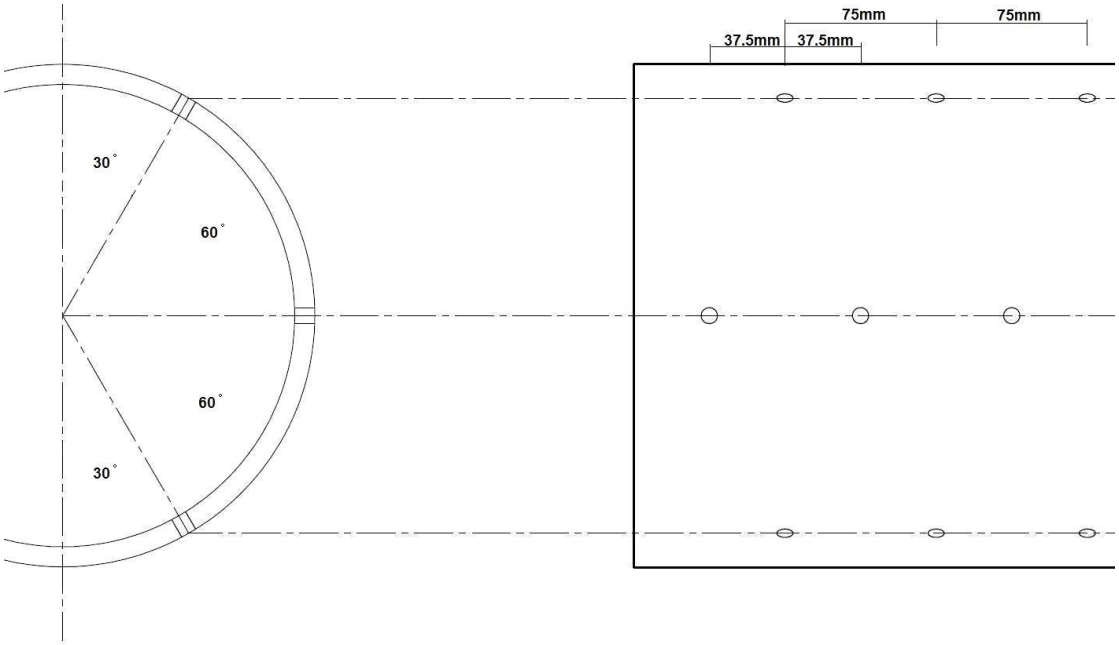

Figure 5.18: Section and Elevation of ø250mm Perforated PVC Pipe

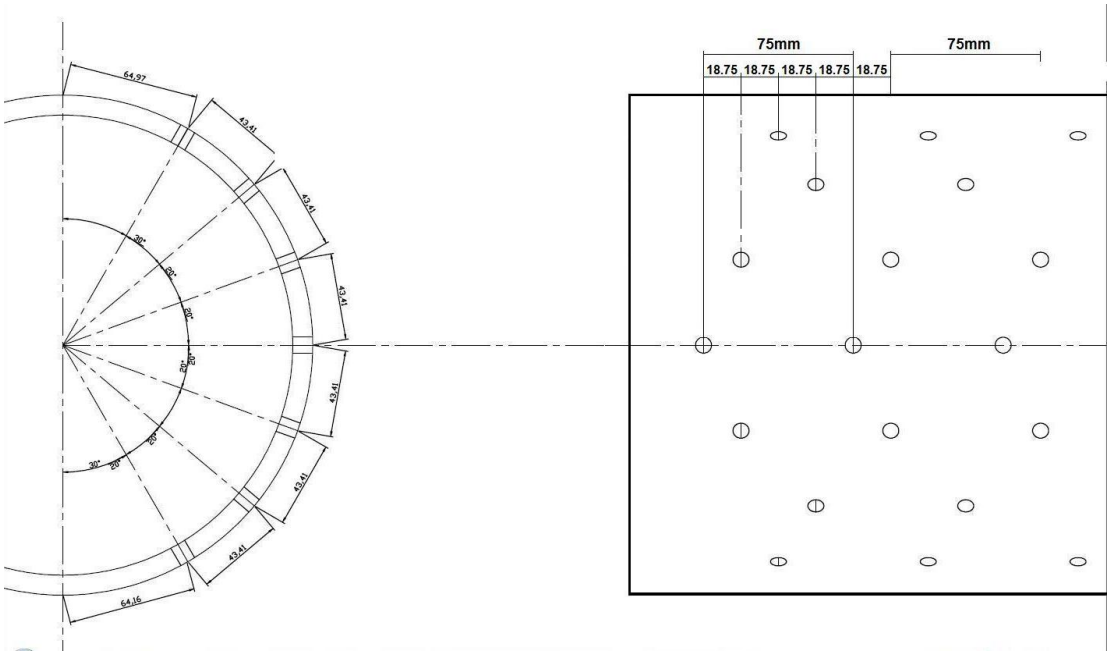

Figure 5.19: Section and Elevation of Extra Perforated ø250mm Perforated PVC Pipe

The first three tests proceeded well. In the fourth test, sand flowed out of the sand and stone mixture and filled the pipeline. Only due to scouring flow was the pipe not blocked. The system of back flushing was not required as the flow between WC1 and WC2 was capable of removing all the sand. The movement of this sand was akin to the migration of Dunes. The front face of the dune progresses forward due to continuous new material being supplied by the flow of water, Figure 5.25

5.2.2 Test 1: Water Only Test

The first test aims to measure the relationship between flowrate and the headloss due to perforation. Figure 5.20 below describes the headloss due to the holes (Loss A) versus the flowrate for a fully flowing ø250mm perforated pipe.

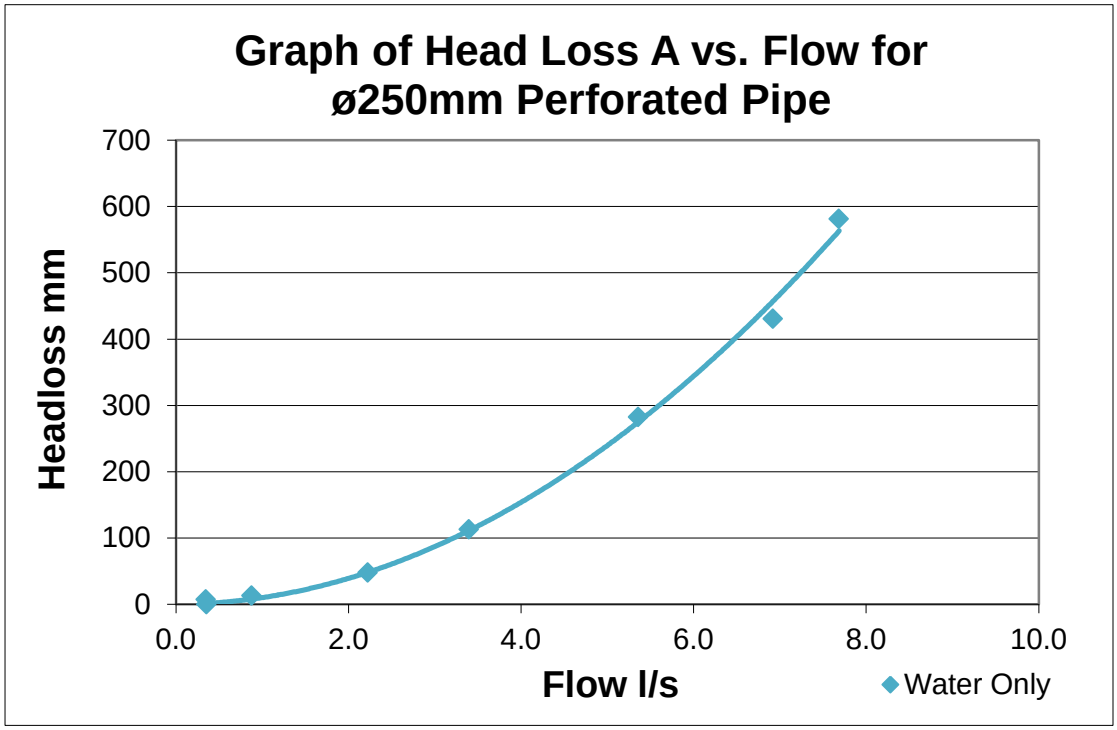

Figure 5.20: Headloss due to perforation (Loss A) versus the flowrate for a fully flowing ø250mm perforated pipe

The equation below describes the relationship between headloss due to slot friction and flowrate

$$\Delta P = 5.464Q^2 + 0.722Q \qquad \text{(Eqn 4)}$$

With

ΔP = Headloss due to slot friction in mm

Q = Flowrate in liters/second

5.2.3 Test 2: Water Only Test with Extra Perforation

The flowrate in the previous test, when compared to test 1 of the Slotted PVC pipe, was low. Hence it was decided to increase the number of holes in the pipeline. Initially the perforated pipeline has three holes per 75mm. Referring to Figure 5.19, four additional holes per 75mm was added. This increased the infiltration area by 133%. Figure 5.21 below describes graphically the headloss due to the holes (Loss A) versus the flowrate for a fully flowing ø250mm Extra Perforated pipe.

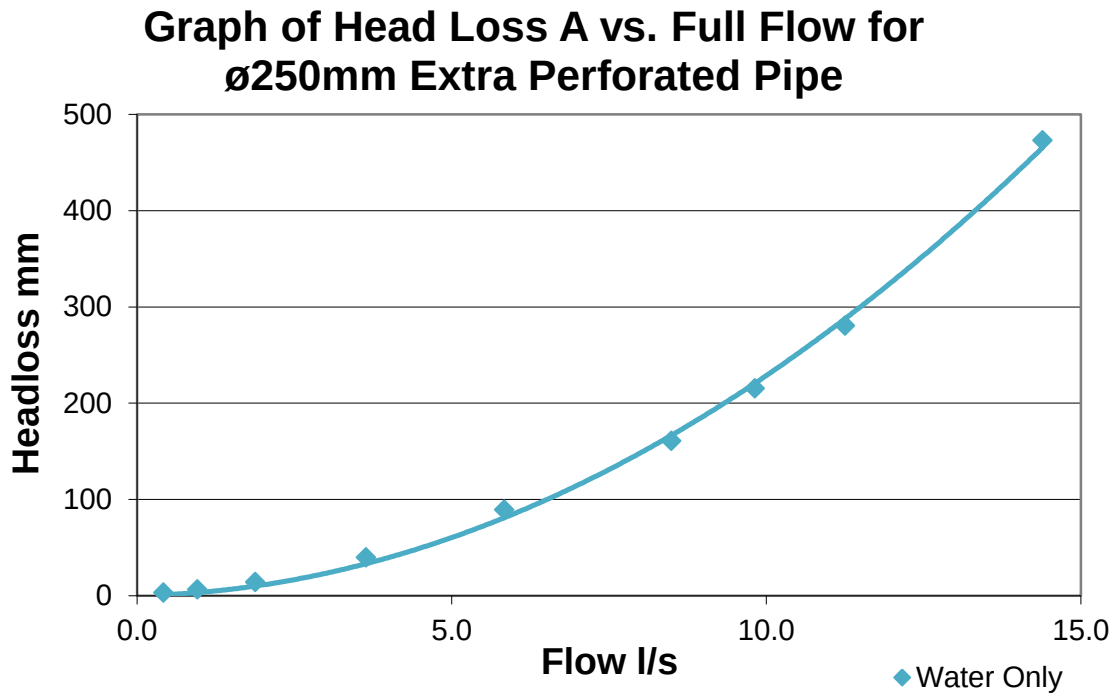

Figure 5.21: Headloss due to extra perforation (Loss A) versus the flowrate for a fully flowing ø250mm Perforated pipe

The equation below describes the relationship between headloss due to perforation friction and flowrate

$$\Delta P = 0.891Q^2 + 1.286Q \qquad \text{(Eqn 6)}$$

With

ΔP = Headloss due to slot friction in mm

Q = Flowrate in liters/second

5.2.4 Test 3: Water and Stone Test

The remaining two tests make use of the extra perforated pipe. In Test 3, 19mm stone is used as bedding and blanketing material. Figure 5.22 below describes graphically the headloss due to the slots (Loss A) and the loss due to 19mm stone and slot friction, versus the flowrate for a fully flowing ø250mm extra perforated pipe.

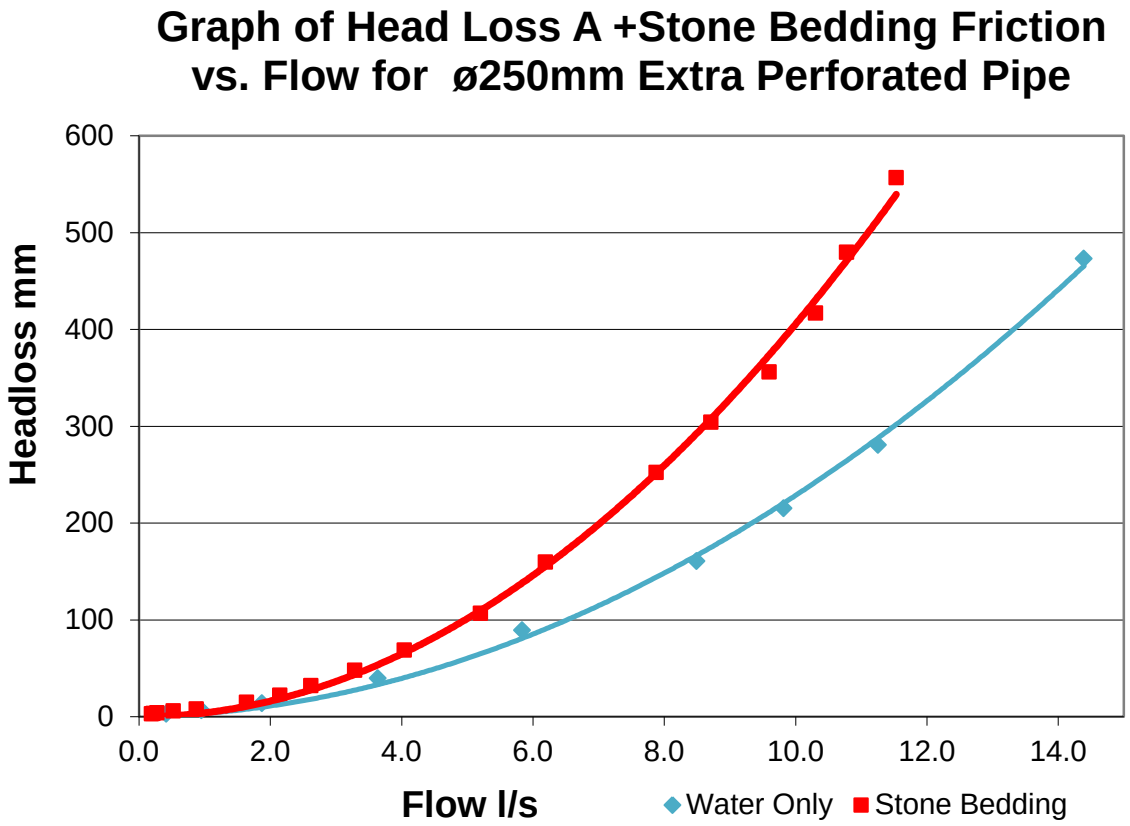

Figure 5.22: Headloss due to Perforation Friction only and Stone bedding including perforation friction

The equation below describes the relationship between headloss due to Stone Bedding and perforation friction versus flowrate

$$\Delta P = 2.066\ Q^2 + 0.019\ Q \qquad \text{(Eqn 7)}$$

The equation below describes the relationship between headloss due perforation friction only versus flowrate

$\Delta P = 0.891Q^2 + 1.286Q$ (Eqn 6)

With

ΔP = Headloss in mm

Q = Flowrate in liters/second

Hence using Method 1, the pressure loss due to the Stone bedding alone Equation 8, would be Equation 6 minus Equation 7

$\Delta P = 1.175Q^2 – 1.267Q$ (Eqn 8)

5.2.5 Test 4: Water, Stone and Sand Test

5.2.5.1 Introduction

Once again the ingress of sand into the seawater intake was considered. The stone bedding surrounding the perforated pipeline was considered to be saturated with sand. The grading of the sand can be found in Appendix C

5.2.5.2 Testing

Pretesting

The test commenced with the sand and stone mixture being insitu. Due to the perforations on the Intake pipe being ø8mm, any sand near a hole was transported into the Intake pipeline while the HPM was being primed. This can be seen in Figure 5.23 below.

Figure 5.23: Sand ingress into Intake Pipeline before testing can commence

Note that the displacement of sand was due to the flow of water and not only gravity. This is evident by the voids in the bedding below the Intake Pipe.

Testing

The test commences with the initial flow into the intake pipeline, occurring closest to WC2. This is evident by the suspended material in Figure 4.36. This is foreseeable as the maximum ingress velocity occurs at a point closest to WC2. With the initial driving pressure head not being changed, the mounds of sand within the Intake Pipe began to grow, Figure 5.24 and 5.25.

Figure 5.24: Sand ingress into Intake Pipeline when testing commences

Figure 5.25: The growth of sand mounds within the Intake Pipeline

The growth of the sand mounds increase until the minimum area required for flow is reached. With the constriction of area, there is an increase in flow velocity in this area. When the flow area becomes too small, the flow starts to scour sand in the region of the constriction. Thereafter the sand falls out of suspension as the flow area increases. This scour and deposition of sand aids the development of the front face of the “sand dune”

The front face of the dune can be seen more clearly in Figure 5.26. The development of this surface in important as it indicates when equilibrium or stability of the sand mounds has been achieved. If the front face of the sand mound does not develop, it implies that for a certain flow rate, there is no net ingress of sand into the Intake Pipeline; hence the driving pressure head can be easily measured.

Figure 5.26: Development of front face of 'dune' seen as angular stratified layers of sand

The driving pressure was incrementally increased 6 times whenever the ingress of sand into the pipeline became insignificant. On the fifth test, the ingress of sand was at a negligible level and the pipe had begun to scour clean, Figure 5.27. In total seven tests were conducted and Figure 5.28 depicts the relationship between flow and 1.) the Headloss due to Perforation Friction; 2.) Headloss due to Perforation friction and Stone bedding and 3) Headloss due to Perforation friction, Stone and Sand bedding

Figure 5.27: Front face of the dune has reached WC1 and the Intake pipeline has started to scour clean

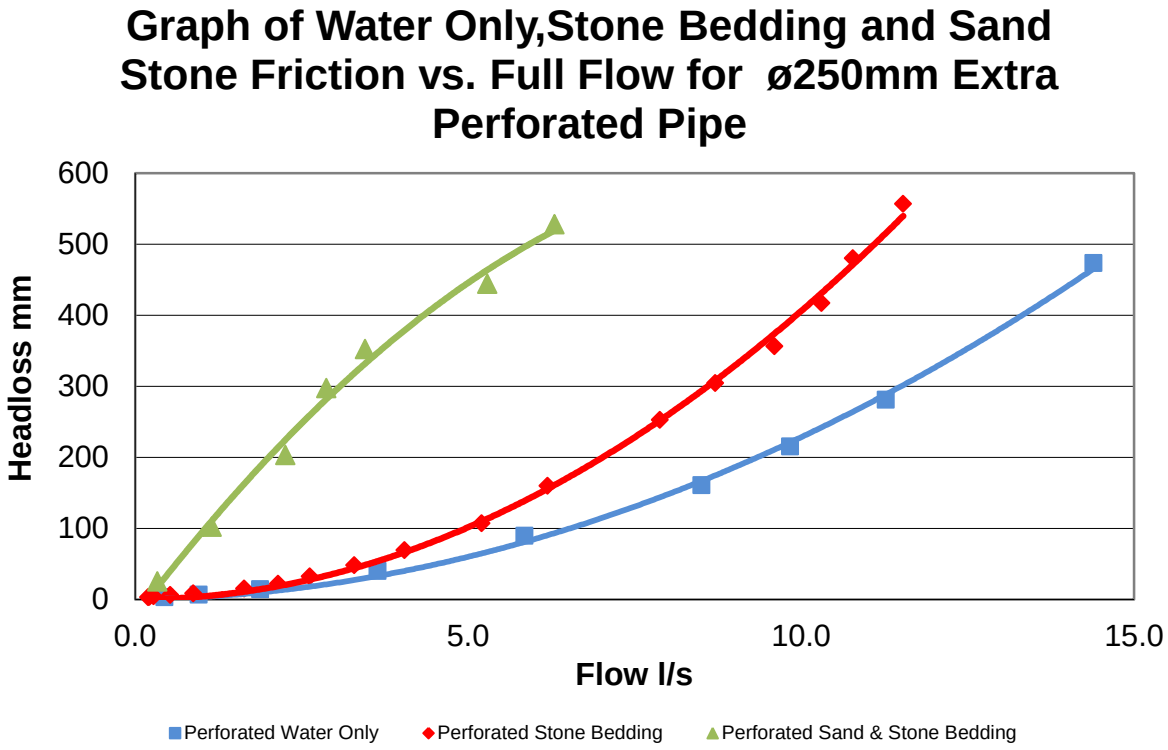

Figure 5.28: Headloss due to Perforation Friction; Headloss due to Perforation friction and Stone bedding; and Headloss due to Perforation friction, Stone and Sand bedding.

This extra perforated pipe with a porosity of 1.27% has the lowest flow rate per headloss in comparison to the Slotted and Metal Wire Pipe. However, this pipe has not blocked up with the addition of sand to the stone bedding. If this pipe is to be used as an intake pipe, the seawater intake design has to allow for sand to be transported from the stone bedding, through the intake pipe and deposited in the collection manhole. Hence a minimum scour flow velocity of 0.7m/s should be maintained to ensure that sand is not deposited on the pipe floor, but transported into the collection chamber.

5.3 Metal Wire Pipe Abstraction Model

5.3.1 Synopsis

Only two tests were conducted on the Metal Wire Pipe, Figure 5.29 and 5.30. The first test was conducted utilising water only. Thereafter 19mm stone bedding was placed around the pipeline for the second test. The test for sand and stone bedding was not considered based on the unsatisfactory results of the test on the Slotted PVC pipe.

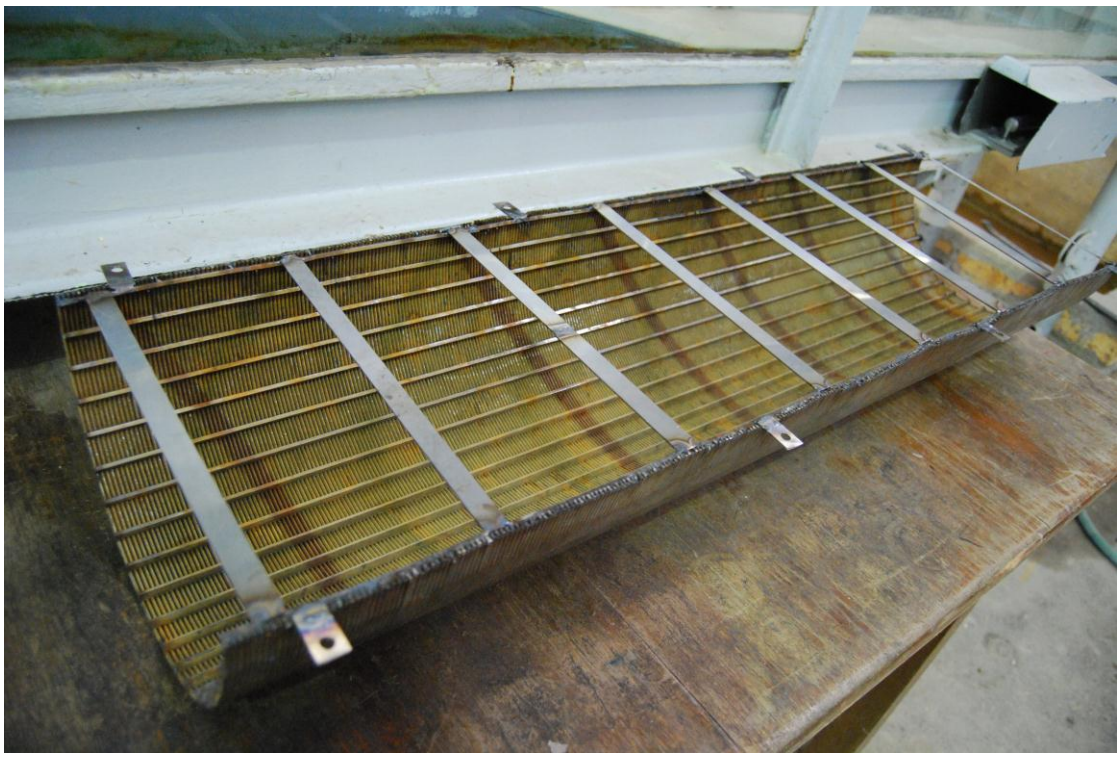

Figure 5.29: Internal View of half a ø250mm Metal Wire Pipe

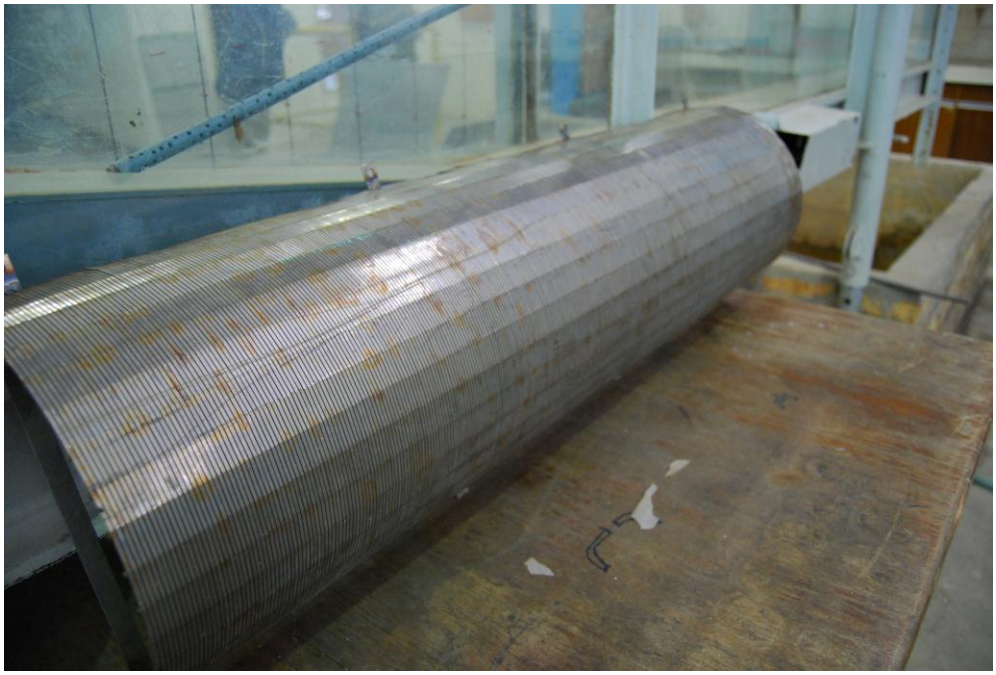

Figure 5.30: External View of half a ø250mm Metal Wire Pipe

5.3.2 Test 1: Water Only Test

The water only test proceeded satisfactorily. Figure 5.31 below describes graphically the headloss due to the grooves (Loss A) versus the flowrate for a fully flowing ø250mm Metal Wire Pipe.

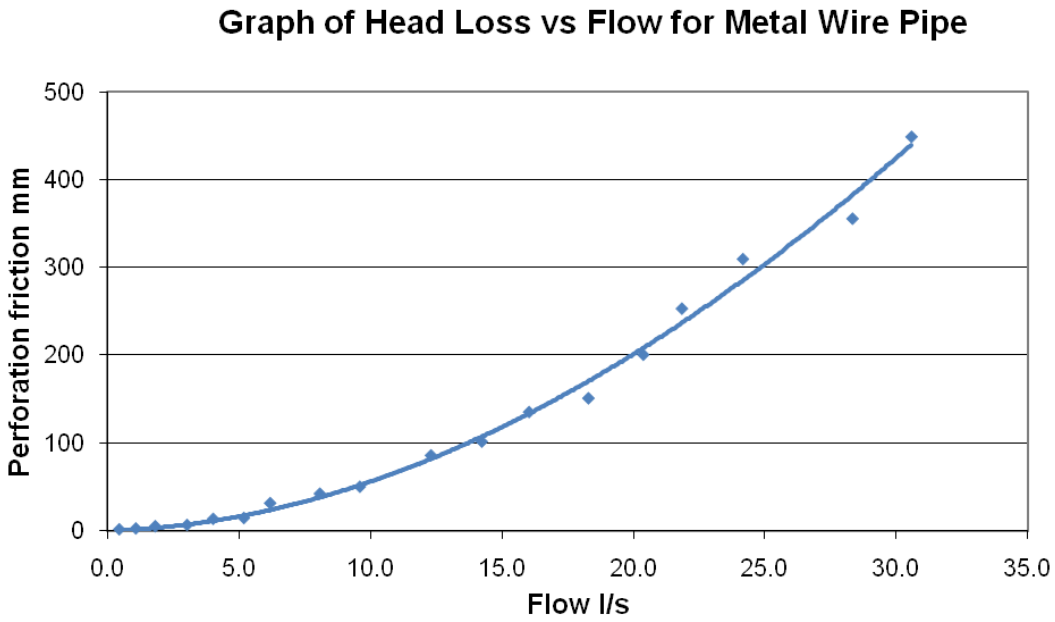

Figure 5.31: Headloss due to the Slots (Loss A) versus the flowrate for a fully flowing ø250mm Metal Wire pipe

The equation below describes the relationship between headloss due to slot friction and flowrate

$\Delta P = 0.494Q^2 + 1.443Q$ (Eqn10)

With

ΔP = Headloss due to perforation friction in mm

Q = Flowrate for full pipeline in litres/second

5.3.3 Test 2: Water and Stone Test

The second experiment saw the intake pipe contained entirely within a 19mm Stone benching medium. This experiment process was straight forward and similar to the previous experiment. Figure 5.32 below describes graphically, the headloss due to the slots (Loss A) and 19mm stone. It also describes the headloss due to perforation friction only, versus the flowrate for a fully flowing ø250mm metal wire pipe.

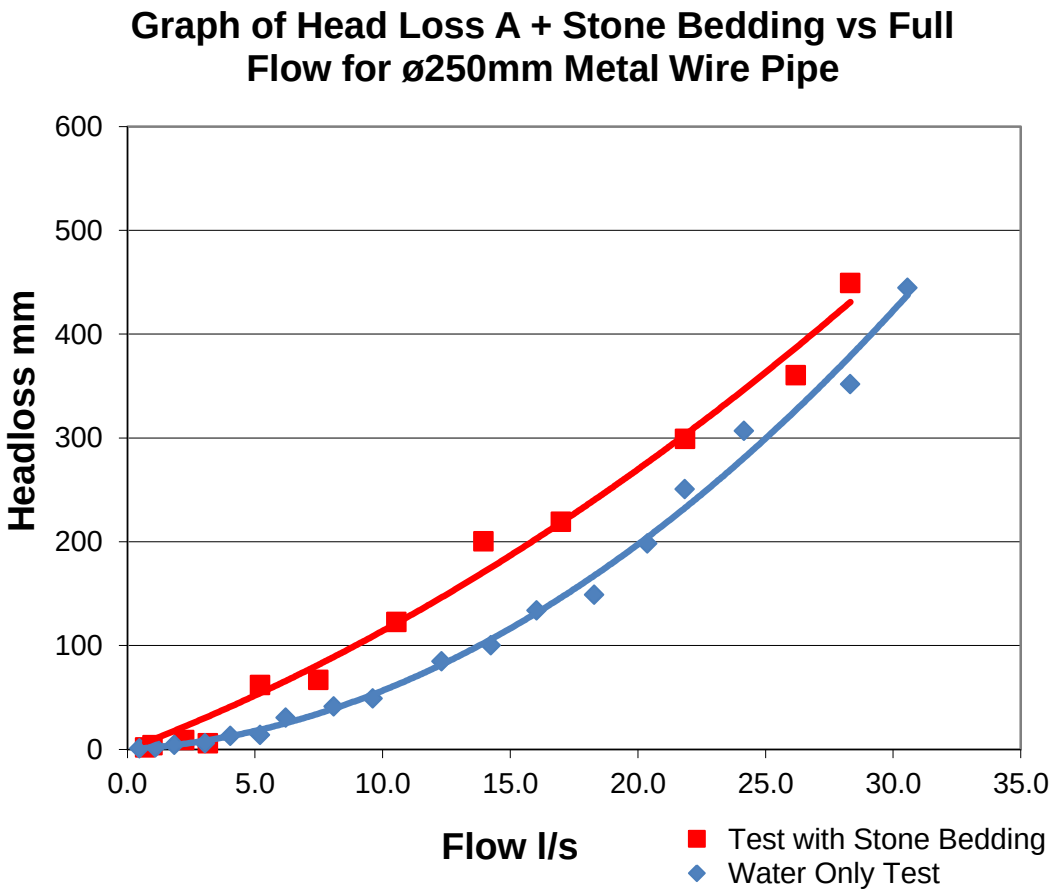

Figure 5.32: Headloss due to Slot Friction and Stone bedding including Slot friction

The equation below describes the relationship between headloss due to Stone Bedding and slot friction versus flowrate

$$\Delta P = 0.2077Q^2 + 9.3323Q \quad \text{(Eqn 11)}$$

The equation below describes the relationship between headloss due slot friction only versus flowrate

$$\Delta P = 0.494Q^2 + 1.443Q \quad \text{(Eqn 10)}$$

Using Method 1, the loss due to the Stone bedding alone, Eqn12, would be Eqn11 minus Eqn10

$$\Delta P = -0.2863Q^2 + 7.8893Q \quad \text{(Eqn 12)}$$

With
ΔP = Headloss due friction in mm
Q = Flowrate in liters/second

The tests on the Metal Wire Wipe proceeded without incident. Test 1: At a particular headloss value, this pipe type had flow values higher than that of the extra perforated pipe but values lower that of the slotted PVC pipe. The headloss values for this pipe was in between the Extra perforated and the Slotted PVC pipes.

Chapter 6

6. DISCUSSION OF CASE STUDY TEST RESULTS

6.1 Introduction

The following is a summary and discussion on the experiments conducted on the three intakes pipes used in a horizontal well configuration. The first sub chapter reviews the water only test for all three pipes; the second sub chapter reviews the tests when 19mm Stone bedding was used. The third chapter reviews the tests when sand was added to the stone bedding.

Note that the term, “Half Flow” refers to the actual flow rates recorded for the tests. As this flow rate is due to only half a pipe being used, the flowrate for a whole can be obtained by doubling the test flowrate. This is termed “Full Flow”. The headloss due to friction would remain the same as the friction effects would be mirrored by the “other half’” of the test pipe. Hence the most applicable practical points are used to substantiate the design recommendations.

6.2 Water Only Tests

6.2.1 Test Results

Slotted PVC Pipe

This slotted pipe is a locally produced conduit that is manufactured in the Johannesburg, South Africa (SA) region. Hence its immediate availability is advantageous. This pipe wall has a porosity of 23.7%, which is the highest for all three pipes tested.

Perforated PVC Pipe

This pipe is commonly used as an agricultural drain. It is locally produced and is manufactured in all major cities in SA. The pipewall with extra perforation has a porosity of 1.27%, the lowest of all three.

Metal Wire Pipe

This pipe is specialised product that is manufactured by Johnson screens in the United States. Hence its availability cannot always be guaranteed. This pipe has a porosity of 19.3% and can be considered highly pervious.

The following Table 6.1 contains the results of the Water Only Test (WOT) carried out on the four test pipe conduits.

Table 6.1 : Results of Water Only Test carried on the four test pipe

Intake Pipe Types	Slotted PVC Pipe		Perforated PVC Pipe		Perforated PVC Pipe with Extra Perforation		Metal Wire Pipe	
Test No.	Loss A	Q Half Pipe	Loss A	Q Half Pipe	Loss A	Q Half Pipe	Loss A	Q Half Pipe
	mm	l/s	mm	l/s	mm	l/s	mm	l/s
1	0	0.8	0	0.1	3	0.2	1	0.2
2	1	1.4	7	0.1	6	0.5	2	0.5
3	3	2.1	13	0.4	14	0.9	4	0.9
4	5	2.6	48	1.1	40	1.8	6	1.5
5	7	3.3	113	1.7	89	2.9	13	2.0
6	9	3.7	282	2.6	161	4.3	14	2.6
7	10	4.3	431	3.4	215	4.9	31	3.1
8	13	5.2	581	3.8	281	5.6	41	4.0
9	16	6.4			473	7.2	49	4.8
10	19	7.3					85	6.2
11	25	8.3					100	7.1
12	30	8.9					134	8.0
13	38	9.8					149	9.1
14	48	10.8					198	10.2
15	61	11.4					251	10.9
16	74	12.6					307	12.1
17	93	14.3					352	14.2
18	133	15.9					445	15.3
19	172	18.3						

The results of Table 6.1 are plotted in Figure 6.1 below. This shows the comparative flowrates the pressure lost through friction, or in other terms, the head required to drive the flow. The worst performing pipe is the Perforated PVC Pipe (PPP). This pipe with a porosity of 0.57%, recorded a maximum flow rate of 3.8l/s with approximately 0.58m pressure head required to drive this flow into the pipe. This flowrate was considered to be very low and hence a perforated pipe with extra holes was produced in order to increase the flowrate.

This was termed the Perforated PVC Pipe with Extra Perforation (PPPEP). This pipe produced more than twice the flow rate as the PPP and required approximately 100mm less driving pressure than the PPP.

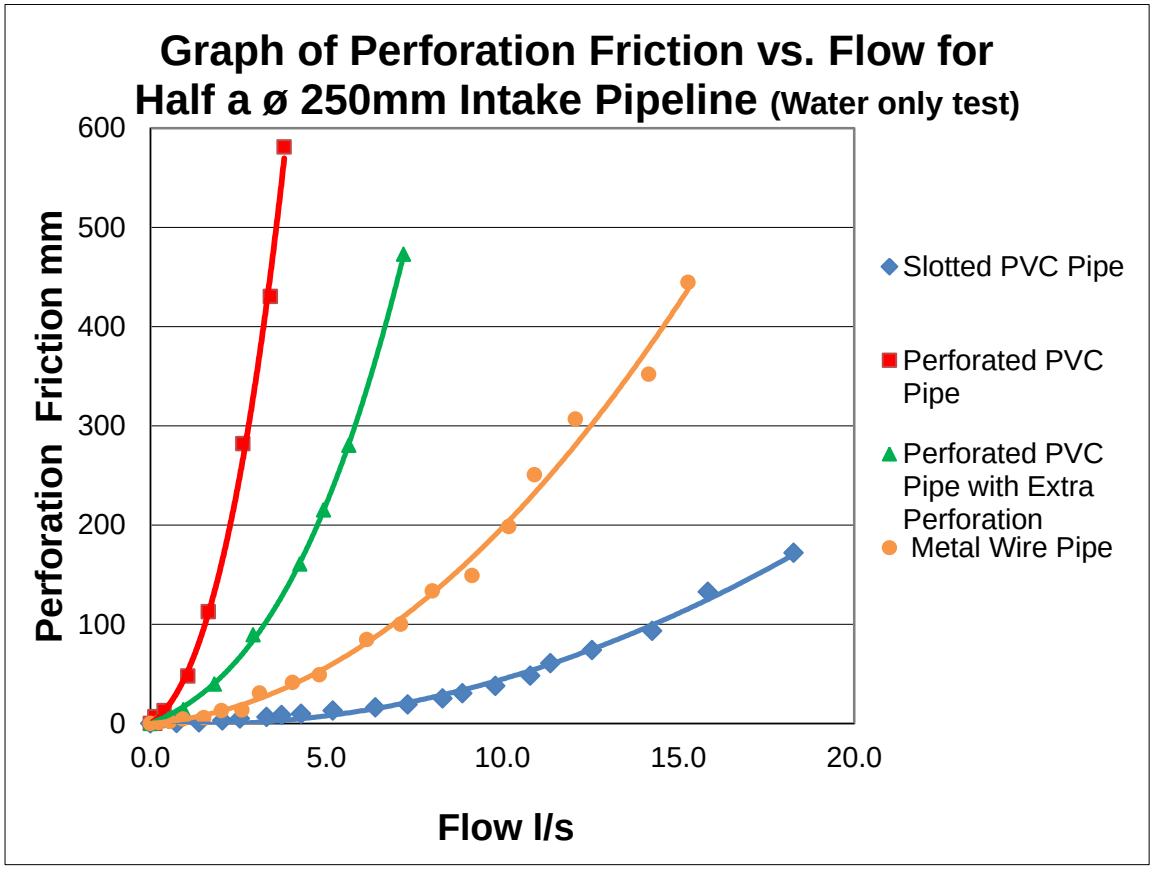

Figure 6.1: Perforation friction for all three intake pipe types

With a porosity of 19.73% the next pipe, according to Figure 6.1, is the Metal Wire Pipe (MWP). This pipe, for a similar driving pressure of 445mm as compared to the PPPEP (473mm) produced more than twice the flowrate as that of the PPPEP (7.2l/s) at 15.3l/s.

Chronologically, the first pipe tested, the Slotted PVC pipe, had the largest perforation area and produced the largest flow for the least amount of the pressure loss. For a driving head of approximately 0.17m, this pipe produced a flowrate of 18.3l/s. Hence on first time observation, the slotted pipe produces the best results.

6.2.2 Porosity versus Flowrate Test

One of the first general speculation made is that the larger the holes in the pipe, the greater the flow. However, when designing an hydraulic structure, the flowrate is only

one of the more important design criteria. Another important factor is the losses in the system. The losses play an essential role in the overall design process. The following Table 6.2 documents the relationship between porosity versus the flowrate divided by the associated headloss for all four intake pipes. Figure 6.2 is a graphical plot of Table 6.2

Table 6.2: Relationship between porosity versus the flowrate divided by the associated headloss for the four test pipes

Description	Unit	Slotted PVC Pipe	Perforated PVC Pipe	Perforated PVC Pipe with Extra Perforation	Metal Wire Pipe
Flow	l/s/m	18.3	3.8	7.2	15.3
Headloss	mm	172	581	473	445
Headloss	m	0.172	0.581	0.473	0.445
Flow/Headloss	l/s/m	106.34	6.54	15.22	34.40
Porosity	%	23.7	0.57	1.27	19.73

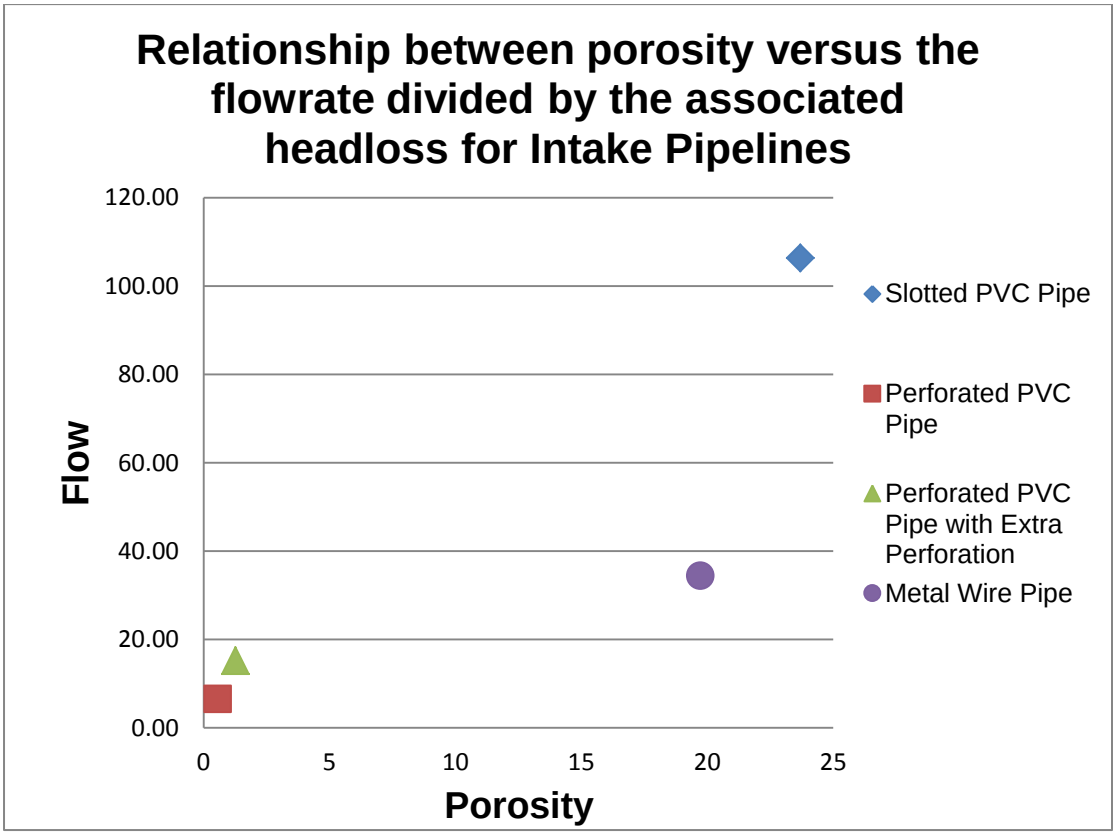

Figure 6.2: Plot of Relationship between porosity and the flowrate divided by the associated headloss for the four test pipes

As can be seen in Figure 6.2, there is no clearly defined relationship between the Flow and headloss and porosity, A general observation is that, the higher the porosity, the larger the flows.

However, the configuration of the perforation / porosity does play a vital role. Comparing the Metal Wire Pipe (MWP) to the Slotted PVC Pipe (SPP), it is found that there is a 4% difference of porosity, however when comparing the Flow/headloss for each pipe, it is found that the maximum flow experience by the SPP is approximately three times that of the MWP. This is mainly attributed to the configuration of the perforation. The slots in the MWP are much smaller. Hence the resultant velocities (Table F7) are larger. The largest velocity V_{max} of 2.954m/s is experienced by the MWP, while the SPP (Table D7) has a lower V_{max} velocity of 1.838m/s. Hence since the headloss is proportional to the velocity squared, the losses in the MWP are much higher than the loss for the SPP for similar flowrates.

6.3 Tests with Stone Bedding

The following Table 6.3 contains the results of the Water and Stone bedding Test (WST) carried out on the three test pipe conduits. The Perforate Pipe was eliminated from further testing as the flowrates where deemed too low and would not yield any better results than the Perforated PVC Pipe with Extra Perforation (PPPEP)

Table 6.3 : Results of Water and Stone bedding Test carried on the 3 test pipes

Intake Pipe Types	Slotted PVC Pipe		Perforated PVC Pipe with Extra Perforation		Metal Wire Pipe	
Test No.	Loss A + Stone BF mm	Q Half Pipe l/s	Loss A + Stone BF mm	Q Half Pipe l/s	Loss A + Stone BF mm	Q Half Pipe l/s
1	0.5	0.33	3	0.219	2	0.35
2	0.99	0.53	6.48	0.478	4	0.49
3	1.98	0.84	13.94	0.939	9	1.11
4	2.95	1.31	39.75	1.822	6	1.58
5	5.82	2.34	89.36	2.923	62	2.60
6	11.21	2.98	160.63	4.253	67	3.74
7	17.95	4.11	215.17	4.919	123	5.27
8	34.64	6.45	280.59	5.638	201	6.98
9	48.04	7.75	473.05	7.196	219	8.49
10	70.14	9.37			299	10.92
11	83.45	10.43			361	13.09
12	105.64	11.55			449	14.16
13	129.52	12.96				
14	155.38	14.24				
15	171.74	14.92				

The results of Table 6.3 are plotted in Figure 6.3 below. This shows the relative flowrates and the pressure lost through friction. This can also be termed the driving head, as it is the pressure head required to drive the flow. The worst performing pipe is the Perforated PVC Pipe with Extra Perforation (PPPEP). This pipe recorded a maximum flow rate of 7.19/s with approximately 0.47m pressure head required to drive this flow into the pipe.

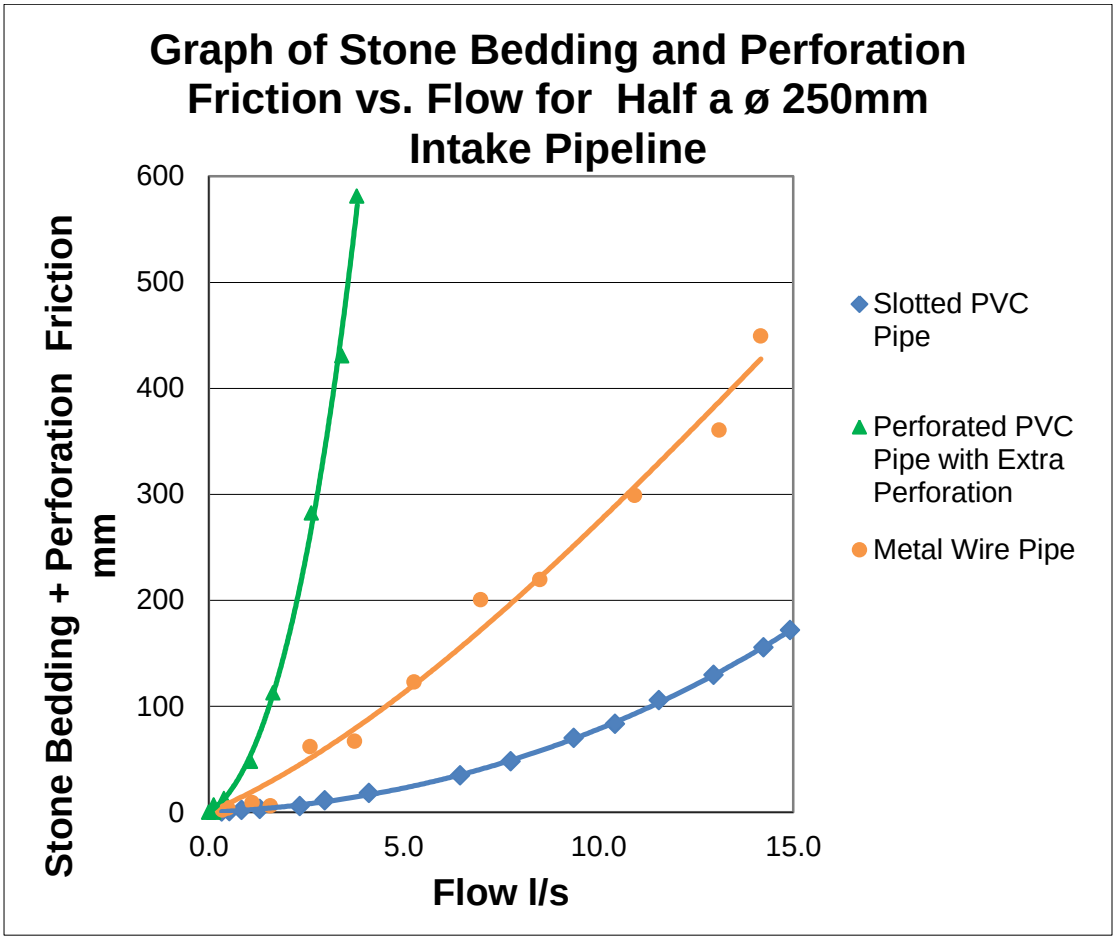

Figure 6.3: Perforation friction for all three intake pipe

The next, better performing pipe is the Metal Wire Pipe (MWP). For a driving pressure of 450mm, this intake pipe produced approximately twice the flowrate as that of the PPPEP at 14.16/s.

Chronologically, the first pipe tested, the Slotted PVC pipe, had the largest perforation area and produced the largest flow for the least amount of the pressure loss. For a driving head of approximately 0.17m, this pipe produced a flowrate of 14.92/s. Hence, in general terms and as can be seen in Figure 6.3 above, the Slotted PVC pipe, once again, produced the largest flow for the least friction/head loss.

6.4 Test with Sand + Stone Bedding

6.4.1 Slotted PVC Pipe

At this point, the normal methods of testing for pressure losses, used so far, ceased. This occurred when the rate of flow in the testing of the Slotted PVC pipe (with sand and stone bedding) became a fraction of the values recorded in previous tests. For the design criteria, these flow values were too low. Hence a flushing system was designed to physically move the sand particles away from the intake pipe surface, using high velocity flows. Refer to Chapter 5.1.5.2. Table 6.4 below shows the results of the tests conducted.

Table 6.4: Pressure loss and Flowrate vs. time relationship for the Slotted PVC Pipe with sand and stone bedding

	Before Back Flushing			After Back Flushing		
Test No.	Time min	BBF Loss A+ sand + stone bedding mm	BBF Q Full Pipe ml/s	Time min	ABF Loss A+ sand + stone bedding mm	ABF Q Full Pipe ml/s
1	0	40	82	0	0	133
2	45	312	291	7	234	107
3	60	335	300	12	255	153
4	70	350	306	16	285	189
5	83	362	302	20	311	204
6	107	374	348	24	324.5	229
7	118	293	313	28	339	227
8	143	220	183	32	350	246
9	149	257	212	36	356	269
10	160.5	266	234	40	360	267
11	171.5	268	233	44	362.5	275
12	178.2	268	233	48	363	286
13	185	268	233	52	366	287
				56	366	289
				60	365.5	293
				66	363.5	259
				72	362.5	260
				78	359.5	263
				101	349.5	203
				150	329.5	192
				170	320.5	205
				192	315.5	203
				230	307.5	195
				280	297.5	192
				326	291.5	193
				377	281.5	192

The first flushing system was of little success and an augmented flushing system was designed (Chapter 5.1.5.3). This system used air in the attempt to create additional buoyancy. It was hoped that this additional buoyancy, coupled with high flows, would dislodge the sand and hence allow for high flow rates into the intake pipe.

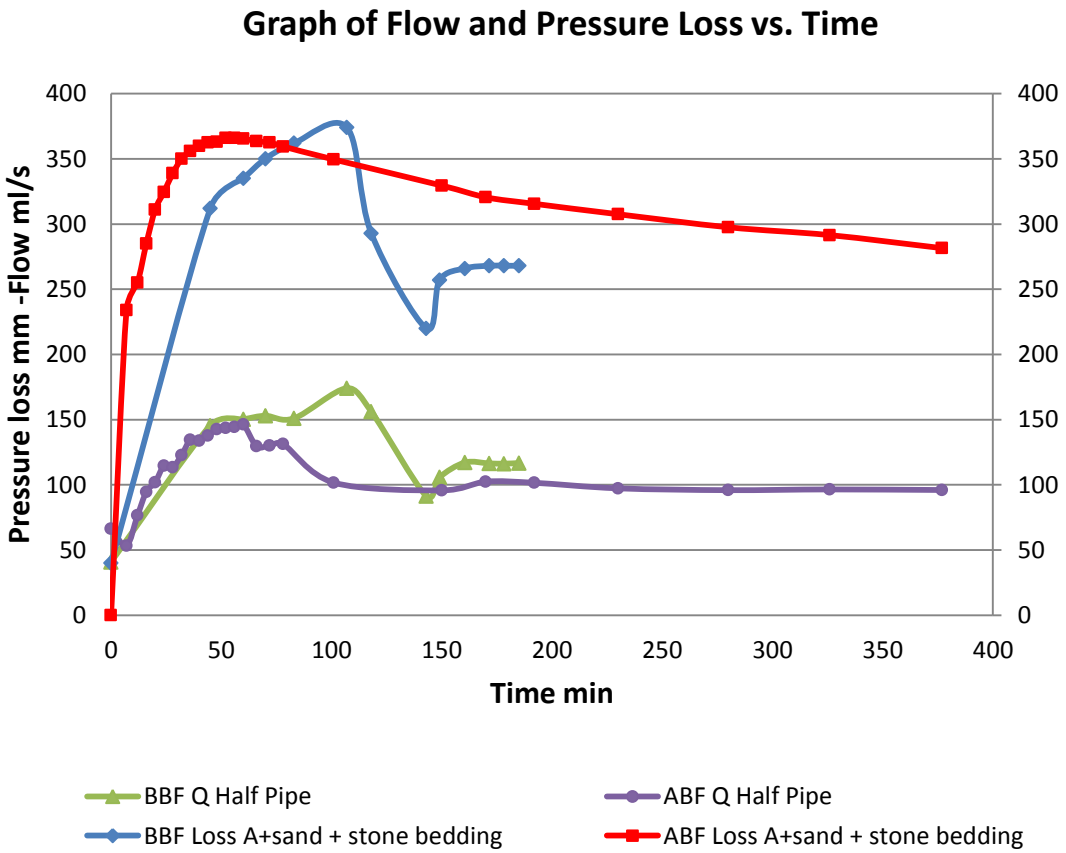

Figure 6.4: Pressure loss and Flowrate vs. time relationship for the Slotted PVC Pipe with sand and stone bedding

Figure 6.4 above below shows the flowrate vs. time relationship in attempt to understand the flowrate over time. Figure 6.4 shows the test results values for the Before Back Flushing (BBF) and the After Back Flushing (ABF) test. The maximum flow encountered was 0.175l/s and 0.15l/s respectively.

As can be seen, there is no marked difference between the headloss and flow rate for before and after Back Flushing. If the BBF test where to be run for 6.5hours, the results would be similar; hence back flushing has not proved successful for the design criteria of these experiments.

When considering low flows encountered, Chapter 2.4.5.6 can be referenced. It notes that in general, the transition for water from laminar to turbulent occurred at approximately Re = 1000. Values lower than 1000 indicated laminar flow and values

greater than 1000 indicated turbulent flow (CIRIA, CUR, CETMEF, 2007). Hence using Equation 13

$$Re = \frac{UD_p}{v} = \frac{4RU}{v} \qquad \text{(Eqn 13)}$$

Where

U = Flow velocity (either Cross sectional averaged or depth averaged) (m/s)

D_p = Diameter of the pipe (m)

v = Kinematic viscosity of the fluid

R = Area of flow/Perimeter of flow = 1 segment of pipe Table D

The identification of the type of flow to be encountered is calculated.

Note that since a full analysis was not done for this pipe, the initial reading from the water and stone bedding test will be used for comparison. This test had a a value of 0.33 l/s which is double that of the maximum flow value in this test (0.15l/s)

Re can be calculated using the flowing values

Vs1 = 0.099 m/s (Table D13)

R = (414087.5mm^2/1207mm) = 0.343m

v = 1.14*10-3 m^2/s

Q = 150ml/s or 0.15l/s

Hence Re = 119 < 1000 Hence the flow is decidedly laminar.

6.4.2 Extra Perforated PVC Pipe

The tests on the perforated pipe do not follow a time sequence as the flow was not similarly small as those in the previous test. This is primarily due to the seepage of sand out of the sand and stone bedding matrix via the ø8mm perforation on the intake pipe. Referring to Figure C3 in Appendix C, the value of D_5 for sand would be is approximately 0.2mm. From Figure E26, this translated to a k of 0.02cm/s or 0.2mm/s.

Considering the Table 6.5 below a *k* value of 0.02 cm/sec is not reflective of the actual flow rates recorded. The best explanation for this can be attributed to the removal of sand from the bedding matrix, Figure 5.23. With the removal of the sand,

the bedding matrix would revert close to its original contents of only 19mm Stone. Hence a D_{50} of 10mm was used. Hence utilising Eqn E5 and E6 a hydraulic conductivity *k* of 0.688m/s was obtained. This was the same *k* used for PPPEP tested with Stone bedding only. Table 6.5 below compares the test results for the Extra perforated PVC Pipe with sand + stone bedding and Extra perforated PVC Pipe with stone bedding only

Table 6.5: Pressure Loss vs. Flowrates for: Extra perforated PVC Pipe with sand + stone bedding and Extra perforated PVC Pipe with stone bedding only (WST + WSST)

Test No.	Loss A+ SAND + stone bedding	Q Half Pipe	Loss A + Stone Bedding	Q Half Pipe
	mm	l/s	mm	l/s
1	24.97	0.167	3	0.219
2	101.61	0.576	6.48	0.478
3	201.51	1.128	13.94	0.939
4	294.59	1.436	39.75	1.822
5	348.51	1.728	89.36	2.923
6	435.82	2.646	160.63	4.253
7	516.4	3.15	215.17	4.919
8			280.59	5.638
9			473.05	7.196

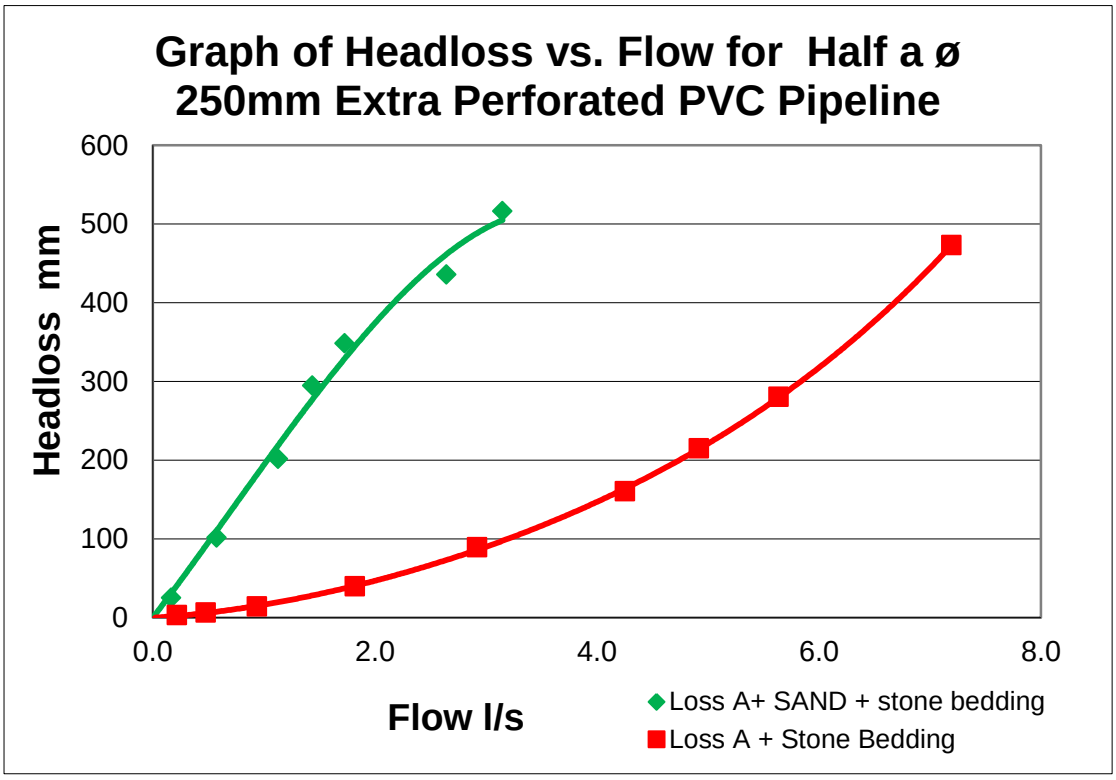

Figure 6.5: Pressure Loss vs. Flowrate for Extra perforated PVC Pipe (WST + WSST)

From Figure 6.5, is it clear that the same hydraulic conductivity *k* cannot be used for both tests. I.e. visual confirmation that all sand was removed from the sand, stone matrix is not conclusive. Hence the *k* value used for a sand stone matrix should obviously lay between that of a minimum value and that of the sand stone matrix. The minimum value *k* will be higher than that of the sand and can be estimated using the information from Chapter : 2.4.7.3 Interface Stability of a Granular Filter.

6.5 Estimating losses due to Stone Bedding

As stated in Chapter 4.4.5, the three methods used to estimate the pressure losses due to stone bedding alone are not similar and are summarised below.

Method 1: Simple method for determining stone bedding loss

In this simplistic method, the results of the "Water Test only: is plotted. Curve line 1 is fitted to the results and an equation characterising the line and hence the pipe, headloss characteristics is formulated.

Thereafter, the results of the "Stone and water test" is plotted. Curve line 2 is fitted to the results and an equation characterising the line and hence the pipe and surrounding bedding, headloss characteristics is formulated.

The loss due to the stone bedding only, Curve line 3, is determined by subtracting Curve line 2 from Curve Line 1. This data is then plotted to show graphically, the relationship between the headloss caused by the 19mm Stone bedding.

Method 2: Method for determining stone bedding loss: Hydraulic conductivity: Kenny, Lau and Ofoegbu

The second method used to determine the loss of pressure due to Stone bedding, looks at the hydraulic conductivity of stone bedding. The equation LR10 and Figures, 2.32 and 2.33 by Kenny, Lau and Ofoegbu are used to estimate stone bedding headloss.

Method 3: Method for determining stone bedding loss : Hydraulic conductivity: Forchheimer

The third method used to determine the loss of pressure due to Stone bedding, stems from work carried out by Forchheimer. The Figure 2.34 was used to estimate the permeability of the stone bedding and hence the headloss.

Detailed calculations with reference to the, Slotted, Perforated and Metal Wire pipe can be found in Appendices D, E and F respectively. The following are comparisons of the three methods used to calculate the Stone bedding friction for each pipe type tested.

Slotted PVC Pipe

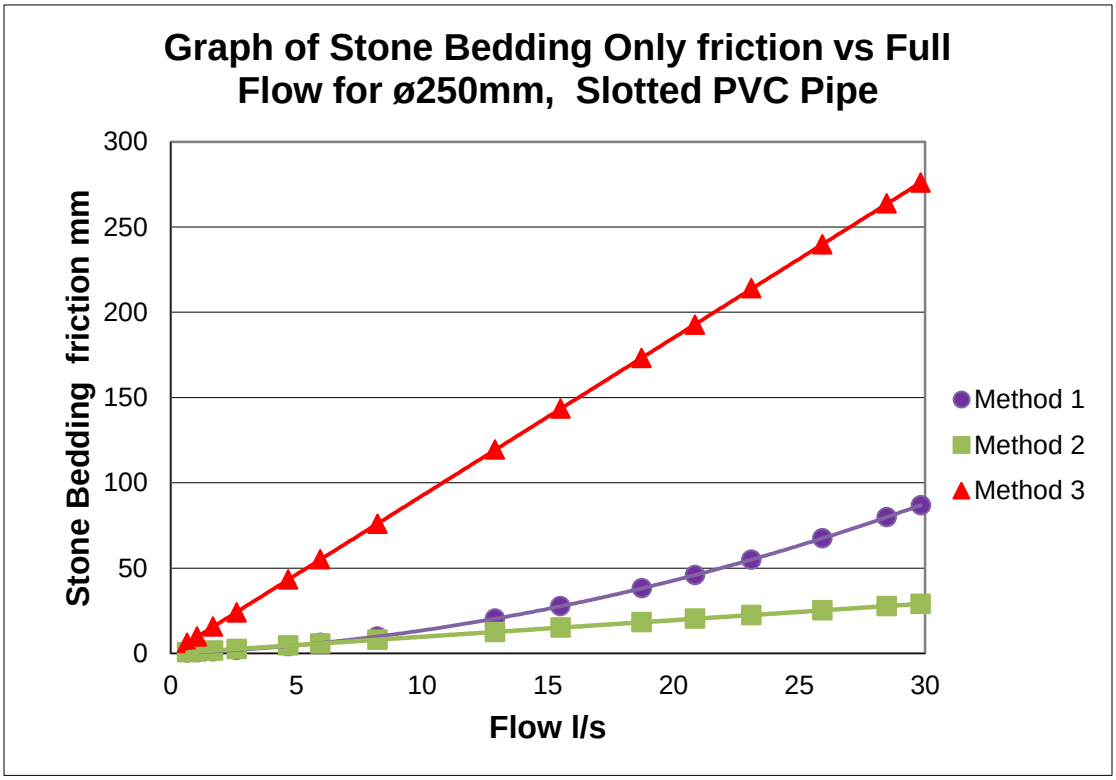

Figure 6.6: Slotted PVC Pipe-Method 1, 2 and 3 : Headloss due to the stone bedding

Extra Perforated PVC Pipe

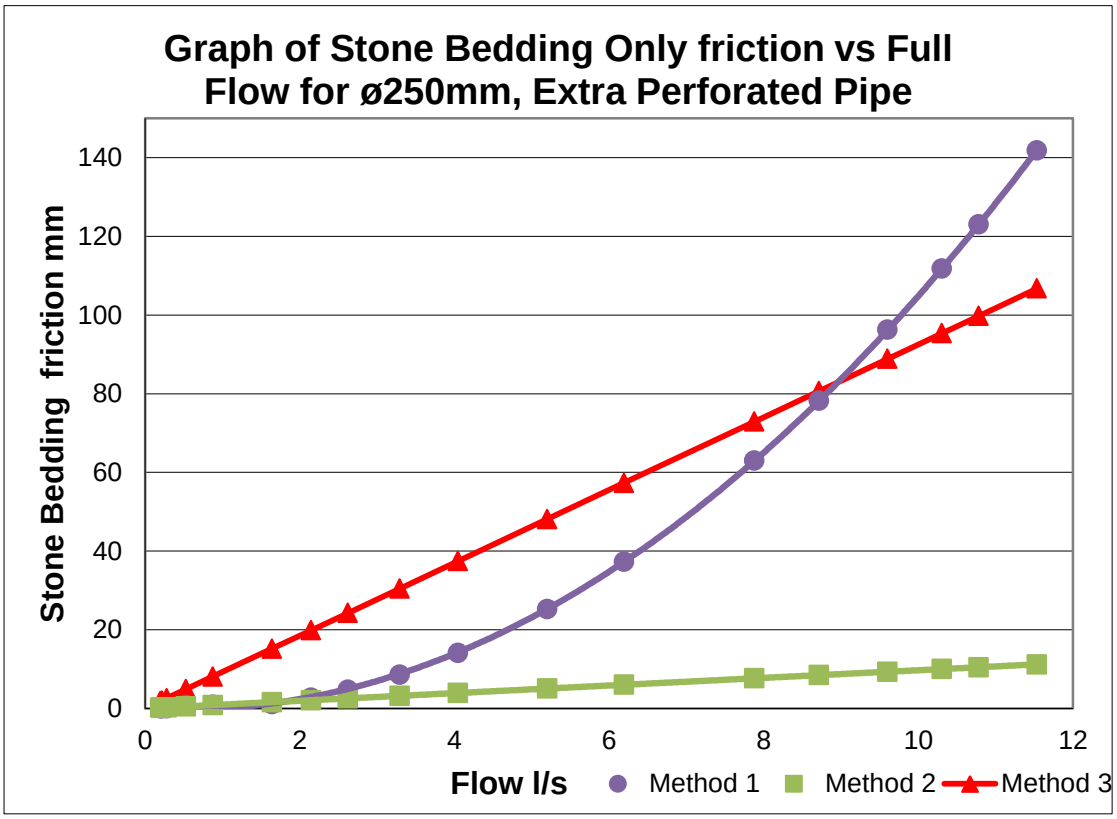

Figure 6.7: Extra Perforated PVC Pipe- Method 1, 2 and 3 : Headloss due to the stone bedding

Metal Wire Pipe

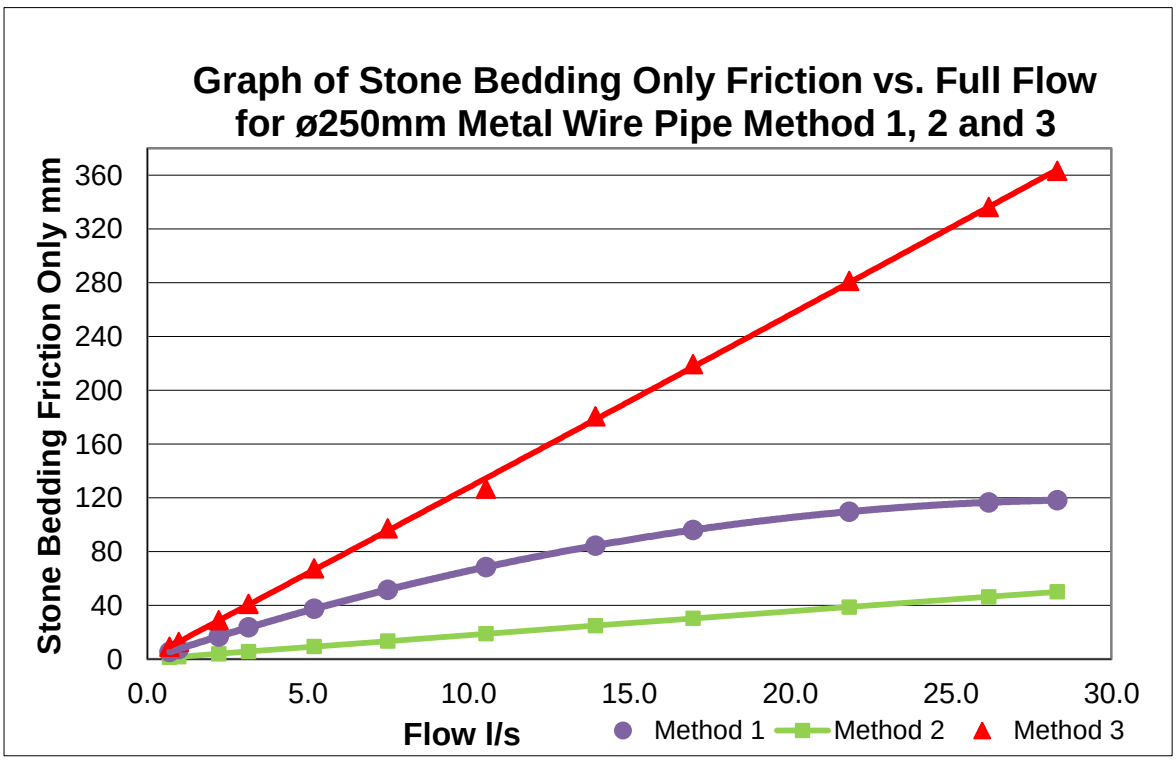

Figure 6.8: Metal Wire Pipe- Method 1, 2 and 3 : Headloss due to the stone bedding

With the exception of Method three in the Extra Perforated PVC test (which is attributed to experimental error), the general pattern indicates that Method 3 approximates the headloss due to stone bedding alone, at three times the value of Method one. Method 2 on the other hand, seems to provide half the Headloss values of Method 1.

The following argument is proposed: First consider the flow through the Stone bedding. It is obvious that there is headloss due to the flow, however, these losses occurs as loss in pressure. Hence the flow does not influence the losses due to the intake pipe. However, as bedding material is placed against the intake, this has a two fold effect on the loss due to the intake pipe.

The first occurs as there is a reduction in perforation area, hence in order to maintain the flow, there is an increase in the flow velocity. This increased velocity implies a greater headloss for a similar flowrate as in the “Water Only tests”

The second occurrence is substantiated by Chapter 6.2.2, With stone bedding up against the intake pipe there is a decrease in perforation area and therefore an increase in the overall perimeter of the little drainage paths. The reduction of this drainage paths, serve to further increase the velocity and hence the friction that cause a loss in pressure head.

Therefore it is proposed that there is an increase in the pressure loss due to the Intake pipe, which shows that Method 2, appears to prevail in most conditions.

Hence is appears that Method 3 seems to overestimate the losses due to stone bedding grossly. Although there has been substantial research conducted on Intake pipes and bedding material on an individual basis, a very limited amount of research has been done on spitting the losses due to stone bedding and the losses due to an Intake pipe line. Hence it is into this region that further research should occur

6.6 Estimating losses due to Sand and Stone Bedding

This test was only undertaken on the Extra Perforated Pipe. This estimation of estimation methods, was not carried out on the other two pipes, as the flow rates through them were far below the required design flows. In this section, the use of Method 3 produced results that were far less than that of Method 1. This is mainly attributed to Method 3 being most appropriate for turbulent flow conditions and not appropriate for the lower flow conditions experienced here.

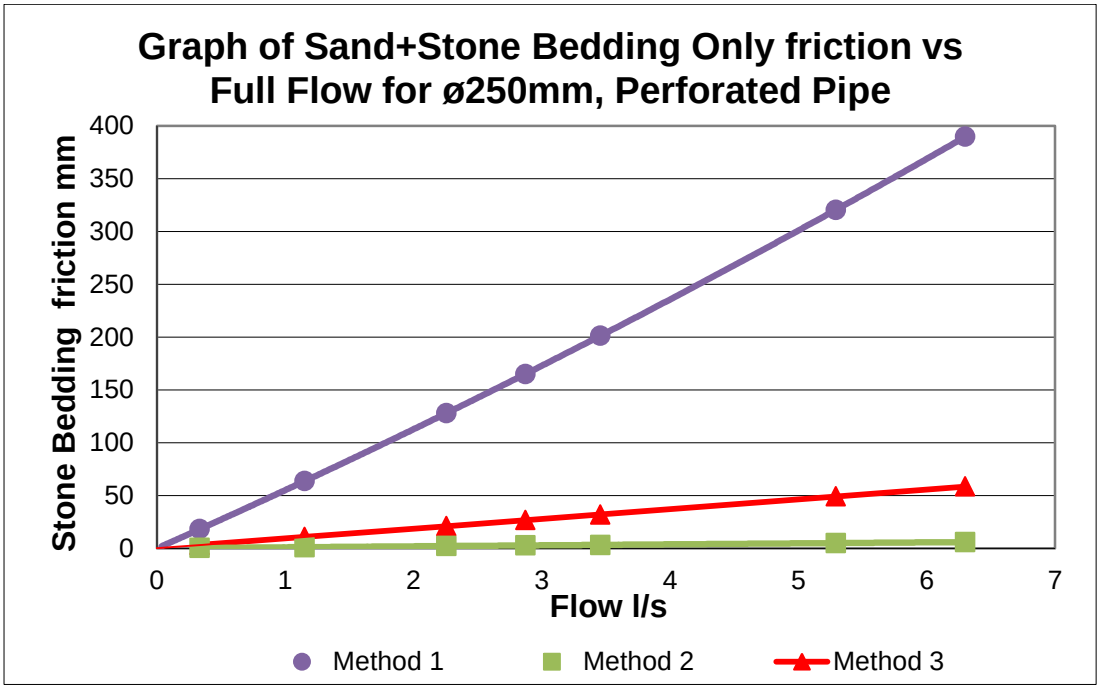

Figure 6.9: Perforated PVC Pipe-Method 1, 2 and 3: Headloss due to the stone bedding

6.7 Comparison of Three methods used to estimate Stone Bedding losses

Method 1

This is a comparison of "Method 1", which was conducted on all three pipe types. As can be seen in Figure 6.10, there seems to be a varying, generally weak correlation between the results of Method 1 used on all three intake pipes. The outcome for the exponential tendency of the extra perforated pipe is attributed to experiment error. Method 1 is not approved and should not be used when trying to determine the losses due to stone bedding surrounding intake pipelines.

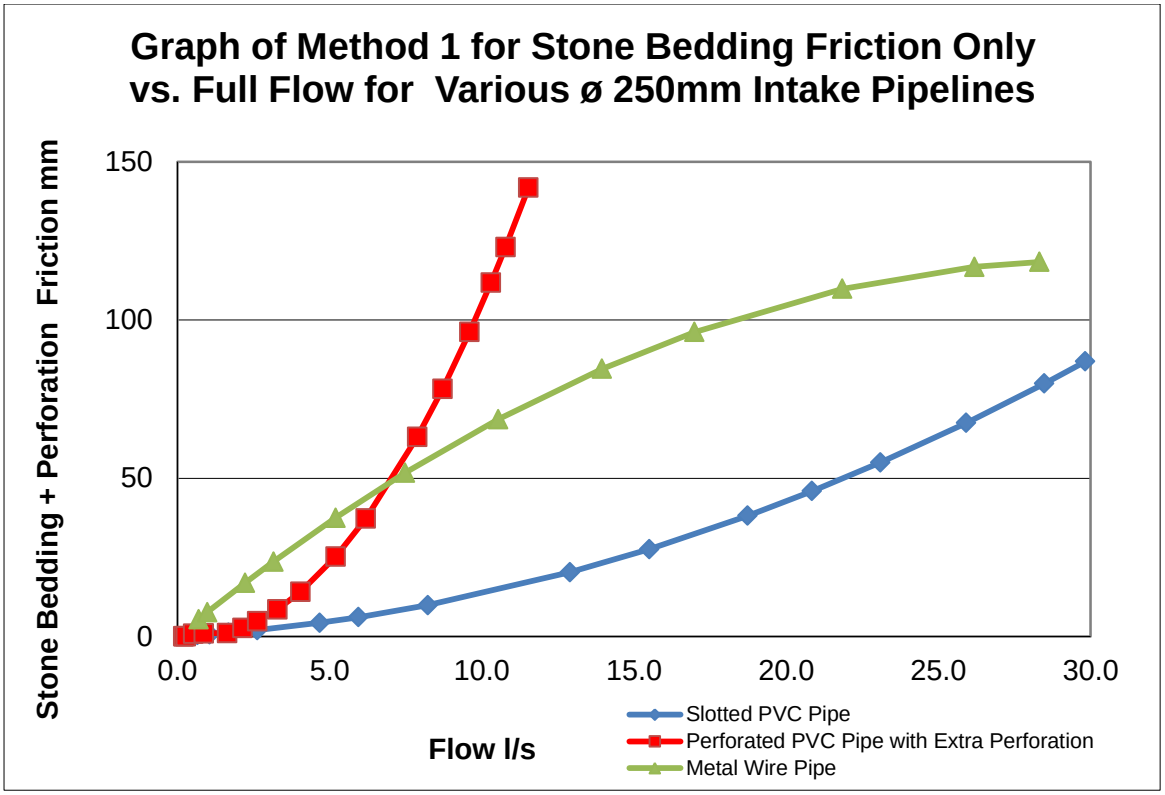

Figure 6.10: Comparison of Method 1 for all three pipe types

Method 2

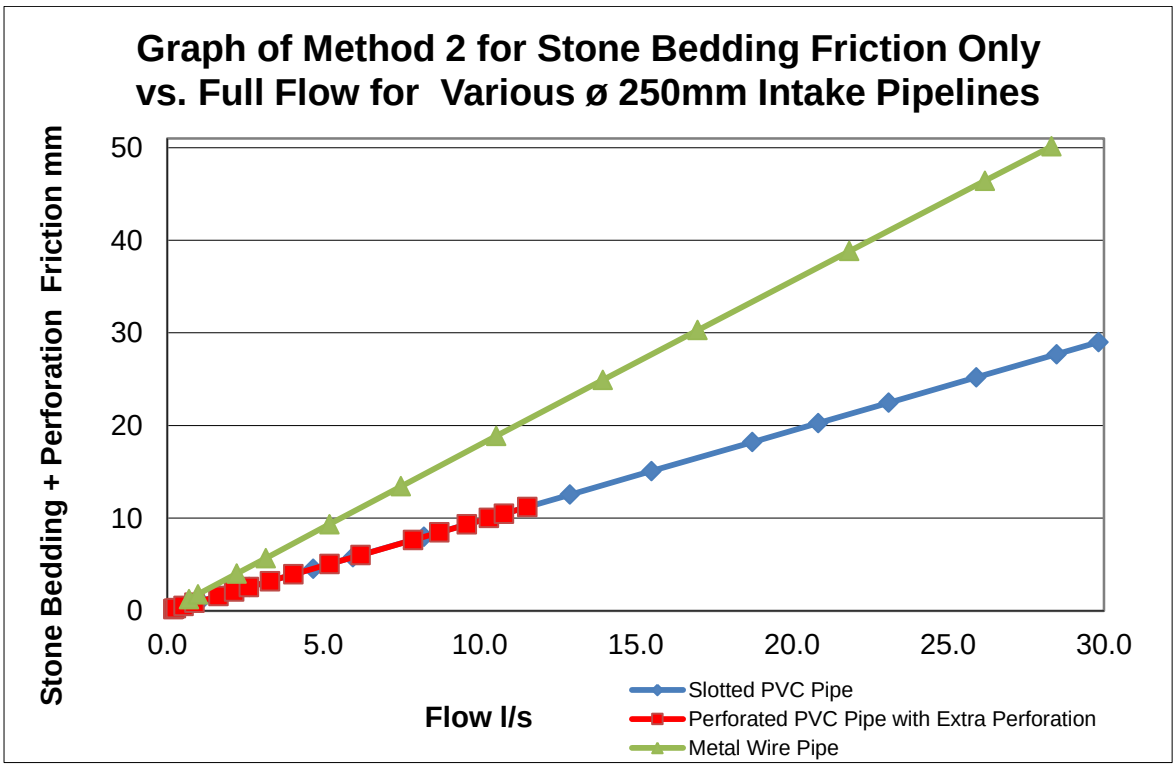

Figure 6.11: Comparison of Method 2 for all three pipe types

Figure 6.11 shows a generally good correlation between the results of Method 2 The Slotted PVC and Metal Wire Pipe show a correlation of approximately unity. The slightly higher values of the extra perforated pipe are attributed to experiment error. However, the generally characteristics are quiet close. Hence Method 2 has proven to produce consistent results regardless of the Intake pipe used.

Method 3

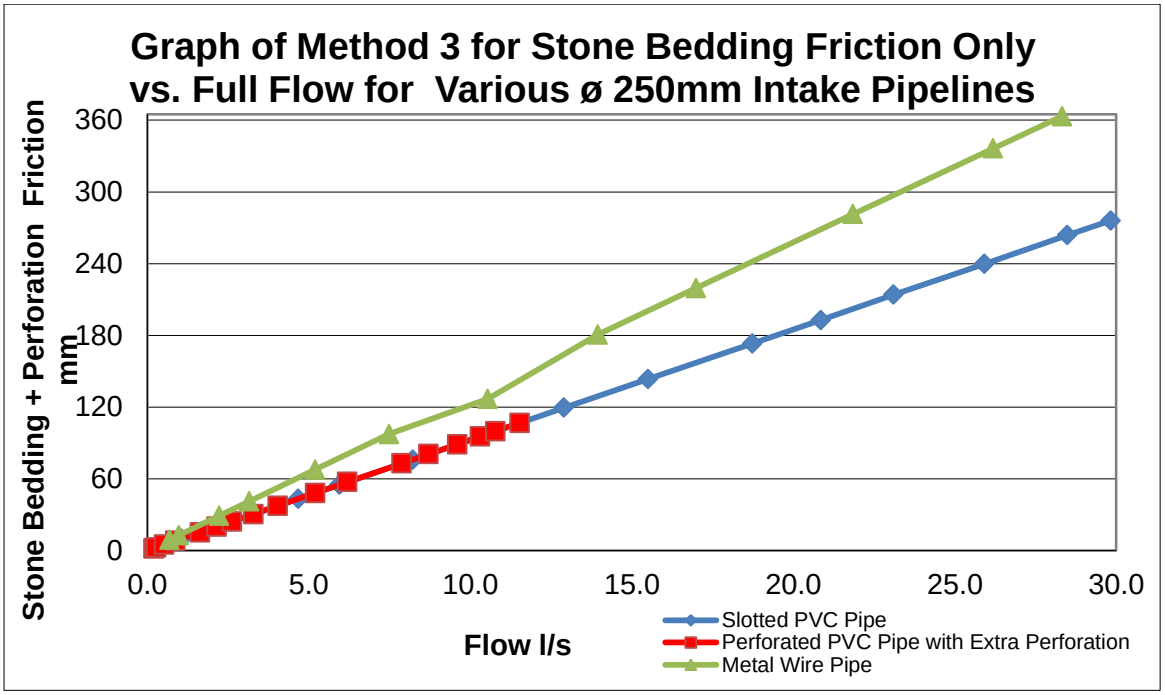

Figure 6.12: Comparison of Method 3 for all three pipe types

Upon examining Figure 6.12, there is good correlation between the results of Method 3. The Slotted PVC and Metal Wire Pipe once again, show a correlation of approximately 100%. The fractionally higher values of the extra perforated pipe (although lower than those of Method 2) are attributed to experiment error. Nevertheless, the general characteristics are quiet close. Hence Method 3 has proven to produce consistent results regardless of the Intake pipe used.

6.8 Concluding Summary and Recommendations

6.7.1 Summary

A larger amount of valuable information was obtained from the experimental work and surveys. From the experimental component, much technical and material specific information, to be used in seawater Intakes, was gained. Numerous technical conclusions can be found in the preceding subsections 6.1 to 6.6. Some of this information and derivations are best presented in the next Chapter 7.

The survey of selected existing seawater intakes provided very valuable information that was very practical in nature. The problems encountered by the seawater intakes and their solutions, regardless of no engineering input, is invaluable information. Chapter 3.9 summaries this adequately.

6.7.2 Recommendations

The following recommendations pertain to the experimental component of this thesis. There are volumes of research that investigate the characteristics of pipes. The experimental work conducted, has produced fruitful results. Hence further investigation into intake pipes only, is not sanctioned.

A large amount of work has been done on bedding material. These vary from fine clays to cobble and even boulders. Most of these tests are conducted as per Figure 2.28. Further investigation into bedding material, is not sanctioned. However, more research is required to determine the headloss when the flow is not singular but is repetitively reversed, as is the case when wave run up and run down occurs..

A further recommendation is that research be conducted into pressure losses due to the intake pipe and the stone bedding, when both are used simultaneously. There is a large repository of work regarding the individual components. However further research can be done in portioning the associated friction losses.

It is recommended that the action of waves on stone bedding (including sand) and pervious pipes be investigated. This will provide valuable information on the displacement of ingressed sand and hence seawater intake and abstraction rates.

Chapter 7

7. DESIGN RECOMMENDATIONS FOR SMALL SCALE SEAWATER INTAKES ON A ROCKY COASTLINE USING THE HORIZONTAL WELL SYSTEM

7.1 Introduction

The following are design step recommendations for a small scale seawater intake on a rocky coastline. Figure 7.1 shows these steps in a chronological order. Note however that these steps need not be followed rigidly. These design steps ultimately consider that the Intake will be a Horizontal/radial well system on a rocky shoreline. This step guide assumes that through the design process, the horizontal well method has proved to be a worthy alternative. Hence each step is referenced to useful information obtained from the preceding chapters. This information is derived from the Literature Review, Experimental results and the Survey of selected Seawater Intakes.

7.2 Design Steps

Step 1: End Usage Requirements

Part of the initial steps is to establishment the exact the water requirements. At this point in the design process, the end water requirement and hence the abstraction rate (m^3/h etc.), should be known. Amongst other parameters, the quality of the water required should also be established. The general guideline is that seawater which is to interact with marine life should be of the best quality.

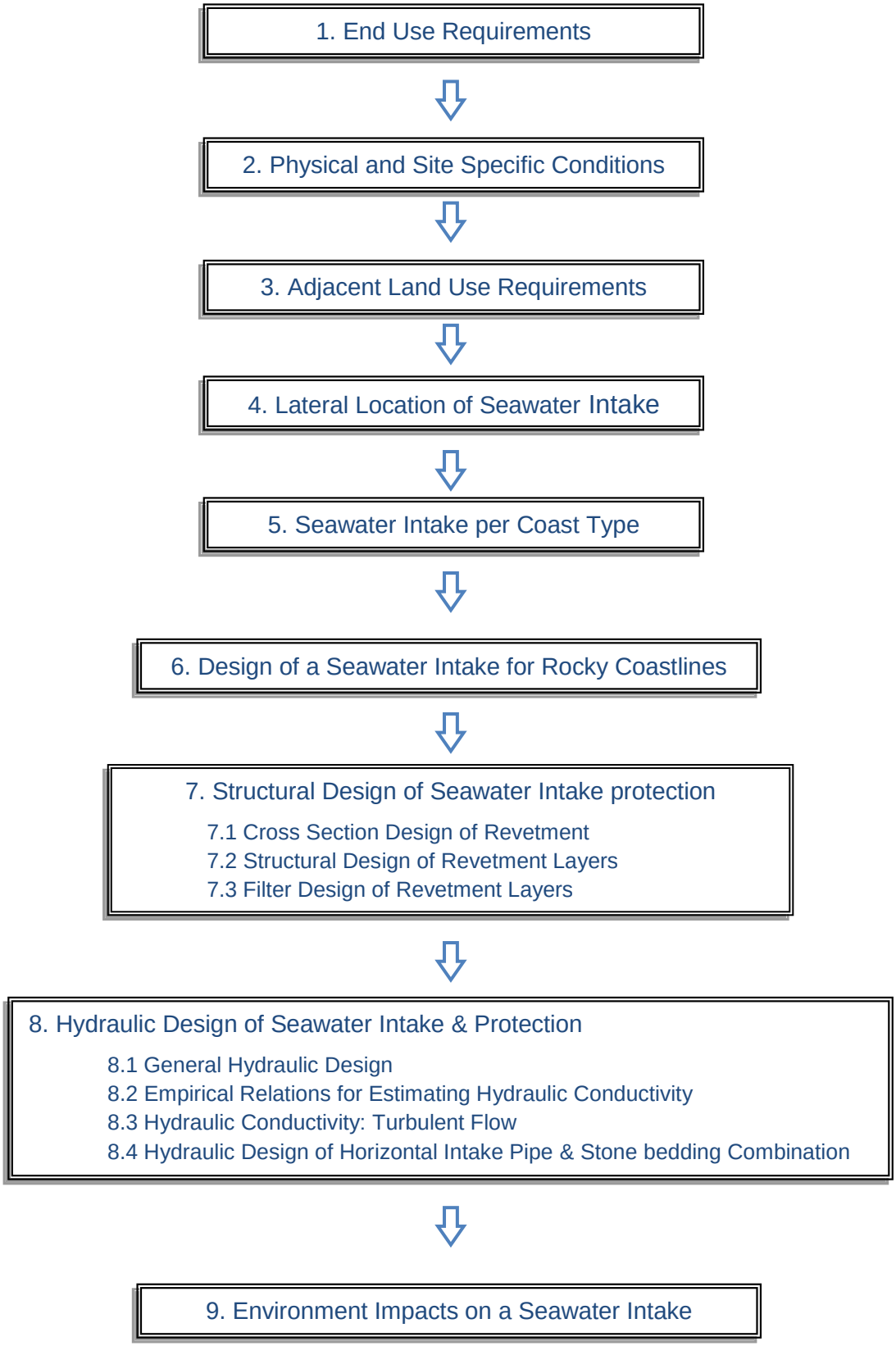

Figure 7.1: Design Step Guide for a Seawater Intake

Step 2: Site Specific and Physical Conditions

After the end user requirements have been established. The site selection process commences. A minimum of three sites should be considered as this allows for flexibility with regard to other constraints.

It is assumed that the seawater intake has already been allocated within a rocky coastline. Information regarding the following physical features, is of vital importance. They should include:

1. the topology of the incurred coastline, i.e. stratified rocky beaches, or cobble beachs or highly dynamic perched beaches.
2. The current, wind and wave climate
3. The quantified movement of sediment via littoral drift or aeolian transport
4. The characteristics of the sand including the grain size distribution.

Step 3: Adjacent Landuse

The quantity of seawater in the region of the proposed seawater intake is affected by land based activities. I.e. Recreational, commercial and industrial activities can pose a potential threat to the water quality.

Another impact can be adjacent sea conditions. The first “natural” impact is from river mouths located close to the propose seawater intake. Rivers bring down sediment and an assortment of chemicals based on the land use of the catchment. During times of flooding, the impact of an adjacent river would be higher than normal.

An impact of water based activities ranges from large ports, down to minor, small craft harbours. For example, the Port of Durban, South Africa, has recently widened the harbour entrance and is proposing a small craft harbour adjacent to the new harbour entrance. These water based activities will have an impact on the closely located Ushaka Marine World, seawater intakes. Due to the activities, there will be an increase of turbidity and the suspension of other material due to dredging. A seawater intake should be designed to accommodate such situations.

Step 4: Lateral location of Seawater Intake

The lateral location of the Seawater Intake refers to its position relative to the surf/swash zone. Offshore positions are not considered. Seawater Intakes placed in these environments are subject to conditions not covered (for design purposes) in this text

A seawater intake can be placed in the surf/swash zone or the back shore. If the intake is in the back shore, the effect of wave action is minimal. This in turn reduces the energy required to protect the seawater intake. If the geology of the area is high permeable, a seawater intake situated a distance from the swash zone, would be an attractive option.

Step 5: Seawater Intake per Coast Type

There are basically two types of coastlines, these are Sandy Coastlines and Rocky Coastlines. The topography, geology and shoreline parameters might differ, however, all shoreline can be categorised into the above two broad descriptions.

Sandy Coastlines

For sandy coastlines, Chapter 2.3.3.1, sub-bottom, horizontal beach wells, are the most common types used. These wells provide clear seawater due to the filtration action of the surrounding sand. Horizontal wells are protected against wave action as they are beneath the sand. The external loading on these pipes would vary with the tide, but not immensely as it would be situated within a sand matrix, hence the intake pipe itself would not require large structural strength. When designing such systems, Chapter 2.4.6.2 defines the general design parameters that should be used.

Rocky Coastlines

In a rocky coastline, any seawater intake designs will deal with inflexible hard ground conditions. These will invariably increase the complexity and cost of a seawater

intake. In a rocky shore, there are three main types of intakes that can be considered. These are mainly:

- Direct
- Partially Direct
- Sub-bottom

In a rocky shoreline, it is inherently hard to construct an *Direct* intake line that will traverse the surfzone. Hence this option is not discussed further as the financial implication does not make it pliable to a small scale seawater intake application.

Step 6: Design of a Seawater Intake for Rocky Coastlines

When designing a seawater intake on a Rocky Coastline, there are two main locations where a seawater intake can be cited. The first is the surfzone and the second would be further inland.

Lateral Location

It is very favourable if a seawater intake is placed away from the surfzone. This is due to the cost savings made as the intake is not subjected to wave forces.. The abstraction of water via well points and associated information is contained in Chapter 2.2.4. If the geology of the coastline does not allow for abstraction via inland well points, then abstraction from the surfzone will have to be considered.

Partially Direct and Sub-bottom

Aa Partially Direct abstraction method is best suited for a coastline that has natural deep gulley's. This allows for water to travel closer inland with no significant wave attack at the end of the gulley. If the rocky shoreline is at a flatter grade then a *Sub-bottom* Horizontal well system can be used. Due to the horizontal well being below the water level, wave attack would occur in the vicinity of the seawater intake. Hence protection against wave action will be required.

The most common form of protection is a rubble mound revetment. This type of structure is normally used for protection purposes only. However as the objective is the design of a seawater intake, a Structural as well as Hydraulic design of the revetment/Seawater Intake should be undertaken. These two components will be discussed further

Step 7: Structural Design of Seawater Intake

If the seawater intake is a radial beach well on a sandy beach or a partially direct seawater intake, then not much protection against wave attack is required. If the seawater intake is on rock then a rock revetment, the most common form of protection, is recommended. The “Structural” design of a Seawater Intake with a rock revetment, can be found in Chapter 4.2.3 and 4.2.4.

Step 8. Hydraulic Design of Seawater Intake & Protection

After the cross section of revetment has been designing, the hydraulics of the seawater intake has to be analysed. The outer armour layer, underlayer and core layer material might be considered to be large enough not to affect the flow of seawater into the intake pipe. However, this should be estimated to obtain a conservative design.

The brief first sub chapter stated a few general hydraulic design principles. The second sub chapter looks at the various methods where the headloss through the revetment can be estimated. The third Chapter looks at headloss occurring through that stone bedding and horizontal screen. This sub chapter uses the data obtained from the tests carried out in this thesis.

Step 8.1 General Hydraulic Design

Numerous guidelines can be applied when designing a seawater intake. However the most important ones look at the bottleneck in the system and attempts to quantify these. One of the most important factors in the design process is to determination of the flow regime of the seawater through the protection and Intake pipe. The type of flow in the Intake will be either laminar or turbulent. For Laminar low, Darcys law is used. Laminar flow is limited to conditions for which the Reynolds number does not exceed approximately 60 to 700. Refer to example in chapter 6.4.1.

Step 8.2 Empirical Relations for Estimating Hydraulic Conductivity

In the past, several empirical methods have been derived for estimating the hydraulic conductivity. Refer to Chapter 2.4.5.3 for the different estimation methods

Step 8.3 Hydraulic Conductivity: Turbulent Flow

The flow of water through most soils is laminar. However, as material size increases for example rockfill, the flow though the larger voids is found to be turbulent. In Darcy's law the Flow velocity *v* and the Hydraulic gradient *i* share a linear relationship. When the flow becomes turbulent, this equation has to be replaced by a non linear relationship. This is summarised by Forchheimer's work which can be found in chapter 2.4.5.4.

Step 8.4 Hydraulic Design of Horizontal Intake Pipe and Stone bedding Combination

This chapter uses the Intake pipe and stone bedding characteristics obtained from results of the experimental work carried out in this thesis. The following Table 7.1 is a table of equations that can be used to calculate the amount of pressure loss for certain flowrate into a 1meter length of seawater intake pipe. It is based on the pressure loss - flow relationship for all three intake pipes derived from Chapter 6

Table 7.16 pressure loss - flow relationship for intake pipes

Intake Pipe	Water Only test	Test with Stone bedding
Slotted PVC Pipe	$\Delta P = 0.0518Q^2 + 0.3206Q$	$\Delta P = 0.1309Q^2 + 0.8725Q$
Extra Perforated Pipe	$\Delta P = 0.891\ Q^2 + 1.286\ Q$	$\Delta P = 2.066\ Q^2 + 0.019\ Q$
Metal Wire Pipe	$\Delta P = 0.494\ Q^2 + 1.443\ Q$	$\Delta P = 0.2077Q^2 + 9.332Q$

ΔP = Headloss due friction in mm, Q = Flowrate in liters/second

Step 9: Environment Impacts on a Seawater Intake

The construction of a seawater intake will have an effect on the environment. An optimum design will seek to minimise the impact of the intake on the environment and vice versa. However in the construction stage, impact on the adjacent environment will occur.

In the surf zone, the growth of marine life impacts the operation of any equipment. “Fouling” will impact negatively on the flow area and effective roughness of the seawater intake pipe. Hence for long term performance, this impact must be considered at design stage.

There are two common design approaches to manage marine growth. The first is the chemical approach and sees the use of antifouling material that hinders the attachment of marine life to a specific surface. The second method is a mechanical cleaning method that physically removes marine growth. This method has a lower impact as no harmful chemicals are used or released into the environment. Hence, this method of maintenance is recommended as it has the least impact on the surrounding environment.

References

African Sky. (2005). *South Africa's Climate*. [Online] October 2006. Available from : http://www.africansky.com/travel/climate.html. [Accessed December 2007]

Alexander, M. & Mindess, S. (2005). *Aggregates in Concrete.* Oxon:Taylor & Francis

Aqualyng AS, (2009) *Fastwater* [Online]. Available from: http://www.aqualyng.com/Solutions/FastWater.aspx. [Accessed: 10 September 2009]

Bakker, K. J., Verheij, H. J. and de Groot, M. B. (1994). Design relationship for filters in bed protection. *J. Hydraulic Engineering,* ASCE, 120(9), 1082-1088.

Basson, G.R. (2005). *Considerations for the Design of River Abstraction Works in South Africa*, *Volume II*. Stellenbosch: University of Stellenbosch

Bundesanstalt für Wasserbau, (1993). *Code of practice : use of geotextile filters on waterways.* Karlsruhe, 18pp

Bornman, T.G. & Klages, N.T.W. (2004), *IECM Report No.C84: Upgrade of Kenton-on-Sea/Bushman's rivermouth. Bulk Water Supply: Environmental Scoping Report.*

Bosman, D.E. (2005). *Fish processing plants close to Elandsbaai harbour and quay wall*.

Busby, A. (2008). *Seawater Intake at Sea Fisheries Aquarium*. [Interview] 20 March 2008.

CBI Consulting Engineers, (2007). Report: *Sea World at uShaka Marine World, Water Intake System, Well Point: Problems identified over the past two years of operation.*

Coastal Engineering Manual, (2006). EM 1110-2-1100. Part VI, Chapter 5, *Fundamentals of Design*. U.S. Army Corps of Engineers, Washington, DC.

CIRIA, CUR, CETMEF (2007). *The Rock Manual. The use of rock in hydraulic engineering*. (2nd edition). C683, CIRIA, London.

Das, B. M. (2000). *Principles of Geotechnical Engineering*. PWS Publishing Company.

Denis, C. (2008). *Seawater Intake at St Helena Abalone.* [Interview] 26 March 2008.

Department of Environmental Affairs and Tourism (DEAT), (2001) *Coastal Care Fact Sheets Series*. Cape Town

Department of Environmental Affairs and Tourism (DEAT), (2001). *Marine Aquaculture in South Africa.* Cape Town.

Department Of Water Affairs And Forestry (DWAF), (1995a). *South African water quality guidelines for coastal marine waters.* Volume 1. Natural Environment. Pretoria.

Department Of Water Affairs And Forestry (DEAT), (1995b). *South African water quality guidelines for coastal marine waters*. Volume 2. Recreation. Pretoria.

Department Of Water Affairs And Forestry (DEAT), (1995c). *South African water quality guidelines for coastal marine waters*. Volume 3. Industrial use. Pretoria.

Desalination Issues Assessment Report, (2003). *Desalination, with a grain of salt – a California perspective*. May 2003.

De Wit, C. (2008). *Seawater Intake at Abagold (PTY) Ltd*. [Interview] 15 May 2008.

Eskom, (2010a). *Understanding Electricity* [Online] October 2002. Available from: http://www.eskom.co.za/c/article/199/understanding-electricity/.[Accessed: May 2008]

Eskom, (2010b). *Operating Methods of Power Stations*. [Online] October 2002. Available from: http://www.eskom.co.za/c/article/96/operating-method/. [Accessed: May 2008]

Eskom, (2010c). *Electricity Generation.* [Online] October 2002. Available from: http://www.eskom.co.za/content/GX_0001GenPlantMixRev11~1.pdf. [Accessed: May 2008]

Google. (2009). *Google Earth Maps* [Online] September 2007. Available from: http://www.googleearth.com. [Accessed : June 2008]

Giroud, J P (1988). Review of geotextile filter criteria. *Proc 1st Indian geotextiles conf on reinforced soil and geotextiles*, Bombay, 8-9 Dec. Oxford and IBH Publishing, Bombay, pp 1-6

Giroud, J. P. (1996). Granular filters and geotextile filters. *Proc 2nd intconfgeofilters '96, Montreal, 29-31 May*, Bitech Publishing, Richmond, BC, pp 565-680

Hatzikos, E.V., et al (2007). *An Empirical Study of Sea Water Quality Prediction.* Elsevier Science.

Kenney, T., and Lau, D. (1985). Internal stability of granular filters. Can. Geotech. J., 22(2), 215–225.

Lafleur, J, Mlynarek, J and Rollin, A L (1993). Filter criteria for well graded cohesionless soils. *Filters in geotechnical and hydraulic engineering*. Proc 1st intconf Geo Filters, Karlsruhe, 20 22 Oct 1922. AA Balkema, Rotterdam

Lafleur, J., Eichenauer, T. and Werner, G. (1996)." Geotextile filter retention criteria for well graded cohesionless soils". *Proc 2nd intconfgeofilters '96, Montreal, 29-31 May*, Bitech Publishing, Richmond, BC pp429-438

Lattermann, S. & Höpner, T. (2007). *Environmental impact and impact assessment of seawater desalination*. Elsevier 2007.

Makai, (2008a). *Cold Seawater Air Conditioning (SWAC)*. [Online] February 2008. Available from: http://www.makai.com/p-swac.htm. [Accessed : May 2008]

Makai, (2008b*). SWAC – Sea Water Air Conditioning*. [Online] February 2008. Available from: http://www.makai.com/e-swac.htm. [Accessed : May 2008]

Mora Associates. (2007). *Water desalination – Tap into the liquid Gold* [Online] December 2007. Available from: http://www.moraassociates.com/publications/0712%20Water%20desalination.pdf. [Accessed May 2008]

Nuclear Power Plants all over the World Page (NPPWP), (2008): *Koeberg Nuclear Station* [Online] Available from : http://www.icjt.org/npp/foto/688_1.jpg [Accessed : May 2008]

Reynolds, P. Maley, M. (2008). *Monterey Bay Water Works Association Desalination Intake Approaches:Open Ocean Intake vs. Subsurface*. [Online] December 2008. Available from: http://www.scwd2desal.org/documents/Presentations/MBWWA%20Intake%20Presentation%2010-16-08-web2.pdf. [Accessed : February 2009]

Roberson, J.A., Cassidy, J.J. & Chaudhry, M.H., (1998). *Hydraulic Engineering*. John Wiley and Sons, Inc.

Roussow, C. (2010). *Seawater Intakes at Sedgefield*. [E-mail]. Message to A. Brahmin. February 2010.

Prankratz, T. (2008). *An overview of seawater intake facilities for seawater desalination.* Alden desalination intake solutions workshop, Massachusetts. October 2008.

Samson, K. (2010). *Augmented flushing of Sandvlei and De Gama Marina, Cape Town*. [E-mail]. Message to A. Brahmin. February 2010.

Smith, M. (2008). *Seawater Intake at Paternoster Oyster Co.* [Interview] 26 March 2008

Schwarz, J. (2000). *Beach well intakes for small seawater reverse osmosis plants*. MEDRC Project 97-BS-015.

Templar, T. (2008). *Seawater Intake at Two Ocean Aquarium.* [Interview] 27 February 2008.

The San Diego Union-Tribune, (2006). *South Bay Power Plant in Chula Vista*, [Online] October 2006. Available from: http://www.signonsandiego.com/uniontrib/20060414/news1n14intake.html. [Accessed November 2008]

Theiss, (2006). *Seawater Intake for the Ravensthorpe Nickel Project*. [Online] October 2006. Available from : http://www.leighton.com.au/verve/_resources/ThiessNewsvol106.pdf. [Accessed May 2008]

Wenlock, H. (2009). *Seawater Intakes Paddling pools on Durban Beachfront.* [Interview] 24 April 2009.

Whyte, D. C. (2008). *Seawater Intake at West Coast Abalone (PTY) Ltd.* [Interview] 26 March 2008.

Wang, S. (2009). *Design and Performance Update of LBWD's Under Ocean Floor Seawater Intake and Discharge System*. Alden Desalination Intake/Outfall Workshop. Alden

WSP Africa Consulting Engineers (WSPACE) (2007), Report No.WSP/co/206822e/1. *Renovations to the existing marine intake jetty for Ikamva Lethu Fishing*, Hout Bay.

Zietsman Lloyd and Hemsted (ZLH), (2007). ZLH Consulting Engineers Report: *Seawater Intake and Extensions to Ikamva Lethu Fishing, Lobster Holding Facility*, Hout Bay.

Zietsman Lloyd and Hemsted (ZLH), (2008). ZLH Consulting Engineers Report: *Kidd's Beach Desalination.*

Zietsman Lloyd and Hemsted (ZLH), (2008a). ZLH Consulting Engineers Report: *Majung Power Station Seawater Intake.*

Appendix A

Design of Model

A.1 Introduction

The main objective of this model is to investigate the relationship between flows, the pressure driving the flow and headloss in the seawater, pipe intake. The second part of the investigation would determine the effect of different material surrounding the intake pipeline, on flow, pressure driving the flow and headloss in the seawater pipe intake.

The model would have to be robust and equally easy to dismantle and assemble in a short period of time. Hence it was decided to used ply board and angle irons, as the main structural elements. Since these materials were easily available, construction followed design immediately.

A.2 Design

The requirements of the model had to satisfy the following conditions.

The model should allow for easy calculation of head loss.
Variable flow should be attainable.
The model should allow for material to surround the intake pipe

It should also:

Ensure that all flow is measured.
Ensure that all losses are accounted for.
Ensure that any material (sand) conveyed by water is measurable.
Maximise visual viewing of flow.

Method

The first idea established, was that water should flow from one compartment to another via the intake pipe, thus the head difference between the two water columns would be the head loss in the pipe.

The second one was that both columns should be sufficiently high enough to accommodate any material that would be placed above and below the intake pipe line. The one fixed measurement would be the bedding of the pipe. This was usually stated by pipe manufacturers as a minimum of 300mm above the pipe and 100mm below. 150mm was allowed in this case as a smooth rock insitu profile could not be guaranteed.

The next concern was any other material that would lie over this bedding. A depth of 1.2m was allowed for this. Thereafter an additional amount of 300mm was allowed for freeboard. The pipe sponsored was in 250mm in diameter hence the minimum height of the water columns would be the sum of the following:

Freeboard:	300mm
Fill Material	1200mm]
Blanket over pipe:	300mm
Diameter of Pipe:	250mm
Bedding:	150mm
Total height:	2200mm.

The next criterion would be the measuring of flow. Hence it was decided that a V Notch weir would to be introduced to the second column. An important note being the V notch would determine the lowest water level.

Ply boards come in the following dimension, 2440mm by 1220mm by 20mm, depending on the thickness you require. In order to maximize the usage of the wood, it was decide that the water column heights would be 2440mm. The length of the main water compartment would be 1220mm and the width at 610mm.

Hence the dimensions of the structure were as follows. The main water column is: 1220mm long * 610mm wide * 2400mm tall (Figure A1). The second compartment is 610mm square, also with a height of 2400mm. However this second part has a partitioning center board, with a 90˚ V notch weir sitting above the board (Figure A2).

It was then decided to use a half pipe and a sheet of Perspex as the conduit between two columns of water. The actual flow through the pipe could then be easily observed. This would be greatly beneficial to understand the flow of e.g. sand in through the model.

IMAGES OF MODEL

Figure A1: Hydraulic Model for testing intake pipework

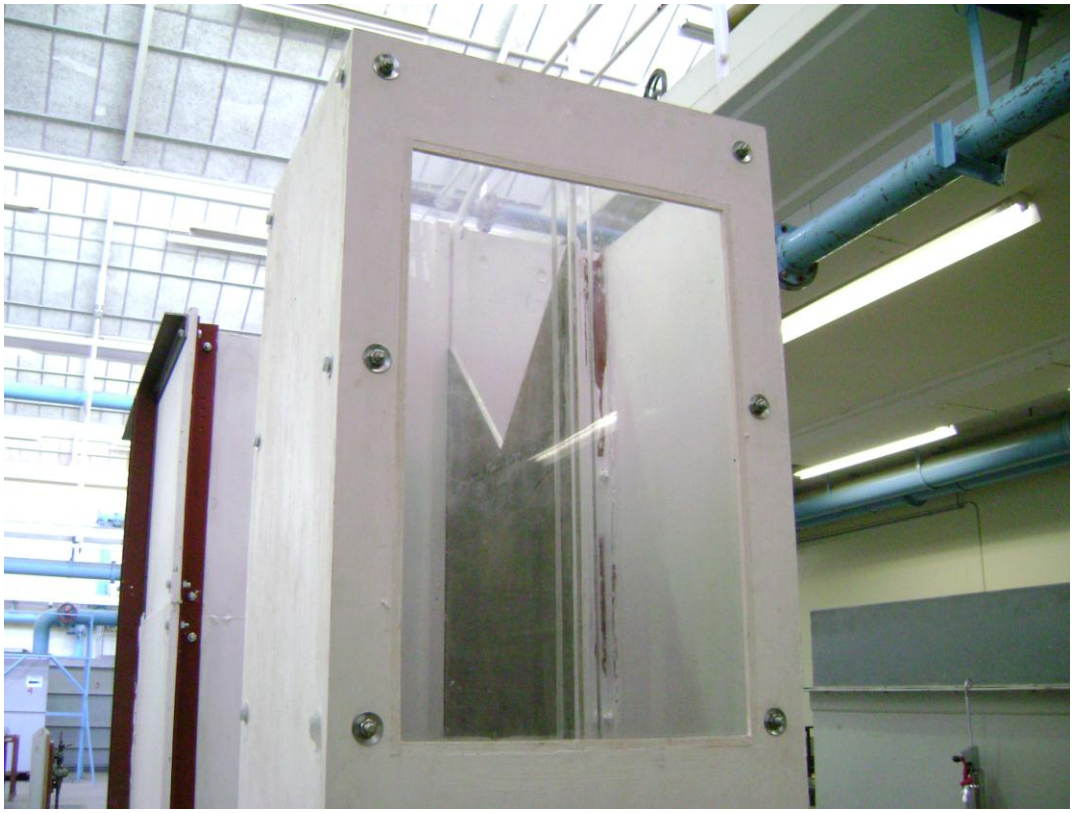

Figure A2: V Notch weir inside the second water column

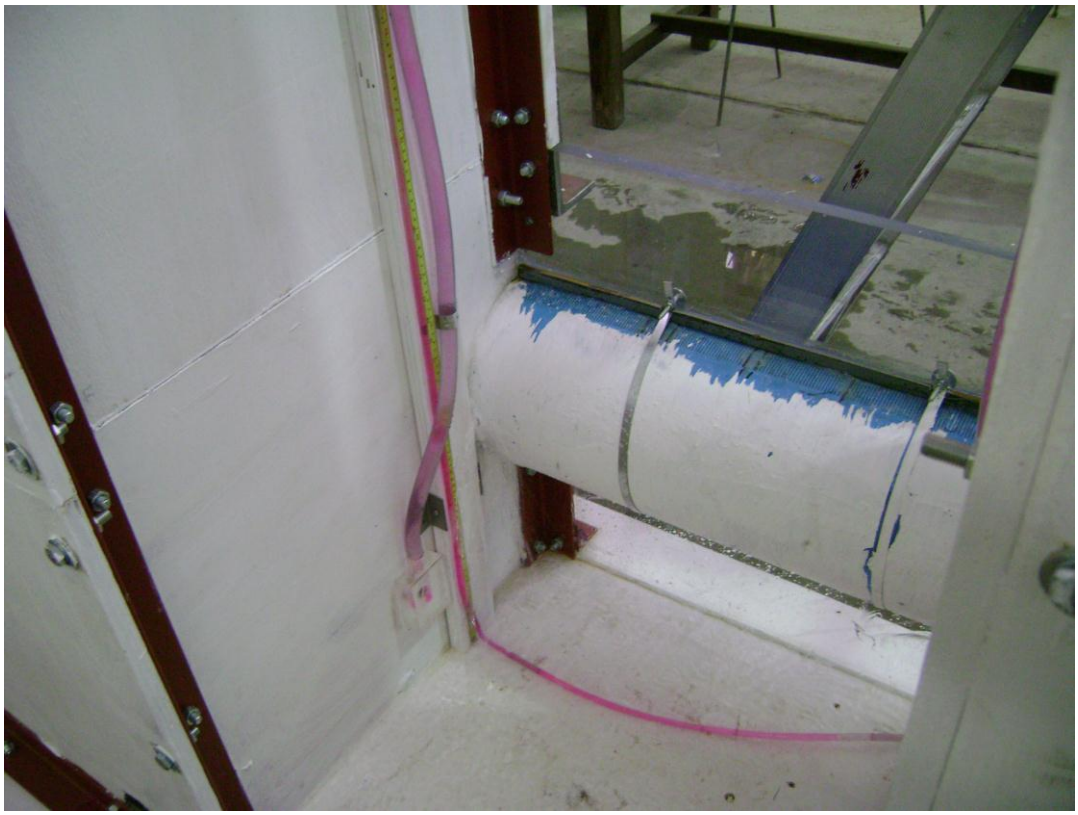

Figure A3: Tubing to measure height of water in a column

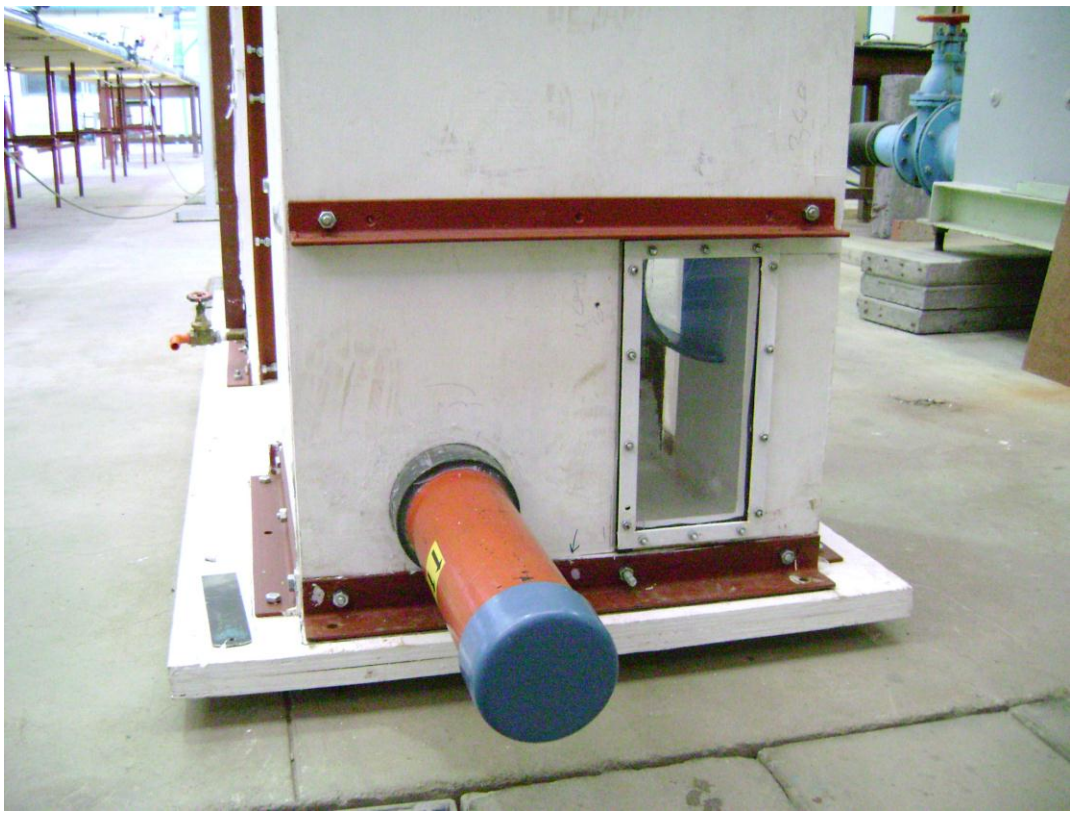

Figure A4: Outlet and Inspection window to Water Column 2

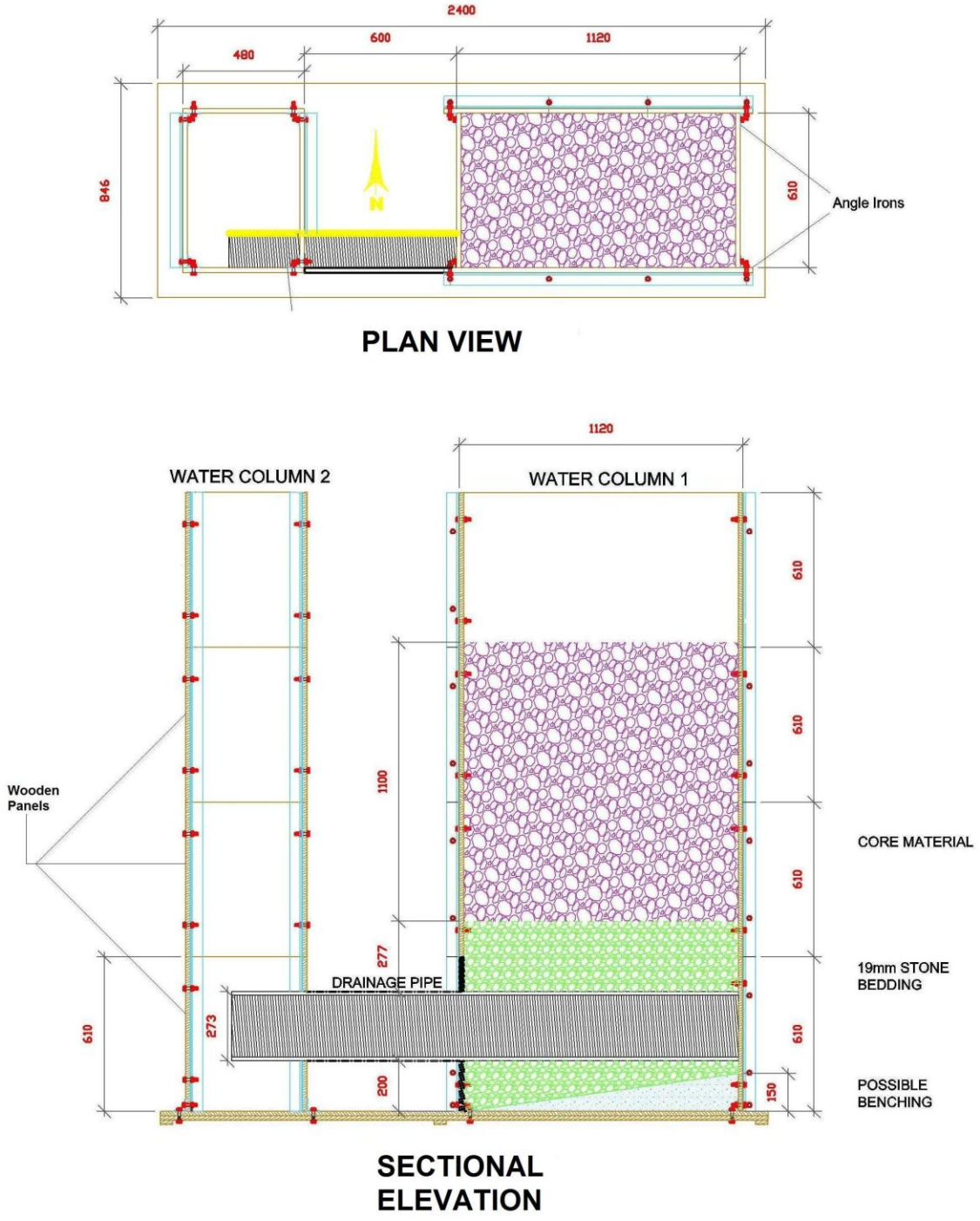

Figure A5: Construction Drawing of Hydraulic Model

Appendix B

Calibration of V Notch Weir

B.1 Introduction

In order to measure the flow, a 90˚ V notch weir was installed in the second water column. Using the appropriate outflow theory, the flow can be estimated by the following Equation B1.

$$q = C_d \cdot \frac{8}{15} \cdot \sqrt{2g} \cdot \tan\frac{\theta}{2} \cdot h^{\frac{5}{2}} \qquad \text{EqnB1}$$

Where

q = flow rate (m^3/s)

h = head on the weir (m)

θ = v-notch angle in degrees

g = 9.81 (m/s^2) - gravity

C_d= discharge constant for the weir

These parameters can be seen in the following Figure B1

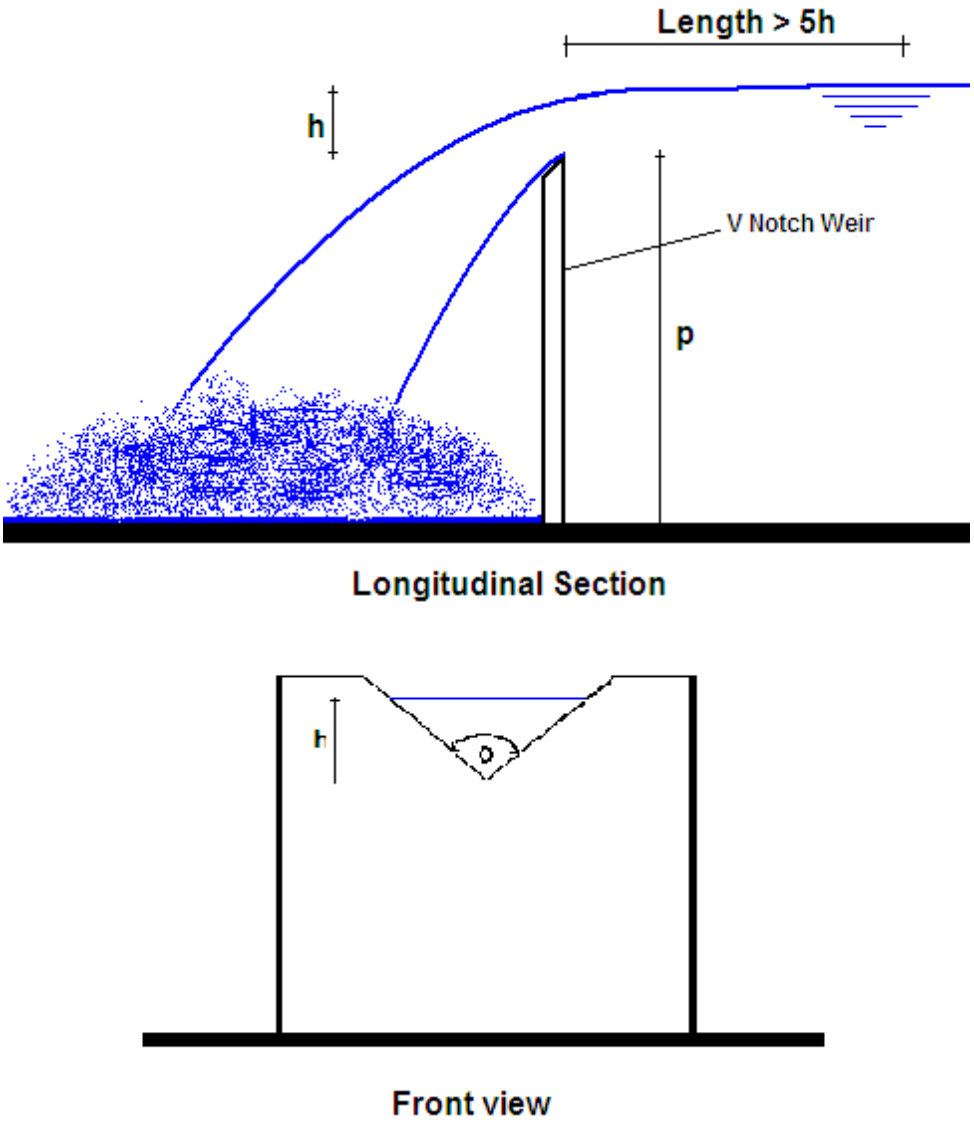

Figure B1: V notch weir used for flow calculations

Referring to Figure B1, when measuring the depth of flow over the V notch, the measuring point should be 5 times the approximated height, upstream of the weir. However when looking at the model, it is found that the inner wall of the second compartment is only 28cm away from the V notch weir. Considering that the maximum height of over the V is 20cm, the length of freeboard required at during peak flow would be 100cm. This is in excess of the 28cm restriction; hence the weir has to be calibrated for the particular model.

The V notch weir was calibrated in a 600mm flume. Figure B2 shows this installed with the appropriate timber and fastenings.

Figure B2a: V Notch Weir

Figure B2b: Flow augmenting structure adjacent to V notch weir on the right

Due to the actual V notch weir being situated within a confined environment and with the model flow being vertical rather than horizontal, a flow augmenting structure was built adjacently upstream of the weir to mimic the constrained environment and the upward direction of flow within the actual model. Figure B2 and Figure B1b give an indication of the structure and implied effects.

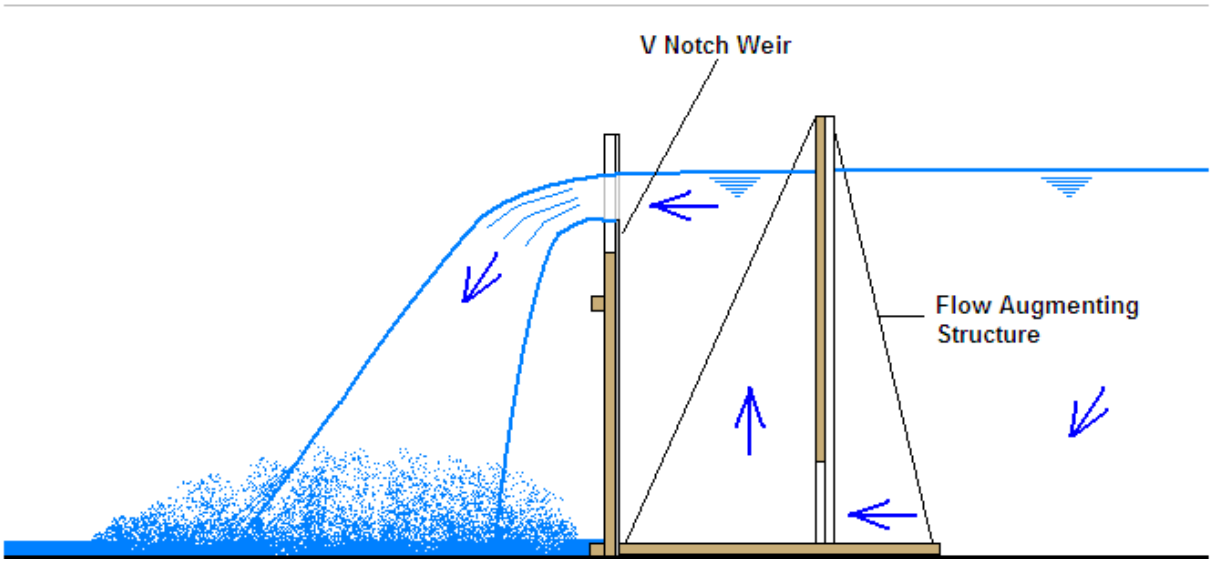

Figure B3: V notch weir and additional structure depicting flow pattern

B.2 Calibration of V Notch Weir

The method used for the calibration of the V notch was a simple one that involved measuring the height of water and then collecting a measurable volume of water in a certain period of time t. From this information a Height vs. Flow relationship was established. For the various heights used, at least 5 samples were taken in order to provide an adequate estimation of the flow.

As explained above, the best way to calibrate the V notch weir is to measure the volume collected over a specific time period. With the measuring vessel calibrated, the next step would be to measure the height of flow at the V notch and also a point 28cm upstream of the V. Here two measuring needles were used as can be seen in Figure B3 and Figure B3.

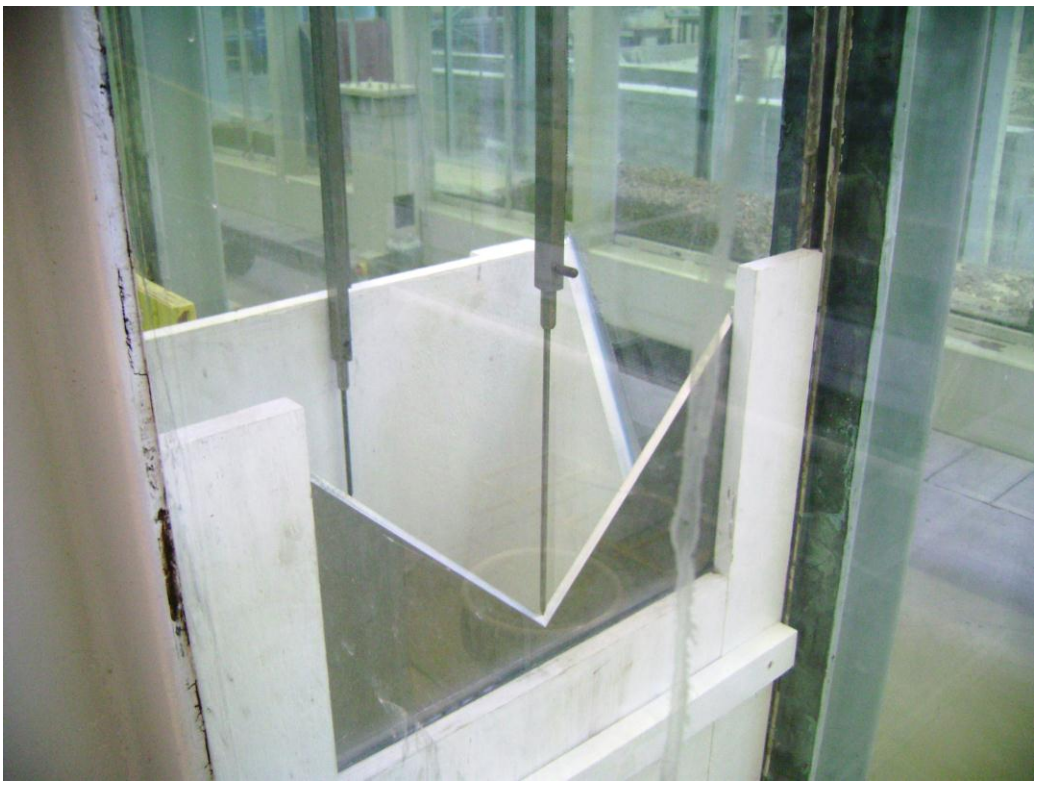

Figure B4: V notch weir with Measuring Needles

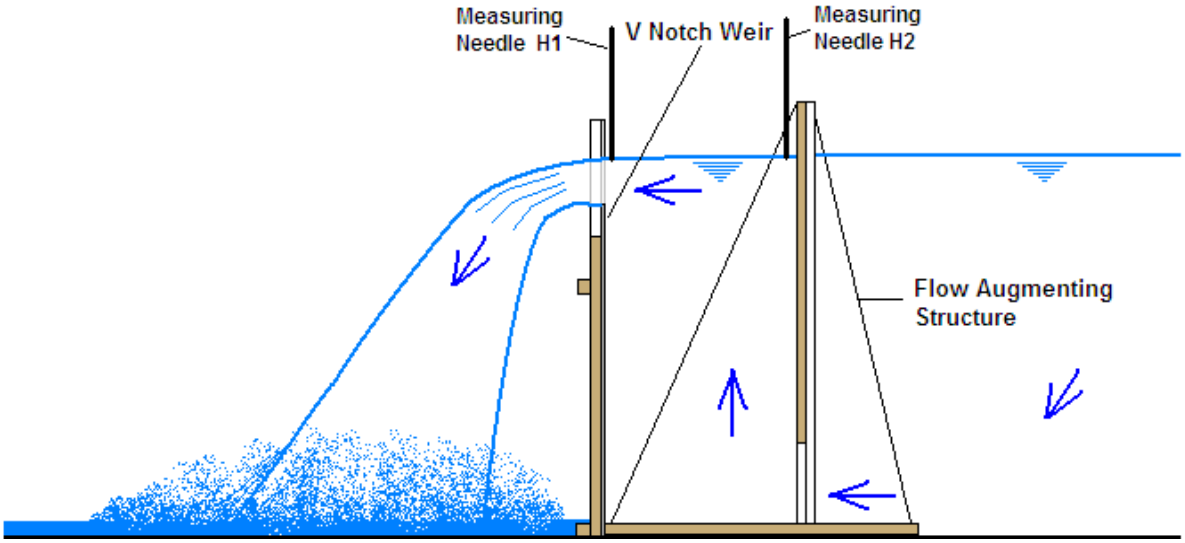

Figure B5: V notch weir, additional structure and measuring needle orientation

The water depth is measured at the V notch and at a point 28cm upstream of the V notch by Needles H1 and H2respectively. This is done so that the Velocity Head can be checked against the actual difference between H1 and H2. The measuring vessel, by means of an overhead crane, was used to collect water for a period of time. Hence the flow was easily calculated. This was done for a minimum of 5 times and the average value noted as the flow for that certain height.

The average flow was calculated from 6 various heights. These are presented in Table B1 below and plotted in Figure B6

Table B1:Flow vs. Height for V Notch Weir

Height mm	Flow q l/s
156	12.84
128	8.28
110	5.71
98	4.31
96	4.12
80	2.61
59	1.15

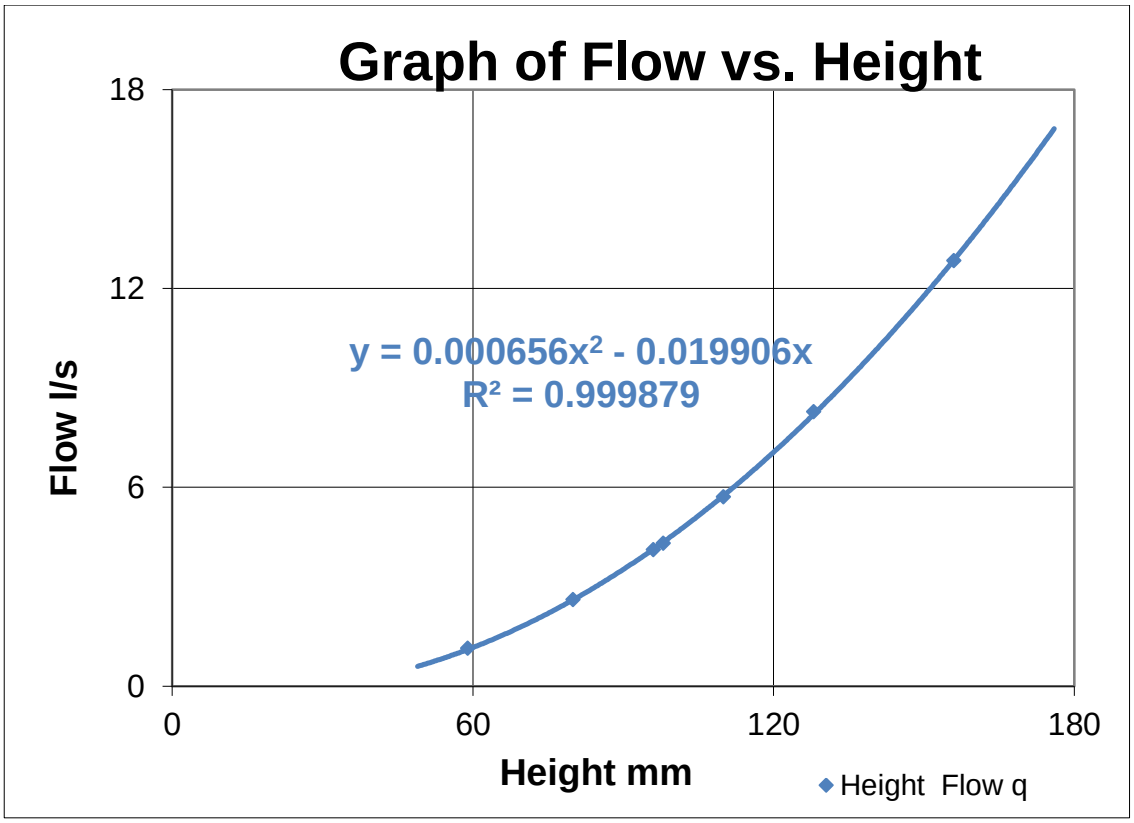

Figure B6:Flow vs. Height for 90 V Notch Weir

Hence the Equation B3 best describes the relationship between height and volume of the measuring vessel.

$$q = 0.000656\,h^2 - 0.019906\,h \qquad \text{Eqn. B2}$$

Where

q= Flow (l/s)

h = depth of water above V Notch (mm)

B 3 Comparison of conventional and calibrated overflow equations

A comparison was made using the convention overflow equation B1 below and the calibrated equation B2 above.

$$q = C_d \cdot \frac{8}{15} \cdot \sqrt{2g} \cdot \tan\frac{\theta}{2} \cdot h^{\frac{5}{2}} \qquad \text{Eqn. B3}$$

Where

C_d= 0.57

A comparison of these results can be seen in Table B2 and Figure B7

Table B2: Flow vs. Height for 90° V Notch Weir

Height mm	Flow q l/s	Flow Equation B1 l/s
156	12.84	12.94
128	8.28	7.89
110	5.71	5.40
98	4.31	4.05
96	4.12	3.84
80	2.61	2.44
59	1.15	1.14

In Table B2, the second column indicates the average values for flow from calibration tests, while the third column indicates the flow calculated from equation B1. Here the recommended value for C_d is 06 to 0.57 is recommended (RCC 1990). A Cd value of 0.57 is used

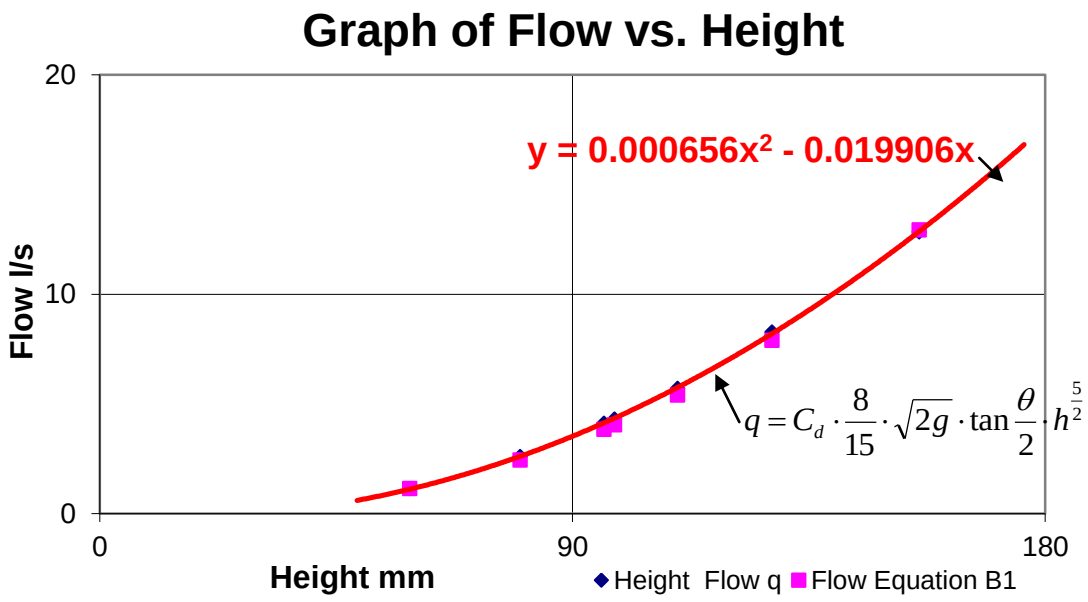

Figure B7: Flow vs. Height curves for Calibrated and Conventional outflow calculation

The plot of this comparison is found on Figure B7. The correlation for both the equations is found to be 0.9991. This shows that the flow can be predicted quite accurately using the conventional formulae with a Cd value of 0.57.

Appendix C

Soil Grading

C.1 Introduction

A combination of two equally weighted soils was used in the testing of the model. This was done so that a larger average grain size achieved. Hence this would compensate for the larger grain sizes found on the east coast of South Africa. The first being a fine grained 'beach' sanded called Phillipi that is found around the Cape. The second was a 'single sized' granular sand which is normally used as filter material. The majority of the fine Phillipi grain size was in between the region of 0.15mm and 0.6mm. This can be seen in the partial grading curve in Figure C1

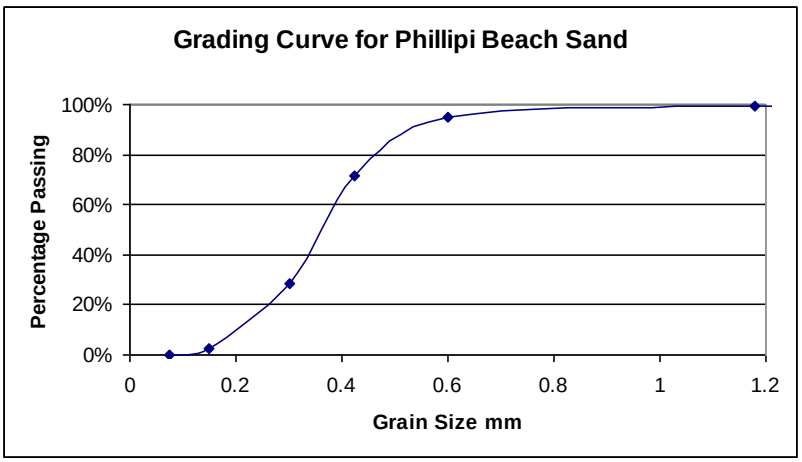

Figure C1: Partial grading curve for Phillipi sand

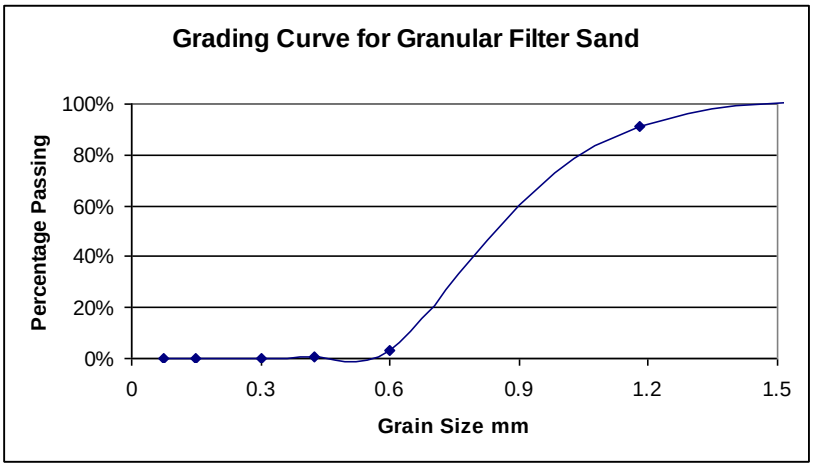

Figure C2: Partial grading curve for Granular Filter sand

The granular filter sand in contrast had a huge gap grading. Approximately 85% of its particles were in between the region of 0.6mm and 1.18mm. This can be seen in the partial grading curve in Figure C2

The combined equal masses of both sands yields the following sand grading as calculated in Table C1 and depicted graphically as a grading curve in Figure C3.

Table C1: Soils grading for combined Phillipi and Granular Filter sand

Percentage Passing	Mass Retained (g)	Percentage Retained	Percentage Passing
100.00%	0.0	0.0%	100.00%
99.80%	2.7	0.1%	99.86%
99.74%	1.9	0.1%	99.75%
99.66%	81.2	4.4%	95.38%
95.00%	857.4	46.2%	49.22%
71.34%	246.5	13.3%	35.95%
28.79%	398.4	21.4%	14.51%
2.35%	247.5	13.3%	1.18%
0.05%	21.5	1.2%	0.02%
0.00%	0.4	0.0%	0.00%
Total	1857.7		

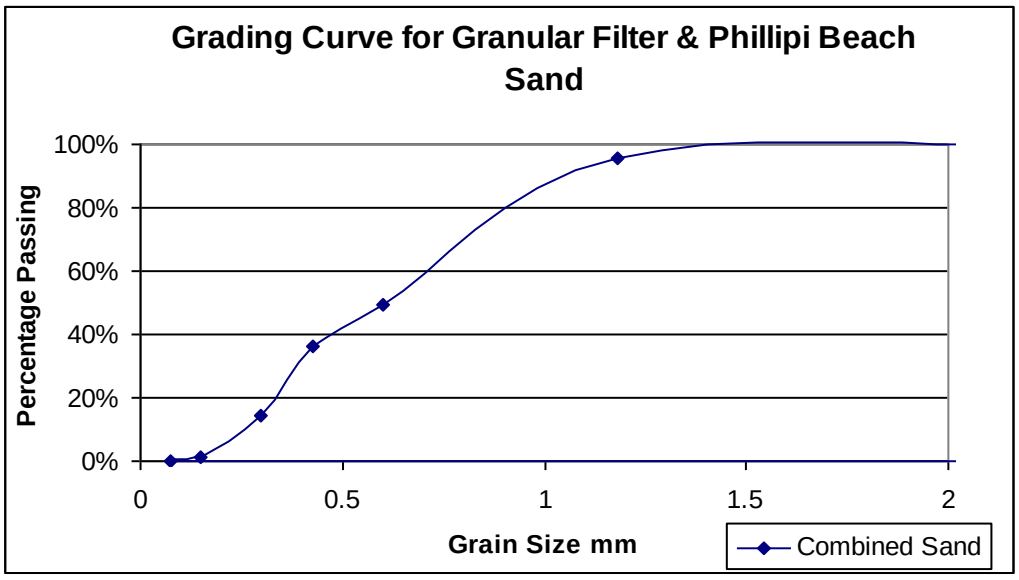

Figure C3: Partial grading curve for combined Phillipi and Granular Filter sand

Appendix D

Slotted PVC Pipe Abstraction Model

Table of Contents

Description	Page
D.1 Introduction	178
D.2 Pressure Losses	178
D.3 Water Losses due to Leakage	179
D.4 Water Test Only	181
D.4.1 Water Leakage losses	184
D.4.2 Water Pressure losses	185
D.4.3 Perforation losses and Flowrate Relationship	186
D.4.4 Segmental Analysis of HPM	188
D.5 Water and Stone Test	193
D.5.1 Water Leakage losses	196
D.5.2 Water Pressure losses	197
D.5.3 Relationship between Flowrate, Perforation and Stone and Bedding friction	198
D.5.4 Segmental Analysis of HPM	200
D.5.4.1 Methodology	201
D.5.4.2 Pressure loss due to Stone Bedding	204
D.5.4.2.1 Method 1: Simple method for determining headloss due to stone bedding	204
D.5.4.2.2 Method 2: Kenny, Lau and Ofoegbu Method for determining headloss due to stone bedding	206
D.5.4.2.3 Method 3: Forchheimer Method for determining headloss due to stone bedding	218
D.5.4.3 Comparison of Results for Method 1, 2 and 3	229
D.6 Water Sand and Stone Bedding Test before Flushing	230
D.6.1 Water Leakage losses	213
D.6.2 Pressure losses	232
D.6.3 Perforation losses and Flowrate Relationship	233
D.7 Water Sand and Stone Bedding Test after Flushing	235
D.7.1 Water Leakage losses	237
D.7.2 Pressure losses	238
D.7.3 Perforation losses and Flowrate Relationship	239

D.1 Introduction

This appendix describes in detail the calculations behind Chapter5.1: Slotted PVC Pipe Abstraction Model. Via the use of figures and tables the most relevant calculations are explained. Neither armour, core nor intermediatelayer materialwere used for the tests. Figure D1 below describes the model and the areas of interest which are used when undertaking calculations.

D. 2 Pressure Losses

Chapter 4.4.6 describes the losses A to E. Note that the datum of the model is the top of the model base.

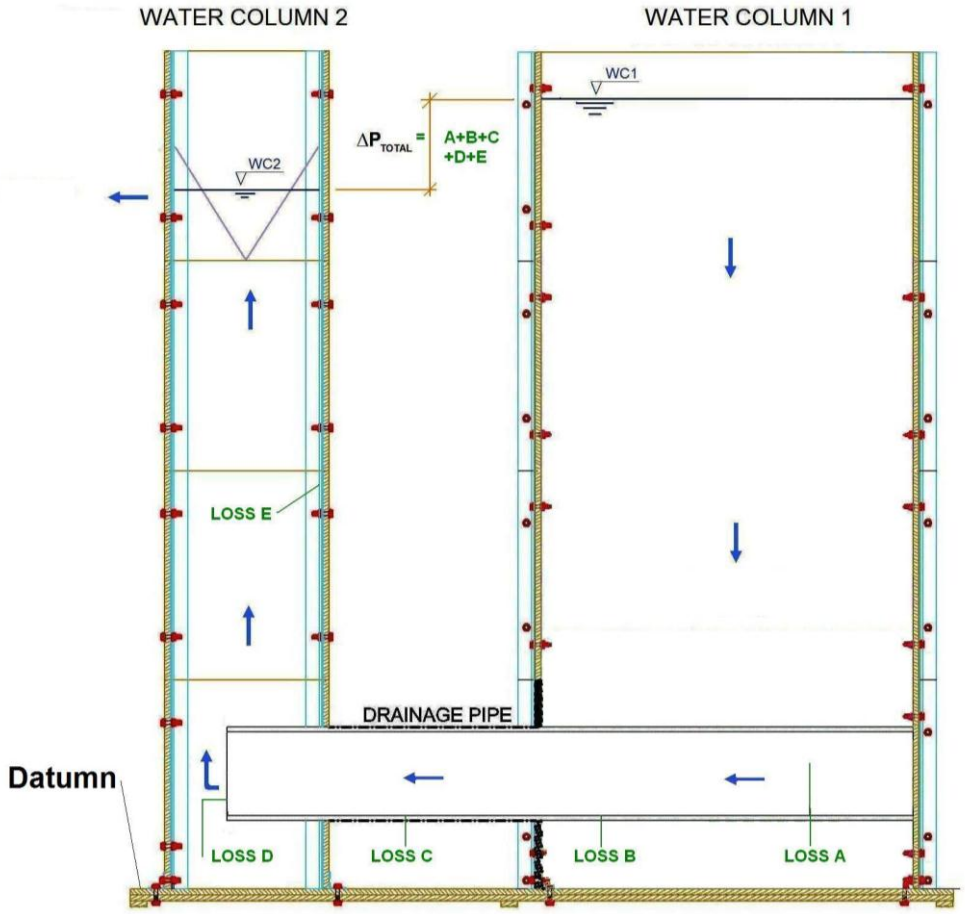

Figure D1: Slotted PVC Pipe Abstraction Model: Areas of interest

The following is a reiteration of the losses A to E. as described in Chapter4.4.6.1

Loss A: This reduction in pressure occurs as water travels from the outside of the pipe, in. Losses B to E can be easily estimated using conventional calculation methods. Loss A accounts for a significantly large portion of the total pressure loss.

Loss B: Skin friction in the portion of intake pipe where there is water ingression and transportation. The skin friction in this chapter is calculated using Manning's Method. A pipe of 250mm is used as the conduit size. However, the skin friction in this area is halved as theoretically the flow is at its maximum as it exits WC1 and zero at the start of the pipeline (Right hand side of Figure D1)

Loss C: Skin friction in the portion of intake pipe where there is water transportation only. The skin friction in this chapter is calculated using Manning's Method. A pipe of 250mm is used as the conduit size.

Loss D: Exit loss as water enters Column 2 (WC2). For the flow exiting the Intake pipe and then turning 90 degrees, the loss is equal to $Ke*V^2/2g$ where Ke = 1

Loss E: Skin friction as water flows up WC2. The skin friction in this chapter is calculated using Manning's Method. A rectangular section of 600mm by 250mm is used as the conduit size.

D. 3 Water Losses due to Leakage

The ability to quantify leakage is crucial especially if the leakage rate becomes a large fraction of the overall flow. Hence the flow rate of the leakage for each increment of the flow through the model was noted.

The entire leakage rate was calculated by constructing a dam around the HPM, and determining the amount of water that left the dam, over a period of time, for a particular increment a test. There were three placesfrom where water could have leaked. These were: WC1, WC2a and WC2b. Figure D2 below describes the emanation of the leak location via a visual inspection, 40% of all leakage was deemed to be out of WC1, 40% out of WC2a and 20% out of WC2b.

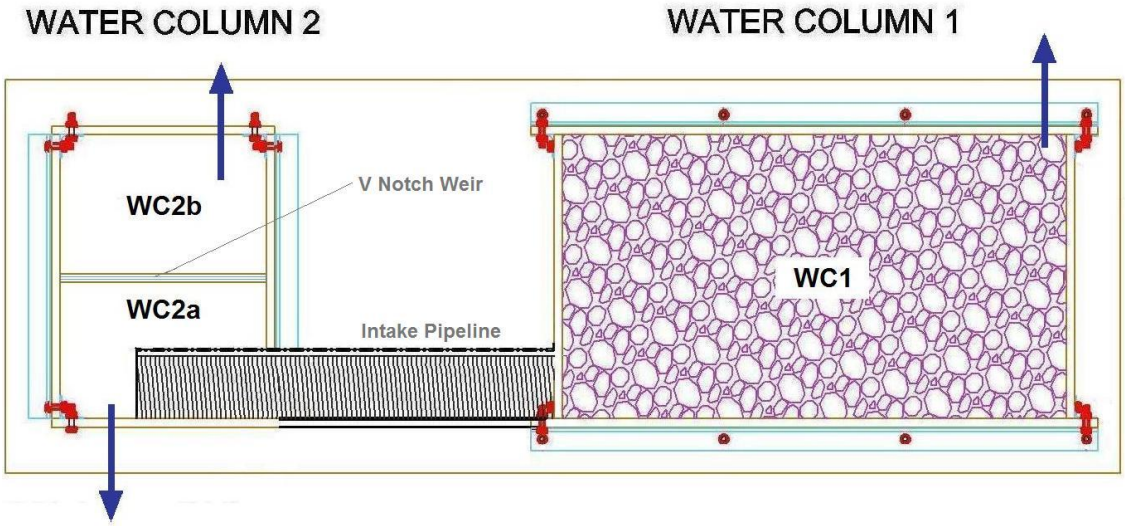

Figure D2: Areas of Water Leakage

D.4: Water Test Only

The following explains the manner in which the 'Water Only Test' (WOT) was conducted and uses tables and equations to illustrate the analysis process. Table D1 details the physical aspects of the model including the Intake pipeline.

Table D1: The physical aspects of the HPM and Intake Pipeline (WOT)

Description	Value	Unit
Physical aspects of the HPM:WC2a		
Angle of V Notch Weir	90	Degrees
Height of V Notch Weir	2015	mm
Length	0.28	m
Breath	0.45	m
Area A	0.126	m^2
Wet Perimeter P	1.46	m
Hydraulic Radius R	0.0863	m
Friction Factor f	0.02	
Loss CoefficientKe	1	
Slotted Pipeline Perforation Configuration		
D Pipe Length	1055	mm
Pipe OD	250	mm
Pipe ID	230	mm
Half Pipe Area	0.0208	m^2
Wet Perimeter	0.5911	m
Hydraulic Radius Pipe HR	0.1405	m
No of Slots per 20cm Length	50	
Area of each Slot	392.5	mm^2
Length of Pipe	1055	mm
No. of Segments	5	
Segment Length	211	mm
Perforation Area of Segment	19625	mm^2
Total Perforation Area	98125	mm^2
Total pipe Wetted Surface Area	414087.5	mm^2
Percentage perforation	23.70%	
Friction Factor f	0.015	

Where:

C_d = Coefficient of Discharge as established in Appendix B

D Pipe Length = Length of Intake pipeline in the HPM

Pipe OD = Outside Diameter of Intake Pipeline

Pipe ID = Inside Diameter of Pipeline

Half Pipe Area = The area of flow when only half a pipe is used

Wet Perimeter = Perimeter of the intake pipeline that has been in contact with the flow

Hydraulic RadiusHR = the Hydraulic Radius of the Intake Pipeline or WC2a

The aim of this experiment is to establish the relationship between the flow and the loss of pressure head as it passes into the Intake pipeline. Using the above information, 19 incremental testwith increasing driving heads, where conducted. Table D2 shows the initial results. The difference between WC1 and WC2 denotes the total headloss. The flow rate was determined from the following Equation B1

$$Q = C_d \cdot \frac{8}{15} \cdot \sqrt{2g} \cdot \tan\frac{\theta}{2} \cdot h^{\frac{5}{2}}$$ Eqn B1

Where

Q = *Flow (l/s)*

C_d= *0.57*

H = *depth of water above V Notch (mm)*

Table D2: Total Headloss and initial flow rate for Water Only test

Test No.	WC1	WC2	Upstream Head	Downstream Head	Total ∆hf	Initial Q Half Pipe
	mm	mm	mm	mm	mm	l/s
1	2064.5	2064	49.5	49	0.5	0.72
2	2079	2078	64	63	1	1.34
3	2092	2089	77	74	3	2.01
4	2101	2096	86	81	5	2.51
5	2112	2105	97	90	7	3.27
6	2118.5	2109.5	103.5	94.5	9	3.70
7	2125.5	2115	110.5	100	10.5	4.26
8	2137	2123	122	108	14	5.16
9	2150	2132.5	135	117.5	17.5	6.37
10	2160	2139	145	124	21	7.29
11	2173	2145.5	158	130.5	27.5	8.28
12	2182	2149	167	134	33	8.85
13	2195.5	2154.5	180.5	139.5	41	9.79
14	2212	2160	197	145	52	10.78
15	2228	2163	213	148	65	11.35
16	2248	2169	233	154	79	12.53
17	2277	2177	262	162	100	14.22
18	2325	2184	310	169	141	15.81
19	2377	2194	362	179	183	18.25

After the total headloss and initial flow rate relationship has been established, Water leakage has to be considered. As per chapter D3, theses losses are incorporated in Table D3 with 40% of all leakage deemed to be out of WC1, 40% out of WC2a and 20% out of WC2b.

D.4.1 Water Leakage losses

In Table D3, the total leakage rate is calculated in Column 6. Columns 7, 8 and 9 calculate the loss for WC1, WC2a and WC2b, respectively. The Total flow rate Q is calculated as the Initial flow rate plus the leakage from WC1 and WC2a

Table D3: Total headloss and flow rate incorporating losses (WOT)

1	2	3	4	5	6	7	8	9	10
Test No.	Q Half Pipe	Bucket Ht	Time	Volume	Total	Loss due to WC1	Loss due to WC2a	Loss due to WC2b	Total Q
	l/s	mm	s	l	l/s	l/s	l/s	l/s	l/s
1	0.72	302	1643.2	80.42	0.049	0.019577	0.019577	0.009789	0.75
2	1.34	314	1685.4	84.00	0.050	0.019935	0.019935	0.009967	1.38
3	2.01	293	1565.8	77.76	0.050	0.019865	0.019865	0.009933	2.05
4	2.51	161	1037.2	40.60	0.039	0.015659	0.015659	0.007830	2.55
5	3.27	163	1049.2	41.14	0.039	0.015685	0.015685	0.007842	3.30
6	3.70	211	1337.8	54.27	0.041	0.016226	0.016226	0.008113	3.73
7	4.26	160	1000.9	40.34	0.040	0.016120	0.016120	0.008060	4.29
8	5.16	168	1076.7	42.49	0.039	0.015784	0.015784	0.007892	5.19
9	6.37	168	1086.1	42.49	0.039	0.015648	0.015648	0.007824	6.40
10	7.29	160	1067.4	40.34	0.038	0.015116	0.015116	0.007558	7.32
11	8.28	132	1056.6	32.91	0.031	0.012458	0.012458	0.006229	8.31
12	8.85	130	1096.2	32.38	0.030	0.011816	0.011816	0.005908	8.87
13	9.79	117	1045	28.99	0.028	0.011098	0.011098	0.005549	9.81
14	10.78	63	631.6	15.27	0.024	0.009671	0.009671	0.004836	10.80
15	11.35	77	763.3	18.77	0.025	0.009838	0.009838	0.004919	11.37
16	12.53	67	465.6	16.27	0.035	0.013976	0.013976	0.006988	12.56
17	14.22	145	672	36.34	0.054	0.021629	0.021629	0.010815	14.27
18	15.81	162	757	40.87	0.054	0.021597	0.021597	0.010799	15.85
19	18.25	125	639.2	31.08	0.049	0.019446	0.019446	0.009723	18.29

D.4.2 Water Pressure losses

After the correct total flow has been established, the next step is the disaggregation of pressure losses. This is done so that Loss A, the loss of pressure as water enters the Intake pipeline, can be established. Chapter D2 states the Pressure Losses A to E with the relevant equations. Table D4 calculates the Losses B to E and hence the remaining total headloss will be Loss A.

Table D4: Disaggregation of pressure losses (WOT)

Test No.	Total ∆hf	Total Q	Loss B+C	Loss D	Loss E	Loss A	%A of Total ∆hf
	mm	l/s	m	m	m	mm	
1	0.5	0.75	0.000010	0.000061	0.0000071	0.48	0.00%
2	1	1.38	0.000034	0.000213	0.0000248	0.94	94.11%
3	3	2.05	0.000076	0.000476	0.0000555	2.87	95.61%
4	5	2.55	0.000120	0.000747	0.0000873	4.79	95.86%
5	7	3.30	0.000203	0.001266	0.0001478	6.65	94.99%
6	9	3.73	0.000259	0.001616	0.0001886	8.55	95.03%
7	10.5	4.29	0.000343	0.002144	0.0002503	9.91	94.35%
8	14	5.19	0.000504	0.003150	0.0003677	13.13	93.77%
9	17.5	6.40	0.000769	0.004801	0.0005605	16.17	92.40%
10	21	7.32	0.001006	0.006284	0.0007337	19.26	91.71%
11	27.5	8.31	0.001299	0.008114	0.0009472	25.25	91.83%
12	33	8.87	0.001483	0.009261	0.0010812	30.44	92.23%
13	41	9.81	0.001813	0.011325	0.0013221	37.86	92.35%
14	52	10.80	0.002200	0.013740	0.0016041	48.20	92.68%
15	65	11.37	0.002438	0.015222	0.0017770	60.79	93.52%
16	79	12.56	0.002973	0.018568	0.0021676	73.86	93.49%
17	100	14.27	0.003830	0.023918	0.0027923	93.38	93.38%
18	141	15.85	0.004732	0.029552	0.0034500	132.82	94.20%
19	183	18.29	0.006308	0.039393	0.0045988	172.09	94.04%

D.4.3 Perforation losses and Flowrate Relationship

Table D5 below shows the Intake pipeline perforation friction (Loss A) and the flowrate for half a pipe and for a full pipeline. Figure D3 show the relationship between the Perforation friction and the flowrate in a 250mm Slotted PVC Pipeline.

Table D5: Perforation friction (Loss A) flowrate Half and Full pipeline (WOT)

Test No.	Loss A	Q Half Pipe	Q Full Pipe
	mm	l/s	l/s
1	0.48	0.75	1.51
2	0.94	1.38	2.76
3	2.87	2.05	4.09
4	4.79	2.55	5.09
5	6.65	3.30	6.61
6	8.55	3.73	7.46
7	9.91	4.29	8.58
8	13.13	5.19	10.39
9	16.17	6.40	12.81
10	19.26	7.32	14.64
11	25.25	8.31	16.62
12	30.44	8.87	17.75
13	37.86	9.81	19.62
14	48.20	10.80	21.60
15	60.79	11.37	22.73
16	73.86	12.56	25.12
17	93.38	14.27	28.53
18	132.82	15.85	31.71
19	172.09	18.29	36.59

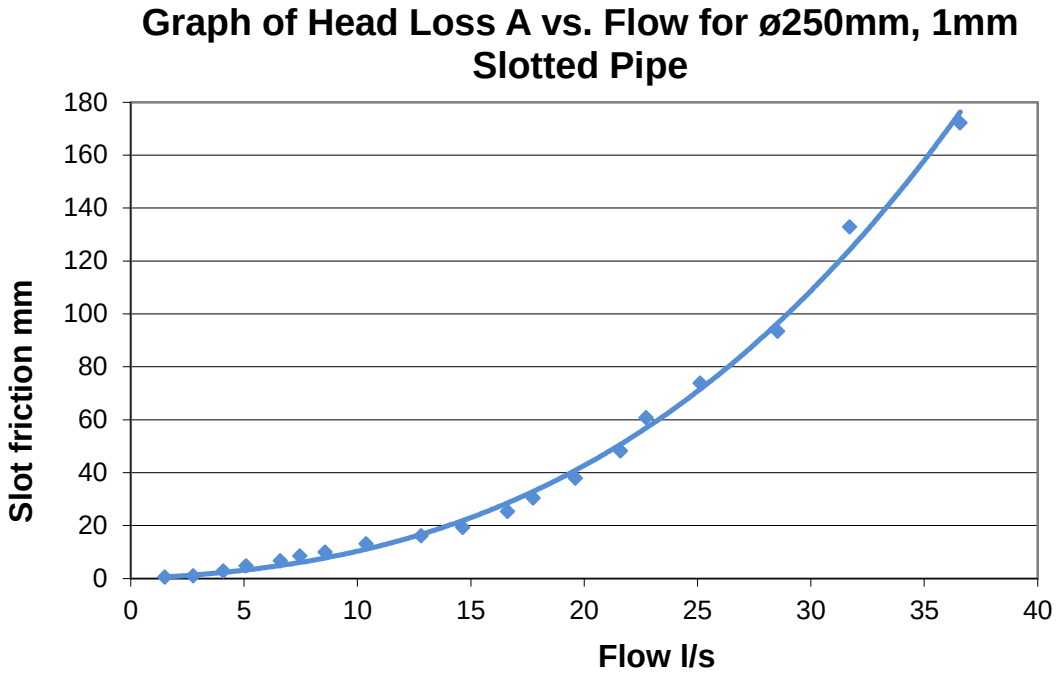

Figure D3: Headloss due to the slots (Loss A) versus the flowrate for a fully flowing ø250mm slotted pipe

The equation below describes the relationship between headloss due to slot friction and flowrate

$$\Delta P = 0.0518Q^2 + 0.3206Q \qquad \text{(Eqn 1)}$$

With

ΔP = Headloss due to slot friction in mm

Q = Flowrate for one full pipeline in liters/second

D.4.4 Segmental Analysis of HPM

Analysing the Slotted/Perforation friction and flow relationship was relatively simple. However in order to understand the flow regime better, it was required that the flow at different points in the HPM be calculated. It was decided that a model would be better understood if it was segmented. Hence the model was portioned into five segments.

As described by Table D4, the Perforation Loss A accounts for the nearly all of the pressure loss. Hence for a point on the Intake pipeline just inside WC1, the velocity of the flow into the pipeline is at its maximum. The velocity at this point is termed V_{max}. The opposite holds true for a point at the start of the Intake pipeline. At this point, V_{min}, the velocity of the inflow is zero. Hence via linear interpolation, the velocity at any point in between both ends can be calculated. Figure D4 below describes the manner in which the HPM is segmented.

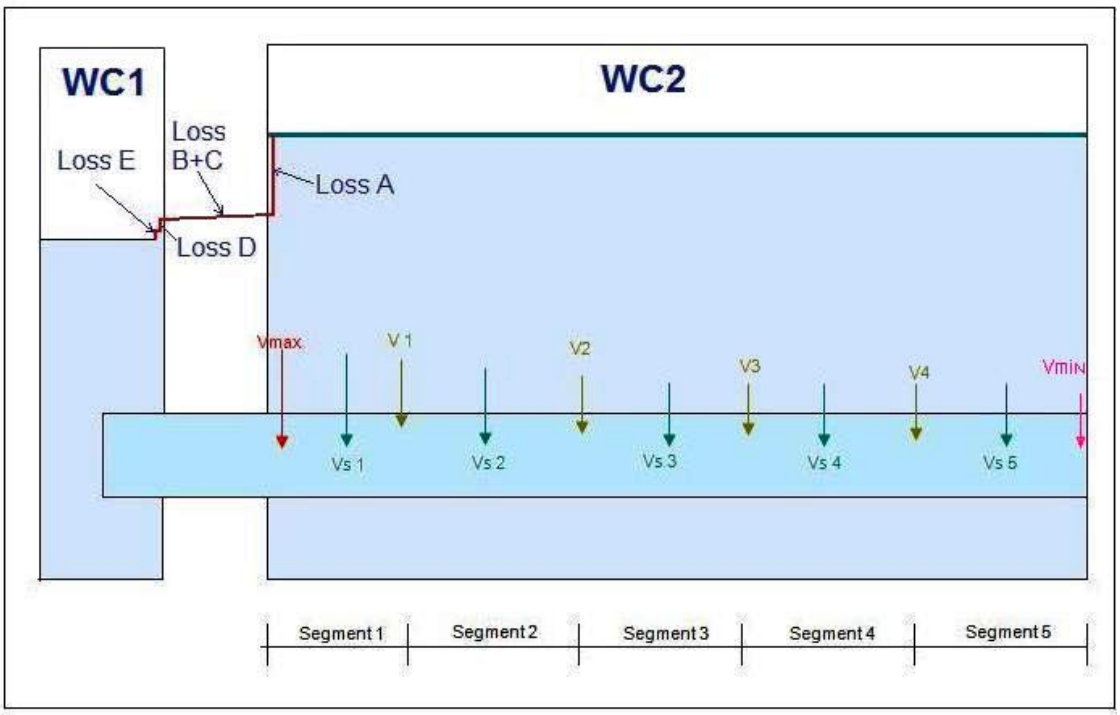

Figure D4: Segmented HPM with notional EGL flow that enters WC1 and exits fromWC2

Methodology

In order to calculate the flow at various points within the model, the HPM was divided into five segments. The velocities V_{MAX}, V_1, V_2, V_3, V_4 and V_{MIN}occur at the border of each segment, hence for each segment, the Average Velocity, V_S1, V_S2, V_S3, V_S4 and V_S5 for each segment is easily calculated.

V_{MAX} is derived from Bernoulli principles where:

$$V = \sqrt{2g\Delta h} \qquad \text{EqnD1}$$

With

V = Velocity in m/s

Δh = is the driving pressure

G = gravitational constant (9.81m/s^2)

Note that the driving pressure Δh is Loss A. The flow from each segment is then calculated by multiplying the velocity with the perforation area and a discharge coefficient, C_d. Table D6 shows the distribution of inflowing velocity over the length of the Intake Pipeline.

Equation D2 was used to calculate the flow from each segment. Table D7contains the flowrate for each segment and the sum of flow from all segments of the pipeline.

$$Q_T = \sum q = \sum C_d A\sqrt{2g\Delta h} \qquad \text{Eqn D2}$$

With

q = Flowrate through for each segment in m^3/s

Q = Sum of Flowrate form each segment in m^3/s

A= The Area through which flow is allowed in m^2

C_d = Coefficient of Discharge

Table D6: Velocity of water flowing into the pipe, over the length of the SPP Intake (WOT)

		Pos. 0	Pos. 1	Pos. 2	Pos. 3	Pos. 4	Pos. 5	Pos. 6	Pos. 7	Pos. 8	Pos. 9	Pos. 10
Test	Loss A	Vmax	Vs 1	V1	Vs 2	V2	Vs 3	V3	Vs 4	V4	Vs 5	Vmin
0	mm	m/s	m/s	m/s	m/s	m/s	m/s	m/s	m/s	m/s	m/s	m/s
1	0.48	0.097	0.088	0.078	0.068	0.058	0.049	0.039	0.029	0.019	0.010	0.0
2	0.94	0.136	0.122	0.109	0.095	0.082	0.068	0.054	0.041	0.027	0.014	0.0
3	2.87	0.237	0.214	0.190	0.166	0.142	0.119	0.095	0.071	0.047	0.024	0.0
4	4.79	0.307	0.276	0.245	0.215	0.184	0.153	0.123	0.092	0.061	0.031	0.0
5	6.65	0.361	0.325	0.289	0.253	0.217	0.181	0.144	0.108	0.072	0.036	0.0
6	8.55	0.410	0.369	0.328	0.287	0.246	0.205	0.164	0.123	0.082	0.041	0.0
7	9.91	0.441	0.397	0.353	0.309	0.265	0.220	0.176	0.132	0.088	0.044	0.0
8	13.13	0.508	0.457	0.406	0.355	0.305	0.254	0.203	0.152	0.102	0.051	0.0
9	16.17	0.563	0.507	0.451	0.394	0.338	0.282	0.225	0.169	0.113	0.056	0.0
10	19.26	0.615	0.553	0.492	0.430	0.369	0.307	0.246	0.184	0.123	0.061	0.0
11	25.25	0.704	0.634	0.563	0.493	0.422	0.352	0.282	0.211	0.141	0.070	0.0
12	30.44	0.773	0.695	0.618	0.541	0.464	0.386	0.309	0.232	0.155	0.077	0.0
13	37.86	0.862	0.776	0.690	0.603	0.517	0.431	0.345	0.259	0.172	0.086	0.0
14	48.20	0.972	0.875	0.778	0.681	0.583	0.486	0.389	0.292	0.194	0.097	0.0
15	60.79	1.092	0.983	0.874	0.764	0.655	0.546	0.437	0.328	0.218	0.109	0.0
16	73.86	1.204	1.083	0.963	0.843	0.722	0.602	0.482	0.361	0.241	0.120	0.0
17	93.38	1.354	1.218	1.083	0.947	0.812	0.677	0.541	0.406	0.271	0.135	0.0
18	132.82	1.614	1.453	1.291	1.130	0.969	0.807	0.646	0.484	0.323	0.161	0.0
19	172.09	1.838	1.654	1.470	1.286	1.103	0.919	0.735	0.551	0.368	0.184	0.0

Of particular concern is the Energy Grade Line (EGL) at the centre of the Intake Pipeline. Figure D5 depicts the EGL for the various tests. The EGL shows the amount of energy that has been lost from water merely entering the Intake Pipeline. For this case the loss of pressure is due to perforation friction only. Hence if the Still Water Level (SWL) is known at a particular position along the Intake pipeline, the new EGL would be the still water level in WC1 minus the perforation friction/ Loss A

Table D7: Calculated Flowrate from all segments of the Pipeline (WOT)

Test	Loss A	C_b	Qs 1	Qs 2	Qs 3	Qs 4	Qs 5	Q Total	Q Total	2Q Total
0	mm		m^3/s	m^3/s	m^3/s	m^3/s	m^3/s	m^3/s	l/s	l/s
1	0.48	0.158	0.0003	0.0002	0.0002	0.0001	0.0000	0.0008	0.76	1.51
2	0.94	0.207	0.0005	0.0004	0.0003	0.0002	0.0001	0.0014	1.38	2.76
3	2.87	0.176	0.0007	0.0006	0.0004	0.0002	0.0001	0.0020	2.05	4.09
4	4.79	0.169	0.0009	0.0007	0.0005	0.0003	0.0001	0.0025	2.55	5.09
5	6.65	0.186	0.0012	0.0009	0.0007	0.0004	0.0001	0.0033	3.30	6.61
6	8.55	0.186	0.0013	0.0010	0.0007	0.0004	0.0001	0.0037	3.73	7.46
7	9.91	0.198	0.0015	0.0012	0.0009	0.0005	0.0002	0.0043	4.29	8.58
8	13.13	0.209	0.0019	0.0015	0.0010	0.0006	0.0002	0.0052	5.19	10.39
9	16.17	0.232	0.0023	0.0018	0.0013	0.0008	0.0003	0.0064	6.40	12.81
10	19.26	0.243	0.0026	0.0020	0.0015	0.0009	0.0003	0.0073	7.32	14.64
11	25.25	0.241	0.0030	0.0023	0.0017	0.0010	0.0003	0.0083	8.31	16.62
12	30.44	0.234	0.0032	0.0025	0.0018	0.0011	0.0004	0.0089	8.87	17.75
13	37.86	0.232	0.0035	0.0027	0.0020	0.0012	0.0004	0.0098	9.81	19.62
14	48.20	0.226	0.0039	0.0030	0.0022	0.0013	0.0004	0.0108	10.80	21.60
15	60.79	0.212	0.0041	0.0032	0.0023	0.0014	0.0005	0.0114	11.37	22.73
16	73.86	0.213	0.0045	0.0035	0.0025	0.0015	0.0005	0.0126	12.56	25.12
17	93.38	0.215	0.0051	0.0040	0.0029	0.0017	0.0006	0.0143	14.27	28.53
18	132.82	0.200	0.0057	0.0044	0.0032	0.0019	0.0006	0.0159	15.85	31.71
19	172.09	0.203	0.0066	0.0051	0.0037	0.0022	0.0007	0.0183	18.29	36.59

Figure D5 below is a plot of EGLs at the centre of the Intake Pipeline. For the 19 tests conducted, the increase in pressure losses occurs closer to the exit point of WC1.

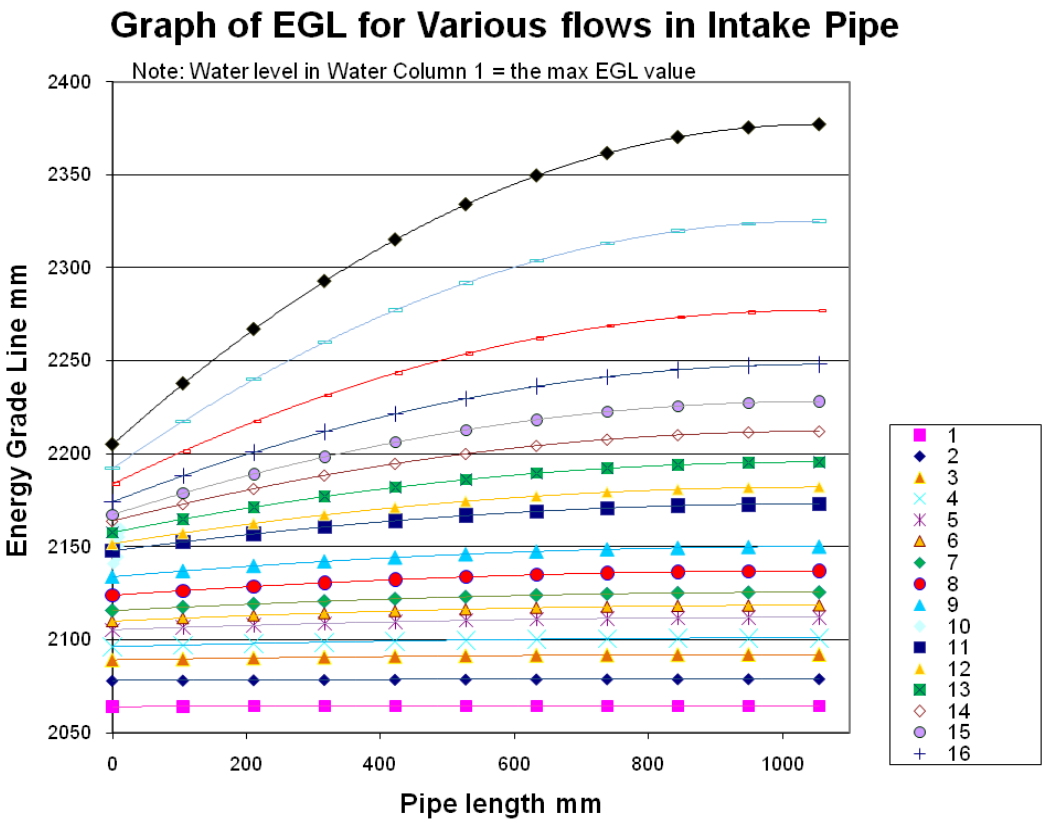

Figure D5: Plot of EGLs at the centre of the Intake Pipeline (WOT)

Combining Figures D4 and D5 produces Figure D6 which shows graphically the EGL as per the Intake pipeline section. With the main Flow versus headloss relationship being the most important, calculation of the EGL might appear of no use, however calculation of EGL at various points in the flow will prove fruitful in future chapters.

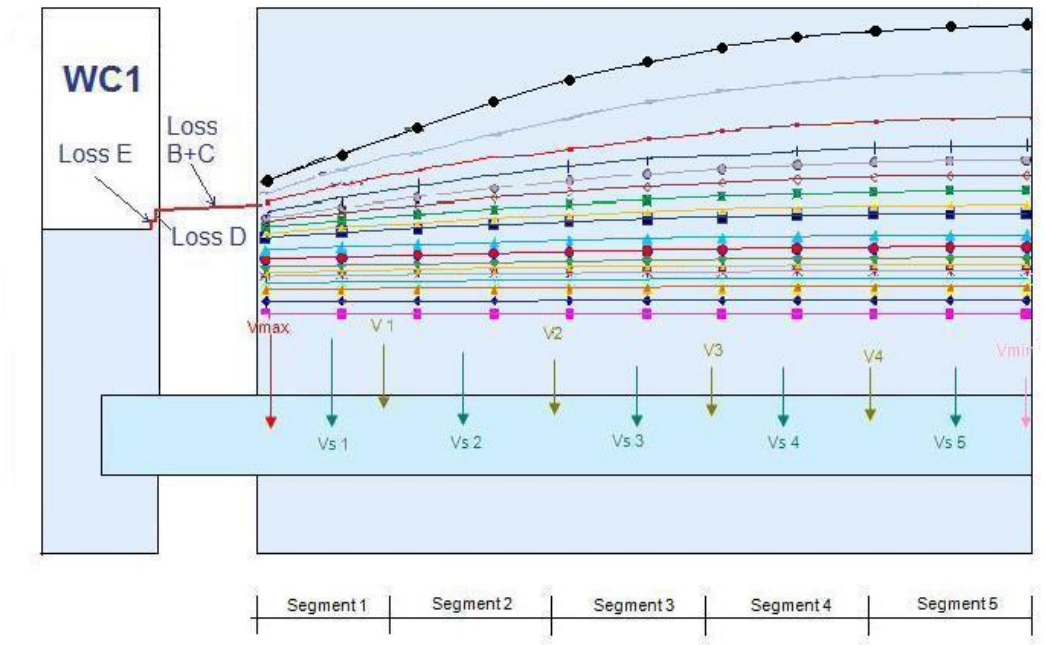

Figure D6: The EGL in the HPM for all nineteen tests (WOT)

D.5: Water and Stone Test

The following elucidates the manner in which the 'Water and Stone Test' (WST)was conducted and uses tables and equations to illustrate the analysis process. Table D8 details the physical aspects of the model including the Intake pipeline.

Table D8: The physical aspects of the HPM and Intake Pipeline (WST)

Description	Value	Unit
Physical aspects of the HPM:WC2a		
Angle of V Notch Weir	90	Degrees
Height of V Notch Weir	2015	mm
Length	0.28	m
Breath	0.45	m
Area A	0.126	m^2
Wet Perimeter P	1.46	m
Hydraulic Radius R	0.0863	m
Friction Factor f	0.02	
Loss Coefficient Ke	1	
Slotted Pipeline Perforation Configuration		
D Pipe Length	1055	mm
Pipe OD	250	mm
Pipe ID	230	mm
Half Pipe Area	0.0208	m^2
Wet Perimeter	0.5911	m
Hydraulic Radius Pipe HR	0.1405	m
No of Slots per 20cm Length	50	
Area of each Slot	392.5	mm^2
Length of Pipe	1055	mm
No. of Segments	5	
Segment Length	211	mm
Perforation Area of Segment	19625	mm^2
Total Perforation Area	98125	mm^2
Total pipe Wetted Surface Area	414087.5	mm^2
Percentage perforation	23.70%	
Friction Factor f	0.015	

Where:

C_d = Coefficient of Discharge as established in Appendix B

D Pipe Length = Length of Intake pipeline in the HPM

Pipe OD = Outside Diameter of Intake Pipeline

Pipe ID = Inside Diameter of Pipeline

Half Pipe Area = The area of flow when only half a pipe is used

Wet Perimeter = Perimeter of the intake pipeline that has been in contact with the flow

Hydraulic Radius HR = The Hydraulic Radius of the Intake Pipeline or WC2a

The aim of this experiment is to:

1) confirm the relationship between the flow and the loss of pressure head as it passes in to the Intake pipeline and to
2) establish the relationship between the flow and the loss of pressure head as it passes through the 19mm Stone bedding.

Using the above information, 15 incremental tests, with increasing driving heads, where conducted. Table D9 shows the initial results. The difference between WC1 and WC2 denotes the total headloss. The flow rate was determined from the following EquationB1

$$Q = C_d \cdot \frac{8}{15} \cdot \sqrt{2g} \cdot \tan\frac{\theta}{2} \cdot h^{\frac{5}{2}} \qquad \text{Eqn B1}$$

Where

Q= Flow (l/s)

C_d= 0.57

h = depth of water above V Notch (mm)

Table D9: Total Headloss and initial flow rate for Water and Stone test (WST)

Test No.	WC1	WC2	Upstream Head	Downstream Head	Total ∆hf	Initial Q Half Pipe
	mm	mm	mm	mm	mm	l/s
1	2050.5	2050	35.5	35	0.5	0.31
2	2059	2058	44	43	1	0.52
3	2069	2067	54	52	2	0.83
4	2080	2077	65	62	3	1.29
5	2099.5	2093.5	84.5	78.5	6	2.32
6	2113	2101.5	98	86.5	11.5	2.96
7	2132	2113.5	117	98.5	18.5	4.10
8	2169	2133	154	118	36	6.44
9	2192	2142	177	127	50	7.74
10	2225	2152	210	137	73	9.35
11	2245	2158	230	143	87	10.41
12	2274	2164	259	149	110	11.54
13	2306	2171	291	156	135	12.94
14	2339	2177	324	162	162	14.22
15	2359	2180	344	165	179	14.89

After the total headloss and initial flow rate relationship has been established, Water leakage has to be considered. As per chapter D3 theses losses are incorporated in Table D10 with 40% of all leakage deemed to be out of WC1, 40% out of WC2a and 20% out of WC2b.

D.5.1 Water Leakage losses

In Table D10, the total leakage rate is calculated in Column 6. Columns 7, 8 and 9 calculate the loss for WC1, WC2a and WC2b, respectively. The Total flow rate Q is calculated as the Initial flow rate plus the leakage from WC1 and WC2a

Table D10: Total headloss and flow rate incorporating losses for Water and Stone Test (WST)

1	2	3	4	5	6	7	8	9	10
Test No.	Q Half Pipe	Bucket Ht	Time	Volume	Total	Loss due to WC1	Loss due to WC2a	Loss due to WC2b	Half PipeQ
	l/s	mm	s	l	l/s	l/s	l/s	l/s	l/s
1	0.31	106	1013.6	26.15	0.026	0.01032	0.010320	0.00516	0.33
2	0.52	62	1055.7	15.02	0.014	0.00569	0.005692	0.00285	0.53
3	0.83	44	758.5	10.58	0.014	0.00558	0.005580	0.00279	0.84
4	1.29	77	654.6	18.77	0.029	0.01147	0.011471	0.00574	1.31
5	2.32	46	725.5	11.07	0.015	0.00610	0.006105	0.00305	2.34
6	2.96	20	316.8	4.76	0.015	0.00601	0.006013	0.00301	2.98
7	4.10	36	560.7	8.63	0.015	0.00616	0.006156	0.00308	4.11
8	6.44	47	858.5	11.32	0.013	0.00527	0.005273	0.00264	6.45
9	7.74	46	657.4	11.07	0.017	0.00674	0.006737	0.00337	7.75
10	9.35	45	635.7	10.83	0.017	0.00681	0.006813	0.00341	9.37
11	10.41	30	418	7.17	0.017	0.00686	0.006864	0.00343	10.43
12	11.54	41	664.5	9.85	0.015	0.00593	0.005928	0.00296	11.55
13	12.94	55	648.4	13.29	0.020	0.00820	0.008197	0.00410	12.96
14	14.22	40	399.4	9.60	0.024	0.00962	0.009618	0.00481	14.24
15	14.89	78	615.9	19.02	0.031	0.01236	0.012355	0.00618	14.92

D.5.2 Water Pressure losses

After the correct total flow has been established, the next step is the disaggregation of pressure losses. This is done so that Loss A, the loss of pressure as water enters the Intake pipeline, can be established. Chapter D2 states the Pressure Losses A to E with the relevant equations. Table D11 calculates the Losses B to E and hence the remaining total headloss will be Loss A.

Table D11: Disaggregation of pressure losses for Water and Stone test (WST)

Test No.	Total ∆hf	Total Half PipeQ	Loss B+C	Loss D	Loss E	Loss A +Stone bedding	%A of Total ∆hf
	mm	l/s	m	m	m	mm	
1	0.5	0.33	0.000002	0.000011	0.0000013	0.50	0.00%
2	1	0.53	0.000005	0.000032	0.0000037	0.99	99.13%
3	2	0.84	0.000013	0.000082	0.0000095	1.98	98.87%
4	3	1.31	0.000031	0.000196	0.0000229	2.95	98.19%
5	6	2.34	0.000102	0.000639	0.0000746	5.82	97.05%
6	11.5	2.98	0.000166	0.001038	0.0001212	11.21	97.50%
7	18.5	4.11	0.000318	0.001988	0.0002320	17.95	97.03%
8	36	6.45	0.000785	0.004904	0.0005725	34.64	96.23%
9	50	7.75	0.001134	0.007082	0.0008268	48.04	96.08%
10	73	9.37	0.001657	0.010346	0.0012078	70.14	96.08%
11	87	10.43	0.002053	0.012818	0.0014965	83.45	95.92%
12	110	11.55	0.002521	0.015743	0.0018379	105.64	96.04%
13	135	12.96	0.003172	0.019805	0.0023121	129.52	95.94%
14	162	14.24	0.003830	0.023918	0.0027923	155.38	95.91%
15	179	14.92	0.004198	0.026217	0.0030606	171.74	95.94%

D.5.3 Relationship between flowrate, Perforation and Stone Bedding friction

Table D12 shows the Intake pipeline perforation friction (Loss A) + stone bedding loss. It also includes the flowrate for half a pipe and for a full pipeline. Figure D7 shows the relationship between the Perforation and stone bedding friction and the flowrate in theø250mm Slotted PVC Pipeline.

Table D12:Perforation (Loss A), and Stone Bedding friction, Half flowrate and Full pipeline flowrate (WST)

Test No.	Loss A +Stone bedding	Q Half Pipe	Q Full Pipe
	mm	l/s	l/s
1	0.50	0.33	0.66
2	0.99	0.53	1.06
3	1.98	0.84	1.68
4	2.95	1.31	2.62
5	5.82	2.34	4.67
6	11.21	2.98	5.95
7	17.95	4.11	8.23
8	34.64	6.45	12.90
9	48.04	7.75	15.51
10	70.14	9.37	18.74
11	83.45	10.43	20.85
12	105.64	11.55	23.10
13	129.52	12.96	25.92
14	155.38	14.24	28.49
15	171.74	14.92	29.83

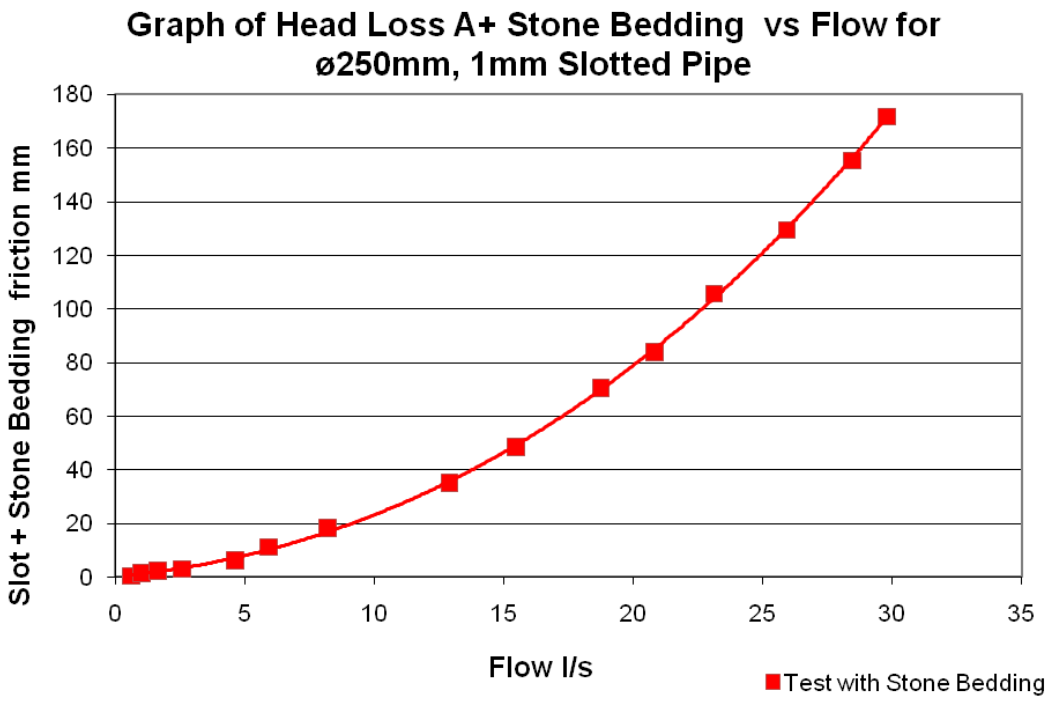

Figure D7: Headloss due to the slots (Loss A) and Stone bedding versus the flowrate for a fullyflowing ø250mm slotted pipe

The equation below describes the relationship between headloss due to slot friction and stone bedding and flowrate

$$\Delta P = 0.1309Q^2 + 0.8725Q \qquad \text{(Eqn 2)}$$

With

ΔP = Headloss due to slot friction in mm

Q = Flowrate for one full pipeline in litres/second

D.5.4 Segmental Analysis of HPM

Analysing the Slotted/Perforation friction + Stone Bedding and flow relationship initially, is as per chapter D.4.4. The flow was calculated at the same points in the HPM.Themodelwasbetter understood when it was portioned into five segments.

As described by Table D11, the Perforation Loss A + Stone Bedding accounts for the nearly all of the pressure loss. Hence for a point on the Intake pipeline just inside WC1, the velocity of the flow into the pipeline is at its maximum. The velocity at this point is termed V_{max}. The opposite holds true for a point at the start of the Intake pipeline. At this point, V_{min}, the velocity of the inflow is zero. Hence via linear interpolation, the velocity at any point in between both ends can be calculated. Figure D8 below describes the manner in which the HPM is segmented.

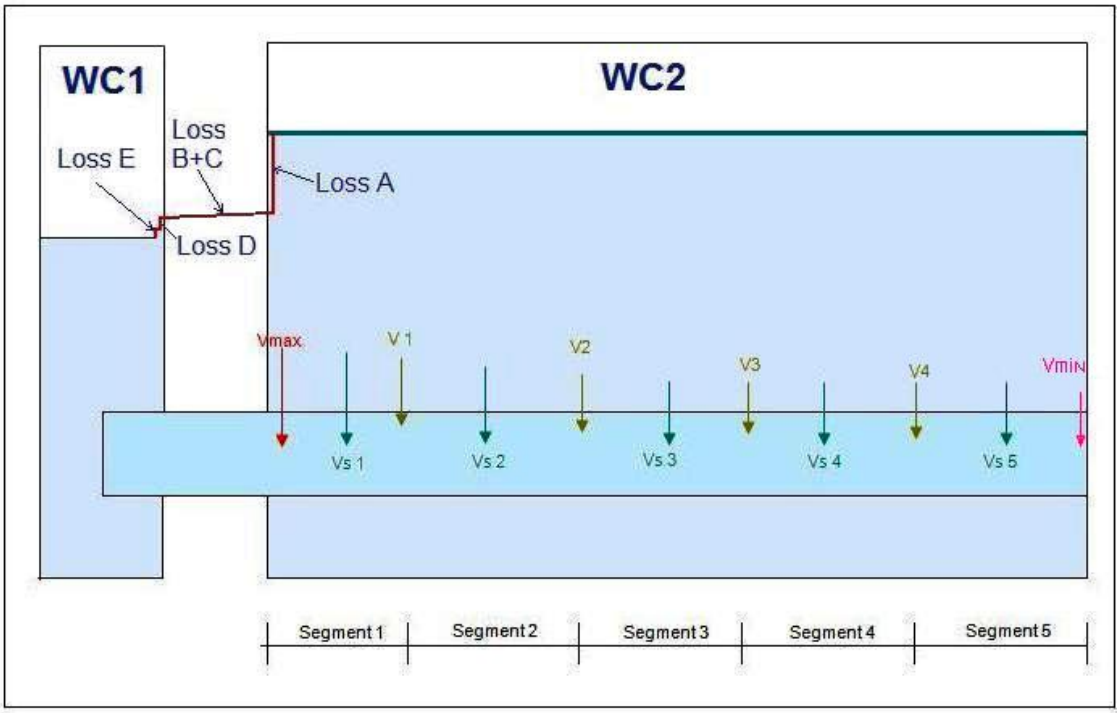

Figure D8: Segmented HPM with notional EGL flow that enters WC1 and exits fromWC2

D.5.4.1 Methodology

In order to calculate the flow at various points within the model, the HPM was divided into five segments. The velocities V_{MAX}, V_1, V_2, V_3, V_4 and V_{MIN} occur at the border of each segment, hence for each segment, the Average Velocity, V_S1, V_S2, V_S3, V_S4 and V_S5 for each segment is easily calculated.

$V_{MAX}$is derived from Bernoulli principles where:

$$V = \sqrt{2g\Delta h} \qquad \text{Eqn D1}$$

With

V = Velocity in m/s

Δh = is the driving pressure

g = gravitational constant (9.81m/s^2)

Note that the driving pressure Δh is Perforation Loss A+ Stone bedding. The flow from each segment is then calculated by multiplying the velocity with the perforation area and a discharge coefficient, C_d. Table D13 shows the distribution of inflowing velocity over the length of the Intake Pipeline.

Equation D2 was used to calculate the flow from each segment. Table D14 contains the flowrate for each segment and the sum of flow from all segments of the pipeline.

$$Q_T = \sum q = \sum C_d A\sqrt{2g\Delta h} \qquad \text{Eqn D2}$$

With

q = Flowrate through for each segment in m^3/s

Q = Sum of Flowrate form each segment in m^3/s

A= The Area through which flow is allowed in m^2

C_d = Coefficient of Discharge

Table D13: Inflowing velocity of water flowing into the pipe, over the length of the Intake Pipeline (WST)

		Pos. 0	Pos. 1	Pos. 2	Pos. 3	Pos. 4	Pos. 5	Pos. 6	Pos. 7	Pos. 8	Pos. 9	Pos. 10
Test	Loss A + Stone Bedding	Vmax	Vs 1	V1	Vs 2	V2	Vs 3	V3	Vs 4	V4	Vs 5	Vmin
0	mm	m/s	m/s	m/s	m/s	m/s	m/s	m/s	m/s	m/s	m/s	m/s
1	0.50	0.099	0.089	0.079	0.069	0.059	0.049	0.039	0.030	0.020	0.010	0.0
2	0.99	0.139	0.126	0.112	0.098	0.084	0.070	0.056	0.042	0.028	0.014	0.0
3	1.98	0.197	0.177	0.158	0.138	0.118	0.098	0.079	0.059	0.039	0.020	0.0
4	2.95	0.240	0.216	0.192	0.168	0.144	0.120	0.096	0.072	0.048	0.024	0.0
5	5.82	0.338	0.304	0.270	0.237	0.203	0.169	0.135	0.101	0.068	0.034	0.0
6	11.21	0.469	0.422	0.375	0.328	0.281	0.235	0.188	0.141	0.094	0.047	0.0
7	17.95	0.593	0.534	0.475	0.415	0.356	0.297	0.237	0.178	0.119	0.059	0.0
8	34.64	0.824	0.742	0.660	0.577	0.495	0.412	0.330	0.247	0.165	0.082	0.0
9	48.04	0.971	0.874	0.777	0.680	0.583	0.485	0.388	0.291	0.194	0.097	0.0
10	70.14	1.173	1.056	0.938	0.821	0.704	0.587	0.469	0.352	0.235	0.117	0.0
11	83.45	1.280	1.152	1.024	0.896	0.768	0.640	0.512	0.384	0.256	0.128	0.0
12	105.64	1.440	1.296	1.152	1.008	0.864	0.720	0.576	0.432	0.288	0.144	0.0
13	129.52	1.594	1.435	1.275	1.116	0.956	0.797	0.638	0.478	0.319	0.159	0.0
14	155.38	1.746	1.571	1.397	1.222	1.048	0.873	0.698	0.524	0.349	0.175	0.0
15	171.74	1.836	1.652	1.469	1.285	1.101	0.918	0.734	0.551	0.367	0.184	0.0

Table D14: Calculated Flowrate from all segments of the Pipeline (WST)

1	2	3	4	5	6	7	8	9	10	11
Test	Loss A + Stone Bedding	C_b	Qs 1	Qs 2	Qs 3	Qs 4	Qs 5	Q Total	Q Total	2Q Total
0	mm		m^3/s	m^3/s	m^3/s	m^3/s	m^3/s	m^3/s	l/s	l/s
1	0.50	0.085	0.00012	0.00009	0.00007	0.00004	0.00001	0.00033	0.33	0.66
2	0.99	0.096	0.00019	0.00015	0.00011	0.00006	0.00002	0.00053	0.53	1.06
3	1.98	0.109	0.00030	0.00024	0.00017	0.00010	0.00003	0.00084	0.84	1.68
4	2.95	0.139	0.00047	0.00037	0.00026	0.00016	0.00005	0.00131	1.31	2.62
5	5.82	0.176	0.00084	0.00065	0.00047	0.00028	0.00009	0.00234	2.34	4.67
6	11.21	0.162	0.00107	0.00083	0.00059	0.00036	0.00012	0.00297	2.98	5.95
7	17.95	0.177	0.00148	0.00115	0.00082	0.00049	0.00016	0.00411	4.11	8.23
8	34.64	0.199	0.00232	0.00181	0.00129	0.00077	0.00026	0.00645	6.45	12.90
9	48.04	0.203	0.00279	0.00217	0.00155	0.00093	0.00031	0.00775	7.75	15.51
10	70.14	0.203	0.00337	0.00262	0.00187	0.00112	0.00037	0.00937	9.37	18.74
11	83.45	0.208	0.00375	0.00292	0.00209	0.00125	0.00042	0.01043	10.43	20.85
12	105.64	0.204	0.00416	0.00323	0.00231	0.00139	0.00046	0.01155	11.55	23.10
13	129.52	0.207	0.00467	0.00363	0.00259	0.00156	0.00052	0.01296	12.96	25.92
14	155.38	0.208	0.00513	0.00399	0.00285	0.00171	0.00057	0.01424	14.24	28.49
15	171.74	0.207	0.00537	0.00418	0.00298	0.00179	0.00060	0.01492	14.92	29.83

Of particular concern is the Energy Grade Line (EGL) at the centre of the Intake Pipeline. The EGL,Figure D9, shows the amount of energy that has been lost from the stone bedding friction and from water entering the Intake Pipeline.For the 15 tests conducted, pressure losses increase closer to the exit point of WC1 as can be seen in Figure D9.

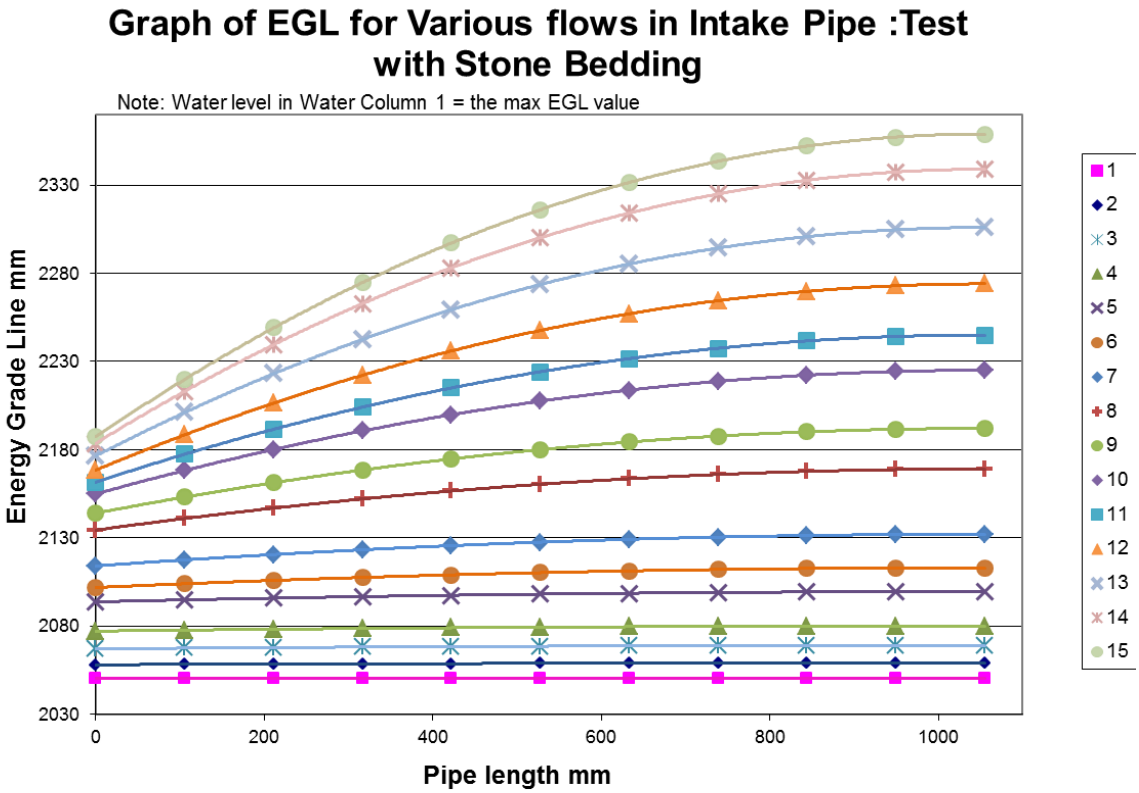

Figure D9: Plot of EGLs at the centre of the Intake Pipeline for Water and Stone Test

The calculation of the EGL at various points within the Intake pipeline is crucial as it aids in determining the loss due to the stone bedding. This can be seen in the flowing section

D.5.4.2 Pressure loss due to Stone Bedding

Calculating the loss of pressure due to stone bedding is critical as it inadvertently determines the design of the seawater Intake. Note that the stone bedding for all tests were standardised with the Intake pipe being 150mm above the bedrock, 300mm below the cover level of the stone bedding and 485mm from an adjacent intake pipeline. Two methods where employed when seeking to determine the pressure loss due the stone bedding.

D.5.4.2.1 Method 1: Simple method for determining headloss due to stone bedding

In this simplistic method, the equation for the "Water Test only: is removed from the equation for "Stone and water test" This is simplified as Eqn 3 equals Eqn1 minus Eqn2 where:

$$\Delta P = 0.1309Q^2 + 0.8725Q \qquad \text{(Eqn2)}$$

Minus

$$\Delta P = 0.0518Q^2 + 0.3206Q \qquad \text{(Eqn1)}$$

Equals

$$\Delta P = 0.0791Q^2 + 0.5519Q \qquad \text{(Eqn3)}$$

Table D15shows the headloss for corresponding flow values while Figure D10 plots these graphically.

Table D15: ø250mm Slotted pipe test: Method 1 :Pressure loss due to Stone Bedding Only

Test No.	Q Half Pipe	Q Full Pipe	Stone Bedding Friction
	l/s	l/s	mm
1	0.33	0.66	0.4
2	0.53	1.06	0.7
3	0.84	1.68	1.2
4	1.31	2.62	2.0
5	2.34	4.68	4.3
6	2.98	5.96	6.1
7	4.11	8.22	9.9
8	6.45	12.9	20.3
9	7.75	15.5	27.6
10	9.37	18.74	38.1
11	10.43	20.86	45.9
12	11.55	23.1	55.0
13	12.96	25.92	67.5
14	14.24	28.48	79.9
15	14.92	29.84	86.9

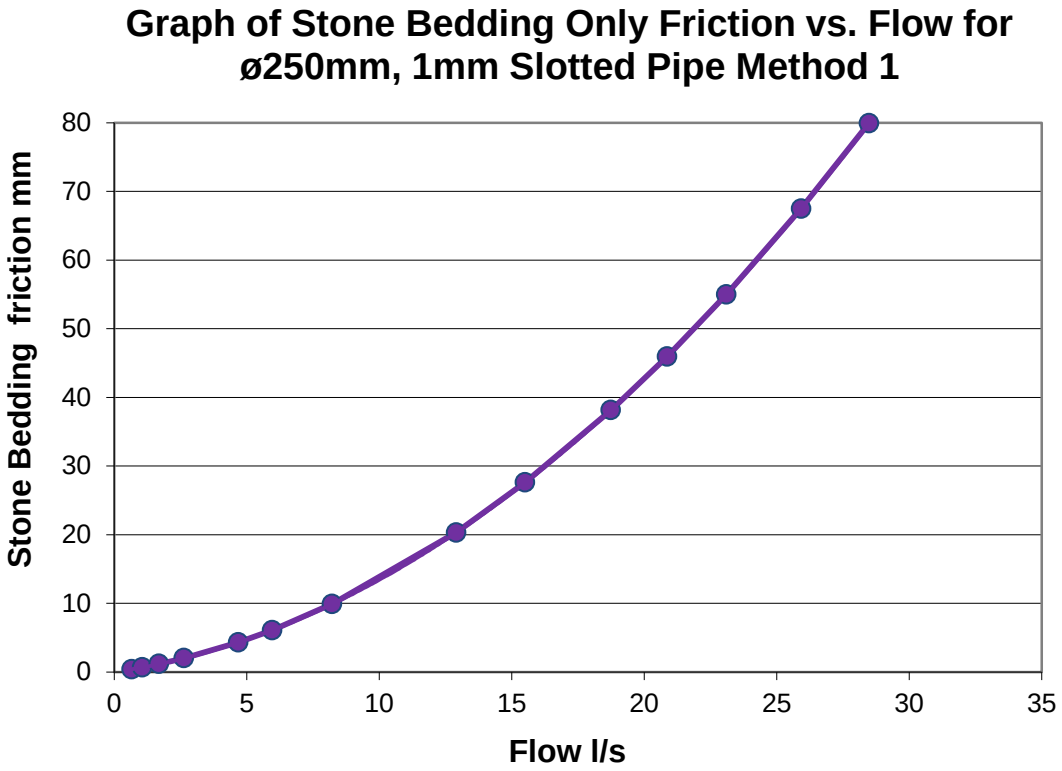

Figure D10: ø250mm Slotted pipe-Water and Stone Bedding Test: Pressure loss due to Stone Bedding Only

D.5.4.2.2 Method 2: Method for determining stone bedding loss : Hydraulic conductivity: Kenny, Lau and Ofoegbu

The second method used to determine the loss of pressure due to Stone bedding, looks at the hydraulic conductivity of the stone bedding based on work by Kenny, Lau and Ofoegbu. From Table D13, the velocity for each segment of the Intake pipeline was determined. However, stone bedding cannot be split into equal segments as well. This is only correct for stone bedding adjacent to the intake pipeline. It does not apply to the flat horizontal surface of the stone bedding.

Flow into the intake pipe line is proportional to the velocity. The maximum velocity occurs at one end of the intake pipeline and the minimum velocity occurs at the start of the intake pipeline. Table D16 below looks at the ratio of the (flowrate) as a proportion of the entire flowrate.

Figure D11, these proportions were then applied to length of the stone bed. This splitting of the stone bedding surface ensured that all flows entering the stone bed were proportional to the flow entering the intake pipeline for all segments.

Table D16:ø250mm Slotted Pipe, Method 2:Water and Stone Bedding Test: Flow through segments(WST)

Test No.	Seg1	Seg2	Seg3	Seg4	Seg5	Seg1	Seg2	Seg3	Seg4	Seg5
	Qs 1	Qs 2	Qs 3	Qs 4	Qs 5	Qs 1	Qs 2	Qs 3	Qs 4	Qs 5
	m^3/s	m^3/s	m^3/s	m^3/s	m^3/s	m^3/s	m^3/s	m^3/s	m^3/s	m^3/s
1	0.00012	0.00009	0.00007	0.00004	0.00001	36%	28%	20%	12%	4%
2	0.00019	0.00015	0.00011	0.00006	0.00002	36%	28%	20%	12%	4%
3	0.00030	0.00024	0.00017	0.00010	0.00003	36%	28%	20%	12%	4%
4	0.00047	0.00037	0.00026	0.00016	0.00005	36%	28%	20%	12%	4%
5	0.00084	0.00065	0.00047	0.00028	0.00009	36%	28%	20%	12%	4%
6	0.00107	0.00083	0.00059	0.00036	0.00012	36%	28%	20%	12%	4%
7	0.00148	0.00115	0.00082	0.00049	0.00016	36%	28%	20%	12%	4%
8	0.00232	0.00181	0.00129	0.00077	0.00026	36%	28%	20%	12%	4%
9	0.00279	0.00217	0.00155	0.00093	0.00031	36%	28%	20%	12%	4%
10	0.00337	0.00262	0.00187	0.00112	0.00037	36%	28%	20%	12%	4%
11	0.00375	0.00292	0.00209	0.00125	0.00042	36%	28%	20%	12%	4%
12	0.00416	0.00323	0.00231	0.00139	0.00046	36%	28%	20%	12%	4%
13	0.00467	0.00363	0.00259	0.00156	0.00052	36%	28%	20%	12%	4%
14	0.00513	0.00399	0.00285	0.00171	0.00057	36%	28%	20%	12%	4%
15	0.00537	0.00418	0.00298	0.00179	0.00060	36%	28%	20%	12%	4%

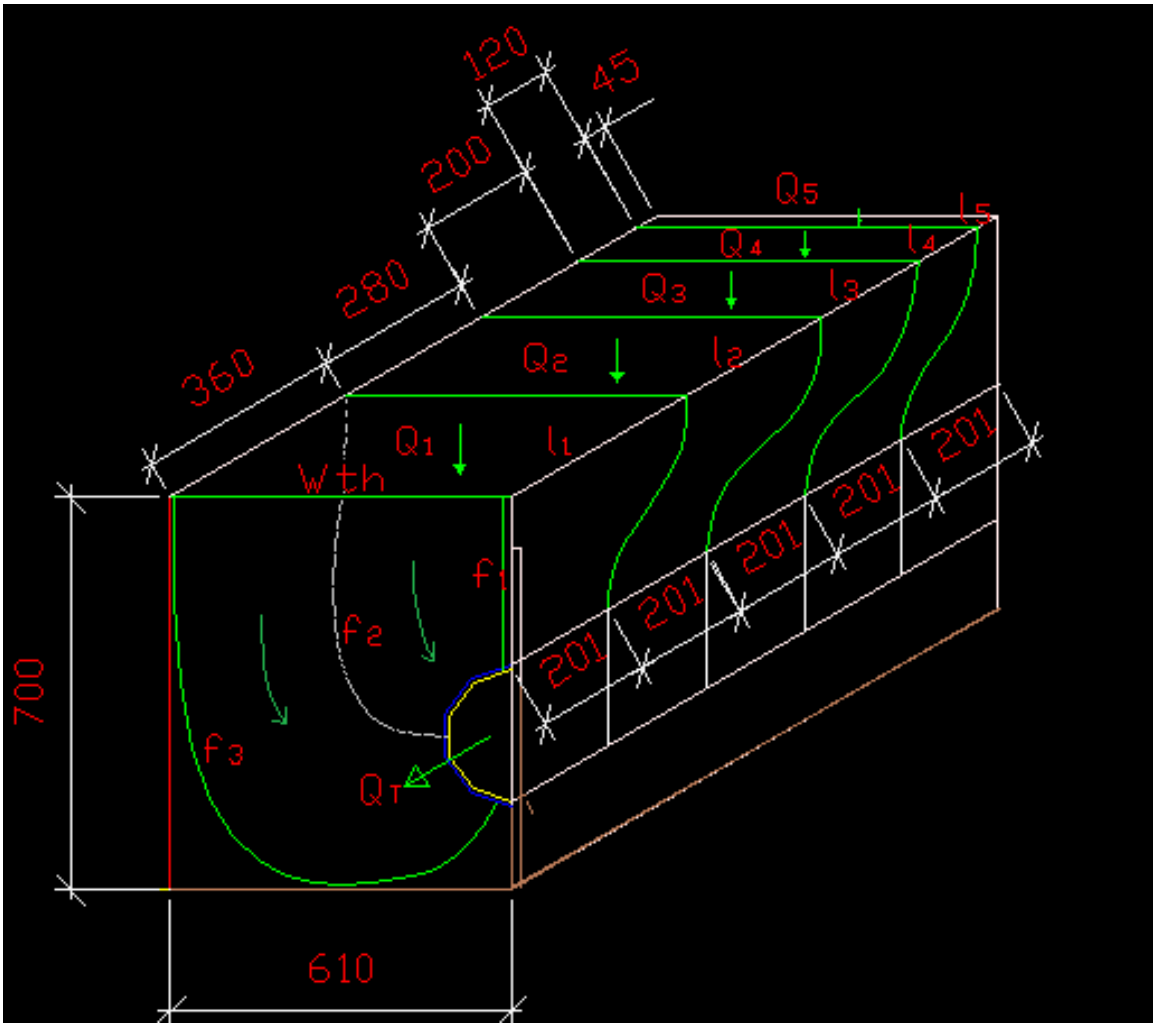

Figure D11: ø250mm Slotted pipe-Water and Stone Bedding Test: Segmentation of Stone Bedding area

Figure D12 shows the simplified version of a single notional segment. Note line f_1, f_2 and f_3 as lines of reference in Figure D11 and D12. As in Figure D12, length (l_1) is multiplied by the standard width (With), to create the area A_1. Area A_4 was easily calculated it is based on the intake pipe dimensions. Areas A_2 and $A_3$are a third of the distance from each end and hence are calculated proportionately. The distances from Area A_1 to A_2 to A_3 to $A_4$are noted as Lengths len_1, len_2 and len_3 respectively.

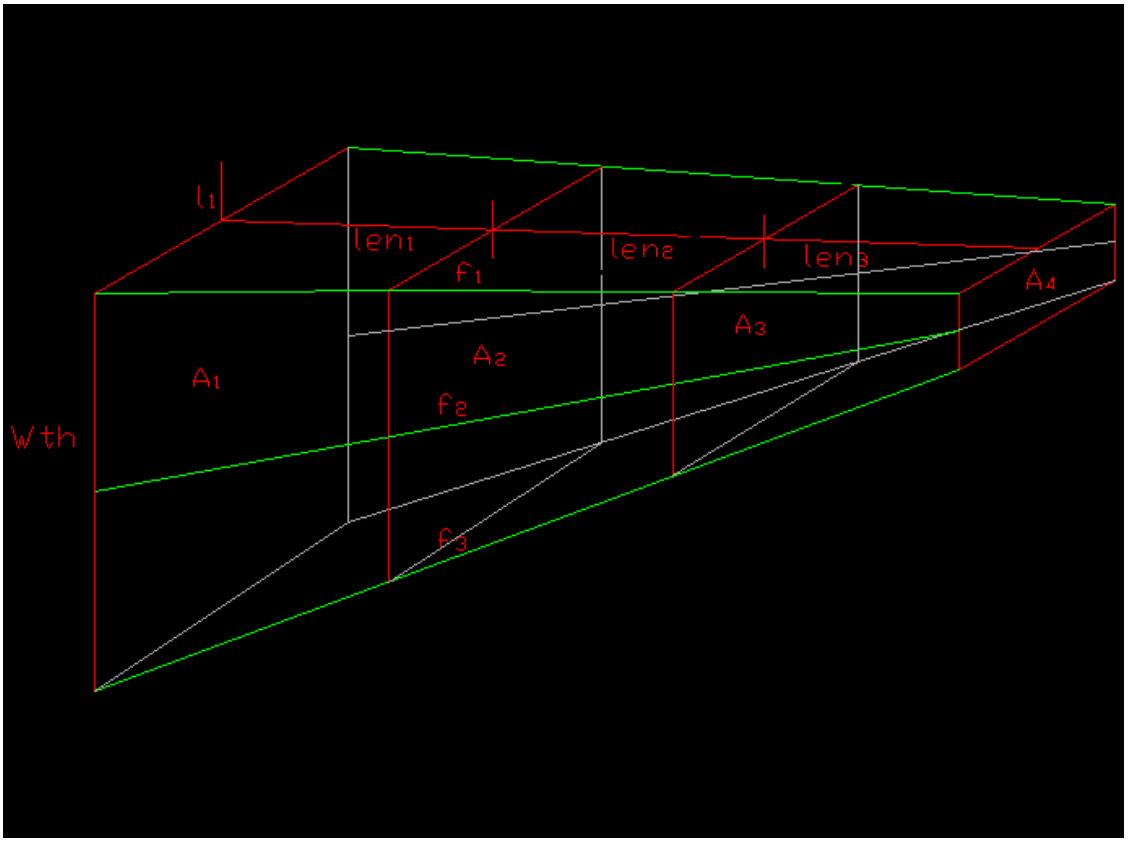

Figure D12: Notional flow path of a stone bedding segment

In order to calculate the pressure loss due to the stone bedding, the hydraulic conductivity is required. The pressure loss is defined as follows:

$$hf(m) = \frac{L * V}{k} \qquad \text{EqnD4}$$

Where:

hf = pressure loss due to friction within stone bedding

L = Length of water path (m)

V = Flow velocity

k = Hydraulic conductivity

The first three variables are easily to calculate however determining the hydraulic conductivity k, requires further investigation.

The hydraulic conductivity is calculated using the following equation

$$k = \frac{\gamma_w}{\eta K} \qquad \text{EqnD5}$$

Where:

k = Hydraulic conductivity

γ_W = Unit Weight of Water

η = Dynamic Viscosity of water

K = Absolute Hydraulic conductivity

The unit weight of water γ_W, and the dynamic viscosity of water η are fairly simple to calculate. However the Absolute Hydraulic conductivity*K* has to be calculated. It is calculated using the following equation:

$$K = C_u D_5^2 \qquad \text{EqnD6}$$

Where:

K = Absolute Hydraulic conductivity

C_u = Coefficient of Uniformity. Varies between 0.05 to 1

D_5 = Dimension of aggregate that has a cumulative percentage passing of 5%

Figure D13 below is a typical grading curve for nominally single-sized 19mm. From the grading curve, a value of D_5 = 10mm was obtained. Hence for a C_u of 0.8, EquationD6 yields a K of 80mm^2. As confirmation, Figure D14 is a graphical plot of EquationD6. Using a D_5 of 10mm, a k value of approximately 0.7m/s is found. Utilising EqnD5 and the following values:

γ_W = 9800 N/m3

η = 0.00014 Ns/m

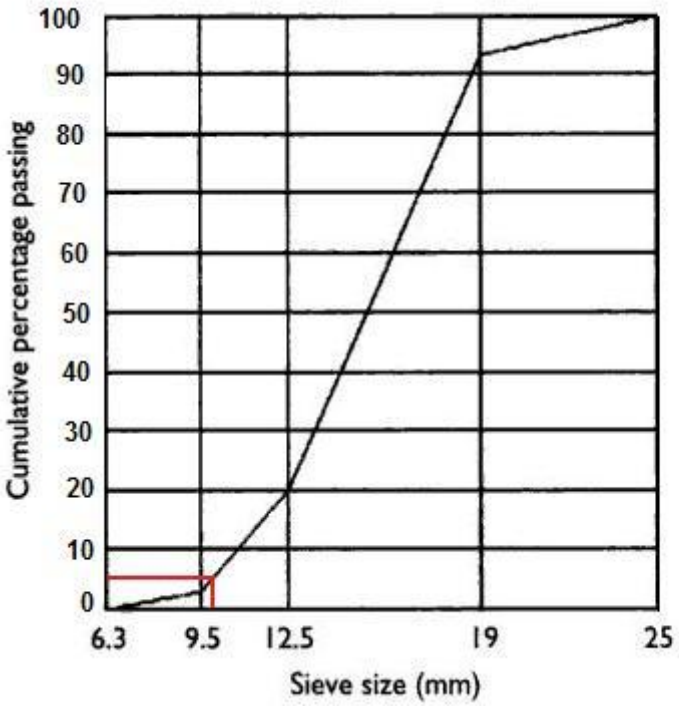

Figure D13: Typical grading curve for nominally single-sized 19mm Stone (Alexander & Mindess, 2005)

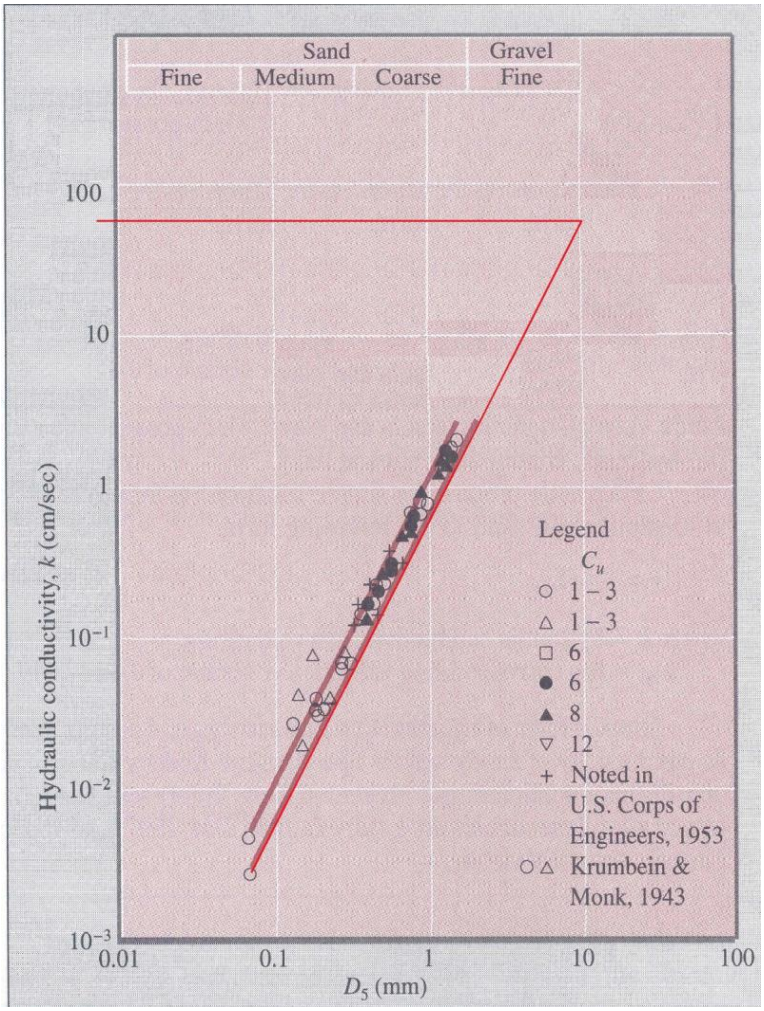

Figure D14: Graphical plot of Hydraulic conductivity Equation (Das 2000)

Table D17: Summary:Calculating the Hydraulic conductivity (WST)

Description	Value	Unit
C_u (0.05 to 1)	0.80	
D_5	10.0	mm
Water Column Width	0.61	m
Absolute Conductivity K	80	mm^2
Unit Weight of Water γ_W	9800	N/m^3
Dynamic Viscosity of water η	1.14E-03	Ns/m^2
Hydraulic Conductivity k	0.688	m/s

Using the values from Table D10 and D13, headloss for segment1 was calculated in the following manner. With the flow through each segment know, it is possible to determine the headloss if the areas through which water flows is uniform.

However, this is not the case. Hence each segment has been split into three equal portions. Table D18 below, describes the manner in which Segment 1 is split into three sub segments. Thereafter, Table D19 determines the average velocity for each sub segment, the associated headloss and finally the cumulative headloss for Segment 1. The following tables describe the headloss calculated for Segments 1, 2, 3, 4 and 5.

Table D18: Segment 1: Averaging of Areas (WST)

Test No.	Len1	A11	A12	A13	A14	Qs 1	Ave A1	Ave A2	Ave A3
	m	m^2	m^2	m^2	m^2	m^3/s	m^2	m^2	m^2
1	0.3618	0.221	0.196	0.170	0.145	0.00012	0.208	0.183	0.158
2	0.3618	0.221	0.196	0.170	0.145	0.00019	0.208	0.183	0.158
3	0.3618	0.221	0.196	0.170	0.145	0.00030	0.208	0.183	0.158
4	0.3618	0.221	0.196	0.170	0.145	0.00047	0.208	0.183	0.158
5	0.3618	0.221	0.196	0.170	0.145	0.00084	0.208	0.183	0.158
6	0.3618	0.221	0.196	0.170	0.145	0.00107	0.208	0.183	0.158
7	0.3618	0.221	0.196	0.170	0.145	0.00148	0.208	0.183	0.158
8	0.3618	0.221	0.196	0.170	0.145	0.00232	0.208	0.183	0.158
9	0.3618	0.221	0.196	0.170	0.145	0.00279	0.208	0.183	0.158
10	0.3618	0.221	0.196	0.170	0.145	0.00337	0.208	0.183	0.158
11	0.3618	0.221	0.196	0.170	0.145	0.00375	0.208	0.183	0.158
12	0.3618	0.221	0.196	0.170	0.145	0.00416	0.208	0.183	0.158
13	0.3618	0.221	0.196	0.170	0.145	0.00467	0.208	0.183	0.158
14	0.3618	0.221	0.196	0.170	0.145	0.00513	0.208	0.183	0.158
15	0.3618	0.221	0.196	0.170	0.145	0.00537	0.208	0.183	0.158

Table D19: Segment 1: Velocity and cumulative headloss (WST)

Test No.	Vel 1A	Vel 1B	Vel 1C	H_l11	H_l12	H_l13	H_{l1} Total	H_l1Total
	m/s	m/s	m/s	m	m	m	m	mm
1	0.0006	0.0006	0.0008	0.0002	0.0002	0.0002	0.0006	0.60
2	0.0009	0.0010	0.0012	0.0003	0.0003	0.0004	0.0010	0.96
3	0.0015	0.0017	0.0019	0.0004	0.0005	0.0006	0.0015	1.54
4	0.0023	0.0026	0.0030	0.0007	0.0008	0.0009	0.0024	2.40
5	0.0040	0.0046	0.0053	0.0012	0.0014	0.0016	0.0043	4.27
6	0.0051	0.0059	0.0068	0.0016	0.0018	0.0021	0.0054	5.43
7	0.0071	0.0081	0.0094	0.0022	0.0025	0.0029	0.0075	7.51
8	0.0112	0.0127	0.0147	0.0034	0.0039	0.0045	0.0118	11.78
9	0.0134	0.0153	0.0177	0.0041	0.0047	0.0054	0.0142	14.16
10	0.0162	0.0184	0.0214	0.0049	0.0056	0.0065	0.0171	17.11
11	0.0180	0.0205	0.0238	0.0055	0.0063	0.0073	0.0190	19.04
12	0.0200	0.0227	0.0264	0.0061	0.0069	0.0080	0.0211	21.09
13	0.0224	0.0255	0.0296	0.0068	0.0078	0.0090	0.0237	23.66
14	0.0246	0.0280	0.0325	0.0075	0.0086	0.0099	0.0260	26.01
15	0.0258	0.0294	0.0340	0.0079	0.0090	0.0104	0.0272	27.24

Table D20: Segment 2: Averaging of Areas (WST)

Test No.	Len1	A11	A12	A13	A14	Qs 1	Ave A1	Ave A2	Ave A3
	m	m^2	m^2	m^2	m^2	m^3/s	m^2	m^2	m^2
1	0.2814	0.172	0.163	0.154	0.145	0.00009	0.167	0.158	0.150
2	0.2814	0.172	0.163	0.154	0.145	0.00015	0.167	0.158	0.150
3	0.2814	0.172	0.163	0.154	0.145	0.00024	0.167	0.158	0.150
4	0.2814	0.172	0.163	0.154	0.145	0.00037	0.167	0.158	0.150
5	0.2814	0.172	0.163	0.154	0.145	0.00065	0.167	0.158	0.150
6	0.2814	0.172	0.163	0.154	0.145	0.00083	0.167	0.158	0.150
7	0.2814	0.172	0.163	0.154	0.145	0.00115	0.167	0.158	0.150
8	0.2814	0.172	0.163	0.154	0.145	0.00181	0.167	0.158	0.150
9	0.2814	0.172	0.163	0.154	0.145	0.00217	0.167	0.158	0.150
10	0.2814	0.172	0.163	0.154	0.145	0.00262	0.167	0.158	0.150
11	0.2814	0.172	0.163	0.154	0.145	0.00292	0.167	0.158	0.150
12	0.2814	0.172	0.163	0.154	0.145	0.00323	0.167	0.158	0.150
13	0.2814	0.172	0.163	0.154	0.145	0.00363	0.167	0.158	0.150
14	0.2814	0.172	0.163	0.154	0.145	0.00399	0.167	0.158	0.150
15	0.2814	0.172	0.163	0.154	0.145	0.00418	0.167	0.158	0.150

Table D21: Segment 2: Velocity and cumulative headloss (WST)

Test No.	Vel 1A	Vel 1B	Vel 1C	H_l11	H_l12	H_l13	H_{l1} Total	H_l1Total
	m/s	m/s	m/s	m	m	m	m	mm
1	0.0006	0.0006	0.0006	0.0002	0.0002	0.0002	0.0005	0.53
2	0.0009	0.0009	0.0010	0.0003	0.0003	0.0003	0.0009	0.86
3	0.0014	0.0015	0.0016	0.0004	0.0005	0.0005	0.0014	1.37
4	0.0022	0.0023	0.0025	0.0007	0.0007	0.0007	0.0021	2.13
5	0.0039	0.0041	0.0044	0.0012	0.0013	0.0013	0.0038	3.79
6	0.0050	0.0053	0.0056	0.0015	0.0016	0.0017	0.0048	4.83
7	0.0069	0.0073	0.0077	0.0021	0.0022	0.0024	0.0067	6.67
8	0.0108	0.0114	0.0121	0.0033	0.0035	0.0037	0.0105	10.47
9	0.0130	0.0137	0.0145	0.0040	0.0042	0.0044	0.0126	12.58
10	0.0157	0.0166	0.0175	0.0048	0.0051	0.0054	0.0152	15.20
11	0.0175	0.0184	0.0195	0.0053	0.0056	0.0060	0.0169	16.92
12	0.0193	0.0204	0.0216	0.0059	0.0062	0.0066	0.0187	18.74
13	0.0217	0.0229	0.0243	0.0066	0.0070	0.0074	0.0210	21.03
14	0.0238	0.0252	0.0267	0.0073	0.0077	0.0081	0.0231	23.11
15	0.0250	0.0264	0.0279	0.0076	0.0081	0.0085	0.0242	24.20

Table D22: Segment 3: Averaging of Areas (WST)

Test No.	Len1	A11	A12	A13	A14	Qs 1	Ave A1	Ave A2	Ave A3
	m	m^2	m^2	m^2	m^2	m^3/s	m^2	m^2	m^2
1	0.201	0.123	0.130	0.138	0.145	0.00007	0.126	0.134	0.141
2	0.201	0.123	0.130	0.138	0.145	0.00011	0.126	0.134	0.141
3	0.201	0.123	0.130	0.138	0.145	0.00017	0.126	0.134	0.141
4	0.201	0.123	0.130	0.138	0.145	0.00026	0.126	0.134	0.141
5	0.201	0.123	0.130	0.138	0.145	0.00047	0.126	0.134	0.141
6	0.201	0.123	0.130	0.138	0.145	0.00059	0.126	0.134	0.141
7	0.201	0.123	0.130	0.138	0.145	0.00082	0.126	0.134	0.141
8	0.201	0.123	0.130	0.138	0.145	0.00129	0.126	0.134	0.141
9	0.201	0.123	0.130	0.138	0.145	0.00155	0.126	0.134	0.141
10	0.201	0.123	0.130	0.138	0.145	0.00187	0.126	0.134	0.141
11	0.201	0.123	0.130	0.138	0.145	0.00209	0.126	0.134	0.141
12	0.201	0.123	0.130	0.138	0.145	0.00231	0.126	0.134	0.141
13	0.201	0.123	0.130	0.138	0.145	0.00259	0.126	0.134	0.141
14	0.201	0.123	0.130	0.138	0.145	0.00285	0.126	0.134	0.141
15	0.201	0.123	0.130	0.138	0.145	0.00298	0.126	0.134	0.141

Table D23: Segment 3: Velocity and cumulative headloss (WST)

Test No.	Vel 1A	Vel 1B	Vel 1C	H_l11	H_l12	H_l13	H_{l1} Total	H_l1Total
	m/s	m/s	m/s	m	m	m	m	mm
1	0.0005	0.0005	0.0005	0.0002	0.0002	0.0001	0.0005	0.45
2	0.0008	0.0008	0.0007	0.0003	0.0002	0.0002	0.0007	0.72
3	0.0013	0.0013	0.0012	0.0004	0.0004	0.0004	0.0012	1.15
4	0.0021	0.0020	0.0019	0.0006	0.0006	0.0006	0.0018	1.80
5	0.0037	0.0035	0.0033	0.0011	0.0011	0.0010	0.0032	3.20
6	0.0047	0.0044	0.0042	0.0014	0.0014	0.0013	0.0041	4.08
7	0.0065	0.0061	0.0058	0.0020	0.0019	0.0018	0.0056	5.64
8	0.0102	0.0096	0.0091	0.0031	0.0029	0.0028	0.0088	8.85
9	0.0123	0.0116	0.0110	0.0037	0.0035	0.0033	0.0106	10.63
10	0.0148	0.0140	0.0132	0.0045	0.0043	0.0040	0.0128	12.85
11	0.0165	0.0156	0.0147	0.0050	0.0048	0.0045	0.0143	14.30
12	0.0183	0.0173	0.0163	0.0056	0.0053	0.0050	0.0158	15.84
13	0.0205	0.0194	0.0183	0.0063	0.0059	0.0056	0.0178	17.77
14	0.0225	0.0213	0.0201	0.0069	0.0065	0.0062	0.0195	19.53
15	0.0236	0.0223	0.0211	0.0072	0.0068	0.0064	0.0205	20.45

Table D24: Segment 4: Averaging of Areas

Test No.	Len1	A11	A12	A13	A14	Qs 1	Ave A1	Ave A2	Ave A3
	m	m^2	m^2	m^2	m^2	m^3/s	m^2	m^2	m^2
1	0.1206	0.074	0.097	0.121	0.145	0.00004	0.085	0.109	0.133
2	0.1206	0.074	0.097	0.121	0.145	0.00006	0.085	0.109	0.133
3	0.1206	0.074	0.097	0.121	0.145	0.00010	0.085	0.109	0.133
4	0.1206	0.074	0.097	0.121	0.145	0.00016	0.085	0.109	0.133
5	0.1206	0.074	0.097	0.121	0.145	0.00028	0.085	0.109	0.133
6	0.1206	0.074	0.097	0.121	0.145	0.00036	0.085	0.109	0.133
7	0.1206	0.074	0.097	0.121	0.145	0.00049	0.085	0.109	0.133
8	0.1206	0.074	0.097	0.121	0.145	0.00077	0.085	0.109	0.133
9	0.1206	0.074	0.097	0.121	0.145	0.00093	0.085	0.109	0.133
10	0.1206	0.074	0.097	0.121	0.145	0.00112	0.085	0.109	0.133
11	0.1206	0.074	0.097	0.121	0.145	0.00125	0.085	0.109	0.133
12	0.1206	0.074	0.097	0.121	0.145	0.00139	0.085	0.109	0.133
13	0.1206	0.074	0.097	0.121	0.145	0.00156	0.085	0.109	0.133
14	0.1206	0.074	0.097	0.121	0.145	0.00171	0.085	0.109	0.133
15	0.1206	0.074	0.097	0.121	0.145	0.00179	0.085	0.109	0.133

Table D25: Segment 4: Velocity and cumulative headloss (WST)

Test No.	Vel 1A	Vel 1B	Vel 1C	H_l11	H_l12	H_l13	H_{l1} Total	H_l1Total
	m/s	m/s	m/s	m	m	m	m	mm
1	0.0005	0.0004	0.0003	0.0001	0.0001	0.0001	0.0003	0.34
2	0.0007	0.0006	0.0005	0.0002	0.0002	0.0001	0.0005	0.55
3	0.0012	0.0009	0.0008	0.0004	0.0003	0.0002	0.0009	0.87
4	0.0018	0.0014	0.0012	0.0006	0.0004	0.0004	0.0014	1.36
5	0.0033	0.0026	0.0021	0.0010	0.0008	0.0006	0.0024	2.43
6	0.0042	0.0033	0.0027	0.0013	0.0010	0.0008	0.0031	3.09
7	0.0058	0.0045	0.0037	0.0018	0.0014	0.0011	0.0043	4.27
8	0.0091	0.0071	0.0058	0.0028	0.0022	0.0018	0.0067	6.70
9	0.0109	0.0085	0.0070	0.0033	0.0026	0.0021	0.0081	8.05
10	0.0132	0.0103	0.0084	0.0040	0.0031	0.0026	0.0097	9.73
11	0.0146	0.0114	0.0094	0.0045	0.0035	0.0029	0.0108	10.83
12	0.0162	0.0127	0.0104	0.0050	0.0039	0.0032	0.0120	12.00
13	0.0182	0.0142	0.0117	0.0056	0.0043	0.0036	0.0135	13.46
14	0.0200	0.0156	0.0128	0.0061	0.0048	0.0039	0.0148	14.79
15	0.0209	0.0164	0.0134	0.0064	0.0050	0.0041	0.0155	15.49

Table D26: Segment 5: Averaging of Areas

Test No.	Len1	A11	A12	A13	A14	Qs 1	Ave A1	Ave A2	Ave A3
	m	m^2	m^2	m^2	m^2	m^3/s	m^2	m^2	m^2
1	0.0402	0.025	0.065	0.105	0.145	0.00001	0.045	0.085	0.125
2	0.0402	0.025	0.065	0.105	0.145	0.00002	0.045	0.085	0.125
3	0.0402	0.025	0.065	0.105	0.145	0.00003	0.045	0.085	0.125
4	0.0402	0.025	0.065	0.105	0.145	0.00005	0.045	0.085	0.125
5	0.0402	0.025	0.065	0.105	0.145	0.00009	0.045	0.085	0.125
6	0.0402	0.025	0.065	0.105	0.145	0.00012	0.045	0.085	0.125
7	0.0402	0.025	0.065	0.105	0.145	0.00016	0.045	0.085	0.125
8	0.0402	0.025	0.065	0.105	0.145	0.00026	0.045	0.085	0.125
9	0.0402	0.025	0.065	0.105	0.145	0.00031	0.045	0.085	0.125
10	0.0402	0.025	0.065	0.105	0.145	0.00037	0.045	0.085	0.125
11	0.0402	0.025	0.065	0.105	0.145	0.00042	0.045	0.085	0.125
12	0.0402	0.025	0.065	0.105	0.145	0.00046	0.045	0.085	0.125
13	0.0402	0.025	0.065	0.105	0.145	0.00052	0.045	0.085	0.125
14	0.0402	0.025	0.065	0.105	0.145	0.00057	0.045	0.085	0.125
15	0.0402	0.025	0.065	0.105	0.145	0.00060	0.045	0.085	0.125

Table D27: Segment 5: Velocity and cumulative headloss (WST)

Test No.	Vel 1A	Vel 1B	Vel 1C	H_l11	H_l12	H_l13	H_{l1} Total	H_l1Total
	m/s	m/s	m/s	m	m	m	m	mm
1	0.0003	0.0002	0.0001	0.0001	0.0000	0.0000	0.0002	0.17
2	0.0005	0.0002	0.0002	0.0001	0.0001	0.0001	0.0003	0.27
3	0.0008	0.0004	0.0003	0.0002	0.0001	0.0001	0.0004	0.43
4	0.0012	0.0006	0.0004	0.0004	0.0002	0.0001	0.0007	0.68
5	0.0021	0.0011	0.0007	0.0006	0.0003	0.0002	0.0012	1.20
6	0.0027	0.0014	0.0010	0.0008	0.0004	0.0003	0.0015	1.53
7	0.0037	0.0019	0.0013	0.0011	0.0006	0.0004	0.0021	2.12
8	0.0058	0.0030	0.0021	0.0018	0.0009	0.0006	0.0033	3.33
9	0.0070	0.0037	0.0025	0.0021	0.0011	0.0008	0.0040	4.00
10	0.0084	0.0044	0.0030	0.0026	0.0013	0.0009	0.0048	4.83
11	0.0093	0.0049	0.0033	0.0029	0.0015	0.0010	0.0054	5.37
12	0.0104	0.0054	0.0037	0.0032	0.0017	0.0011	0.0060	5.95
13	0.0116	0.0061	0.0041	0.0035	0.0019	0.0013	0.0067	6.68
14	0.0128	0.0067	0.0046	0.0039	0.0021	0.0014	0.0073	7.34
15	0.0134	0.0070	0.0048	0.0041	0.0021	0.0015	0.0077	7.69

Table D28 below, summaries the results of Tables 18 to 27.Figure D15 plots these graphically. A trendline is added to the results in order to predict the headloss, due to stone bedding, at the most downstream point of WC1. It is at this point that the largest magnitude of headloss occurs. Table D29 summaries these results.

Table D28: Summary of Method 2 Headloss Tests. Results from Tables 18 to 27 (WST)

Test No.	Total Q	Total 2Q	Segment 1	Segment 2	Segment 3	Segment 4	Segment 5
	l/s	l/s	mm	mm	mm	mm	mm
1	0.33	0.66	0.60	0.53	0.45	0.34	0.17
2	0.53	1.06	0.96	0.86	0.72	0.55	0.27
3	0.84	1.68	1.54	1.37	1.15	0.87	0.43
4	1.31	2.62	2.40	2.13	1.80	1.36	0.68
5	2.34	4.67	4.27	3.79	3.20	2.43	1.20
6	2.98	5.95	5.43	4.83	4.08	3.09	1.53
7	4.11	8.23	7.51	6.67	5.64	4.27	2.12
8	6.45	12.90	11.78	10.47	8.85	6.70	3.33
9	7.75	15.51	14.16	12.58	10.63	8.05	4.00
10	9.37	18.74	17.11	15.20	12.85	9.73	4.83
11	10.43	20.85	19.04	16.92	14.30	10.83	5.37
12	11.55	23.10	21.09	18.74	15.84	12.00	5.95
13	12.96	25.92	23.66	21.03	17.77	13.46	6.68
14	14.24	28.49	26.01	23.11	19.53	14.79	7.34
15	14.92	29.83	27.24	24.20	20.45	15.49	7.69

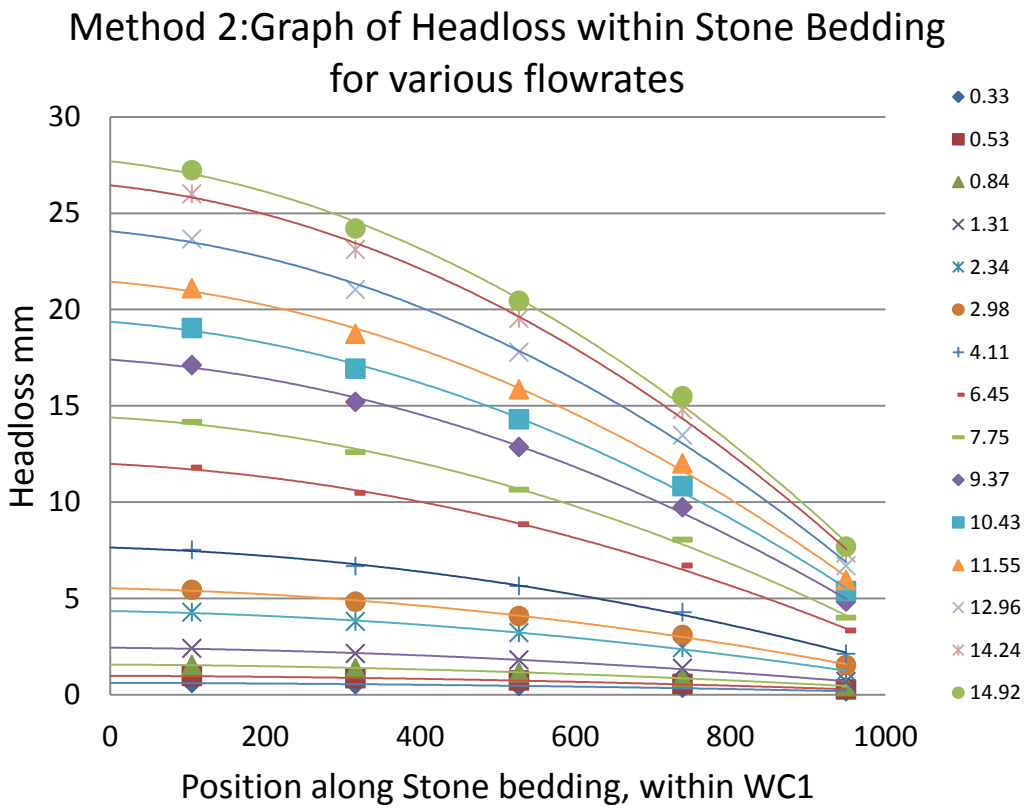

Figure D15: Method 2: Results ofHeadloss estimation due to Stone Bedding, within WC1

Table D29:Method 2:Summary of maximum headloss versus flow rates (WST)

Test No.	Total Q	Total 2Q	Maximum Headloss due to Stone Bedding
	l/s	l/s	mm
1	0.33	0.66	0.64
2	0.53	1.06	1.03
3	0.84	1.68	1.64
4	1.31	2.62	2.55
5	2.34	4.67	4.54
6	2.98	5.95	5.78
7	4.11	8.23	8.00
8	6.45	12.90	12.54
9	7.75	15.51	15.07
10	9.37	18.74	18.21
11	10.43	20.85	20.27
12	11.55	23.10	22.46
13	12.96	25.92	25.20
14	14.24	28.49	27.69
15	14.92	29.83	29.00

D.5.4.2.3 Method 3: Method for determining stone bedding loss : Hydraulic conductivity: Forchheimer

The third method used to determine the loss of pressure due to Stone bedding, looks at the hydraulic conductivity of the stone bedding. This is based on work carried out by Forchheimer. From Table D31, the velocity for each segment of the Intake pipeline was determined. However, stone bedding cannot be split into equal segments as well. This is only correct for stone bedding adjacent to the intake pipeline. It does not apply to the flat horizontal surface of the stone bedding.

Flow into the intake pipe line is proportional to the velocity. The maximum velocity occurs at one end of the intake pipeline and the minimum velocity occurs at the start of the intake pipeline. Table D30 below looks at the ratio of the (flowrate) as a proportion of the entire flowrate.

Figure D16, these proportions were then applied to length of the stone bed. This splitting of the stone bedding surface ensured that all flows entering the stone bed were proportional to the flow entering the intake pipeline for all segments.

Table D30:ø250mm Slotted Pipe, Water and Stone Bedding Test: Flow through segments (WST)

Test No.	Seg1	Seg2	Seg3	Seg4	Seg5	Seg1	Seg2	Seg3	Seg4	Seg5
	Qs 1	Qs 2	Qs 3	Qs 4	Qs 5	Qs 1	Qs 2	Qs 3	Qs 4	Qs 5
	m^3/s	m^3/s	m^3/s	m^3/s	m^3/s	m^3/s	m^3/s	m^3/s	m^3/s	m^3/s
1	0.00012	0.00009	0.00007	0.00004	0.00001	36%	28%	20%	12%	4%
2	0.00019	0.00015	0.00011	0.00006	0.00002	36%	28%	20%	12%	4%
3	0.00030	0.00024	0.00017	0.00010	0.00003	36%	28%	20%	12%	4%
4	0.00047	0.00037	0.00026	0.00016	0.00005	36%	28%	20%	12%	4%
5	0.00084	0.00065	0.00047	0.00028	0.00009	36%	28%	20%	12%	4%
6	0.00107	0.00083	0.00059	0.00036	0.00012	36%	28%	20%	12%	4%
7	0.00148	0.00115	0.00082	0.00049	0.00016	36%	28%	20%	12%	4%
8	0.00232	0.00181	0.00129	0.00077	0.00026	36%	28%	20%	12%	4%
9	0.00279	0.00217	0.00155	0.00093	0.00031	36%	28%	20%	12%	4%
10	0.00337	0.00262	0.00187	0.00112	0.00037	36%	28%	20%	12%	4%
11	0.00375	0.00292	0.00209	0.00125	0.00042	36%	28%	20%	12%	4%
12	0.00416	0.00323	0.00231	0.00139	0.00046	36%	28%	20%	12%	4%
13	0.00467	0.00363	0.00259	0.00156	0.00052	36%	28%	20%	12%	4%
14	0.00513	0.00399	0.00285	0.00171	0.00057	36%	28%	20%	12%	4%
15	0.00537	0.00418	0.00298	0.00179	0.00060	36%	28%	20%	12%	4%

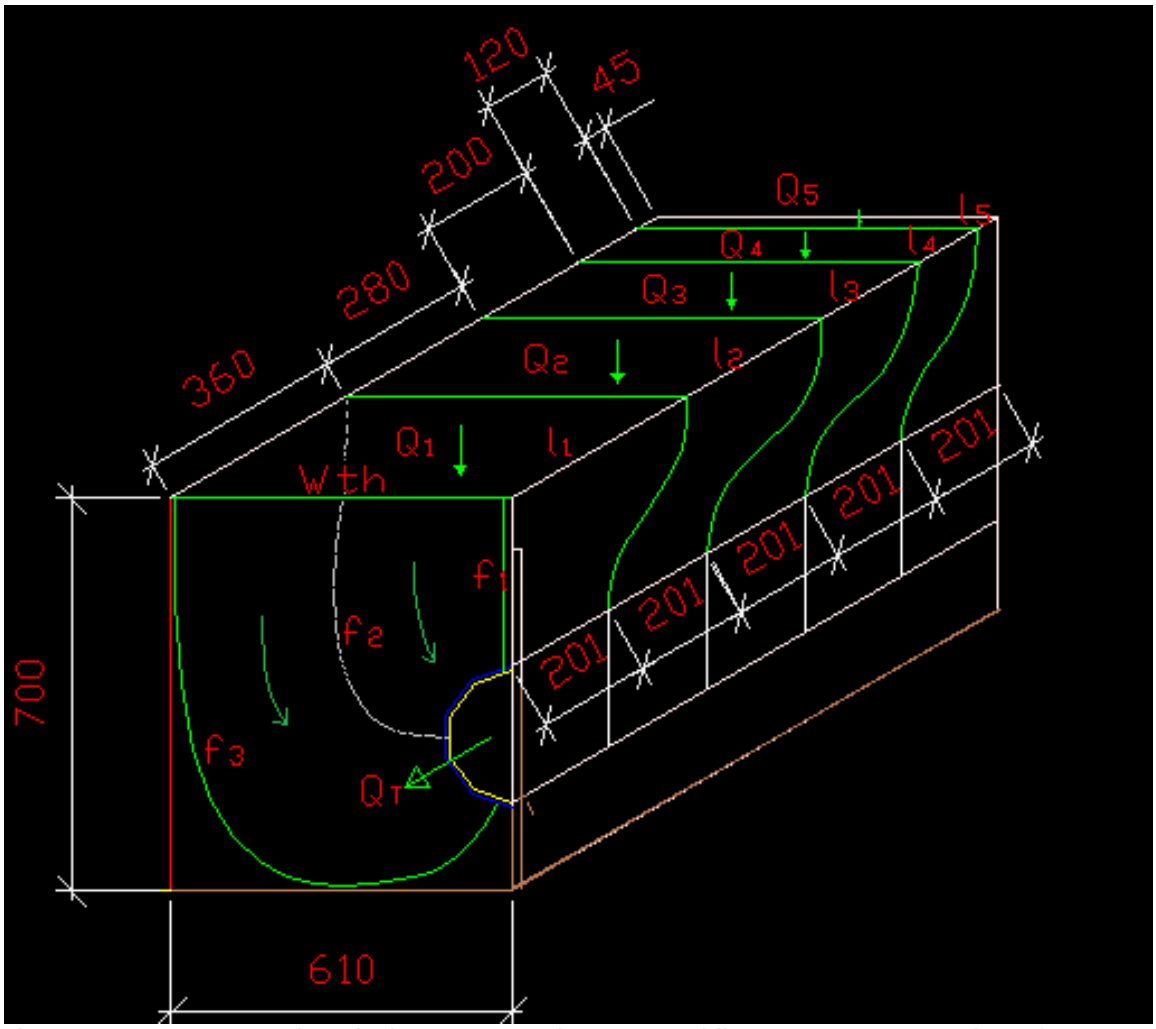

Figure D16: ø250mm Slotted pipe-Water and Stone Bedding Test: Segmentation of Stone Bedding area

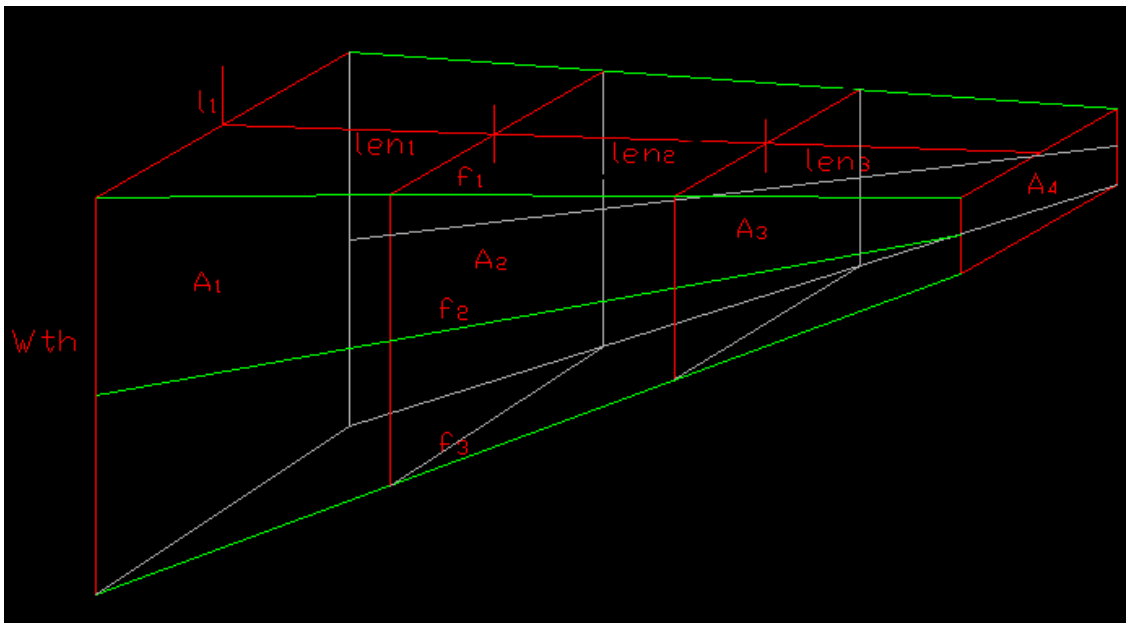

Figure D17: Notional flow path of a stone bedding segment

Figure D17 shows the simplified version of a single notional segment. Note line f_1, f_2 and f_3 as lines of reference in Figure D16 and D17. As in Figure D17, length (l_1) is multiplied by the standard width (With), to create the area A_1. Area A_4 was easily calculated it is based on the intake pipe dimensions. Areas A_2 and $A_3$are a third of the distance from each end and hence are calculated proportionately. The distances from Area A_1 to A_2 to A_3 to $A_4$are noted as Lengths len_1, len_2 and len_3 respectively.

In order to calculate the pressure loss due to the stone bedding, the hydraulic conductivity is required. The pressure loss is defined as per Equation 4 below:

$$hf\,(m) = \frac{L * V}{k} \qquad \text{EqnD4}$$

Where:

hf = pressure loss due to friction within stone bedding

L = Length of water path (m)

V = Flow velocity

k = Hydraulic conductivity

The first two variables are easily to calculate however the hydraulic conductivity is calculated fromFigure D19.

Figure D18 below is a typical grading curve for nominally single-sized 19mm. From the grading curve, a value of D_{50} = 15.7mm was obtained. Table 31 summaries the parameters when obtaining the hydraulic conductivity k value.

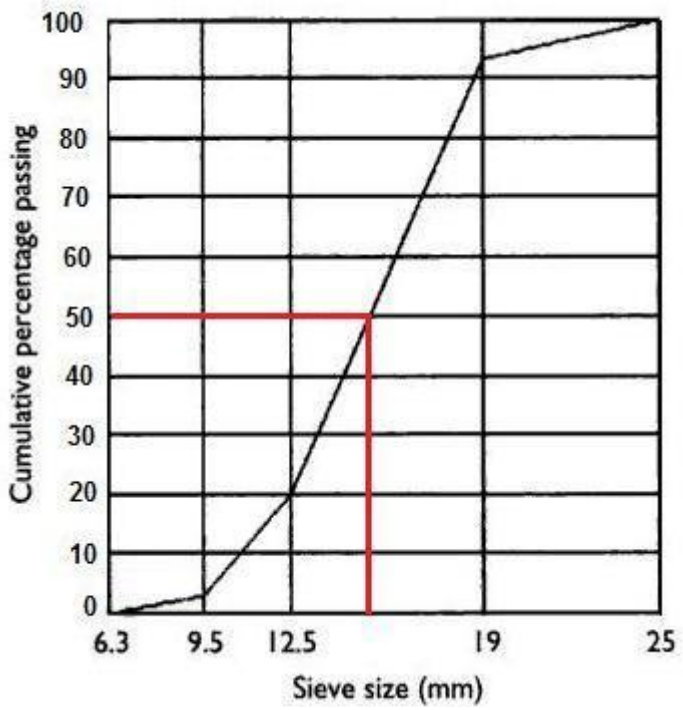

Figure D18: Grading curve for nominally single-sized 19mm Stone (Alexander & Mindess, 2005)

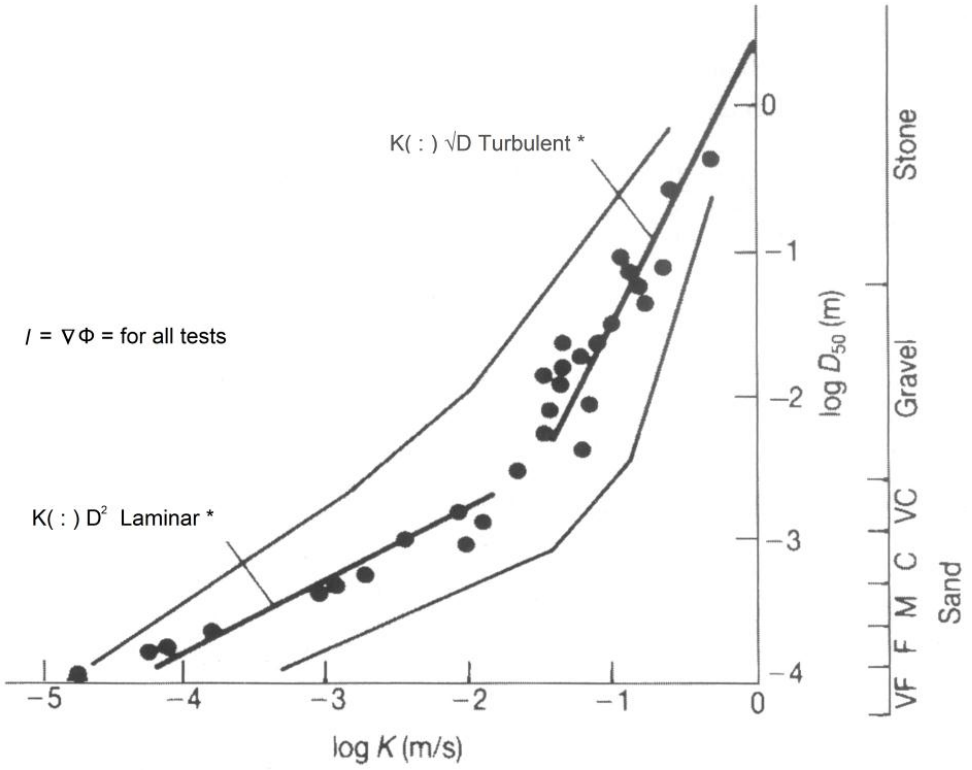

Figure D19: Permeability versus grain or stone sieve size (CIRIA, CUR, CETMEF,2007)

Table D31: Calculation of Permeability for19mm Bedding of seawater Intake (WST)

Description	Unit	Bedding
D_{n50}	m	0.0157
Log (D_{50})	m	-1.80
Log *k* (from fig. 2.39)	m/s	-1.16
k	m/s	0.069

Using the values from Table D31 and D31, headloss for Segment1 was calculated in the following manner. With the flow through each segment know, it is possible to determine the headloss if the areas through which water flows is uniform.

However, this is not the case. Hence each segment has been split into three equal portions. Table D32 below, describes the manner in which Segment 1 is split into three sub segments. Thereafter, Table D33 determines the average velocity for each sub segment, the associated headloss and finally the cumulative headloss for Segment 1. The following tables describe the headloss calculated for Segments 1, 2, 3, 4 and 5.

Table D32: Segment 1: Averaging of Areas (WST)

Test No.	Len1	A11	A12	A13	A14	Qs 1	Ave A1	Ave A2	Ave A3
	m	m^2	m^2	m^2	m^2	m3/s	m^2	m^2	m^2
1	0.3618	0.221	0.196	0.170	0.145	0.00012	0.208	0.183	0.158
2	0.3618	0.221	0.196	0.170	0.145	0.00019	0.208	0.183	0.158
3	0.3618	0.221	0.196	0.170	0.145	0.00030	0.208	0.183	0.158
4	0.3618	0.221	0.196	0.170	0.145	0.00047	0.208	0.183	0.158
5	0.3618	0.221	0.196	0.170	0.145	0.00084	0.208	0.183	0.158
6	0.3618	0.221	0.196	0.170	0.145	0.00107	0.208	0.183	0.158
7	0.3618	0.221	0.196	0.170	0.145	0.00148	0.208	0.183	0.158
8	0.3618	0.221	0.196	0.170	0.145	0.00232	0.208	0.183	0.158
9	0.3618	0.221	0.196	0.170	0.145	0.00279	0.208	0.183	0.158
10	0.3618	0.221	0.196	0.170	0.145	0.00337	0.208	0.183	0.158
11	0.3618	0.221	0.196	0.170	0.145	0.00375	0.208	0.183	0.158
12	0.3618	0.221	0.196	0.170	0.145	0.00416	0.208	0.183	0.158
13	0.3618	0.221	0.196	0.170	0.145	0.00467	0.208	0.183	0.158
14	0.3618	0.221	0.196	0.170	0.145	0.00513	0.208	0.183	0.158
15	0.3618	0.221	0.196	0.170	0.145	0.00537	0.208	0.183	0.158

Table D33: Segment 1: Velocity and cumulative headloss (WST)

Test No.	Vel 1A	Vel 1B	Vel 1C	H_l11	H_l12	H_l13	H_{l1} Total	H_l1Total
	m/s	m/s	m/s	m	m	m	m	mm
1	0.0006	0.0006	0.0008	0.0017	0.0020	0.0023	0.0060	6.00
2	0.0009	0.0010	0.0012	0.0028	0.0032	0.0037	0.0096	9.61
3	0.0015	0.0017	0.0019	0.0044	0.0050	0.0058	0.0153	15.32
4	0.0023	0.0026	0.0030	0.0069	0.0079	0.0091	0.0239	23.88
5	0.0040	0.0046	0.0053	0.0123	0.0140	0.0162	0.0425	42.53
6	0.0051	0.0059	0.0068	0.0157	0.0178	0.0207	0.0541	54.14
7	0.0071	0.0081	0.0094	0.0217	0.0246	0.0286	0.0749	74.86
8	0.0112	0.0127	0.0147	0.0340	0.0386	0.0448	0.1174	117.41
9	0.0134	0.0153	0.0177	0.0408	0.0464	0.0539	0.1411	141.10
10	0.0162	0.0184	0.0214	0.0493	0.0561	0.0651	0.1705	170.50
11	0.0180	0.0205	0.0238	0.0549	0.0624	0.0724	0.1898	189.75
12	0.0200	0.0227	0.0264	0.0608	0.0692	0.0802	0.2102	210.23
13	0.0224	0.0255	0.0296	0.0682	0.0776	0.0900	0.2359	235.85
14	0.0246	0.0280	0.0325	0.0750	0.0853	0.0989	0.2592	259.22
15	0.0258	0.0294	0.0340	0.0785	0.0893	0.1036	0.2715	271.47

Table D34: Segment 2: Averaging of Areas (WST)

Test No.	Len1	A11	A12	A13	A14	Qs 1	Ave A1	Ave A2	Ave A3
	m	m^2	m^2	m^2	m^2	m3/s	m^2	m^2	m^2
1	0.2814	0.172	0.163	0.154	0.145	0.00009	0.167	0.158	0.150
2	0.2814	0.172	0.163	0.154	0.145	0.00015	0.167	0.158	0.150
3	0.2814	0.172	0.163	0.154	0.145	0.00024	0.167	0.158	0.150
4	0.2814	0.172	0.163	0.154	0.145	0.00037	0.167	0.158	0.150
5	0.2814	0.172	0.163	0.154	0.145	0.00065	0.167	0.158	0.150
6	0.2814	0.172	0.163	0.154	0.145	0.00083	0.167	0.158	0.150
7	0.2814	0.172	0.163	0.154	0.145	0.00115	0.167	0.158	0.150
8	0.2814	0.172	0.163	0.154	0.145	0.00181	0.167	0.158	0.150
9	0.2814	0.172	0.163	0.154	0.145	0.00217	0.167	0.158	0.150
10	0.2814	0.172	0.163	0.154	0.145	0.00262	0.167	0.158	0.150
11	0.2814	0.172	0.163	0.154	0.145	0.00292	0.167	0.158	0.150
12	0.2814	0.172	0.163	0.154	0.145	0.00323	0.167	0.158	0.150
13	0.2814	0.172	0.163	0.154	0.145	0.00363	0.167	0.158	0.150

14	0.2814	0.172	0.163	0.154	0.145	0.00399	0.167	0.158	0.150
15	0.2814	0.172	0.163	0.154	0.145	0.00418	0.167	0.158	0.150

Table D35: Segment 2: Velocity and cumulative headloss (WST)

Test No.	Vel 1A	Vel 1B	Vel 1C	H_l21	H_l22	H_l23	H_l2 Total	H_l2 Total
	m/s	m/s	m/s	m	m	m	m	mm
1	0.0006	0.0006	0.0006	0.0017	0.0018	0.0019	0.0053	5.33
2	0.0009	0.0009	0.0010	0.0027	0.0028	0.0030	0.0085	8.54
3	0.0014	0.0015	0.0016	0.0043	0.0045	0.0048	0.0136	13.62
4	0.0022	0.0023	0.0025	0.0067	0.0071	0.0075	0.0212	21.22
5	0.0039	0.0041	0.0044	0.0119	0.0126	0.0133	0.0378	37.79
6	0.0050	0.0053	0.0056	0.0152	0.0160	0.0169	0.0481	48.11
7	0.0069	0.0073	0.0077	0.0210	0.0221	0.0234	0.0665	66.52
8	0.0108	0.0114	0.0121	0.0329	0.0347	0.0368	0.1043	104.33
9	0.0130	0.0137	0.0145	0.0395	0.0417	0.0442	0.1254	125.38
10	0.0157	0.0166	0.0175	0.0477	0.0504	0.0534	0.1515	151.50
11	0.0175	0.0184	0.0195	0.0531	0.0561	0.0594	0.1686	168.61
12	0.0193	0.0204	0.0216	0.0589	0.0621	0.0658	0.1868	186.81
13	0.0217	0.0229	0.0243	0.0660	0.0697	0.0738	0.2096	209.58
14	0.0238	0.0252	0.0267	0.0726	0.0766	0.0811	0.2303	230.34
15	0.0250	0.0264	0.0279	0.0760	0.0802	0.0850	0.2412	241.23

Table D36: Segment 3: Averaging of Areas (WST)

Test No.	Len1	A11	A12	A13	A14	Qs 1	Ave A1	Ave A2	Ave A3
	m	m^2	m^2	m^2	m^2	m3/s	m^2	m^2	m^2
1	0.201	0.123	0.130	0.138	0.145	0.00007	0.126	0.134	0.141
2	0.201	0.123	0.130	0.138	0.145	0.00011	0.126	0.134	0.141
3	0.201	0.123	0.130	0.138	0.145	0.00017	0.126	0.134	0.141
4	0.201	0.123	0.130	0.138	0.145	0.00026	0.126	0.134	0.141
5	0.201	0.123	0.130	0.138	0.145	0.00047	0.126	0.134	0.141
6	0.201	0.123	0.130	0.138	0.145	0.00059	0.126	0.134	0.141
7	0.201	0.123	0.130	0.138	0.145	0.00082	0.126	0.134	0.141
8	0.201	0.123	0.130	0.138	0.145	0.00129	0.126	0.134	0.141
9	0.201	0.123	0.130	0.138	0.145	0.00155	0.126	0.134	0.141
10	0.201	0.123	0.130	0.138	0.145	0.00187	0.126	0.134	0.141
11	0.201	0.123	0.130	0.138	0.145	0.00209	0.126	0.134	0.141
12	0.201	0.123	0.130	0.138	0.145	0.00231	0.126	0.134	0.141
13	0.201	0.123	0.130	0.138	0.145	0.00259	0.126	0.134	0.141

14	0.201	0.123	0.130	0.138	0.145	0.00285	0.126	0.134	0.141
15	0.201	0.123	0.130	0.138	0.145	0.00298	0.126	0.134	0.141

Table D37: Segment 3: Velocity and cumulative headloss (WST)

Test No.	Vel 1A	Vel 1B	Vel 1C	H_l31	H_l32	H_l33	H_l3 Total	H_l3 Total
	m/s	m/s	m/s	m	m	m	m	mm
1	0.0005	0.0005	0.0005	0.0016	0.0015	0.0014	0.0045	4.50
2	0.0008	0.0008	0.0007	0.0025	0.0024	0.0023	0.0072	7.22
3	0.0013	0.0013	0.0012	0.0041	0.0038	0.0036	0.0115	11.51
4	0.0021	0.0020	0.0019	0.0063	0.0060	0.0056	0.0179	17.93
5	0.0037	0.0035	0.0033	0.0113	0.0106	0.0101	0.0319	31.94
6	0.0047	0.0044	0.0042	0.0143	0.0135	0.0128	0.0407	40.66
7	0.0065	0.0061	0.0058	0.0198	0.0187	0.0177	0.0562	56.22
8	0.0102	0.0096	0.0091	0.0311	0.0293	0.0278	0.0882	88.17
9	0.0123	0.0116	0.0110	0.0373	0.0352	0.0334	0.1060	105.97
10	0.0148	0.0140	0.0132	0.0451	0.0426	0.0403	0.1280	128.04
11	0.0165	0.0156	0.0147	0.0502	0.0474	0.0449	0.1425	142.50
12	0.0183	0.0173	0.0163	0.0556	0.0525	0.0497	0.1579	157.88
13	0.0205	0.0194	0.0183	0.0624	0.0589	0.0558	0.1771	177.12
14	0.0225	0.0213	0.0201	0.0686	0.0648	0.0613	0.1947	194.67
15	0.0236	0.0223	0.0211	0.0718	0.0678	0.0642	0.2039	203.87

Table D38: Segment 4: Averaging of Areas (WST)

Test No.	Len1	A11	A12	A13	A14	Qs 1	Ave A1	Ave A2	Ave A3
	m	m^2	m^2	m^2	m^2	m3/s	m^2	m^2	m^2
1	0.1206	0.074	0.097	0.121	0.145	0.00004	0.085	0.109	0.133
2	0.1206	0.074	0.097	0.121	0.145	0.00006	0.085	0.109	0.133
3	0.1206	0.074	0.097	0.121	0.145	0.00010	0.085	0.109	0.133
4	0.1206	0.074	0.097	0.121	0.145	0.00016	0.085	0.109	0.133
5	0.1206	0.074	0.097	0.121	0.145	0.00028	0.085	0.109	0.133
6	0.1206	0.074	0.097	0.121	0.145	0.00036	0.085	0.109	0.133
7	0.1206	0.074	0.097	0.121	0.145	0.00049	0.085	0.109	0.133
8	0.1206	0.074	0.097	0.121	0.145	0.00077	0.085	0.109	0.133
9	0.1206	0.074	0.097	0.121	0.145	0.00093	0.085	0.109	0.133
10	0.1206	0.074	0.097	0.121	0.145	0.00112	0.085	0.109	0.133
11	0.1206	0.074	0.097	0.121	0.145	0.00125	0.085	0.109	0.133
12	0.1206	0.074	0.097	0.121	0.145	0.00139	0.085	0.109	0.133

13	0.1206	0.074	0.097	0.121	0.145	0.00156	0.085	0.109	0.133
14	0.1206	0.074	0.097	0.121	0.145	0.00171	0.085	0.109	0.133
15	0.1206	0.074	0.097	0.121	0.145	0.00179	0.085	0.109	0.133

Table D39: Segment 4: Velocity and cumulative headloss (WST)

Test No.	Vel 1A	Vel 1B	Vel 1C	H_l41	H_l42	H_l43	H_l4 Total	H_l4 Total
	m/s	m/s	m/s	m	m	m	m	mm
1	0.0005	0.0004	0.0003	0.0014	0.0011	0.0009	0.0034	3.41
2	0.0007	0.0006	0.0005	0.0023	0.0018	0.0014	0.0055	5.47
3	0.0012	0.0009	0.0008	0.0036	0.0028	0.0023	0.0087	8.72
4	0.0018	0.0014	0.0012	0.0056	0.0044	0.0036	0.0136	13.58
5	0.0033	0.0026	0.0021	0.0100	0.0078	0.0064	0.0242	24.19
6	0.0042	0.0033	0.0027	0.0127	0.0099	0.0082	0.0308	30.80
7	0.0058	0.0045	0.0037	0.0176	0.0137	0.0113	0.0426	42.58
8	0.0091	0.0071	0.0058	0.0276	0.0215	0.0177	0.0668	66.79
9	0.0109	0.0085	0.0070	0.0331	0.0259	0.0213	0.0803	80.26
10	0.0132	0.0103	0.0084	0.0400	0.0313	0.0257	0.0970	96.98
11	0.0146	0.0114	0.0094	0.0445	0.0348	0.0286	0.1079	107.94
12	0.0162	0.0127	0.0104	0.0493	0.0386	0.0317	0.1196	119.58
13	0.0182	0.0142	0.0117	0.0554	0.0433	0.0355	0.1342	134.16
14	0.0200	0.0156	0.0128	0.0608	0.0476	0.0390	0.1475	147.45
15	0.0209	0.0164	0.0134	0.0637	0.0498	0.0409	0.1544	154.42

Table D40: Segment 5: Averaging of Areas (WST)

Test No.	Len1	A11	A12	A13	A14	Qs 1	Ave A1	Ave A2	Ave A3
	m	m^2	m^2	m^2	m^2	m3/s	m^2	m^2	m^2
1	0.0402	0.025	0.065	0.105	0.145	0.00001	0.045	0.085	0.125
2	0.0402	0.025	0.065	0.105	0.145	0.00002	0.045	0.085	0.125
3	0.0402	0.025	0.065	0.105	0.145	0.00003	0.045	0.085	0.125
4	0.0402	0.025	0.065	0.105	0.145	0.00005	0.045	0.085	0.125
5	0.0402	0.025	0.065	0.105	0.145	0.00009	0.045	0.085	0.125
6	0.0402	0.025	0.065	0.105	0.145	0.00012	0.045	0.085	0.125
7	0.0402	0.025	0.065	0.105	0.145	0.00016	0.045	0.085	0.125
8	0.0402	0.025	0.065	0.105	0.145	0.00026	0.045	0.085	0.125
9	0.0402	0.025	0.065	0.105	0.145	0.00031	0.045	0.085	0.125
10	0.0402	0.025	0.065	0.105	0.145	0.00037	0.045	0.085	0.125
11	0.0402	0.025	0.065	0.105	0.145	0.00042	0.045	0.085	0.125

12	0.0402	0.025	0.065	0.105	0.145	0.00046	0.045	0.085	0.125
13	0.0402	0.025	0.065	0.105	0.145	0.00052	0.045	0.085	0.125
14	0.0402	0.025	0.065	0.105	0.145	0.00057	0.045	0.085	0.125
15	0.0402	0.025	0.065	0.105	0.145	0.00060	0.045	0.085	0.125

Table D41: Segment 5: Velocity and cumulative headloss (WST)

Test No.	Vel 1A	Vel 1B	Vel 1C	H_l51	H_l52	H_l53	H_l5 Total	H_l5 Total
	m/s	m/s	m/s	m	m	m	m	mm
1	0.0003	0.0002	0.0001	0.0009	0.0005	0.0003	0.0017	1.69
2	0.0005	0.0002	0.0002	0.0014	0.0008	0.0005	0.0027	2.71
3	0.0008	0.0004	0.0003	0.0023	0.0012	0.0008	0.0043	4.33
4	0.0012	0.0006	0.0004	0.0036	0.0019	0.0013	0.0067	6.74
5	0.0021	0.0011	0.0007	0.0064	0.0034	0.0023	0.0120	12.01
6	0.0027	0.0014	0.0010	0.0081	0.0043	0.0029	0.0153	15.28
7	0.0037	0.0019	0.0013	0.0112	0.0059	0.0040	0.0211	21.13
8	0.0058	0.0030	0.0021	0.0176	0.0093	0.0063	0.0331	33.14
9	0.0070	0.0037	0.0025	0.0212	0.0111	0.0075	0.0398	39.83
10	0.0084	0.0044	0.0030	0.0256	0.0134	0.0091	0.0481	48.13
11	0.0093	0.0049	0.0033	0.0285	0.0150	0.0101	0.0536	53.56
12	0.0104	0.0054	0.0037	0.0315	0.0166	0.0112	0.0593	59.34
13	0.0116	0.0061	0.0041	0.0354	0.0186	0.0126	0.0666	66.57
14	0.0128	0.0067	0.0046	0.0389	0.0204	0.0139	0.0732	73.17
15	0.0134	0.0070	0.0048	0.0407	0.0214	0.0145	0.0766	76.63

Table D42 below, summaries the results of Tables 32 to 41.Figure D20plots these graphically. A trendline is added to the results in order to predict the headloss, due to stone bedding, at the most downstream point of WC1. The largest headloss occurs at this point. Table D43 summaries these extrapolatedresults.

Table D42: Summary of Method 3 Headloss Tests. Results from Tables 32 to 41 (WST)

Test No.	Total Q	Total 2Q	Segment 1	Segment 2	Segment 3	Segment 4	Segment 5
	l/s	l/s	mm	mm	mm	mm	mm
1	0.33	0.66	6.00	5.33	4.50	3.41	1.69
2	0.53	1.06	9.61	8.54	7.22	5.47	2.71
3	0.84	1.68	15.32	13.62	11.51	8.72	4.33
4	1.31	2.62	23.88	21.22	17.93	13.58	6.74
5	2.34	4.67	42.53	37.79	31.94	24.19	12.01
6	2.98	5.95	54.14	48.11	40.66	30.80	15.28
7	4.11	8.23	74.86	66.52	56.22	42.58	21.13
8	6.45	12.90	117.41	104.33	88.17	66.79	33.14
9	7.75	15.51	141.10	125.38	105.97	80.26	39.83

10	9.37	18.74	170.50	151.50	128.04	96.98	48.13
11	10.43	20.85	189.75	168.61	142.50	107.94	53.56
12	11.55	23.10	210.23	186.81	157.88	119.58	59.34
13	12.96	25.92	235.85	209.58	177.12	134.16	66.57
14	14.24	28.49	259.22	230.34	194.67	147.45	73.17
15	14.92	29.83	271.47	241.23	203.87	154.42	76.63

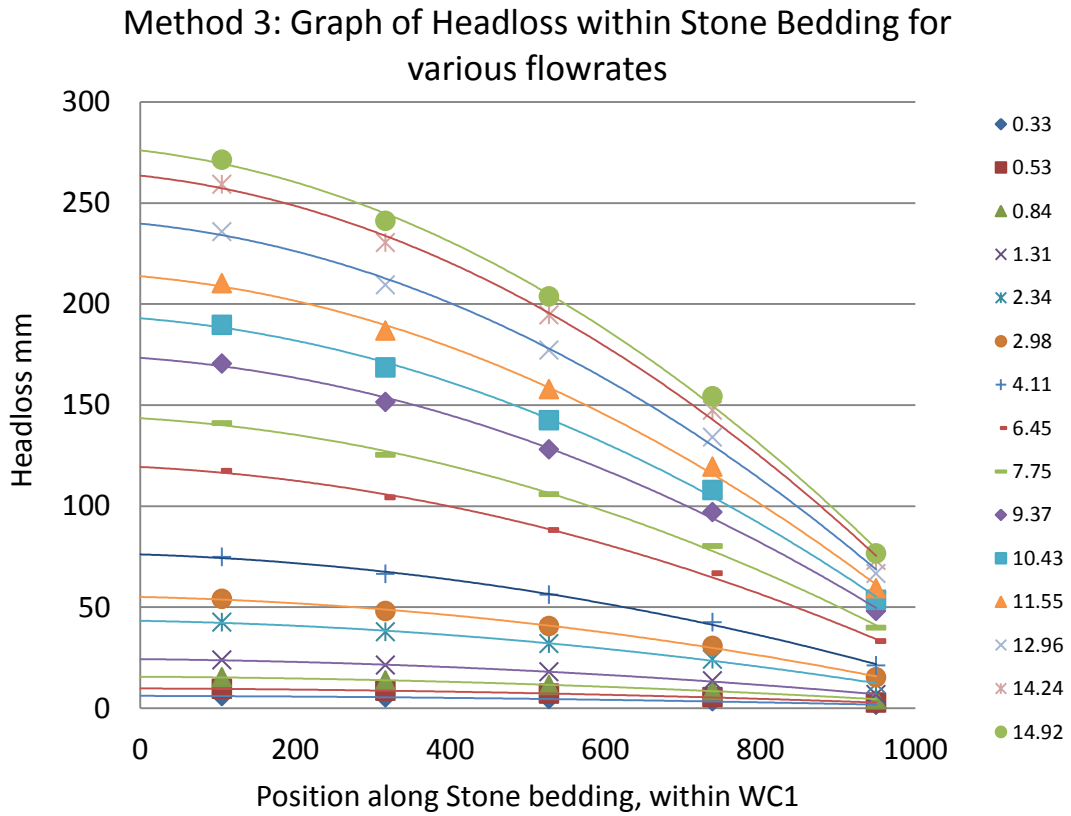

Figure D20: Results of Method 3:Headloss estimation due to Stone Bedding, within WC1

Table D43: Method 3:Summary of maximum headloss versus flow rates (WST)

Test No.	Total Q	Total 2Q	Maximum Headloss due to Stone Bedding
	l/s	l/s	mm
1	0.33	0.66	6.02
2	0.53	1.06	9.85
3	0.84	1.68	15.75
4	1.31	2.62	23.95
5	2.34	4.67	43.25
6	2.98	5.95	55
7	4.11	8.23	76
8	6.45	12.90	119.5
9	7.75	15.51	143.5
10	9.37	18.74	173.2
11	10.43	20.85	192.7
12	11.55	23.10	214

13	12.96	25.92	239.7
14	14.24	28.49	263.8
15	14.92	29.83	276

D.5.4.3 Comparison of Results for Method 1, 2 and 3

The following Figure D21 shows the results for Method 1, 2 and 3 for the calculation of Headloss due to the stone bedding, Results for Method1, 2 and 3 are derived from Table D12, D29 and D43. Note that for flows less than 8l/s, the results of Method 1 and 2 are in the same ballpark. The values for Method 3 appear to overestimate the pressure loss due to the stone bedding.

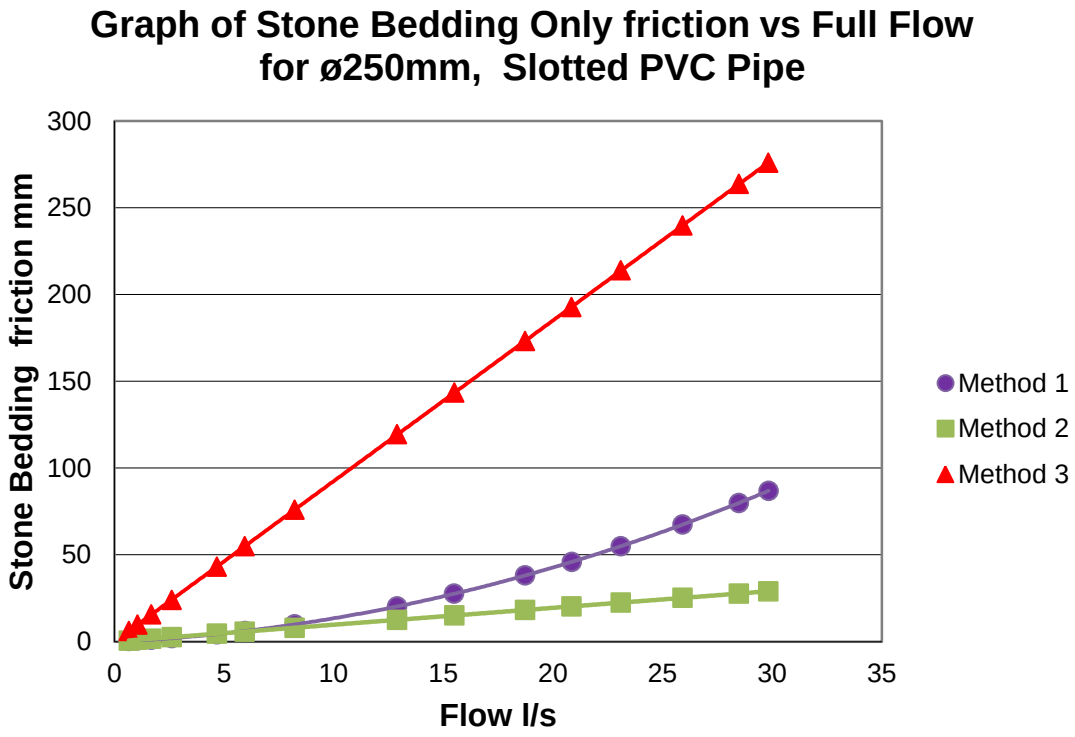

Figure D16: Method 1, 2 and 3: Headloss due to the stone bedding

D.6: Water, Sand and Stone Bedding Test before Flushing

The following Water, Sand and Stone test(WSST) is aimed at finding the headloss due the Sand and stone bedding that surrounds the intake pipe. For design and academic purposes, a conservative approach was taken. In the HPM, the stone bedding surrounding the slotted pipeline was considered to be saturated with sand. The sand is a mixture of a fine grained 'beach' sanded called Philippi and a 'single sized' granular filter sand which is normally used as filter material. Details concerning the sand added to the stone bedding can be found in Appendix C

The following explains the manner in which the Sand and Stone Bedding Test was conducted and uses tables and equations to illustrate the analysis process. Table D1 details the physical aspects of the model including the Intake pipeline and can found in Chapter D1.

The aim of this experiment is to establish the relationship between the flow and the loss of pressure head as it passes in to the Intake pipeline Using the above information, 13 tests, where conducted. Table D30 shows the initial results. The difference between WC1 and WC2 denotes the total headloss. The flow rate was determined from the following EquationB1

$$Q = C_d \cdot \frac{8}{15} \cdot \sqrt{2g} \cdot \tan\frac{\theta}{2} \cdot h^{\frac{5}{2}} \qquad \text{Eqn B1}$$

Where

Q= Flow (l/s)

C_d*= 0.57*

h = depth of water above V Notch (mm)

Table D44: Total Headloss and initial flow rate for Sand and Stone Bedding (WSST)

Test No.	Time min	WC1	WC2	Upstream Head	Downstream Head	Total Δhf	Initial Q Half Pipe
		mm	mm	mm	mm	mm	l/s
1	0	2070	2030	55	15	40	0.0371
2	45	2352	2040	337	25	312	0.1331
3	60	2375	2040	360	25	335	0.1331
4	70	2390	2040	375	25	350	0.1331
5	83	2402	2040	387	25	362	0.1331
6	107	2414	2040	399	25	374	0.1331
7	118	2333	2040	318	25	293	0.1331
8	143	2255	2035	240	20	220	0.0762
9	149	2293	2036	278	21	257	0.0861
10	160.5	2303	2037	288	22	266	0.0967
11	171.5	2305	2037	290	22	268	0.0967
12	178.2	2305	2037	290	22	268	0.0967
13	185	2305	2037	290	22	268	0.0967

Next, Water leakage has to be considered. As per chapter D3 theses losses are incorporated in Table D45. 40% of all leakage is estimated to emanate from WC1, 40% from WC2a and 20% from WC2b.

D.6.1 Water Leakage losses

Table D31: Total headloss and flow rate incorporating losses (WSST)

1	2	3	4	5	6	7	8	9	10
Test No.	Q Half Pipe	Bucket Ht	Time	Volume	Total	Loss due to WC1	Loss due to WC2a	Loss due to WC2b	Total Q
	l/s	mm	s	l	l/s	l/s	l/s	l/s	l/s
1	0.0371	67	344.0	16.27	0.005	0.00189	0.00189	0.00095	0.0409
2	0.1331	67	1055.7	16.27	0.015	0.00616	0.00616	0.00308	0.1454
3	0.1331	67	758.5	16.27	0.021	0.00858	0.00858	0.00429	0.1502
4	0.1331	67	654.6	16.27	0.025	0.00994	0.00994	0.00497	0.1529
5	0.1331	67	725.5	16.27	0.022	0.00897	0.00897	0.00448	0.1510
6	0.1331	67	316.8	16.27	0.051	0.02054	0.02054	0.01027	0.1741
7	0.1331	67	560.7	16.27	0.029	0.01161	0.01161	0.00580	0.1563
8	0.0762	67	858.5	16.27	0.019	0.00758	0.00758	0.00379	0.0913
9	0.0861	67	657.4	16.27	0.025	0.00990	0.00990	0.00495	0.1059
10	0.0967	67	635.7	16.27	0.026	0.01024	0.01024	0.00512	0.1171
11	0.0967	67	658	16.27	0.025	0.00989	0.00989	0.00494	0.1164
12	0.0967	67	664.5	16.27	0.024	0.00979	0.00979	0.00490	0.1163
13	0.0967	67	648.4	16.27	0.025	0.01004	0.01004	0.00502	0.1167

In Table D45, the total leakage rate is calculated in Column 6. Columns 7, 8 and 9 calculate the loss for WC1, WC2a and WC2b, respectively. The Total flow rate Q is calculated as the Initial flow rate plus the leakage from WC1 and WC2a

D.6.2 Pressure losses

After the correct total flow has been established, the next step is the disaggregation of pressure losses. This is done so that Loss A and the loss for sand and stone bedding can be established. Chapter D2 states the Pressure Losses A to E with the relevant equations. Table D46 calculates the Losses B to E and hence the remaining total headloss will be Loss A plus sand and stone bedding.

Table D46: Disaggregation of pressure losses (WSST)

Test No.	Total ∆hf	Total Q	Loss B+C	Loss D	Loss E	Loss A + sand + stone bedding	%A of Total ∆hf
	mm	l/s	m	m	m	mm	
1	40	0.75	2.735E-08	8.139E-08	1.900E-08	40.0	0.00%
2	312	1.38	3.458E-07	1.047E-06	2.444E-07	312.0	~100%
3	335	2.05	3.691E-07	1.047E-06	2.444E-07	335.0	~100%
4	350	2.55	3.826E-07	1.047E-06	2.444E-07	350.0	~100%
5	362	3.30	3.730E-07	1.047E-06	2.444E-07	362.0	~100%
6	374	3.73	4.960E-07	1.047E-06	2.444E-07	374.0	~100%
7	293	4.29	3.995E-07	1.047E-06	2.444E-07	293.0	100%
8	220	5.19	1.364E-07	3.430E-07	8.008E-08	220.0	~100%
9	257	6.40	1.833E-07	4.377E-07	1.022E-07	257.0	~100%
10	266	7.32	2.244E-07	5.524E-07	1.290E-07	266.0	~100%
11	268	8.31	2.218E-07	5.524E-07	1.290E-07	268.0	~100%
12	268	8.87	2.210E-07	5.524E-07	1.290E-07	268.0	~100%
13	268	9.81	2.229E-07	5.524E-07	1.290E-07	268.0	~100%

D.6.3 Perforation losses and Flowrate Relationship

Table D47 shows relationship between LossA+sand + stone bedding and the flowrate for half a pipe and for a full pipeline. Figure D17 show the plot of various flows rate and their corresponding pressure loss. Note that due to the scatter of the data, a strongly defined relationship between the Pressure loss and flowrate could not be established.

Table D33: Loss A + sand + stone bedding with correspondingflowrates (WSST)

Test No.	Loss A+sand + stone bedding	Q Half Pipe	Q Full Pipe
	mm	l/s	l/s
1	40.0	l/s	ml/s
2	312.0	0.082	81.78
3	335.0	0.291	290.79
4	350.0	0.300	300.45
5	362.0	0.306	305.90
6	374.0	0.302	302.01
7	293.0	0.348	348.30
8	220.0	0.313	312.56
9	257.0	0.183	182.66
10	266.0	0.212	211.70
11	268.0	0.234	234.28
12	268.0	0.233	232.89
13	268.0	0.233	232.50

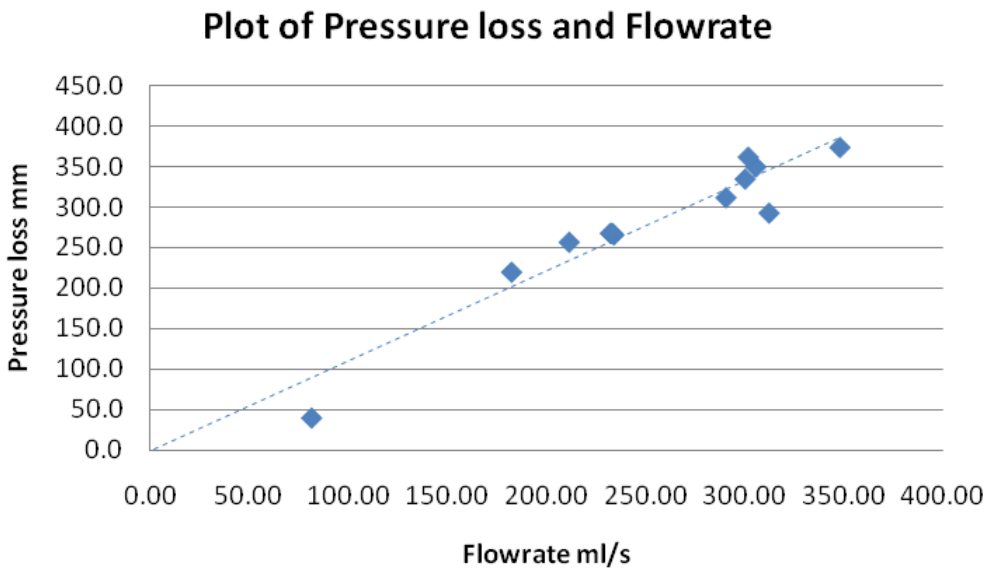

Figure D22: Plot of Pressure due to the slots, +sand + stone beddingand corresponding flowrate for a fully flowing ø250mm slotted pipe

The test commenced with the sand and stone mixture insitu. However prior to the test starting, the seawater intake experienced accelerated clogging. Increasing the driving head had no effect on the rate of flow through the HPM. Figure D23 shows the headloss and rate of flow for the 3hour test.

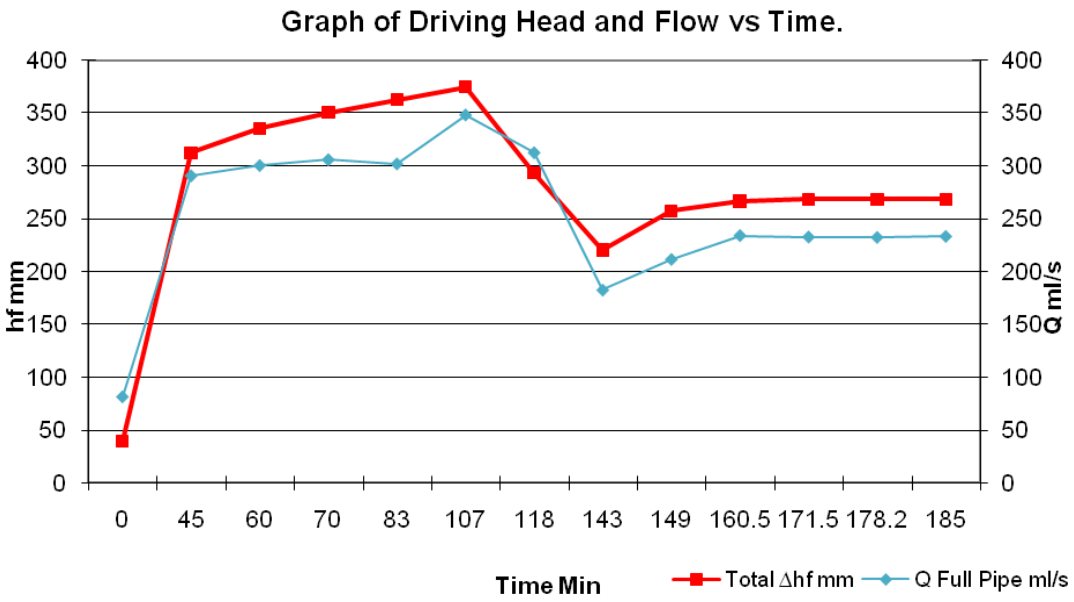

Figure D23: Headloss and rate of flow for a 3hour test period

Due to the severely restricted flow, and the design of such a Seawater Intake pipeline was considered a failure as the tested flow rate was not relatively close to the design flow of 48l/s. Due to this restricted flow, backflushing was considered next.

D.7: Water Sand and Stone Bedding Test after Backflushing

The followingWater Sand and Stone test after Backflushing(WSST-ABF) is similar to the previous one. This test is conducted after the back flushing. The first aim is to find the headloss due to the Sand and stone bedding that surrounds the intake pipe. The second aim is to compare the results with the previous test in order to understand the effect of the back flushing

The following explains the manner in which the Sand and Stone Bedding Test was conducted and uses tables and equations to illustrate the analysis process. Table D1 which can be found in previous chapters details the physical aspects of the model including the Intake pipeline.

26 tests, where conducted. Table D48 shows the initial results. The difference between WC1 and WC2 denotes the total headloss. The flow rate was determined from the following EquationB1

$$Q = C_d \cdot \frac{8}{15} \cdot \sqrt{2g} \cdot \tan\frac{\theta}{2} \cdot h^{\frac{5}{2}} \qquad \text{Eqn B1}$$

Where

Q= Flow (l/s)

C_d= 0.57

h = depth of water above V Notch (mm)

Table D48: Total Headloss and initial flow rate for Sand and Stone Bedding (WSST-ABF)

Test No.	Time min	WC1	WC2	Upstream Head	Downstream Head	Total ∆hf	Initial Q Half Pipe
		mm	mm	mm	mm	mm	l/s
1	0	2015	2015	0	0	0	0.0000
2	7	2261	2027	246	12	234	0.0212
3	12	2284	2029	269	14	255	0.0312
4	16	2315	2030	300	15	285	0.0371
5	20	2342	2031	327	16	311	0.0436
6	24	2357	2032.5	342	17.5	324.5	0.0546
7	28	2372	2033	357	18	339	0.0585
8	32	2384	2034	369	19	350	0.0670
9	36	2391	2035	376	20	356	0.0762
10	40	2395	2035	380	20	360	0.0762
11	44	2398	2035.5	383	20.5	362.5	0.0810
12	48	2399	2036	384	21	363	0.0861
13	52	2402	2036	387	21	366	0.0861
14	56	2402	2036	387	21	366	0.0861
15	60	2402	2036.5	387	21.5	365.5	0.0913
16	66	2400	2036.5	385	21.5	363.5	0.0913
17	72	2399	2036.5	384	21.5	362.5	0.0913
18	78	2396	2036.5	381	21.5	359.5	0.0913
19	101	2386	2036.5	371	21.5	349.5	0.0913
20	150	2366	2036.5	351	21.5	329.5	0.0913
21	170	2357	2036.5	342	21.5	320.5	0.0913
22	192	2352	2036.5	337	21.5	315.5	0.0913
23	230	2344	2036.5	329	21.5	307.5	0.0913
24	280	2334	2036.5	319	21.5	297.5	0.0913
25	326	2328	2036.5	313	21.5	291.5	0.0913
26	377	2318	2036.5	303	21.5	281.5	0.0913

Next, Water leakage has to be considered. As per chapter D3 theses losses are incorporated in Table D49. 40% of all leakage is estimated to emanate from WC1, 40% from WC 2a and 20% from WC2b.

D.7.1 Water Leakage losses

In Table D32, the total leakage rate is calculated in Column 6. Columns 7, 8 and 9 calculate the loss for WC1, WC2a and WC2b, respectively. The Total flow rate Q is calculated as the Initial flow rate plus the leakage from WC1 and WC2a

Table D49: Total headloss and flow rate incorporating losses (WSST-ABF)

1	2	3	4	5	6	7	8	9	10
Test No.	Q Half Pipe	Bucket Ht	Time	Volume	Total	Loss due to WC1	Loss due to WC2a	Loss due to WC2b	Total Q
	l/s	mm	s	l	l/s	l/s	l/s	l/s	l/s
1	0.0000	68.2	200	16.57	0.083	0.03313	0.03313	0.01657	0.0663
2	0.0212	69.5	420	16.89	0.040	0.01609	0.01609	0.00804	0.0534
3	0.0312	70	300	17.02	0.057	0.02269	0.02269	0.01134	0.0766
4	0.0371	71	240	17.27	0.072	0.02878	0.02878	0.01439	0.0947
5	0.0436	72	240	17.52	0.073	0.02920	0.02920	0.01460	0.1020
6	0.0546	74	240	18.02	0.075	0.03003	0.03003	0.01502	0.1146
7	0.0585	68	240	16.52	0.069	0.02753	0.02753	0.01376	0.1136
8	0.0670	69	240	16.77	0.070	0.02795	0.02795	0.01397	0.1229
9	0.0762	72	240	17.52	0.073	0.02920	0.02920	0.01460	0.1346
10	0.0762	71	240	17.27	0.072	0.02878	0.02878	0.01439	0.1337
11	0.0810	70	240	17.02	0.071	0.02836	0.02836	0.01418	0.1377
12	0.0861	70	240	17.02	0.071	0.02836	0.02836	0.01418	0.1428
13	0.0861	71	240	17.27	0.072	0.02878	0.02878	0.01439	0.1436
14	0.0861	72	240	17.52	0.073	0.02920	0.02920	0.01460	0.1444
15	0.0913	68	240	16.52	0.069	0.02753	0.02753	0.01376	0.1463
16	0.0913	71	360	17.27	0.048	0.01919	0.01919	0.00959	0.1296
17	0.0913	72	360	17.52	0.049	0.01946	0.01946	0.00973	0.1302
18	0.0913	74	360	18.02	0.050	0.02002	0.02002	0.01001	0.1313
19	0.0913	74	1380	18.02	0.013	0.00522	0.00522	0.00261	0.1017
20	0.0913	68	2940	16.52	0.006	0.00225	0.00225	0.00112	0.0958
21	0.0913	69	1200	16.77	0.014	0.00559	0.00559	0.00279	0.1024
22	0.0913	70	1320	17.02	0.013	0.00516	0.00516	0.00258	0.1016
23	0.0913	71	2280	17.27	0.008	0.00303	0.00303	0.00151	0.0973
24	0.0913	72	3000	17.52	0.006	0.00234	0.00234	0.00117	0.0959
25	0.0913	74	2760	18.02	0.007	0.00261	0.00261	0.00131	0.0965
26	0.0913	75	3060	18.27	0.006	0.00239	0.00239	0.00119	0.0960

D.7.2 Pressure losses

After the correct total flow has been established, the next step is the disaggregation of pressure losses. This is done so that Loss A and the loss for sand and stone bedding can be established. Chapter D2 states the Pressure Losses A to E with the relevant equations. Table D50 calculates the Losses B to E and hence the remaining total headloss will be Loss A plus sand and stone bedding.

Table D50: Disaggregation of pressure losses (WSST-ABF)

Test No.	Total Δhf	Total Q	Loss B+C	Loss D	Loss E	Loss A+sand + stone bedding	%A of Total Δhf
	mm	l/s	m	m	m	mm	
1	0	0.1325	7.183E-08	0.000E+0	0.000E+0	0.00	0.00%
2	234	0.1068	4.667E-08	2.667E-08	6.227E-09	234.00	~100%
3	255	0.1532	9.599E-08	5.765E-08	1.346E-08	255.00	~100%
4	285	0.1893	1.466E-07	8.139E-08	1.900E-08	285.00	~100%
5	311	0.2040	1.702E-07	1.124E-07	2.624E-08	311.00	~100%
6	324.5	0.2292	2.149E-07	1.759E-07	4.107E-08	324.50	~100%
7	339	0.2272	2.110E-07	2.025E-07	4.729E-08	339.00	100%
8	350	0.2458	2.470E-07	2.654E-07	6.197E-08	350.00	~100%
9	356	0.2691	2.962E-07	3.430E-07	8.008E-08	356.00	~100%
10	360	0.2675	2.925E-07	3.430E-07	8.008E-08	360.00	~100%
11	362.5	0.2755	3.103E-07	3.881E-07	9.061E-08	362.50	~100%
12	363	0.2856	3.334E-07	4.377E-07	1.022E-07	363.00	~100%
13	366	0.2872	3.373E-07	4.377E-07	1.022E-07	366.00	~100%
14	366	0.2889	3.413E-07	4.377E-07	1.022E-07	366.00	~100%
15	365.5	0.2927	3.502E-07	4.924E-07	1.150E-07	365.50	~100%
16	363.5	0.2593	2.749E-07	4.924E-07	1.150E-07	363.50	~100%
17	362.5	0.2604	2.773E-07	4.924E-07	1.150E-07	362.50	~100%
18	359.5	0.2626	2.820E-07	4.924E-07	1.150E-07	359.50	~100%
19	349.5	0.2034	1.692E-07	4.924E-07	1.150E-07	349.50	100%
20	329.5	0.1915	1.500E-07	4.924E-07	1.150E-07	329.50	~100%
21	320.5	0.2049	1.717E-07	4.924E-07	1.150E-07	320.50	~100%
22	315.5	0.2032	1.688E-07	4.924E-07	1.150E-07	315.50	~100%
23	307.5	0.1947	1.549E-07	4.924E-07	1.150E-07	307.50	~100%
24	297.5	0.1919	1.505E-07	4.924E-07	1.150E-07	297.50	~100%
25	291.5	0.1930	1.523E-07	4.924E-07	1.150E-07	291.50	~100%
26	281.5	0.1921	1.509E-07	4.924E-07	1.150E-07	281.50	~100%

D.7.3 Perforation losses and Flowrate Relationship

Table D51 shows relationship between LossA+sand + stone bedding and the flowrate for half a pipe and for a full pipeline. Figure D24 shows the plot of various flows rate and their corresponding pressure loss. Note that due to the scatter of the data, a strongly defined relationship between the Pressure loss and flowrate could not be established.

Table D51: Loss A+ sand + stone bedding with correspondingflowrates (WSST-ABF)

Test No.	Loss A+sand + stone bedding	Q Half Pipe	Q Full Pipe
	mm	l/s	l/s
1	0.00	0.066	0.1325
2	234.00	0.053	0.1068
3	255.00	0.077	0.1532
4	285.00	0.095	0.1893
5	311.00	0.102	0.2040
6	324.50	0.115	0.2292
7	339.00	0.114	0.2272
8	350.00	0.123	0.2458
9	356.00	0.135	0.2691
10	360.00	0.134	0.2675
11	362.50	0.138	0.2755
12	363.00	0.143	0.2856
13	366.00	0.144	0.2872
14	366.00	0.144	0.2889
15	365.50	0.146	0.2927
16	363.50	0.130	0.2593
17	362.50	0.130	0.2604
18	359.50	0.131	0.2626
19	349.50	0.102	0.2034
20	329.50	0.096	0.1915
21	320.50	0.102	0.2049
22	315.50	0.102	0.2032
23	307.50	0.097	0.1947
24	297.50	0.096	0.1919
25	291.50	0.096	0.1930
26	281.50	0.096	0.1921

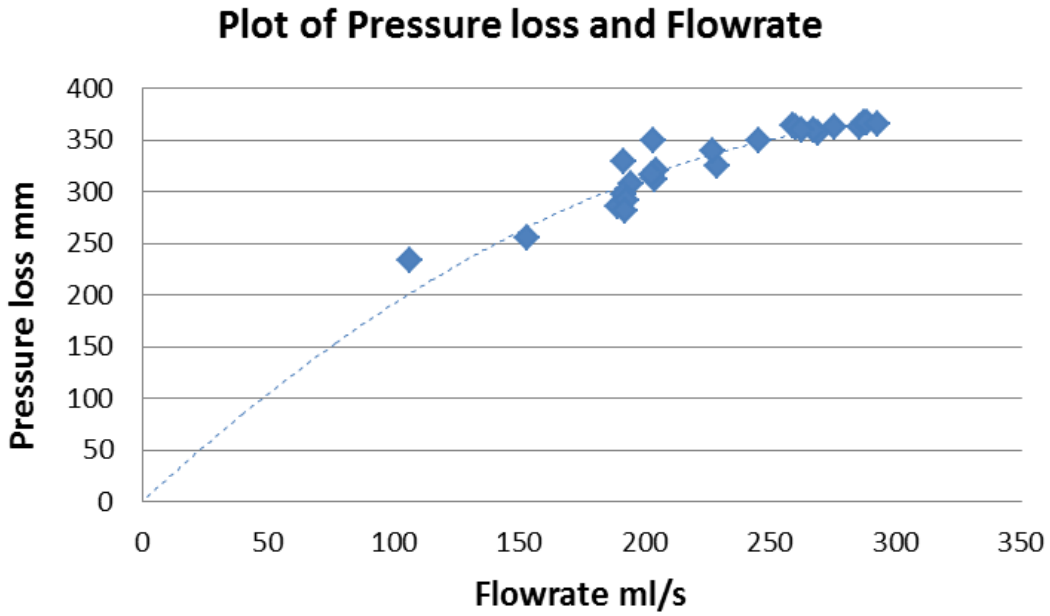

Figure D19: Plot of Pressure due to the slots, +sand + stone bedding and corresponding flowrate for a fully flowing ø250mm slotted pipe after flushing

The test commenced with the sand and stone mixture insitu and the back flushing completed at the onset, the seawater intake experienced clogging. Increasing the driving head had no effect on the rate of flow through the HPM. Figure D25 shows the loss on head (left axis) and rate of flow (right axis) over a 6.5 hour test period.

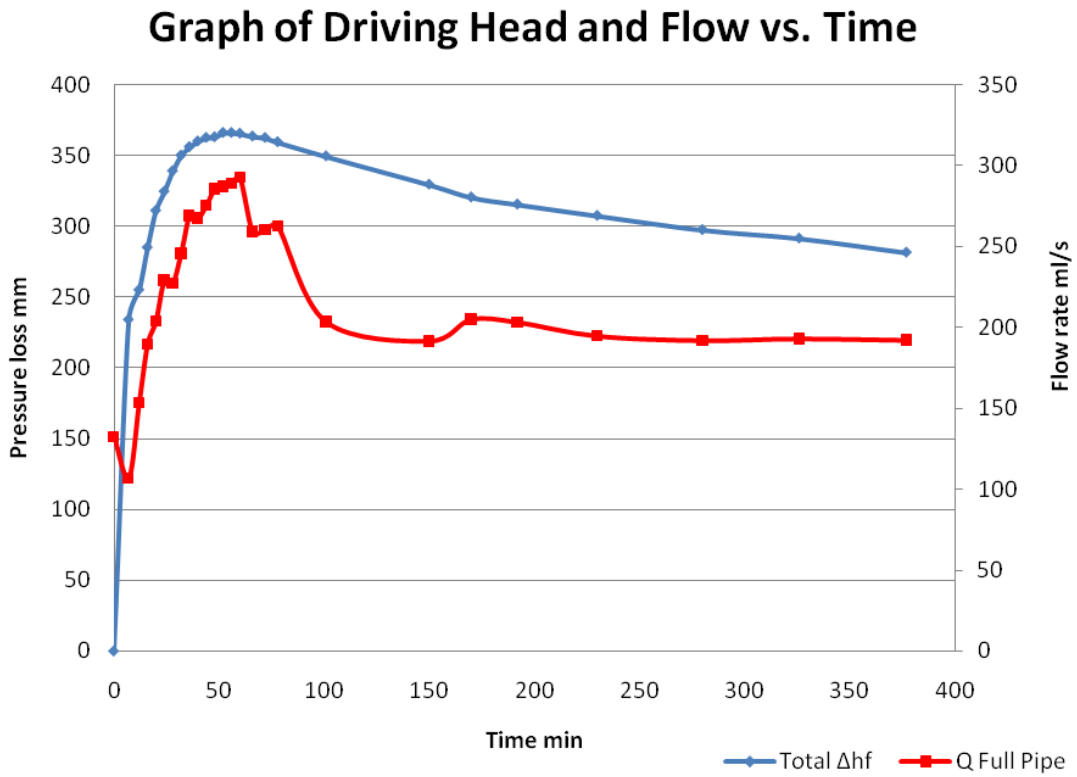

Figure D25: Headloss and rate of flow for a 6.5hour test period (WSST-ABF)

Due the severely restricted flow, and the design and subsequent backflushing of such a Seawater Intake pipeline was considered a failure as well. This was due to the flow rate of 48l/s not being achieved. Figure D22 below plots the time series for the test before the back flushing and after the back flushing.

At approximately 180min the pressure loss before back flushing, was lower than that after back flushing. The flowrate after flushing was lower than that before flushing. However considering that former test had a shorter duration of 3 hours it does not imply that these conditions would prevail after 6.5 hours.

The pressure loss and flow rate for the former test seem to have plateaued, hence in in approximately 7 hours the pressure loss for the former test would be similar to that of the latter test.

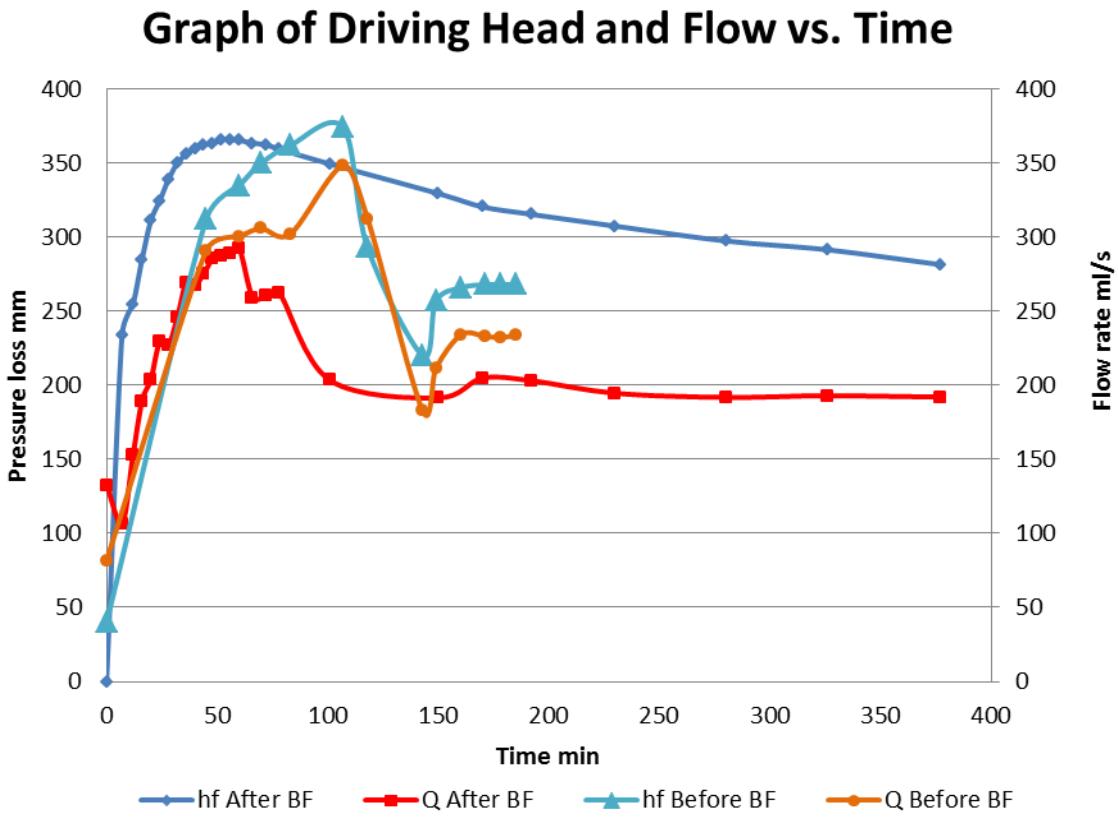

Figure D26: Headloss and rate of flow for test Before Back Flushing (BBF) and After Back Flushing (ABF)

Appendix E

Perforated PVC Pipe Abstraction Model

Table of Contents

Description	Page
E.1 Introduction	244
E.2 Pressure Losses	245
E.3 Water Losses due to Leakage	246
E.4 Water Test Only	247
E.4.1 Water Leakage losses	249
E.4.2 Water Pressure losses	250
E.4.3 Perforation losses and Flowrate Relationship	250
E.5 Water Test with Extra Perforation	252
E.5.1 Water Leakage losses	254
E.5.2 Water Pressure losses	255
E.5.3 Perforation losses and Flowrate Relationship	255
E.5.4 Segmental Analysis of HPM	257
E.6 Water and Stone Test	262
E.6.1 Water Leakage losses	269
E.6.2 Water Pressure losses	265
E.6.3 Relationship between Flowrate, Perforation and Stone Bedding friction	266
E.6.4 Segmental Analysis of HPM	268
E.6.4.1 Methodology	269
E.6.4.2 Pressure loss due to Stone Bedding	273
E.6.4.2.1 Method 1: Simple method for determining headloss due to stone bedding	273
E.6.4.2.2 Method 2: Kenny, Lau and Ofoegbu Method for determining headloss due to stone bedding	275
E.6.4.2.3 Method 3: Forchheimer Method for determining headloss due to stone bedding	287

E.6.4.3 Comparison of Results for Method 1, 2 and 3 299
E.7 Water, Sand and Stone Bedding Test 300
E.7.1 Water Leakage losses 301
E.7.2 Pressure losses 302
E.7.3 Perforation losses and Flowrate Relationship 302
E.7.4 Segmental Analysis of HPM 304
E.7.4.1 Methodology 304
E.7.4.2 Pressure loss due to Sand and Stone Bedding 308
E.7.4.2.1 Method 1: Simple method for determining headloss due to sand and stone bedding 308
E.7.4.2.2 Method 2: Kenny, Lau and Ofoegbu Method for determining headloss due to sand and stone bedding 310
E.7.4.2.3 Method 3: Forchheimer Method for determining headloss due to sand and stone bedding 319
E.7.4.3 Comparison of Results for Method 1, 2 and 3 327

E.1 Introduction

This appendix describes in detail the calculations behind Chapter 5.2 and 6: Perforated PVC Pipe Abstraction Model. Via the use of figures and tables is explains the most relevant calculations. Note that for all tests, no core material was used. Figure E1 below describes the model and the areas of interest which are used when undertaking calculations.

Table E1: Perforated PVC Pipe: Variables and Values

Perforated PVC Pipe- Perforation Configuration	Value	Unit	Value	Unit
No of Holes per 20cm Length	9			
Area of each Hole	50.24	mm^2	5.024E-05	m^2
Length of Pipe	1055	mm	1.055	m
No. of Segments	5			
Segment Length	201	mm	0.201	m
Perforation Area of Segment	452.16	mm^2	0.000452	m^2
Total Perforation Area	2260.8	mm^2	0.002261	m^2
Total pipe Wetted Surface Area	394462.5	mm2	0.394463	m2
Percentage perforation	0.57%			

Table E2: Extra Perforated PVC Pipe: Variables and Values

Extra Perforated PVC Pipe- Perforation Configuration	Value	Unit	Value	Unit
No of Hole/Slots per 20cm Length	20			
Area of each Hole	50.24	mm^2	5.024E-05	m^2
Length of Pipe	1005	mm	1.005	m
No. of Segments	5			
Segment Length	201	mm	0.201	m
Perforation Area of Segment	1004.8	mm^2	0.0010048	m^2
Total Perforation Area	5024	mm^2	0.005024	m^2
Total pipe Wetted Surface Area	394462.5	mm2	0.3944625	m^2
Percentage perforation	1.27%			

E. 2 Pressure Losses

Chapter 4.4.6.1 describes the losses A to E. Note the datum of the model is the top of the model base.

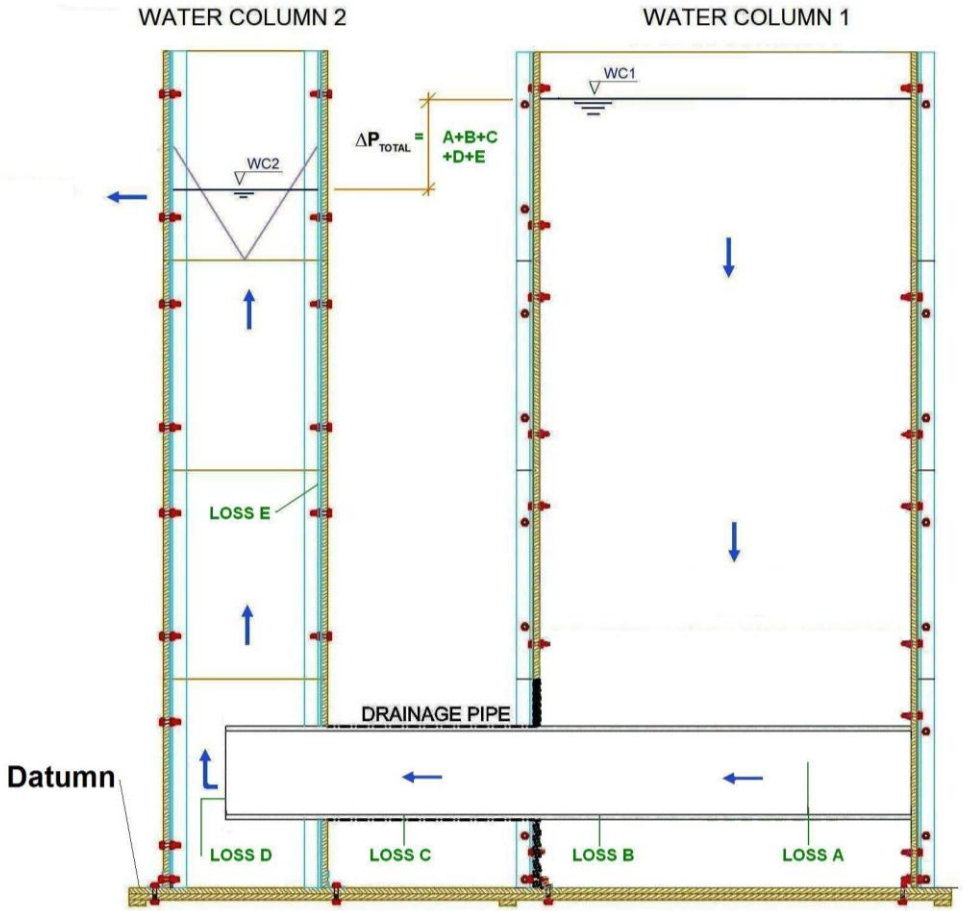

Figure E1: Perforated PVC Pipe Abstraction Model: Areas of interest

The following is a reiteration of the losses A to E. as described in Chapter 4.4.6.1

Loss A: This reduction in pressure occurs as water travels from the outside of the pipe, in. Losses B to E can easily be estimated using conventional calculation methods. Loss A accounts for a significantly large portion of the total pressure losses.

Loss B: Skin friction in the portion of intake pipe where there is water ingression and transportation. The skin friction in this chapter is calculated using Manning's Method. A pipe of 250mm is used as the conduit size. However, the skin friction in this area is halved as theoretically the flow is at its maximum as it exits WC1 and zero at the start of the pipeline (Right hand side of Figure E1)

Loss C: Skin friction in the portion of intake pipe where there is water transportation only. The skin friction in this chapter is calculated using Manning's Method. A pipe of 250mm is used as the conduit size.

Loss D: Exit loss as water enters Column 2 (WC2). For the flow exiting the Intake pipe and then turning 90 degrees, the loss equal to $Ke*V^2/2g$ where Ke = 1

Loss E: Skin friction as water flows up WC2. The skin friction in this chapter is calculated using Manning's Method. A rectangular section of 600mm by 250mm is used as the conduit size.

E. 3 Water Losses due to Leakage

The ability to quantify leakage is crucial especially if the leakage rate becomes a large fraction of the overall flow. Hence the flow rate of the leakage for each increment of the flow through the model was noted.

The entire leakage rate was calculated by constructing a dam around the HPM, and determining the amount of water that left the dam, over a period of time, for a particular increment a test. There were three places that water could have leaked out. These are WC1, WC2a and WC2b. Figure E2 below describes where the leaks emanate from. Via visual inspection 40% of all leakage was deemed to be out of WC1, 40% out of WC2a and 20% out of WC2b.

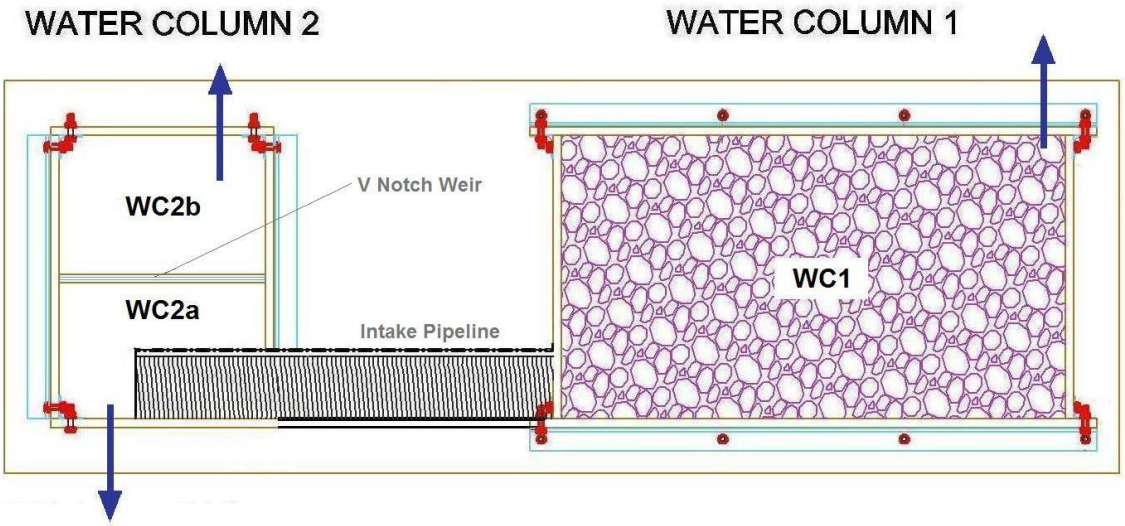

Figure E2: Areas of Water Leakage

E.4 Water Test Only

The following explains the manner in which the first 'Water Only Test' was conducted and uses tables and equations to illustrate the analysis process. Table E3 details the physical aspects of the Hydraulic Physical Model (HPM) including the Intake pipeline.

Table E3: The physical aspects of the HPM and Initial Intake Pipeline

Description	Value	Unit
Physical aspects of the HPM:WC2a		
Angle of V Notch Weir	90	Degrees
Height of V Notch Weir	1708.5	mm
Length	0.28	m
Breath	0.45	m
Area A	0.126	m^2
Wet Perimeter P	1.46	m
Hydraulic Radius R	0.0863	m
Friction Factor f	0.02	
Loss Coefficient Ke	1	
Perforated Pipeline Perforation Configuration		
D Pipe Length	1050	mm
Pipe OD	250	mm
Pipe ID	230	mm
Half Pipe Area	0.0208	m^2
Wet Perimeter	0.5911	m
Hydraulic Radius Pipe HR	0.1405	m
No of Holes per 20cm Length	9	
Area of each Hole	50.24	mm^2
Length of Pipe	1050	mm
No. of Segments	5	
Segment Length	210	mm
Perforation Area of Segment	452.16	mm^2
Total Perforation Area	2260.8	mm^2
Total pipe Wetted Surface Area	394462.5	mm^2
Percentage perforation	0.57%	
Friction Factor f	0.015	

Where:

C_d = Coefficient of Discharge as established in Appendix B

D Pipe Length = Length of Intake pipeline in the HPM

Pipe OD = Outside Diameter of Intake Pipeline

Pipe ID = Inside Diameter of Pipeline

Half Pipe Area = The area of flow when only half a pipe is used

Wet Perimeter = Perimeter of the intake pipeline that has been in contact with the flow

Hydraulic Radius HR = The Hydraulic Radius of the Intake Pipeline or WC2a

The aim of this experiment is to establish the relationship between the flow and the loss of pressure head as it passes in to the Intake pipeline Using the above information, 8 incremental tests, with increasing driving heads, where conducted. Table E4 shows the initial results. The difference between WC1 and WC2 denotes the total headloss. The flow rate was determined from the following Equation: B1

$$Q = C_d \cdot \frac{8}{15} \cdot \sqrt{2g} \cdot \tan\frac{\theta}{2} \cdot h^{\frac{5}{2}}$$ Eqn B1

where

Q= Flow (l/s)

C_d= 0.57

h = depth of water above V Notch (mm)

Table E4: Total Headloss and initial flow rate for Initial Water Only test

Test No.	WC1	WC2	Upstream Head	Downstream Head	Total Δhf	Initial Q Half Pipe
	mm	mm	mm	mm	mm	l/s
1	1739	1733	30.5	24.5	6	0.13
2	1740	1733	31.5	24.5	7	0.13
3	1760	1747	51.5	38.5	13	0.39
4	1814	1766	105.5	57.5	48	1.07
5	1890	1777	181.5	68.5	113	1.65
6	2074	1791	365.5	82.5	283	2.63
7	2232	1800	523.5	91.5	432	3.41
8	2387	1804	678.5	95.5	583	3.80

After the total headloss and initial flow rate relationship has been established, Water leakage has to be considered. As per ChapterE3 theses losses are incorporated in Table E5 with 80% of all leakage deemed to be out of WC1, 10% out of WC 2a and 10% out of WC2b. This new ratio was due to WC2 being sealed in several places

E.4.1 Water Leakage losses

In Table E5, the total leakage rate is calculated in Column 6. Columns 7, 8 and 9 calculate the loss for WC1, WC2a and WC2b, respectively. The Total flow rate Q is calculated as the Initial flow rate plus the leakage from WC1 and WC2a

Table E5: Total headloss and flow rate incorporating losses

1	2	3	4	5	6	7	8	9	10
Test No.	Q Half Pipe	Bucket Ht	Time	Volume	Total	Loss due to WC1	Loss due to WC2a	Loss due to WC2b	Total Q
	l/s	mm	s	l	l/s	l/s	l/s	l/s	l/s
1	0.13	170	771	43.03	0.056	0.044645	0.005581	0.005581	0.177
2	0.13	112	524	27.70	0.053	0.042286	0.005286	0.005286	0.174
3	0.39	72	334	17.52	0.052	0.041958	0.005245	0.005245	0.439
4	1.07	106	529	26.15	0.049	0.039547	0.004943	0.004943	1.112
5	1.65	96	470	23.59	0.050	0.040148	0.005019	0.005019	1.699
6	2.63	87	404	21.30	0.053	0.042173	0.005272	0.005272	2.680
7	3.41	90	390	22.06	0.057	0.045249	0.005656	0.005656	3.461
8	3.80	88	406	21.55	0.053	0.042465	0.005308	0.005308	3.843

E.4.2 Water Pressure losses

After the correct total flow has been established, the next step is the disaggregation of pressure losses. This is done so that Loss A, the loss of pressure as water enters the Intake pipeline, can be established. ChapterE2 states the Pressure Losses A to E with the relevant equations. Table E6 calculates the Losses B to E and hence the remaining total headloss will be Loss A.

Table E6: Disaggregation of pressure losses

Test No.	Total ∆hf	Total Q	Loss B+C	Loss D	Loss E	Loss A	%A of Total ∆hf
	mm	l/s	m	m	m	mm	
1	6	0.177	0.000001	0.000001	0.0000007	0.00	0.00%
2	7	0.174	0.000000	0.000001	0.0000007	7.00	94.11%
3	13	0.439	0.000003	0.000009	0.0000065	12.98	95.61%
4	48	1.112	0.000020	0.000067	0.0000487	47.86	95.86%
5	113	1.699	0.000047	0.000162	0.0001168	112.67	94.99%
6	283	2.680	0.000117	0.000410	0.0002959	282.18	95.03%
7	432	3.461	0.000196	0.000687	0.0004966	430.62	94.35%
8	583	3.843	0.000242	0.000851	0.0006150	581.29	93.77%

E.4.3 Perforation losses and Flowrate Relationship

Table E7 shows the Intake pipeline perforation friction (Loss A) and the flowrate for half a pipe and for a full pipeline. Figure E3 show the relationship between the Perforation friction and the flowrate in a 250mm Perforated PVC Pipeline.

Table E7: Perforation friction (Loss A) flowrate Half and Full pipeline

Test No.	Loss A	Q Half Pipe	Q Full Pipe
	mm	l/s	l/s
1	0.00	0.13	0.353
2	7.00	0.13	0.348
3	12.98	0.39	0.878
4	47.86	1.07	2.224
5	112.67	1.65	3.398
6	282.18	2.63	5.360
7	430.62	3.41	6.922
8	581.29	3.80	7.686

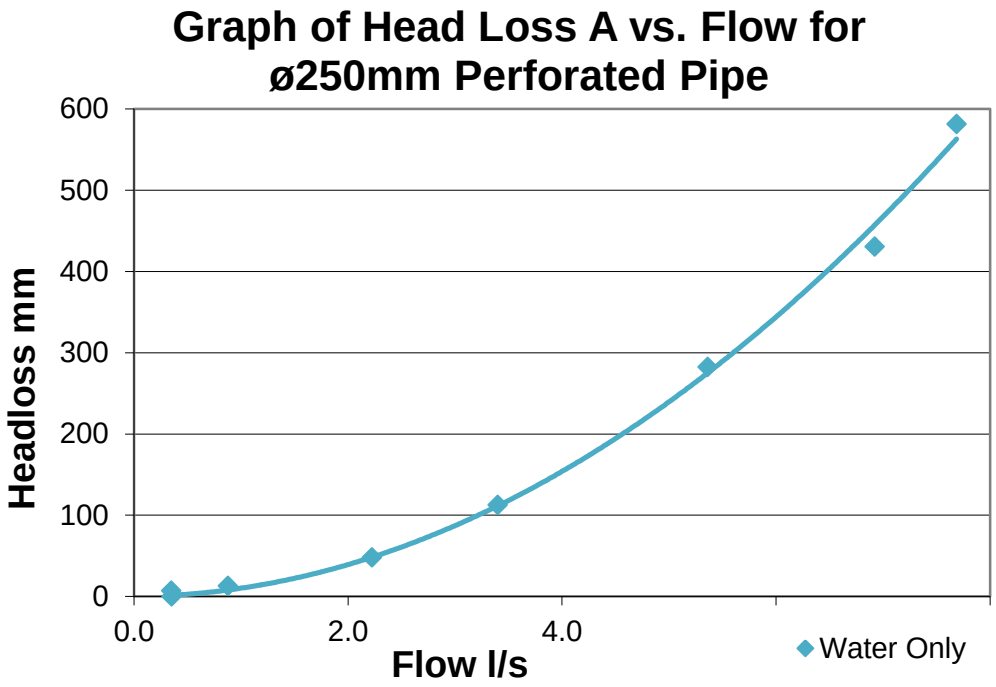

Figure E3: Headloss due to perforation (Loss A) versus the flowrate for a fully flowing ø250mm Perforated pipe

The equation below describes the relationship between headloss due to perforation friction and flowrate

$$\Delta P = 5.456Q^2 + 0.722Q \qquad \text{(Eqn 4)}$$

With

ΔP = Headloss due to slot friction in mm

Q = Flowrate for one full ø250mm pipeline in liters/second

E.5: Water Test with Extra Perforation

The following explains the manner in which the Water Test with Extra Perforation was conducted and uses tables and equations to illustrate the analysis process. Table E8 details the physical aspects of the Hydraulic Physical Model (HPM) including the Intake pipeline.

Table E8: The physical aspects of the HPM and Initial Intake Pipeline

Description	Value	Unit
Physical aspects of the HPM:WC2a		
Angle of V Notch Weir	90	Degrees
Height of V Notch Weir	1708.5	mm
Length	0.28	m
Breath	0.45	m
Area A	0.126	m^2
Wet Perimeter P	1.46	m
Hydraulic Radius R	0.0863	m
Friction Factor f	0.02	
Loss Coefficient Ke	Varies	
Perforated Pipeline Perforation Configuration		
D Pipe Length	1050	mm
Pipe OD	250	mm
Pipe ID	230	mm
Half Pipe Area	0.0208	m^2
Wet Perimeter	0.5911	m
Hydraulic Radius Pipe HR	0.1405	m
No of Holes per 20cm Length	20	
Area of each Hole	50.24	mm^2
Length of Pipe	1050	mm
No. of Segments	5	
Segment Length	210	mm
Perforation Area of Segment	452.16	mm^2
Total Perforation Area	5024	mm^2
Total pipe Wetted Surface Area	394462.5	mm^2
Percentage perforation	1.27%	
Friction Factor f	0.015	

Where:

C_d = Coefficient of Discharge as established in Appendix B

D Pipe Length = Length of Intake pipeline in the HPM

Pipe OD = Outside Diameter of Intake Pipeline

Pipe ID = Inside Diameter of Pipeline

Half Pipe Area = The area of flow when only half a pipe is used

Wet Perimeter = Perimeter of the intake pipeline that has been in contact with the flow

Hydraulic Radius HR = The Hydraulic Radius of the Intake Pipeline or WC2a

The aim of this experiment is to establish the relationship between the flow and the loss of pressure head as it passes in to the Intake pipeline Using the above information, 9 incremental tests, with increasing driving heads, where conducted. Table E9 shows the initial results. The difference between WC1 and WC2 denotes the total headloss. The flow rate was determined from the following Equation: B1

$$Q = C_d \cdot \frac{8}{15} \cdot \sqrt{2g} \cdot \tan\frac{\theta}{2} \cdot h^{\frac{5}{2}} \qquad \text{Eqn B1}$$

where

Q= Flow (l/s)

C_d= 0.57

h = depth of water above V Notch (mm)

Table E9: Total Headloss and initial flow rate for Initial Water Only test

Test No.	WC1	WC2	Upstream Head	Downstream Head	Total Δhf	Initial Q Half Pipe
	mm	mm	mm	mm	mm	l/s
1	1739	1736	30.5	27.5	3	0.17
2	1755	1748.5	46.5	40	6.5	0.43
3	1776	1762	67.5	53.5	14	0.89
4	1819	1779	110.5	70.5	40	1.78
5	1884	1794	175.5	85.5	90	2.88
6	1970	1808	261.5	99.5	162	4.21
7	2031	1814	322.5	105.5	217	4.87
8	2103	1820	394.5	111.5	283	5.59
9	2310	1831.5	1831.5	123	478.5	7.14

After the total headloss and initial flow rate relationship has been established, Water leakage has to be considered. As per chapter E3 theses losses are incorporated in Table E10 with 80% of all leakage deemed to be out of WC1, 10% out of WC 2a and 10% out of WC2b. This new ratio was due to WC2 being sealed in several places

E.5.1 Water Leakage losses

In Table E10, the total leakage rate is calculated in Column 6. Columns 7, 8 and 9 calculate the loss for WC1, WC2a and WC2b, respectively. The Total flow rate Q is calculated as the Initial flow rate plus the leakage from WC1 and WC2a

Table E10: Total headloss and flow rate incorporating losses

1	2	3	4	5	6	7	8	9	10
Test No.	Q Half Pipe	Bucket Ht	Time	Volume	Total	Loss due to WC1	Loss due to WC2a	Loss due to WC2b	Total Q
	l/s	mm	s	l	l/s	l/s	l/s	l/s	l/s
1	0.17	170	771	43.03	0.056	0.044645	0.005581	0.005581	0.219
2	0.43	112	524	27.70	0.053	0.042286	0.005286	0.005286	0.478
3	0.89	72	334	17.52	0.052	0.041958	0.005245	0.005245	0.939
4	1.78	106	529	26.15	0.049	0.039547	0.004943	0.004943	1.822
5	2.88	96	470	23.59	0.050	0.040148	0.005019	0.005019	2.923
6	4.21	87	404	21.30	0.053	0.042173	0.005272	0.005272	4.253
7	4.87	90	390	22.06	0.057	0.045249	0.005656	0.005656	4.919
8	5.59	88	406	21.55	0.053	0.042465	0.005308	0.005308	5.638
9	7.14	90	390	22.06	0.057	0.045249	0.005656	0.005656	7.196

E.5.2 Water Pressure losses

After the correct total flow has been established, the next step is the disaggregation of pressure losses. This is done so that Loss A, the loss of pressure as water enters the Intake pipeline, can be established. Chapter E2 states the Pressure Losses A to E with the relevant equations. Table E11 calculates the Losses B to E and hence the remaining total headloss will be Loss A.

Table E11: Disaggregation of pressure losses

Test No.	Total ∆hf	Total Q	Loss B+C	Loss D	Loss E	Loss A	%A of Total ∆hf
	mm	l/s	m	m	m	mm	
1	3	0.219	0.000002	0.000003	0.0000012	3.00	99.91%
2	6.5	0.478	0.000008	0.000022	0.0000079	6.48	99.76%
3	14	0.939	0.000030	0.000094	0.0000339	13.94	99.54%
4	40	1.822	0.000113	0.000373	0.0001348	39.75	99.38%
5	90	2.923	0.000290	0.000979	0.0003538	89.36	99.28%
6	162	4.253	0.000615	0.002091	0.0007551	160.63	99.15%
7	217	4.919	0.000822	0.002802	0.0010119	215.17	99.15%
8	283	5.638	0.001080	0.003694	0.0013343	280.59	99.15%
9	478.5	7.196	0.001760	0.006035	0.0036908	473.05	98.86%

E.5.3 Perforation losses and Flowrate Relationship

Table E12 shows the Intake pipeline, extra perforation friction (Loss A) and the flowrate for half a pipe and for a full pipeline. Figure E4 shows the relationship between the Perforation friction and the flowrate in a ø250mm Extra-Perforated PVC Pipeline.

Table E12: Extra Perforation friction (Loss A) flowrate for Half and Full pipeline

Test No.	Loss A	Q Half Pipe	Q Full Pipe
	mm	l/s	l/s
1	3.00	0.219	0.44
2	6.48	0.478	0.96
3	13.94	0.939	1.88
4	39.75	1.822	3.64
5	89.36	2.923	5.85
6	160.63	4.253	8.51
7	215.17	4.919	9.84
8	280.59	5.638	11.28
9	473.05	7.196	14.39

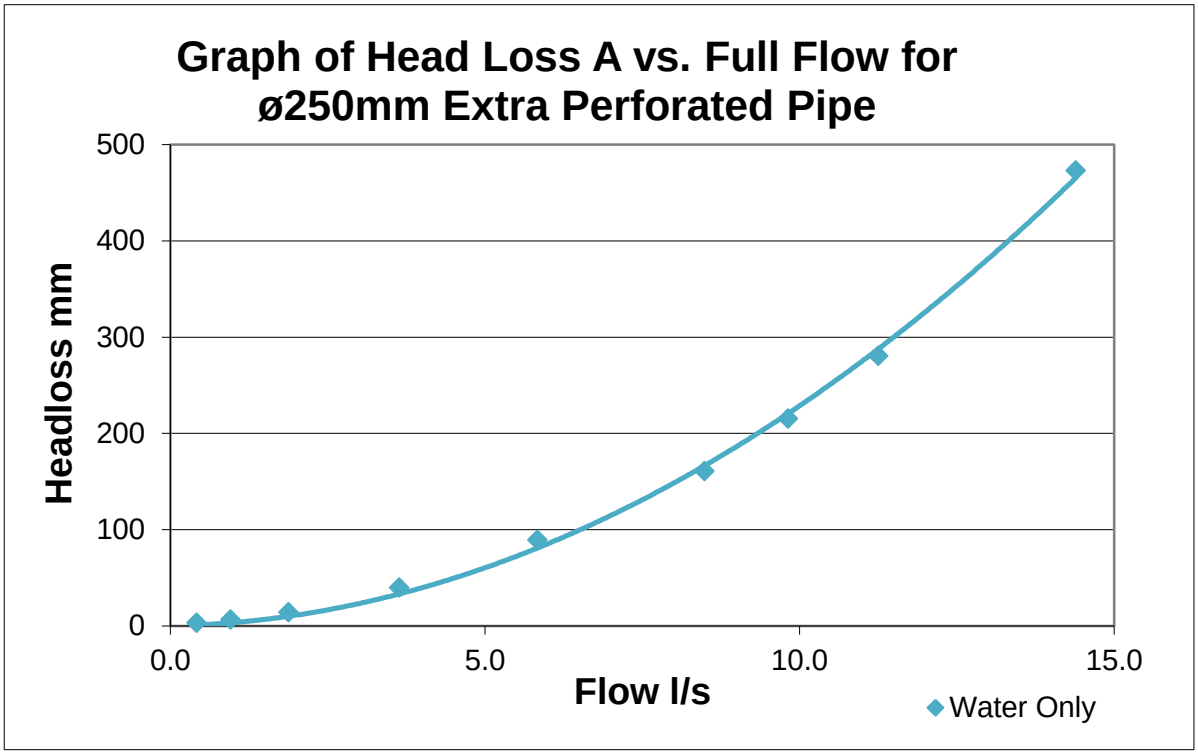

Figure E4: Headloss due to extra perforation (Loss A) versus the flowrate for a fully flowing ø250mm Extra Perforated pipe.

The equation below describes the relationship between headloss due to perforation friction and flowrate

$\Delta P = 0.891Q^2 + 1.286Q$ (Eqn5)

With

ΔP = Headloss due to slot friction in mm

Q = Flowrate for one full ø250mm pipeline in liters/second

E.5.4 Segmental Analysis of HPM

Analysing the Perforation friction and flow relationship was relatively simple. However in order to understand the flow regime better, it was required that the flow at different points in the HPM be calculated. It was decided that a model would be better understood if it was segmented. Hence the model was portioned into five segments.

As described by Table E11, the Perforation Loss A accounts for the nearly all of the pressure loss. Hence for a point on the Intake pipeline just inside WC1, the velocity of the flow into the pipeline is at its maximum. The velocity at this point is termed V_{max}. The opposite holds true for a point at the start of the Intake pipeline. At this point, V_{min}, the velocity of the inflow is zero. Hence via linear interpolation, the velocity at any point in between both ends, can be calculated Figure E5 below describes the manner in which the HPM is segmented.

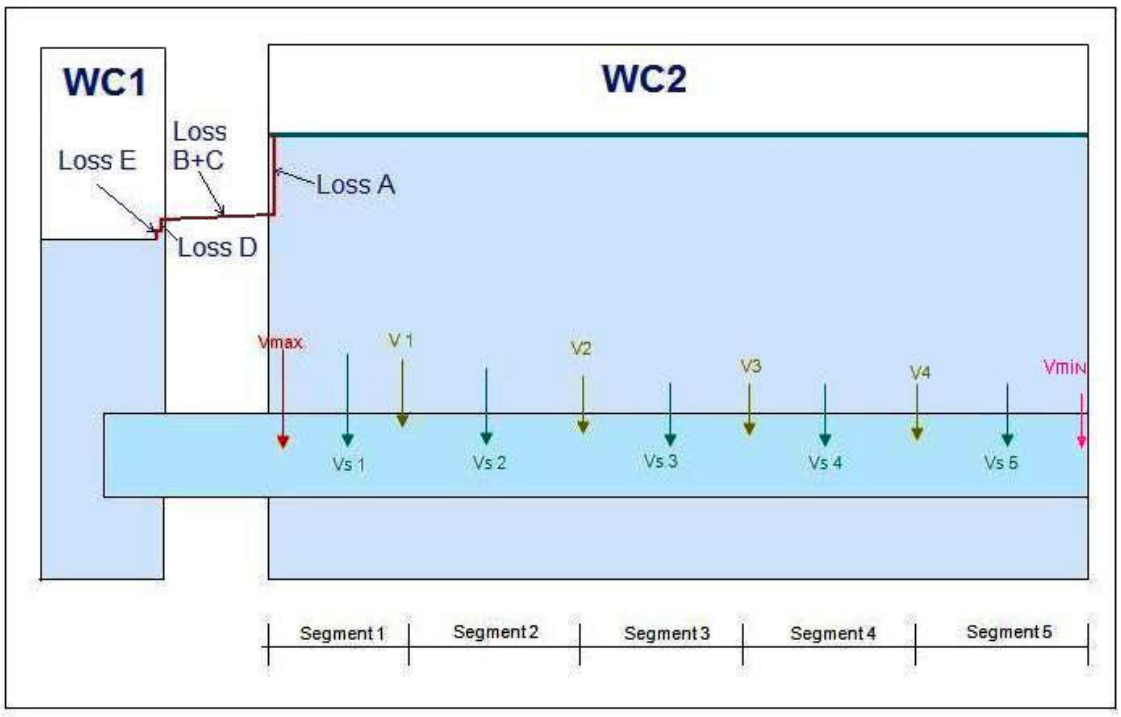

Figure E5: Segmented HPM with notional EGL flow that enters WC1 and exits from WC2

Methodology

In order to calculate the flow at various points within the model, the HPM was divided into five segments. The velocities V_{MAX}, V_1, V_2 , V_3, V_4 and V_{MIN} occur at the border of each segment, hence for each segment, the Average Velocities, V_S1, V_S2, V_S3, V_S4 and V_S5 are easily calculated.

V_{MAX} is derived from Bernoulli principles where:

$$V = \sqrt{2g\Delta h} \qquad \text{(EqnE1)}$$

With

V = Velocity in m/s

Δh = = is the driving pressure

g = gravitational constant (9.81m/s^2)

Note that the driving pressure Δh is Loss A. The flow from each segment is then calculated by multiplying the velocity with the perforation area and a discharge coefficient, C_d. Table E8 shows the distribution of inflowing velocity over the length of the Intake Pipeline.

Equation E2 was used to calculate the flow from each segment. Table E13 contains the flowrate for each segment and the sum of flow from all segments of the pipeline. Note: Position 0 is the most downstream point in WC1

$$Q_T = \sum q = \sum C_d A\sqrt{2g\Delta h} \qquad \text{(EqnE2)}$$

With

q = Flowrate through for each segment in m^3/s

Q = Sum of Flowrate form each segment in m^3/s

A= The Area through which flow is allowed in m^2

C_d = Coefficient of Discharge

Table E13: Inflowing velocity of water flowing into the pipe, over the length of the Intake Pipeline

		Pos. 0	Pos. 1	Pos. 2	Pos. 3	Pos. 4	Pos. 5	Pos. 6	Pos. 7	Pos. 8	Pos. 9	Pos. 10
Test	Loss A	Vmax	Vs 1	V1	Vs 2	V2	Vs 3	V3	Vs 4	V4	Vs 5	Vmin
	mm	m/s	m/s	m/s	m/s	m/s	m/s	m/s	m/s	m/s	m/s	m/s
1	3.0	0.087	0.078	0.070	0.061	0.052	0.044	0.035	0.026	0.017	0.009	0.0
2	6.5	0.190	0.171	0.152	0.133	0.114	0.095	0.076	0.057	0.038	0.019	0.0
3	13.9	0.373	0.336	0.299	0.261	0.224	0.187	0.149	0.112	0.075	0.037	0.0
4	39.8	0.725	0.653	0.580	0.508	0.435	0.363	0.290	0.218	0.145	0.073	0.0
5	89.4	1.164	1.047	0.931	0.815	0.698	0.582	0.465	0.349	0.233	0.116	0.0
6	160.6	1.693	1.524	1.354	1.185	1.016	0.847	0.677	0.508	0.339	0.169	0.0
7	215.2	1.958	1.762	1.567	1.371	1.175	0.979	0.783	0.587	0.392	0.196	0.0
8	280.6	2.244	2.020	1.796	1.571	1.347	1.122	0.898	0.673	0.449	0.224	0.0
9	473.0	2.865	2.578	2.292	2.005	1.719	1.432	1.146	0.859	0.573	0.286	0.0

Table E14: Calculated Flowrate from all segments of the Pipeline

Test	Loss A	C_b	Qs 1	Qs 2	Qs 3	Qs 4	Qs 5	Q Total	Q Total	2Q Total
0	mm		m^3/s	m^3/s	m^3/s	m^3/s	m^3/s	m^3/s	l/s	l/s
1	3.0	0.360	0.0001	0.0001	0.0000	0.0000	0.0000	0.0002	0.219	0.438
2	6.5	0.533	0.0002	0.0001	0.0001	0.0001	0.0000	0.0005	0.478	0.956
3	13.9	0.714	0.0003	0.0003	0.0002	0.0001	0.0000	0.0009	0.938	1.876
4	39.8	0.821	0.0007	0.0005	0.0004	0.0002	0.0001	0.0018	1.822	3.644
5	89.4	0.879	0.0011	0.0008	0.0006	0.0004	0.0001	0.0029	2.923	5.846
6	160.6	0.954	0.0015	0.0012	0.0009	0.0005	0.0002	0.0043	4.253	8.506
7	215.2	0.953	0.0018	0.0014	0.0010	0.0006	0.0002	0.0049	4.919	9.838
8	280.6	0.957	0.0020	0.0016	0.0011	0.0007	0.0002	0.0056	5.638	11.276
9	473.0	0.940	0.0026	0.0020	0.0014	0.0009	0.0003	0.0072	7.196	14.392

For this case the loss of pressure is due to perforation friction only. Hence if the EGL is required at a particular position along the Intake pipeline, the new EGL would be the still water level in WC1 minus the perforation friction/ Loss A

Table E 15 below calculates the headloss along the intake pipeline using the following equation:

$$hf = Ke * \frac{V^2}{2g} \qquad \text{(Eqn E3)}$$

With

Ke = Loss Coefficient

V = Velocity in m/s

Hf= Pressure loss

g = gravitational constant (9.81m/s^2)

Table E15: Pressure losses over length of Intake Pipeline

		Pos. 0	Pos. 1	Pos. 2	Pos. 3	Pos. 4	Pos. 5	Pos. 6	Pos. 7	Pos. 8	Pos. 9	Pos. 10
Test	Loss A	hf max	hf	hf	hf	hf	hf	hf	hf	hf	hf	hf
	mm	mm	mm	mm	mm	mm	mm	mm	mm	mm	mm	mm
1	3.0	3.0	2.4	1.9	1.5	1.1	0.8	0.5	0.3	0.1	0.009	0.0
2	6.5	6.5	5.2	4.1	3.2	2.3	1.6	1.0	0.6	0.3	0.019	0.1
3	13.9	13.9	11.3	8.9	6.8	5.0	3.5	2.2	1.3	0.6	0.037	0.1
4	39.8	39.8	32.2	25.4	19.5	14.3	9.9	6.4	3.6	1.6	0.073	0.4
5	89.4	89.4	72.4	57.2	43.8	32.2	22.3	14.3	8.0	3.6	0.116	0.9
6	160.6	160.6	130.1	102.8	78.7	57.8	40.2	25.7	14.5	6.4	0.169	1.6
7	215.2	215.2	174.3	137.7	105.4	77.5	53.8	34.4	19.4	8.6	0.196	2.2
8	280.6	280.6	227.3	179.6	137.5	101.0	70.1	44.9	25.3	11.2	0.224	2.8
9	473.0	473.0	383.2	302.8	231.8	170.3	118.3	75.7	42.6	18.9	0.286	4.7

Figure E6 below shows Energy Grade Line (EGL) at the centre of the Intake Pipeline. The EGL shows the amount of energy that has been lost from water entering the Intake Pipeline. For the 9 tests conducted, the increase in pressure losses closer to the exit point of WC1 can be clearly seen.

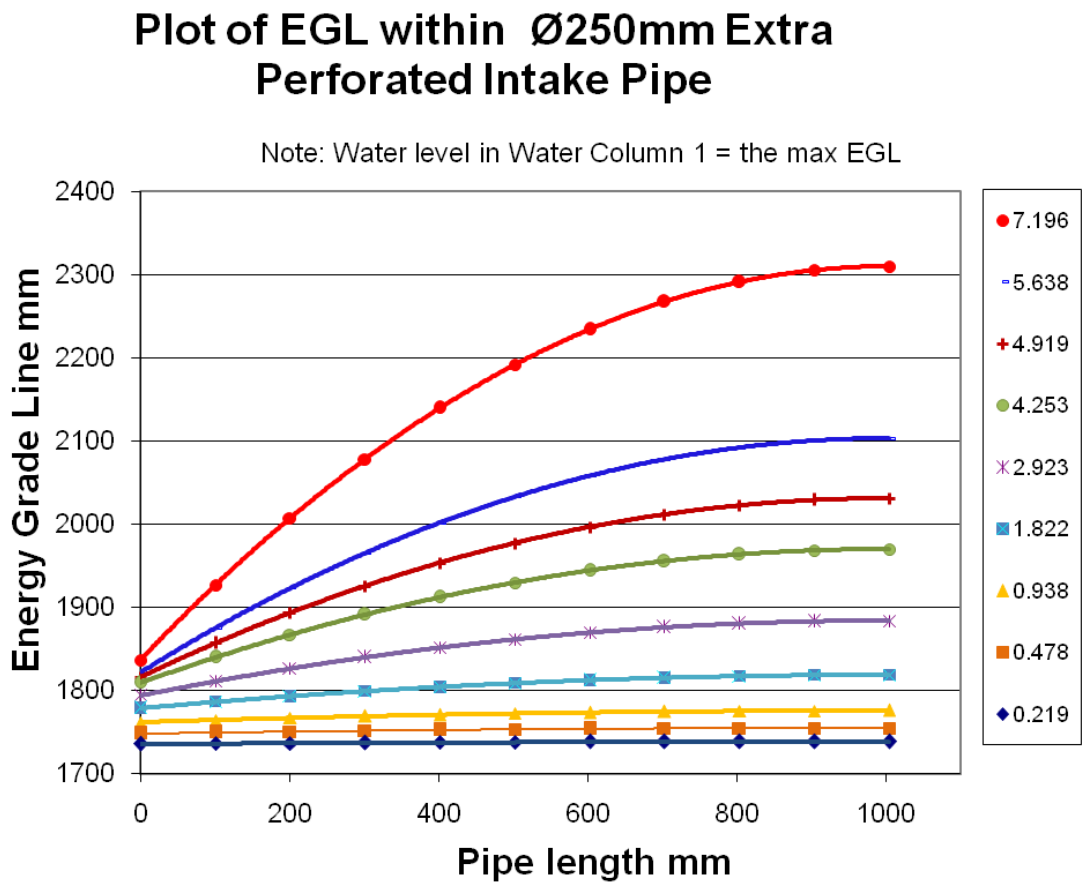

Figure E6: Plot of EGLs at the centre of the Intake Pipeline. Legend: Flowrates

The Flow versus Pressure loss relationship is the most important. Calculation of the EGL at various points' aid in the visualisation of the losses incurred.

E.6 Water and Stone Test

The following elucidates the manner in which the 'Water and Stone Test' was conducted and uses tables and equations to illustrate the analysis process. Table E3, from the previous Chapter E4 details the physical aspects of the model including the Intake pipeline.

The aim of this experiment is to:

1) confirm the relationship between the flow and the loss of pressure head as it passes in to the Intake pipeline and to
2) establish the relationship between the flow and the loss of pressure head as it passes through the 19mm Stone bedding.

Using the above information, 18 incremental tests, with increasing driving heads, where conducted. Table E11 shows the initial results. The difference between WC1 and WC2 denotes the total headloss. The flow rate was determined from the following Equation: B1

$$Q = C_d \cdot \frac{8}{15} \cdot \sqrt{2g} \cdot \tan\frac{\theta}{2} \cdot h^{\frac{5}{2}} \qquad \text{(Eqn B1)}$$

where

Q= Flow (l/s)

C_d*= 0.57*

h = depth of water above V Notch (mm)

Table E16: Total Headloss and initial flow rate for Water and Stone test

Test No.	WC1	WC2	Upstream Head	Downstream Head	Total ∆hf	Initial Q Half Pipe
	mm	mm	mm	mm	mm	l/s
1	1728	1725	19.5	16.5	3	0.05
2	1730	1726.75	21.5	18.25	3.25	0.06
3	1734	1730	25.5	21.5	4	0.09
4	1745	1739	36.5	30.5	6	0.22
5	1755	1747	46.5	38.5	8	0.39
6	1774	1759	65.5	50.5	15	0.77
7	1787	1765	78.5	56.5	22	1.02
8	1802	1770	93.5	61.5	32	1.26
9	1824	1776	115.5	67.5	48	1.59
10	1851	1782	142.5	73.5	69	1.97
11	1897	1790	188.5	81.5	107	2.55
12	1956	1796	247.5	87.5	160	3.05
13	2058	1805	349.5	96.5	253	3.90
14	2114	1809	405.5	100.5	305	4.31
15	2170	1813	461.5	104.5	357	4.75
16	2234	1816	525.5	107.5	418	5.10
17	2299	1818	590.5	109.5	481	5.34
18	2381	1821	1831.5	112.5	560	5.72

After the total headloss and initial flow rate relationship has been established, Water leakage has to be considered. As per chapterE3 theses losses are incorporated in Table E17 with 80% of all leakage deemed to be out of WC1, 100% out of WC2a and 10% out of WC2b.

E.6.1 Water Leakage losses

In Table E17, the total leakage rate is calculated in Column 6. Columns 7, 8 and 9 calculate the loss for WC1, WC2a and WC2b, respectively. The Total flow rate Q is calculated as the Initial flow rate plus the leakage from WC1 and WC2a

Table E17: Total headloss and flow rate incorporating losses for Water and Stone Test

1	2	3	4	5	6	7	8	9	10
Test No.	Q Half Pipe	Bucket Ht	Time	Volume	Total	Loss due to WC1	Loss due to WC2a	Loss due to WC2b	Half Pipe Q
	l/s	mm	s	l	l/s	l/s	l/s	l/s	l/s
1	0.05	170	771	43.03	0.056	0.04465	0.00558	0.00558	0.097
2	0.06	112	524	27.70	0.053	0.04229	0.00529	0.00529	0.108
3	0.09	72	334	17.52	0.052	0.04196	0.00524	0.00524	0.138
4	0.22	106	529	26.15	0.049	0.03955	0.00494	0.00494	0.263
5	0.39	96	470	23.59	0.050	0.04015	0.00502	0.00502	0.437
6	0.77	87	404	21.30	0.053	0.04217	0.00527	0.00527	0.819
7	1.02	90	390	22.06	0.057	0.04525	0.00566	0.00566	1.073
8	1.26	88	406	21.55	0.053	0.04247	0.00531	0.00531	1.311
9	1.59	90	390	22.06	0.057	0.04525	0.00566	0.00566	1.645
10	1.97	170	771	43.03	0.056	0.04465	0.00558	0.00558	2.022
11	2.55	112	524	27.70	0.053	0.04229	0.00529	0.00529	2.601
12	3.05	72	334	17.52	0.052	0.04196	0.00524	0.00524	3.097
13	3.90	106	529	26.15	0.049	0.03955	0.00494	0.00494	3.940
14	4.31	96	470	23.59	0.050	0.04015	0.00502	0.00502	4.357
15	4.75	87	404	21.30	0.053	0.04217	0.00527	0.00527	4.801
16	5.10	90	390	22.06	0.057	0.04525	0.00566	0.00566	5.153
17	5.34	88	406	21.55	0.053	0.04247	0.00531	0.00531	5.390
18	5.72	90	390	22.06	0.057	0.04525	0.00566	0.00566	5.767

E.6.2 Water Pressure losses

After the correct total flow has been established, the next step is the disaggregation of pressure losses. This is done so that Loss A, the loss of pressure due to water and stone bedding, can be established. ChapterE2 states the Pressure Losses A to E with the relevant equations. Table E18 calculates the Losses B to E and hence the remaining total headloss will be Loss A.

Table E18: Disaggregation of pressure losses for Water and Stone test

Test No.	Total ∆hf	Total Half Pipe Q	Loss B+C	Loss D	Loss E	Loss A +Stone bedding	%A of Total ∆hf
	mm	l/s	m	m	m	mm	
1	3	0.097	0.000000	0.000000	0.0000000	3.00	99.99%
2	3.25	0.108	0.000000	0.000000	0.0000000	3.25	99.99%
3	4	0.138	0.000001	0.000001	0.0000001	4.00	99.98%
4	6	0.263	0.000002	0.000006	0.0000005	6.00	99.95%
5	8	0.437	0.000006	0.000018	0.0000016	7.99	99.90%
6	15	0.819	0.000023	0.000070	0.0000064	14.97	99.81%
7	22	1.073	0.000039	0.000123	0.0000111	21.95	99.77%
8	32	1.311	0.000058	0.000189	0.0000170	31.92	99.76%
9	48	1.645	0.000092	0.000300	0.0001837	47.72	99.43%
10	69	2.022	0.000139	0.000460	0.0000415	68.82	99.74%
11	107	2.601	0.000230	0.000771	0.0000696	106.70	99.72%
12	160	3.097	0.000326	0.001100	0.0000993	159.57	99.73%
13	253	3.940	0.000527	0.001794	0.0001620	252.31	99.73%
14	305	4.357	0.000645	0.002198	0.0001984	304.16	99.72%
15	357	4.801	0.000783	0.002671	0.0002412	355.98	99.71%
16	418	5.153	0.000902	0.003078	0.0002779	416.82	99.72%
17	481	5.390	0.000987	0.003375	0.0003047	479.71	99.73%
18	560	5.767	0.001130	0.003863	0.0023624	556.51	99.38%

E.6.3 Relationship between flowrate, Perforation and Stone Bedding friction

Table E19 shows the Intake pipeline perforation friction (Loss A) + stone bedding loss. It also includes the flowrate for half a pipe and for a full pipeline. Figure E7 shows the relationship between the Perforation and stone bedding friction and the flowrate in a 250mm Perforated PVC Pipeline.

Table E19: Perforation (Loss A), and Stone Bedding friction, flowrate for Half and Full pipeline

Test No.	Loss A +Stone bedding	Q Half Pipe	Q Full Pipe
	mm	l/s	l/s
1	3.00	0.097	0.19
2	3.25	0.108	0.22
3	4.00	0.138	0.28
4	6.00	0.263	0.53
5	7.99	0.437	0.87
6	14.97	0.819	1.64
7	21.95	1.073	2.15
8	31.92	1.311	2.62
9	47.72	1.645	3.29
10	68.82	2.022	4.04
11	106.70	2.601	5.20
12	159.57	3.097	6.19
13	252.31	3.940	7.88
14	304.16	4.357	8.71
15	355.98	4.801	9.60
16	416.82	5.153	10.31
17	479.71	5.390	10.78
18	556.51	5.767	11.53

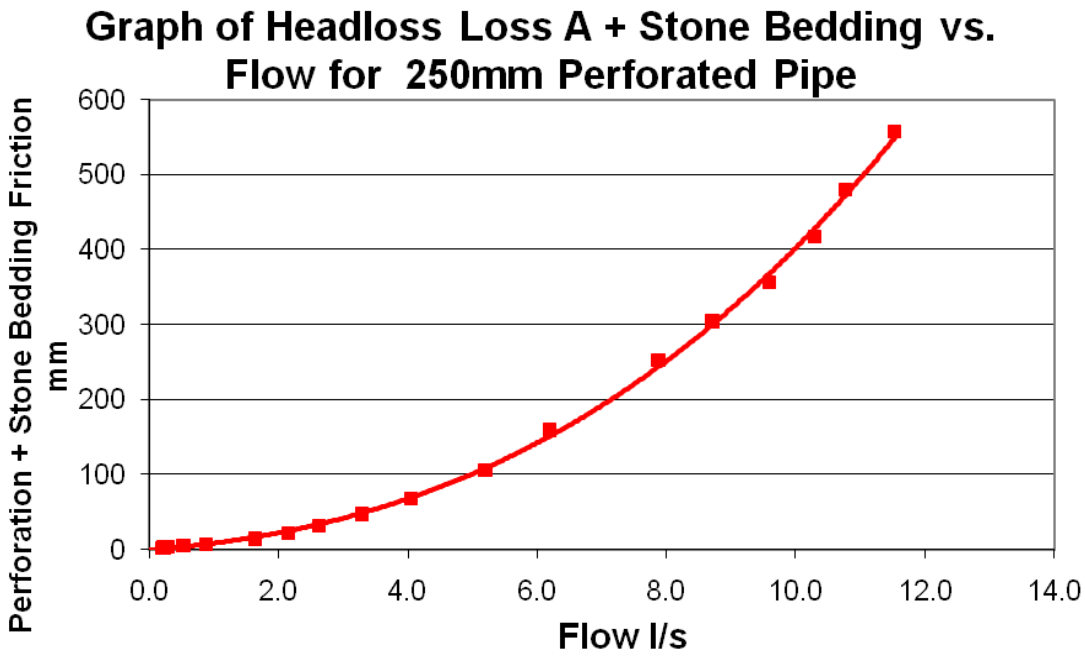

Figure E7: Headloss due to perforation (Loss A) and Stone bedding versus the flowrate for a fully flowing ø250mm Perforated pipe

The equation below describes the relationship between headloss due to slot friction and stone bedding and flowrate

$$\Delta P = 2.066\ Q^2 + 0.019\ Q \qquad \text{(Eqn6)}$$

With

ΔP = Headloss due to slot friction in mm

Q = Flowrate for one full pipeline in litres/second

E.6.4 Segmental Analysis of HPM

Analysing the Perforation friction + Stone Bedding and flow relationship initially, is as per ChapterE5.4. The model is better understood when portioned into five segments. The flow was calculated at the same points in the HPM

As described by Table E18, the Perforation Loss A + Stone Bedding accounts for the vast majority of the pressure loss. Hence for a point on the Intake pipeline just inside WC1 (Pos 0), the velocity of the flow into the pipeline is at its maximum. The velocity at this point is termed V_{max}. The opposite holds true for a point at the start of the Intake pipeline. At this point, V_{min}, the velocity of the inflow is zero. Hence via **linear interpolation,** the velocity at any point in between both ends, can be calculated Figure E8below describes the manner in which the HPM is segmented.

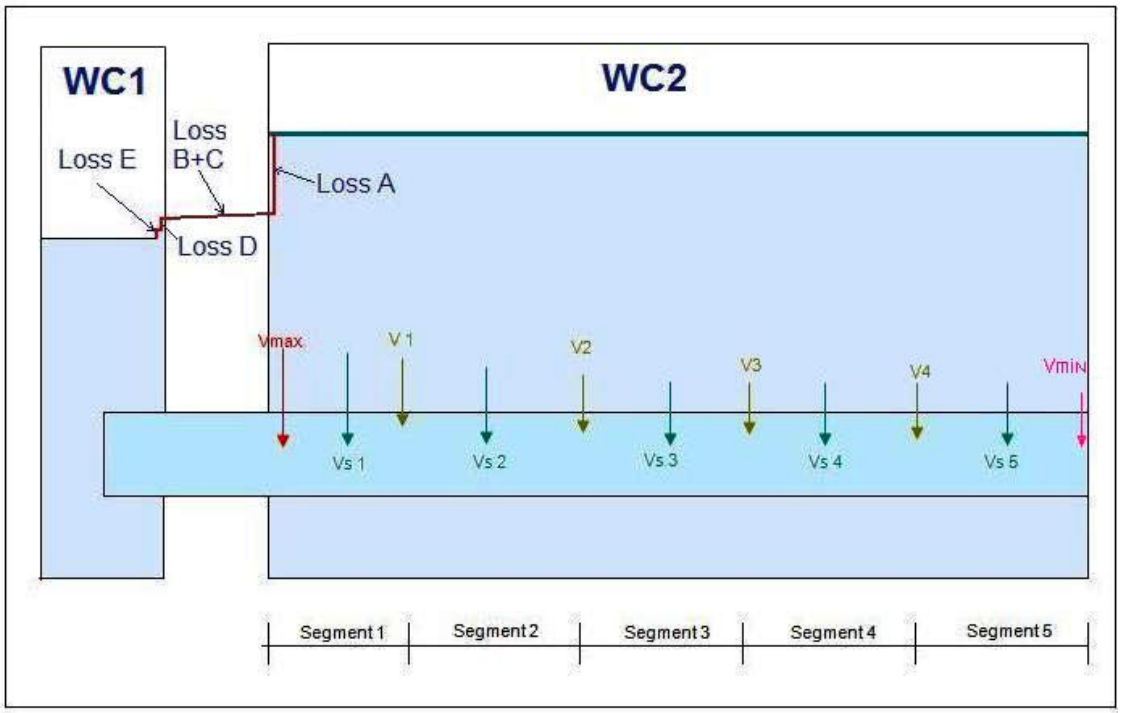

Figure E8: Segmented HPM with notional EGL flow that enters WC1 and exits from WC2

E.6.4.1 Methodology

In order to calculate the flow at various points within the model, the HPM was divided into five segments. The velocities V_{MAX}, V_1, V_2 , V_3, V_4 and V_{MIN} occur at the border of each segment, Hence for each segment, the Average Velocity, V_S1, V_S2, V_S3, V_S4 and V_S5 for each segment is easily calculated.

V_{MAX} is derived from Bernoulli principles where:

$$V = \sqrt{2g\Delta h} \qquad \text{EqnE1}$$

With

V = Velocity in m/s

Δh = = is the driving pressure

g = gravitational constant (9.81m/s^2)

Note that the driving pressure Δh is Perforation Loss A+ Stone bedding. The flow from each segment is then calculated by multiplying the velocity with the perforation area and a discharge coefficient, C_d. Table E20 shows the distribution of inflowing velocity over the length of the Intake Pipeline.

Equation E2 was used to calculate the flow from each segment. Table E21 contains the flowrate for each segment and the sum of flow from all segments of the pipeline.

$$Q_T = \sum q = \sum C_d A\sqrt{2g\Delta h} \qquad \text{(EqnE2)}$$

With

q = Flowrate through for each segment in m^3/s

Q = Sum of Flowrate form each segment in m^3/s

A= The Area through which flow is allowed in m^2

C_d = Coefficient of Discharge

Table E20: Inflowing velocity of water flowing into the pipe, over the length of the Intake Pipeline

		Pos. 0	Pos. 1	Pos. 2	Pos. 3	Pos. 4	Pos. 5	Pos. 6	Pos. 7	Pos. 8	Pos. 9	Pos. 10
Test	Loss A + Stone Bed.	Vmax	Vs 1	V1	Vs 2	V2	Vs 3	V3	Vs 4	V4	Vs 5	Vmin
0	mm	m/s	m/s	m/s	m/s	m/s	m/s	m/s	m/s	m/s	m/s	m/s
1	3.00	0.000	0.000	0.000	0.000	0.000	0.000	0.000	0.000	0.000	0.000	0.00
2	3.25	0.000	0.000	0.000	0.000	0.000	0.000	0.000	0.000	0.000	0.000	0.00
3	4.00	0.001	0.001	0.001	0.000	0.000	0.000	0.001	0.001	0.000	0.000	0.00
4	6.00	0.006	0.005	0.003	0.002	0.001	0.000	0.005	0.004	0.003	0.002	0.001
5	7.99	0.018	0.015	0.011	0.007	0.004	0.000	0.016	0.013	0.009	0.005	0.002
6	14.97	0.070	0.056	0.042	0.028	0.014	0.000	0.063	0.049	0.035	0.021	0.007
7	21.95	0.123	0.099	0.074	0.049	0.025	0.000	0.111	0.086	0.062	0.037	0.012
8	31.92	0.189	0.151	0.113	0.075	0.038	0.000	0.170	0.132	0.094	0.057	0.019
9	47.72	0.300	0.240	0.180	0.120	0.060	0.000	0.270	0.210	0.150	0.090	0.030
10	68.82	0.460	0.368	0.276	0.184	0.092	0.000	0.414	0.322	0.230	0.138	0.046
11	106.7	0.771	0.617	0.462	0.308	0.154	0.000	0.694	0.540	0.385	0.231	0.077
12	159.5	1.100	0.880	0.660	0.440	0.220	0.000	0.990	0.770	0.550	0.330	0.110
13	252.3	1.794	1.435	1.076	0.718	0.359	0.000	1.614	1.256	0.897	0.538	0.179
14	304.1	2.198	1.758	1.319	0.879	0.440	0.000	1.978	1.538	1.099	0.659	0.220
15	355.9	2.671	2.137	1.603	1.069	0.534	0.000	2.404	1.870	1.336	0.801	0.267
16	416.8	3.078	2.462	1.847	1.231	0.616	0.000	2.770	2.154	1.539	0.923	0.308
17	479.7	3.375	2.700	2.025	1.350	0.675	0.000	3.037	2.362	1.687	1.012	0.337
18	556.5	3.863	3.090	2.318	1.545	0.773	0.000	3.477	2.704	1.931	1.159	0.386

Table E21: Calculated Flowrate from all segments of the Pipeline

1	2	3	4	5	6	7	8	9	10	11
Test	Loss A + Stone Bedding	C_b	Qs 1	Qs 2	Qs 3	Qs 4	Qs 5	Q Total	Q Total	2Q Total
0	mm		m^3/s	m^3/s	m^3/s	m^3/s	m^3/s	m^3/s	l/s	l/s
1	3.00	0.159	0.00003	0.00003	0.00002	0.00001	0.00000	0.00010	0.10	0.19
2	3.25	0.170	0.00004	0.00003	0.00002	0.00001	0.00000	0.00011	0.11	0.22
3	4.00	0.196	0.00005	0.00004	0.00003	0.00002	0.00001	0.00014	0.14	0.28
4	6.00	0.305	0.00009	0.00007	0.00005	0.00003	0.00001	0.00026	0.26	0.53
5	7.99	0.440	0.00016	0.00012	0.00009	0.00005	0.00002	0.00044	0.44	0.87
6	14.97	0.602	0.00029	0.00023	0.00016	0.00010	0.00003	0.00082	0.82	1.64
7	21.95	0.651	0.00039	0.00030	0.00021	0.00013	0.00004	0.00107	1.07	2.15
8	31.92	0.659	0.00047	0.00037	0.00026	0.00016	0.00005	0.00131	1.31	2.62
9	47.72	0.677	0.00059	0.00046	0.00033	0.00020	0.00007	0.00165	1.64	3.29
10	68.82	0.693	0.00073	0.00057	0.00040	0.00024	0.00008	0.00202	2.02	4.04
11	106.70	0.716	0.00094	0.00073	0.00052	0.00031	0.00010	0.00260	2.60	5.20
12	159.57	0.697	0.00111	0.00087	0.00062	0.00037	0.00012	0.00310	3.10	6.19
13	252.31	0.705	0.00142	0.00110	0.00079	0.00047	0.00016	0.00394	3.94	7.88
14	304.16	0.710	0.00157	0.00122	0.00087	0.00052	0.00017	0.00436	4.36	8.71
15	355.98	0.723	0.00173	0.00134	0.00096	0.00058	0.00019	0.00480	4.80	9.60
16	416.82	0.717	0.00186	0.00144	0.00103	0.00062	0.00021	0.00515	5.15	10.31
17	479.71	0.699	0.00194	0.00151	0.00108	0.00065	0.00022	0.00539	5.39	10.78
18	556.51	0.695	0.00208	0.00161	0.00115	0.00069	0.00023	0.00577	5.77	11.53

With incoming velocities calculated, the next step is the estimation of the pressure loss due to the above velocities. Equation E3 calculates the headloss along the intake pipeline using the following equation:

$$hf = Ke * \frac{V^2}{2g} \qquad \text{(Eqn E3)}$$

With

Ke = Loss Coefficient

V = Velocity in m/s

Hf= Pressure los

g = gravitational constant (9.81m/s^2)

Table E 22 below calculates the headloss along the intake pipeline using the above equation:

Table E22: Pressure losses over length of Intake Pipeline

		Pos. 0	Pos. 1	Pos. 2	Pos. 3	Pos. 4	Pos. 5	Pos. 6	Pos. 7	Pos. 8	Pos. 9	Pos. 10
Test	Loss A	hf max	hf	hf	hf	hf	hf	hf	hf	hf	hf	hf
	mm	mm	mm	mm	mm	mm	mm	mm	mm	mm	mm	mm
1	3.0	3.0	2.4	1.9	1.5	1.1	0.8	0.5	0.3	0.1	0.009	0.0
2	6.5	6.5	5.2	4.1	3.2	2.3	1.6	1.0	0.6	0.3	0.019	0.1
3	13.9	13.9	11.3	8.9	6.8	5.0	3.5	2.2	1.3	0.6	0.037	0.1
4	39.8	39.8	32.2	25.4	19.5	14.3	9.9	6.4	3.6	1.6	0.073	0.4
5	89.4	89.4	72.4	57.2	43.8	32.2	22.3	14.3	8.0	3.6	0.116	0.9
6	160.6	160.6	130.1	102.8	78.7	57.8	40.2	25.7	14.5	6.4	0.169	1.6
7	215.2	215.2	174.3	137.7	105.4	77.5	53.8	34.4	19.4	8.6	0.196	2.2
8	280.6	280.6	227.3	179.6	137.5	101.0	70.1	44.9	25.3	11.2	0.224	2.8
9	473.0	473.0	383.2	302.8	231.8	170.3	118.3	75.7	42.6	18.9	0.286	4.7

Figure E9 below is a plot of EGLs at the centre of the Intake Pipeline. The EGL shows the amount of energy that has been lost from stone bedding friction and from water entering the Intake Pipeline.For the 18 tests conducted, the increase in pressure losses closer to the exit point of WC1, is clearly visible. The calculation of the EGL at various points within the Intake pipeline is crucial as it aids in determining the loss due to the stone bedding alone. This can be seen in the flowing chapter

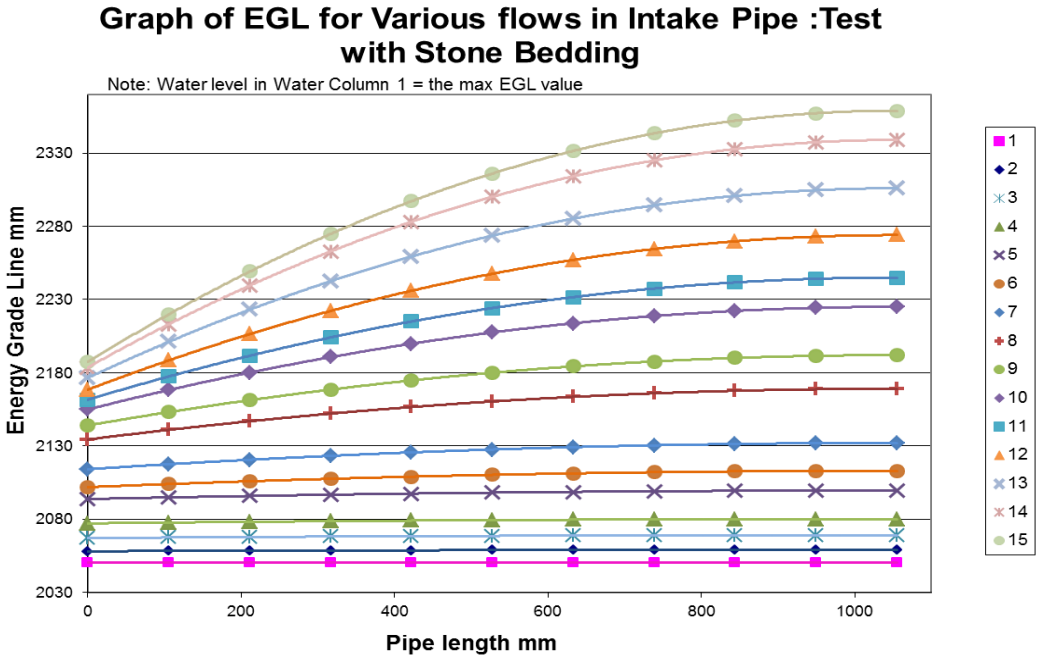

Figure E9: Plot of EGLs at the centre of the Intake Pipeline for Water and Stone Bedding Test

E.6.4.2 Pressure loss due to Stone Bedding

Calculating the loss of pressure due to stone bedding is critical as it inadvertently influences the design of the seawater Intake. Note that the stone bedding for all tests were standardised with the Intake pipe being 150mm above the bedrock, 300mm below the cover level of the stone bedding and 485mm from an adjacent intake pipeline. Three methods where employed when seeking to determine the pressure loss due the stone bedding.

E.6.4.2.1 Method 1: Simple method for determining stone bedding loss

In this simplistic method, the equation for the "Water Test with Extra Perforation": is removed from the equation for "Stone and water test" This is simplified as Eqn7 equals Eqn6 minus Eqn5 where:

$$\Delta P = 2.066\ Q^2 + 0.019\ Q \qquad \text{(Eqn6)}$$

minus

$$\Delta P = 0.891Q^2 + 1.286Q \qquad \text{(Eqn5)}$$

Hence the loss due to the Stone bedding alone would be

$$\Delta P = 1.175Q^2 - 1.267Q \qquad \text{(Eqn7)}$$

Table E23 below calculates the amount of headloss for notional flow values while Figure E10 plots these graphically.

Table E23: ø250mm Slotted pipe test: Method 1 :Pressure loss due to Stone Bedding Only

Test No	Q Half Pipe	Q Full Pipe	Stone Bedding Friction
	l/s	l/s	mm
1	0.10	0.19	0.002
2	0.11	0.22	0.009
3	0.14	0.28	0.02
4	0.26	0.53	0.8
5	0.44	0.87	0.96
6	0.82	1.64	1.08
7	1.07	2.15	2.69
8	1.31	2.62	4.76
9	1.64	3.29	8.56
10	2.02	4.04	14.11
11	2.60	5.20	25.23
12	3.10	6.19	37.27
13	3.94	7.88	63.03
14	4.36	8.71	78.25
15	4.80	9.60	96.26
16	5.15	10.31	111.85
17	5.39	10.78	123.02
18	5.77	11.53	141.84

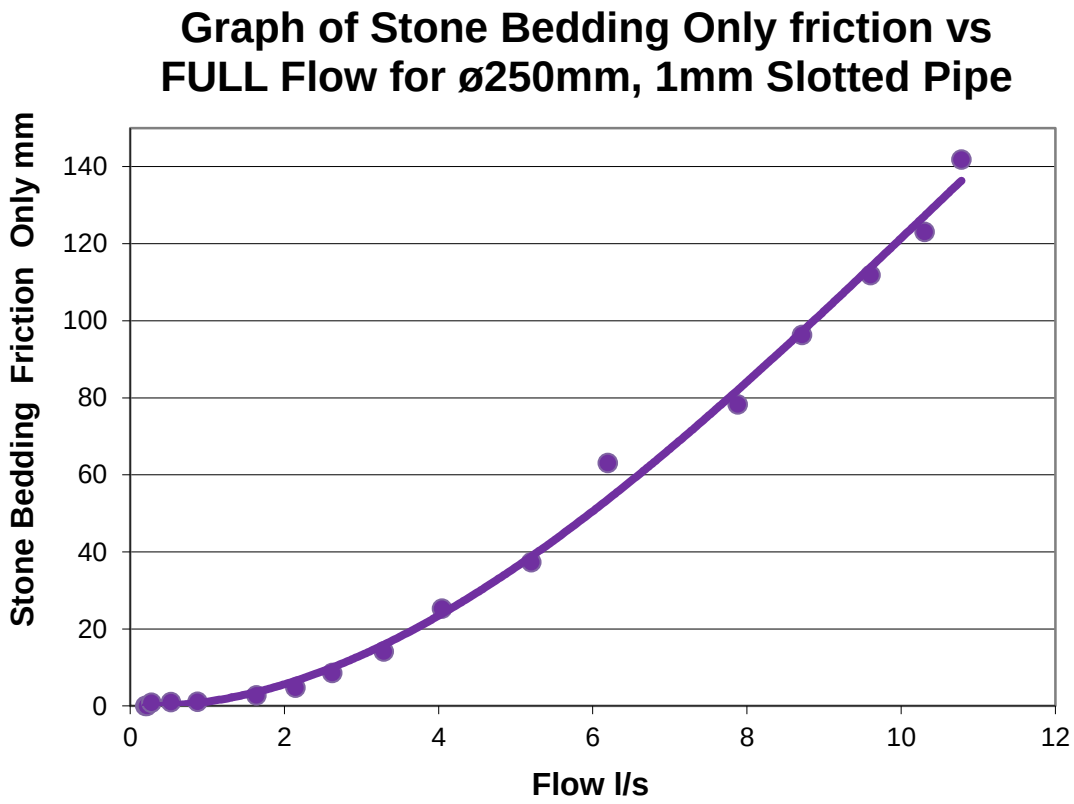

Figure E10: Method 1- ø250mm Perforated pipe, Water and Stone Bedding Test: Pressure loss due to Stone Bedding ONLY

E.6.4.2.2 Method 2: Method for determining stone bedding loss : Hydraulic conductivity: Kenny, Lau and Ofoegbu

The second method used to determine the loss of pressure due to Stone bedding, looks at the hydraulic conductivity of the stone bedding. From Table E20, the velocity for each segment of the Intake pipeline was determined. However the stone bedding cannot be split into equal segments as well. This is only correct for stone bedding adjacent to the intake pipeline. It does not apply to the flat horizontal surface of the stone bedding.

Table E24:ø250mm Perforated pipe, Water and Stone Bedding Test: Flow through segments

Test No.	Seg1	Seg2	Seg3	Seg4	Seg5	Seg1	Seg2	Seg3	Seg4	Seg5
	Qs 1	Qs 2	Qs 3	Qs 4	Qs 5	Qs 1	Qs 2	Qs 3	Qs 4	Qs 5
	m^3/s	m^3/s	m^3/s	m^3/s	m^3/s	m^3/s	m^3/s	m^3/s	m^3/s	m^3/s
1	0.00003	0.00003	0.00002	0.00001	0.00000	36%	28%	20%	12%	4%
2	0.00004	0.00003	0.00002	0.00001	0.00000	36%	28%	20%	12%	4%
3	0.00005	0.00004	0.00003	0.00002	0.00001	36%	28%	20%	12%	4%
4	0.00009	0.00007	0.00005	0.00003	0.00001	36%	28%	20%	12%	4%
5	0.00016	0.00012	0.00009	0.00005	0.00002	36%	28%	20%	12%	4%
6	0.00029	0.00023	0.00016	0.00010	0.00003	36%	28%	20%	12%	4%
7	0.00039	0.00030	0.00021	0.00013	0.00004	36%	28%	20%	12%	4%
8	0.00047	0.00037	0.00026	0.00016	0.00005	36%	28%	20%	12%	4%
9	0.00059	0.00046	0.00033	0.00020	0.00007	36%	28%	20%	12%	4%
10	0.00073	0.00057	0.00040	0.00024	0.00008	36%	28%	20%	12%	4%
11	0.00094	0.00073	0.00052	0.00031	0.00010	36%	28%	20%	12%	4%
12	0.00111	0.00087	0.00062	0.00037	0.00012	36%	28%	20%	12%	4%
13	0.00142	0.00110	0.00079	0.00047	0.00016	36%	28%	20%	12%	4%
14	0.00157	0.00122	0.00087	0.00052	0.00017	36%	28%	20%	12%	4%
15	0.00173	0.00134	0.00096	0.00058	0.00019	36%	28%	20%	12%	4%
16	0.00186	0.00144	0.00103	0.00062	0.00021	36%	28%	20%	12%	4%
17	0.00194	0.00151	0.00108	0.00065	0.00022	36%	28%	20%	12%	4%
18	0.00208	0.00161	0.00115	0.00069	0.00023	36%	28%	20%	12%	4%

Flow into the intake pipe line is proportional to the velocity. The maximum velocity occurs at one end of the intake pipeline and the minimum velocity occurs at the start of the intake pipeline. Table E24above looks at the ratio of the (flowrate) as a proportion of the entire flowrate.

Figure E11 provides a graphical description of how proportions were then applied to length of the stone bed. This splitting of the stone bedding surface ensured that all flows entering the stone bed were proportional to the flow entering the intake pipeline for all segments.

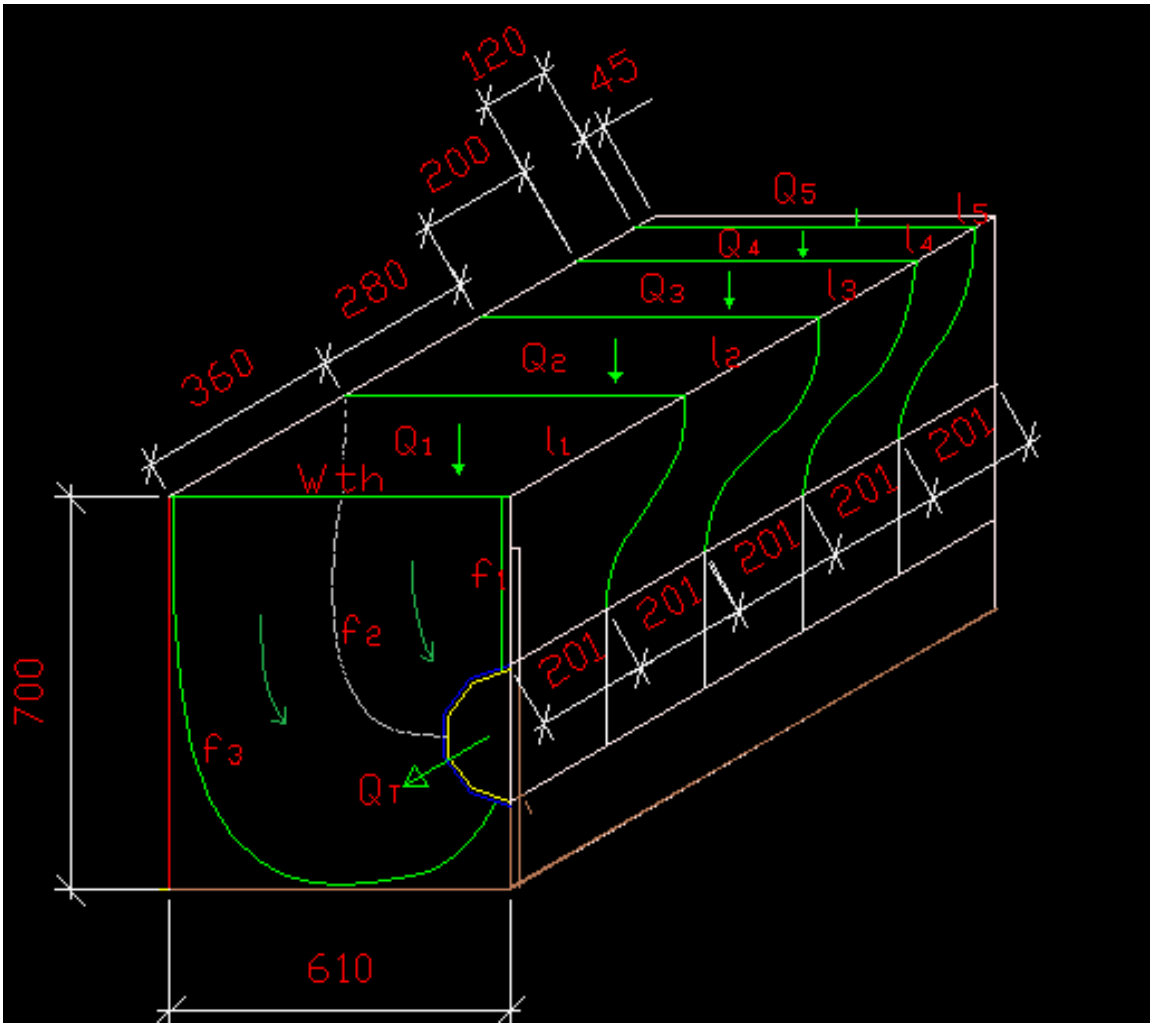

Figure E11: ø250mm Perforated pipe, Water and Stone Bedding Test: Segmentation of Stone Bedding area

Figure E12 shows the simplified version of a single notional segment. Note line f_1, f_2 and f_3 as lines of reference in Figure E12 and E13. As in Figure E11, length (l_1) is multiplied by the standard width (With), to create the area A_1. Area A_4 was easily calculated it is based on the intake pipe dimensions. Areas A_2 and A_3 are a third of the

distance from each end and hence are calculated proportionately. The distances from Area A_1 to A_2 to A_3 to A_4 are noted as Lengths len_1, len_2 and len_3 respectively.

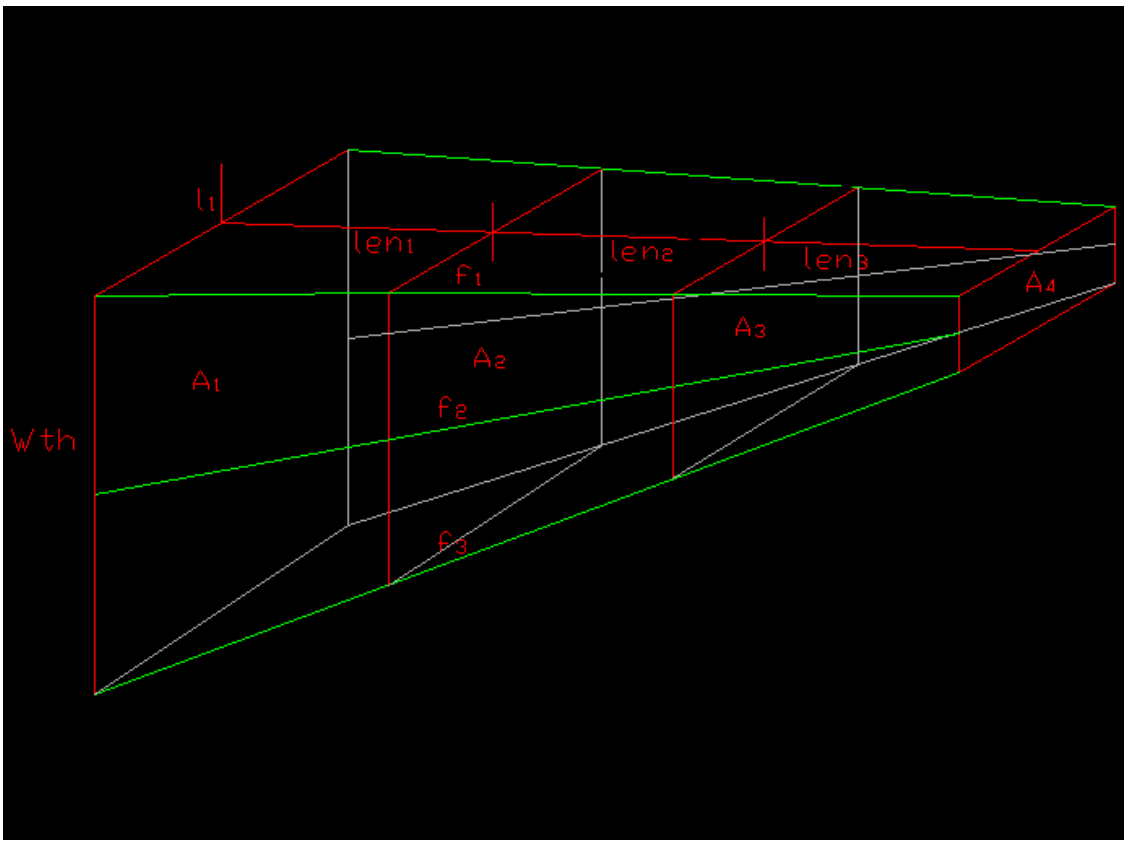

Figure E12: Notional flow path of a stone bedding segment

In order to calculate the pressure loss due to the stone bedding, the hydraulic conductivity is required. The pressure loss is defined as follows:

$$hf\,(m) = \frac{L * V}{k} \qquad \text{(Eqn E4)}$$

Where:

hf = pressure loss due to friction within stone bedding

L = Length of water path (m)

V = Flow velocity

k = Hydraulic conductivity

The first three variables are easily to calculate however determining the hydraulic conductivity k, requires further investigation.

The hydraulic conductivity is calculated using the following equation

$$k = \frac{\gamma_w}{\eta K} \qquad \text{(EqnE5)}$$

Where:

k = Hydraulic conductivity

γ_W = Unit Weight of Water

η = Dynamic Viscosity of water

K = Absolute Hydraulic conductivity

The unit weight of water γ_W,' and the dynamic viscosity of water η are fairly simple to calculate. However the Absolute Hydraulic conductivity K has to be calculated. It is calculated using the following equation:

$$\overline{K} = C_u D_5^2 \qquad \text{(Eqn E6)}$$

Where:

K = Absolute Hydraulic conductivity

C_u = Coefficient of Uniformity. Varies between 0.05 to 1

D_5 = Dimension of aggregate that has a cumulative percentage passing of 5%

Figure E13 below is a typical grading curve for nominally single-sized 19mm. From the grading curve, a value of D_5 = 10mm was obtained. Hence for a C_u of 0.8, Eqn E6 yields a K of 80mm^2. Utilising Eqn E6 and the following values:

γ_W = 9800 N/m^3

η = 0.00014 Ns/m

A hydraulic conductivity k of 0.688m/s was obtained. Table E20 summaries these results. As confirmation, Figure E15 is a graphical plot of Equation E6. Using a D_5 of 10mm, a k value of approximately 0.7m/s is found.

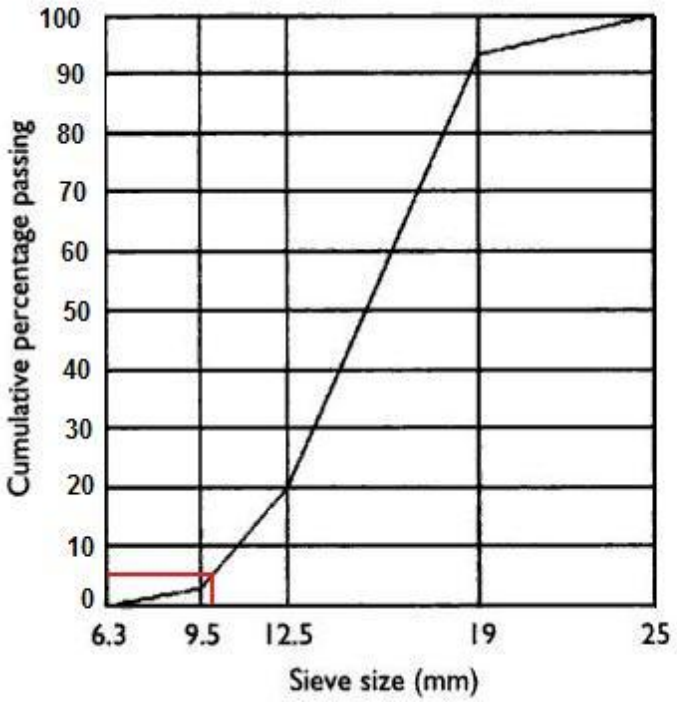

Figure E13: Typical grading curve for nominally single-sized 19mm Stone (Alexander & Mindess, 2005)

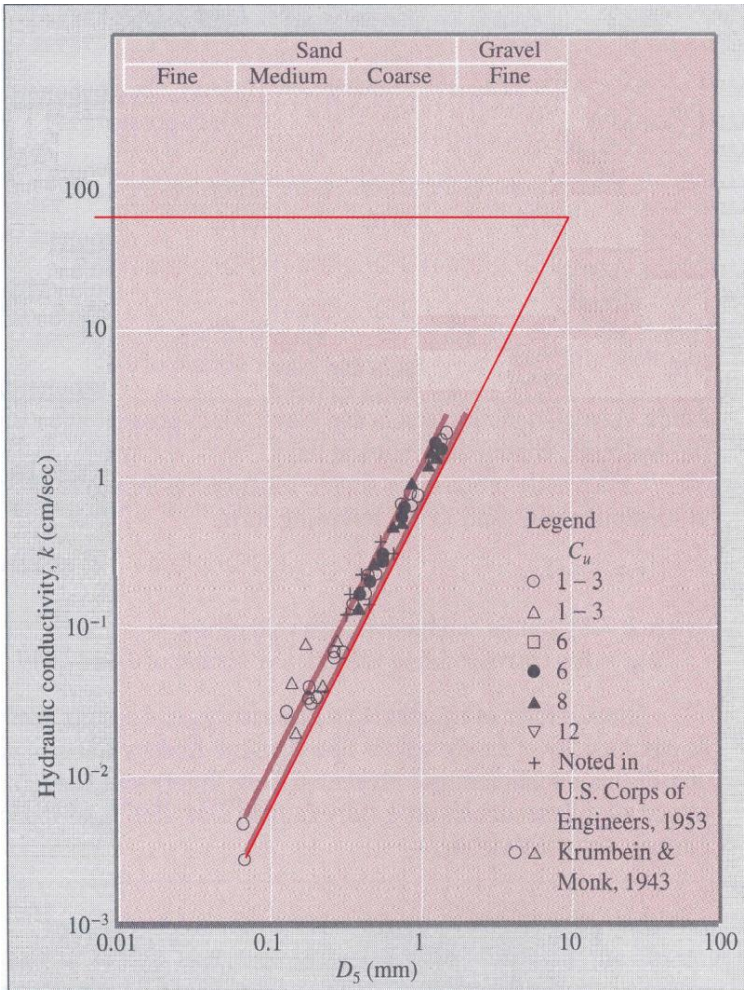

Figure E14: Graphical plot of Hydraulic conductivity Equation (Das 2000)

Table E25: Summary: Calculating the Hydraulic conductivity

Description	Value	Unit
C_u (0.05 to 1)	0.80	
D_5	10.0	mm
Water Column Width	0.61	m
Absolute Conductivity K	80	mm^2
Unit Weight of Water γ_W	9800	N/m^3
Dynamic Viscosity of water η	1.14E-03	Ns/m^2
Hydraulic Conductivity k	0.688	m/s

Using the values from Table E24 and E25, headloss for segment1 was calculated in the following manner. With the flow through each segment know, it is possible to determine the headloss if the areas through which water flows is uniform.

However, this is not the case. Hence each segment has been split into three equal portions. Table E26 below, describes the manner in which Segment 1 is split into three sub segments. Thereafter, Table E27 determines the average velocity for each sub segment, the associated headloss and finally the cumulative headloss for Segment 1. The following tables describe the headloss calculated for Segments, 2, 3, 4 and 5.

Table E26: Segment 1: Averaging of Areas

Test No.	Len1	A11	A12	A13	A14	Qs 1	Ave A11	Ave A12	Ave A13
	m	m^2	m^2	m^2	m^2	m3/s	m^2	m^2	m^2
1	0.3618	0.221	0.196	0.170	0.145	3.E-05	0.208	0.183	0.158
2	0.3618	0.221	0.196	0.170	0.145	4.E-05	0.208	0.183	0.158
3	0.3618	0.221	0.196	0.170	0.145	5.E-05	0.208	0.183	0.158
4	0.3618	0.221	0.196	0.170	0.145	9.E-05	0.208	0.183	0.158
5	0.3618	0.221	0.196	0.170	0.145	2.E-04	0.208	0.183	0.158
6	0.3618	0.221	0.196	0.170	0.145	3.E-04	0.208	0.183	0.158
7	0.3618	0.221	0.196	0.170	0.145	4.E-04	0.208	0.183	0.158
8	0.3618	0.221	0.196	0.170	0.145	5.E-04	0.208	0.183	0.158
9	0.3618	0.221	0.196	0.170	0.145	6.E-04	0.208	0.183	0.158
10	0.3618	0.221	0.196	0.170	0.145	7.E-04	0.208	0.183	0.158
11	0.3618	0.221	0.196	0.170	0.145	9.E-04	0.208	0.183	0.158
12	0.3618	0.221	0.196	0.170	0.145	1.E-03	0.208	0.183	0.158
13	0.3618	0.221	0.196	0.170	0.145	1.E-03	0.208	0.183	0.158
14	0.3618	0.221	0.196	0.170	0.145	2.E-03	0.208	0.183	0.158
15	0.3618	0.221	0.196	0.170	0.145	2.E-03	0.208	0.183	0.158
16	0.3618	0.221	0.196	0.170	0.145	2.E-03	0.208	0.183	0.158
17	0.3618	0.221	0.196	0.170	0.145	2.E-03	0.208	0.183	0.158
18	0.3618	0.221	0.196	0.170	0.145	2.E-03	0.208	0.183	0.158

Table E27: Segment 1: Velocity and cumulative headloss

Test No.	Vel 1A	Vel 1B	Vel 1C	H_l11	H_l12	H_l13	$H_l1Total$	$H_l1Total$
	m/s	m/s	m/s	m	m	m	m	mm
1	2.E-04	2.E-04	2.E-04	0.0001	0.0001	0.0001	0.0002	0.18
2	2.E-04	2.E-04	2.E-04	0.0001	0.0001	0.0001	0.0002	0.20
3	2.E-04	3.E-04	3.E-04	0.0001	0.0001	0.0001	0.0003	0.25
4	5.E-04	5.E-04	6.E-04	0.0001	0.0002	0.0002	0.0005	0.48
5	8.E-04	9.E-04	1.E-03	0.0002	0.0003	0.0003	0.0008	0.80
6	1.E-03	2.E-03	2.E-03	0.0004	0.0005	0.0006	0.0015	1.50
7	2.E-03	2.E-03	2.E-03	0.0006	0.0006	0.0007	0.0020	1.96
8	2.E-03	3.E-03	3.E-03	0.0007	0.0008	0.0009	0.0024	2.39
9	3.E-03	3.E-03	4.E-03	0.0009	0.0010	0.0011	0.0030	3.00
10	3.E-03	4.E-03	5.E-03	0.0011	0.0012	0.0014	0.0037	3.69
11	4.E-03	5.E-03	6.E-03	0.0014	0.0016	0.0018	0.0047	4.75
12	5.E-03	6.E-03	7.E-03	0.0016	0.0019	0.0022	0.0057	5.66
13	7.E-03	8.E-03	9.E-03	0.0021	0.0024	0.0027	0.0072	7.19
14	8.E-03	9.E-03	1.E-02	0.0023	0.0026	0.0030	0.0080	7.96
15	8.E-03	9.E-03	1.E-02	0.0025	0.0029	0.0033	0.0088	8.77
16	9.E-03	1.E-02	1.E-02	0.0027	0.0031	0.0036	0.0094	9.41
17	9.E-03	1.E-02	1.E-02	0.0028	0.0032	0.0038	0.0098	9.84
18	1.E-02	1.E-02	1.E-02	0.0030	0.0035	0.0040	0.0105	10.53

Table E28: Segment 2: Averaging of Areas

Test No.	Len2	A21	A22	A23	A24	Qs 2	Ave A21	Ave A22	Ave A23
	m	m^2	m^2	m^2	m^2	m3/s	m^2	m^2	m^2
1	0.2814	0.172	0.163	0.154	0.145	3.E-05	0.167	0.158	0.150
2	0.2814	0.172	0.163	0.154	0.145	3.E-05	0.167	0.158	0.150
3	0.2814	0.172	0.163	0.154	0.145	4.E-05	0.167	0.158	0.150
4	0.2814	0.172	0.163	0.154	0.145	7.E-05	0.167	0.158	0.150
5	0.2814	0.172	0.163	0.154	0.145	1.E-04	0.167	0.158	0.150
6	0.2814	0.172	0.163	0.154	0.145	2.E-04	0.167	0.158	0.150
7	0.2814	0.172	0.163	0.154	0.145	3.E-04	0.167	0.158	0.150
8	0.2814	0.172	0.163	0.154	0.145	4.E-04	0.167	0.158	0.150
9	0.2814	0.172	0.163	0.154	0.145	5.E-04	0.167	0.158	0.150
10	0.2814	0.172	0.163	0.154	0.145	6.E-04	0.167	0.158	0.150
11	0.2814	0.172	0.163	0.154	0.145	7.E-04	0.167	0.158	0.150
12	0.2814	0.172	0.163	0.154	0.145	9.E-04	0.167	0.158	0.150
13	0.2814	0.172	0.163	0.154	0.145	1.E-03	0.167	0.158	0.150
14	0.2814	0.172	0.163	0.154	0.145	1.E-03	0.167	0.158	0.150
15	0.2814	0.172	0.163	0.154	0.145	1.E-03	0.167	0.158	0.150
16	0.2814	0.172	0.163	0.154	0.145	1.E-03	0.167	0.158	0.150
17	0.2814	0.172	0.163	0.154	0.145	2.E-03	0.167	0.158	0.150
18	0.2814	0.172	0.163	0.154	0.145	2.E-03	0.167	0.158	0.150

Table E29: Segment 2: Velocity and cumulative headloss

Test No.	Vel2A	Vel2B	Vel2C	H_l21	H_l22	H_l23	H_l2 Total	H_l2 Total
	m/s	m/s	m/s	m	m	m	m	mm
1	2.E-04	2.E-04	2.E-04	0.0000	0.0001	0.0001	0.0002	0.16
2	2.E-04	2.E-04	2.E-04	0.0001	0.0001	0.0001	0.0002	0.18
3	2.E-04	2.E-04	3.E-04	0.0001	0.0001	0.0001	0.0002	0.22
4	4.E-04	5.E-04	5.E-04	0.0001	0.0001	0.0002	0.0004	0.43
5	7.E-04	8.E-04	8.E-04	0.0002	0.0002	0.0003	0.0007	0.71
6	1.E-03	1.E-03	2.E-03	0.0004	0.0004	0.0005	0.0013	1.33
7	2.E-03	2.E-03	2.E-03	0.0005	0.0006	0.0006	0.0017	1.74
8	2.E-03	2.E-03	2.E-03	0.0007	0.0007	0.0007	0.0021	2.13
9	3.E-03	3.E-03	3.E-03	0.0008	0.0009	0.0009	0.0027	2.67
10	3.E-03	4.E-03	4.E-03	0.0010	0.0011	0.0012	0.0033	3.28
11	4.E-03	5.E-03	5.E-03	0.0013	0.0014	0.0015	0.0042	4.22
12	5.E-03	5.E-03	6.E-03	0.0016	0.0017	0.0018	0.0050	5.03
13	7.E-03	7.E-03	7.E-03	0.0020	0.0021	0.0023	0.0064	6.39
14	7.E-03	8.E-03	8.E-03	0.0022	0.0024	0.0025	0.0071	7.07
15	8.E-03	8.E-03	9.E-03	0.0025	0.0026	0.0027	0.0078	7.79
16	9.E-03	9.E-03	1.E-02	0.0026	0.0028	0.0029	0.0084	8.36
17	9.E-03	1.E-02	1.E-02	0.0028	0.0029	0.0031	0.0087	8.75
18	1.E-02	1.E-02	1.E-02	0.0029	0.0031	0.0033	0.0094	9.36

Table E30: Segment 3: Averaging of Areas

Test No.	Len3	A31	A32	A33	A34	Qs 3	Ave A31	Ave A32	Ave A33
	m	m^2	m^2	m^2	m^2	m3/s	m^2	m^2	m^2
1	0.201	0.123	0.130	0.138	0.145	2.E-05	0.126	0.134	0.141
2	0.201	0.123	0.130	0.138	0.145	2.E-05	0.126	0.134	0.141
3	0.201	0.123	0.130	0.138	0.145	3.E-05	0.126	0.134	0.141
4	0.201	0.123	0.130	0.138	0.145	5.E-05	0.126	0.134	0.141
5	0.201	0.123	0.130	0.138	0.145	9.E-05	0.126	0.134	0.141
6	0.201	0.123	0.130	0.138	0.145	2.E-04	0.126	0.134	0.141
7	0.201	0.123	0.130	0.138	0.145	2.E-04	0.126	0.134	0.141
8	0.201	0.123	0.130	0.138	0.145	3.E-04	0.126	0.134	0.141
9	0.201	0.123	0.130	0.138	0.145	3.E-04	0.126	0.134	0.141
10	0.201	0.123	0.130	0.138	0.145	4.E-04	0.126	0.134	0.141
11	0.201	0.123	0.130	0.138	0.145	5.E-04	0.126	0.134	0.141
12	0.201	0.123	0.130	0.138	0.145	6.E-04	0.126	0.134	0.141
13	0.201	0.123	0.130	0.138	0.145	8.E-04	0.126	0.134	0.141
14	0.201	0.123	0.130	0.138	0.145	9.E-04	0.126	0.134	0.141
15	0.201	0.123	0.130	0.138	0.145	1.E-03	0.126	0.134	0.141
16	0.201	0.123	0.130	0.138	0.145	1.E-03	0.126	0.134	0.141
17	0.201	0.123	0.130	0.138	0.145	1.E-03	0.126	0.134	0.141
18	0.201	0.123	0.130	0.138	0.145	1.E-03	0.126	0.134	0.141

Table E31: Segment 3: Velocity and cumulative headloss

Test No.	Vel3A	Vel3B	Vel3C	H_l31	H_l32	H_l33	$H_l3Total$	$H_l3Total$
	m/s	m/s	m/s	m	m	m	m	mm
1	2.E-04	1.E-04	1.E-04	0.0000	0.0000	0.0000	0.0001	0.13
2	2.E-04	2.E-04	2.E-04	0.0001	0.0000	0.0000	0.0001	0.15
3	2.E-04	2.E-04	2.E-04	0.0001	0.0001	0.0001	0.0002	0.19
4	4.E-04	4.E-04	4.E-04	0.0001	0.0001	0.0001	0.0004	0.36
5	7.E-04	7.E-04	6.E-04	0.0002	0.0002	0.0002	0.0006	0.60
6	1.E-03	1.E-03	1.E-03	0.0004	0.0004	0.0004	0.0011	1.12
7	2.E-03	2.E-03	2.E-03	0.0005	0.0005	0.0005	0.0015	1.47
8	2.E-03	2.E-03	2.E-03	0.0006	0.0006	0.0006	0.0018	1.80
9	3.E-03	2.E-03	2.E-03	0.0008	0.0008	0.0007	0.0023	2.26
10	3.E-03	3.E-03	3.E-03	0.0010	0.0009	0.0009	0.0028	2.77
11	4.E-03	4.E-03	4.E-03	0.0013	0.0012	0.0011	0.0036	3.57
12	5.E-03	5.E-03	4.E-03	0.0015	0.0014	0.0013	0.0042	4.25
13	6.E-03	6.E-03	6.E-03	0.0019	0.0018	0.0017	0.0054	5.40
14	7.E-03	7.E-03	6.E-03	0.0021	0.0020	0.0019	0.0060	5.97
15	8.E-03	7.E-03	7.E-03	0.0023	0.0022	0.0021	0.0066	6.58
16	8.E-03	8.E-03	7.E-03	0.0025	0.0024	0.0022	0.0071	7.07
17	9.E-03	8.E-03	8.E-03	0.0026	0.0025	0.0023	0.0074	7.39
18	9.E-03	9.E-03	8.E-03	0.0028	0.0026	0.0025	0.0079	7.91

Table E32: Segment 4: Averaging of Areas

Test No.	Len4	A41	A42	A43	A44	Qs 4	Ave A41	Ave A42	Ave A43
	m	m^2	m^2	m^2	m^2	m3/s	m^2	m^2	m^2
1	0.1206	0.074	0.097	0.121	0.145	1.E-05	0.085	0.109	0.133
2	0.1206	0.074	0.097	0.121	0.145	1.E-05	0.085	0.109	0.133
3	0.1206	0.074	0.097	0.121	0.145	2.E-05	0.085	0.109	0.133
4	0.1206	0.074	0.097	0.121	0.145	3.E-05	0.085	0.109	0.133
5	0.1206	0.074	0.097	0.121	0.145	5.E-05	0.085	0.109	0.133
6	0.1206	0.074	0.097	0.121	0.145	1.E-04	0.085	0.109	0.133
7	0.1206	0.074	0.097	0.121	0.145	1.E-04	0.085	0.109	0.133
8	0.1206	0.074	0.097	0.121	0.145	2.E-04	0.085	0.109	0.133
9	0.1206	0.074	0.097	0.121	0.145	2.E-04	0.085	0.109	0.133
10	0.1206	0.074	0.097	0.121	0.145	2.E-04	0.085	0.109	0.133
11	0.1206	0.074	0.097	0.121	0.145	3.E-04	0.085	0.109	0.133
12	0.1206	0.074	0.097	0.121	0.145	4.E-04	0.085	0.109	0.133
13	0.1206	0.074	0.097	0.121	0.145	5.E-04	0.085	0.109	0.133
14	0.1206	0.074	0.097	0.121	0.145	5.E-04	0.085	0.109	0.133
15	0.1206	0.074	0.097	0.121	0.145	6.E-04	0.085	0.109	0.133
16	0.1206	0.074	0.097	0.121	0.145	6.E-04	0.085	0.109	0.133
17	0.1206	0.074	0.097	0.121	0.145	6.E-04	0.085	0.109	0.133
18	0.1206	0.074	0.097	0.121	0.145	7.E-04	0.085	0.109	0.133

Table E33: Segment 4: Velocity and cumulative headloss

Test No.	Vel4A	Vel4B	Vel4C	H_l41	H_l42	H_l43	H_l4 Total	H_l4 Total
	m/s	m/s	m/s	m	m	m	m	mm
1	1.E-04	1.E-04	9.E-05	0.0000	0.0000	0.0000	0.0001	0.10
2	2.E-04	1.E-04	1.E-04	0.0000	0.0000	0.0000	0.0001	0.11
3	2.E-04	2.E-04	1.E-04	0.0001	0.0000	0.0000	0.0001	0.14
4	4.E-04	3.E-04	2.E-04	0.0001	0.0001	0.0001	0.0003	0.27
5	6.E-04	5.E-04	4.E-04	0.0002	0.0001	0.0001	0.0005	0.45
6	1.E-03	9.E-04	7.E-04	0.0004	0.0003	0.0002	0.0009	0.85
7	2.E-03	1.E-03	1.E-03	0.0005	0.0004	0.0003	0.0011	1.11
8	2.E-03	1.E-03	1.E-03	0.0006	0.0004	0.0004	0.0014	1.36
9	2.E-03	2.E-03	1.E-03	0.0007	0.0006	0.0005	0.0017	1.71
10	3.E-03	2.E-03	2.E-03	0.0009	0.0007	0.0006	0.0021	2.10
11	4.E-03	3.E-03	2.E-03	0.0011	0.0009	0.0007	0.0027	2.70
12	4.E-03	3.E-03	3.E-03	0.0013	0.0010	0.0009	0.0032	3.22
13	6.E-03	4.E-03	4.E-03	0.0017	0.0013	0.0011	0.0041	4.09
14	6.E-03	5.E-03	4.E-03	0.0019	0.0015	0.0012	0.0045	4.53
15	7.E-03	5.E-03	4.E-03	0.0021	0.0016	0.0013	0.0050	4.99
16	7.E-03	6.E-03	5.E-03	0.0022	0.0017	0.0014	0.0054	5.35
17	8.E-03	6.E-03	5.E-03	0.0023	0.0018	0.0015	0.0056	5.60
18	8.E-03	6.E-03	5.E-03	0.0025	0.0019	0.0016	0.0060	5.99

Table E34: Segment 5: Averaging of Areas

Test No.	Len5	A51	A52	A53	A54	Qs 5	Ave A51	Ave A52	Ave A53
	m	m^2	m^2	m^2	m^2	m3/s	m^2	m^2	m^2
1	0.0402	0.025	0.065	0.105	0.145	4.E-06	0.045	0.085	0.125
2	0.0402	0.025	0.065	0.105	0.145	4.E-06	0.045	0.085	0.125
3	0.0402	0.025	0.065	0.105	0.145	6.E-06	0.045	0.085	0.125
4	0.0402	0.025	0.065	0.105	0.145	1.E-05	0.045	0.085	0.125
5	0.0402	0.025	0.065	0.105	0.145	2.E-05	0.045	0.085	0.125
6	0.0402	0.025	0.065	0.105	0.145	3.E-05	0.045	0.085	0.125
7	0.0402	0.025	0.065	0.105	0.145	4.E-05	0.045	0.085	0.125
8	0.0402	0.025	0.065	0.105	0.145	5.E-05	0.045	0.085	0.125
9	0.0402	0.025	0.065	0.105	0.145	7.E-05	0.045	0.085	0.125
10	0.0402	0.025	0.065	0.105	0.145	8.E-05	0.045	0.085	0.125
11	0.0402	0.025	0.065	0.105	0.145	1.E-04	0.045	0.085	0.125
12	0.0402	0.025	0.065	0.105	0.145	1.E-04	0.045	0.085	0.125
13	0.0402	0.025	0.065	0.105	0.145	2.E-04	0.045	0.085	0.125
14	0.0402	0.025	0.065	0.105	0.145	2.E-04	0.045	0.085	0.125
15	0.0402	0.025	0.065	0.105	0.145	2.E-04	0.045	0.085	0.125
16	0.0402	0.025	0.065	0.105	0.145	2.E-04	0.045	0.085	0.125
17	0.0402	0.025	0.065	0.105	0.145	2.E-04	0.045	0.085	0.125
18	0.0402	0.025	0.065	0.105	0.145	2.E-04	0.045	0.085	0.125

Table E35: Segment 5: Velocity and cumulative headloss

Test No.	Vel5A	Vel5B	Vel5C	H_l51	H_l52	H_l53	$H_l5Total$	$H_l5Total$
	m/s	m/s	m/s	m	m	m	m	mm
1	9.E-05	5.E-05	3.E-05	0.0000	0.0000	0.0000	0.0000	0.05
2	1.E-04	5.E-05	3.E-05	0.0000	0.0000	0.0000	0.0001	0.06
3	1.E-04	7.E-05	4.E-05	0.0000	0.0000	0.0000	0.0001	0.07
4	2.E-04	1.E-04	8.E-05	0.0001	0.0000	0.0000	0.0001	0.14
5	4.E-04	2.E-04	1.E-04	0.0001	0.0001	0.0000	0.0002	0.23
6	7.E-04	4.E-04	3.E-04	0.0002	0.0001	0.0001	0.0004	0.42
7	1.E-03	5.E-04	3.E-04	0.0003	0.0002	0.0001	0.0006	0.55
8	1.E-03	6.E-04	4.E-04	0.0004	0.0002	0.0001	0.0007	0.68
9	1.E-03	8.E-04	5.E-04	0.0005	0.0002	0.0002	0.0008	0.85
10	2.E-03	1.E-03	6.E-04	0.0006	0.0003	0.0002	0.0010	1.04
11	2.E-03	1.E-03	8.E-04	0.0007	0.0004	0.0003	0.0013	1.34
12	3.E-03	1.E-03	1.E-03	0.0008	0.0004	0.0003	0.0016	1.60
13	4.E-03	2.E-03	1.E-03	0.0011	0.0006	0.0004	0.0020	2.03
14	4.E-03	2.E-03	1.E-03	0.0012	0.0006	0.0004	0.0022	2.25
15	4.E-03	2.E-03	2.E-03	0.0013	0.0007	0.0005	0.0025	2.47
16	5.E-03	2.E-03	2.E-03	0.0014	0.0007	0.0005	0.0027	2.66
17	5.E-03	3.E-03	2.E-03	0.0015	0.0008	0.0005	0.0028	2.78
18	5.E-03	3.E-03	2.E-03	0.0016	0.0008	0.0006	0.0030	2.97

Table E36:Summary of Method 2 Headloss Tests. Results from Tables26 to 35 (WST)

Test No.	Total Q	Segment 1	Segment 2	Segment 3	Segment 4	Segment 5
	l/s	mm	mm	mm	mm	mm
1	0.10	0.18	0.16	0.13	0.10	0.05
2	0.11	0.20	0.18	0.15	0.11	0.06
3	0.14	0.25	0.22	0.19	0.14	0.07
4	0.26	0.48	0.43	0.36	0.27	0.14
5	0.44	0.80	0.71	0.60	0.45	0.23
6	0.82	1.50	1.33	1.12	0.85	0.42
7	1.07	1.96	1.74	1.47	1.11	0.55
8	1.31	2.39	2.13	1.80	1.36	0.68
9	1.64	3.00	2.67	2.26	1.71	0.85
10	2.02	3.69	3.28	2.77	2.10	1.04
11	2.60	4.75	4.22	3.57	2.70	1.34
12	3.10	5.66	5.03	4.25	3.22	1.60
13	3.94	7.19	6.39	5.40	4.09	2.03
14	4.36	7.96	7.07	5.97	4.53	2.25
15	4.80	8.77	7.79	6.58	4.99	2.47
16	5.15	9.41	8.36	7.07	5.35	2.66
17	5.39	9.84	8.75	7.39	5.60	2.78
18	5.77	10.53	9.36	7.91	5.99	2.97

Figure E15 plots Table E36 graphically. A trendline is added to the results in order to predict the headloss, due to stone bedding, at the most downstream point of WC1. It is at this point that the largest magnitude of headloss occurs. Table E37 summaries these results.

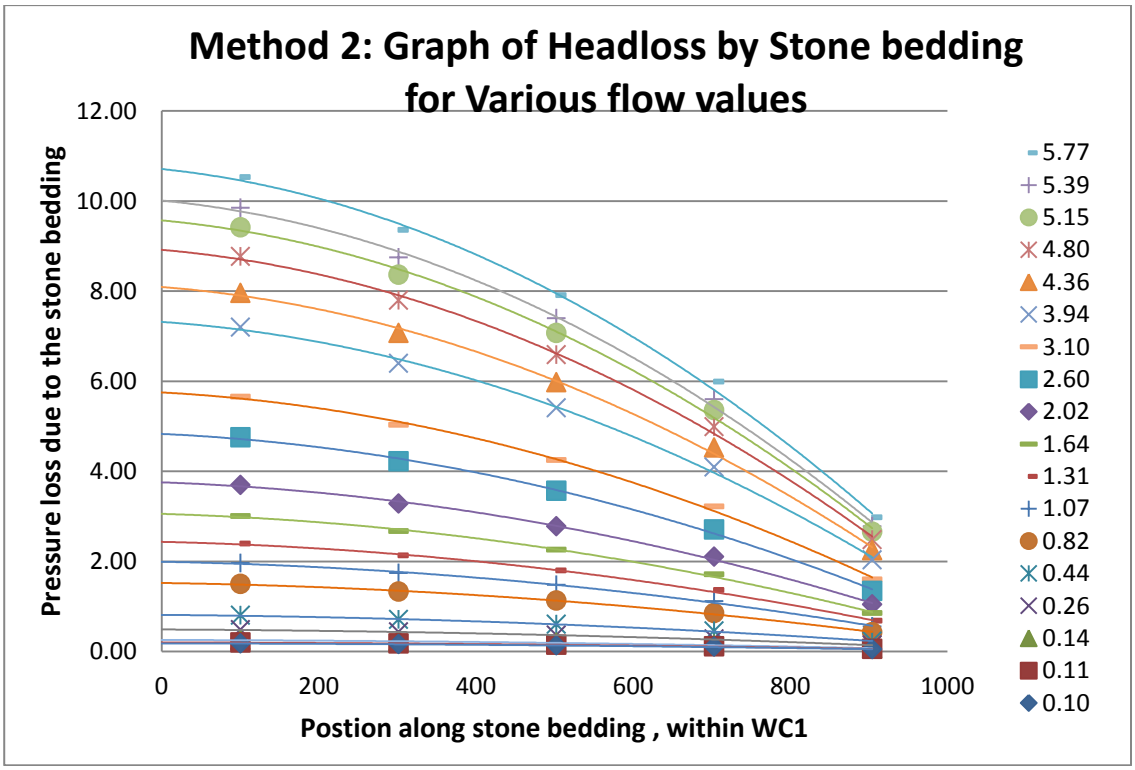

Figure E15: Results of Headloss due to Stone Bedding, within WC1

Table E37: Method 2: Summary of maximum headloss versus flow rates

Test No.	Total Q	Total 2Q	Maximum Headloss due to Stone Bedding
	l/s	l/s	mm
1	0.10	0.19	0.18
2	0.11	0.22	0.21
3	0.14	0.28	0.27
4	0.26	0.53	0.51
5	0.44	0.87	0.85
6	0.82	1.64	1.59
7	1.07	2.15	2.08
8	1.31	2.62	2.55
9	1.65	3.29	3.19
10	2.02	4.04	3.93
11	2.60	5.20	5.05
12	3.10	6.19	6.01
13	3.94	7.88	7.65
14	4.36	8.71	8.46
15	4.80	9.60	9.32
16	5.15	10.31	10.01
17	5.39	10.78	10.47
18	5.77	11.53	11.20

E.5.4.2.3 Method 3: Method for determining stone bedding loss : Hydraulic conductivity: Forchheimer

The third method used to determine the loss of pressure due to Stone bedding, looks at the hydraulic conductivity of the stone bedding. This is based on work carried out by Forchheimer. From Table E38, the velocity for each segment of the Intake pipeline was determined. However, stone bedding cannot be split into equal segments as well. This is only correct for stone bedding adjacent to the intake pipeline. It does not apply to the flat horizontal surface of the stone bedding.

Flow into the intake pipe line is proportional to the velocity. The maximum velocity occurs at one end of the intake pipeline and the minimum velocity occurs at the start of the intake pipeline. Table E38 below looks at the ratio of the (flowrate) as a proportion of the entire flowrate.

In Figure E16, these proportions were applied to the length of the stone bed. This splitting of the stone bedding surface ensured that all flows entering the stone bed were proportional to the flow entering the intake pipeline for all segments.

Table E38:ø250mm Perforated pipe, Water and Stone Bedding Test: Flow through segments

Test No.	Seg1	Seg2	Seg3	Seg4	Seg5	Seg1	Seg2	Seg3	Seg4	Seg5
	Qs 1	Qs 2	Qs 3	Qs 4	Qs 5	Qs 1	Qs 2	Qs 3	Qs 4	Qs 5
	m^3/s	m^3/s	m^3/s	m^3/s	m^3/s	m^3/s	m^3/s	m^3/s	m^3/s	m^3/s
1	0.00003	0.00003	0.00002	0.00001	0.00000	36%	28%	20%	12%	4%
2	0.00004	0.00003	0.00002	0.00001	0.00000	36%	28%	20%	12%	4%
3	0.00005	0.00004	0.00003	0.00002	0.00001	36%	28%	20%	12%	4%
4	0.00009	0.00007	0.00005	0.00003	0.00001	36%	28%	20%	12%	4%
5	0.00016	0.00012	0.00009	0.00005	0.00002	36%	28%	20%	12%	4%
6	0.00029	0.00023	0.00016	0.00010	0.00003	36%	28%	20%	12%	4%
7	0.00039	0.00030	0.00021	0.00013	0.00004	36%	28%	20%	12%	4%
8	0.00047	0.00037	0.00026	0.00016	0.00005	36%	28%	20%	12%	4%
9	0.00059	0.00046	0.00033	0.00020	0.00007	36%	28%	20%	12%	4%
10	0.00073	0.00057	0.00040	0.00024	0.00008	36%	28%	20%	12%	4%
11	0.00094	0.00073	0.00052	0.00031	0.00010	36%	28%	20%	12%	4%
12	0.00111	0.00087	0.00062	0.00037	0.00012	36%	28%	20%	12%	4%
13	0.00142	0.00110	0.00079	0.00047	0.00016	36%	28%	20%	12%	4%
14	0.00157	0.00122	0.00087	0.00052	0.00017	36%	28%	20%	12%	4%
15	0.00173	0.00134	0.00096	0.00058	0.00019	36%	28%	20%	12%	4%
16	0.00186	0.00144	0.00103	0.00062	0.00021	36%	28%	20%	12%	4%
17	0.00194	0.00151	0.00108	0.00065	0.00022	36%	28%	20%	12%	4%
18	0.00208	0.00161	0.00115	0.00069	0.00023	36%	28%	20%	12%	4%

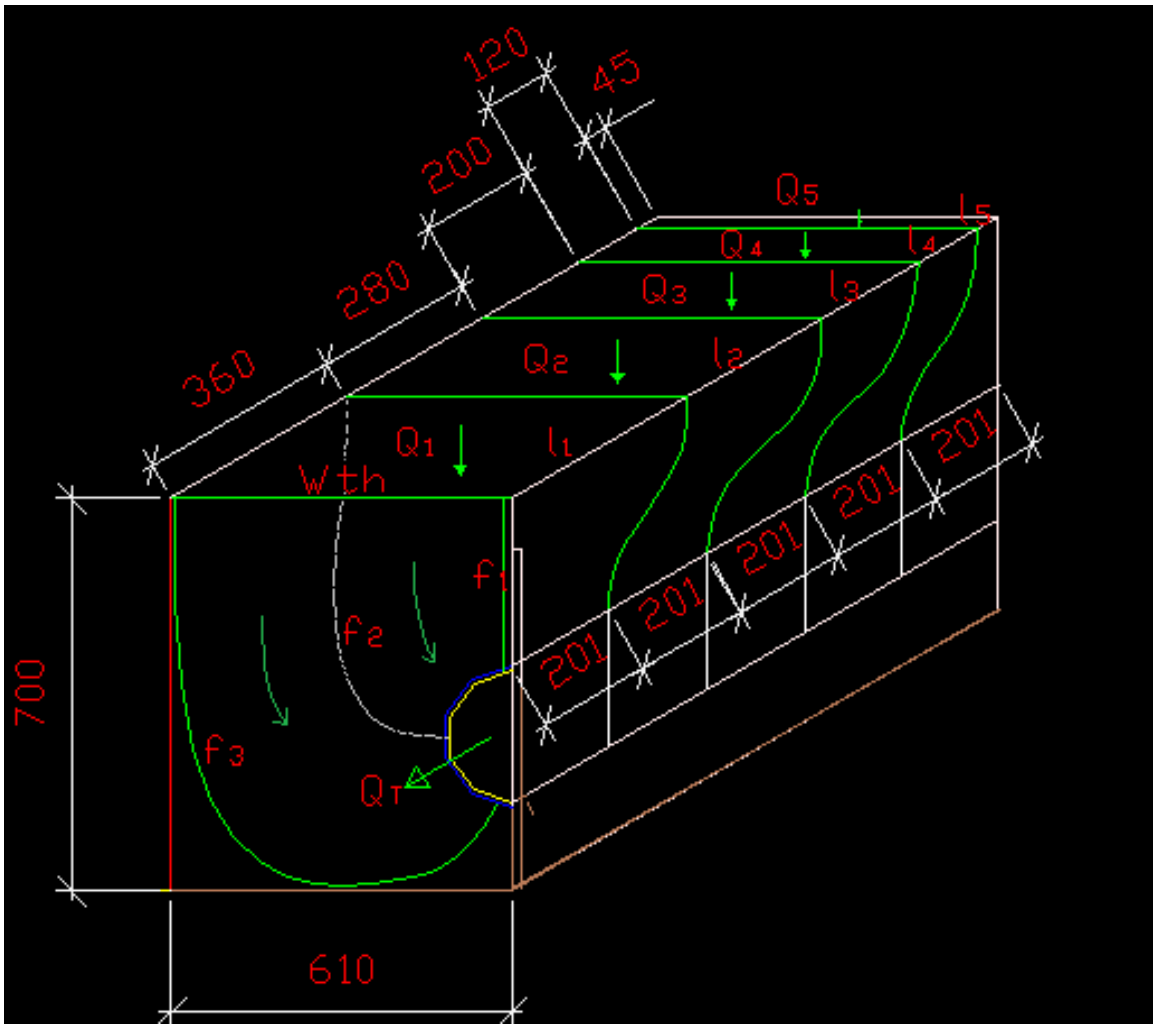

Figure E16: ø250mm Slotted pipe-Water and Stone Bedding Test: Segmentation of Stone Bedding area

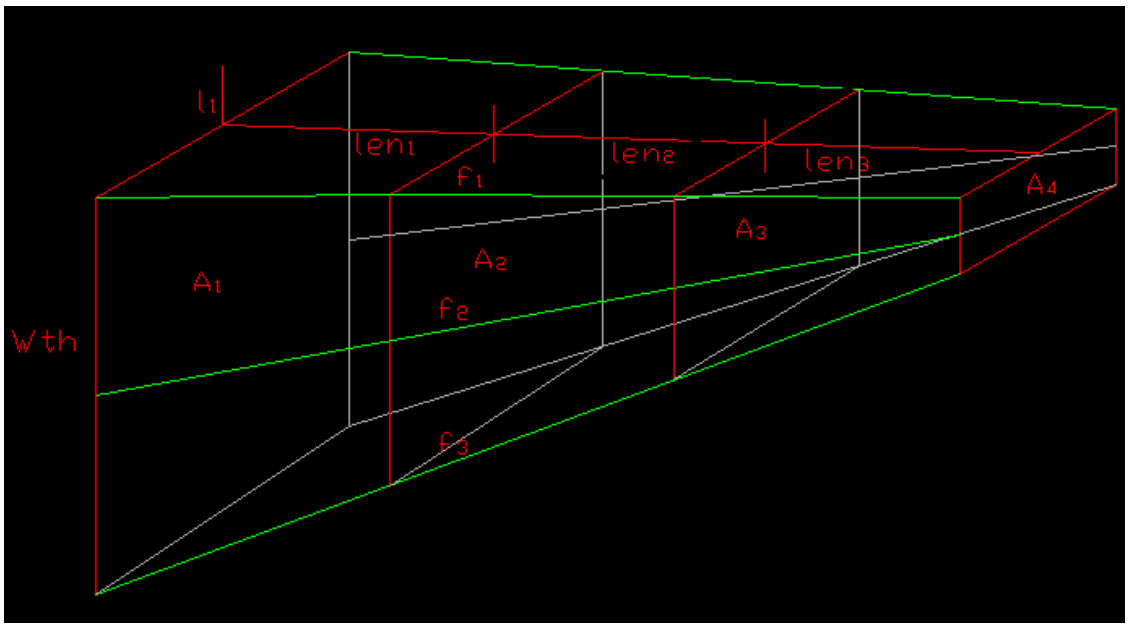

Figure E17: Notional flow path of a stone bedding segment

Figure E17 shows the simplified version of a single notional segment. Note line f_1, f_2 and f_3 as lines of reference in Figure E16 and E17. As in Figure E17, length (l_1) is multiplied by the standard width (With), to create the area A_1. Area A_4 was easily calculated it is based on the intake pipe dimensions. Areas A_2 and $A_3$are a third of the distance from each end and hence are calculated proportionately. The distances from Area A_1 to A_2 to A_3 to $A_4$are noted as Lengths len_1, len_2 and len_3 respectively.

In order to calculate the pressure loss due to the stone bedding, the hydraulic conductivity is required. The pressure loss is defined as per Equation 4 below:

$$hf(m) = \frac{L * V}{k} \qquad \text{Eqn E4}$$

Where:

hf = pressure loss due to friction within stone bedding

L = Length of water path (m)

V = Flow velocity

k = Hydraulic conductivity

Figure E18 below is a typical grading curve for nominally single-sized 19mm. From the grading curve, a value of D_{50} = 15.7mm was obtained. The hydraulic conductivity is calculated from Figure E19. Table E31 summaries the parameters when obtaining the hydraulic conductivity k value.

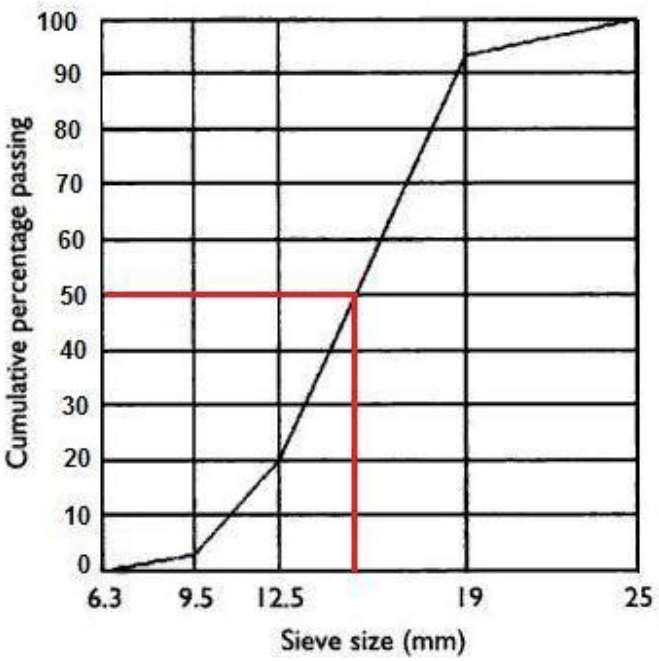

Figure E18: Grading curve for nominally single-sized 19mm Stone (Alexander & Mindess, 2005)

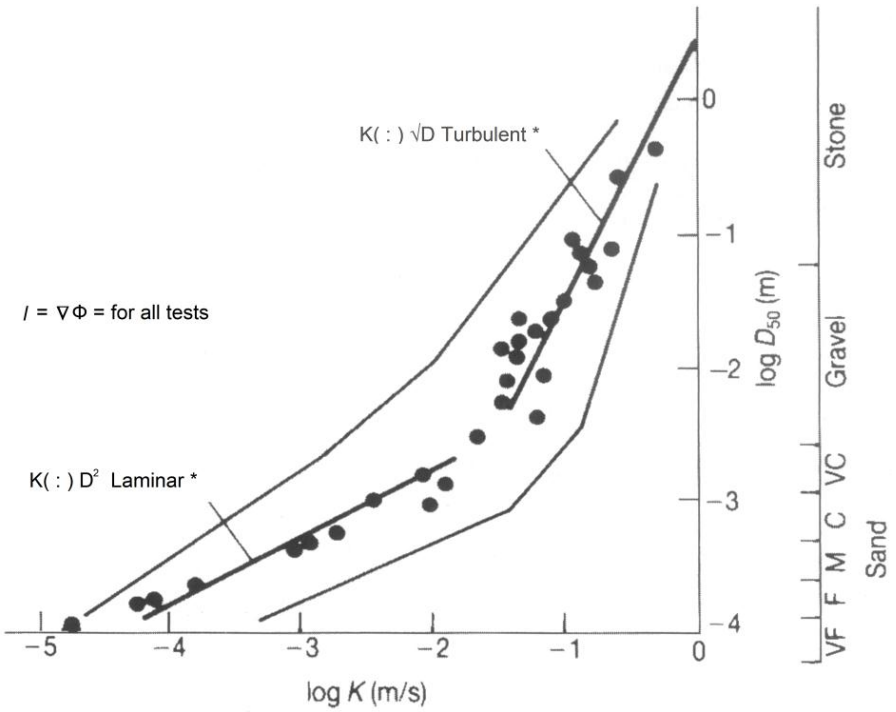

Figure E19: Permeability versus grain or stone sieve size (CIRIA, CUR, CETMEF,2007)

Table E39: Calculation of Permeability for19mm Bedding of seawater Intake (WST)

Description	Unit	Bedding
D_{n50}	m	0.0157
Log (D_{50})	m	-1.80
Log *k* (from fig. 2.39)	m/s	-1.16
k	m/s	0.069

Using the values from Table E38 and E39, headloss for Segment 1 was calculated in the following manner. With the flow through each segment know, it is possible to determine the headloss if the areas through which water flows is uniform.

However, this is not the case. Hence each segment has been split into three equal portions. Table E40 below, describes the manner in which Segment 1 is split into three sub segments. Thereafter, Table E41 determines the average velocity for each sub segment, the associated headloss and finally the cumulative headloss for Segment 1. The following tables describe the headloss calculated for Segments 1, 2, 3, 4 and 5.

Table E40: Segment 1: Averaging of Areas

Test No.	Len1	A11	A12	A13	A14	Qs 1	Ave A11	Ave A12	Ave A13
	m	m^2	m^2	m^2	m^2	m3/s	m^2	m^2	m^2
1	0.3618	0.221	0.196	0.170	0.145	3.E-05	0.208	0.183	0.158
2	0.3618	0.221	0.196	0.170	0.145	4.E-05	0.208	0.183	0.158
3	0.3618	0.221	0.196	0.170	0.145	5.E-05	0.208	0.183	0.158
4	0.3618	0.221	0.196	0.170	0.145	9.E-05	0.208	0.183	0.158
5	0.3618	0.221	0.196	0.170	0.145	2.E-04	0.208	0.183	0.158
6	0.3618	0.221	0.196	0.170	0.145	3.E-04	0.208	0.183	0.158
7	0.3618	0.221	0.196	0.170	0.145	4.E-04	0.208	0.183	0.158
8	0.3618	0.221	0.196	0.170	0.145	5.E-04	0.208	0.183	0.158
9	0.3618	0.221	0.196	0.170	0.145	6.E-04	0.208	0.183	0.158
10	0.3618	0.221	0.196	0.170	0.145	7.E-04	0.208	0.183	0.158
11	0.3618	0.221	0.196	0.170	0.145	9.E-04	0.208	0.183	0.158
12	0.3618	0.221	0.196	0.170	0.145	1.E-03	0.208	0.183	0.158
13	0.3618	0.221	0.196	0.170	0.145	1.E-03	0.208	0.183	0.158
14	0.3618	0.221	0.196	0.170	0.145	2.E-03	0.208	0.183	0.158
15	0.3618	0.221	0.196	0.170	0.145	2.E-03	0.208	0.183	0.158
16	0.3618	0.221	0.196	0.170	0.145	2.E-03	0.208	0.183	0.158
17	0.3618	0.221	0.196	0.170	0.145	2.E-03	0.208	0.183	0.158
18	0.3618	0.221	0.196	0.170	0.145	2.E-03	0.208	0.183	0.158

Table E41: Segment 1: Velocity and cumulative headloss

Test No.	Vel 1A	Vel 1B	Vel 1C	H_l11	H_l12	H_l13	$H_l1Total$	$H_l1Total$
	m/s	m/s	m/s	m	m	m	m	mm
1	2.E-04	2.E-04	2.E-04	0.0005	0.0006	0.0007	0.0018	1.77
2	2.E-04	2.E-04	2.E-04	0.0006	0.0006	0.0008	0.0020	1.97
3	2.E-04	3.E-04	3.E-04	0.0007	0.0008	0.0010	0.0025	2.51
4	5.E-04	5.E-04	6.E-04	0.0014	0.0016	0.0018	0.0048	4.79
5	8.E-04	9.E-04	1.E-03	0.0023	0.0026	0.0030	0.0080	7.96
6	1.E-03	2.E-03	2.E-03	0.0043	0.0049	0.0057	0.0149	14.91
7	2.E-03	2.E-03	2.E-03	0.0056	0.0064	0.0075	0.0195	19.53
8	2.E-03	3.E-03	3.E-03	0.0069	0.0079	0.0091	0.0239	23.86
9	3.E-03	3.E-03	4.E-03	0.0087	0.0099	0.0114	0.0299	29.94
10	3.E-03	4.E-03	5.E-03	0.0106	0.0121	0.0140	0.0368	36.80
11	4.E-03	5.E-03	6.E-03	0.0137	0.0156	0.0181	0.0473	47.34
12	5.E-03	6.E-03	7.E-03	0.0163	0.0185	0.0215	0.0564	56.37
13	7.E-03	8.E-03	9.E-03	0.0207	0.0236	0.0274	0.0717	71.71
14	8.E-03	9.E-03	1.E-02	0.0229	0.0261	0.0303	0.0793	79.30
15	8.E-03	9.E-03	1.E-02	0.0253	0.0288	0.0333	0.0874	87.38
16	9.E-03	1.E-02	1.E-02	0.0271	0.0309	0.0358	0.0938	93.78
17	9.E-03	1.E-02	1.E-02	0.0284	0.0323	0.0374	0.0981	98.10
18	1.E-02	1.E-02	1.E-02	0.0304	0.0345	0.0401	0.1050	104.96

Table E42: Segment 2: Averaging of Areas

Test No.	Len2	A21	A22	A23	A24	Qs 2	Ave A21	Ave A22	Ave A23
	m	m^2	m^2	m^2	m^2	m3/s	m^2	m^2	m^2
1	0.2814	0.172	0.163	0.154	0.145	3.E-05	0.167	0.158	0.150
2	0.2814	0.172	0.163	0.154	0.145	3.E-05	0.167	0.158	0.150
3	0.2814	0.172	0.163	0.154	0.145	4.E-05	0.167	0.158	0.150
4	0.2814	0.172	0.163	0.154	0.145	7.E-05	0.167	0.158	0.150
5	0.2814	0.172	0.163	0.154	0.145	1.E-04	0.167	0.158	0.150
6	0.2814	0.172	0.163	0.154	0.145	2.E-04	0.167	0.158	0.150
7	0.2814	0.172	0.163	0.154	0.145	3.E-04	0.167	0.158	0.150
8	0.2814	0.172	0.163	0.154	0.145	4.E-04	0.167	0.158	0.150
9	0.2814	0.172	0.163	0.154	0.145	5.E-04	0.167	0.158	0.150
10	0.2814	0.172	0.163	0.154	0.145	6.E-04	0.167	0.158	0.150
11	0.2814	0.172	0.163	0.154	0.145	7.E-04	0.167	0.158	0.150
12	0.2814	0.172	0.163	0.154	0.145	9.E-04	0.167	0.158	0.150
13	0.2814	0.172	0.163	0.154	0.145	1.E-03	0.167	0.158	0.150
14	0.2814	0.172	0.163	0.154	0.145	1.E-03	0.167	0.158	0.150
15	0.2814	0.172	0.163	0.154	0.145	1.E-03	0.167	0.158	0.150
16	0.2814	0.172	0.163	0.154	0.145	1.E-03	0.167	0.158	0.150
17	0.2814	0.172	0.163	0.154	0.145	2.E-03	0.167	0.158	0.150
18	0.2814	0.172	0.163	0.154	0.145	2.E-03	0.167	0.158	0.150

Table E43: Segment 2: Velocity and cumulative headloss

Test No.	Vel2A	Vel2B	Vel2C	H_l21	H_l22	H_l23	H_l2 Total	H_l2 Total
	m/s	m/s	m/s	m	m	m	m	mm
1	2.E-04	2.E-04	2.E-04	0.0005	0.0005	0.0006	0.0016	1.57
2	2.E-04	2.E-04	2.E-04	0.0006	0.0006	0.0006	0.0017	1.75
3	2.E-04	2.E-04	3.E-04	0.0007	0.0007	0.0008	0.0022	2.23
4	4.E-04	5.E-04	5.E-04	0.0013	0.0014	0.0015	0.0043	4.26
5	7.E-04	8.E-04	8.E-04	0.0022	0.0024	0.0025	0.0071	7.08
6	1.E-03	1.E-03	2.E-03	0.0042	0.0044	0.0047	0.0132	13.25
7	2.E-03	2.E-03	2.E-03	0.0055	0.0058	0.0061	0.0174	17.35
8	2.E-03	2.E-03	2.E-03	0.0067	0.0071	0.0075	0.0212	21.20
9	3.E-03	3.E-03	3.E-03	0.0084	0.0088	0.0094	0.0266	26.60
10	3.E-03	4.E-03	4.E-03	0.0103	0.0109	0.0115	0.0327	32.70
11	4.E-03	5.E-03	5.E-03	0.0133	0.0140	0.0148	0.0421	42.06
12	5.E-03	5.E-03	6.E-03	0.0158	0.0167	0.0176	0.0501	50.09
13	7.E-03	7.E-03	7.E-03	0.0201	0.0212	0.0224	0.0637	63.72
14	7.E-03	8.E-03	8.E-03	0.0222	0.0234	0.0248	0.0705	70.46
15	8.E-03	8.E-03	9.E-03	0.0245	0.0258	0.0274	0.0776	77.64
16	9.E-03	9.E-03	1.E-02	0.0263	0.0277	0.0294	0.0833	83.34
17	9.E-03	1.E-02	1.E-02	0.0275	0.0290	0.0307	0.0872	87.17
18	1.E-02	1.E-02	1.E-02	0.0294	0.0310	0.0329	0.0933	93.27

Table E44: Segment 3: Averaging of Areas

Test No.	Len3	A31	A32	A33	A34	Qs 3	Ave A31	Ave A32	Ave A33
	m	m^2	m^2	m^2	m^2	m3/s	m^2	m^2	m^2
1	0.201	0.123	0.130	0.138	0.145	2.E-05	0.126	0.134	0.141
2	0.201	0.123	0.130	0.138	0.145	2.E-05	0.126	0.134	0.141
3	0.201	0.123	0.130	0.138	0.145	3.E-05	0.126	0.134	0.141
4	0.201	0.123	0.130	0.138	0.145	5.E-05	0.126	0.134	0.141
5	0.201	0.123	0.130	0.138	0.145	9.E-05	0.126	0.134	0.141
6	0.201	0.123	0.130	0.138	0.145	2.E-04	0.126	0.134	0.141
7	0.201	0.123	0.130	0.138	0.145	2.E-04	0.126	0.134	0.141
8	0.201	0.123	0.130	0.138	0.145	3.E-04	0.126	0.134	0.141
9	0.201	0.123	0.130	0.138	0.145	3.E-04	0.126	0.134	0.141
10	0.201	0.123	0.130	0.138	0.145	4.E-04	0.126	0.134	0.141
11	0.201	0.123	0.130	0.138	0.145	5.E-04	0.126	0.134	0.141
12	0.201	0.123	0.130	0.138	0.145	6.E-04	0.126	0.134	0.141
13	0.201	0.123	0.130	0.138	0.145	8.E-04	0.126	0.134	0.141
14	0.201	0.123	0.130	0.138	0.145	9.E-04	0.126	0.134	0.141
15	0.201	0.123	0.130	0.138	0.145	1.E-03	0.126	0.134	0.141
16	0.201	0.123	0.130	0.138	0.145	1.E-03	0.126	0.134	0.141
17	0.201	0.123	0.130	0.138	0.145	1.E-03	0.126	0.134	0.141
18	0.201	0.123	0.130	0.138	0.145	1.E-03	0.126	0.134	0.141

Table E45: Segment 3: Velocity and cumulative headloss

Test No.	Vel3A	Vel3B	Vel3C	H_l31	H_l32	H_l33	H_l3Total	H_l3Total
	m/s	m/s	m/s	m	m	m	m	mm
1	2.E-04	1.E-04	1.E-04	0.0005	0.0004	0.0004	0.0013	1.33
2	2.E-04	2.E-04	2.E-04	0.0005	0.0005	0.0005	0.0015	1.48
3	2.E-04	2.E-04	2.E-04	0.0007	0.0006	0.0006	0.0019	1.89
4	4.E-04	4.E-04	4.E-04	0.0013	0.0012	0.0011	0.0036	3.60
5	7.E-04	7.E-04	6.E-04	0.0021	0.0020	0.0019	0.0060	5.98
6	1.E-03	1.E-03	1.E-03	0.0039	0.0037	0.0035	0.0112	11.19
7	2.E-03	2.E-03	2.E-03	0.0052	0.0049	0.0046	0.0147	14.67
8	2.E-03	2.E-03	2.E-03	0.0063	0.0060	0.0056	0.0179	17.92
9	3.E-03	2.E-03	2.E-03	0.0079	0.0075	0.0071	0.0225	22.48
10	3.E-03	3.E-03	3.E-03	0.0097	0.0092	0.0087	0.0276	27.64
11	4.E-03	4.E-03	4.E-03	0.0125	0.0118	0.0112	0.0356	35.55
12	5.E-03	5.E-03	4.E-03	0.0149	0.0141	0.0133	0.0423	42.33
13	6.E-03	6.E-03	6.E-03	0.0190	0.0179	0.0170	0.0539	53.85
14	7.E-03	7.E-03	6.E-03	0.0210	0.0198	0.0188	0.0596	59.55
15	8.E-03	7.E-03	7.E-03	0.0231	0.0218	0.0207	0.0656	65.62
16	8.E-03	8.E-03	7.E-03	0.0248	0.0234	0.0222	0.0704	70.43
17	9.E-03	8.E-03	8.E-03	0.0260	0.0245	0.0232	0.0737	73.67
18	9.E-03	9.E-03	8.E-03	0.0278	0.0262	0.0248	0.0788	78.82

Table E46: Segment 4: Averaging of Areas

Test No.	Len4	A41	A42	A43	A44	Qs 4	Ave A41	Ave A42	Ave A43
	m	m^2	m^2	m^2	m^2	m3/s	m^2	m^2	m^2
1	0.1206	0.074	0.097	0.121	0.145	1.E-05	0.085	0.109	0.133
2	0.1206	0.074	0.097	0.121	0.145	1.E-05	0.085	0.109	0.133
3	0.1206	0.074	0.097	0.121	0.145	2.E-05	0.085	0.109	0.133
4	0.1206	0.074	0.097	0.121	0.145	3.E-05	0.085	0.109	0.133
5	0.1206	0.074	0.097	0.121	0.145	5.E-05	0.085	0.109	0.133
6	0.1206	0.074	0.097	0.121	0.145	1.E-04	0.085	0.109	0.133
7	0.1206	0.074	0.097	0.121	0.145	1.E-04	0.085	0.109	0.133
8	0.1206	0.074	0.097	0.121	0.145	2.E-04	0.085	0.109	0.133
9	0.1206	0.074	0.097	0.121	0.145	2.E-04	0.085	0.109	0.133
10	0.1206	0.074	0.097	0.121	0.145	2.E-04	0.085	0.109	0.133
11	0.1206	0.074	0.097	0.121	0.145	3.E-04	0.085	0.109	0.133
12	0.1206	0.074	0.097	0.121	0.145	4.E-04	0.085	0.109	0.133
13	0.1206	0.074	0.097	0.121	0.145	5.E-04	0.085	0.109	0.133
14	0.1206	0.074	0.097	0.121	0.145	5.E-04	0.085	0.109	0.133
15	0.1206	0.074	0.097	0.121	0.145	6.E-04	0.085	0.109	0.133
16	0.1206	0.074	0.097	0.121	0.145	6.E-04	0.085	0.109	0.133
17	0.1206	0.074	0.097	0.121	0.145	6.E-04	0.085	0.109	0.133
18	0.1206	0.074	0.097	0.121	0.145	7.E-04	0.085	0.109	0.133

Table E47: Segment 4: Velocity and cumulative headloss

Test No.	Vel4A	Vel4B	Vel4C	H_l41	H_l42	H_l43	H_l4 Total	H_l4 Total
	m/s	m/s	m/s	m	m	m	m	mm
1	1.E-04	1.E-04	9.E-05	0.0004	0.0003	0.0003	0.0010	1.00
2	2.E-04	1.E-04	1.E-04	0.0005	0.0004	0.0003	0.0011	1.12
3	2.E-04	2.E-04	1.E-04	0.0006	0.0005	0.0004	0.0014	1.43
4	4.E-04	3.E-04	2.E-04	0.0011	0.0009	0.0007	0.0027	2.72
5	6.E-04	5.E-04	4.E-04	0.0019	0.0015	0.0012	0.0045	4.53
6	1.E-03	9.E-04	7.E-04	0.0035	0.0027	0.0022	0.0085	8.48
7	2.E-03	1.E-03	1.E-03	0.0046	0.0036	0.0029	0.0111	11.11
8	2.E-03	1.E-03	1.E-03	0.0056	0.0044	0.0036	0.0136	13.57
9	2.E-03	2.E-03	1.E-03	0.0070	0.0055	0.0045	0.0170	17.03
10	3.E-03	2.E-03	2.E-03	0.0086	0.0068	0.0055	0.0209	20.93
11	4.E-03	3.E-03	2.E-03	0.0111	0.0087	0.0071	0.0269	26.93
12	4.E-03	3.E-03	3.E-03	0.0132	0.0103	0.0085	0.0321	32.06
13	6.E-03	4.E-03	4.E-03	0.0168	0.0132	0.0108	0.0408	40.79
14	6.E-03	5.E-03	4.E-03	0.0186	0.0146	0.0119	0.0451	45.11
15	7.E-03	5.E-03	4.E-03	0.0205	0.0160	0.0132	0.0497	49.70
16	7.E-03	6.E-03	5.E-03	0.0220	0.0172	0.0141	0.0533	53.35
17	8.E-03	6.E-03	5.E-03	0.0230	0.0180	0.0148	0.0558	55.80
18	8.E-03	6.E-03	5.E-03	0.0246	0.0193	0.0158	0.0597	59.70

Table E48: Segment 5: Averaging of Areas

Test No.	Len5	A51	A52	A53	A54	Qs 5	Ave A51	Ave A52	Ave A53
	m	m^2	m^2	m^2	m^2	m3/s	m^2	m^2	m^2
1	0.0402	0.025	0.065	0.105	0.145	4.E-06	0.045	0.085	0.125
2	0.0402	0.025	0.065	0.105	0.145	4.E-06	0.045	0.085	0.125
3	0.0402	0.025	0.065	0.105	0.145	6.E-06	0.045	0.085	0.125
4	0.0402	0.025	0.065	0.105	0.145	1.E-05	0.045	0.085	0.125
5	0.0402	0.025	0.065	0.105	0.145	2.E-05	0.045	0.085	0.125
6	0.0402	0.025	0.065	0.105	0.145	3.E-05	0.045	0.085	0.125
7	0.0402	0.025	0.065	0.105	0.145	4.E-05	0.045	0.085	0.125
8	0.0402	0.025	0.065	0.105	0.145	5.E-05	0.045	0.085	0.125
9	0.0402	0.025	0.065	0.105	0.145	7.E-05	0.045	0.085	0.125
10	0.0402	0.025	0.065	0.105	0.145	8.E-05	0.045	0.085	0.125
11	0.0402	0.025	0.065	0.105	0.145	1.E-04	0.045	0.085	0.125
12	0.0402	0.025	0.065	0.105	0.145	1.E-04	0.045	0.085	0.125
13	0.0402	0.025	0.065	0.105	0.145	2.E-04	0.045	0.085	0.125
14	0.0402	0.025	0.065	0.105	0.145	2.E-04	0.045	0.085	0.125
15	0.0402	0.025	0.065	0.105	0.145	2.E-04	0.045	0.085	0.125
16	0.0402	0.025	0.065	0.105	0.145	2.E-04	0.045	0.085	0.125
17	0.0402	0.025	0.065	0.105	0.145	2.E-04	0.045	0.085	0.125
18	0.0402	0.025	0.065	0.105	0.145	2.E-04	0.045	0.085	0.125

Table E49: Segment 5: Velocity and cumulative headloss

Test No.	Vel5A	Vel5B	Vel5C	H_l51	H_l52	H_l53	$H_l5Total$	$H_l5Total$
	m/s	m/s	m/s	m	m	m	m	mm
1	9.E-05	5.E-05	3.E-05	0.0003	0.0001	0.0001	0.0005	0.50
2	1.E-04	5.E-05	3.E-05	0.0003	0.0002	0.0001	0.0006	0.55
3	1.E-04	7.E-05	4.E-05	0.0004	0.0002	0.0001	0.0007	0.71
4	2.E-04	1.E-04	8.E-05	0.0007	0.0004	0.0003	0.0014	1.35
5	4.E-04	2.E-04	1.E-04	0.0012	0.0006	0.0004	0.0022	2.25
6	7.E-04	4.E-04	3.E-04	0.0022	0.0012	0.0008	0.0042	4.21
7	1.E-03	5.E-04	3.E-04	0.0029	0.0015	0.0010	0.0055	5.51
8	1.E-03	6.E-04	4.E-04	0.0036	0.0019	0.0013	0.0067	6.73
9	1.E-03	8.E-04	5.E-04	0.0045	0.0024	0.0016	0.0085	8.45
10	2.E-03	1.E-03	6.E-04	0.0055	0.0029	0.0020	0.0104	10.39
11	2.E-03	1.E-03	8.E-04	0.0071	0.0037	0.0025	0.0134	13.36
12	3.E-03	1.E-03	1.E-03	0.0085	0.0044	0.0030	0.0159	15.91
13	4.E-03	2.E-03	1.E-03	0.0108	0.0057	0.0038	0.0202	20.24
14	4.E-03	2.E-03	1.E-03	0.0119	0.0063	0.0042	0.0224	22.38
15	4.E-03	2.E-03	2.E-03	0.0131	0.0069	0.0047	0.0247	24.66
16	5.E-03	2.E-03	2.E-03	0.0141	0.0074	0.0050	0.0265	26.47
17	5.E-03	3.E-03	2.E-03	0.0147	0.0077	0.0052	0.0277	27.69
18	5.E-03	3.E-03	2.E-03	0.0157	0.0083	0.0056	0.0296	29.63

Table 50: Summary of Method 3 Headloss Tests. Results from Tables 40 to 49 (WST)

Test No.	Total Q	Segment 1	Segment 2	Segment 3	Segment 4	Segment 5
	l/s	mm	mm	mm	mm	mm
1	0.10	1.77	1.57	1.33	1.00	0.50
2	0.11	1.97	1.75	1.48	1.12	0.55
3	0.14	2.51	2.23	1.89	1.43	0.71
4	0.26	4.79	4.26	3.60	2.72	1.35
5	0.44	7.96	7.08	5.98	4.53	2.25
6	0.82	14.91	13.25	11.19	8.48	4.21
7	1.07	19.53	17.35	14.67	11.11	5.51
8	1.31	23.86	21.20	17.92	13.57	6.73
9	1.64	29.94	26.60	22.48	17.03	8.45
10	2.02	36.80	32.70	27.64	20.93	10.39
11	2.60	47.34	42.06	35.55	26.93	13.36
12	3.10	56.37	50.09	42.33	32.06	15.91
13	3.94	71.71	63.72	53.85	40.79	20.24
14	4.36	79.30	70.46	59.55	45.11	22.38
15	4.80	87.38	77.64	65.62	49.70	24.66
16	5.15	93.78	83.34	70.43	53.35	26.47
17	5.39	98.10	87.17	73.67	55.80	27.69
18	5.77	104.96	93.27	78.82	59.70	29.63

Figure E20 plots Table E50 graphically. A trendline is added to the results in order to predict the headloss, due to stone bedding. This occursat the most downstream point of WC1. It is at this point that the largest magnitude of headloss occurs. Table E51 summaries these results.

Table E51: Summary of Method 3: maximum headloss versus flow rates (WST)

Test No.	Total Q	Total 2Q	Maximum Headloss due to Stone Bedding
	l/s	l/s	mm
1	0.10	0.19	1.795
2	0.11	0.22	1.999
3	0.14	0.28	2.554
4	0.26	0.53	4.87
5	0.44	0.87	8.098
6	0.82	1.64	15.16
7	1.07	2.15	19.86
8	1.31	2.62	24.26
9	1.65	3.29	30.45
10	2.02	4.04	37.42
11	2.60	5.20	48.14
12	3.10	6.19	57.32
13	3.94	7.88	72.93
14	4.36	8.71	80.65
15	4.80	9.60	88.87
16	5.15	10.31	95.38
17	5.39	10.78	99.77
18	5.77	11.53	106.75

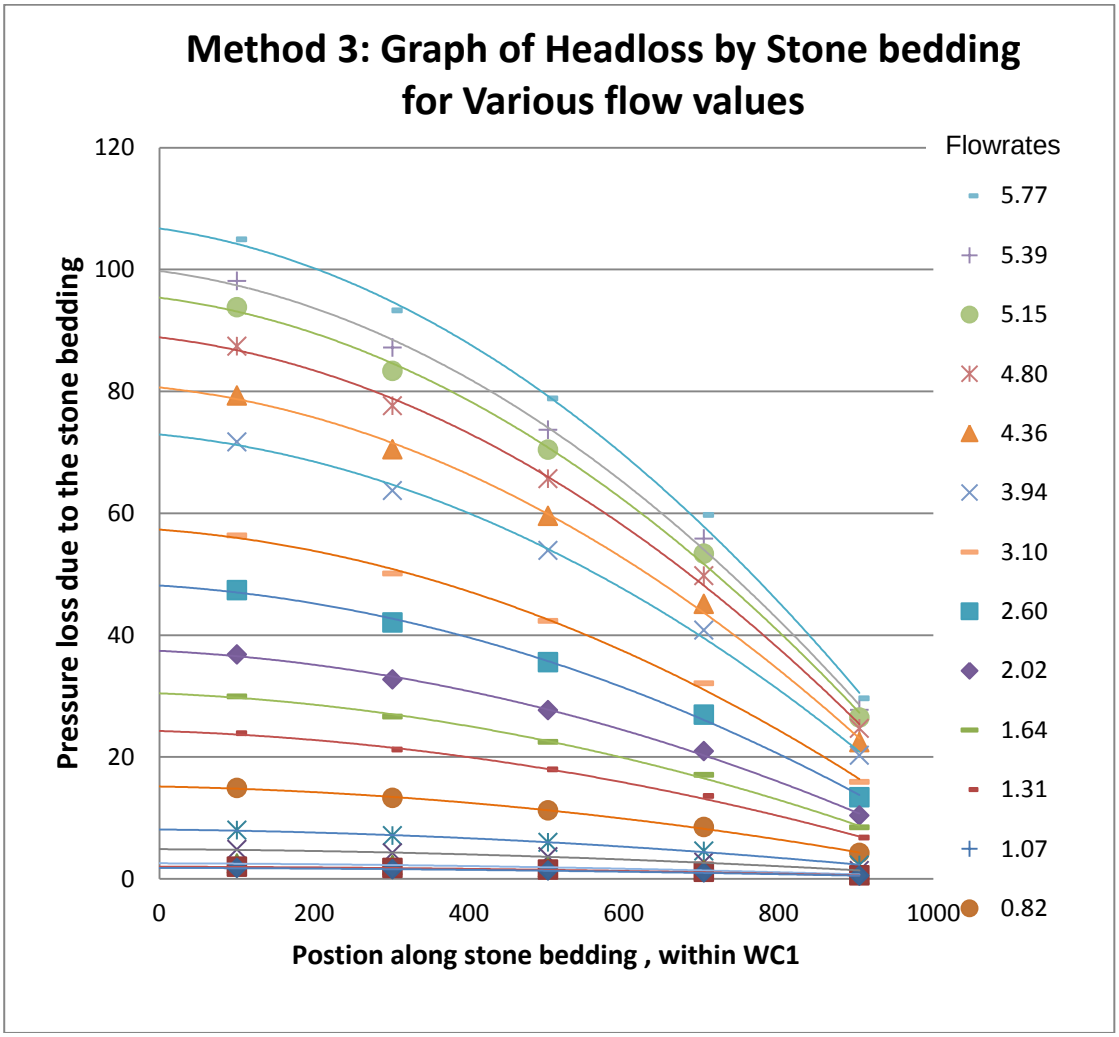

Figure E15: Method 3:Results of Headloss due to Stone Bedding, within WC1

E.6.4.3 Comparison of Results for Method 1, 2 and 3

The following Figure E21 shows the results for Method 1, 2 and 3 for the calculation of Headloss due to the stone bedding, Results for Method1, 2 and 3 are derived from TablesE23, E37 and E51.

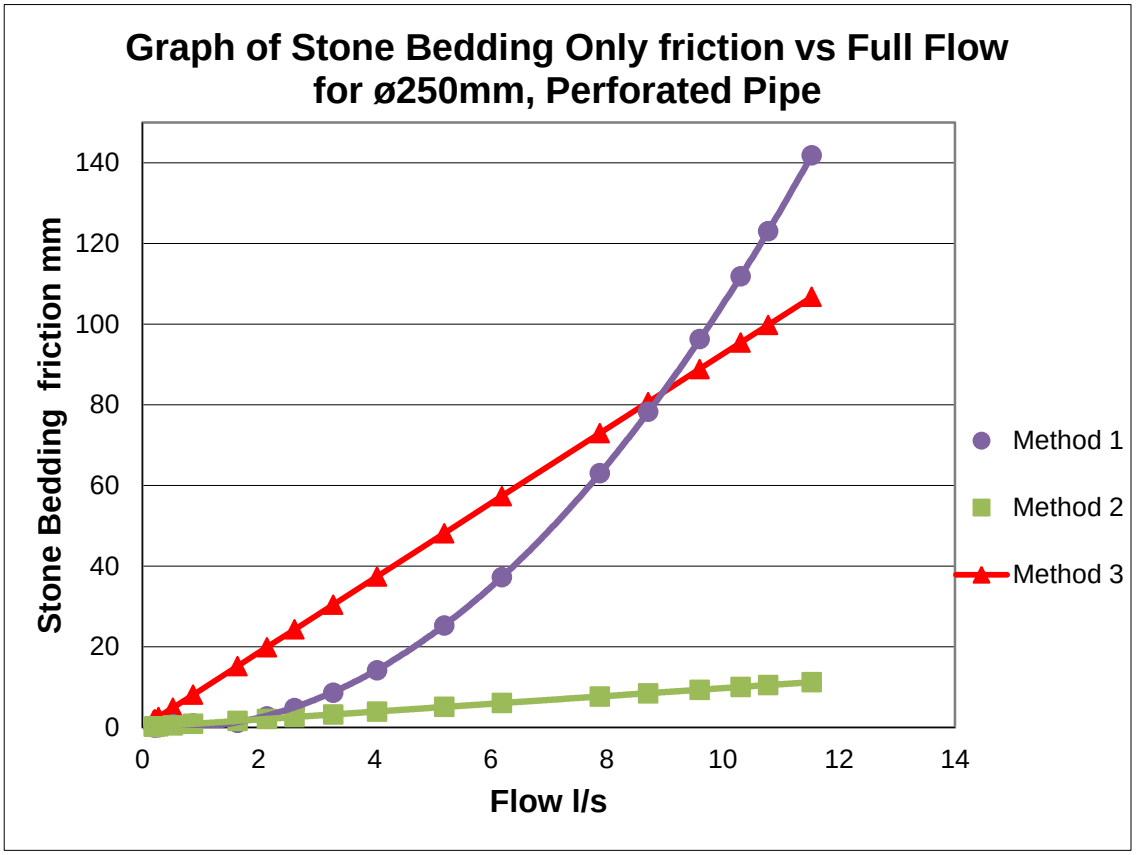

Figure E21: Method 1, 2 and 3: Headloss due to the stone bedding

E.7:Water, Sand and Stone Bedding Test

The following test is similar to the previous one and the addition of sand aims to create a worst case scenario where all voids are assumed to be filled to 100% with sand. Details for the sand can be found in Appendix C. The main aim is quantify the headloss due to the sand and stone bedding matrix that surround the intake pipe

The following explains the manner in which the Sand and Stone Bedding Test was conducted and uses tables and equations to illustrate the analysis process. Table E1 which can be found in previous chapters details the physical aspects of the model including the Intake pipeline.

Table E52 shows the initial results of the 7 tests that where conducted. The difference between WC1 and WC2 denotes the total headloss. The flow rate was determined from the following Equation: B1

$$Q = C_d \cdot \frac{8}{15} \cdot \sqrt{2g} \cdot \tan\frac{\theta}{2} \cdot h^{\frac{5}{2}} \qquad \text{Eqn B1}$$

where

Q= Flow (l/s)

C_d= 0.57

h = depth of water above V Notch (mm)

Table E52: Total Headloss and initial flow rate for Sand and Stone Bedding

Test No.	WC1	WC2	Upstream Head	Downstream Head	Total ∆hf	Q Half Pipe	Q Half Pipe
	mm	mm	mm	mm	mm	l/s	m3/s
1	1760	1735	51.5	26.5	25	0.15	0.000154
2	1855	1753	146.5	44.5	102	0.56	0.000563
3	1970	1767	261.5	58.5	203	1.11	0.001115
4	2070	1773	361.5	64.5	297	1.42	0.001423
5	2130	1778	421.5	69.5	352	1.71	0.001715
6	2235	1791	526.5	82.5	444	2.63	0.002632
7	2325	1797	616.5	88.5	528	3.14	0.003137

Water leakage is considered next. As per ChapterE3 theses losses are incorporated in Table E53. 80% of all leakage is estimated to emanate from WC1, 10% from WC 2a and 10% from WC2b.

E.7.1 Water Leakage losses

In Table E53, the total leakage rate is calculated in Column 6. Columns 7, 8 and 9 calculate the loss for WC1, WC2a and WC2b, respectively. The Total flow rate Q is calculated as the Initial flow rate plus the leakage from WC1 and WC2a

Table E53: Total headloss and flow rate incorporating losses

1	2	3	4	5	6	7	8	9	10
Test No.	Q Half Pipe	Bucket Ht	Time	Volume	Total	Loss due to WC1	Loss due to WC2a	Loss due to WC2b	Total Q
	l/s	mm	s	l	l/s	l/s	l/s	l/s	l/s
1	0.15	277	4911	73.07	0.015	0.011903	0.001488	0.001488	0.167
2	0.56	272	4902	71.62	0.015	0.011688	0.001461	0.001461	0.576
3	1.11	267	4857	70.17	0.014	0.011557	0.001445	0.001445	1.128
4	1.42	280	4907	73.95	0.015	0.012056	0.001507	0.001507	1.436
5	1.71	275	4934	72.49	0.015	0.011754	0.001469	0.001469	1.728
6	2.63	288	5187	76.29	0.015	0.011767	0.001471	0.001471	2.646
7	3.14	273	5002	71.91	0.014	0.011501	0.001438	0.001438	3.150

E.7.2 Pressure losses

After the correct total flow has been established, the next step is the disaggregation of pressure losses. This is done so that Loss A and the loss for sand and stone bedding, can be established. ChapterE2 states the Pressure Losses A to E with the relevant equations. Table E54 calculates the Losses B to E and hence the remaining total headloss will be Loss A plus the losses due to sand and stone bedding.

Table E54: Disaggregation of pressure losses

Test No.	Total Δhf	Total Q	Loss B+C	Loss D	Loss E	Loss A + sand + stone bedding	%A of Total Δhf
	mm	l/s	m	m	m	mm	
1	25	0.17	3.0.E-05	2.80E-06	2.27E-06	24.97	99.87%
2	102	0.58	3.6.E-04	3.74E-05	2.68E-05	101.61	99.62%
3	203	1.13	1.4.E-03	1.47E-04	1.03E-04	201.51	99.27%
4	297	1.44	2.2.E-03	2.39E-04	1.67E-04	294.59	99.19%
5	352	1.73	3.2.E-03	3.48E-04	2.42E-04	348.51	99.01%
6	444	2.65	7.6.E-03	8.19E-04	5.67E-04	435.82	98.16%
7	528	3.15	1.1.E-02	1.16E-03	8.04E-04	516.40	97.80%

E.7.3 Perforation losses and Flowrate Relationship

Table E55 shows relationship between Loss A + sand + stone bedding and the flowrate for half a pipe and for a full pipeline. Figure E22 plots the various flows rate and their corresponding pressure loss. There is a small scatter of data, Hence a strongly defined relationship between the Pressure loss and flowrate could be established.

Table E55: Loss A+ sand + stone bedding with corresponding flowrates

Test No.	Loss A + sand + stone bedding	Q Half Pipe	Q Full Pipe
	mm	l/s	l/s
1	24.97	0.167	0.33
2	101.61	0.576	1.15
3	201.51	1.128	2.26
4	294.59	1.436	2.87
5	348.51	1.728	3.46
6	435.82	2.646	5.29
7	516.40	3.150	6.30

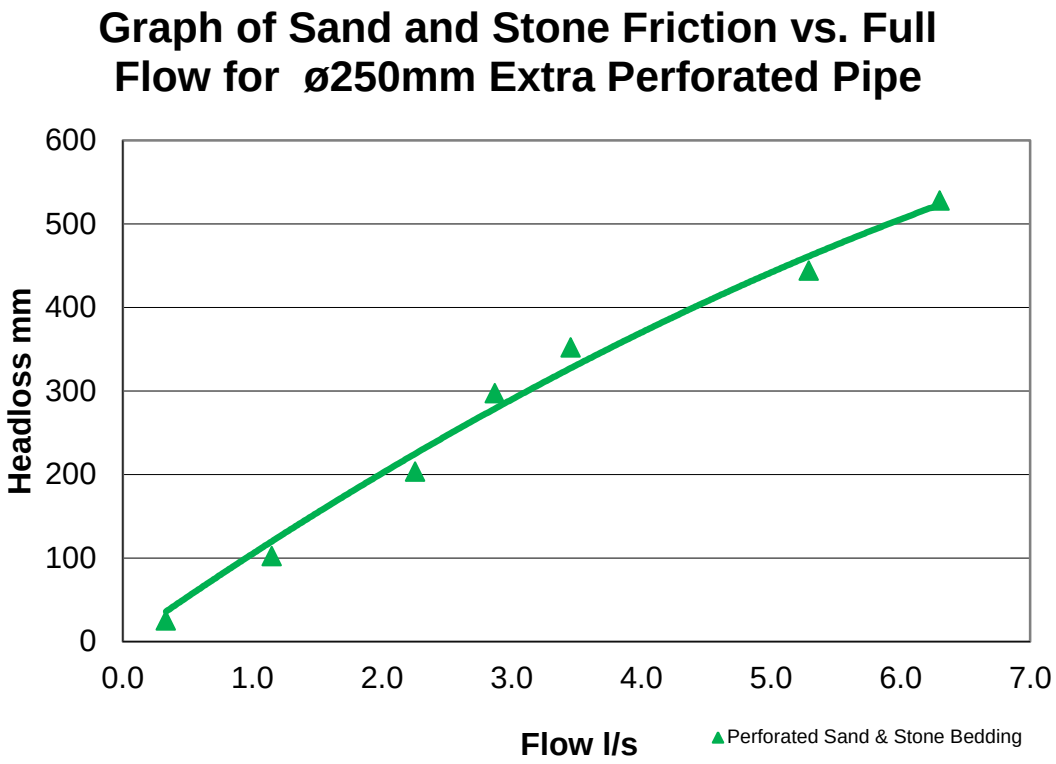

Figure E22: Plot of Pressure loss due to the slots, +sand + stone bedding flowrate for Full flowing ø250mm perforated pipe

The equation below describes the relationship between headloss due to perforation friction, sand and stone bedding and flowrate

$\Delta P = 4.214Q^2 + 108.9Q$ Eqn8

With

ΔP = Headloss due to slot friction in mm

Q = Flowrate for one full ø250mm pipeline in liters/second

E.7.4 Segmental Analysis of HPM

Analysing the Perforation friction + Stone Bedding and flow relationship initially, is as per chapter E5.4. The model is portioned into five segments. The flow was calculated at the same points in the HPM

As described by Table E54, the Perforation Loss A + Stone Bedding accounts for the vast majority of the pressure loss. Hence for a point on the Intake pipeline just inside WC1 (Pos 0), the velocity of the flow into the pipeline is at its maximum. The velocity at this point is termed V_{max}. The opposite holds true for a point at the start of the Intake pipeline. At this point, V_{min}, the velocity of the inflow is zero. Hence via **linear interpolation,** the velocity at any point in between both ends, can be calculated Figure E8 in chapter E6.4 above, describes the manner in which the HPM is segmented.

E.7.4.1 Methodology

In order to calculate the flow at various points within the model, the HPM was divided into five segments. The velocities V_{MAX}, V_1, V_2 , V_3, V_4 and V_{MIN} occur at the border of each segment, Hence for each segment, the Average Velocity, V_S1, V_S2, V_S3, V_S4 and V_S5 for each segment is easily calculated.

V_{MAX} is derived from Bernoulli principles where:

$$V = \sqrt{2g\Delta h} \qquad \text{Eqn E1}$$

With

V = Velocity in m/s

Δh = = is the driving pressure

g = gravitational constant (9.81m/s^2)

Note that the driving pressure Δh is Perforation Loss A+ Stone bedding. The flow from each segment is then calculated by multiplying the velocity with the perforation area

and a discharge coefficient, C_d. Table E56 shows the distribution of inflowing velocity over the length of the Intake Pipeline.

Equation E2 was used to calculate the flow from each segment. Table E57 contains the flowrate for each segment and the sum of flow from all segments of the pipeline.

$$Q_T = \sum q = \sum C_d A \sqrt{2g\Delta h} \qquad \text{Eqn E2}$$

With

q = Flowrate through for each segment in m^3/s

Q = Sum of Flowrate form each segment in m^3/s

A= The Area through which flow is allowed in m^2

C_d = Coefficient of Discharge

Table E56: Inflowing velocity of water flowing into the pipe, over the length of the Intake Pipeline

		Pos. 0	Pos. 1	Pos. 2	Pos. 3	Pos. 4	Pos. 5	Pos. 6	Pos. 7	Pos. 8	Pos. 9	Pos. 10
Test	Loss A , sand +Stone	Vmax	Vs 1	V1	Vs 2	V2	Vs 3	V3	Vs 4	V4	Vs 5	Vmin
	mm	m/s	m/s	m/s	m/s	m/s	m/s	m/s	m/s	m/s	m/s	m/s
1	25.0	0.700	0.630	0.560	0.490	0.420	0.350	0.280	0.210	0.140	0.070	0.000
2	101.6	1.412	1.271	1.130	0.988	0.847	0.706	0.565	0.424	0.282	0.141	0.000
3	201.5	1.988	1.790	1.591	1.392	1.193	0.994	0.795	0.597	0.398	0.199	0.000
4	294.6	2.404	2.164	1.923	1.683	1.442	1.202	0.962	0.721	0.481	0.240	0.000
5	348.5	2.615	2.353	2.092	1.830	1.569	1.307	1.046	0.784	0.523	0.261	0.000
6	435.8	2.924	2.632	2.339	2.047	1.755	1.462	1.170	0.877	0.585	0.292	0.000
7	516.4	3.183	2.865	2.546	2.228	1.910	1.592	1.273	0.955	0.637	0.318	0.000

Table E57: Calculated Flowrate from all segments of the Pipeline

1	2	3	4	5	6	7	8	9	10	11
Test	Loss A + Stone Bedding	C_b	Qs 1	Qs 2	Qs 3	Qs 4	Qs 5	Q Total	Q Total	2Q Total
0	mm		m^3/s	m^3/s	m^3/s	m^3/s	m^3/s	m^3/s	l/s	l/s
1	25.0	0.09	0.00006	0.00005	0.00003	0.00002	0.00001	0.00017	0.17	0.33
2	101.6	0.16	0.00021	0.00016	0.00012	0.00007	0.00002	0.00058	0.58	1.15
3	201.5	0.23	0.00041	0.00032	0.00023	0.00014	0.00005	0.00113	1.13	2.26
4	294.6	0.24	0.00052	0.00040	0.00029	0.00017	0.00006	0.00144	1.44	2.87
5	348.5	0.26	0.00062	0.00048	0.00035	0.00021	0.00007	0.00173	1.73	3.46
6	435.8	0.36	0.00095	0.00074	0.00053	0.00032	0.00011	0.00265	2.65	5.29
7	516.4	0.39	0.00113	0.00088	0.00063	0.00038	0.00013	0.00315	3.15	6.30

With incoming velocities calculated, the next step is the estimation of the pressure loss due to the above velocities. Equation E3 calculates the headloss along the intake pipeline using the following equation:

$$hf = Ke * \frac{V^2}{2g} \qquad \text{Eqn E3}$$

With

Ke = Loss Coefficient

V = Velocity in m/s

hf = Pressure loss

g = gravitational constant ($9.81 m/s^2$)

Table E58 below calculates the headloss along the intake pipeline using the above equation:

Table E58: Pressure losses over length of Intake Pipeline

		Pos. 0	Pos. 1	Pos. 2	Pos. 3	Pos. 4	Pos. 5	Pos. 6	Pos. 7	Pos. 8	Pos. 9	Pos. 10
Test	Total Losses	hf max	hf	hf	hf	hf	hf	hf	hf	hf	hf	hf
	mm	mm	mm	mm	mm	mm	mm	mm	mm	mm	mm	mm
1	24.97	24.9	20	16	12	9	6	4	2	1	0	0
2	101.61	101	82	65	50	37	25	16	9	4	1	0
3	201.51	201	163	129	99	73	50	32	18	8	2	0
4	294.59	294	239	189	144	106	74	47	27	12	3	0
5	348.51	348	282	223	171	125	87	56	31	14	3	0
6	435.82	435	353	279	214	157	109	70	39	17	4	0
7	516.40	516	418	330	253	186	129	83	46	21	5	0

Figure E23 below is a plot of EGLs at the centre of the Intake Pipeline. The EGL shows the amount of energy that has been lost from the sand and stone bedding friction and from water entering the Intake.

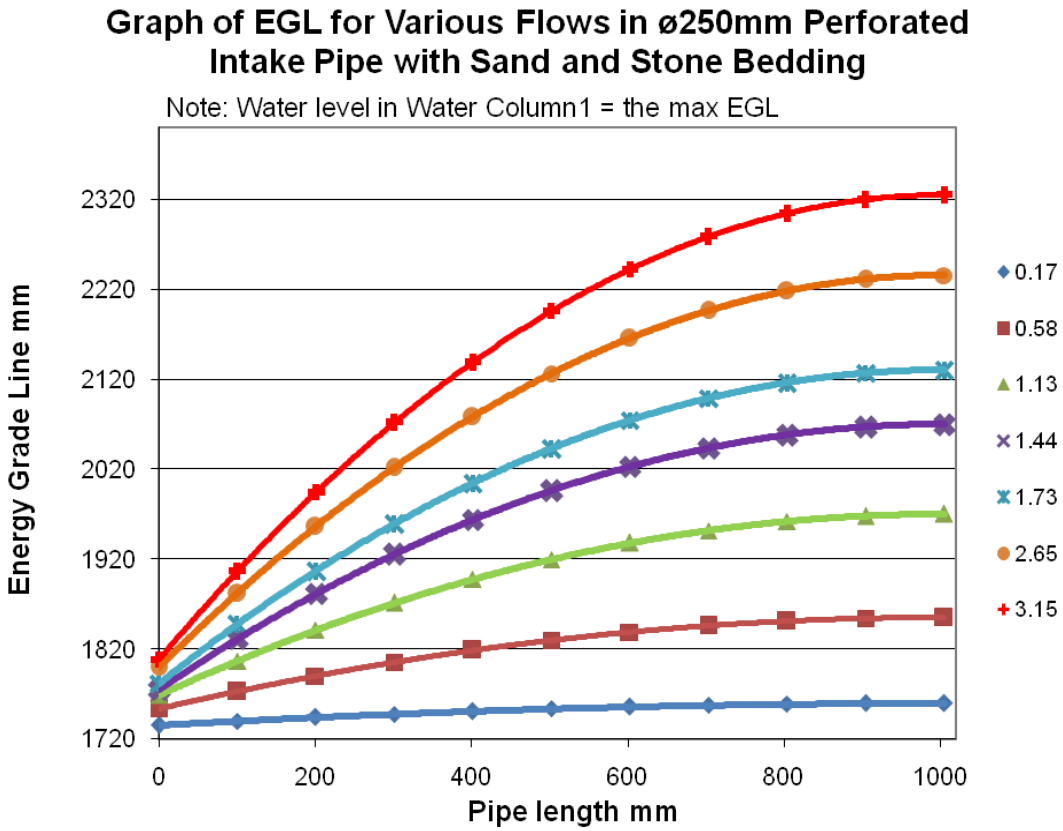

Figure E23: Plot of EGLs at the centre of the Intake Pipeline for Sand and Stone Bedding Test

For the 7 tests conducted, the increase in pressure losses closer to the exit point of WC1, is clearly visible. The calculation of the EGL at various points within the Intake pipeline is crucial as it aids in determining the loss due to the sand and stone bedding. This can be seen in the flowing chapter

E.7.4.2 Pressure loss due to Sand and Stone Bedding

Calculating the loss of pressure due to sand and stone bedding is critical as it influences the design of the seawater intake. Note that the stone bedding for all tests were standardised with the Intake pipe being 150mm above the bedrock, 300mm below the cover level of the stone bedding and 485mm from an adjacent intake pipeline. Three methods where employed when seeking to determine the pressure loss due the stone bedding. They are termed, Method 1, 2 and 3 are explained in further below.

E.7.4.2.1 Method 1: Simple method for determining sand and stone bedding loss

In this simplistic method, the equation for the “Water Test with Extra Perforation”: is removed from the equation for “Sand and Stone Test” This is simplified as Eqn 9 equals Eqn 8 minus Eqn 5 where:

$\Delta P = 4.214Q^2 + 108.9Q$ (Eqn8)

minus

$\Delta P = -0.891Q^2 + 1.286Q$ (Eqn5)

equals

$\Delta P = 5.105Q^2 + 107.614Q$ (Eqn9)

Table E59 below calculates the amount of headloss for notional flow values while Figure E24 plots these graphically.

Table E59: Method 1: ø250mm perforated pipe test: Pressure loss due to Stone Bedding only

Test No	Q Half Pipe	Q Full Pipe	Sand and Stone Bedding Friction
	l/s	l/s	mm
1	0.167	0.335	18
2	0.576	1.151	64
3	1.128	2.255	128
4	1.436	2.873	165
5	1.728	3.456	201
6	2.646	5.291	320
7	3.150	6.301	390

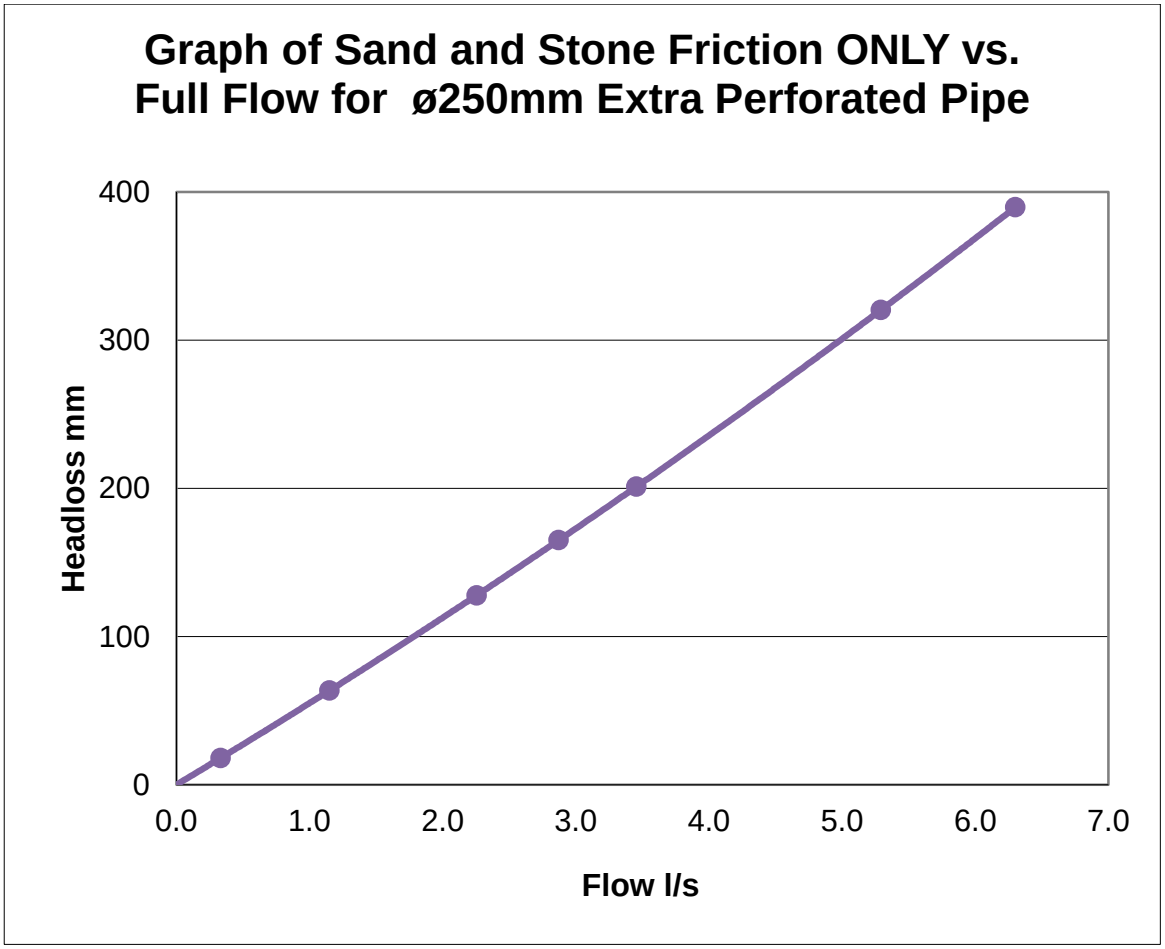

Figure E24: ø250mm Perforated pipe, Sand and Stone Bedding Test: Pressure loss due to sand and Stone Bedding ONLY

E.7.4.2.2 Method 2: Method for determining stone bedding loss : Hydraulic conductivity: Kenny, Lau and Ofoegbu

The second method used to determine the loss of pressure due to Stone bedding, looks at the hydraulic conductivity of the sand stone bedding. From Table E56, the velocity for each segment of the Intake pipeline was determined. However the stone bedding cannot be split into equal segments as well. This is only correct for stone bedding adjacent to the intake pipeline. It does not apply to the flat horizontal surface of the stone bedding.

Table E60:ø250mm Perforated pipe, Sand and Stone Bedding Test: Flow through segments

Test No.	Seg1	Seg2	Seg3	Seg4	Seg5	Seg1	Seg2	Seg3	Seg4	Seg5
	Qs 1	Qs 2	Qs 3	Qs 4	Qs 5	Qs 1	Qs 2	Qs 3	Qs 4	Qs 5
	m^3/s	m^3/s	m^3/s	m^3/s	m^3/s	m^3/s	m^3/s	m^3/s	m^3/s	m^3/s
1	0.00006	0.00005	0.00003	0.00002	0.00001	36%	28%	20%	12%	4%
2	0.00021	0.00016	0.00012	0.00007	0.00002	36%	28%	20%	12%	4%
3	0.00040	0.00031	0.00022	0.00013	0.00004	36%	28%	20%	12%	4%
4	0.00052	0.00040	0.00029	0.00017	0.00006	36%	28%	20%	12%	4%
5	0.00062	0.00048	0.00034	0.00021	0.00007	36%	28%	20%	12%	4%
6	0.00095	0.00074	0.00053	0.00032	0.00011	36%	28%	20%	12%	4%
7	0.00112	0.00087	0.00062	0.00037	0.00012	36%	28%	20%	12%	4%

Flow into the intake pipe line is proportional to the velocity. The maximum velocity occurs at one end of the intake pipeline and the minimum velocity occurs at the start of the intake pipeline. Table E60above looks at the ratio of the (flowrate) as a proportion of the entire flowrate.

Figure E16 provides a graphical description of how proportions were then applied to length of the stone bed. This splitting of the stone bedding surface ensured that all flows entering the stone bed were proportional to the flow entering the intake pipeline for all segments.

Figure E17 shows the simplified version of a single notional segment. Note line f_1, f_2 and f_3 as lines of reference in Figure E16 and E17. As in Figure E16, length (l_1) is multiplied by the standard width (With), to create the area A_1. Area A_4 was easily

calculated it is based on the intake pipe dimensions. Areas A_2 and A_3 are a third of the distance from each end and hence are calculated proportionately. The distances from Area A_1 to A_2 to A_3 to A_4 are noted as Lengths len_1, len_2 and len_3 respectively.

In order to calculate the pressure loss due to the stone bedding, the hydraulic conductivity is required. The pressure loss is defined as follows:

$$hf(m) = \frac{L * V}{k} \qquad \text{Eqn E4}$$

Where:

hf = pressure loss due to friction within stone bedding

L = Length of water path (m)

V = Flow velocity

k = Hydraulic conductivity

The first three variables are easily to calculate however determining the hydraulic conductivity k, requires further investigation.

The hydraulic conductivity is calculated using the following equation

$$k = \frac{\gamma_w}{\eta K} \qquad \text{Eqn E5}$$

Where:

k = Hydraulic conductivity

γ_W = Unit Weight of Water

η = Dynamic Viscosity of water

K = Absolute Hydraulic conductivity

The unit weight of water γ_W ,' and the dynamic viscosity of water η are fairly simple to calculate. However the Absolute Hydraulic conductivity K has to be calculated. It is calculated using the following equation:

$$K = C_u D_5^2 \qquad \text{Eqn E6}$$

Where:

K = Absolute Hydraulic conductivity

C_u = Coefficient of Uniformity. Varies between 0.05 to 1

D_5 = Dimension of aggregate that has a cumulative percentage passing of 5%

Figure E25 below is a typical grading curve for nominally single-sized 19mm. From the grading curve, a value of D_5 = 10mm was obtained. This was adequate for the previous Chapter E7.3. With the inclusion of sand, this would decrease D_5 significantly.

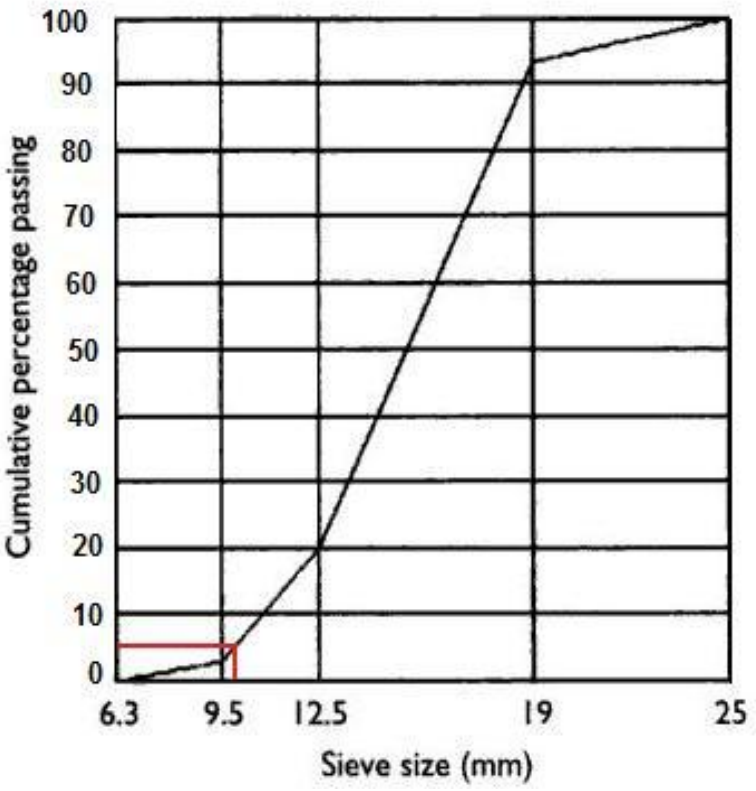

Figure E25: Typical grading curve for nominally single-sized 19mm Stone (Alexander & Mindess, 2005)

Referring to Figure C3 in Appendix C, the value of D_5 is approximately 0.2mm. From Figure E26 below, this translated to a k of 0.02cm/s or 0.2mm/s. Considering the tests within the HPM, a k value of 0.02 cm/sec is not reflective of the actual flow rates recorded.

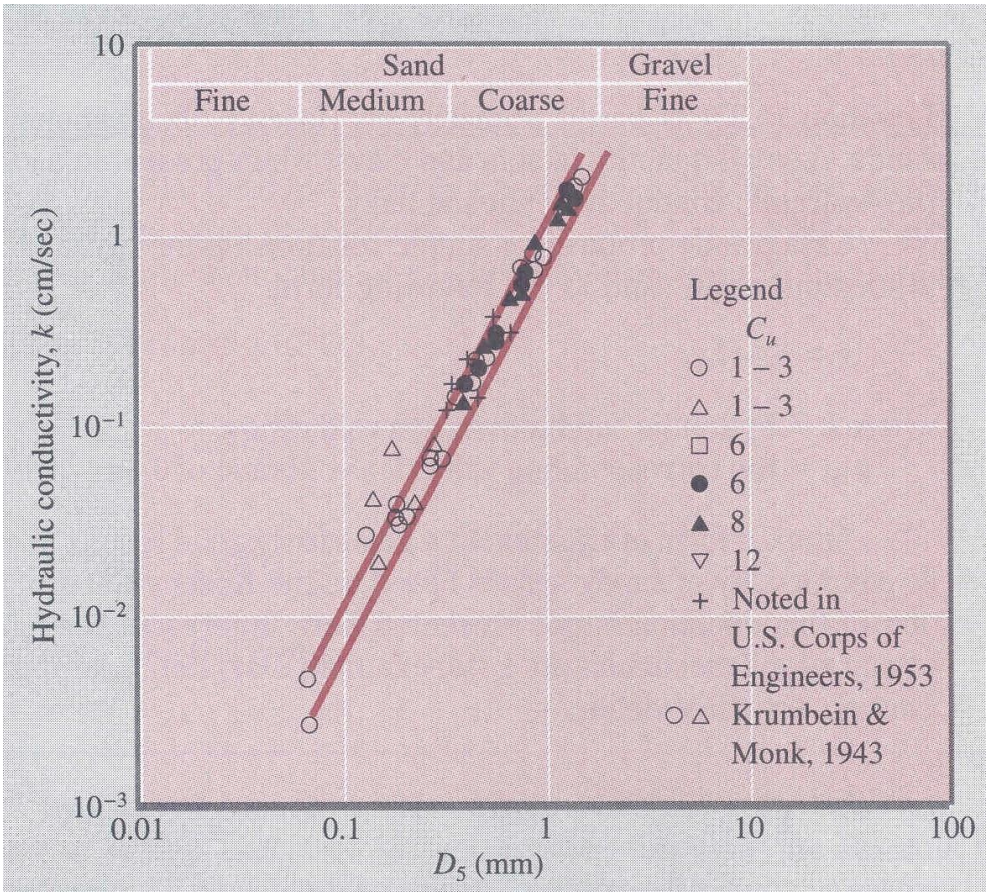

Figure E26: Graphical plot of Hydraulic conductivity Equation (Das 2000)

The best explanation for this can be attributed to the removal of sand from the bedding matrix, Figure 42. With the removal of the sand, the bedding matrix would revert close to its original contents of only 19mm Stone. Hence a $D_5$of 10mm will be used again.

Hence for a C_u of 0.8, Eqn E6 yields a K of 80mm^2. Utilising Eqn E5 and the following values:

γ_W = 9800 N/m^3

η = 0.00014 Ns/m

A hydraulic conductivity k of 0.688m/s was obtained. Table E61 summaries these results. Using a D_5 of 10mm, a k value of approximately 0.7m/s is found.

Table E61: Summary: Calculating the Hydraulic conductivity

Description	Value	Unit
C_u (0.05 to 1)	0.80	
D_5	10.0	mm
Water Column Width	0.61	m
Absolute Conductivity K	80	mm^2
Unit Weight of Water γ_W	9800	N/m^3
Dynamic Viscosity of water η	1.14E-03	Ns/m^2
Hydraulic Conductivity k	0.688	m/s

Using the values from Table E60 and E61, headloss for segment 1 was calculated in the following manner. With the flow through each segment know, it is possible to determine the headloss if the areas through which water flows is uniform.

However, this is not the case. Hence each segment has been split into three equal portions. Table E62 below, describes the manner in which Segment 1 is split into three sub segments. Thereafter, Table E63 determines the average velocity for each sub segment, the associated headloss and finally the cumulative headloss for Segment 1. The following tables describe the headloss calculated for Segments, 2, 3, 4 and 5.

Table E62: Segment 1: Averaging of Areas

Test No.	Len1	A11	A12	A13	A14	Qs 1	Ave A11	Ave A12	Ave A13
	m	m^2	m^2	m^2	m^2	m3/s	m^2	m^2	m^2
1	0.3618	0.221	0.196	0.170	0.145	0.00006	0.208	0.183	0.158
2	0.3618	0.221	0.196	0.170	0.145	0.00021	0.208	0.183	0.158
3	0.3618	0.221	0.196	0.170	0.145	0.00040	0.208	0.183	0.158
4	0.3618	0.221	0.196	0.170	0.145	0.00052	0.208	0.183	0.158
5	0.3618	0.221	0.196	0.170	0.145	0.00062	0.208	0.183	0.158
6	0.3618	0.221	0.196	0.170	0.145	0.00095	0.208	0.183	0.158
7	0.3618	0.221	0.196	0.170	0.145	0.00112	0.208	0.183	0.158

Table E63: Segment 1: Velocity and cumulative headloss

Test No.	Vel 1A	Vel 1B	Vel 1C	H_l11	H_l12	H_l13	H_l1Total	H_l1Total
	m/s	m/s	m/s	m	m	m	m	mm
1	0.0003	0.0003	0.0004	0.0001	0.0001	0.0001	0.0003	0.30
2	0.0010	0.0011	0.0013	0.0003	0.0003	0.0004	0.0011	1.05
3	0.0019	0.0022	0.0026	0.0006	0.0007	0.0008	0.0021	2.05
4	0.0025	0.0028	0.0033	0.0008	0.0009	0.0010	0.0026	2.61
5	0.0030	0.0034	0.0039	0.0009	0.0010	0.0012	0.0031	3.14
6	0.0045	0.0052	0.0060	0.0014	0.0016	0.0018	0.0048	4.80
7	0.0054	0.0061	0.0071	0.0016	0.0019	0.0022	0.0057	5.70

Table E64: Segment 2: Averaging of Areas

Test No.	Len2	A21	A22	A23	A24	Qs 2	Ave A21	Ave A22	Ave A23
	m	m^2	m^2	m^2	m^2	m3/s	m^2	m^2	m^2
1	0.2814	0.172	0.163	0.154	0.145	0.00005	0.167	0.158	0.150
2	0.2814	0.172	0.163	0.154	0.145	0.00016	0.167	0.158	0.150
3	0.2814	0.172	0.163	0.154	0.145	0.00031	0.167	0.158	0.150
4	0.2814	0.172	0.163	0.154	0.145	0.00040	0.167	0.158	0.150
5	0.2814	0.172	0.163	0.154	0.145	0.00048	0.167	0.158	0.150
6	0.2814	0.172	0.163	0.154	0.145	0.00074	0.167	0.158	0.150
7	0.2814	0.172	0.163	0.154	0.145	0.00087	0.167	0.158	0.150

Table E65: Segment 2: Velocity and cumulative headloss

Test No.	Vel 2A	Vel 2B	Vel 2C	H_l21	H_l22	H_l23	H_l2 Total	H_l2 Total
	m/s	m/s	m/s	m	m	m	m	mm
1	0.0003	0.0003	0.0003	0.0001	0.0001	0.0001	0.0003	0.27
2	0.0010	0.0010	0.0011	0.0003	0.0003	0.0003	0.0009	0.93
3	0.0019	0.0020	0.0021	0.0006	0.0006	0.0006	0.0018	1.82
4	0.0024	0.0025	0.0027	0.0007	0.0008	0.0008	0.0023	2.32
5	0.0029	0.0030	0.0032	0.0009	0.0009	0.0010	0.0028	2.79
6	0.0044	0.0046	0.0049	0.0013	0.0014	0.0015	0.0043	4.26
7	0.0052	0.0055	0.0058	0.0016	0.0017	0.0018	0.0051	5.07

Table E66: Segment 3: Averaging of Areas

Test No.	Len3	A31	A32	A33	A34	Qs 3	Ave A31	Ave A32	Ave A33
	m	m^2	m^2	m^2	m^2	m3/s	m^2	m^2	m^2
1	0.201	0.123	0.130	0.138	0.145	0.00003	0.126	0.134	0.141
2	0.201	0.123	0.130	0.138	0.145	0.00012	0.126	0.134	0.141
3	0.201	0.123	0.130	0.138	0.145	0.00022	0.126	0.134	0.141
4	0.201	0.123	0.130	0.138	0.145	0.00029	0.126	0.134	0.141
5	0.201	0.123	0.130	0.138	0.145	0.00034	0.126	0.134	0.141
6	0.201	0.123	0.130	0.138	0.145	0.00053	0.126	0.134	0.141
7	0.201	0.123	0.130	0.138	0.145	0.00062	0.126	0.134	0.141

Table E67: Segment 3: Velocity and cumulative headloss

Test No.	Vel 3A	Vel 3B	Vel 3C	H_l31	H_l32	H_l33	H_l3Total	H_l3Total
	m/s	m/s	m/s	m	m	m	m	mm
1	0.0003	0.0002	0.0002	0.0001	0.0001	0.0001	0.0002	0.23
2	0.0009	0.0009	0.0008	0.0003	0.0003	0.0002	0.0008	0.79
3	0.0018	0.0017	0.0016	0.0005	0.0005	0.0005	0.0015	1.54
4	0.0023	0.0021	0.0020	0.0007	0.0007	0.0006	0.0020	1.96
5	0.0027	0.0026	0.0024	0.0008	0.0008	0.0007	0.0024	2.36
6	0.0042	0.0039	0.0037	0.0013	0.0012	0.0011	0.0036	3.60
7	0.0049	0.0047	0.0044	0.0015	0.0014	0.0013	0.0043	4.28

Table E68: Segment 4: Averaging of Areas

Test No.	Len4	A41	A42	A43	A44	Qs 4	Ave A41	Ave A42	Ave A43
	m	m^2	m^2	m^2	m^2	m3/s	m^2	m^2	m^2
1	0.1206	0.074	0.097	0.121	0.145	0.00002	0.085	0.109	0.133
2	0.1206	0.074	0.097	0.121	0.145	0.00007	0.085	0.109	0.133
3	0.1206	0.074	0.097	0.121	0.145	0.00013	0.085	0.109	0.133
4	0.1206	0.074	0.097	0.121	0.145	0.00017	0.085	0.109	0.133
5	0.1206	0.074	0.097	0.121	0.145	0.00021	0.085	0.109	0.133
6	0.1206	0.074	0.097	0.121	0.145	0.00032	0.085	0.109	0.133
7	0.1206	0.074	0.097	0.121	0.145	0.00037	0.085	0.109	0.133

Table E69: Segment 4: Velocity and cumulative headloss

Test No.	Vel 4A	Vel 4B	Vel 4C	H_l41	H_l42	H_l43	H_l4 Total	H_l4 Total
	m/s	m/s	m/s	m	m	m	m	mm
1	0.0002	0.0002	0.0002	0.0001	0.0001	0.0000	0.0002	0.17
2	0.0008	0.0006	0.0005	0.0002	0.0002	0.0002	0.0006	0.60
3	0.0016	0.0012	0.0010	0.0005	0.0004	0.0003	0.0012	1.17
4	0.0020	0.0016	0.0013	0.0006	0.0005	0.0004	0.0015	1.49
5	0.0024	0.0019	0.0016	0.0007	0.0006	0.0005	0.0018	1.79
6	0.0037	0.0029	0.0024	0.0011	0.0009	0.0007	0.0027	2.73
7	0.0044	0.0034	0.0028	0.0013	0.0010	0.0009	0.0032	3.24

Table E70: Segment 5: Averaging of Areas

Test No.	Len5	A51	A52	A53	A54	Qs 5	Ave A51	Ave A52	Ave A53
	m	m^2	m^2	m^2	m^2	m3/s	m^2	m^2	m^2
1	0.0402	0.025	0.065	0.105	0.145	0.00001	0.045	0.085	0.125
2	0.0402	0.025	0.065	0.105	0.145	0.00002	0.045	0.085	0.125
3	0.0402	0.025	0.065	0.105	0.145	0.00004	0.045	0.085	0.125
4	0.0402	0.025	0.065	0.105	0.145	0.00006	0.045	0.085	0.125
5	0.0402	0.025	0.065	0.105	0.145	0.00007	0.045	0.085	0.125
6	0.0402	0.025	0.065	0.105	0.145	0.00011	0.045	0.085	0.125
7	0.0402	0.025	0.065	0.105	0.145	0.00012	0.045	0.085	0.125

Table E71: Segment 5: Velocity and cumulative headloss

Test No.	Vel 5A	Vel 5B	Vel 5C	H_l51	H_l52	H_l53	H_l5Total	H_l5Total
	m/s	m/s	m/s	m	m	m	m	mm
1	0.0001	0.0001	0.0001	0.0000	0.0000	0.0000	0.0001	0.09
2	0.0005	0.0003	0.0002	0.0002	0.0001	0.0001	0.0003	0.30
3	0.0010	0.0005	0.0004	0.0003	0.0002	0.0001	0.0006	0.58
4	0.0013	0.0007	0.0005	0.0004	0.0002	0.0001	0.0007	0.74
5	0.0015	0.0008	0.0006	0.0005	0.0002	0.0002	0.0009	0.89
6	0.0024	0.0012	0.0008	0.0007	0.0004	0.0003	0.0014	1.35
7	0.0028	0.0015	0.0010	0.0009	0.0004	0.0003	0.0016	1.61

Table E72: Summary of results for Tables 62 to 71

Test No.	Total Q	Segment 1	Segment 2	Segment 3	Segment 4	Segment 5
	l/s	mm	mm	mm	mm	mm
1	0.17	0.30	0.27	0.23	0.17	0.09
2	0.58	1.05	0.93	0.79	0.60	0.30
3	1.13	2.05	1.82	1.54	1.17	0.58
4	1.44	2.61	2.32	1.96	1.49	0.74
5	1.73	3.14	2.79	2.36	1.79	0.89
6	2.65	4.80	4.26	3.60	2.73	1.35
7	3.15	5.70	5.07	4.28	3.24	1.61
8	0.17	0.30	0.27	0.23	0.17	0.09

Figure E72 plots Table E27 graphically. A trendline is added to the results in order to predict the headloss, due to stone bedding, at the most downstream point of WC1. It is at this point that the largest magnitude of headloss occurs. Table E73 summaries these results.

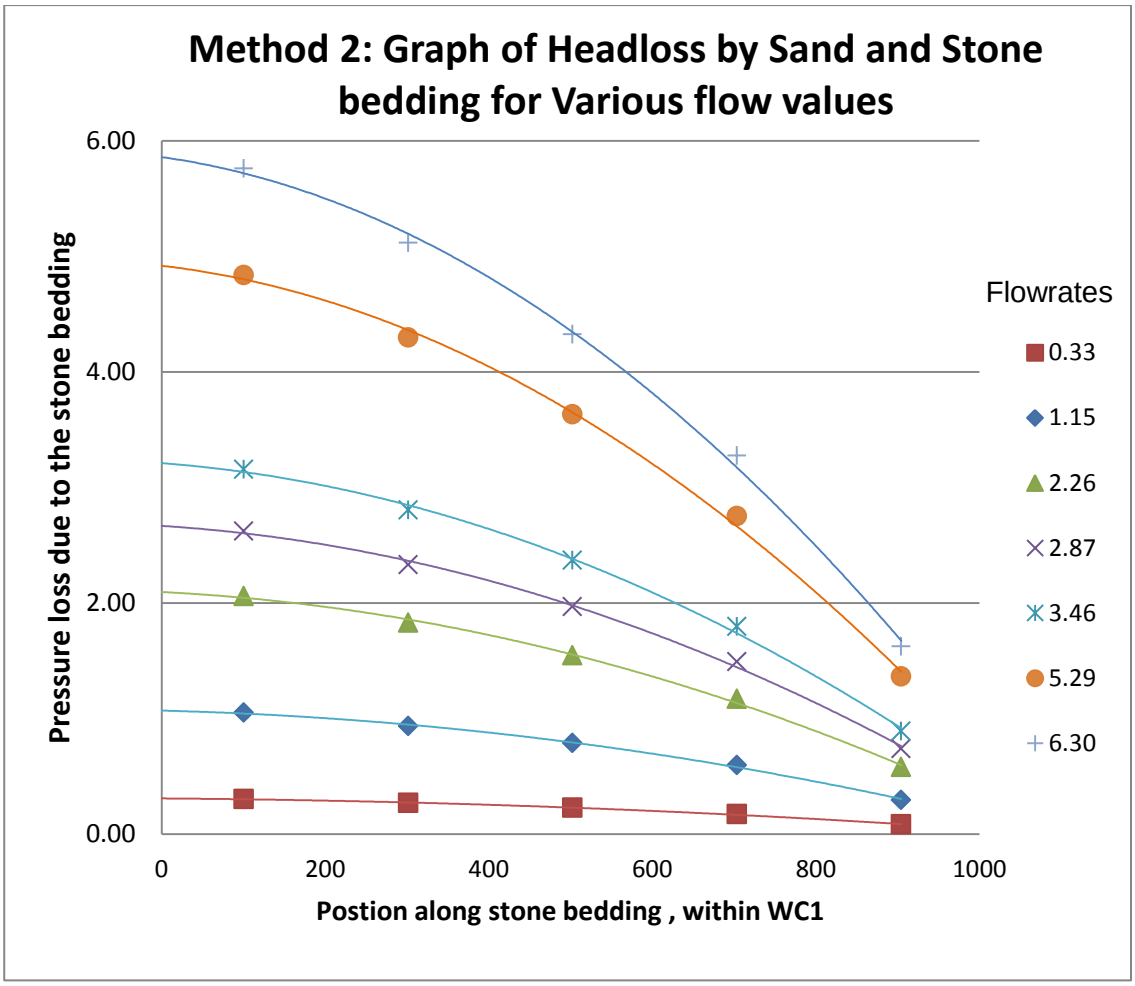

Figure E27: Method 2 :Results of Headloss due to (sand and) Stone Bedding, within WC1 (Legend: Flowrates)

Table E73: Method 2 : Summary of maximum headloss versus flow rates(WSST)

Test No.	Total Q	Total 2Q	Maximum Headloss due to Stone Bedding
	l/s	l/s	mm
1	0.17	0.33	0.31
2	0.58	1.15	1.069
3	1.13	2.26	2.095
4	1.44	2.87	2.668
5	1.73	3.46	3.21
6	2.65	5.29	4.918
7	3.15	6.30	5.858

The results of the above table will be represented with the results of Method 1 and 3 in section E.7.4.3

E.7.4.2.2 Method 3: Method for determining stone bedding loss : Hydraulic conductivity: Forchheimer

The third method used to determine the loss of pressure due to Stone bedding, also looks at the hydraulic conductivity of the stone bedding. This is based on work carried out by Forchheimer. From Table E56, the velocity for each segment of the Intake pipeline was determined. However, stone bedding cannot be split into equal segments as well. This is only correct for stone bedding adjacent to the intake pipeline. It does not apply to the flat horizontal surface of the stone bedding.

Flow into the intake pipe line is proportional to the velocity. The maximum velocity occurs at one end of the intake pipeline and the minimum velocity occurs at the start of the intake pipeline. Table E74 below looks at the ratio of the (flowrate) as a proportion of the entire flowrate.

In Figure E28, these proportions were then applied to length of the stone bed. This splitting of the stone bedding surface ensured that all flows entering the stone bed were proportional to the flow entering the intake pipeline for all segments.

Table E74:ø250mm Perforated pipe, Water and Stone Bedding Test: Flow through segments

Test No.	Seg1	Seg2	Seg3	Seg4	Seg5	Seg1	Seg2	Seg3	Seg4	Seg5
	Qs 1	Qs 2	Qs 3	Qs 4	Qs 5	Qs 1	Qs 2	Qs 3	Qs 4	Qs 5
	m^3/s	m^3/s	m^3/s	m^3/s	m^3/s	m^3/s	m^3/s	m^3/s	m^3/s	m^3/s
1	0.00006	0.00005	0.00003	0.00002	0.00001	36%	28%	20%	12%	4%
2	0.00021	0.00016	0.00012	0.00007	0.00002	36%	28%	20%	12%	4%
3	0.00040	0.00031	0.00022	0.00013	0.00004	36%	28%	20%	12%	4%
4	0.00052	0.00040	0.00029	0.00017	0.00006	36%	28%	20%	12%	4%
5	0.00062	0.00048	0.00034	0.00021	0.00007	36%	28%	20%	12%	4%
6	0.00095	0.00074	0.00053	0.00032	0.00011	36%	28%	20%	12%	4%
7	0.00112	0.00087	0.00062	0.00037	0.00012	36%	28%	20%	12%	4%

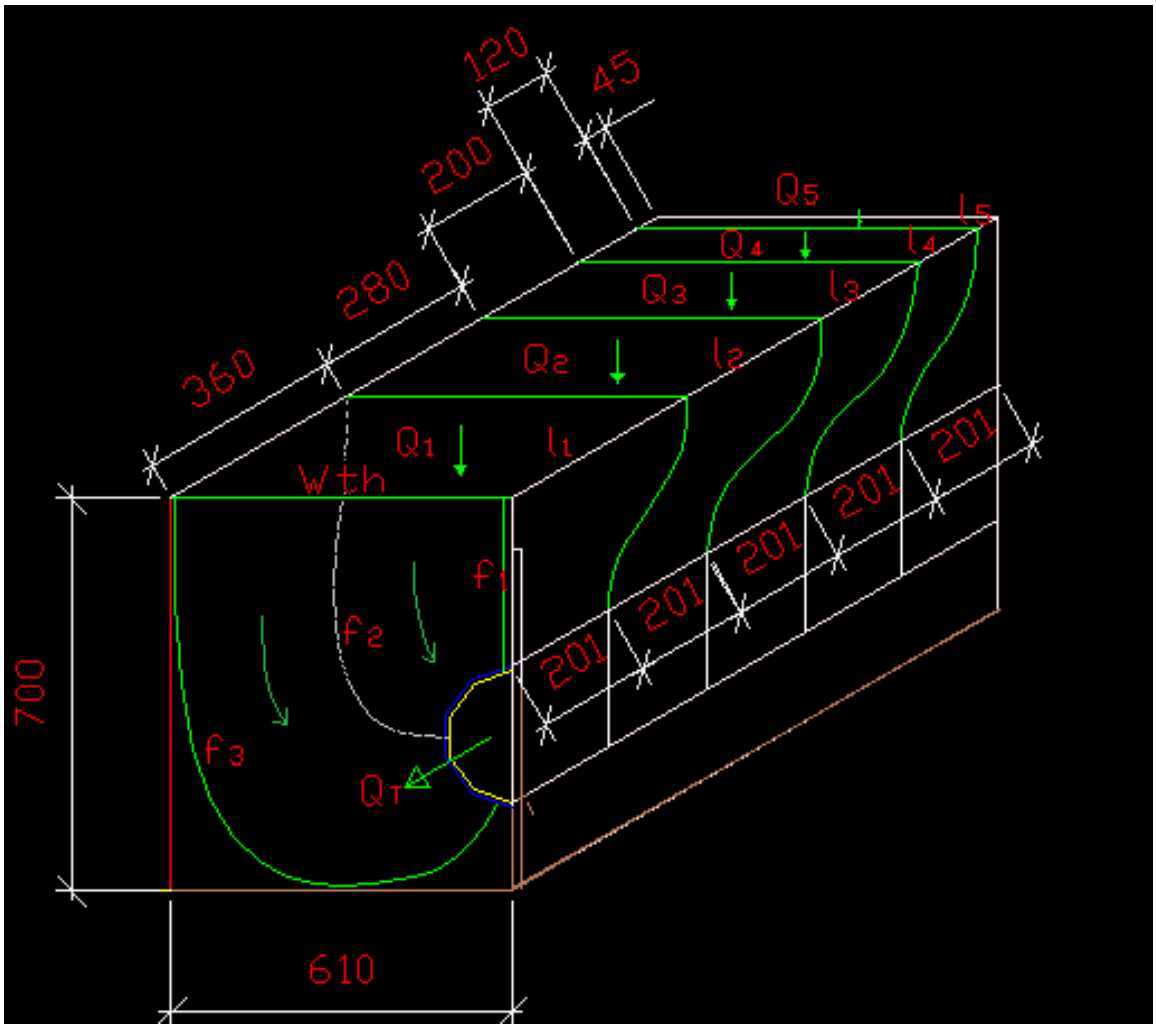

Figure E28: ø250mm Slotted pipe-Water and Stone Bedding Test: Segmentation of Stone Bedding area

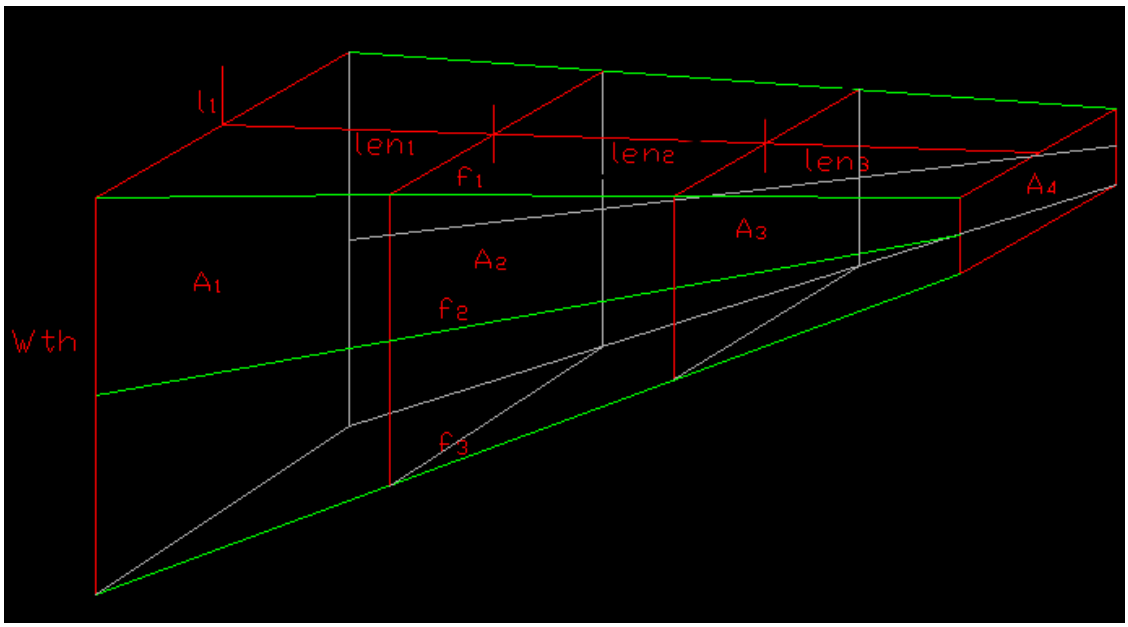

Figure E29: Notional flow path of a stone bedding segment

Figure E28 shows the simplified version of a single notional segment. Note line f_1, f_2 and f_3 as lines of reference in Figure E28 and E29. As in Figure E28, length (l_1) is multiplied by the standard width (With), to create the area A_1. Area A_4 was easily calculated it is based on the intake pipe dimensions. Areas A_2 and $A_3$are a third of the distance from each end and hence are calculated proportionately. The distances from Area A_1 to A_2 to A_3 to $A_4$are noted as Lengths len_1, len_2 and len_3 respectively.

In order to calculate the pressure loss due to the stone bedding, the hydraulic conductivity is required. The pressure loss is defined as per Equation 4 below:

$$hf(m) = \frac{L * V}{k} \qquad \text{Eqn E4}$$

Where:

hf = pressure loss due to friction within stone bedding

L = Length of water path (m)

V = Flow velocity

k = Hydraulic conductivity

The first two variables are easily to calculate however the hydraulic conductivity is calculated from Figure E31.

Referring to Figure C3 in Appendix C, the value of $D_{50}$of the SAND is approximately 0.2mm. Hence as per the previous section, the k value is of 0.02 cm/sec is not reflective of the actual flow rates recorded.

This is due to the removal of sand from the bedding matrix, Figure 42, during the test. With the removal of the sand, the bedding matrix would revert close to its original contents of only 19mm Stone. Hence a D_{50} of 15.7mm will be used again.

Table E75 summaries the parameters when obtaining the hydraulic conductivity k value.

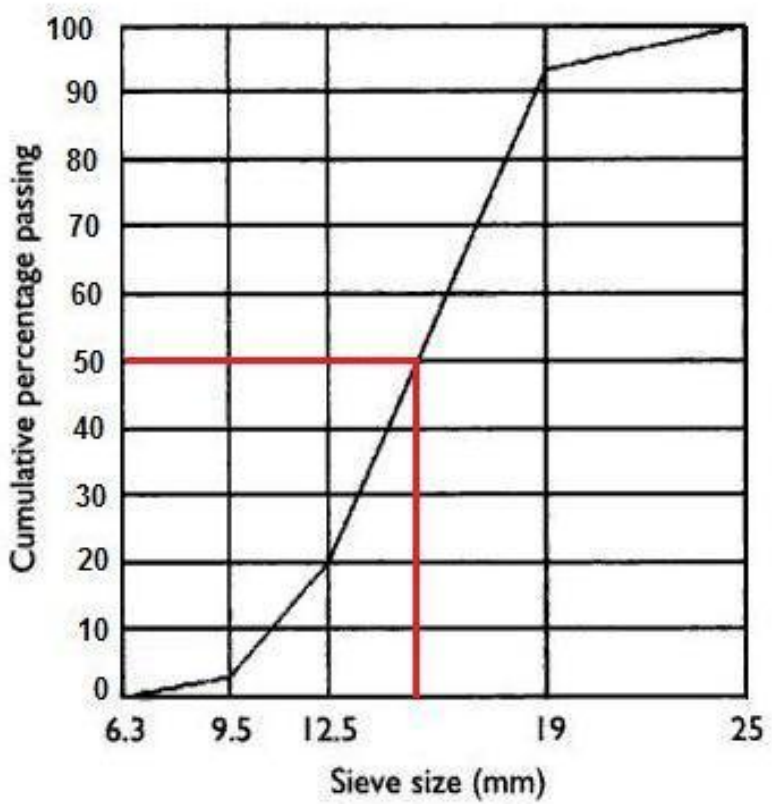

Figure E30: Grading curve for nominally single-sized 19mm Stone (Alexander & Mindess, 2005)

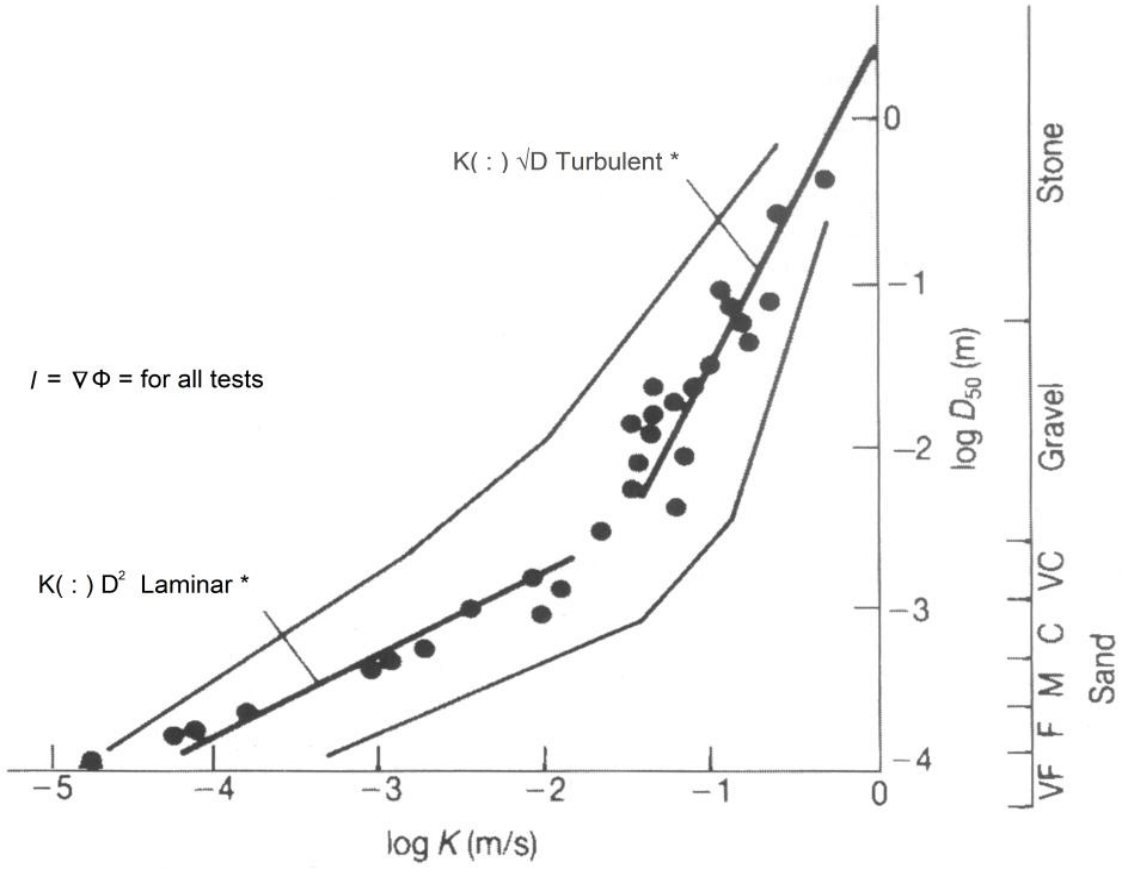

Figure E31: Permeability versus grain or stone sieve size (CIRIA, CUR, CETMEF,2007)

Table D75: Calculation of Permeability for 19mm Bedding of seawater Intake (WST)

Description	Unit	Bedding
D_{n50}	m	0.0157
Log (D_{50})	m	-1.80
Log *k*	m/s	-1.16
k	m/s	0.069

Using the values from Table E74 and E75, headloss for Segment 1 was calculated in the following manner. With the flow through each segment know, it is possible to determine the headloss if the areas through which water flows is uniform.

However, this is not the case. Hence each segment has been split into three equal portions. Table E76 below, describes the manner in which Segment 1 is split into three sub segments. Thereafter, Table E77 determines the average velocity for each sub segment, the associated headloss and finally the cumulative headloss for Segment 1. The following tables describe the headloss calculated for Segments 1, 2, 3, 4 and 5.

Table E76: Segment 1: Averaging of Areas

Test No.	Len1	A11	A12	A13	A14	Qs 1	Ave A11	Ave A12	Ave A13
	m	m^2	m^2	m^2	m^2	m3/s	m^2	m^2	m^2
1	0.3618	0.221	0.196	0.170	0.145	0.00006	0.208	0.183	0.158
2	0.3618	0.221	0.196	0.170	0.145	0.00021	0.208	0.183	0.158
3	0.3618	0.221	0.196	0.170	0.145	0.00040	0.208	0.183	0.158
4	0.3618	0.221	0.196	0.170	0.145	0.00052	0.208	0.183	0.158
5	0.3618	0.221	0.196	0.170	0.145	0.00062	0.208	0.183	0.158
6	0.3618	0.221	0.196	0.170	0.145	0.00095	0.208	0.183	0.158
7	0.3618	0.221	0.196	0.170	0.145	0.00112	0.208	0.183	0.158

Table E77: Segment 1: Velocity and cumulative headloss

Test No.	Vel 1A	Vel 1B	Vel 1C	H_l11	H_l12	H_l13	H_l1Total	H_l1Total
	m/s	m/s	m/s	m	m	m	m	mm
1	0.0003	0.0003	0.0004	0.00088	0.00100	0.00116	0.00304	3.04
2	0.0010	0.0011	0.0013	0.00303	0.00345	0.00400	0.01049	10.49
3	0.0019	0.0022	0.0026	0.00594	0.00676	0.00784	0.02054	20.54
4	0.0025	0.0028	0.0033	0.00756	0.00860	0.00998	0.02615	26.15
5	0.0030	0.0034	0.0039	0.00910	0.01035	0.01201	0.03147	31.47
6	0.0045	0.0052	0.0060	0.01394	0.01586	0.01840	0.04820	48.20
7	0.0054	0.0061	0.0071	0.01661	0.01889	0.02191	0.05741	57.41

Table E78: Segment 2: Averaging of Areas

Test No.	Len2	A21	A22	A23	A24	Qs 2	Ave A21	Ave A22	Ave A23
	m	m^2	m^2	m^2	m^2	m3/s	m^2	m^2	m^2
1	0.2814	0.172	0.163	0.154	0.145	0.00005	0.167	0.158	0.150
2	0.2814	0.172	0.163	0.154	0.145	0.00016	0.167	0.158	0.150
3	0.2814	0.172	0.163	0.154	0.145	0.00031	0.167	0.158	0.150
4	0.2814	0.172	0.163	0.154	0.145	0.00040	0.167	0.158	0.150
5	0.2814	0.172	0.163	0.154	0.145	0.00048	0.167	0.158	0.150
6	0.2814	0.172	0.163	0.154	0.145	0.00074	0.167	0.158	0.150
7	0.2814	0.172	0.163	0.154	0.145	0.00087	0.167	0.158	0.150

Table E79: Segment 2: Velocity and cumulative headloss

Test No.	Vel 2A	Vel 2B	Vel 2C	H_l21	H_l22	H_l23	H_l2 Total	H_l2 Total
	m/s	m/s	m/s	m	m	m	m	mm
1	0.0003	0.0003	0.0003	0.00085	0.00090	0.00095	0.00270	2.70
2	0.0010	0.0010	0.0011	0.00294	0.00310	0.00328	0.00932	9.32
3	0.0019	0.0020	0.0021	0.00575	0.00607	0.00643	0.01825	18.25
4	0.0024	0.0025	0.0027	0.00732	0.00773	0.00818	0.02323	23.23
5	0.0029	0.0030	0.0032	0.00881	0.00930	0.00985	0.02796	27.96
6	0.0044	0.0046	0.0049	0.01349	0.01425	0.01509	0.04283	42.83
7	0.0052	0.0055	0.0058	0.01607	0.01697	0.01797	0.05102	51.02

Table E80: Segment 3: Averaging of Areas

Test No.	Len3	A31	A32	A33	A34	Qs 3	Ave A31	Ave A32	Ave A33
	m	m^2	m^2	m^2	m^2	m3/s	m^2	m^2	m^2
1	0.201	0.123	0.130	0.138	0.145	0.00003	0.126	0.134	0.141
2	0.201	0.123	0.130	0.138	0.145	0.00012	0.126	0.134	0.141
3	0.201	0.123	0.130	0.138	0.145	0.00022	0.126	0.134	0.141
4	0.201	0.123	0.130	0.138	0.145	0.00029	0.126	0.134	0.141
5	0.201	0.123	0.130	0.138	0.145	0.00034	0.126	0.134	0.141
6	0.201	0.123	0.130	0.138	0.145	0.00053	0.126	0.134	0.141
7	0.201	0.123	0.130	0.138	0.145	0.00062	0.126	0.134	0.141

Table E81: Segment 3: Velocity and cumulative headloss

Test No.	Vel 3A	Vel 3B	Vel 3C	H_l31	H_l32	H_l33	H_l3Total	H_l3Total
	m/s	m/s	m/s	m	m	m	m	mm
1	0.0003	0.0002	0.0002	0.00080	0.00076	0.00072	0.00228	2.28
2	0.0009	0.0009	0.0008	0.00278	0.00262	0.00248	0.00787	7.87
3	0.0018	0.0017	0.0016	0.00544	0.00513	0.00486	0.01542	15.42
4	0.0023	0.0021	0.0020	0.00692	0.00653	0.00618	0.01964	19.64
5	0.0027	0.0026	0.0024	0.00833	0.00786	0.00744	0.02363	23.63
6	0.0042	0.0039	0.0037	0.01276	0.01204	0.01140	0.03620	36.20
7	0.0049	0.0047	0.0044	0.01520	0.01434	0.01358	0.04312	43.12

Table E82: Segment 4: Averaging of Areas

Test No.	Len4	A41	A42	A43	A44	Qs 4	Ave A41	Ave A42	Ave A43
	m	m^2	m^2	m^2	m^2	m3/s	m^2	m^2	m^2
1	0.1206	0.074	0.097	0.121	0.145	0.00002	0.085	0.109	0.133
2	0.1206	0.074	0.097	0.121	0.145	0.00007	0.085	0.109	0.133
3	0.1206	0.074	0.097	0.121	0.145	0.00013	0.085	0.109	0.133
4	0.1206	0.074	0.097	0.121	0.145	0.00017	0.085	0.109	0.133
5	0.1206	0.074	0.097	0.121	0.145	0.00021	0.085	0.109	0.133
6	0.1206	0.074	0.097	0.121	0.145	0.00032	0.085	0.109	0.133
7	0.1206	0.074	0.097	0.121	0.145	0.00037	0.085	0.109	0.133

Table E83: Segment 4: Velocity and cumulative headloss

Test No.	Vel 4A	Vel 4B	Vel 4C	H_l41	H_l42	H_l43	$H_l4Total$	$H_l4Total$
	m/s	m/s	m/s	m	m	m	m	mm
1	0.0002	0.0002	0.0002	0.00071	0.00056	0.00046	0.00173	1.73
2	0.0008	0.0006	0.0005	0.00246	0.00192	0.00158	0.00596	5.96
3	0.0016	0.0012	0.0010	0.00482	0.00377	0.00309	0.01168	11.68
4	0.0020	0.0016	0.0013	0.00614	0.00480	0.00394	0.01487	14.87
5	0.0024	0.0019	0.0016	0.00739	0.00577	0.00474	0.01790	17.90
6	0.0037	0.0029	0.0024	0.01131	0.00884	0.00726	0.02742	27.42
7	0.0044	0.0034	0.0028	0.01348	0.01053	0.00865	0.03266	32.66

Table E84: Segment 5: Averaging of Areas

Test No.	Len5	A51	A52	A53	A54	Qs 5	Ave A51	Ave A52	Ave A53
	m	m^2	m^2	m^2	m^2	m3/s	m^2	m^2	m^2
1	0.0402	0.025	0.065	0.105	0.145	0.00001	0.045	0.085	0.125
2	0.0402	0.025	0.065	0.105	0.145	0.00002	0.045	0.085	0.125
3	0.0402	0.025	0.065	0.105	0.145	0.00004	0.045	0.085	0.125
4	0.0402	0.025	0.065	0.105	0.145	0.00006	0.045	0.085	0.125
5	0.0402	0.025	0.065	0.105	0.145	0.00007	0.045	0.085	0.125
6	0.0402	0.025	0.065	0.105	0.145	0.00011	0.045	0.085	0.125
7	0.0402	0.025	0.065	0.105	0.145	0.00012	0.045	0.085	0.125

Table E85: Segment 5: Velocity and cumulative headloss

Test No.	Vel 5A	Vel 5B	Vel 5C	H_l51	H_l52	H_l53	$H_l5Total$	$H_l5Total$
	m/s	m/s	m/s	m	m	m	m	mm
1	0.0001	0.0001	0.0001	0.00046	0.00024	0.00016	0.00086	0.86
2	0.0005	0.0003	0.0002	0.00157	0.00083	0.00056	0.00296	2.96
3	0.0010	0.0005	0.0004	0.00308	0.00162	0.00110	0.00580	5.80
4	0.0013	0.0007	0.0005	0.00392	0.00206	0.00140	0.00738	7.38
5	0.0015	0.0008	0.0006	0.00472	0.00248	0.00168	0.00888	8.88
6	0.0024	0.0012	0.0008	0.00723	0.00380	0.00258	0.01361	13.61
7	0.0028	0.0015	0.0010	0.00861	0.00453	0.00307	0.01621	16.21

Table E86: Method 3: Summary of results for Tables 48 to 57

Test No.	Total Q	Segment 1	Segment 2	Segment 3	Segment 4	Segment 5
	l/s	mm	mm	mm	mm	mm
1	0.33	3.04	2.70	2.28	1.73	0.86
2	1.15	10.49	9.32	7.87	5.96	2.96
3	2.26	20.54	18.25	15.42	11.68	5.80
4	2.87	26.15	23.23	19.64	14.87	7.38
5	3.46	31.47	27.96	23.63	17.90	8.88
6	5.29	48.20	42.83	36.20	27.42	13.61
7	6.30	57.41	51.02	43.12	32.66	16.21

Figure E32 plots Table E86 these graphically. A trendline is added to the results in order to predict the headloss, due to stone bedding, at the most downstream point of WC1. It is at this point that the largest magnitude of headloss occurs. Table E87 summaries these results.

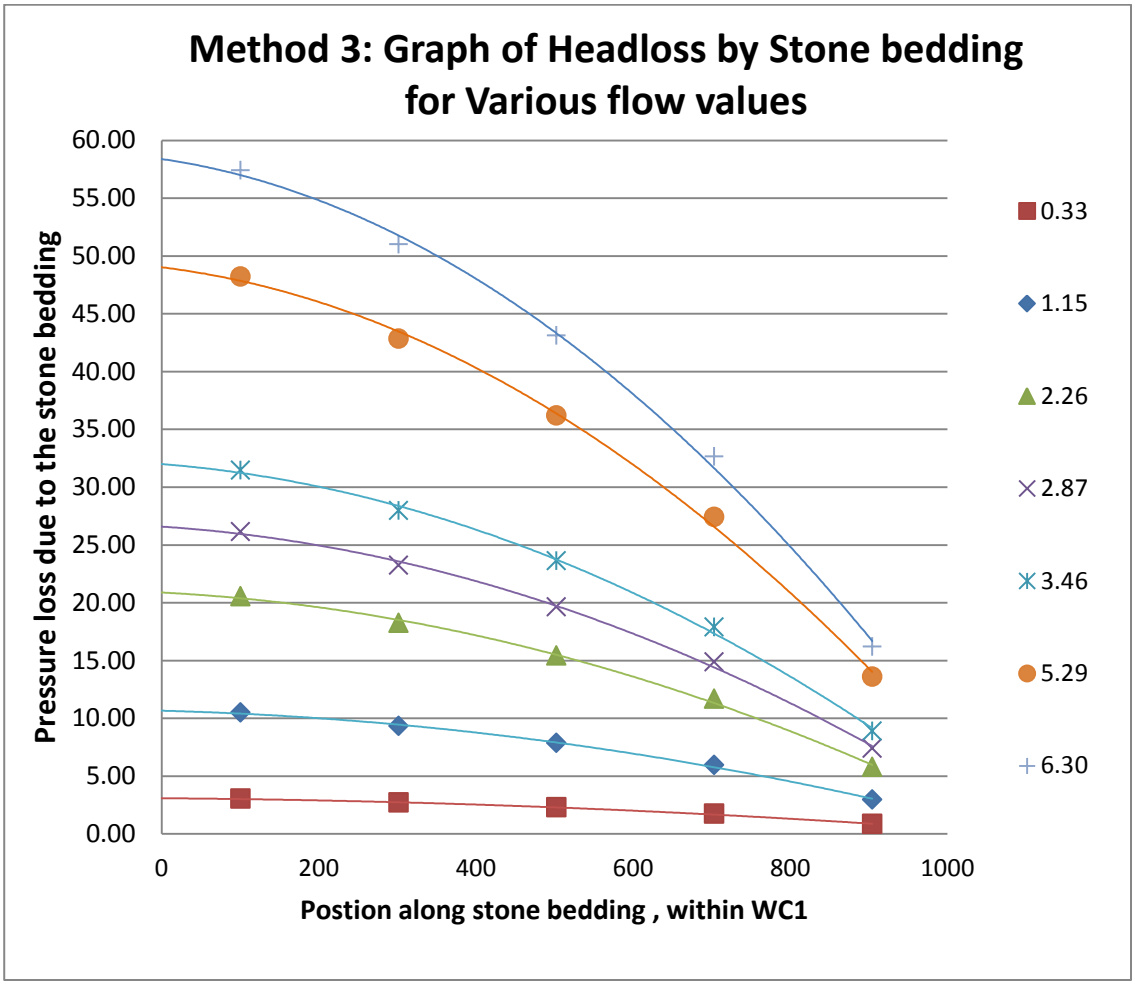

Figure E32: Results of Headloss due to (sand and) Stone Bedding, within WC1 (Legend: Flowrates)

Table E87: Summary of maximum headloss versus flow rates

Test No.	Total Q	Total 2Q	Maximum Headloss due to Stone Bedding
	l/s	l/s	mm
1	0.17	0.33	3.091
2	0.58	1.15	10.66
3	1.13	2.26	20.88
4	1.44	2.87	26.59
5	1.73	3.46	32
6	2.65	5.29	49.02
7	3.15	6.30	58.39

The results of the above table will be represented along with the results of Method 1 and 2 in the following section E.7.4.3.

E.7.4.3 Comparison of Results for Method 1, 2 and 3

The following Figure E33 shows the results for Method 1, 2 and 3 for the calculation of Headloss due to the stone bedding, Results for Method1, 2 and 3 are derived from Tables E59, E73 and E87.

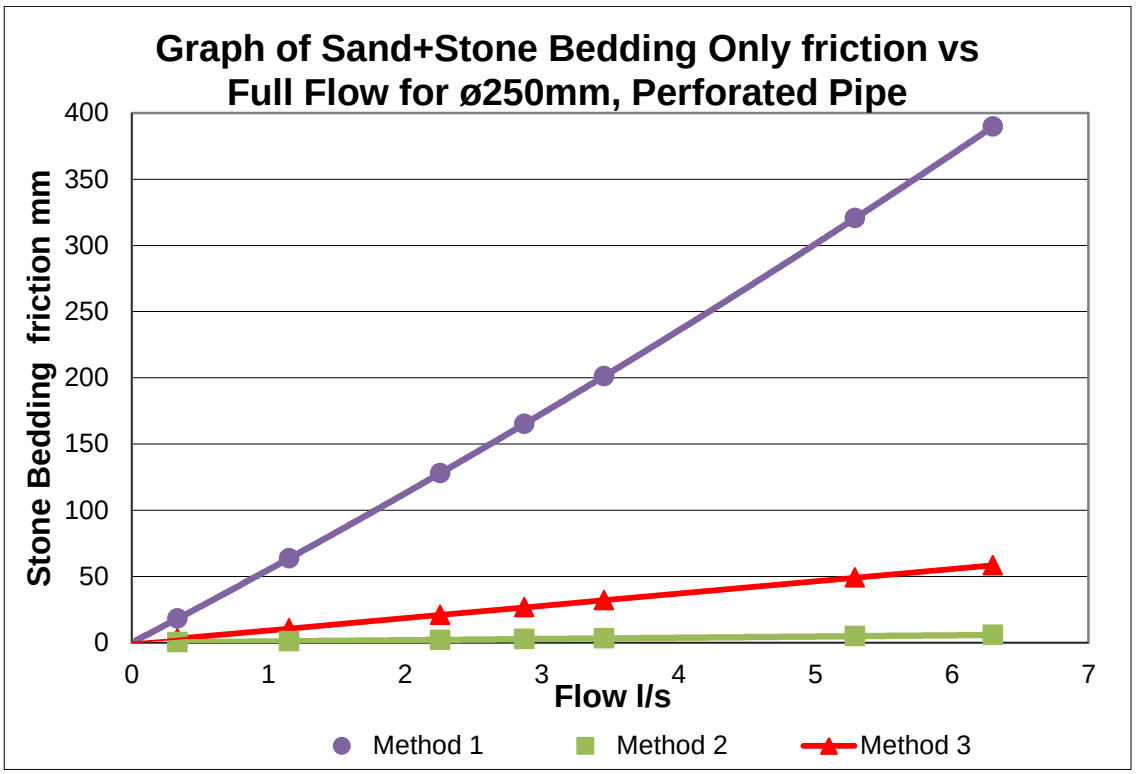

Figure E33: Method 1, 2 and 3 : Headloss due to the sand and stone bedding

Appendix F

Metal Wire Pipe Abstraction Model

Table of Contents

Description	Page
F.1 Introduction	329
F.2 Pressure Losses	330
F.3 Water Losses due to Leakage	331
F.4 Water Test Only	332
F.4.1 Water Leakage losses	335
F.4.2 Water Pressure losses	336
F.4.3 Perforation losses and Flowrate Relationship	337
F.4.4 Segmental Analysis of HPM	339
F.5 Water and Stone Test	344
F.5.1 Water Leakage losses	345
F.5.2 Water Pressure losses	346
F.5.3 Relationship between Flowrate, Perforation and Stone Bedding friction	346
F.5.4 Segmental Analysis of HPM	348
F.5.4.1 Methodology	348
F.5.4.2 Pressure loss due to Stone Bedding	351
F.5.4.2.1 Method 1: Simple method for determining headloss due to stone bedding	351
F.5.4.2.2 Method 2: Kenny, Lau and Ofoegbu Method for determining headloss due to stone bedding	353
F.5.4.2.3 Method 3: Forchheimer Method for determining headloss due to stone bedding	365
F.5.4.3 Comparison of Results for Method 1, 2 and 3	376

F.1 Introduction

This appendix describes in detail the calculations behind Chapter 5.3: Metal Wire Pipe Abstraction Model. Via the use of figures and tables it explains the most relevant calculations. Note that for all tests, no core material was used. Figure F1 below describes the model and the areas of interest. Table F1 below list parameters of the Metal Wire pipe (MWP).

Table F1: Metal Wire Pipe: Variables and Values

Metal Wire Pipeline Perforation Configuration	Value	Unit	Value	Unit
No of Hole/Slots per 20cm Length	38.18			
Area of each Slot	423.9	mm^2	0.0004239	m^2
Length of Pipe	1005	mm	1.005	m
No. of Segments	5			
Segment Length	201	mm	0.201	m
Perforation Area of Segment	16185	mm^2	0.0161856	m^2
Total Perforation Area	80927	mm^2	0.0809278	m^2
Total pipe Wetted Surface Area	410241		0.410241	m^2
Percentage perforation	19.73%			
Coefficient of Discharge Cd				
Coefficient Loss Ke	1			

F. 2 Pressure Losses

Chapter 4.4.6.1 describes the losses A to E. Note the datum of the model is the top of the model base.

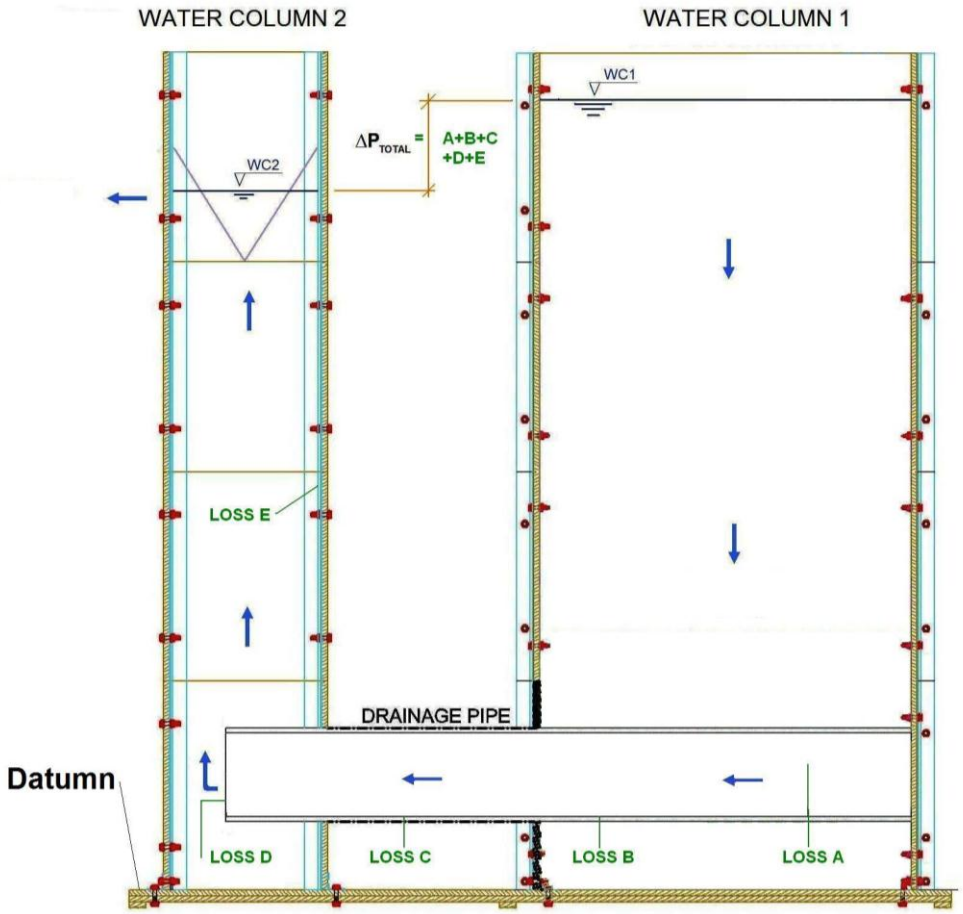

Figure F1: Metal Wire Pipe Abstraction Model: Areas of interest

The following is a reiteration of the losses A to E. as described in Chapter 4.4.6.1

Loss A: This reduction in pressure occurs as water travels from the outside of the pipe, in. Losses B to E is easily estimated using conventional calculation methods. Loss A accounts for a significantly large portion of the total pressure loss.

Loss B: Skin friction in the portion of intake pipe where there is water ingression and transportation. The skin friction in this chapter is calculated using Manning's Method. A pipe of 250mm is used as the conduit size. However, the skin friction in this area is halved as theoretically the flow is at its maximum as it exits WC1 and zero at the start of the pipeline (Right hand side of Figure F1)

Loss C: Skin friction in the portion of intake pipe where there is water transportation only. The skin friction in this chapter is calculated using Manning's Method. A pipe of 250mm is used as the conduit size.

Loss D: Exit loss as water enters Column 2 (WC2). For the flow exiting the Intake pipe and then turning 90 degrees, the loss equal to $Ke*V^2/2g$ where Ke = 1

Loss E: Skin friction as water flows up WC2. The skin friction in this chapter is calculated using Manning's Method. A rectangular section of 600mm by 250mm is used as the conduit size.

F. 3 Water Losses due to Leakage

The ability to quantify leakage is crucial especially if the leakage rate becomes a large fraction of the overall flow. Hence the flow rate of the leakage for each increment of the flow through the model was noted.

The entire leakage rate was calculated by constructing a dam around the HPM, and determining the amount of water that left the dam, over a period of time, for a particular increment a test. There were three places that water could have leaked out. These were : WC1, WC2a and WC2b. Figure F2 describes these. Via visual inspection 80% of all leakage was deemed to be out of WC1, 10% out of WC2a and 10% out of WC2b.

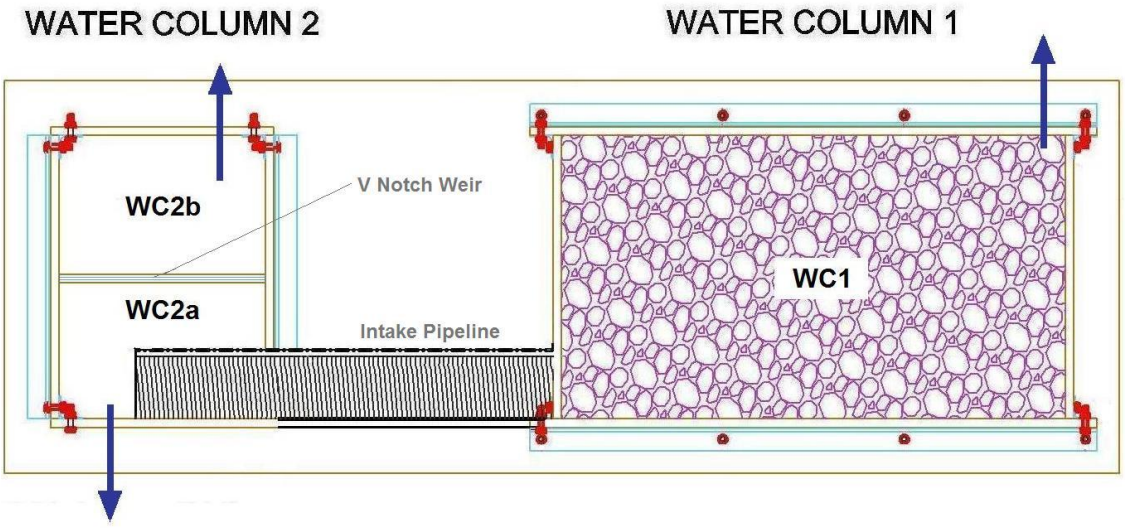

Figure F2: Areas of Water Leakage

F.4: Water Only Test

The following explains the manner in which the 'Water Only Test' (WOT) was conducted. It uses tables and equations to illustrate the analysis process. Table F2 details the physical aspects of the model including the Intake pipeline.

Table F2: The physical aspects of the HPM and Intake Pipeline

Description	Value	Unit
Physical aspects of the HPM:WC2a		
Angle of V Notch Weir	90	Degrees
Height of V Notch Weir	1708.5	mm
Length	0.28	m
Breath	0.45	m
Area A	0.126	m^2
Wet Perimeter P	1.46	m
Hydraulic Radius R	0.0863	m
Friction Factor f	0.02	
Loss Coefficient Ke	1	
Metal Wire Pipeline Perforation Configuration		
D Pipe Length	1005	mm
Pipe OD	270	mm
Pipe ID	260	mm
Half Pipe Area	0.026533	m^2
Wet Perimeter	0.6682	m
Hydraulic Radius Pipe HR	0.1588	m
No of Slots per 20cm Length	38.15	
Area of each Slot	423.9	mm^2
Length of Pipe	1005	mm
No. of Segments	5	
Segment Length	201	mm
Perforation Area of Segment	16186	mm^2
Total Perforation Area	80928	mm^2
Total pipe Wetted Surface Area	410241	mm^2
Percentage perforation	19.73	%
Friction Factor f	0.015	

Where :

C_d = Coefficient of Discharge as established in Appendix B

D Pipe Length = Length of Intake pipeline in the HPM

Pipe OD = Outside Diameter of Intake Pipeline

Pipe ID = Inside Diameter of Pipeline

Half Pipe Area = The area of flow when only half a pipe is used

Wet Perimeter = Perimeter of the intake pipeline that has been in contact with the flow

Hydraulic Radius HR = The Hydraulic Radius of the Intake Pipeline or WC2a

The aim of this experiment is to establish the relationship between the flow and the loss of pressure head as it passes in to the Intake pipeline Using the above information, 18 incremental tests, with increasing driving heads, where conducted. Table F3 shows the initial results. The difference between WC1 and WC2 denotes the total headloss. The flow rate was determined from the following Equation:B1

$$Q = C_d \cdot \frac{8}{15} \cdot \sqrt{2g} \cdot \tan\frac{\theta}{2} \cdot h^{\frac{5}{2}} \qquad \text{Eqn B1}$$

where

Q= Flow (l/s)

C_d= 0.57

h = depth of water above V Notch (mm)

Table F3: Total Headloss and initial flow rate for Water Only test

Test No.	WC1	WC2	Upstream Head	Downstream Head	Total ∆hf	Initial Q Half Pipe
	mm	mm	mm	mm	mm	l/s
1	1738	1737	29.5	28.5	1	0.18
2	1753	1751	44.5	42.5	2	0.50
3	1766	1761.5	57.5	53	4.5	0.87
4	1780	1774	71.5	65.5	6	1.48
5	1795	1782	86.5	73.5	13	1.97
6	1804	1790	95.5	81.5	14	2.55
7	1827	1796	118.5	87.5	31	3.05
8	1848	1806	139.5	97.5	42	4.00
9	1863	1813	154.5	104.5	50	4.75
10	1910	1824	201.5	115.5	86	6.10
11	1933	1831	224.5	122.5	102	7.07
12	1973	1837	264.5	128.5	136	7.97
13	1996	1844	287.5	135.5	152	9.10
14	2052	1850	343.5	141.5	202	10.14
15	2109	1854	400.5	145.5	255	10.87
16	2172	1860	463.5	151.5	312	12.03
17	2229	1870	520.5	161.5	359	14.11
18	2328	1875	619.5	166.5	453	15.23

After the total headloss and initial flow rate relationship has been established, Water leakage has to be considered. As per Chapter F3, theses losses are incorporated in Table F4 with 80% of all leakage deemed to be out of WC1, 10% out of WC2a and 10% out of WC2b.

F.4.1 Water Leakage losses

In Table F4, the total leakage rate is calculated in Column 6. Columns 7, 8 and 9 calculates the loss for WC1, WC2a and WC2b, respectively. The Total flow rate Q is calculated as the Initial flow rate plus the leakage from WC1 and WC2a

Table F4: Total headloss and flow rate incorporating losses

1	2	3	4	5	6	7	8	9	10
Test No.	Q Half Pipe	Bucket Ht	Time	Volume	Total	Loss due to WC1	Loss due to WC2a	Loss due to WC2b	Total Q
	l/s	mm	s	l	l/s	l/s	l/s	l/s	l/s
1	0.18	170	771	43.03	0.056	0.044645	0.005581	0.005581	0.23
2	0.50	112	524	27.70	0.053	0.042286	0.005286	0.005286	0.55
3	0.87	72	334	17.52	0.052	0.041958	0.005245	0.005245	0.92
4	1.48	106	529	26.15	0.049	0.039547	0.004943	0.004943	1.52
5	1.97	96	470	23.59	0.050	0.040148	0.005019	0.005019	2.02
6	2.55	87	404	21.30	0.053	0.042173	0.005272	0.005272	2.60
7	3.05	90	390	22.06	0.057	0.045249	0.005656	0.005656	3.10
8	4.00	88	406	21.55	0.053	0.042465	0.005308	0.005308	4.04
9	4.75	90	390	22.06	0.057	0.045249	0.005656	0.005656	4.80
10	6.10	170	771	43.03	0.056	0.044645	0.005581	0.005581	6.16
11	7.07	112	524	27.70	0.053	0.042286	0.005286	0.005286	7.12
12	7.97	72	334	17.52	0.052	0.041958	0.005245	0.005245	8.02
13	9.10	106	529	26.15	0.049	0.039547	0.004943	0.004943	9.15
14	10.14	96	470	23.59	0.050	0.040148	0.005019	0.005019	10.19
15	10.87	87	404	21.30	0.053	0.042173	0.005272	0.005272	10.92
16	12.03	90	390	22.06	0.057	0.045249	0.005656	0.005656	12.08
17	14.11	88	406	21.55	0.053	0.042465	0.005308	0.005308	14.16
18	15.23	90	390	22.06	0.057	0.045249	0.005656	0.005656	15.28

F.4.2 Water Pressure losses

After the correct total flow has been established, the next step is the disaggregation of pressure losses. This is done so that Loss A, the loss of pressure as water enters the Intake pipeline, can be established. Chapter F2 states the Pressure Losses A to E with the relevant equations. Table F5 calculates the Losses B to E and hence the remaining total headloss will be Loss A.

Table F5: Disaggregation of pressure losses

Test No.	Total ∆hf	Total Q	Loss B+C	Loss D	Loss E	Loss A	%A of Total ∆hf
	mm	l/s	m	m	m	mm	
1	1	0.23	0.000001	0.000002	0.0000009	1.00	99.86%
2	2	0.55	0.000003	0.000018	0.0000066	1.99	99.53%
3	4.5	0.92	0.000008	0.000055	0.0000198	4.47	99.39%
4	6	1.52	0.000021	0.000158	0.0000572	5.92	98.69%
5	13	2.02	0.000038	0.000282	0.0001017	12.86	98.93%
6	14	2.60	0.000063	0.000472	0.0001705	13.77	98.34%
7	31	3.10	0.000089	0.000673	0.0002432	30.67	98.93%
8	42	4.04	0.000151	0.001157	0.0004178	41.43	98.65%
9	50	4.80	0.000214	0.001636	0.0005908	49.20	98.39%
10	86	6.16	0.000350	0.002698	0.0009745	84.67	98.46%
11	102	7.12	0.000469	0.003621	0.0013079	100.22	98.26%
12	136	8.02	0.000595	0.004599	0.0016612	133.74	98.34%
13	152	9.15	0.000774	0.005996	0.0021657	149.06	98.07%
14	202	10.19	0.000960	0.007447	0.0026895	198.35	98.19%
15	255	10.92	0.001103	0.008560	0.0030918	250.80	98.35%
16	312	12.08	0.001350	0.010477	0.0037840	306.87	98.35%
17	359	14.16	0.001855	0.014422	0.0052090	351.94	98.03%
18	453	15.28	0.002161	0.016798	0.0060669	444.77	98.18%

F.4.3 Perforation losses and Flowrate Relationship

Table F6 shows the Intake pipeline perforation friction (Loss A) and the flowrate for half a pipe and for a full pipeline. Figure F3 shows the relationship between the Perforation friction and the flowrate in a 250mm Metal Wire Pipeline.

Table F6: Perforation friction (Loss A) flowrate for Half and Full pipeline(MWP-WOT)

Test No.	Loss A	Q Half Pipe	Q Full Pipe
	mm	l/s	l/s
1	1.00	0.235	0.470
2	1.99	0.549	1.098
3	4.47	0.918	1.836
4	5.92	1.523	3.046
5	12.86	2.017	4.035
6	13.77	2.601	5.202
7	30.67	3.101	6.201
8	41.43	4.045	8.090
9	49.20	4.804	9.609
10	84.67	6.155	12.310
11	100.22	7.120	14.240
12	133.74	8.018	16.035
13	149.06	9.145	18.290
14	198.35	10.187	20.374
15	250.80	10.921	21.842
16	306.87	12.081	24.161
17	351.94	14.162	28.324
18	444.77	15.283	30.566

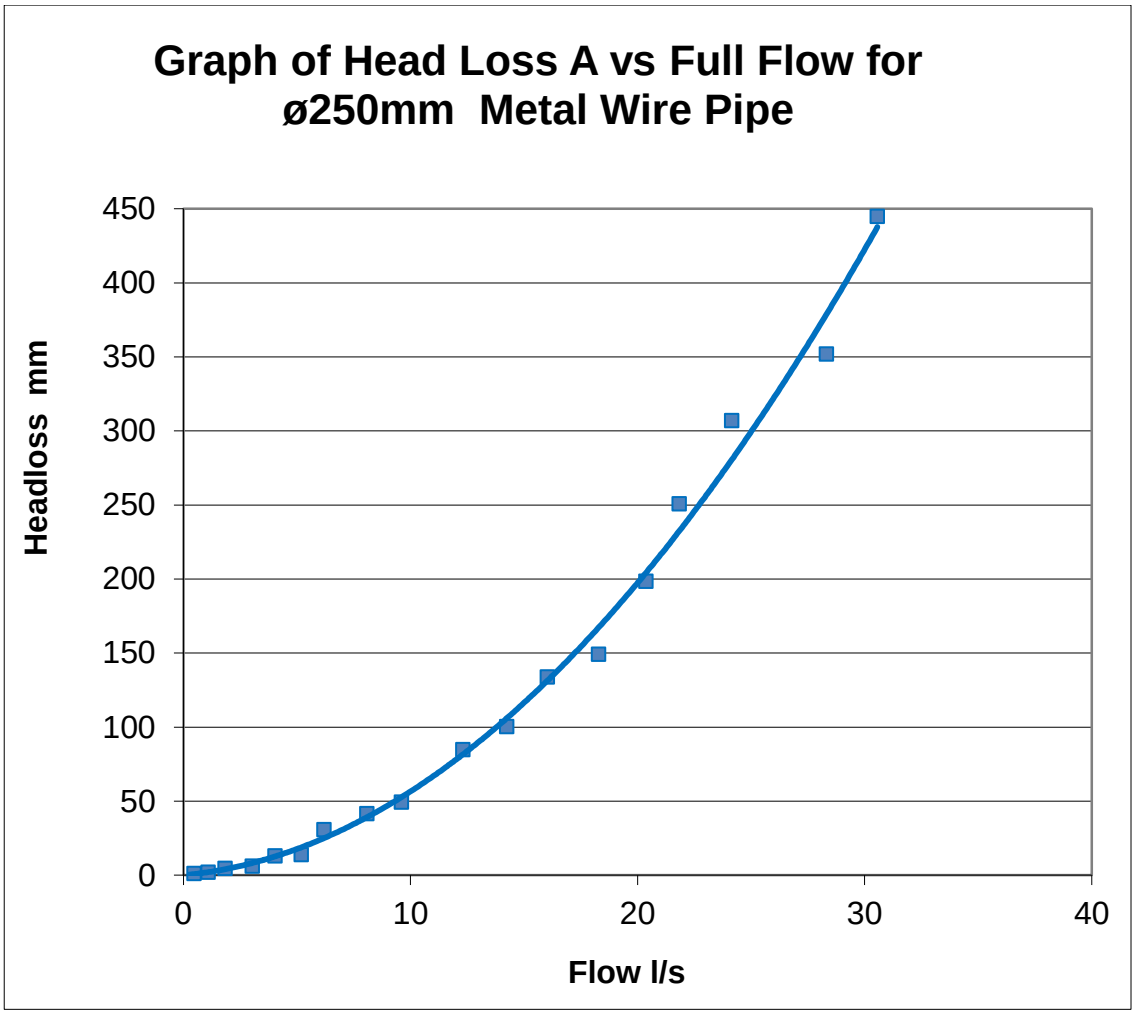

Figure F3: Headloss due to the slots (Loss A) versus the flowrate for a fully flowing ø250mm Metal Wire pipe

The equation below describes the relationship between headloss due to slot friction and flowrate

$$\Delta P = 0.494Q^2 + 1.443Q \qquad \text{Eqn 10}$$

With

ΔP = Headloss due to perforation friction in mm

Q = Flowrate for full pipeline in litres/second

F.4.4 Segmental Analysis of HPM

Analysing the Metal Wire/Perforation friction and flow relationship was relatively simple. However in order to understand the flow regime better, it was required that the flow at different points in the HPM be calculated. It was decided that a model would be better understood if it was segmented. Hence the model was portioned into five segments.

As described by Table F5, the Perforation Loss A accounts for the nearly all of the pressure loss. Hence for a point on the Intake pipeline just inside WC1, the velocity of the flow into the pipeline is at its maximum. The velocity at this point is termed V_{max}. The opposite holds true for a point at the start of the Intake pipeline. At this point, V_{min}, the velocity of the inflow is zero. Hence via linear interpolation, the velocity at any point in between both ends, can be calculated Figure F4 below describes the manner in which the HPM is segmented.

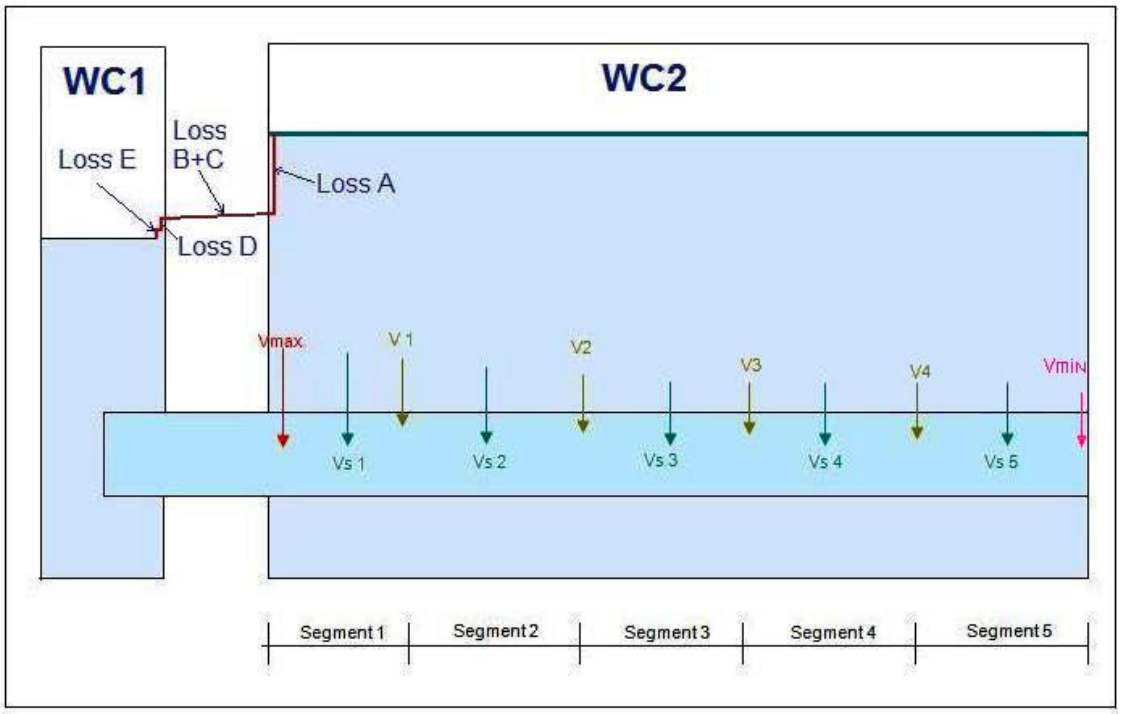

Figure F4: Segmented HPM with notional EGL flow that enters WC1 and exits from WC2

Methodology

In order to calculate the flow at various point within the model, the HPM was divided into five segments. The velocities V_{MAX}, V_1, V_2 , V_3, V_4 and V_{MIN} occur at the border of each segment, Hence for each segment, the Average Velocity, V_S1, V_S2, V_S3, V_S4 and V_S5 for each segment is easily calculated.

V_{MAX} is derived from Bernoulli principles where :

$$V = \sqrt{2g\Delta h} \qquad \text{Eqn F1}$$

With

V = Velocity in m/s

Δh = = is the driving pressure

g = gravitational constant (9.81m/s^2)

Note that the driving pressure Δh is Loss A. The flow from each segment is then calculated by multiplying the velocity with the perforation area and a discharge coefficient, C_d. Table F7 shows the distribution of inflowing velocity over the length of the Intake Pipeline.

Equation F2 was used to calculate the flow from each segment. Table F8 contains the flowrate for each segment and the sum of flow from all segments of the pipeline.

$$Q_T = \Sigma q = \Sigma C_d A\sqrt{2g\Delta h} \qquad \text{Eqn F2}$$

With

q = Flowrate through for each segment in m^3/s

Q = Sum of Flowrate form each segment in m^3/s

A= The Area through which flow is allowed in m^2

C_d = Coefficient of Discharge

Table F7: Inflowing velocity of water flowing into the pipe, over the length of the Intake Pipeline

		Pos. 0	Pos. 1	Pos. 2	Pos. 3	Pos. 4	Pos. 5	Pos. 6	Pos. 7	Pos. 8	Pos. 9	Pos. 10
Test	Loss A	Vmax	Vs1	V1	Vs 2	V2	Vs 3	V3	Vs 4	V4	Vs 5	Vmin
0	mm	m/s	m/s	m/s	m/s	m/s	m/s	m/s	m/s	m/s	m/s	m/s
1	1.00	0.140	0.126	0.112	0.098	0.084	0.070	0.056	0.042	0.028	0.014	0.000
2	1.99	0.198	0.178	0.158	0.138	0.119	0.099	0.079	0.059	0.040	0.020	0.000
3	4.47	0.296	0.267	0.237	0.207	0.178	0.148	0.118	0.089	0.059	0.030	0.000
4	5.92	0.341	0.307	0.273	0.239	0.205	0.170	0.136	0.102	0.068	0.034	0.000
5	12.86	0.502	0.452	0.402	0.352	0.301	0.251	0.201	0.151	0.100	0.050	0.000
6	13.77	0.520	0.468	0.416	0.364	0.312	0.260	0.208	0.156	0.104	0.052	0.000
7	30.67	0.776	0.698	0.621	0.543	0.465	0.388	0.310	0.233	0.155	0.078	0.000
8	41.43	0.902	0.811	0.721	0.631	0.541	0.451	0.361	0.270	0.180	0.090	0.000
9	49.20	0.982	0.884	0.786	0.688	0.589	0.491	0.393	0.295	0.196	0.098	0.000
10	84.67	1.289	1.160	1.031	0.902	0.773	0.644	0.516	0.387	0.258	0.129	0.000
11	100.22	1.402	1.262	1.122	0.982	0.841	0.701	0.561	0.421	0.280	0.140	0.000
12	133.74	1.620	1.458	1.296	1.134	0.972	0.810	0.648	0.486	0.324	0.162	0.000
13	149.06	1.710	1.539	1.368	1.197	1.026	0.855	0.684	0.513	0.342	0.171	0.000
14	198.35	1.973	1.775	1.578	1.381	1.184	0.986	0.789	0.592	0.395	0.197	0.000
15	250.80	2.218	1.996	1.775	1.553	1.331	1.109	0.887	0.665	0.444	0.222	0.000
16	306.87	2.454	2.208	1.963	1.718	1.472	1.227	0.981	0.736	0.491	0.245	0.000
17	351.94	2.628	2.365	2.102	1.839	1.577	1.314	1.051	0.788	0.526	0.263	0.000
18	444.77	2.954	2.659	2.363	2.068	1.772	1.477	1.182	0.886	0.591	0.295	0.000

Of particular concern is the Energy Grade Line (EGL) at the centre of the Intake Pipeline. The EGL shows the amount of energy that has been lost from water merely entering the Intake Pipeline.

For this case the loss of pressure is due to perforation friction only. Hence to calculate the EGL a particular position along the Intake pipeline, would be the still water level in WC1 minus the perforation friction/ Loss A. Table F8 below describes this calculation.

Table F8: Calculated Flowrate from all segments of the Pipeline

Test	Loss A	C_b	Qs 1	Qs 2	Qs 3	Qs 4	Qs 5	Q Total	Q Total	2Q Total
	mm		m^3/s	m^3/s	m^3/s	m^3/s	m^3/s	m^3/s	l/s	l/s
1	1.00	0.207	0.002	0.002	0.001	0.001	0.000	0.0002	0.23	0.47
2	1.99	0.343	0.005	0.004	0.003	0.002	0.001	0.0005	0.55	1.10
3	4.47	0.383	0.008	0.006	0.005	0.003	0.001	0.0009	0.92	1.84
4	5.92	0.552	0.014	0.011	0.008	0.005	0.002	0.0015	1.52	3.05
5	12.86	0.496	0.018	0.014	0.010	0.006	0.002	0.0020	2.02	4.03
6	13.77	0.618	0.023	0.018	0.013	0.008	0.003	0.0026	2.60	5.20
7	30.67	0.494	0.028	0.022	0.016	0.009	0.003	0.0031	3.10	6.20
8	41.43	0.554	0.036	0.028	0.020	0.012	0.004	0.0040	4.04	8.09
9	49.20	0.604	0.043	0.034	0.024	0.014	0.005	0.0048	4.80	9.61
10	84.67	0.590	0.055	0.043	0.031	0.018	0.006	0.0062	6.16	12.31
11	100.22	0.627	0.064	0.050	0.036	0.021	0.007	0.0071	7.12	14.24
12	133.74	0.612	0.072	0.056	0.040	0.024	0.008	0.0080	8.02	16.04
13	149.06	0.661	0.082	0.064	0.046	0.027	0.009	0.0091	9.15	18.29
14	198.35	0.638	0.092	0.071	0.051	0.031	0.010	0.0102	10.19	20.37
15	250.80	0.608	0.098	0.076	0.055	0.033	0.011	0.0109	10.92	21.84
16	306.87	0.608	0.109	0.085	0.060	0.036	0.012	0.0121	12.08	24.16
17	351.94	0.666	0.127	0.099	0.071	0.042	0.014	0.0142	14.16	28.32
18	444.77	0.639	0.138	0.107	0.076	0.046	0.015	0.0153	15.28	30.57

Figure F5 below is a plot of EGLs at the centre of the Intake Pipeline. For the 18 tests conducted, the increase in pressure losses closer to the exit point of WC1, can be clearly seen.

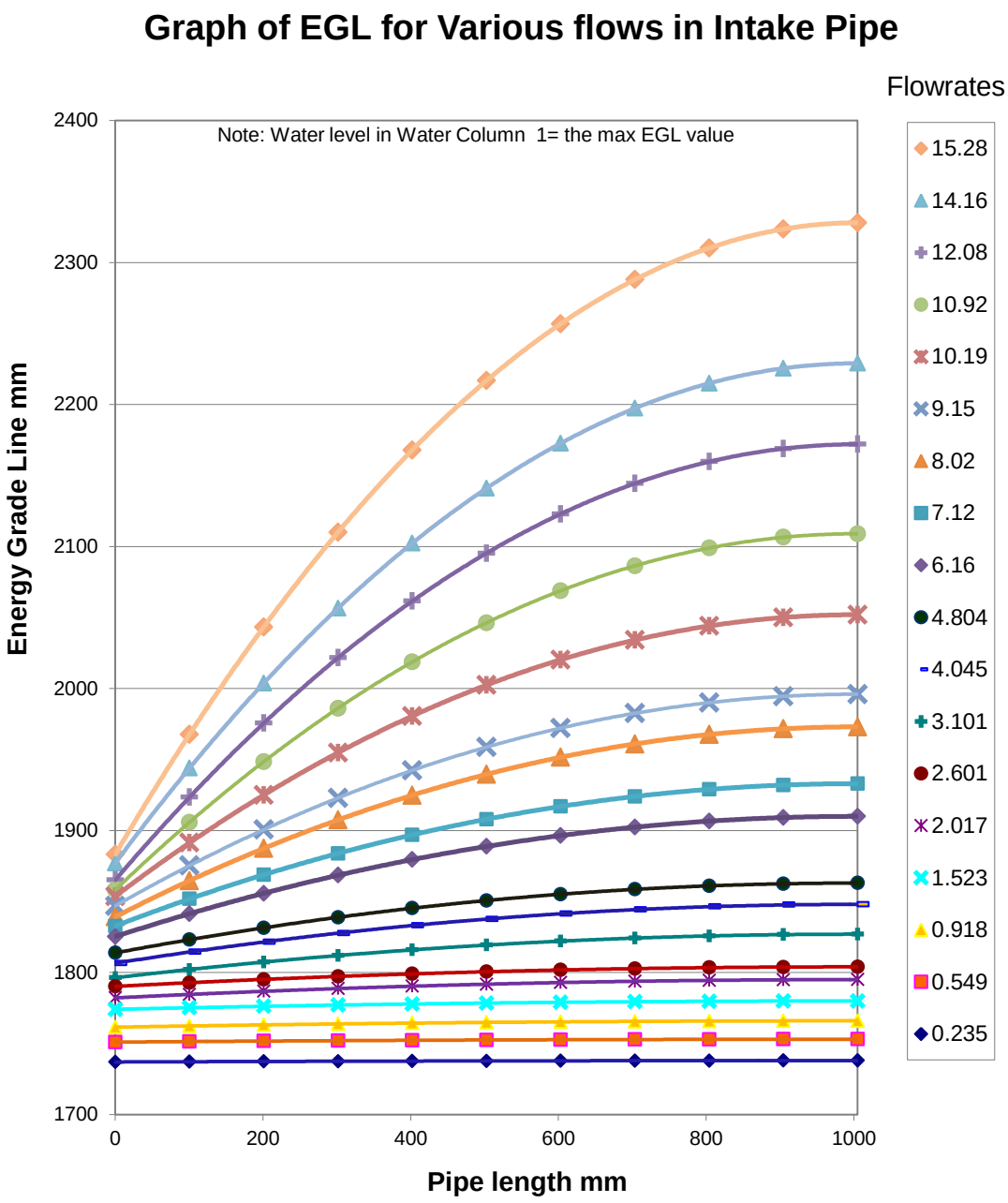

Figure F5: Plot of EGLs at the centre of the Intake Pipeline Legend : Flowrate

With the main Flow versus headloss relationship being the most important, calculation of the EGL might appear of no use, however calculation of EGL at various points in the flow will prove fruitful in future chapters.

F.5: Water and Stone Test

The following explains the manner in which the 'Water and Stone Test' was conducted and uses tables and equations to illustrate the analysis process. Table F1 details the physical aspects of the model. This includes the Intake pipeline and can be found in Chapter F.4 above

The aim of this experiment is to:

1) confirm the relationship between the flow and the loss of pressure head as it passes in to the Intake pipeline and to
2) establish the relationship between the flow and the loss of pressure head as it passes through the 19mm Stone bedding.

Using the above information, 18 incremental tests, with increasing driving heads, where conducted. Table F9 shows the initial results. The difference between WC1 and WC2 denotes the total headloss. The flow rate was determined from the following Equation:B1

$$Q = C_d \cdot \frac{8}{15} \cdot \sqrt{2g} \cdot \tan\frac{\theta}{2} \cdot h^{\frac{5}{2}} \qquad \text{Eqn B1}$$

where

Q= Flow (l/s)

C_d= 0.57

h = depth of water above V Notch (mm)

Table F9: Total Headloss and initial flow rate for Water and Stone test

Test No.	WC1	WC2	Upstream Head	Downstream Head	Total Δhf	Initial Q Half Pipe
	mm	mm	mm	mm	mm	l/s
1	1745	1743	36.5	34.5	2	0.30
2	1753	1749	44.5	40.5	4	0.44
3	1775	1766	66.5	57.5	9	1.07
4	1781	1775	72.5	66.5	6	1.54
5	1852	1790	143.5	81.5	62	2.55
6	1870	1803	161.5	94.5	67	3.70
7	1940	1817	231.5	108.5	123	5.22
8	2031	1830	322.5	121.5	201	6.93
9	2060	1840	351.5	131.5	220	8.44
10	2154	1854	445.5	145.5	300	10.87
11	2227	1865	518.5	156.5	362	13.05
12	2321	1870	612.5	161.5	451	14.11

After the total headloss and initial flow rate relationship has been established, Water leakage is considered. As per chapter F3 theses losses are incorporated in Table F10 with 80% of all leakage deemed to be from WC1, 10% out of WC2a and 10% out of WC2b.

F.5.1 Water Leakage losses

In Table F10, the total leakage rate is calculated in Column 6. Columns 7, 8 and 9 calculates the loss for WC1, WC2a and WC2b, respectively. The Total flow rate Q is calculated as the Initial flow rate plus the leakage from WC1 and WC2a.

Table F10: Total headloss and flow rate incorporating losses for Water and Stone Test

1	2	3	4	5	6	7	8	9	10
Test No.	Q Half Pipe	Bucket Ht	Time	Volume	Total	Loss due to WC1	Loss due to WC2a	Loss due to WC2b	Half Pipe Q
	l/s	mm	s	l	l/s	l/s	l/s	l/s	l/s
1	0.30	170	771	43.03	0.056	0.044645	0.00558	0.00558	0.35
2	0.44	112	524	27.70	0.053	0.042286	0.00529	0.00529	0.49
3	1.07	72	334	17.52	0.052	0.041958	0.00524	0.00524	1.11
4	1.54	106	529	26.15	0.049	0.039547	0.00494	0.00494	1.58
5	2.55	96	470	23.59	0.050	0.040148	0.00502	0.00502	2.60
6	3.70	87	404	21.30	0.053	0.042173	0.00527	0.00527	3.74
7	5.22	90	390	22.06	0.057	0.045249	0.00566	0.00566	5.27
8	6.93	88	406	21.55	0.053	0.042465	0.00531	0.00531	6.98
9	8.44	90	390	22.06	0.057	0.045249	0.00566	0.00566	8.49
10	10.87	170	771	43.03	0.056	0.044645	0.00558	0.00558	10.92
11	13.05	112	524	27.70	0.053	0.042286	0.00529	0.00529	13.09
12	14.11	72	334	17.52	0.052	0.041958	0.00524	0.00524	14.16

F.5.2 Water Pressure losses

After the correct total flow has been established, the next step is the disaggregation of pressure losses. This is done so that Loss A, the loss of pressure as water enters the Intake pipeline, can be established. Chapter F2 states the Pressure Losses A to E with the relevant equations. Table F11 calculates the Losses B to E and hence the remaining total headloss will be Loss A.

Table F11: Disaggregation of pressure losses for Water and Stone test

Test No.	Total ∆hf	Total Half Pipe Q	Loss B+C	Loss D	Loss E	Loss A +Stone bedding	%A of Total ∆hf
	mm	l/s	m	m	m	mm	
1	2.0	0.35	0.000001	0.000006	0.0000001	2.00	99.95%
2	4.0	0.49	0.000002	0.000014	0.0000003	4.00	99.95%
3	9.0	1.11	0.000009	0.000083	0.0000018	8.99	99.88%
4	6.0	1.58	0.000018	0.000171	0.0000036	5.98	99.65%
5	62.0	2.60	0.000047	0.000472	0.0000101	61.94	99.91%
6	67.0	3.74	0.000098	0.000989	0.0000211	66.88	99.82%
7	123.0	5.27	0.000195	0.001974	0.0000421	122.76	99.81%
8	201.0	6.98	0.000342	0.003476	0.0000742	200.58	99.79%
9	220.0	8.49	0.000507	0.005162	0.0001102	219.38	99.72%
10	300.0	10.92	0.000838	0.008560	0.0001828	298.98	99.66%
11	362.0	13.09	0.001204	0.012324	0.0002631	360.53	99.59%
12	451.0	14.16	0.001408	0.014422	0.0003079	449.28	99.62%

F.5.3 Relationship between flowrate, Perforation and Stone Bedding friction

Table F12 shows the Intake pipeline perforation friction (Loss A)+ stone bedding loss. It also includes the flowrate for half a pipe and for a full pipeline. Figure F5 shows the relationship between the Perforation + stone bedding friction and the flowrate in a ø250mm Metal Wire Pipe.

Table F12: Perforation (Loss A), and Stone Bedding friction, flowrate for Half and Full pipeline

Test No.	Loss A +Stone bedding	Q Half Pipe	Q Full Pipe
	mm	l/s	l/s
1	2.00	0.35	0.70
2	4.00	0.49	0.98
3	8.99	1.11	2.23
4	5.98	1.58	3.16
5	61.94	2.60	5.20
6	66.88	3.74	7.49
7	122.76	5.27	10.54
8	200.58	6.98	13.95
9	219.38	8.49	16.99
10	298.98	10.92	21.85
11	360.53	13.09	26.19
12	449.28	14.16	28.32

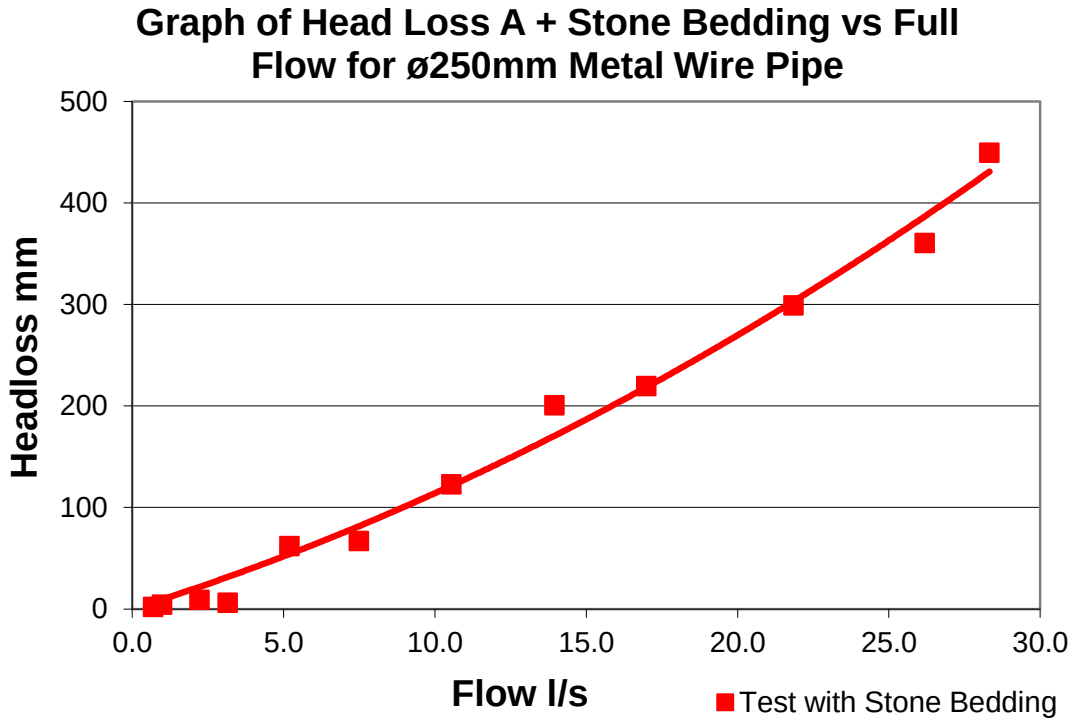

Figure F6: Headloss due to the slots (Loss A) and Stone bedding versus the flowrate for a Full flowing ø250mm Metal Wire pipe

Equation 11 below describes the relationship between headloss due to slot friction and stone bedding and flowrate:

$$\Delta P = 0.369Q^2 + 9.3323Q \qquad \text{Eqn 11}$$

With

ΔP = Headloss due to slot friction in mm

Q = Flowrate for one full pipeline in litres/second

F.5.4 Segmental Analysis of HPM

Analysing the Metal Wire/Perforation pipe friction + Stone Bedding and initial flow relationship, is as per Chapter F4.4. The flow was calculated at the same points in the HPM. The model was once again was portioned into five segments.

As described by Table F11, the Perforation Loss A + Stone Bedding accounts for the nearly all of the pressure loss. Hence for a point on the Intake pipeline just inside WC1, the velocity of the flow into the pipeline is at its maximum. The velocity at this point is termed V_{max}. The opposite holds true for a point at the start of the Intake pipeline. At this point, V_{min}, the velocity of the inflow is zero. Hence via linear interpolation, the velocity at any point in between both ends, can be calculated. Figure F4, in Chapter F4.4 describes the manner in which the HPM is segmented.

F.5.4.1 Methodology

In order to calculate the flow at various points within the model, the HPM was divided into five segments. The velocities V_{MAX}, V_1, V_2 , V_3, V_4 and V_{MIN} occur at the border of each segment, Hence for each segment, the Average Velocity, V_S1, V_S2, V_S3, V_S4 and V_S5 for is easily calculated.

V_{MAX} is derived from Bernoulli principles where :

$$V = \sqrt{2g\Delta h} \qquad \text{Eqn F1}$$

With

V = Velocity in m/s

Δh = = is the driving pressure

g = gravitational constant (9.81m/s^2)

Note that the driving pressure Δh is Perforation Loss A+ Stone bedding. The flow from each segment is then calculated by multiplying the velocity with the perforation area and a discharge coefficient, C_d. Table F13 shows the distribution of inflowing velocity over the length of the Intake Pipeline.

Equation F2 was used to calculate the flow from each segment. Table F14 contains the flowrate for each segment and the sum of flow from all segments of the pipeline.

$$Q_T = \sum q = \sum C_d A \sqrt{2g\Delta h} \qquad \text{Eqn F2}$$

With

q = Flowrate through for each segment in m^3/s

Q = Sum of Flowrate form each segment in m^3/s

A= The Area through which flow is allowed in m^2

C_d = Coefficient of Discharge

Table F13: Inflowing velocity - water flowing into the pipe, over the length of the Intake Pipeline

		Pos. 0	Pos. 1	Pos. 2	Pos. 3	Pos. 4	Pos. 5	Pos. 6	Pos. 7	Pos. 8	Pos. 9	Pos. 10
Test	Loss A + Stone Bedding	Vmax	Vs 1	V1	Vs 2	V2	Vs 3	V3	Vs 4	V4	Vs 5	Vmin
0	mm	m/s	m/s	m/s	m/s	m/s	m/s	m/s	m/s	m/s	m/s	m/s
1	2.00	0.198	0.178	0.158	0.139	0.119	0.099	0.079	0.059	0.040	0.020	0.000
2	4.00	0.280	0.252	0.224	0.196	0.168	0.140	0.112	0.084	0.056	0.028	0.000
3	8.99	0.420	0.378	0.336	0.294	0.252	0.210	0.168	0.126	0.084	0.042	0.000
4	5.98	0.342	0.308	0.274	0.240	0.205	0.171	0.137	0.103	0.068	0.034	0.000
5	61.94	1.102	0.992	0.882	0.772	0.661	0.551	0.441	0.331	0.220	0.110	0.000
6	66.88	1.146	1.031	0.916	0.802	0.687	0.573	0.458	0.344	0.229	0.115	0.000
7	122.76	1.552	1.397	1.242	1.086	0.931	0.776	0.621	0.466	0.310	0.155	0.000
8	200.58	1.984	1.785	1.587	1.389	1.190	0.992	0.794	0.595	0.397	0.198	0.000
9	219.38	2.075	1.867	1.660	1.452	1.245	1.037	0.830	0.622	0.415	0.207	0.000
10	298.98	2.422	2.180	1.938	1.695	1.453	1.211	0.969	0.727	0.484	0.242	0.000
11	360.53	2.660	2.394	2.128	1.862	1.596	1.330	1.064	0.798	0.532	0.266	0.000
12	449.28	2.969	2.672	2.375	2.078	1.781	1.484	1.188	0.891	0.594	0.297	0.000

Table F14: Calculated Flowrate from all segments of the Pipeline

1	2	3	4	5	6	7	8	9	10	11
Test	Loss A + Stone Bedding	C_b	Qs 1	Qs 2	Qs 3	Qs 4	Qs 5	Q Total	Q Total	2Q Total
0	mm		m^3/s	m^3/s	m^3/s	m^3/s	m^3/s	m^3/s	l/s	l/s
1	2.00	0.043	0.00013	0.00010	0.00007	0.00004	0.00001	0.0003	0.35	0.70
2	4.00	0.043	0.00018	0.00014	0.00010	0.00006	0.00002	0.0005	0.49	0.98
3	8.99	0.066	0.00040	0.00031	0.00022	0.00013	0.00004	0.0011	1.11	2.23
4	5.98	0.114	0.00057	0.00044	0.00032	0.00019	0.00006	0.0016	1.58	3.16
5	61.94	0.058	0.00094	0.00073	0.00052	0.00031	0.00010	0.0026	2.60	5.20
6	66.88	0.081	0.00135	0.00105	0.00075	0.00045	0.00015	0.0037	3.74	7.49
7	122.76	0.084	0.00190	0.00148	0.00105	0.00063	0.00021	0.0053	5.27	10.54
8	200.58	0.087	0.00251	0.00195	0.00140	0.00084	0.00028	0.0070	6.98	13.95
9	219.38	0.101	0.00306	0.00238	0.00170	0.00102	0.00034	0.0085	8.49	16.99
10	298.98	0.111	0.00393	0.00306	0.00218	0.00131	0.00044	0.0109	10.92	21.85
11	360.53	0.122	0.00471	0.00367	0.00262	0.00157	0.00052	0.0131	13.09	26.19
12	449.28	0.118	0.00510	0.00397	0.00283	0.00170	0.00057	0.0142	14.16	28.32

Of particular concern is the Energy Grade Line (EGL) at the centre of the Intake Pipeline. The EGL shows the amount of energy that has been lost from the stone bedding friction and from water entering the Intake Pipeline

Figure F13 below is a plot of EGLs at the centre of the Intake Pipeline. For the 18 tests conducted, the increase in pressure losses closer to the exit point of WC1, can be clearly seen.

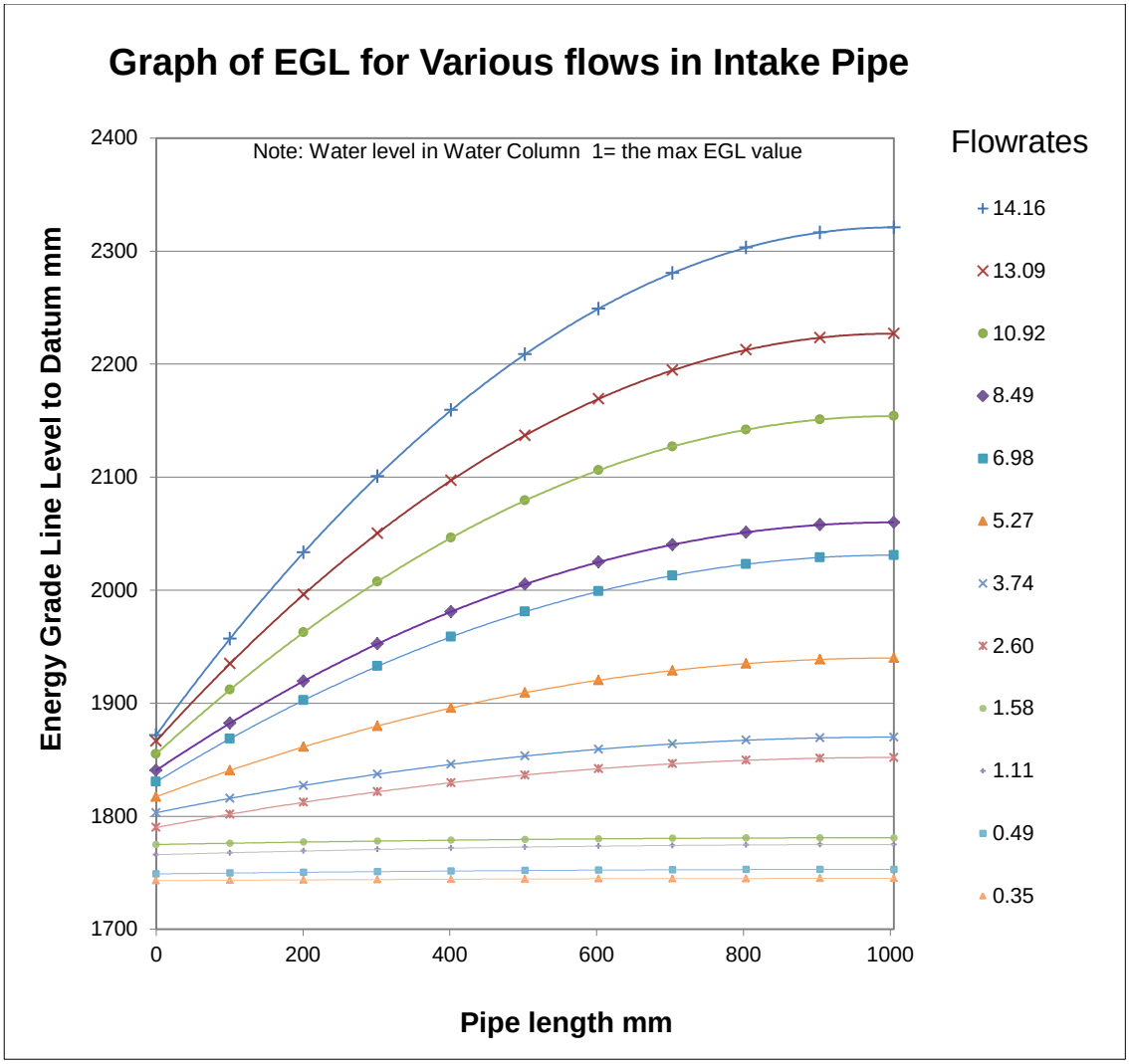

Figure F7: Plot of EGLs at the centre of the Intake Pipeline for Water and Stone Bedding Test

The calculation of the EGL at various points within the Intake pipeline is crucial as it aids in determining the loss due to the stone bedding. This can be seen in the flowing chapter.

F.5.4.2 Pressure loss due to Stone Bedding

Calculating the loss of pressure due to stone bedding is critical as it inadvertently determines the design of the seawater Intake. Note that the stone bedding for all tests were standardised with the Intake pipe being 150mm above the bedrock, 300mm below the cover level of the stone bedding and 2*485mm clearance from an adjacent intake pipeline. Three methods where employed when seeking to determine the pressure loss due the stone bedding.

F.5.4.2.1 Method 1: Simple method for determining stone bedding loss

In this simplistic method, the equation for the “Water Test only: is removed from the equation for “Water and Stone test” This is simplified as Eqn 12 equals Eqn 11 minus Eqn 10 where:

$$\Delta P = .369Q^2 + 9.3323Q \qquad \text{Eqn11}$$

minus

$$\Delta P = 0.494Q^2 + 1.443Q \qquad \text{Eqn10}$$

equals

$$\Delta P = -0.131Q^2 + 7.8893Q \qquad \text{Eqn12}$$

Table F11 shows the headloss for corresponding flow values while Figure F14 plots these graphically.

Table F15: Method1:ø250mm Metal Wire Pipe Test: Stone bedding friction only

Test No.	Q Half Pipe	Q Full Pipe	Stone Bedding Friction
	l/s	l/s	mm
1	0.35	0.70	5.42
2	0.49	0.98	7.63
3	1.11	2.23	16.93
4	1.58	3.16	23.61
5	2.60	5.20	37.45
6	3.74	7.49	51.71
7	5.27	10.54	68.60
8	6.98	13.95	84.54
9	8.49	16.99	96.18
10	10.92	21.85	109.77
11	13.09	26.19	116.69
12	14.16	28.32	118.28

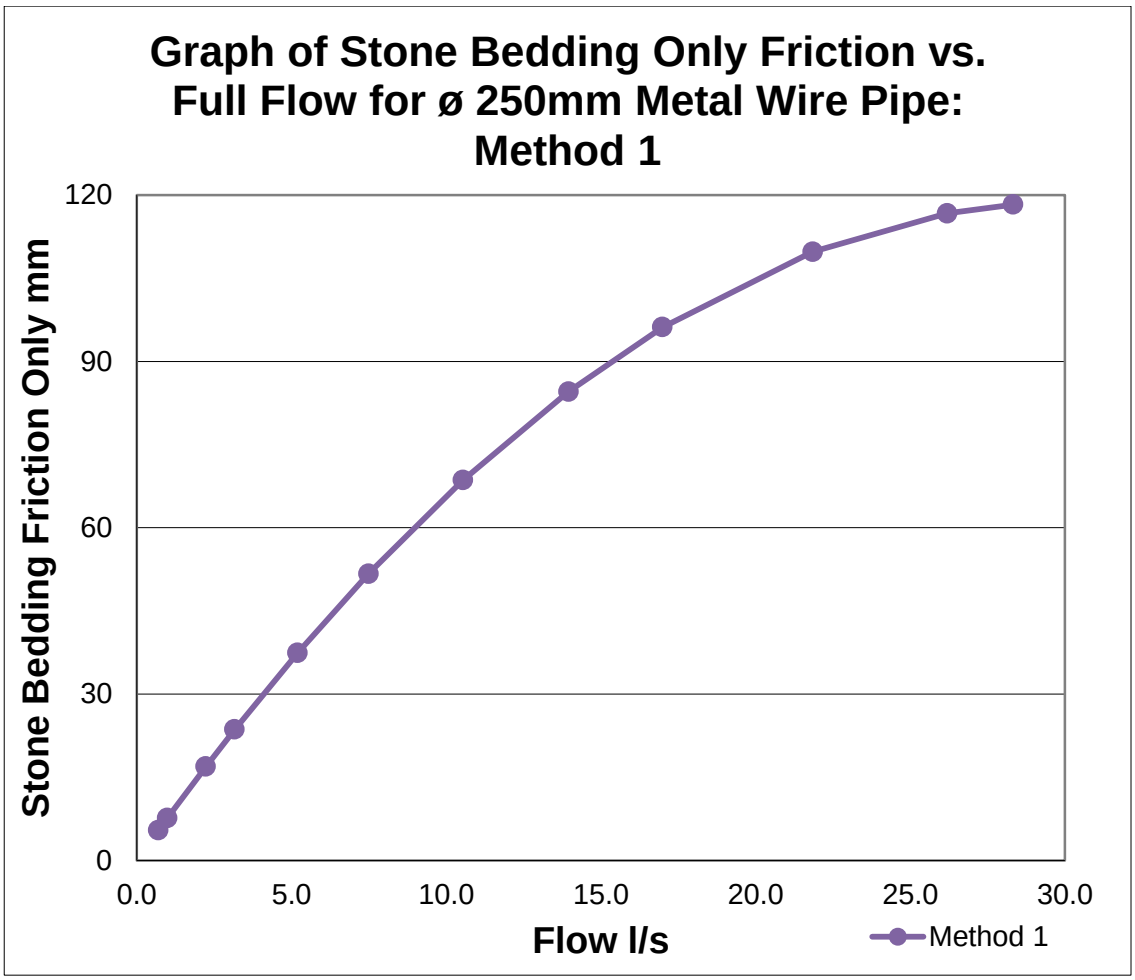

Figure F8:ø250mm Metal Wire Pipe,(WST): Pressure loss due to Stone Bedding Only-Method1

F.5.4.2.2 Method 2: Kenny, Lau and Ofoegbu Method for determining headloss due to stone bedding

The second method used to determine the loss of pressure due to Stone bedding, looks at the hydraulic conductivity of the stone bedding. From Table F14, the velocity for each segment of the Intake pipeline was determined. However stone bedding cannot be split into equal segments as well. This is only correct for stone bedding adjacent to the intake pipeline. It does not apply to the flat, horizontal surface of the stone bedding.

Flow into the intake pipe line is proportional to the velocity. The maximum velocity occurs at one end of the intake pipeline and the minimum velocity occurs at the start of the intake pipeline. Table F16 below looks at the ratio of the (flowrate) as a proportion of the entire flowrate.

As seen in Figure F9, these proportions were then applied to length of the stone bed. This splitting of the stone bedding surface ensured that all flows entering the stone bed were proportional to the flow entering the intake pipeline for all segments.

Table F16:ø250mm Metal Wire Pipe, Water and Stone Bedding Test: Flow through segments

Test No.	Seg1	Seg2	Seg3	Seg4	Seg5	Seg1	Seg2	Seg3	Seg4	Seg5
	Qs 1	Qs 2	Qs 3	Qs 4	Qs 5	Qs 1	Qs 2	Qs 3	Qs 4	Qs 5
	m^3/s	m^3/s	m^3/s	m^3/s	m^3/s	m^3/s	m^3/s	m^3/s	m^3/s	m^3/s
1	0.00013	0.00010	0.00007	0.00004	0.00001	36%	28%	20%	12%	4%
2	0.00018	0.00014	0.00010	0.00006	0.00002	36%	28%	20%	12%	4%
3	0.00040	0.00031	0.00022	0.00013	0.00004	36%	28%	20%	12%	4%
4	0.00057	0.00044	0.00032	0.00019	0.00006	36%	28%	20%	12%	4%
5	0.00094	0.00073	0.00052	0.00031	0.00010	36%	28%	20%	12%	4%
6	0.00135	0.00105	0.00075	0.00045	0.00015	36%	28%	20%	12%	4%
7	0.00190	0.00148	0.00105	0.00063	0.00021	36%	28%	20%	12%	4%
8	0.00251	0.00195	0.00140	0.00084	0.00028	36%	28%	20%	12%	4%
9	0.00306	0.00238	0.00170	0.00102	0.00034	36%	28%	20%	12%	4%
10	0.00393	0.00306	0.00218	0.00131	0.00044	36%	28%	20%	12%	4%
11	0.00471	0.00367	0.00262	0.00157	0.00052	36%	28%	20%	12%	4%
12	0.00510	0.00397	0.00283	0.00170	0.00057	36%	28%	20%	12%	4%

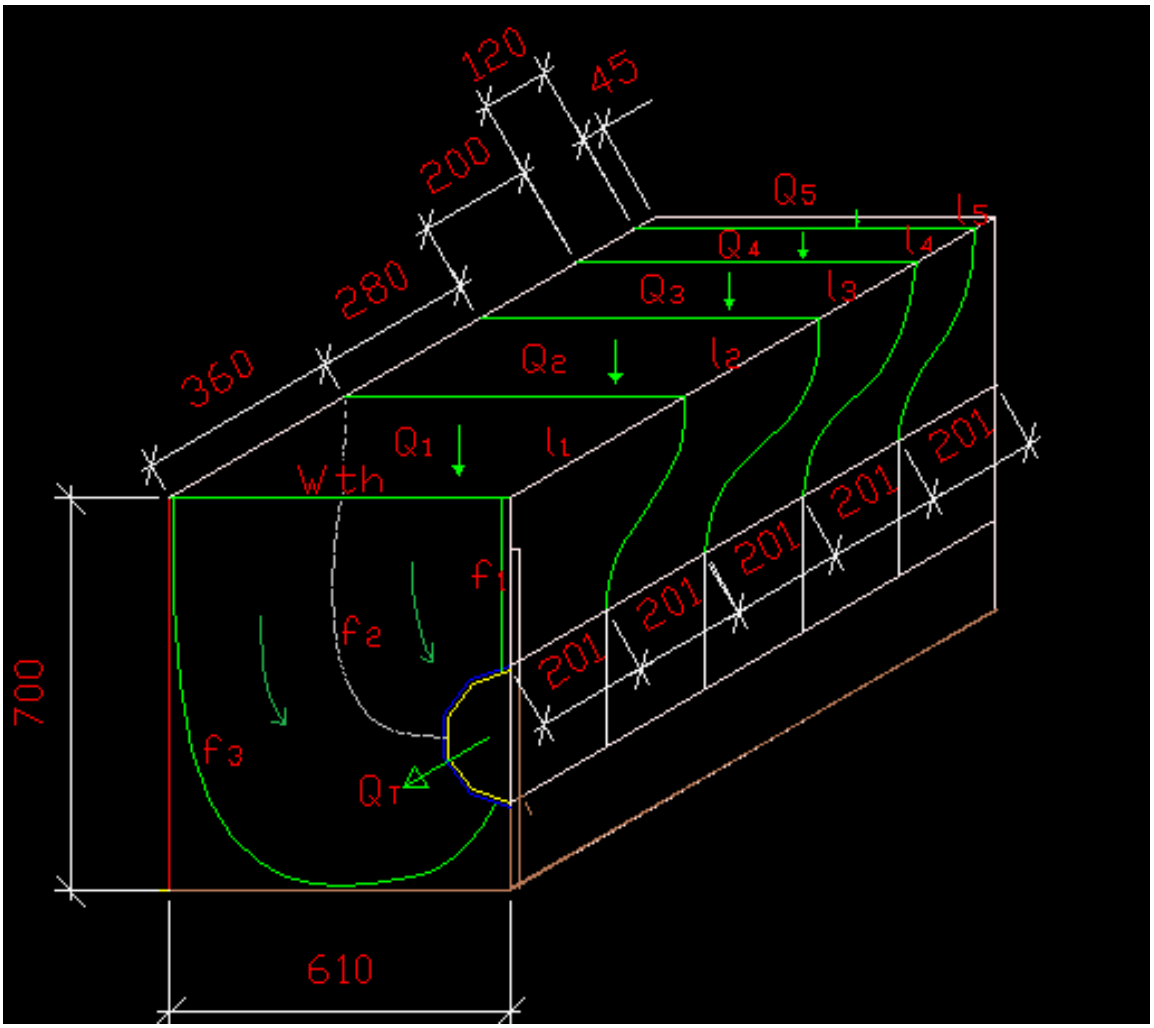

Figure F9: ø250mm Metal Wire pipe, Water and Stone Bedding Test: Segmentation of Stone Bedding area

Figure F9 shows the simplified version of a single notional segment. Note line f_1, f_2 and f_3 as lines of reference in Figure F9 and F10. As in Figure F10, length (l_1) is multiplied by the standard width (With), to create the area A_1. Area A_4 was easily calculated it is based on the intake pipe dimensions. Areas A_2 and A_3 are a third of the distance from each end and hence are calculated proportionately. The distances from Area A_1 to A_2 to A_3 to A_4 are noted as Lengths len_1, len_2 and len_3 respectively.

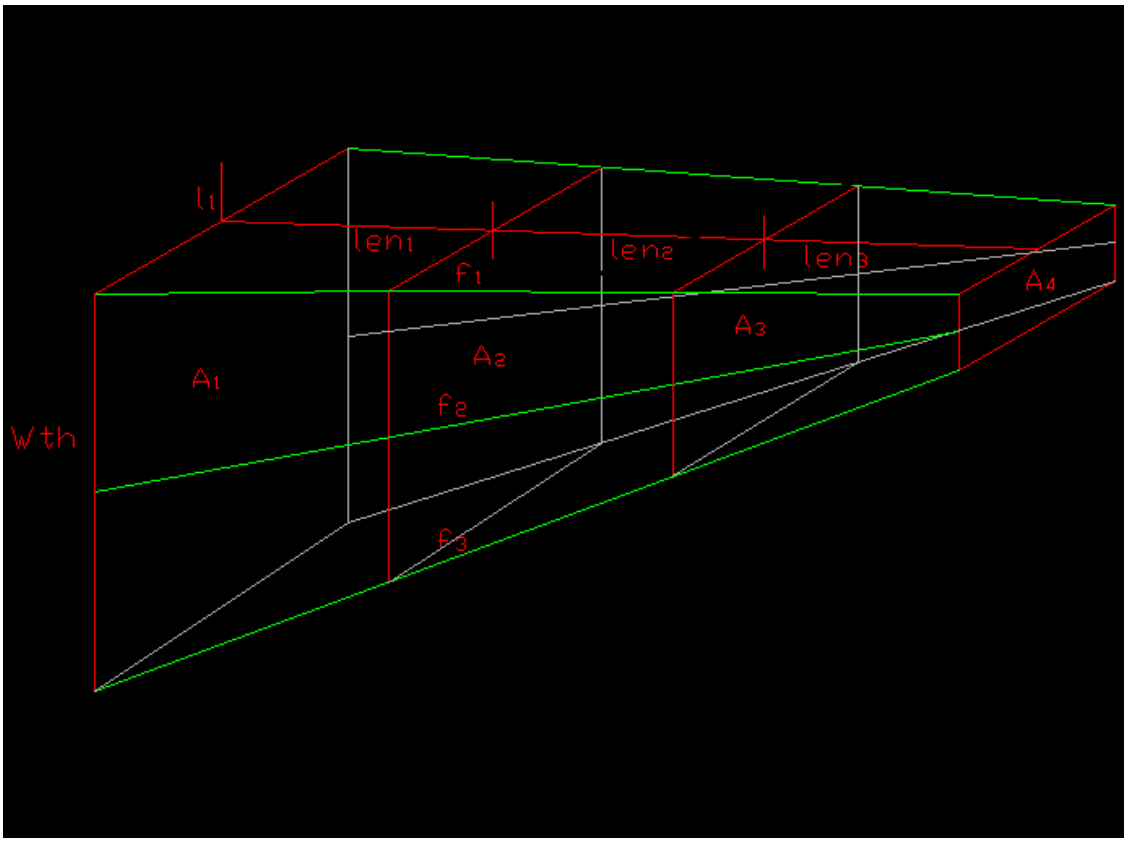

Figure F10: Notional flow path of a stone bedding segment

In order to calculate the pressure loss due to the stone bedding, the hydraulic conductivity is required. The pressure loss is defined as follows:

$$hf(m) = \frac{L * V}{k} \qquad \text{Eqn 4}$$

Where:

Hf = pressure loss due to friction within stone bedding

L = Length of water path (m)

V = Flow velocity

k = Hydraulic conductivity

The first three variables are easily to calculate however determining the hydraulic conductivity k, requires further investigation.

The hydraulic conductivity is calculated using the following equation

$$k = \frac{\gamma_w}{\eta K} \qquad \text{Eqn 5}$$

Where:

k = Hydraulic conductivity

γ_W = Unit Weight of Water

η = Dynamic Viscosity of water

K = Absolute Hydraulic conductivity

The unit weight of water γ_W ,' and the dynamic viscosity of water η are fairly simple to calculate. However the Absolute Hydraulic conductivity K has to be calculated. It is calculated using the following equation:

$$K = C_u D_5^2 \qquad \text{Eqn 6}$$

Where:

K = Absolute Hydraulic conductivity

C_u = Coefficient of Uniformity. Varies between 0.05 to 1

D_5 = Dimension of aggregate that has a cumulative percentage passing of 5%

Figure F11 below is a typical grading curve for nominally single-sized 19mm. From the grading curve, a value of D_5 = 10mm was obtained. Hence for a C_u of 0.8, Eqn E6 yields a K of 80mm^2. As confirmation, Figure E16 is a graphical plot of Equation10. Utilising eqn 5 and the following values:

D_5 = 10mm

γ_W = 9800 N/m3

η = 0.00014 Ns/m

a k value of approximately 0.7m/s is found.

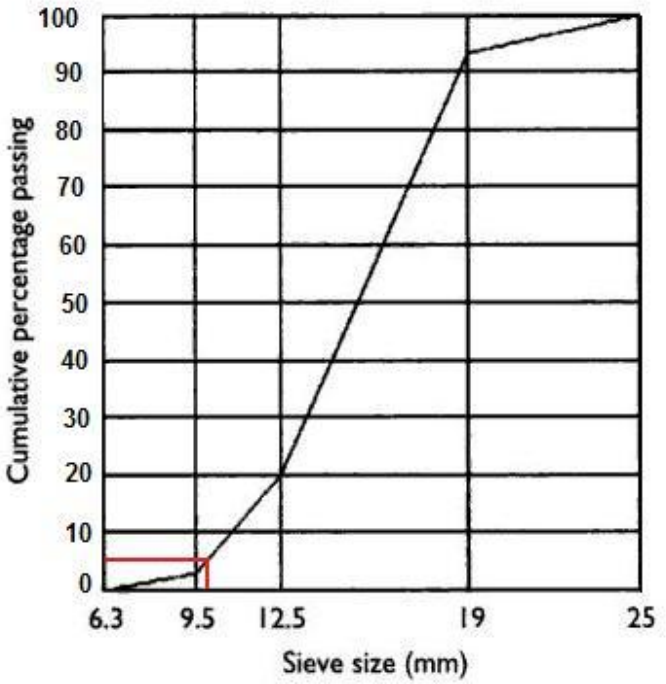

Figure F11: Typical grading curve for nominally single-sized 19mm Stone (Alexander & Mindess, 2005)

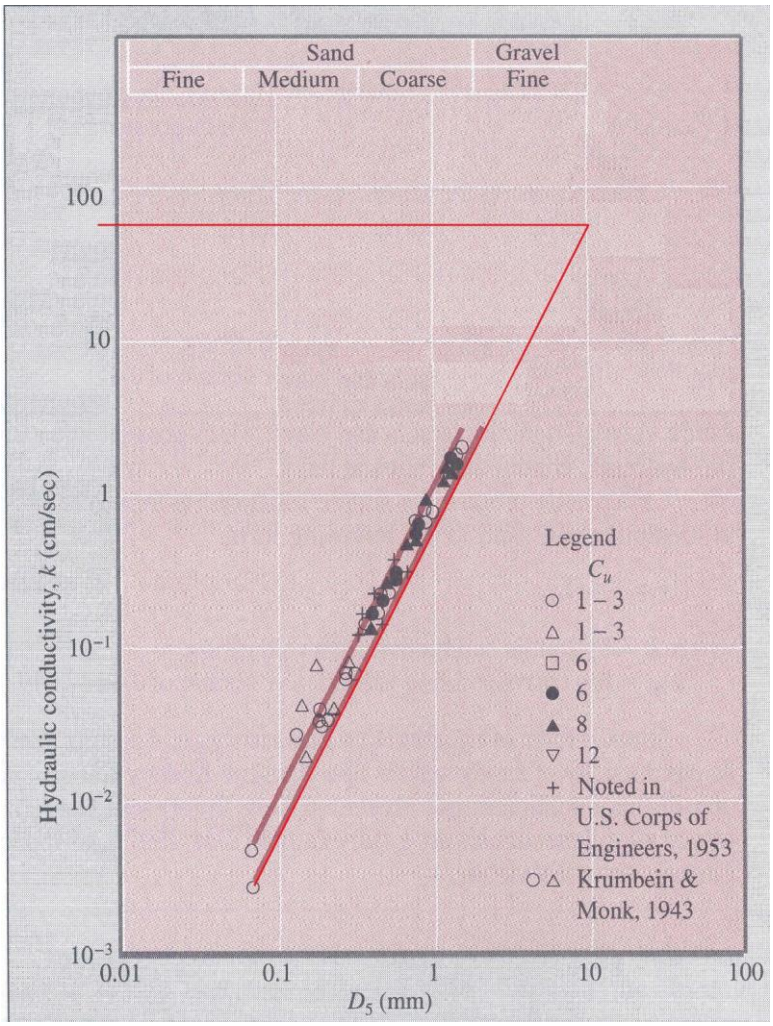

Figure F12: Graphical plot of Hydraulic Conductivity Equation (Das 2000)

Table F17: Summary : Calculating the Hydraulic conductivity

Description	Value	Unit
C_u (0.05 to 1)	0.80	
D_5	10.0	mm
Water Column Width	0.61	m
Absolute Conductivity K	80	mm^2
Unit Weight of Water γ_W	9800	N/m^3
Dynamic Viscosity of water η	1.14E-03	Ns/m^2
Hydraulic Conductivity k	0.688	m/s

Using the values from Table F16 and F17, headloss for segment 1 was calculated in the following manner. With the flow through each segment know, it is possible to determine the headloss if the areas through which water flows, is uniform.

However, this is not the case. Hence each segment has been split into three equal portions. Table F18 below, describes the manner in which Segment 1 is split into three sub segments. Thereafter, Table F19 determines the average velocity for each sub segment, the associated headloss and finally the cumulative headloss for Segment 1. The subsequent tables describe the headloss calculated for Segments, 2, 3, 4 and 5.

Table F18: Segment 1: Averaging of Areas

Test No.	Len1	A11	A12	A13	A14	Qs 1	Ave A1	Ave A2	Ave A3
	m	m^2	m^2	m^2	m^2	m^3/s	m^2	m^2	m^2
1	0.3618	0.221	0.202	0.183	0.164	0.0001	0.192	0.174	0.082
2	0.3618	0.221	0.202	0.183	0.164	0.0002	0.192	0.174	0.082
3	0.3618	0.221	0.202	0.183	0.164	0.0004	0.192	0.174	0.082
4	0.3618	0.221	0.202	0.183	0.164	0.0006	0.192	0.174	0.082
5	0.3618	0.221	0.202	0.183	0.164	0.0009	0.192	0.174	0.082
6	0.3618	0.221	0.202	0.183	0.164	0.0013	0.192	0.174	0.082
7	0.3618	0.221	0.202	0.183	0.164	0.0019	0.192	0.174	0.082
8	0.3618	0.221	0.202	0.183	0.164	0.0025	0.192	0.174	0.082
9	0.3618	0.221	0.202	0.183	0.164	0.0031	0.192	0.174	0.082
10	0.3618	0.221	0.202	0.183	0.164	0.0039	0.192	0.174	0.082
11	0.3618	0.221	0.202	0.183	0.164	0.0047	0.192	0.174	0.083
12	0.3618	0.221	0.202	0.183	0.164	0.0051	0.192	0.174	0.083

Table F19: Segment 1: Velocity and cumulative headloss

Test No.	Vel 1A	Vel 1B	Vel 1C	H_l11	H_l12	H_l13	$H_l1Total$	$H_l1Total$
	m/s	m/s	m/s	m	m	m	m	mm
1	0.0007	0.0007	0.0015	0.0003	0.0003	0.0006	0.0012	1.16
2	0.0009	0.0010	0.0022	0.0004	0.0004	0.0009	0.0016	1.64
3	0.0021	0.0023	0.0049	0.0008	0.0009	0.0020	0.0037	3.71
4	0.0030	0.0033	0.0069	0.0012	0.0013	0.0028	0.0053	5.26
5	0.0049	0.0054	0.0113	0.0019	0.0022	0.0045	0.0086	8.64
6	0.0070	0.0078	0.0163	0.0028	0.0031	0.0065	0.0124	12.43
7	0.0099	0.0109	0.0229	0.0039	0.0044	0.0091	0.0175	17.47
8	0.0131	0.0145	0.0301	0.0052	0.0058	0.0121	0.0231	23.07
9	0.0159	0.0176	0.0366	0.0064	0.0070	0.0146	0.0280	28.04
10	0.0204	0.0227	0.0468	0.0082	0.0091	0.0187	0.0360	35.97
11	0.0245	0.0272	0.0558	0.0098	0.0109	0.0223	0.0430	43.01
12	0.0265	0.0294	0.0603	0.0106	0.0118	0.0241	0.0465	46.46

Table F20: Segment 2: Averaging of Areas

Test No.	Len2	A21	A22	A23	A24	Qs 2	Ave A1	Ave A2	Ave A3
	m	m^2	m^2	m^2	m^2	m^3/s	m^2	m^2	m^2
1	0.2814	0.172	0.169	0.167	0.164	0.0001	0.168	0.165	0.082
2	0.2814	0.172	0.169	0.167	0.164	0.0001	0.168	0.165	0.082
3	0.2814	0.172	0.169	0.167	0.164	0.0003	0.168	0.165	0.082
4	0.2814	0.172	0.169	0.167	0.164	0.0004	0.168	0.165	0.082
5	0.2814	0.172	0.169	0.167	0.164	0.0007	0.168	0.165	0.082
6	0.2814	0.172	0.169	0.167	0.164	0.0010	0.168	0.165	0.083
7	0.2814	0.172	0.169	0.167	0.164	0.0015	0.168	0.165	0.083
8	0.2814	0.172	0.169	0.167	0.164	0.0020	0.168	0.165	0.083
9	0.2814	0.172	0.169	0.167	0.164	0.0024	0.168	0.165	0.083
10	0.2814	0.172	0.169	0.167	0.164	0.0031	0.168	0.165	0.084
11	0.2814	0.172	0.169	0.167	0.164	0.0037	0.168	0.165	0.084
12	0.2814	0.172	0.169	0.167	0.164	0.0040	0.168	0.165	0.084

Table F21: Segment 2: Velocity and cumulative headloss

Test No.	Vel 2A	Vel 2B	Vel 2C	H_l21	H_l22	H_l23	H_l2Total	H_l2 Total
	m/s	m/s	m/s	m	m	m	m	mm
1	0.0006	0.0006	0.0012	0.0002	0.0002	0.0005	0.0009	0.94
2	0.0008	0.0008	0.0017	0.0003	0.0003	0.0007	0.0013	1.33
3	0.0019	0.0019	0.0038	0.0007	0.0008	0.0015	0.0030	3.02
4	0.0026	0.0027	0.0054	0.0011	0.0011	0.0022	0.0043	4.28
5	0.0043	0.0044	0.0088	0.0017	0.0018	0.0035	0.0070	7.03
6	0.0062	0.0063	0.0127	0.0025	0.0025	0.0051	0.0101	10.11
7	0.0088	0.0089	0.0178	0.0035	0.0036	0.0071	0.0142	14.22
8	0.0116	0.0118	0.0235	0.0047	0.0047	0.0094	0.0188	18.79
9	0.0142	0.0144	0.0286	0.0057	0.0058	0.0114	0.0229	22.85
10	0.0182	0.0185	0.0366	0.0073	0.0074	0.0146	0.0293	29.33
11	0.0218	0.0222	0.0437	0.0087	0.0089	0.0175	0.0351	35.09
12	0.0236	0.0240	0.0472	0.0094	0.0096	0.0189	0.0379	37.91

Table F22: Segment 3: Averaging of Areas

Test No.	Len3	A31	A32	A33	A34	Qs 3	Ave A1	Ave A2	Ave A3
	m	m^2	m^2	m^2	m^2	m^3/s	m^2	m^2	m^2
1	0.201	0.123	0.136	0.150	0.164	0.0001	0.143	0.157	0.082
2	0.201	0.123	0.136	0.150	0.164	0.0001	0.143	0.157	0.082
3	0.201	0.123	0.136	0.150	0.164	0.0002	0.143	0.157	0.082
4	0.201	0.123	0.136	0.150	0.164	0.0003	0.143	0.157	0.082
5	0.201	0.123	0.136	0.150	0.164	0.0005	0.143	0.157	0.082
6	0.201	0.123	0.136	0.150	0.164	0.0007	0.143	0.157	0.082
7	0.201	0.123	0.136	0.150	0.164	0.0011	0.143	0.157	0.083
8	0.201	0.123	0.136	0.150	0.164	0.0014	0.143	0.157	0.083
9	0.201	0.123	0.136	0.150	0.164	0.0017	0.143	0.157	0.083
10	0.201	0.123	0.136	0.150	0.164	0.0022	0.143	0.157	0.083
11	0.201	0.123	0.136	0.150	0.164	0.0026	0.143	0.157	0.083
12	0.201	0.123	0.136	0.150	0.164	0.0028	0.143	0.157	0.083

Table F23: Segment 3: Velocity and cumulative headloss

Test No.	Vel 3A	Vel 3B	Vel 3C	H_l31	H_l32	H_l33	$H_l3Total$	$H_l3Total$
	m/s	m/s	m/s	m	m	m	m	mm
1	0.0005	0.0004	0.0008	0.0002	0.0002	0.0003	0.0007	0.71
2	0.0007	0.0006	0.0012	0.0003	0.0003	0.0005	0.0010	1.00
3	0.0016	0.0014	0.0027	0.0006	0.0006	0.0011	0.0023	2.27
4	0.0022	0.0020	0.0038	0.0009	0.0008	0.0015	0.0032	3.22
5	0.0036	0.0033	0.0063	0.0015	0.0013	0.0025	0.0053	5.30
6	0.0052	0.0048	0.0091	0.0021	0.0019	0.0036	0.0076	7.63
7	0.0074	0.0067	0.0128	0.0029	0.0027	0.0051	0.0107	10.73
8	0.0097	0.0089	0.0169	0.0039	0.0036	0.0067	0.0142	14.19
9	0.0119	0.0108	0.0205	0.0047	0.0043	0.0082	0.0173	17.26
10	0.0152	0.0139	0.0263	0.0061	0.0056	0.0105	0.0222	22.17
11	0.0183	0.0167	0.0314	0.0073	0.0067	0.0126	0.0265	26.54
12	0.0198	0.0180	0.0339	0.0079	0.0072	0.0136	0.0287	28.68

Table F24: Segment 4: Averaging of Areas

Test No.	Len4	A41	A42	A43	A44	Qs 4	Ave A1	Ave A2	Ave A3
	m	m^2	m^2	m^2	m^2	m^3/s	m^2	m^2	m^2
1	0.121	0.074	0.104	0.134	0.164	0.0000	0.119	0.149	0.082
2	0.121	0.074	0.104	0.134	0.164	0.0001	0.119	0.149	0.082
3	0.121	0.074	0.104	0.134	0.164	0.0001	0.119	0.149	0.082
4	0.121	0.074	0.104	0.134	0.164	0.0002	0.119	0.149	0.082
5	0.121	0.074	0.104	0.134	0.164	0.0003	0.119	0.149	0.082
6	0.121	0.074	0.104	0.134	0.164	0.0004	0.119	0.149	0.082
7	0.121	0.074	0.104	0.134	0.164	0.0006	0.119	0.149	0.082
8	0.121	0.074	0.104	0.134	0.164	0.0008	0.119	0.149	0.082
9	0.121	0.074	0.104	0.134	0.164	0.0010	0.119	0.149	0.082
10	0.121	0.074	0.104	0.134	0.164	0.0013	0.119	0.149	0.082
11	0.121	0.074	0.104	0.134	0.164	0.0016	0.119	0.149	0.082
12	0.121	0.074	0.104	0.134	0.164	0.0017	0.119	0.149	0.082

Table F25: Segment 4: Velocity and cumulative headloss

Test No.	Vel 4A	Vel 4B	Vel 4C	H_l41	H_l42	H_l43	$H_l4Total$	$H_l4Total$
	m/s	m/s	m/s	m	m	m	m	mm
1	0.0004	0.0003	0.0005	0.0001	0.0001	0.0002	0.0005	0.46
2	0.0005	0.0004	0.0007	0.0002	0.0002	0.0003	0.0006	0.65
3	0.0011	0.0009	0.0016	0.0005	0.0004	0.0007	0.0015	1.46
4	0.0016	0.0013	0.0023	0.0006	0.0005	0.0009	0.0021	2.07
5	0.0026	0.0021	0.0038	0.0010	0.0008	0.0015	0.0034	3.40
6	0.0038	0.0030	0.0055	0.0015	0.0012	0.0022	0.0049	4.90
7	0.0053	0.0042	0.0077	0.0021	0.0017	0.0031	0.0069	6.90
8	0.0070	0.0056	0.0102	0.0028	0.0022	0.0041	0.0091	9.13
9	0.0086	0.0068	0.0123	0.0034	0.0027	0.0049	0.0111	11.11
10	0.0110	0.0088	0.0159	0.0044	0.0035	0.0063	0.0143	14.27
11	0.0132	0.0105	0.0190	0.0053	0.0042	0.0076	0.0171	17.09
12	0.0143	0.0114	0.0205	0.0057	0.0046	0.0082	0.0185	18.48

Table F26: Segment 5: Averaging of Areas

Test No.	Len5	A51	A52	A53	A54	Qs 5	Ave A1	Ave A2	Ave A3
	m	m^2	m^2	m^2	m^2	m^3/s	m^2	m^2	m^2
1	0.0402	0.025	0.071	0.118	0.164	0.0000	0.094	0.141	0.082
2	0.0402	0.025	0.071	0.118	0.164	0.0000	0.094	0.141	0.082
3	0.0402	0.025	0.071	0.118	0.164	0.0000	0.094	0.141	0.082
4	0.0402	0.025	0.071	0.118	0.164	0.0001	0.094	0.141	0.082
5	0.0402	0.025	0.071	0.118	0.164	0.0001	0.094	0.141	0.082
6	0.0402	0.025	0.071	0.118	0.164	0.0001	0.094	0.141	0.082
7	0.0402	0.025	0.071	0.118	0.164	0.0002	0.094	0.141	0.082
8	0.0402	0.025	0.071	0.118	0.164	0.0003	0.094	0.141	0.082
9	0.0402	0.025	0.071	0.118	0.164	0.0003	0.094	0.141	0.082
10	0.0402	0.025	0.071	0.118	0.164	0.0004	0.094	0.141	0.082
11	0.0402	0.025	0.071	0.118	0.164	0.0005	0.094	0.141	0.082
12	0.0402	0.025	0.071	0.118	0.164	0.0006	0.094	0.141	0.082

Table F27: Segment 5: Velocity and cumulative headloss

Test No.	Vel 5A	Vel 5B	Vel 5C	H_l51	H_l52	H_l53	$H_l5Total$	$H_l5Total$
	m/s	m/s	m/s	m	m	m	m	mm
1	0.0001	0.0001	0.0002	0.0001	0.0000	0.0001	0.0002	0.17
2	0.0002	0.0001	0.0002	0.0001	0.0001	0.0001	0.0002	0.24
3	0.0005	0.0003	0.0005	0.0002	0.0001	0.0002	0.0005	0.53
4	0.0007	0.0004	0.0008	0.0003	0.0002	0.0003	0.0008	0.76
5	0.0011	0.0007	0.0013	0.0004	0.0003	0.0005	0.0012	1.24
6	0.0016	0.0011	0.0018	0.0006	0.0004	0.0007	0.0018	1.79
7	0.0022	0.0015	0.0026	0.0009	0.0006	0.0010	0.0025	2.52
8	0.0030	0.0020	0.0034	0.0012	0.0008	0.0014	0.0033	3.33
9	0.0036	0.0024	0.0041	0.0014	0.0010	0.0017	0.0041	4.06
10	0.0046	0.0031	0.0053	0.0019	0.0012	0.0021	0.0052	5.22
11	0.0056	0.0037	0.0064	0.0022	0.0015	0.0025	0.0063	6.25
12	0.0060	0.0040	0.0069	0.0024	0.0016	0.0028	0.0068	6.76

Table F28 below summaries the results of Tables F18 to F27. Figure F13 plots these graphically. A trendline is added to the results in order to predict the headloss, due to stone bedding, at the most downstream point of WC1. It is at this point that the largest magnitude of headloss occurs. Table F29 summaries these results.

Table F28: Summary of 15 Headloss Tests. Results from Tables F18 to F27

Test No.	Total Q	Total 2Q	Segment 1	Segment 2	Segment 3	Segment 4	Segment 5
	l/s	l/s	mm	mm	mm	mm	mm
1	0.35	0.70	1.16	0.94	0.71	0.46	0.17
2	0.49	0.98	1.64	1.33	1.00	0.65	0.24
3	1.11	2.23	3.71	3.02	2.27	1.46	0.53
4	1.58	3.16	5.26	4.28	3.22	2.07	0.76
5	2.60	5.20	8.64	7.03	5.30	3.40	1.24
6	3.74	7.49	12.43	10.11	7.63	4.90	1.79
7	5.27	10.54	17.47	14.22	10.73	6.90	2.52
8	6.98	13.95	23.07	18.79	14.19	9.13	3.33
9	8.49	16.99	28.04	22.85	17.26	11.11	4.06
10	10.92	21.85	35.97	29.33	22.17	14.27	5.22
11	13.09	26.19	43.01	35.09	26.54	17.09	6.25
12	14.16	28.32	46.46	37.91	28.68	18.48	6.76

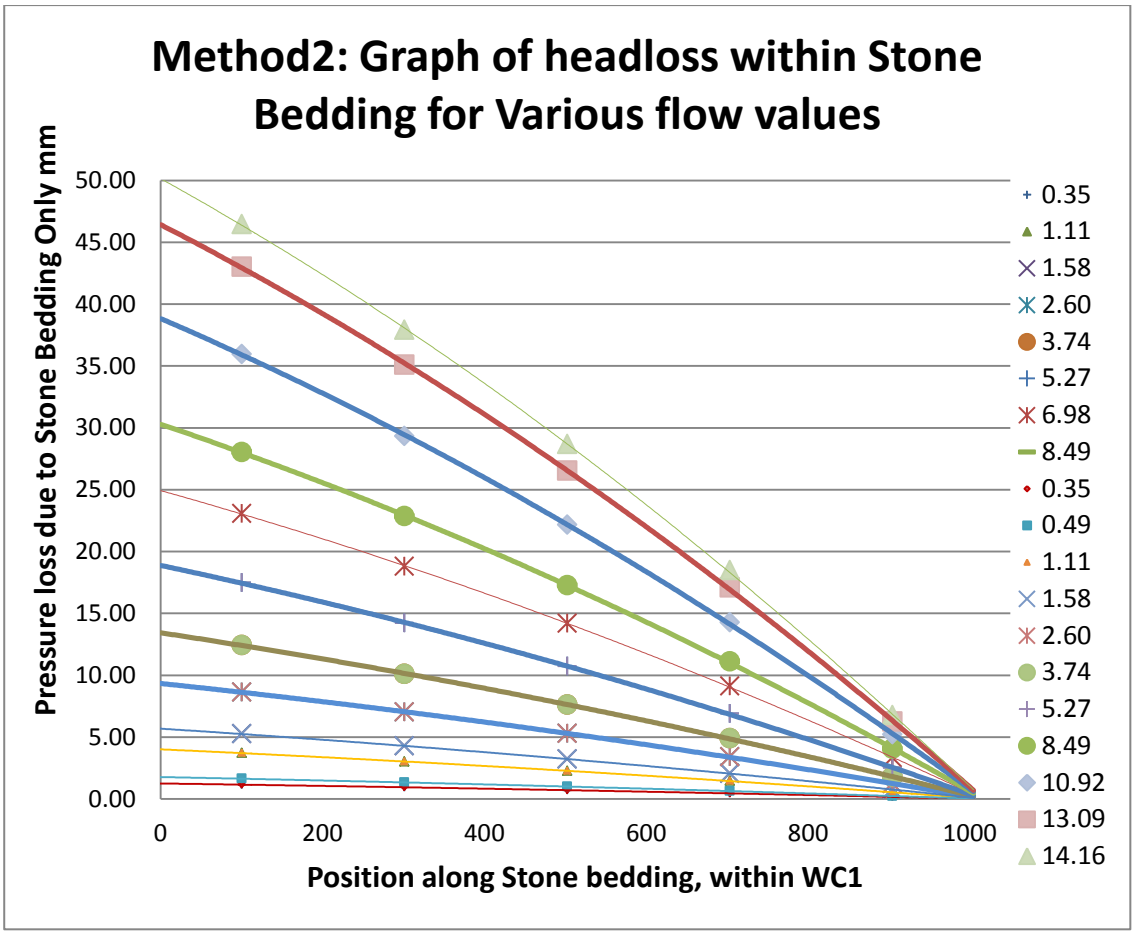

Figure F13: Method2:Results of Headloss due to Stone Bedding, within WC1

Table F29: Method 2:Summary of maximum headloss versus flow rates(WST)

Test No.	Total Q	Total 2Q	Maximum Headloss due to Stone Bedding
	l/s	l/s	mm
1	0.35	0.70	1.25
2	0.49	0.98	1.77
3	1.11	2.23	4.01
4	1.58	3.16	5.69
5	2.60	5.20	9.34
6	3.74	7.49	13.44
7	5.27	10.54	18.88
8	6.98	13.95	24.93
9	8.49	16.99	30.30
10	10.92	21.85	38.84
11	13.09	26.19	46.43
12	14.16	28.32	50.14

F.5.4.2.3 Method 3: Forchheimer Method for determining headloss due to stone bedding

The third method used to determine the loss of pressure due to Stone bedding, looks at the hydraulic conductivity of the stone bedding. This is based on work carried out by Forchheimer. From Table F14, the velocity for each segment of the Intake pipeline was determined. However, stone bedding cannot be split into equal segments as well. This is only correct for stone bedding adjacent to the intake pipeline. It does not apply to the flat horizontal surface of the stone bedding.

Flow into the intake pipe line is proportional to the velocity. The maximum velocity occurs at one end of the intake pipeline and the minimum velocity occurs at the start of the intake pipeline. Table F30 below looks at the ratio of the (flowrate) as a proportion of the entire flowrate.

Figure F15, these proportions were then applied to length of the stone bed. This splitting of the stone bedding surface ensured that all flows entering the stone bed were proportional to the flow entering the intake pipeline for all segments.

Table F30:ø250mm Metal Wire pipe, Water and Stone Bedding Test: Flow through segments

Test No.	Seg1	Seg2	Seg3	Seg4	Seg5	Seg1	Seg2	Seg3	Seg4	Seg5
	Qs 1	Qs 2	Qs 3	Qs 4	Qs 5	Qs 1	Qs 2	Qs 3	Qs 4	Qs 5
	m^3/s	m^3/s	m^3/s	m^3/s	m^3/s	m^3/s	m^3/s	m^3/s	m^3/s	m^3/s
1	0.00013	0.00010	0.00007	0.00004	0.00001	36%	28%	20%	12%	4%
2	0.00018	0.00014	0.00010	0.00006	0.00002	36%	28%	20%	12%	4%
3	0.00040	0.00031	0.00022	0.00013	0.00004	36%	28%	20%	12%	4%
4	0.00057	0.00044	0.00032	0.00019	0.00006	36%	28%	20%	12%	4%
5	0.00094	0.00073	0.00052	0.00031	0.00010	36%	28%	20%	12%	4%
6	0.00135	0.00105	0.00075	0.00045	0.00015	36%	28%	20%	12%	4%
7	0.00190	0.00148	0.00105	0.00063	0.00021	36%	28%	20%	12%	4%
8	0.00251	0.00195	0.00140	0.00084	0.00028	36%	28%	20%	12%	4%
9	0.00306	0.00238	0.00170	0.00102	0.00034	36%	28%	20%	12%	4%
10	0.00393	0.00306	0.00218	0.00131	0.00044	36%	28%	20%	12%	4%
11	0.00471	0.00367	0.00262	0.00157	0.00052	36%	28%	20%	12%	4%
12	0.00510	0.00397	0.00283	0.00170	0.00057	36%	28%	20%	12%	4%

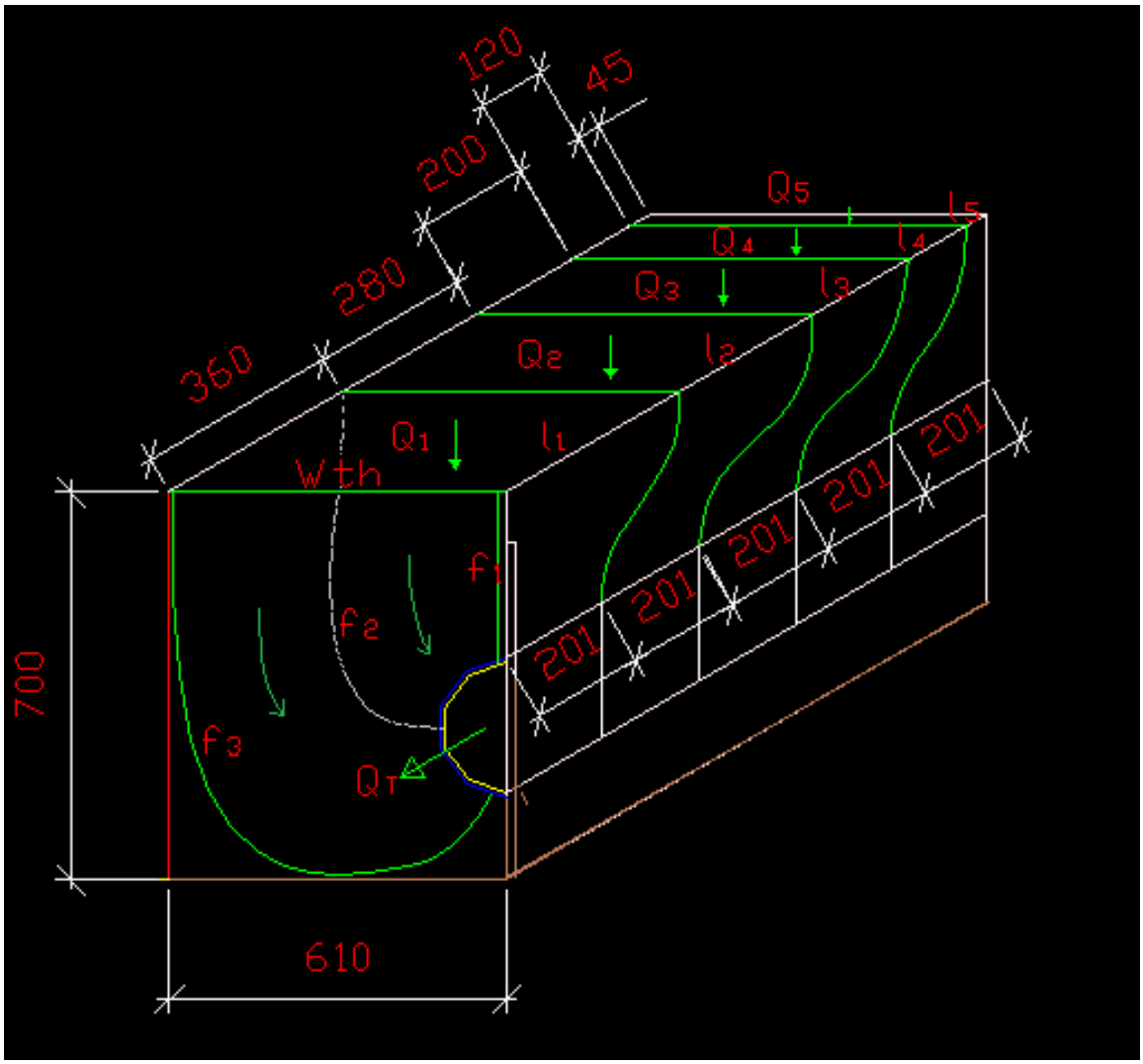

Figure F15: ø250mm Slotted pipe-Water and Stone Bedding Test: Segmentation of Stone Bedding area

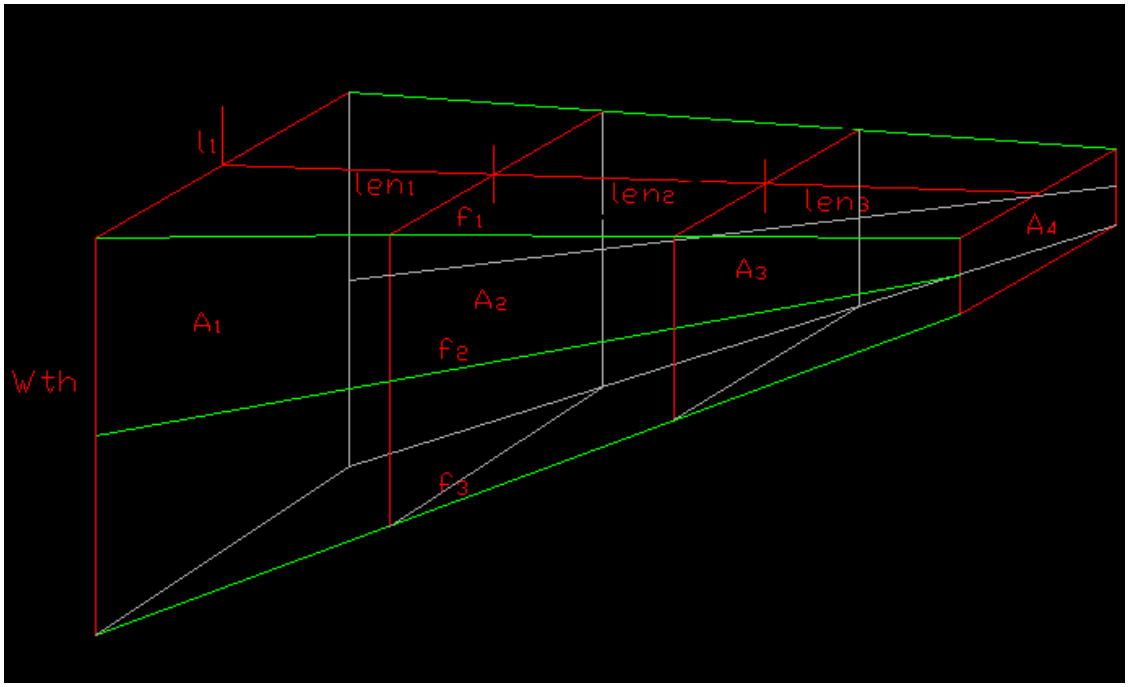

Figure F16: Notional flow path of a stone bedding segment

Figure F16 shows the simplified version of a single notional segment. Note line f_1, f_2 and f_3 as lines of reference in Figure F15 and F167. As in Figure F16, length (l_1) is multiplied by the standard width (With), to create the area A_1. Area A_4 was easily calculated it is based on the intake pipe dimensions. Areas A_2 and $A_3$are a third of the distance from each end and hence are calculated proportionately. The distances from Area A_1 to A_2 to A_3 to $A_4$are noted as Lengths len_1, len_2 and len_3 respectively.

In order to calculate the pressure loss due to the stone bedding, the hydraulic conductivity is required. The pressure loss is defined as per Equation F4 below:

$$hf(m) = \frac{L * V}{k} \qquad \text{Eqn F4}$$

Where:

hf = pressure loss due to friction within stone bedding

L = Length of water path (m)

V = Flow velocity

k = Hydraulic conductivity

The first two variables are easily to calculate however the hydraulic conductivity is calculated from Figure F18.

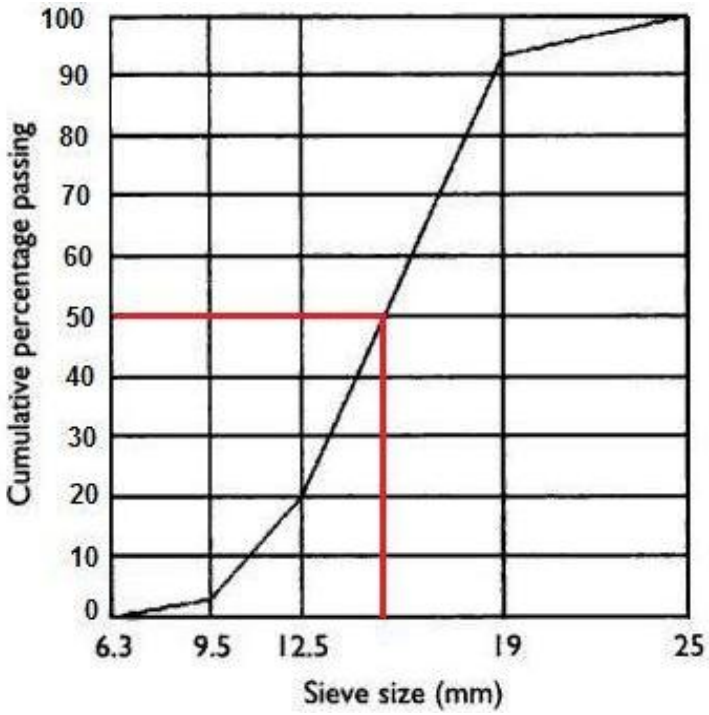

Figure F17: Grading curve for nominally single-sized 19mm Stone (Alexander & Mindess, 2005)

Figure F17 above is a typical grading curve for nominally single-sized 19mm. From the grading curve, a value of D_{50} = 15.7mm was obtained. Table F31 summaries the parameters when obtaining the hydraulic conductivity k value.

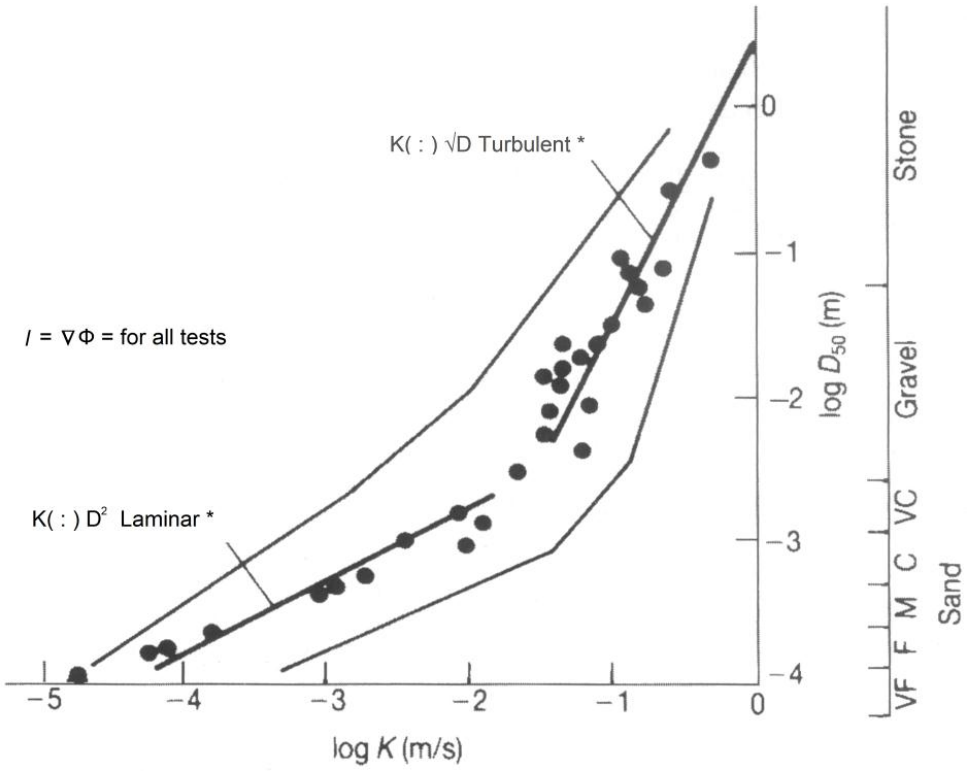

Figure F18: Permeability versus grain or stone sieve size (CIRIA, CUR, CETMEF,2007)

Table F31: Calculation of Permeability for19mm Bedding of seawater Intake (WST)

Description	Unit	Bedding
D_{n50}	m	0.0157
Log (D_{50})	m	-1.80
Log *k* (from fig. 2.39)	m/s	-1.16
k	m/s	0.069

Using the values from Table F30 and F31, headloss for Segment 1 was calculated in the following manner. With the flow through each segment know, it is possible to determine the headloss if the areas through which water flows is uniform.

However, this is not the case. Hence each segment has been split into three equal portions. Table F32 below, describes the manner in which Segment 1 is split into three sub segments. Thereafter, Table F33 determines the average velocity for each sub segment, the associated headloss and finally the cumulative headloss for Segment 1. The subsequent tables describe the headloss calculated for Segments 1, 2, 3, 4 and 5.

Table F32: Segment 1: Averaging of Areas

Test No.	Len1	A11	A12	A13	A14	Qs 1	Ave A1	Ave A2	Ave A3
	m	m^2	m^2	m^2	m^2	m^3/s	m^2	m^2	m^2
1	0.3618	0.221	0.202	0.183	0.164	0.0001	0.192	0.174	0.082
2	0.3618	0.221	0.202	0.183	0.164	0.0002	0.192	0.174	0.082
3	0.3618	0.221	0.202	0.183	0.164	0.0004	0.192	0.174	0.082
4	0.3618	0.221	0.202	0.183	0.164	0.0006	0.192	0.174	0.082
5	0.3618	0.221	0.202	0.183	0.164	0.0009	0.192	0.174	0.083
6	0.3618	0.221	0.202	0.183	0.164	0.0013	0.192	0.174	0.083
7	0.3618	0.221	0.202	0.183	0.164	0.0019	0.192	0.174	0.083
8	0.3618	0.221	0.202	0.183	0.164	0.0025	0.192	0.174	0.083
9	0.3618	0.221	0.202	0.183	0.164	0.0031	0.192	0.174	0.084
10	0.3618	0.221	0.202	0.183	0.164	0.0039	0.192	0.174	0.084
11	0.3618	0.221	0.202	0.183	0.164	0.0047	0.192	0.174	0.084
12	0.3618	0.221	0.202	0.183	0.164	0.0051	0.192	0.174	0.085

Table F33: Segment 1: Velocity and cumulative headloss

Test No.	Vel 1A	Vel 1B	Vel 1C	H_l11	H_l12	H_l13	H_l1Total	H_l1Total
	m/s	m/s	m/s	m	m	m	m	mm
1	0.0007	0.0007	0.0015	0.00189	0.00209	0.00442	0.00840	8.40
2	0.0009	0.0010	0.0022	0.00267	0.00296	0.00625	0.01188	11.88
3	0.0021	0.0023	0.0049	0.00605	0.00670	0.01414	0.02689	26.89
4	0.0030	0.0033	0.0069	0.00857	0.00950	0.02003	0.03810	38.10
5	0.0049	0.0054	0.0113	0.01409	0.01563	0.03286	0.06258	62.58
6	0.0070	0.0078	0.0163	0.02031	0.02252	0.04723	0.09005	90.05
7	0.0099	0.0109	0.0229	0.02860	0.03171	0.06629	0.12659	126.59
8	0.0131	0.0145	0.0301	0.03784	0.04195	0.08739	0.16718	167.18
9	0.0159	0.0176	0.0366	0.04607	0.05108	0.10606	0.20321	203.21
10	0.0204	0.0227	0.0468	0.05925	0.06569	0.13568	0.26062	260.62
11	0.0245	0.0272	0.0558	0.07102	0.07874	0.16188	0.31165	311.65
12	0.0265	0.0294	0.0603	0.07680	0.08516	0.17468	0.33664	336.64

Table F34: Segment 2: Averaging of Areas

Test No.	Len2	A21	A22	A23	A24	Qs 2	Ave A1	Ave A2	Ave A3
	m	m^2	m^2	m^2	m^2	m^3/s	m^2	m^2	m^2
1	0.2814	0.172	0.169	0.167	0.164	0.0001	0.168	0.165	0.082
2	0.2814	0.172	0.169	0.167	0.164	0.0001	0.168	0.165	0.082
3	0.2814	0.172	0.169	0.167	0.164	0.0003	0.168	0.165	0.082
4	0.2814	0.172	0.169	0.167	0.164	0.0004	0.168	0.165	0.082
5	0.2814	0.172	0.169	0.167	0.164	0.0007	0.168	0.165	0.082
6	0.2814	0.172	0.169	0.167	0.164	0.0010	0.168	0.165	0.083
7	0.2814	0.172	0.169	0.167	0.164	0.0015	0.168	0.165	0.083
8	0.2814	0.172	0.169	0.167	0.164	0.0020	0.168	0.165	0.083
9	0.2814	0.172	0.169	0.167	0.164	0.0024	0.168	0.165	0.083
10	0.2814	0.172	0.169	0.167	0.164	0.0031	0.168	0.165	0.084
11	0.2814	0.172	0.169	0.167	0.164	0.0037	0.168	0.165	0.084
12	0.2814	0.172	0.169	0.167	0.164	0.0040	0.168	0.165	0.084

Table F35: Segment 2: Velocity and cumulative headloss

Test No.	Vel 2A	Vel 2B	Vel 2C	H_l21	H_l22	H_l23	H_l2Total	H_l2 Total
	m/s	m/s	m/s	m	m	m	m	mm
1	0.0006	0.0006	0.0012	0.00168	0.00171	0.00344	0.00683	6.83
2	0.0008	0.0008	0.0017	0.00238	0.00242	0.00486	0.00966	9.66
3	0.0019	0.0019	0.0038	0.00539	0.00547	0.01101	0.02187	21.87
4	0.0026	0.0027	0.0054	0.00764	0.00776	0.01559	0.03098	30.98
5	0.0043	0.0044	0.0088	0.01256	0.01275	0.02559	0.05091	50.91
6	0.0062	0.0063	0.0127	0.01810	0.01838	0.03680	0.07328	73.28
7	0.0088	0.0089	0.0178	0.02549	0.02588	0.05169	0.10306	103.06
8	0.0116	0.0118	0.0235	0.03373	0.03424	0.06820	0.13617	136.17
9	0.0142	0.0144	0.0286	0.04107	0.04169	0.08283	0.16559	165.59
10	0.0182	0.0185	0.0366	0.05281	0.05362	0.10608	0.21251	212.51
11	0.0218	0.0222	0.0437	0.06331	0.06427	0.12670	0.25427	254.27
12	0.0236	0.0240	0.0472	0.06846	0.06951	0.13677	0.27474	274.74

Table F36: Segment 3: Averaging of Areas

Test No.	Len3	A31	A32	A33	A34	Qs 3	Ave A1	Ave A2	Ave A3
	m	m^2	m^2	m^2	m^2	m^3/s	m^2	m^2	m^2
1	0.201	0.123	0.136	0.150	0.164	0.0001	0.143	0.157	0.082
2	0.201	0.123	0.136	0.150	0.164	0.0001	0.143	0.157	0.082
3	0.201	0.123	0.136	0.150	0.164	0.0002	0.143	0.157	0.082
4	0.201	0.123	0.136	0.150	0.164	0.0003	0.143	0.157	0.082
5	0.201	0.123	0.136	0.150	0.164	0.0005	0.143	0.157	0.082
6	0.201	0.123	0.136	0.150	0.164	0.0007	0.143	0.157	0.082
7	0.201	0.123	0.136	0.150	0.164	0.0011	0.143	0.157	0.083
8	0.201	0.123	0.136	0.150	0.164	0.0014	0.143	0.157	0.083
9	0.201	0.123	0.136	0.150	0.164	0.0017	0.143	0.157	0.083
10	0.201	0.123	0.136	0.150	0.164	0.0022	0.143	0.157	0.083
11	0.201	0.123	0.136	0.150	0.164	0.0026	0.143	0.157	0.083
12	0.201	0.123	0.136	0.150	0.164	0.0028	0.143	0.157	0.083

Table F31: Segment 3: Velocity and cumulative headloss

Test No.	Vel 3A	Vel 3B	Vel 3C	H_l31	H_l32	H_l33	H_l3Total	H_l3Total
	m/s	m/s	m/s	m	m	m	m	mm
1	0.0005	0.0004	0.0008	0.00141	0.00128	0.00246	0.00515	5.15
2	0.0007	0.0006	0.0012	0.00199	0.00181	0.00347	0.00728	7.28
3	0.0016	0.0014	0.0027	0.00451	0.00411	0.00787	0.01648	16.48
4	0.0022	0.0020	0.0038	0.00639	0.00583	0.01114	0.02336	23.36
5	0.0036	0.0033	0.0063	0.01051	0.00958	0.01830	0.03839	38.39
6	0.0052	0.0048	0.0091	0.01514	0.01381	0.02633	0.05528	55.28
7	0.0074	0.0067	0.0128	0.02132	0.01944	0.03701	0.07778	77.78
8	0.0097	0.0089	0.0169	0.02821	0.02573	0.04888	0.10282	102.82
9	0.0119	0.0108	0.0205	0.03435	0.03133	0.05940	0.12508	125.08
10	0.0152	0.0139	0.0263	0.04418	0.04029	0.07617	0.16063	160.63
11	0.0183	0.0167	0.0314	0.05295	0.04829	0.09107	0.19231	192.31
12	0.0198	0.0180	0.0339	0.05727	0.05223	0.09836	0.20785	207.85

Table F38: Segment 4: Averaging of Areas

Test No.	Len4	A41	A42	A43	A44	Qs 4	Ave A1	Ave A2	Ave A3
	m	m^2	m^2	m^2	m^2	m^3/s	m^2	m^2	m^2
1	0.121	0.074	0.104	0.134	0.164	0.0000	0.119	0.149	0.082
2	0.121	0.074	0.104	0.134	0.164	0.0001	0.119	0.149	0.082
3	0.121	0.074	0.104	0.134	0.164	0.0001	0.119	0.149	0.082
4	0.121	0.074	0.104	0.134	0.164	0.0002	0.119	0.149	0.082
5	0.121	0.074	0.104	0.134	0.164	0.0003	0.119	0.149	0.082
6	0.121	0.074	0.104	0.134	0.164	0.0004	0.119	0.149	0.082
7	0.121	0.074	0.104	0.134	0.164	0.0006	0.119	0.149	0.082
8	0.121	0.074	0.104	0.134	0.164	0.0008	0.119	0.149	0.082
9	0.121	0.074	0.104	0.134	0.164	0.0010	0.119	0.149	0.083
10	0.121	0.074	0.104	0.134	0.164	0.0013	0.119	0.149	0.083
11	0.121	0.074	0.104	0.134	0.164	0.0016	0.119	0.149	0.083
12	0.121	0.074	0.104	0.134	0.164	0.0017	0.119	0.149	0.083

Table F39: Segment 4: Velocity and cumulative headloss

Test No.	Vel 4A	Vel 4B	Vel 4C	H_l41	H_l42	H_l43	H_l4Total	H_l4Total
	m/s	m/s	m/s	m	m	m	m	mm
1	0.0004	0.0003	0.0005	0.00102	0.00081	0.00147	0.00331	3.31
2	0.0005	0.0004	0.0007	0.00144	0.00115	0.00209	0.00467	4.67
3	0.0011	0.0009	0.0016	0.00326	0.00260	0.00472	0.01059	10.59
4	0.0016	0.0013	0.0023	0.00463	0.00369	0.00669	0.01500	15.00
5	0.0026	0.0021	0.0038	0.00761	0.00607	0.01100	0.02467	24.67
6	0.0038	0.0030	0.0055	0.01096	0.00874	0.01583	0.03553	35.53
7	0.0053	0.0042	0.0077	0.01543	0.01231	0.02227	0.05000	50.00
8	0.0070	0.0056	0.0102	0.02042	0.01628	0.02943	0.06613	66.13
9	0.0086	0.0068	0.0123	0.02486	0.01983	0.03579	0.08048	80.48
10	0.0110	0.0088	0.0159	0.03198	0.02550	0.04594	0.10342	103.42
11	0.0132	0.0105	0.0190	0.03833	0.03056	0.05498	0.12388	123.88
12	0.0143	0.0114	0.0205	0.04145	0.03305	0.05942	0.13392	133.92

Table F40: Segment 5: Averaging of Areas

Test No.	Len5	A51	A52	A53	A54	Qs 5	Ave A1	Ave A2	Ave A3
	m	m^2	m^2	m^2	m^2	m^3/s	m^2	m^2	m^2
1	0.0402	0.025	0.071	0.118	0.164	0.0000	0.094	0.141	0.082
2	0.0402	0.025	0.071	0.118	0.164	0.0000	0.094	0.141	0.082
3	0.0402	0.025	0.071	0.118	0.164	0.0000	0.094	0.141	0.082
4	0.0402	0.025	0.071	0.118	0.164	0.0001	0.094	0.141	0.082
5	0.0402	0.025	0.071	0.118	0.164	0.0001	0.094	0.141	0.082
6	0.0402	0.025	0.071	0.118	0.164	0.0001	0.094	0.141	0.082
7	0.0402	0.025	0.071	0.118	0.164	0.0002	0.094	0.141	0.082
8	0.0402	0.025	0.071	0.118	0.164	0.0003	0.094	0.141	0.082
9	0.0402	0.025	0.071	0.118	0.164	0.0003	0.094	0.141	0.082
10	0.0402	0.025	0.071	0.118	0.164	0.0004	0.094	0.141	0.082
11	0.0402	0.025	0.071	0.118	0.164	0.0005	0.094	0.141	0.082
12	0.0402	0.025	0.071	0.118	0.164	0.0006	0.094	0.141	0.082

Table F41: Segment 5: Velocity and cumulative headloss

Test No.	Vel 5A	Vel 5B	Vel 5C	H_l51	H_l52	H_l53	$H_l5Total$	$H_l5Total$
	m/s	m/s	m/s	m	m	m	m	mm
1	0.0001	0.0001	0.0002	0.00043	0.00029	0.00049	0.00121	1.21
2	0.0002	0.0001	0.0002	0.00060	0.00041	0.00070	0.00171	1.71
3	0.0005	0.0003	0.0005	0.00137	0.00092	0.00157	0.00386	3.86
4	0.0007	0.0004	0.0008	0.00194	0.00130	0.00223	0.00548	5.48
5	0.0011	0.0007	0.0013	0.00319	0.00214	0.00367	0.00900	9.00
6	0.0016	0.0011	0.0018	0.00460	0.00308	0.00529	0.01297	12.97
7	0.0022	0.0015	0.0026	0.00648	0.00434	0.00744	0.01826	18.26
8	0.0030	0.0020	0.0034	0.00858	0.00574	0.00984	0.02416	24.16
9	0.0036	0.0024	0.0041	0.01044	0.00699	0.01198	0.02941	29.41
10	0.0046	0.0031	0.0053	0.01343	0.00899	0.01540	0.03782	37.82
11	0.0056	0.0037	0.0064	0.01610	0.01078	0.01844	0.04532	45.32
12	0.0060	0.0040	0.0069	0.01741	0.01166	0.01994	0.04901	49.01

Table F42: Summary of Method 3 Headloss Tests. Results from Tables 32 to 41 (WST)

Test No.	Total Q	Total 2Q	Segment 1	Segment 2	Segment 3	Segment 4	Segment 5
	l/s	l/s	mm	mm	mm	mm	mm
1	0.35	0.70	8.40	6.83	5.15	3.31	1.21
2	0.49	0.98	11.88	9.66	7.28	4.67	1.71
3	1.11	2.23	26.89	21.87	16.48	10.59	3.86
4	1.58	3.16	38.10	30.98	23.36	15.00	5.48
5	2.60	5.20	62.58	50.91	38.39	24.67	9.00
6	3.74	7.49	90.05	73.28	55.28	35.53	12.97
7	5.27	10.54	126.59	103.06	77.78	50.00	18.26
8	6.98	13.95	167.18	136.17	102.82	66.13	24.16
9	8.49	16.99	203.21	165.59	125.08	80.48	29.41
10	10.92	21.85	260.62	212.51	160.63	103.42	37.82
11	13.09	26.19	311.65	254.27	192.31	123.88	45.32
12	14.16	28.32	336.64	274.74	207.85	133.92	49.01

Figure F19 plots these graphically. A trendline is added to the results in order to predict the headloss, due to stone bedding. This occurs at the most downstream point of WC1. It is at this point that the largest magnitude of headloss occurs. Table F43 summaries these results.

Table F43: Method 3: Summary of maximum headloss versus flow rates (WST)

Test No.	Total Q	Total 2Q	Maximum Headloss due to Stone Bedding
	l/s	l/s	mm
1	0.35	0.70	9.09
2	0.49	0.98	12.85
3	1.11	2.23	29.09
4	1.58	3.16	41.20
5	2.60	5.20	67.67
6	3.74	7.49	97.35
7	5.27	10.54	126.82
8	6.98	13.95	180.65
9	8.49	16.99	219.53
10	10.92	21.85	281.43
11	13.09	26.19	336.42
12	14.16	28.32	363.34

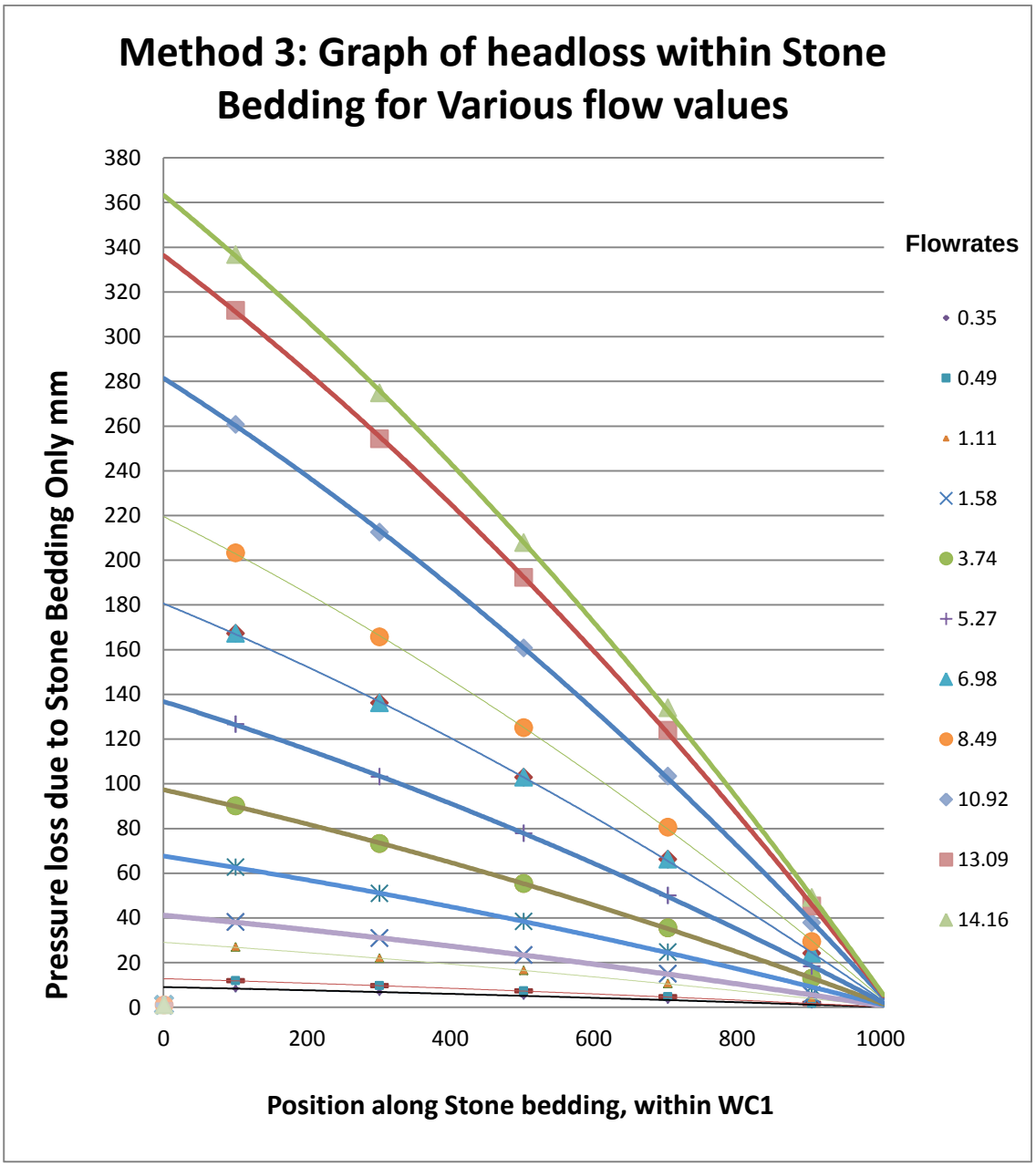

Figure F19: Method 3:Results of Headloss due to Stone Bedding, within WC1

F.5.4.3 Comparison of Results for Method 1, 2 and 3

The following Figure F20 shows the results for Method 1, 2 and 3 for the calculation of Headloss due to the stone bedding only, Results for Method1 is derived from Table F15, Method 2 from Table F29 and Method 3 from Table F43.

Table F30:Summary of maximum headloss versus flow rates for Methods 1, 2 and 3

Test No.	Total Q	Total 2Q	Method 1: Stone Bedding Headloss	Method 2: Stone Bedding Headloss	Method 3: Stone Bedding Headloss
	l/s	l/s	mm	mm	mm
1	0.35	0.70	5.43	1.25	9.09
2	0.49	0.98	7.64	1.77	12.85
3	1.11	2.23	16.94	4.01	29.09
4	1.58	3.16	23.62	5.69	41.20
5	2.60	5.20	37.46	9.34	67.67
6	3.74	7.49	51.73	13.44	97.35
7	5.27	10.54	68.63	18.88	126.82
8	6.98	13.95	84.58	24.93	180.65
9	8.49	16.99	96.22	30.30	219.53
10	10.92	21.85	109.83	38.84	281.43
11	13.09	26.19	116.76	46.43	336.42
12	14.16	28.32	118.36	50.14	363.34

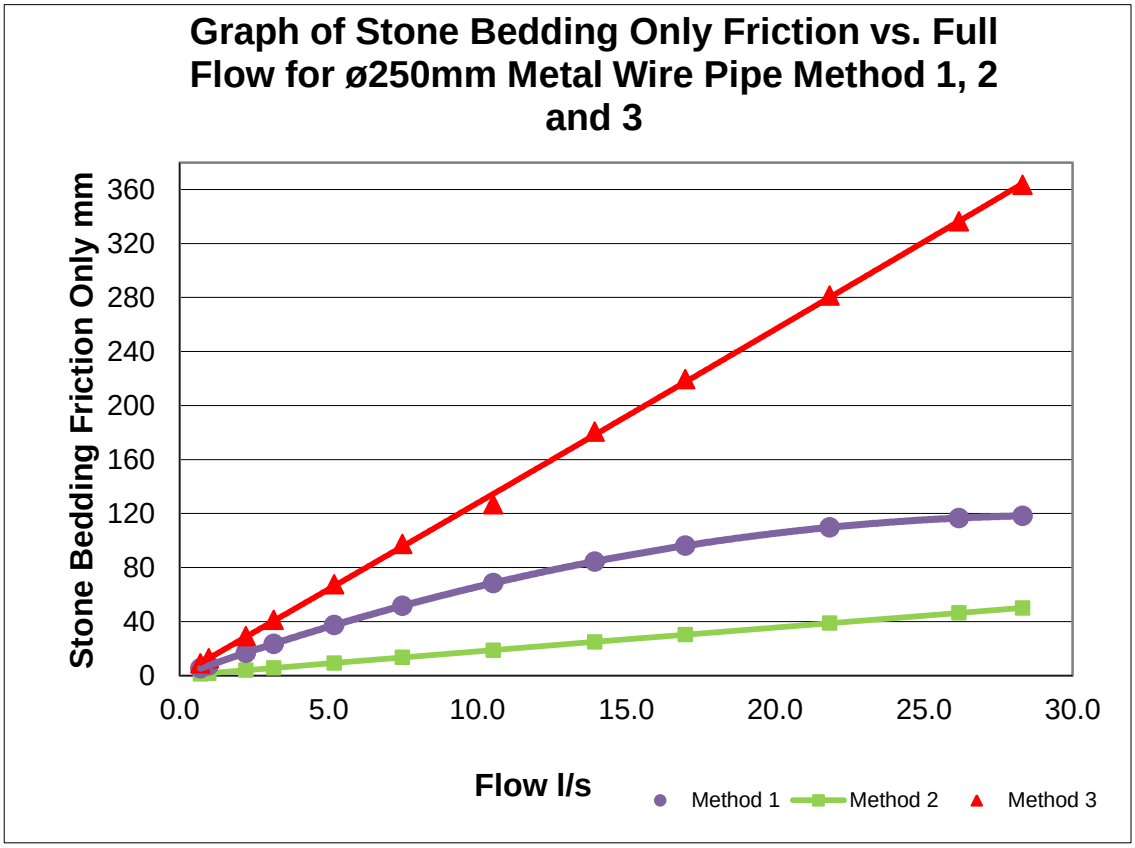

Figure F20: Method 1, 2 and 3: Headloss due to the stone bedding only

Appendix G

Table of Contents

Description	Page
G.1 Water Only Tests	378
G.2 Stone Bedding Tests	379
G.3 Sand + Stone Bedding Test	381
G.3.1 Slotted PVC Pipe	381
G.3.2 Perforated PVC Pipe	382
G.4 Estimating losses due to Stone Bedding	383
G.4.1 Slotted PVC Pipe	384
G.4.2 Perforated PVC Pipe	385
G.4.3 Metal Wire Pipe	386
G.4.4 Results Summary of Method 1	388
G.4.4 Results Summary of Method 2	389
G.4.4 Results Summary of Method 3	390
G5 Estimating Pressure losses due to Sand and Stone Bedding	391
G5.1 Perforated PVC Pipe	392

Summary of Results

The following is a summary of the results and is presented as per type of test. The following chapter summaries the methods used in estimating the Stone Bedding Friction only.

G.1 Water Only Tests

The following is a summary of the water only test that was performed on all three pipes. The flows shown are as per the experiments. These flow numbers can be double as a whole pipe would be used in practical applications. Table G1 contains the values for the test for all three pipes. Figure G1 Perforation friction for all three intake pipe types

Table G1: Summary of results for all the Water only tests

Intake Pipe Types	Slotted PVC Pipe		Perforated PVC Pipe		Perforated PVC Pipe with Extra Perforation		Metal Wire Pipe	
Test No.	Loss A mm	Q Full Pipe l/s	Loss A mm	Q Full Pipe l/s	Loss A mm	Q Full Pipe l/s	Loss A mm	Q Full Pipe l/s
0	0	0.0	0	0.0	0	0.0	0	0.0
1	0	1.5	0	0.3	3	0.4	1	0.5
2	1	2.8	7	0.3	6	1.0	2	1.1
3	3	4.1	13	0.8	14	1.9	4	1.8
4	5	5.1	48	2.1	40	3.6	6	3.0
5	7	6.6	113	3.3	89	5.8	13	4.0
6	9	7.5	282	5.3	161	8.5	14	5.2
7	10	8.6	431	6.8	215	9.8	31	6.2
8	13	10.4	581	7.6	281	11.3	41	8.1
9	16	12.8			473	14.4	49	9.6
10	19	14.6					85	12.3
11	25	16.6					100	14.2
12	30	17.7					134	16.0
13	38	19.6					149	18.3
14	48	21.6					198	20.4
15	61	22.7					251	21.8
16	74	25.1					307	24.2
17	93	28.5					352	28.3
18	133	31.7					445	30.6
19	172	36.6						

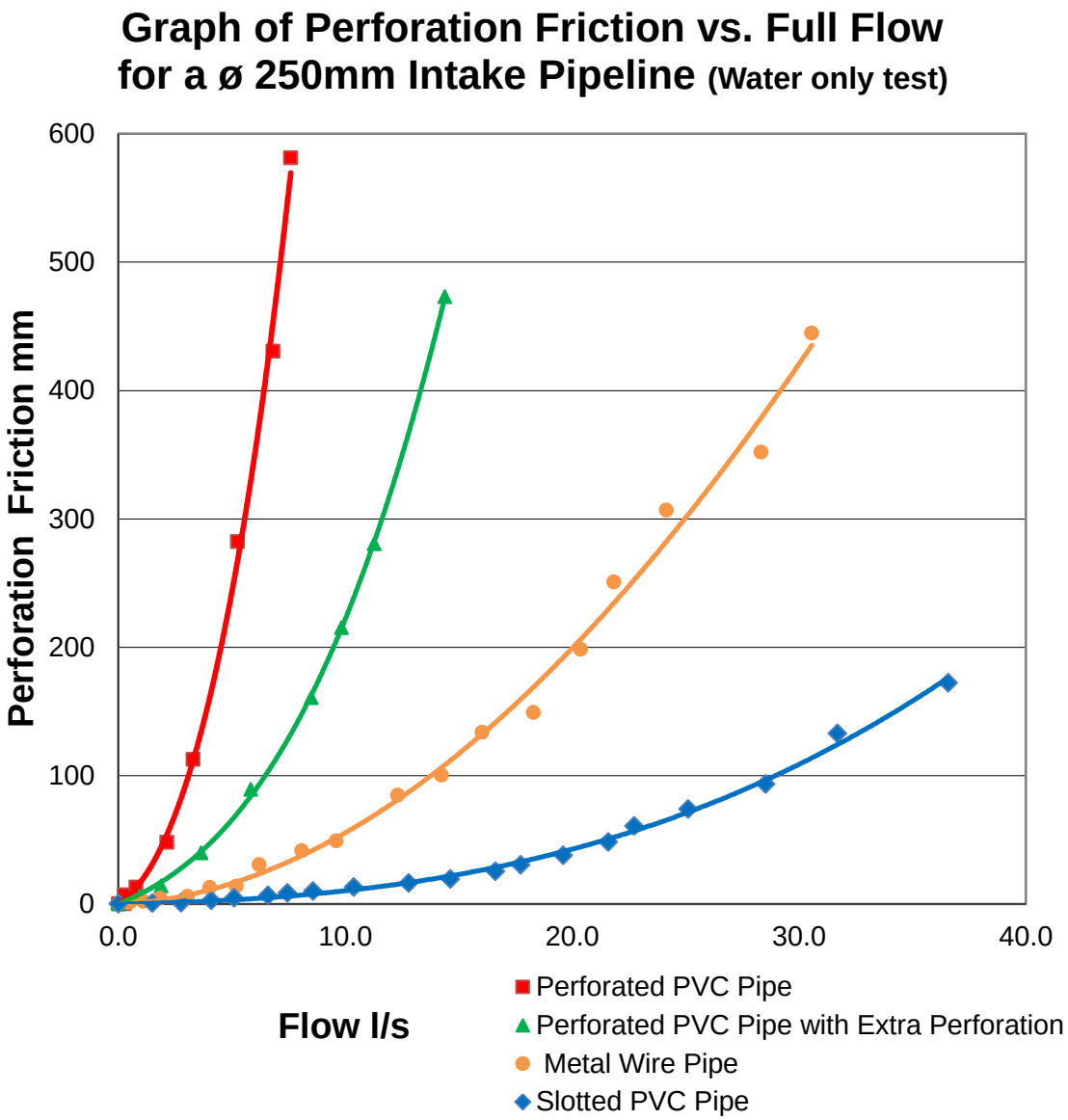

Figure G1: Perforation friction for all three intake pipe types

G.2 Stone Bedding Tests

The following is a summary of the stone test that was performed on all three pipes. The flows shown are as per the experiments. These flow numbers can be double as a whole pipe would be used in practical applications. Table G2 contains the test values for all three pipes. Figure G2 shows the Perforation friction + Stone Bedding friction for all three intake pipe3.

Table G2: Summary of results for the Stone Bedding tests

Intake Pipe Types	Slotted PVC Pipe		Perforated PVC Pipe with Extra Perforation		Metal Wire Pipe	
Test No.	Loss A + Stone BF mm	Q Full Pipe l/s	Loss A + Stone BF mm	Q Full Pipe l/s	Loss A + Stone BF mm	Q Full Pipe l/s
1	0.5	0.66	3	0.44	2	0.70
2	0.99	1.06	6.5	0.96	4	0.98
3	1.98	1.68	13.9	1.88	9	2.23
4	2.95	2.62	39.8	3.64	6	3.16
5	5.82	4.68	89.4	5.85	62	5.20
6	11.2	5.96	160.6	8.51	67	7.49
7	18.0	8.22	215.2	9.84	123	10.54
8	34.6	12.9	280.6	11.28	201	13.95
9	48.0	15.5	473.1	14.39	219	16.99
10	70.1	18.7			299	21.85
11	83.5	20.9			361	26.19
12	105.6	23.1			449	28.32
13	129.5	25.9				
14	155.4	28.5				
15	171.7	29.8				

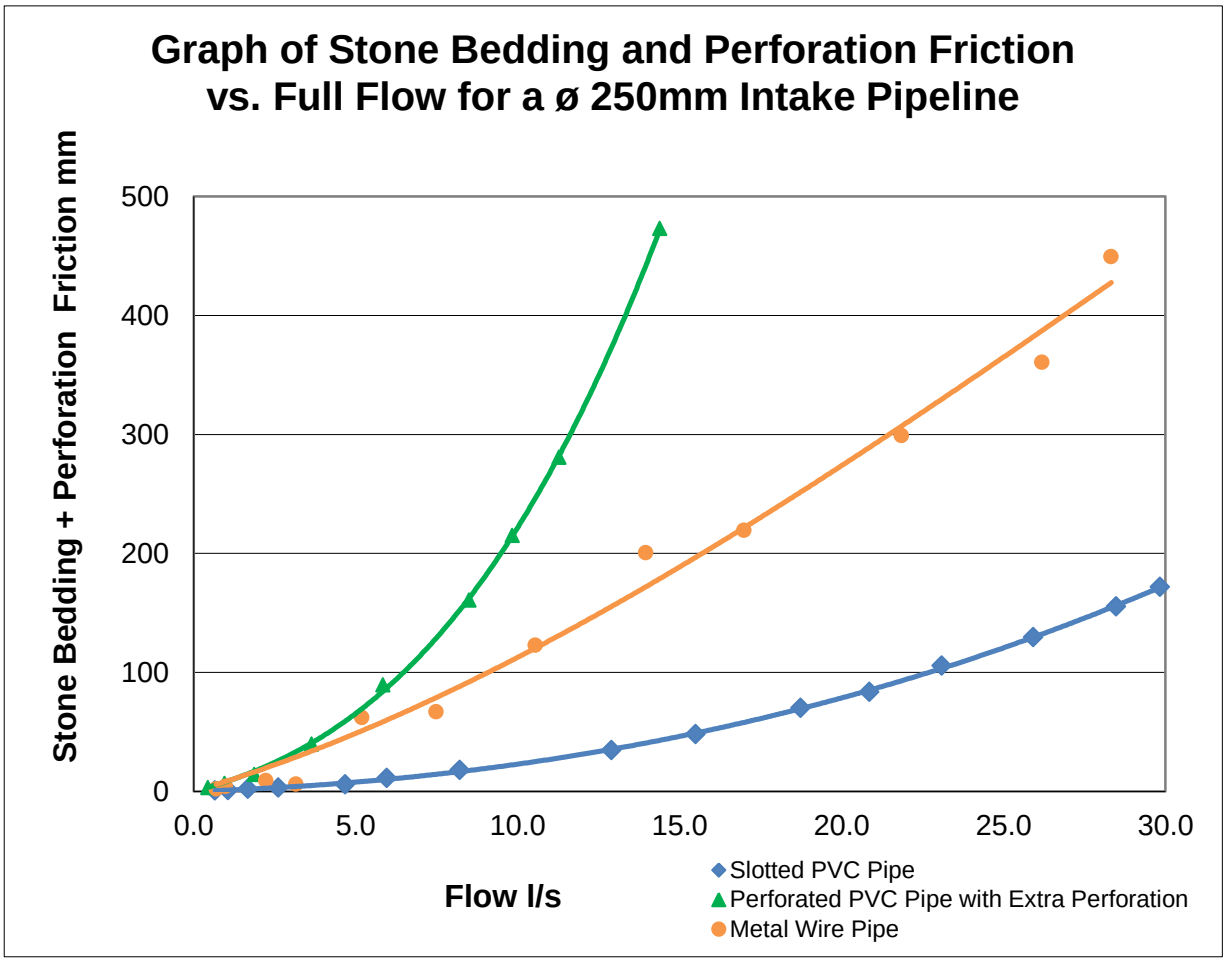

Figure G2: Perforation and Stone Bedding Friction for all three intake pipe types

G.3 Sand + Stone Bedding Test

G.3.1 Slotted PVC Pipe

The following is a summary of the sand and stone tests that was performed on the Slotted PVC Pipe pipes. The flows shown are as per the experiments. These flow numbers can be double as a whole pipe would be used in practical applications. Table G3 contains the test results values for the Before Back Flushing (BBF) and the After Back Flushing (ABF) test Figure G3 plots the results of Table G3

Table G3: Summary of results for the Slotted PVC Pipe :Sand + Stone Bedding tests

	Before Back Flushing			After Back Flushing		
Test No.	Time min	BBF Loss A+sand + stone bedding mm	BBF Q Full Pipe ml/s	Time min	ABF Loss A+sand + stone bedding mm	ABF Q Full Pipe l/s
1	0	40	82	0	0	133
2	45	312	291	7	234	107
3	60	335	300	12	255	153
4	70	350	306	16	285	189
5	83	362	302	20	311	204
6	107	374	348	24	324.5	229
7	118	293	313	28	339	227
8	143	220	183	32	350	246
9	149	257	212	36	356	269
10	160.5	266	234	40	360	267
11	171.5	268	233	44	362.5	275
12	178.2	268	233	48	363	286
13	185	268	233	52	366	287
				56	366	289
				60	365.5	293
				66	363.5	259
				72	362.5	260
				78	359.5	263
				101	349.5	203
				150	329.5	192
				170	320.5	205
				192	315.5	203
				230	307.5	195
				280	297.5	192
				326	291.5	193
				377	281.5	192

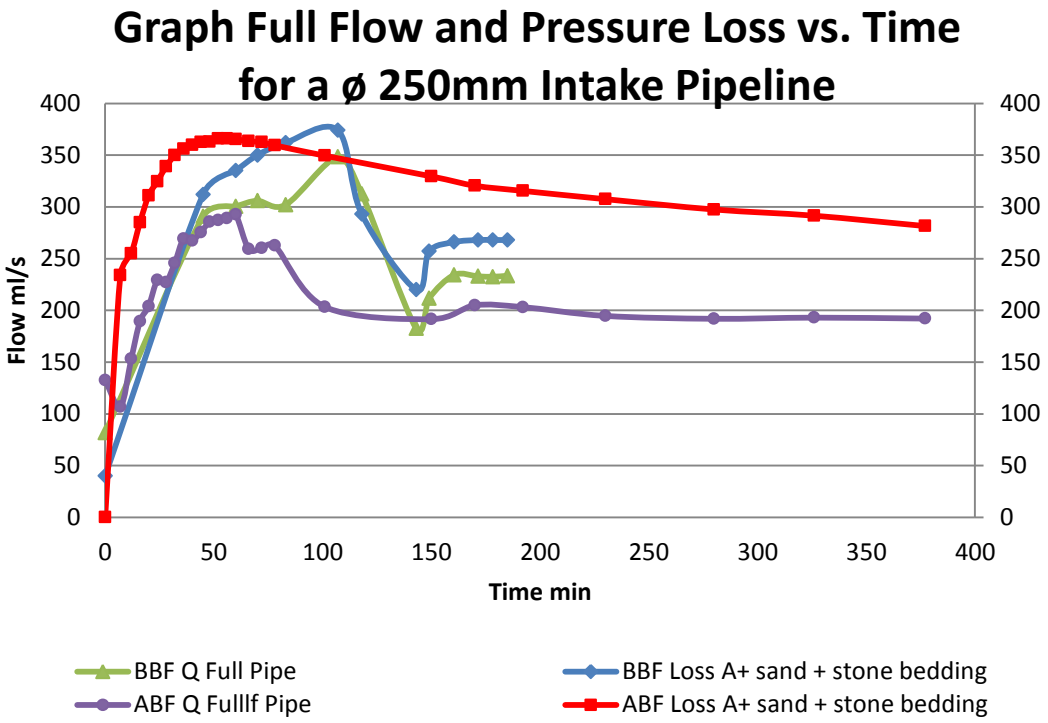

Figure G3: Pressure loss and Flowrate vs. time relationship for the Slotted PVC Pipe with sand and stone bedding

G.3.2 Perforated PVC Pipe

The following is a summary of the sand and stone tests that was performed on the Extra Perforated PVC Pipe pipes. The flows shown are as per the experiments. These flow numbers can be double as a whole pipe would be used in practical applications. Table G4 contains the test results values for Perforation friction + Sand and Stone Bedding friction. Figure G4 plots the results of Table G4

Table G4: Summary of results for the Extra Perforated PVC Pipe:Sand + Stone bedding tests

Test No.	Loss A+sand + stone bedding	Q Half Pipe
	mm	l/s
1	25.00	0.33
2	101.99	1.15
3	202.94	2.26
4	296.91	2.87
5	351.87	3.46
6	443.69	5.29
7	527.56	6.30

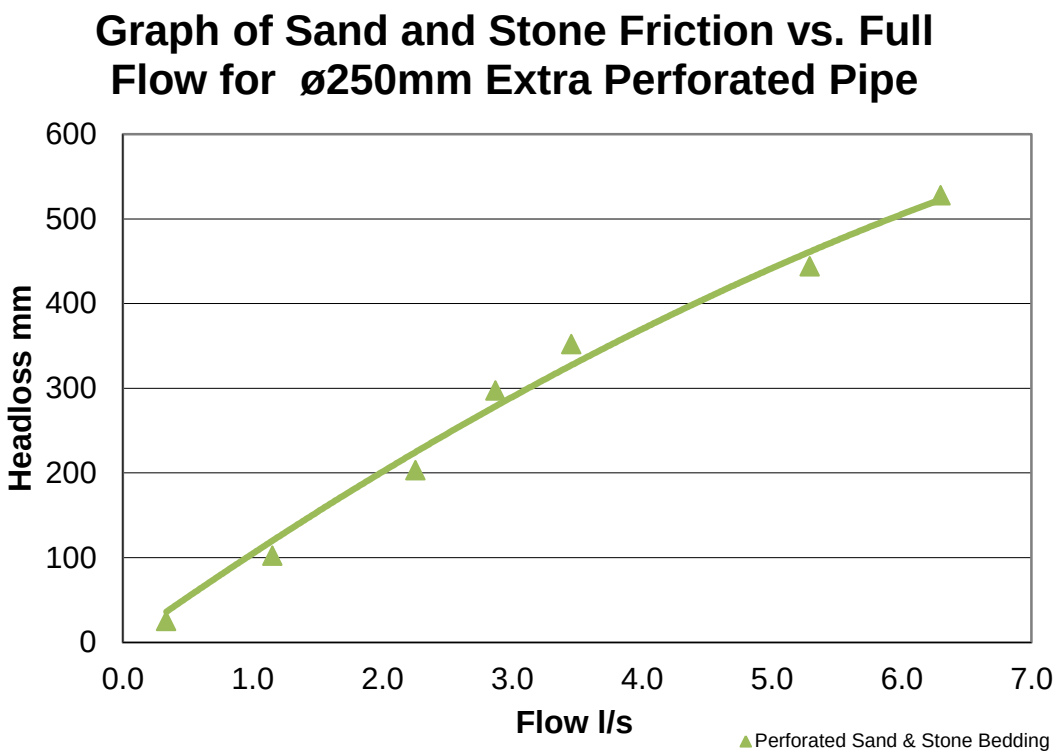

Figure G4: Pressure Loss vs. Flowrate for Extra perforated PVC Pipe with sand and stone bedding

G.4 Estimating losses due to Stone Bedding

Three methods were used to estimate the pressure losses due to stone bedding only. They were as follows:

Method 1: Simple method for determining stone bedding loss

In this simplistic method, the results of the "Water Test only: is plotted. Curve line 1 is fitted to the results and an equation characterising the line and hence the pipe, headloss characteristics is formulated.

Thereafter, the results of the "Stone and water test" is plotted. Curve line 2 is fitted to the results and an equation characterising the line and hence the pipe and surrounding bedding, headloss characteristics is formulated.

The loss due to the stone bedding only, Curve line 3, is determined by subtracting Curve line 2 from Curve Line 1. This data is then plotted to show graphically the relationship between the headloss caused by the stone bedding.

Method 2: Method for determining stone bedding loss : Hydraulic conductivity: Kenny, Lau and Ofoegbu

The second method used to determine the loss of pressure due to Stone bedding, looks at the hydraulic conductivity of stone bedding. Equation by Kenny, Lau and Ofoegbuare used to estimate stone bedding headloss.

Method 3: Method for determining stone bedding loss : Hydraulic conductivity: Forchheimer

The third method used to determine the loss of pressure due to Stone bedding, stems from work carried out by Forchheimer. This method use Figure 2.35 to estimate the permeability of the stone bedding and hence the headloss.

The following Table and Figures show the results of Method 1, 2and 3 that were used to calculate the stone bedding friction for all three intake pipes. The full flow is used in this sub chapter.

G.4.1 Slotted PVC Pipe

Table G5: Slotted PVC Pipe :Method 1, 2 and 3:Headloss due to Stone bedding

Test No.	Total Q	Total 2Q	Method 1 Stone bedding Headloss	Method 2 Stone bedding Headloss	Method 3 Stone bedding Headloss
	l/s	l/s	mm	mm	mm
1	0.33	0.66	0.4	0.64	6.02
2	0.53	1.06	0.7	1.03	9.85
3	0.84	1.68	1.2	1.64	15.75
4	1.31	2.62	2.0	2.55	23.95
5	2.34	4.67	4.3	4.54	43.25
6	2.98	5.95	6.1	5.78	55.00
7	4.11	8.23	9.9	8.00	76.00
8	6.45	12.90	20.3	12.54	119.5
9	7.75	15.51	27.6	15.07	143.5
10	9.37	18.74	38.1	18.21	173.2
11	10.43	20.85	45.9	20.27	192.7
12	11.55	23.10	55.0	22.46	214.0
13	12.96	25.92	67.5	25.20	239.7
14	14.24	28.49	79.9	27.69	263.8
15	14.92	29.83	86.9	29.01	276.0

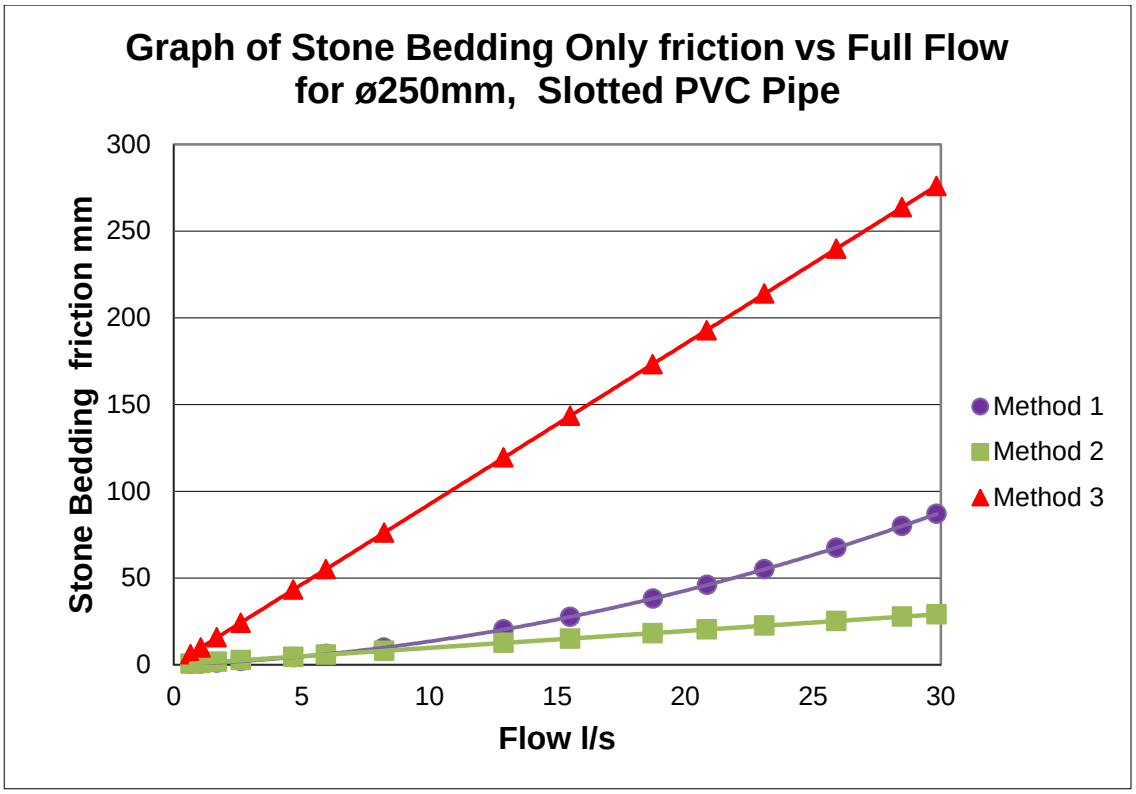

Figure G5: Slotted PVC Pipe-Method 1,2 and 3: Headloss due to the stone bedding

G.4.2 Perforated PVC Pipe

Table G6: Perforated PVC Pipe :Method 1, 2 and 3:Headloss due to Stone bedding

Test No.	Total Q	Total 2Q	Method 1 Stone bedding Headloss	Method 2 Stone bedding Headloss	Method 3 Stone bedding Headloss
	l/s	l/s	mm	mm	mm
1	0.10	0.19	0.002	0.18	1.795
2	0.11	0.22	0.009	0.21	1.999
3	0.14	0.28	0.02	0.27	2.554
4	0.26	0.53	0.8	0.51	4.87
5	0.44	0.87	0.96	0.85	8.098
6	0.82	1.64	1.08	1.59	15.16
7	1.07	2.15	2.69	2.08	19.86
8	1.31	2.62	4.76	2.55	24.26
9	1.64	3.29	8.56	3.19	30.45
10	2.02	4.04	14.11	3.93	37.42
11	2.60	5.20	25.23	5.05	48.14
12	3.10	6.19	37.27	6.01	57.32
13	3.94	7.88	63.03	7.65	72.93
14	4.36	8.71	78.25	8.46	80.65
15	4.80	9.60	96.26	9.32	88.87
16	5.15	10.31	111.85	10.01	95.38
17	5.39	10.78	123.02	10.47	99.77
18	5.77	11.53	141.84	11.2	106.75

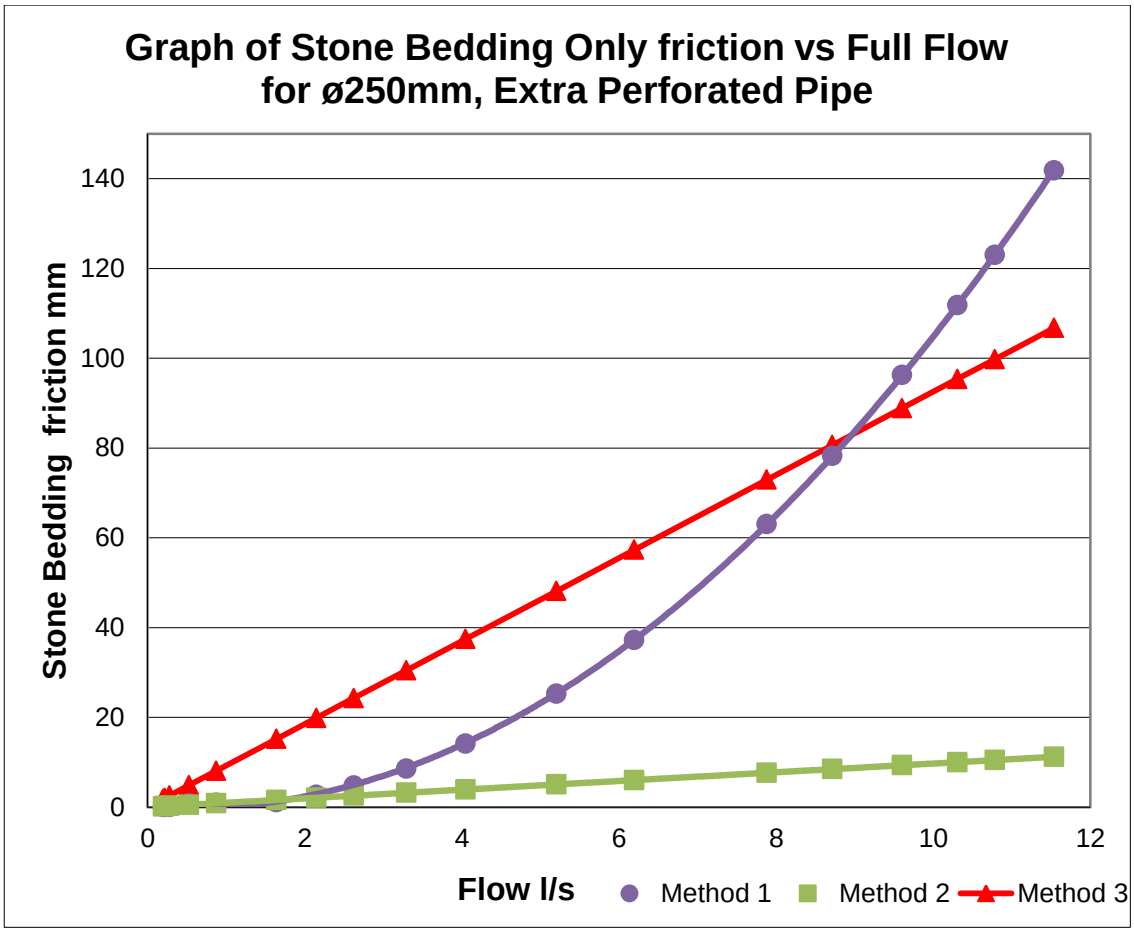

Figure G6: Perforated PVC Pipe-Method 1, 2 and 3: Headloss due to the stone bedding

G.4.3 Metal Wire Pipe

Table G7: Metal Wire Pipe :Method 1, 2 and 3:Headloss due to Stone bedding

Test No.	Total Q	Total 2Q	Method 1 Stone bedding Headloss	Method 2 Stone bedding Headloss	Method 3 Stone bedding Headloss
	l/s	l/s	mm	mm	mm
1	0.35	0.70	5.43	1.25	9.09
2	0.49	0.98	7.64	1.77	12.85
3	1.11	2.23	16.94	4.01	29.09
4	1.58	3.16	23.62	5.69	41.20
5	2.60	5.20	37.46	9.34	67.67
6	3.74	7.49	51.73	13.44	97.35
7	5.27	10.54	68.63	18.88	126.82
8	6.98	13.95	84.58	24.93	180.65
9	8.49	16.99	96.22	30.30	219.53
10	10.92	21.85	109.83	38.84	281.43
11	13.09	26.19	116.76	46.43	336.42
12	14.16	28.32	118.36	50.14	363.34

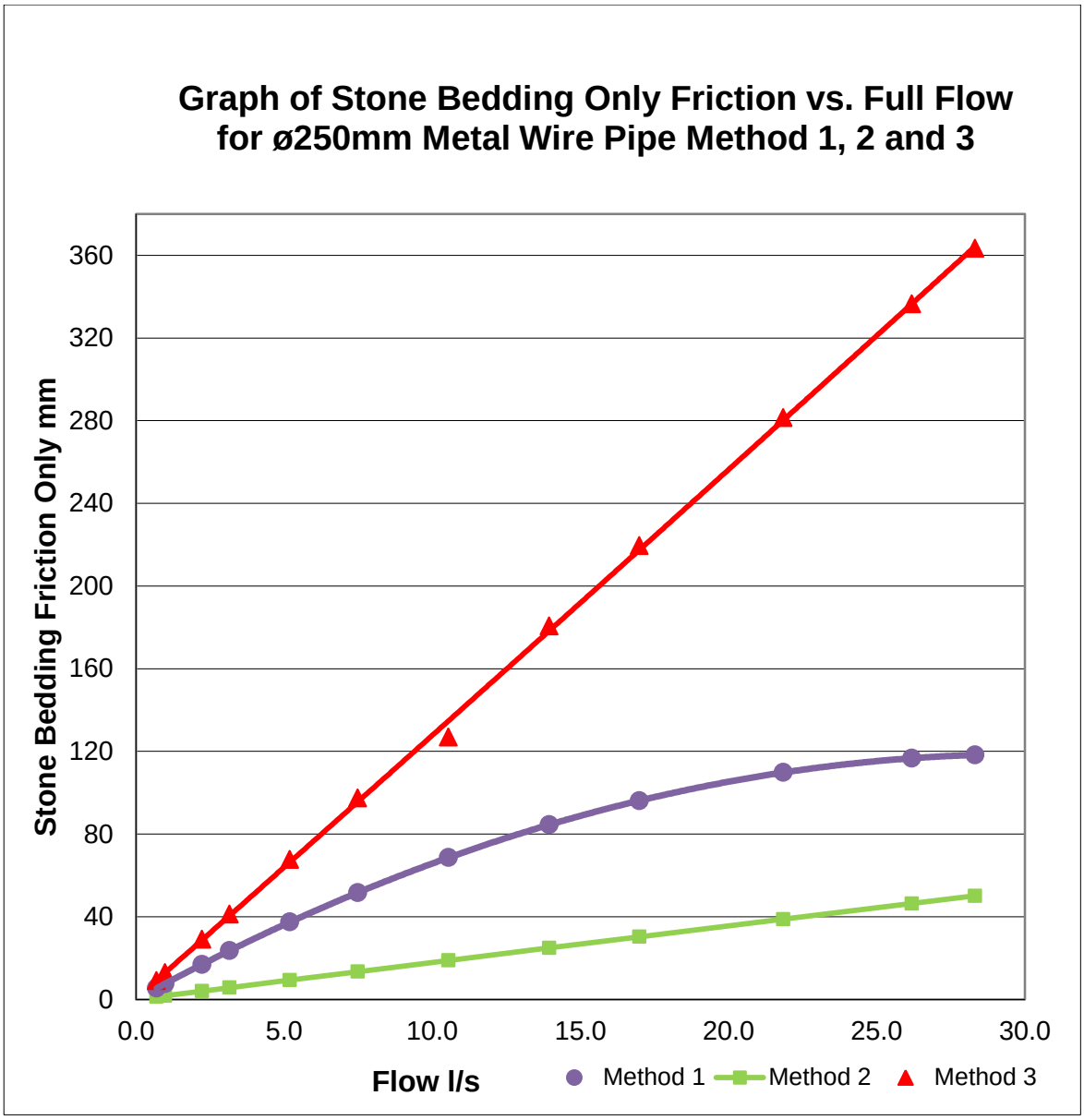

Figure G7: Metal Wire Pipe, Method 1, 2 and 3: Headloss due to the stone bedding

G.4.4 Results Summary of Method 1

This is a summary of "Method 1", which was conducted on all three pipe types. Table G8 contains the data for Figure G8 which is a graphical comparison of the results

Table G8: Comparison of Method 1 for all three pipe types.

Slotted PVC Pipe		Perforated PVC Pipe with Extra Perforation		Metal Wire Pipe	
Method 1 Stone Bedding loss mm	Q Full Pipe l/s	Method 1 Stone Bedding loss mm	Q Full Pipe l/s	Method 1 Stone Bedding loss mm	Q Full Pipe l/s
0.40	0.66	0.00	0.19	5.43	0.70
0.67	1.06	0.01	0.22	7.64	0.98
1.15	1.68	0.02	0.28	16.94	2.23
1.99	2.62	0.80	0.53	23.62	3.16
4.31	4.67	0.96	0.87	37.46	5.20
6.09	5.95	1.08	1.64	51.73	7.49
9.89	8.23	2.69	2.15	68.63	10.54
20.30	12.90	4.76	2.62	84.58	13.95
27.59	15.51	8.56	3.29	96.22	16.99
38.12	18.74	14.11	4.04	109.83	21.85
45.92	20.85	25.23	5.20	116.76	26.19
54.99	23.10	37.27	6.19	118.36	28.32
67.47	25.92	63.03	7.88		
79.94	28.49	78.25	8.71		
86.90	29.83	96.26	9.60		
		111.85	10.31		
		123.02	10.78		
		141.84	11.53		

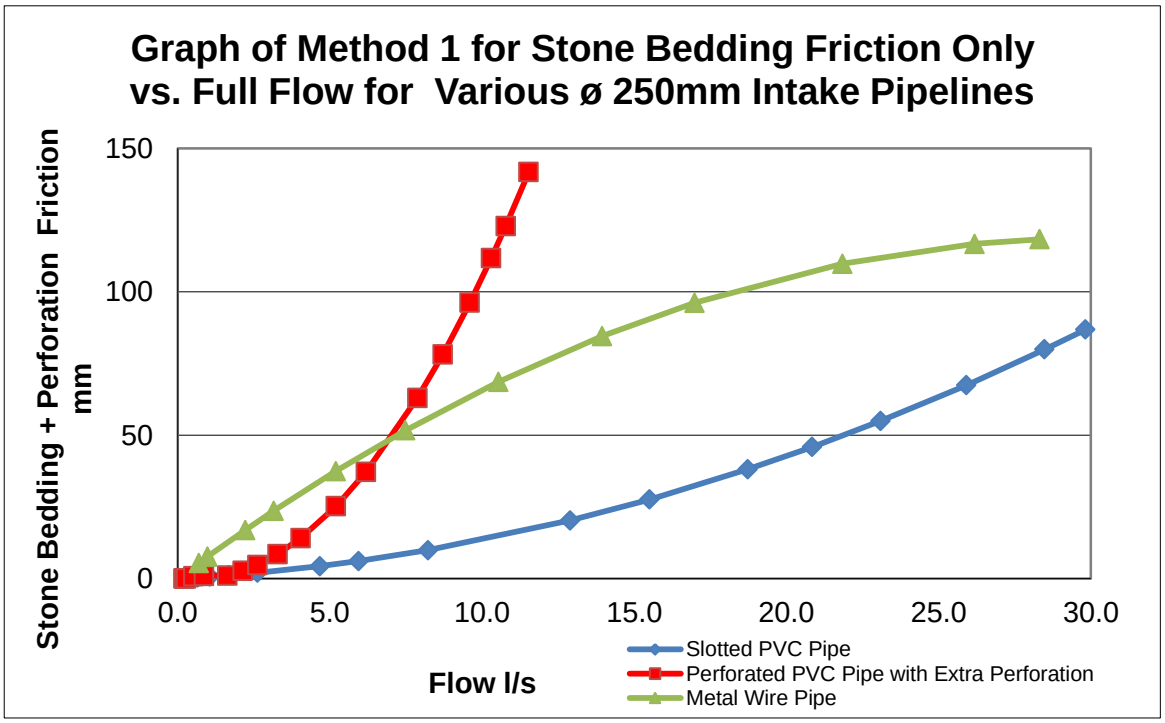

Figure G8: Comparison of Method 1 for all three pipe types

G.4.5 Results Summary of Method 2

This is a summary of Method 2, which was conducted on all three pipe types. Table G9 contains the data for Figure G9 which is a graphical comparison of the results

Table G9: Comparison of Method 2 for all three pipe types.

Intake Pipe Types	Slotted PVC Pipe		Perforated PVC Pipe with Extra Perforation		Metal Wire Pipe	
Test No.	Method 2 Stone Bedding loss mm	Q Full Pipe l/s	Method 2 Stone Bedding loss mm	Q Full Pipe l/s	Method 2 Stone Bedding loss mm	Q Full Pipe l/s
1	0.64	0.66	0.18	0.19	1.25	0.70
2	1.03	1.06	0.21	0.22	1.77	0.98
3	1.64	1.68	0.27	0.28	4.01	2.23
4	2.55	2.62	0.51	0.53	5.69	3.16
5	4.54	4.67	0.85	0.87	9.34	5.20
6	5.78	5.95	1.59	1.64	13.44	7.49
7	8.00	8.23	2.08	2.15	18.88	10.54
8	12.54	12.90	2.55	2.62	24.93	13.95
9	15.07	15.51	3.19	3.29	30.30	16.99
10	18.21	18.74	3.93	4.04	38.84	21.85
11	20.27	20.85	5.05	5.20	46.43	26.19
12	22.46	23.10	6.01	6.19	50.14	28.32
13	25.20	25.92	7.65	7.88		
14	27.69	28.49	8.46	8.71		
15	29.01	29.83	9.32	9.60		
			10.01	10.31		
			10.47	10.78		
			11.2	11.53		

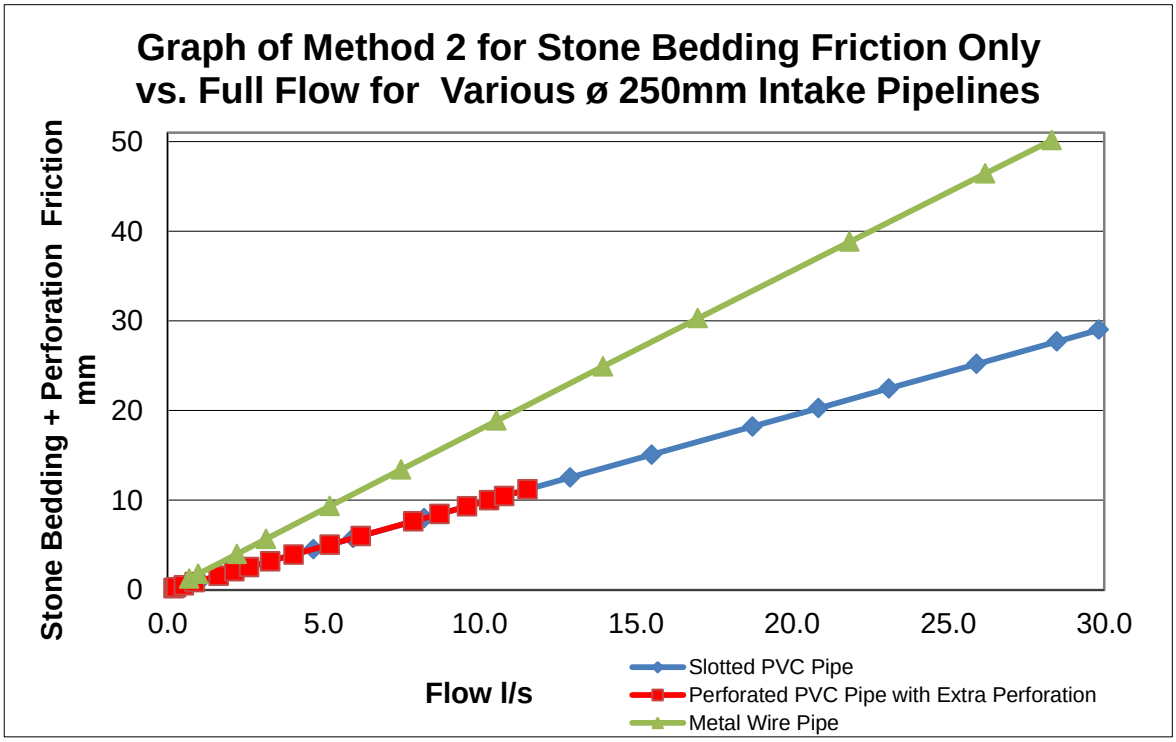

Figure G9: Comparison of Method 2 for all three pipe types

G.4.6 Results Summary of Method 3

This is a summary of Method 3, which was conducted on all three pipe types. Table G10 contains the data for Figure G10 which is a graphical comparison of the results

Table G10: Comparison of Method 3 for all three pipe types.

Intake Pipe Types	Slotted PVC Pipe		Perforated PVC Pipe with Extra Perforation		Metal Wire Pipe	
Test No.	Method 2 Stone Bedding loss mm	Q Full Pipe l/s	Method 2 Stone Bedding loss mm	Q Full Pipe l/s	Method 2 Stone Bedding loss mm	Q Full Pipe l/s
1	6.02	0.66	1.795	0.19	9.09	0.70
2	9.85	1.06	1.999	0.22	12.85	0.98
3	15.75	1.68	2.554	0.28	29.09	2.23
4	23.95	2.62	4.87	0.53	41.20	3.16
5	43.25	4.67	8.098	0.87	67.67	5.20
6	55.00	5.95	15.16	1.64	97.35	7.49
7	76.00	8.23	19.86	2.15	126.82	10.54
8	119.50	12.90	24.26	2.62	180.65	13.95
9	143.50	15.51	30.45	3.29	219.53	16.99
10	173.20	18.74	37.42	4.04	281.43	21.85
11	192.70	20.85	48.14	5.20	336.42	26.19
12	214.00	23.10	57.32	6.19	363.34	28.32
13	239.70	25.92	72.93	7.88		
14	263.80	28.49	80.65	8.71		
15	276.00	29.83	88.87	9.60		
			95.38	10.31		
			99.77	10.78		
			106.75	11.53		

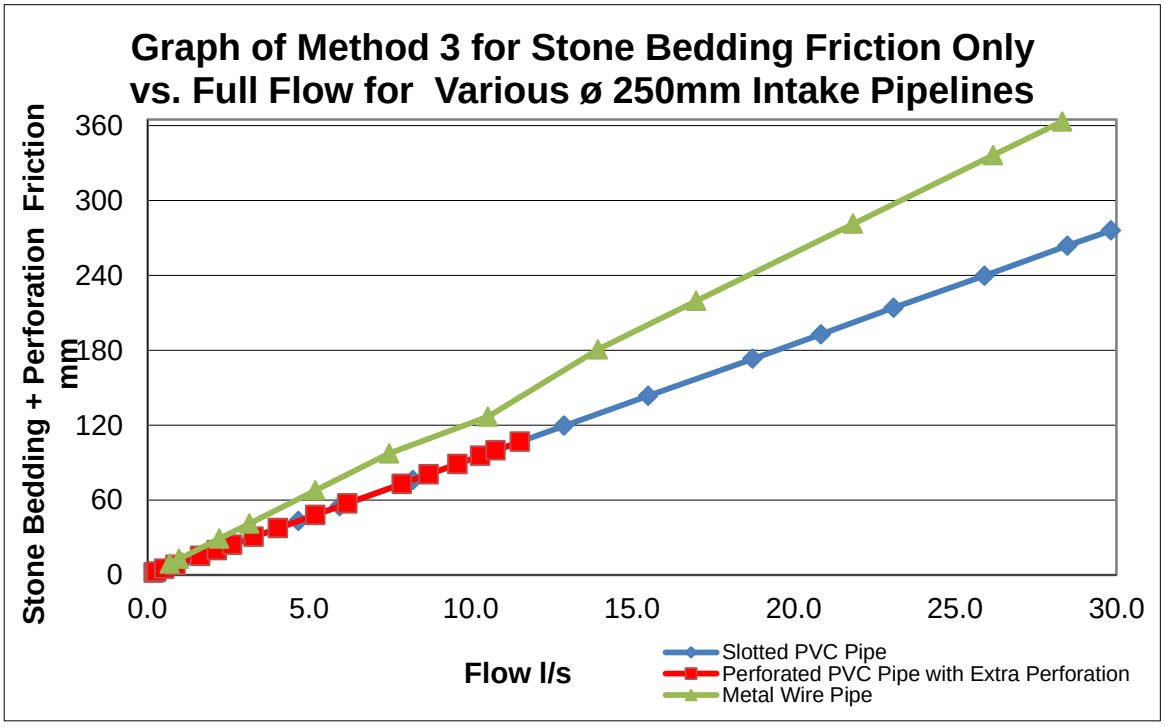

Figure G10: Comparison of Method 3 for all three pipe types

G5 Estimating Pressure losses due to Sand and Stone Bedding

This test was only undertaken on the Perforated Pipe. These tests could have been carried out on the other two pipes, however since the flow rates through them was far below the required design flows. If the aim was to test the horizontal well for sandy beaches, then these tests would prove essential.

Method 1: Simple method for determining stone bedding loss

This simplistic method, is basically the result of the “Stone and water test” minus the “Water Only test”

Method 2: Method for determining stone bedding loss : Hydraulic conductivity: Kenny, Lau and Ofoegbu

The second method used to determine the loss of pressure due to Stone bedding, looks at the hydraulic conductivity of stone bedding. Equation by Kenny, Lau and Ofoegbuare used to estimate stone bedding headloss.

Method 3: Method for determining stone bedding loss : Hydraulic conductivity: Forchheimer

The third method used to determine the loss of pressure due to Stone bedding, stems from work carried out by Forchheimer. This method use Figure 2.35 to estimate the permeability of the stone bedding and hence the headloss.

The following Table and Figures show the results of Method 1, 2 and 3 that were used to calculate the stone bedding friction for all three intake pipes. The full flow is used in this sub chapter.

G5.1 Perforated PVC Pipe

Table G11: Method 1, 2 and 3:Headloss due to Sand and Stone bedding

Test No.	Total Q	Total 2Q	Method 1 Stone bedding Headloss	Method 2 Stone bedding Headloss	Method 3 Stone bedding Headloss
	l/s	l/s	mm	mm	mm
1	0.17	0.33	18	0.31	3.09
2	0.58	1.15	64	1.069	10.66
3	1.13	2.26	128	2.094	20.88
4	1.44	2.87	165	2.667	26.59
5	1.73	3.46	201	3.208	32.00
6	2.65	5.29	320	4.914	49.02
7	3.15	6.30	390	5.85	58.39

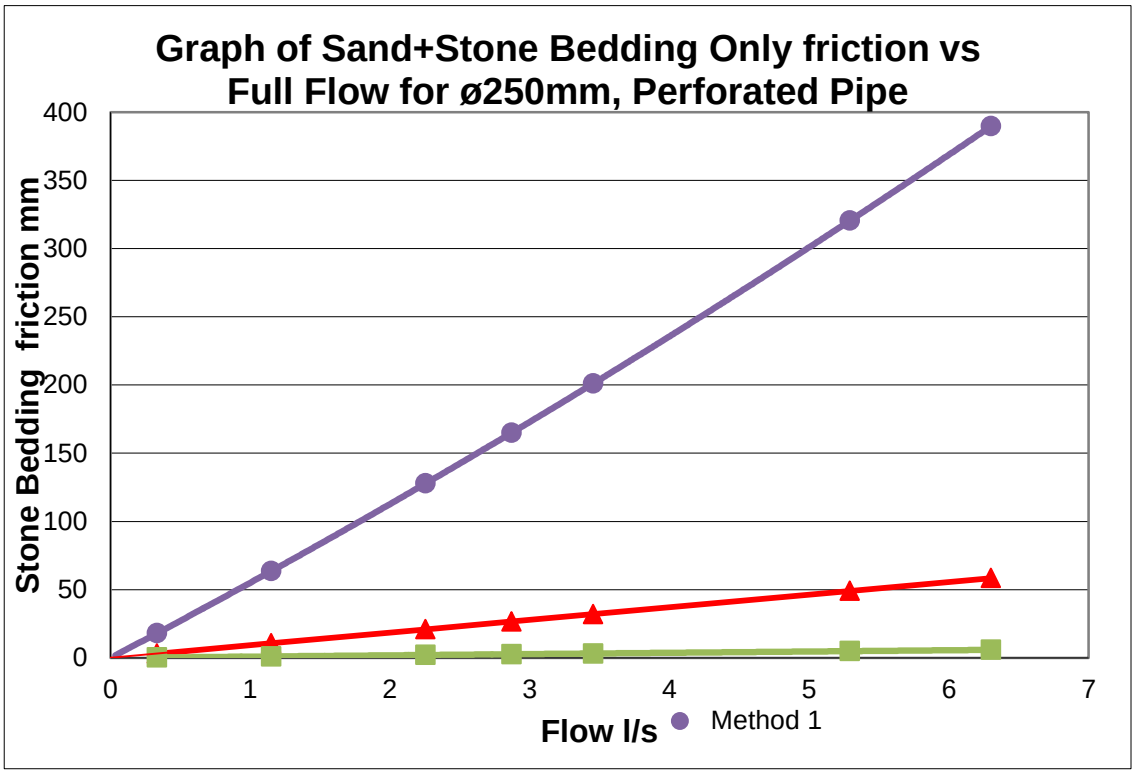

Figure G11: Perforated PVC Pipe Method 1, 2 and 3: Headloss due to the sand and stone bedding